# EVALUATION OF SHALLOW FOUNDATION DISPLACEMENTS USING SOIL SMALL-STRAIN STIFFNESS

A Dissertation
Presented to
The Academic Faculty

by

Amr Farouk Elhakim

In Partial Fulfillment
Of the Requirements for the Degree
Doctor of Philosophy in Civil and Environmental Engineering

Georgia Institute of Technology
August 2005

**EVALUATION OF SHALLOW FOUNDATION DISPLACEMENTS USING SOIL SMALL-STRAIN STIFFNESS**

Approved by:


Prof. Paul W. Mayne, Advisor
College of Engineering
*Georgia Institute of Technology*

Prof. Glenn J. Rix
College of Engineering
*Georgia Institute of Technology*

Prof. Alexander Puzrin
Institute of Geotechnical Engineering
*Swiss Federal Institute* of Technology

Prof. Robert Lowell
College of Sciences
*Georgia Institute of Technology*

Prof. Leonid Germanovich
College of Engineering
*Georgia Institute of Technology*


Date Approved: June 14th, 2005

This dissertation is dedicated to my family: my mother, father, wife and kids

## ACKNOWLEDGMENTS

First and foremost, I would like to thank Allah for giving me the opportunity to expand my knowledge and horizons. I am also grateful to Allah for the successful completion of my doctoral degree.

I would like to recognize Prof. Paul Mayne for all his guidance through my graduate studies at Georgia Tech. He helped me appreciate the importance of practicality in analyzing problems and to simplify solutions for convenient use. I would also like to thank Prof. Alexander Puzrin for all his advice and comments that were essential for the completion of this dissertation. I would also like to thank my committee members: Prof. Bob Lowell, Prof. Leonid Germanovich, and Prof. Glenn Rix for their time and effort. I would also like to acknowledge Prof. David Frost for lending me his version of the finite difference program FLAC for use in this research.

I would like to thank my parents and wife for all their support. Without their support, I would have never been able to finish my dissertation. I would also like to thank my son Abdullah and daughter Amina and apologize for all the time I spent away from them because of my work.

I would also like to acknowledge the people who helped me in different ways during my time at Georgia Tech: Mohamed Hilali, Ahmed Bayoumi, Kathryn Aguilar, Alec McGillivary, Guillermo Zavala, Tianfei Liao, and Maria Guimaraes.

I am sure I have forgotten to mention many people so I would like to extend my thanks to all of them.

## TABLE OF CONTENTS

## LIST OF TABLES

## LIST OF FIGURES

## SUMMARY

Foundation performance is controlled significantly by the stress-strain-strength behavior of the underlying soils which is complex and affected by stress level, direction of loading, anisotropy, strain rate, age, and drainage. For geomaterials, the small-strain shear modulus $G_{max}$ is a fundamental stiffness applicable to both monotonic static and dynamic loading conditions, as well to both drained and undrained loading. Yet, $G_{max}$ is too stiff for direct use in computing foundation displacements using either simple elastic analytical methods or linear elastic-plastic constitutive models contained within geotechnical finite element codes. The main objectives of this research are to: (1) explore the scaled parallelism between the stress-strain-strength behavior of the single soil element response and the load-displacement-capacity of a shallow foundation system supported on soil; (2) develop a methodology for evaluating the performance of vertically-loaded footings using a rational framework based on the small-strain modulus $G_{max}$, large-strain strength ($\tau_{max}$ or $s_u$) and strain at failure; and (3) calibrate the proposed method using a foundation database of full-scale load tests under both undrained and drained conditions.

In geotechnical practice, foundation bearing capacity is handled as a limit plasticity calculation, while footing displacements are evaluated separately via elastic continuum solutions. Herein, a hybrid approach is derived that combines these two facets into a closed-form analytical solution for vertical load-deflection-capacity based on numerical studies. Here, a non-linear elastic-plastic soil model was developed to simulate the stress-strain-strength curves for simple shearing mode (LOGNEP) for each soil element.

The model was encoded into a subroutine within the finite difference program FLAC. A large mesh was used to generate load-displacement curves under circular and strip footings for undrained and drained loading conditions. With proper normalization, parametric foundation response curves were generated for a variety of initial stiffnesses, shear strengths, and degrees of non-linearity in the soil stress-strain-strength response. In all cases, the fundamental small-strain stiffness $G_{max}$ has been used as the initial reference. Soil stress-strain non-linearity is described by a logarithmic function (Puzrin & Burland, 1996, 1998) that utilizes a normalized strain $x_L$ that relates strain at failure $\gamma_f$, shear strength ($\tau_{max}$ or $s_u$), and small-strain stiffness $G_{max}$, all having physical meaning. A closed-form algorithm is proposed for generating non-linear load-displacement curves for footings and mats within an equivalent elastic framework. The proposed method was calibrated using a database of well-documented footing load tests where soil input parameters were available from laboratory and/or in-situ field test results.

# CHAPTER I

# INTRODUCTION

*"Foundations represent about 30 percent of the cost of highway bridges in typical applications; however, this cost can be even higher where bridges are built near or on difficult soil conditions. The total annual expenditure of (U.S.) public funds for bridge construction is conservatively estimated to be more than $2 billion, which means that foundations are costing more than [600 million] dollars per year" (DiMillio, 2004).*

## 1.1 Background

With the rapid growth of urban areas and world population now exceeding 6 billion, there is an ever greater need to build more civil structures including buildings, bridges, walls, dams, ports, towers, and other facilities. For example, each year about 6,000 new bridges are built in the United States alone (Briaud and Gibbens, 1999). In Asia, construction of new infrastructure is at a rapid pace that is unparalleled in the history of mankind. There is an excessive dependence on driven pile foundations, mainly because of lack of confidence in other foundation types such as spread footings (DiMillio, 2004). Any successful design must guarantee the structure is safe under maximum loads. In addition, the designer must ensure the superstructure does not suffer from excessive displacements. Massarsch (2004) notes that geotechnical engineers are traditionally better trained to deal with stability and bearing capacity problems, while the design of a structure under operating working conditions usually requires more sophisticated analyses. Fahey (1998)

points to the limited accuracy in predicting soil displacements due to foundation loading, caused primarily by neglecting the effects of non-linear soil stress-strain response. Therefore, improvements in methods to evaluate shallow foundation displacements are important and should be pursued.

The stress-strain-strength behavior of soils is complex and depends on many factors including: stress level, direction of loading, anisotropy, strain rate of loading, ageing, and drainage. Small-strain stiffness represents a reference value for a specific confining stress. The small-strain shear modulus $G_{max}$ is a fundamental stiffness applicable to both static and dynamic loading (e.g. Burland, 1989; Tatsuoka et al., 2001). Moreover, the stiffness $G_{max}$ applies to both drained and undrained loading, because excess porewater pressures do not yet develop at such small strains. The value of $G_{max}$ can be measured using a variety of laboratory and/or in-situ tests (e.g. Stokoe and Santamarina, 2000), or alternatively assessed using empirical correlations (e.g. Hardin and Drnevich, 1972).

However, $G_{max}$ is too stiff for direct use in computing foundation displacements using either simple elastic analytical methods or linear elastic-plastic constitutive models that are built-in to many commercial finite element programs. Therefore, a variety of non-linear elastic-plastic models have been proposed to better represent the true soil stress-strain behavior (e.g. Jardine et al., 1986; Fahey and Carter, 1993), yet the parameters of a good number of these models generally lack physical meaning (e.g. Lee and Salgado, 1999). Available constitutive models that can capture the full suite of sophisticated nuances of complex soil response often require many parameters, e.g. 15 separate input values for each soil layer in the case of MIT-E3 framework (Whittle, 1993). Barbour and

Krahn (2004) highlight that geotechnical engineers always have to deal with under-constrained systems with more unknowns than equations, which means that we must never increase the complexity of theories beyond the amount of available data. Until geotechnical site characterization is more fully developed to efficiently and economically provide these input parameters, engineering practice needs an intermediate step based in simpler algorithms that apply to both analytical and numerical solutions.

## 1.2 Main objectives

The main objectives of this research are: (1) to explore the scaled parallelism between loading of a single soil element and a foundation system supported on soil; (2) to develop a methodology that enables geotechnical engineers to predict the non-linear load-displacement behavior of shallow foundations under vertical loading based on a rational framework using the small-strain modulus ($G_{max}$) to large-strain strength ($\tau_{max}$ or $s_u$); and (3) to calibrate the proposed method using a database of the load-displacement response of shallow footings under both undrained and drained conditions. Non-linearity is described by a normalized strain ($x_L$) which relates strain at failure ($\gamma_f$), shear strength ($\tau_{max}$ or $s_u$), and small-strain stiffness, all having physical meaning. In routine practice, bearing capacity is handled as one calculation, while foundation displacements are evaluated separately via elastic continuum solutions. Herein, a hybrid approach that integrates these two facets to facilitate a closed-form analytical solution for vertical load-deflection-capacity that is supported by numerical studies.

In order to achieve this goal, a non-linear elastic-plastic model was developed to simulate the load-displacement curves under circular and strip footings for undrained and drained loading conditions. The model is encoded into a subroutine within the commercial finite difference program FLAC (Itasca Consulting Group Inc., 2001c). With proper normalization, generalized load-displacement curves are generated for a variety of initial stiffnesses, shear strengths, and degrees of non-linearity in the soil stress-strain-strength response. In all cases, the fundamental small-strain stiffness $G_{max}$ has been used as the initial reference.

A new approximate closed-form analytical solution is proposed for generating non-linear load-displacement curves for footings and mats within an equivalent elastic framework. The proposed method was calibrated using a database of well-documented footing load tests where soil input parameters could be evaluated from laboratory and/or in-situ field test results. Figure 1-1 provides a schematic diagram illustrating the proposed method for simulating load-displacement foundation response.

## 1.3 Thesis outline

The dissertation is composed of eleven chapters and seven appendices.

In Chapter 2, the definition of foundation bearing capacity is established. Different criteria for interpreting bearing capacity from load-displacement data are reviewed. Analytical solutions for computing bearing capacity are reviewed and compared.

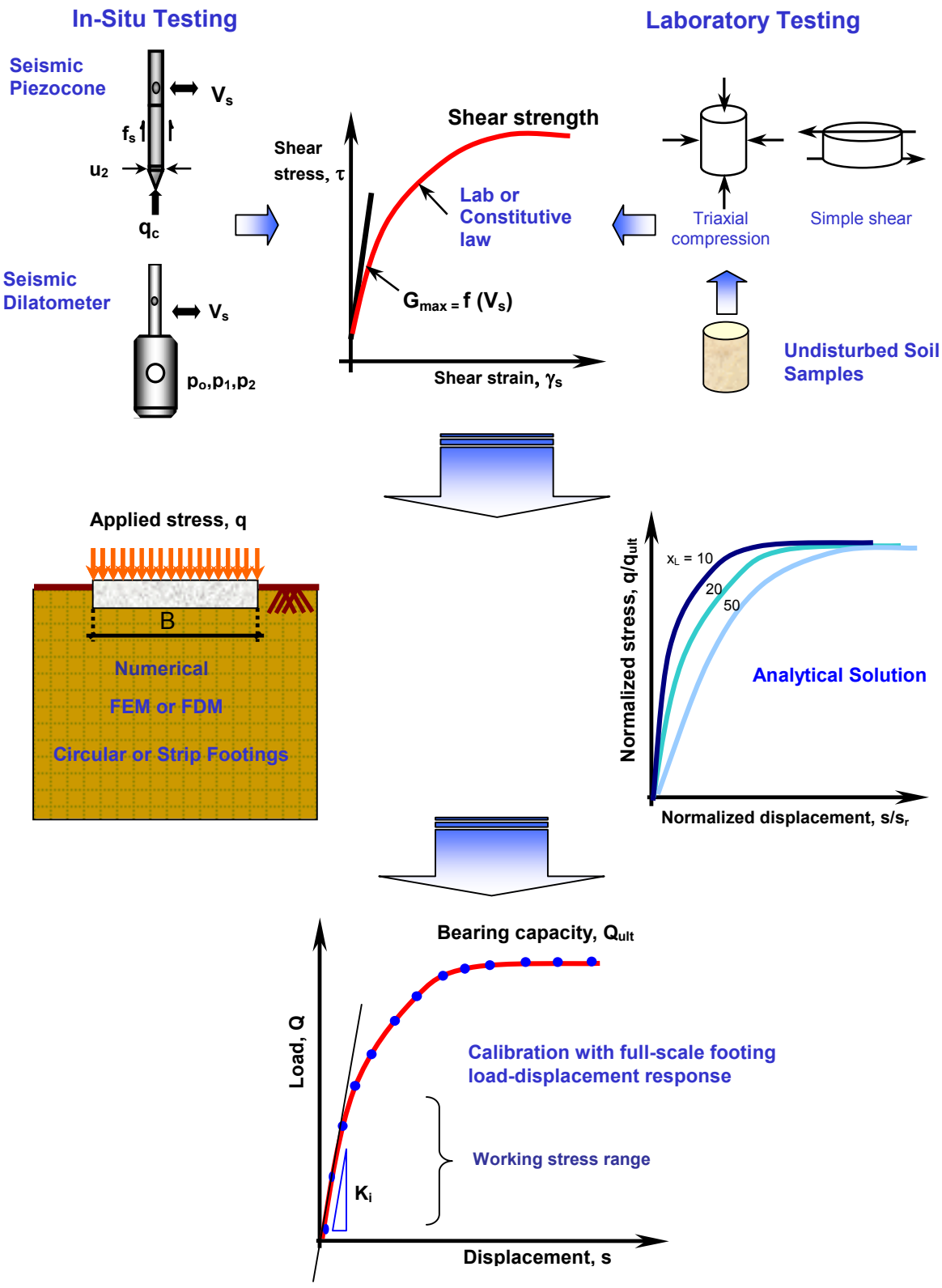


**Figure 1-1.** Schematic diagram illustrating the purpose of the current study of relating soil behavior on the element level to the overall behavior of a soil mass under loading

The use of elastic theory solutions for computing footing displacements is discussed in Chapter 3. A new approximate closed-form solution for calculating the displacement influence factors for circular shallow footings is presented. Results compare favorably with published rigorous solutions and numerical methods.

In Chapter 4, different measures of soil stiffness are reviewed. The concept of the variation of soil stiffness with the strain level is discussed in context with the initial shear modulus ($G_{max}$) as this represents the fundamental beginning of all stress-strain-strength curves of geomaterials (e.g. Burland, 1989). Available analytical modulus reduction schemes for representing the non-linear stress-strain-strength regime are reviewed.

In Chapter 5, the logarithmic modulus reduction scheme (Puzrin and Burland, 1998) is presented in details. Factors influencing the degree of stress-strain non-linearity are investigated. Relationships between index soil properties and non-linear stress-strain behavior are explored.

The logarithmic non-linear elastic-plastic soil model LOGNEP used in this study is presented in Chapter 6. Model results are verified by comparison with the linear elastic-plastic model.

In Chapter 7, the load-displacement responses beneath circular and strip footings are simulated under undrained loading conditions are modeled using LOGNEP model. A new normalization scheme for load-displacement results is proposed. The new

normalization scheme allows the representation of the stress-displacement curves are developed that are solely dependent on the non-linear stress-strain-strength response of a single soil element.

Chapter 8 covers the modeling of circular and strip footings under drained loading conditions. The normalization scheme proposed in Chapter 7 is applied to simulated stress-displacement response under drained conditions. Generalized stress-displacement curves are created that are functions of angle of internal friction $\phi$' and the non-linear stress-strain response of a soil element.

In Chapter 9, an approximate closed-form solution for generating non-linear stress-displacement curves starting at initial stiffness $G_{max}$. Parallelism between the stress-strain behavior of a single soil element and footing stress-displacement response is highlighted.

In Chapter 10, the proposed model is applied to a database of actual and model footing load tests under both undrained and drained conditions for calibration.

Conclusions learned from this study are summarized in Chapter 11. Recommendations for future research are provided.

Appendix A provides the load-displacement data of the footing used in the bearing capacity database presented in Chapter 2.

The normalized limiting strain $x_L$ is calibrated using a database of laboratory stress-strain response as presented in Appendix B. The appendix also contains a database of failure strains from direct simple shear tests.

Appendix C contains the load-displacement data and relevant soil parameters at used in analyzing the footing load tests of Chapter 10.

The use of the seismic piezocone in evaluating soil properties needed for foundation design is presented in Appendix D.

A review the bearing capacity factors for shallow foundations is included in Appendix E.

A database of modulus reduction data from triaxial and plane strain compression test results is compiled and presented in Appendix F.

The user-defined non-linear elastic plastic model LOGNEP, written in FISH language, is presented in Appendix G.

# CHAPTER II

# BEARING CAPACITY OF SHALLOW FOUNDATIONS

## 2.1 Introduction

The bearing capacity of a shallow foundation can be defined conceptually as the ultimate stress ($q_{ult}$) as the footing approaches infinite settlement. The onset of failure is associated with the full mobilization of shear strength along a prescribed failure surface and excessive displacement as the soil target stiffness approaches zero. A schematic diagram of the stress-displacement-capacity relationship of an axially-loaded footing is shown in Figure 2-1.

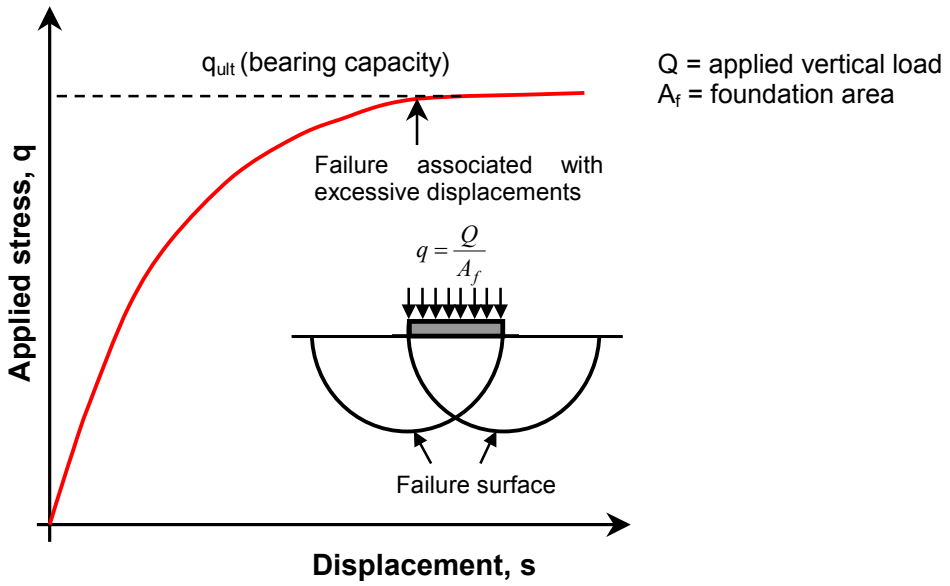


**Figure 2-1.** Idealized axial load-displacement-capacity response of shallow foundations

In full-scale loading of foundations, a reality check must be brought under consideration as "bearing capacity" may be construed at loads less than ultimate due to constraints of performance and/or equipment limitations. In this chapter, traditional methods for determining the bearing capacity using analytical, numerical, empirical, and experimental methods are reviewed. Usually, in geotechnical practice, either analytical or empirical solutions are used to provide an evaluation of the ultimate bearing capacity. The bearing capacity is subsequently reduced using a factor of safety ($FS \geq 3$) to obtain the allowable foundation bearing stress ($q_{allow} = q_{ult}/FS$) for which all footings of the structure are sized.

## 2.2 Evaluation of bearing capacity from experimental data

The most definitive means for determining the bearing capacity is to conduct full-scale load tests (e.g. Briaud and Gibbens, 1999). Because load tests are very expensive and time consuming, they are essentially restricted to research programs or large special projects involving very poor ground conditions and/or critical structures. Conducting plate load tests (e.g. Andersen and Stenhamar, 1982), which are smaller scaled-down versions at full-scale tests, are easier and more economical. Nevertheless, plate load test data need to be manipulated to account for the difference in size between the prototype and plate. This could especially be problematic in layered soil profiles or ground conditions with varying stiffness with depth because of the variation in soil properties with depth, as shown in Figure 2-2, and small plate load tests would not scale up conservatively. Employment of a field compressometer (screw plate) could be used at different depths (Strout, 1998) to alleviate this concern.

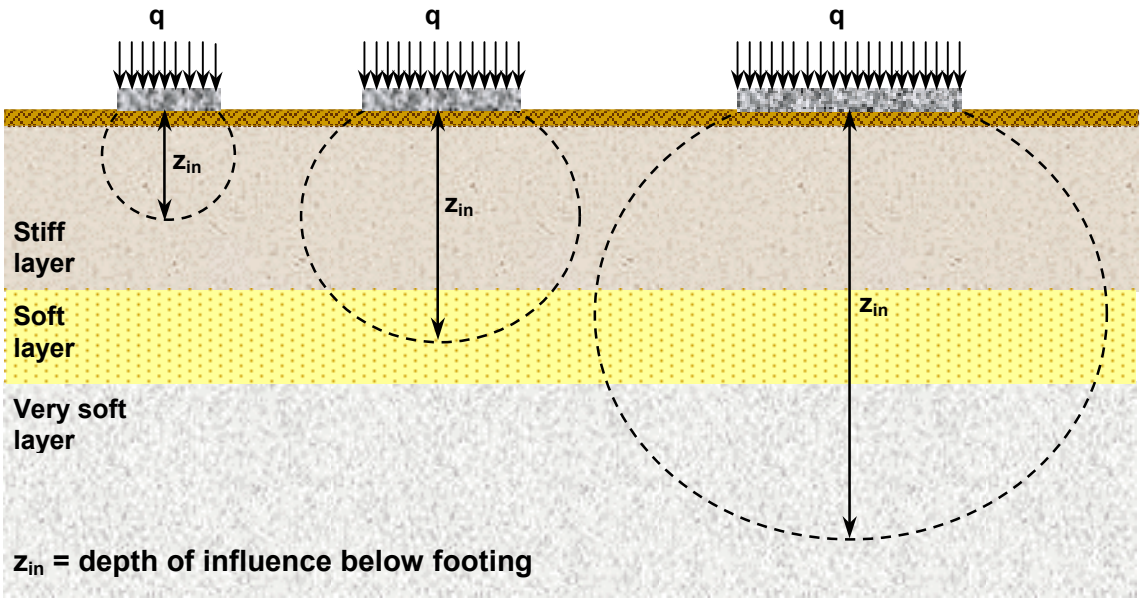


**Figure 2-2.** Effect of footing size on the zone of influence beneath shallow footings in layered soil profiles

Other experimental methods for determining bearing capacity include 1-g model tests (e.g. Kinner and Ladd, 1973), calibration chamber tests (e.g. Lee, 1999), and centrifuge testing, as used in the offshore industry (e.g. Stallebrass and Taylor, 1997). Yet such methods are suitable only for research purposes, as it is impossible to reproduce exact site conditions in the laboratory. Most laboratory setups require reconstituted or remolded soil "deposits" that do not reflect the complete stress history, aging, time effects, fine stratigraphical detailing, and inherent structural fabric, amongst other facets. Due to time and cost restrictions, practitioners resort to simpler procedures including empirical, analytical, or numerical methods. Figure 2-3 summarizes selected methods for evaluating the bearing capacity of shallow footings. Most commonly, geotechnical engineers in practice employ limit plasticity solutions or empirical guidelines involving spread footings on level ground.

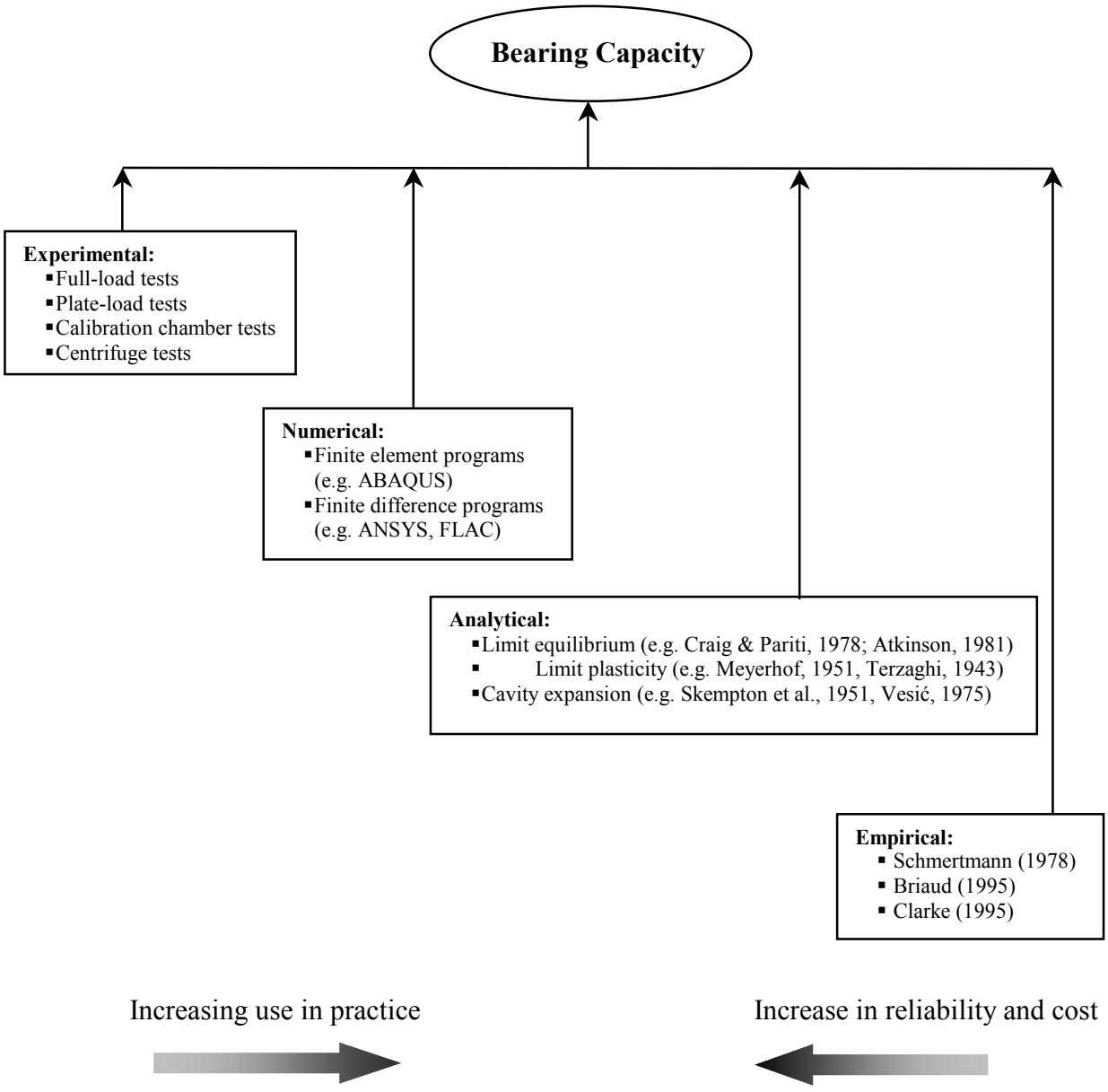


**Figure 2-3.** Methods for determining the bearing capacities of shallow foundations

With the growing surge in computing power, the inevitable simulation by numerical finite element or finite difference modeling for routine bearing capacity calculations is near. Moreover, as rather generous factors of safety are used in practice (generally $FS \geq 3$), the consequences of an accurate bearing capacity evaluation are somewhat unimportant. Only a "good" estimate is needed, as working stresses are much lower. Consequently, an increased accuracy in foundation displacements becomes a prime concern. In this dissertation, a continuous linkage from small-strain displacements to intermediate values to bearing capacity is developed.

### *2.2.1 Defining bearing capacity*

Conceptually, bearing capacity "failure" is defined when a constant stress is reached (see Figure 2-1). However, foundation load tests do not always reach a well-defined peak stress because of practical limitations on field equipment and test setups, or because a progressive failure allows repositioning of soil particles beneath the foundation, thereby the highest stress is not fully achieved. This creates ambiguity in defining the "true" bearing capacity, as illustrated by the stress-displacement load data from Texas A and M (Briaud and Jeanjean, 1994) presented in Figure 2-4. Towards the elucidation of defining "bearing capacity" from a more practical standpoint, a database of the measured load-displacement responses from 29 load tests conducted on full-scale footings and large plates was compiled. The full set of data is from 14 test sites, as presented in Figure 2-5.

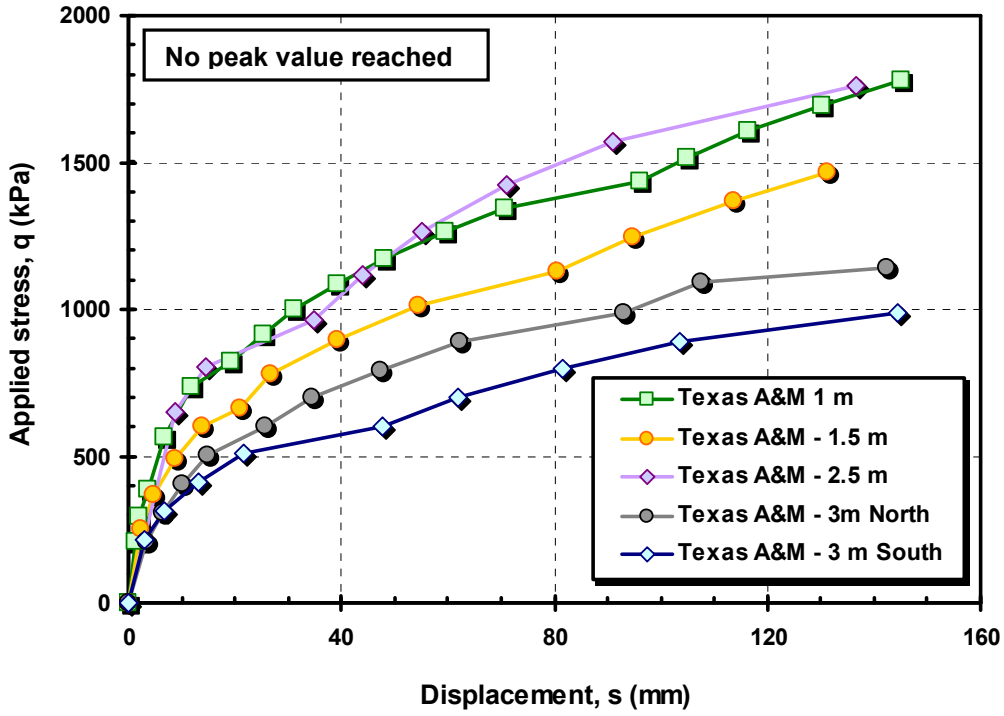


**Figure 2-4.** Stress-displacement load test data from five footings resting on sand at Texas A and M (Briaud and Jeanjean, 1994)

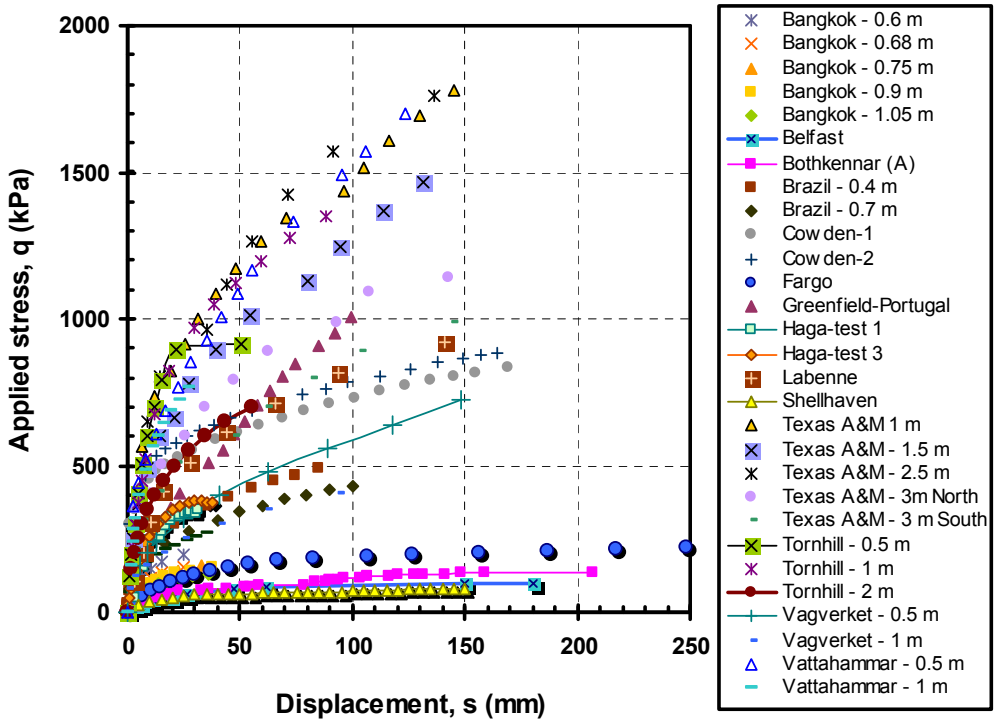


**Figure 2-5.** Measured stress versus displacement for 29 footings on different soil types (clays, silts and sands)

**Table 2-1.** Database of shallow footing load tests

| *Site* | *Soil Type* | *GWT (m)* | *Foundation dimensions B x L (m x m)* | *Test No.* | *Drainage Conditions during loading* | *Reference* |
|---|---|---|---|---|---|---|
| Bangkok, Thailand | Soft clay | 0 | 1.05 x 1.05 | BK-1 | Undrained | Brand et al. (1972) |
| | | | 0.9 x 0.9 | BK-2 | | |
| | | | 0.75 x 0.75 | BK-3 | | |
| | | | 0.675 x 0.675 | BK-4 | | |
| | | | 0.6 x 0.6 | BK-5 | | |
| Belfast, Ireland | Soft clayey silt | 0 | 2 x 2 | BL-1 | Undrained | Lehane (2003) |
| Bothkennar, UK | Soft marine to estuarine clay | 0.2 | 2.2 x 2.2 | BO-1 | Undrained | Hight et al. (1997) Jardine et al. (1995) |
| Cowden, UK | Glacial till | 1[a] | 0.865 x 0.865 | CO-1 | Undrained | Marsland & Powell (1980) |
| | | | 0.865 x 0.865 | CO-2 | | |
| Fargo, USA (Grain Elevator) | Silty clay (sand layer 4.5 to 6m) | 2.2 | 66.5 x 15.9 | FO-1 | Undrained | Nordlund and Deere (1972) |
| Federal University of Rio Grande do Sul, Brazil | Silty sand residuum | 4 | 0.4 x 0.4 | BR-1 | Partially Saturated | Consoli et al. (1998) |
| | | | 0.7 x 0.7 | BR-2 | | |
| Greenfield, Portugal | Silty sand to silty clayey Sand | variable | 1.2 x 1.2 (Circular) | GR-1 | Partially Saturated | Viana da Fonseca (2001) |
| Haga, Norway | Medium stiff OC clay | > 8 | 1 x 1 | HA-1 | Undrained | Andersen and Stenhamar (1982) |
| | | | 1 x 1 | HA-2 | | |
| Labenne, France | Dune sand | 3 | 0.7 x 0.7 | LA-1 | Drained | Amar, et al (1984) |
| Shellhaven, UK | Soft clay | 0.75 | 5 x 14 | SN-1 | Undrained | Schnaid et al. (1993) |
| Texas A & M, USA | Eocene deltaic sand | 4.9 | 1 x 1 | TX-1 | Drained | Briaud and Gibbens (1999) |
| | | | 1.5 x 1.5 | TX-2 | | |
| | | | 2.5 x 2.5 | TX-3 | | |
| | | | 3 x 3 | TX-4 | | |
| | | | 3 x 3 | TX-5 | | |
| Tornhill, Sweden | Clay till | 0.2 | 0.5 x 0.5 | TL-1 | Drained | Larsson (1997) |
| | | | 1 x 1 | TL-2 | | |
| | | | 2 x 2 | TL-3 | | |
| Vagverket, Sweden | Silt | 0.2 | 0.5 x 0.5 | VT-1 | Drained | Larsson (1997) |
| | | | 1 x 1 | VT-2 | | |
| Vattahammar, Sweden | Silt to clayey silt | 12.65 | 0.5 x 0.5 | VR-1 | Drained | Larsson (1997) |
| | | | 1 x 1 | VR-2 | | |

Notes:

[a] Underdrainage to lower chalk layer. Ground water table is not fully hydrostatic.

GWT = groundwater table below foundation level

B = footing width

L = footing length

The tests were conducted under different drainage conditions varying from fully drained (e.g. Texas A & M, USA; and Tornhill, Sweden) to undrained conditions (e.g. Belfast), as well as partially unsaturated states (e.g. Greenfield, Portugal; and Rio Grande do Sul, Brazil). The maximum applied stresses at "failure" were as low as 79 kPa to as high as 1800 kPa.

Several definitions of bearing capacity have been proposed in an attempt to have consistent evaluations (e.g., Brinch Hansen, 1963; De Beer, 1970; Vesić, 1973; Fellenius, 1980; Amar et al., 1998; Decourt, 1999). These methods are reviewed and applied to the case histories compiled in the database, with comparisons made between the interpreted bearing capacities from the different criteria.

#### *2.2.1.1 Brinch Hansen's method*

Brinch Hansen (1963) defined bearing capacity as the achieved stress $q_{cap}$ that produces a displacement twice that produced at 90% of $q_{cap}$, as shown in Figure 2-6. This is an iterative procedure where assumptions of $q_{cap}$ are made until this condition is satisfied.

#### *2.2.1.2 De Beer's method*

De Beer (1970) suggested plotting the load-displacement data on a log-log plot as shown in Figure 2-7. The bearing capacity is defined as the intersection of the two linear portions of the curve as demonstrated in Figure 2-7. Vesić (1973) noted that this method

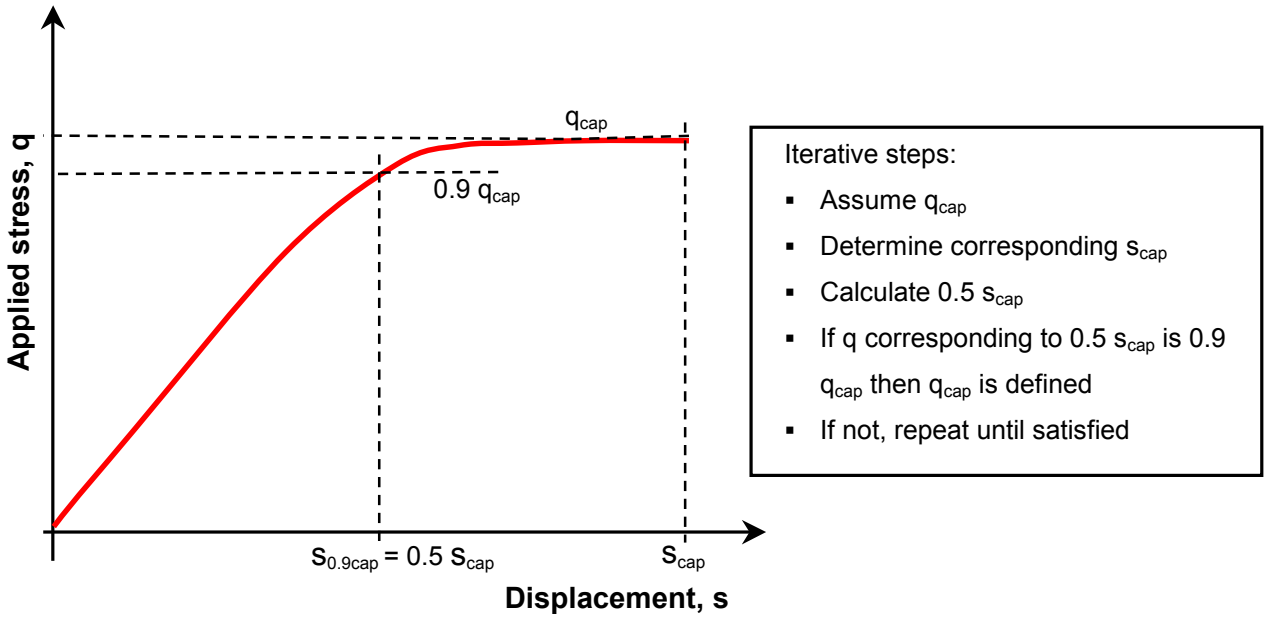


**Figure 2-6.** Brinch Hansen (1963) failure criterion

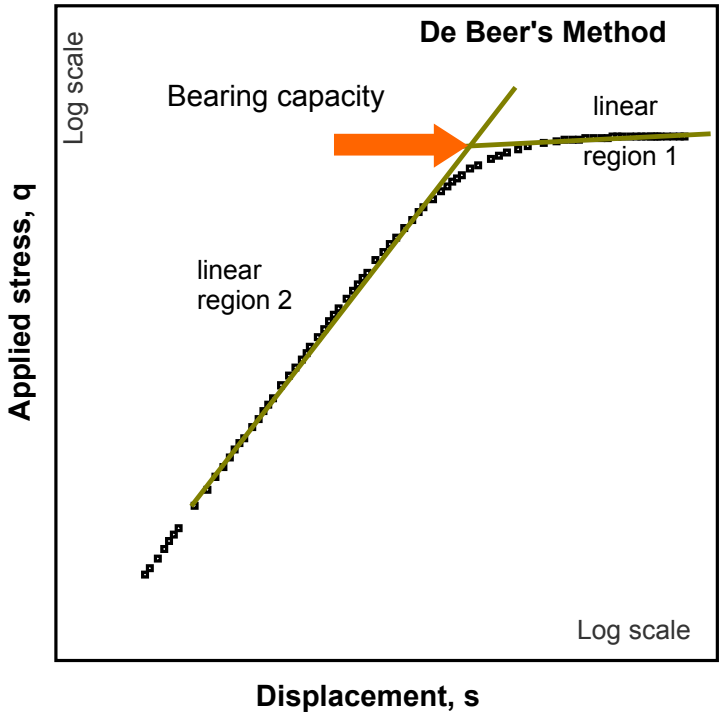


**Figure 2-7.** Determination of bearing capacity criterion according to De Beer (1970)

required loading the footing to a displacement of at least 50 % of the foundation width ($s/B \geq 0.5$). Although such high displacements are achievable for very small model tests (e.g. Vesić, 1973; Nakase et al., 1988), it is impossible to realize these very large deformations for full-scale footings that have widths between $0.3\ \text{m} \leq B \leq 6\ \text{m}$, nor for mat foundations with $B \geq 6$ m.

#### *2.2.1.3 s/B = 10% criterion*

The Laboratoires des Ponts et Chaussees (LPC) conducted a series of full-scale loading tests to update the French standards for shallow foundation design (Amar et al., 1994). Different types of loading (static and dynamic; short term and long term; eccentric and inclined loading) were applied to the foundations. Based on the LPC load tests, the bearing capacity of vertically-loaded footings was consistently defined as the load corresponding to a vertical displacement equal to 10 % of the foundation width (s/B = 0.1). The s/B ratio represents a pseudo-strain for surface loaded foundations. A similar criterion is also used for defining mobilized bearing capacity of deep foundations (e.g. Ghionna et al., 1994; Reese and O'Neill, 1988).

#### *2.2.1.4 Decourt's zero stiffness method*

Decourt (1999) proposed a graph of secant stiffness ($K_s = Q/s$) versus load Q to obtain the ultimate load for bearing capacity $Q_u$ when $K_s = 0$, as shown in Figure 2-8. According to this definition, no foundation has ever reached physical failure. Hence, by this criterion, bearing capacity can only be evaluated by extrapolation. Decourt (1999)

suggests that physical failure is only approached for displacement piles and shallow foundations resting on clays.

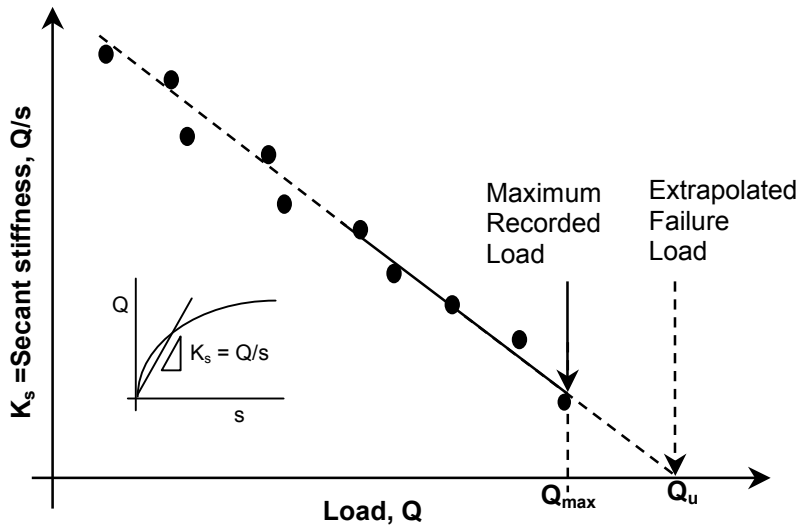


**Figure 2-8.** Schematic diagram demonstrating the use of footing-soil secant stiffness $K_s$ in determining the ultimate capacity according to Decourt's method (1999)

### *2.2.1.5 Hyperbolic asymptote*

One of the simplest forms to represent non-linear curves is the hyperbola as only two constants are required. Fitting a simple hyperbola to load-displacement test data has been used for evaluating the bearing capacity of piles **(**Chin, 1971**)** as well as representing laboratory stress-strain data (Kondner, 1963; Duncan and Chang, 1970). The simple hyperbolic relationship between stress q and pseudo-strain $\varepsilon_s$ (s/B) is:

$$q = \frac{\varepsilon_s}{\frac{1}{k_i} + \frac{\varepsilon_s}{q_{ult}}} \quad \text{.....(2-1)}$$

where $k_i$ = initial stiffness at zero displacement and $q_{ult}$ = ultimate load (asymptote of the hyperbola), as shown in Figure 2-9-a. The parameters $k_i$ and $q_{ult}$ are determined objectively by plotting the transformed axes: $\varepsilon_s/q$ versus $\varepsilon_s$, which is represented by a straight line given by:

$$\frac{\varepsilon_s}{q} = \frac{1}{q_{ult}} \cdot \varepsilon_s + \frac{1}{k_i} \quad \text{.....(2-2)}$$

where $1/k_i$ = y-intercept for zero displacement, and $1/q_{ult}$ is the slope of the straight line (see Figure 2-9-b). Thus, the hyperbola requires two constants ($k_i$ and $q_{ult}$) that are determined and have physical significance: the initial stiffness $k_i = q/s$ at $s = 0$, and the asymptote $q_{ult}$ at infinite displacements $(s \to \infty)$. A complete non-linear representation for all q and s can be generated, as depicted in Figure 2-9-a.

For comparison to Decourt's criterion, the hyperbola is presented graphically in Figure 2-9-c using Decourt's transformed axes stiffness $q/\varepsilon_s$ versus q. The equation describing the relationship is given by:

$$\frac{q}{\varepsilon_s} = k_i \left[ 1 - \frac{q}{q_{ult}} \right] \quad \text{.....(2-3)}$$

The initial stiffness $k_i$ represents stiffness at zero load. The ultimate stress $q_{ult}$ (which is achieved at infinite displacement) corresponds to zero stiffness $k_s$.

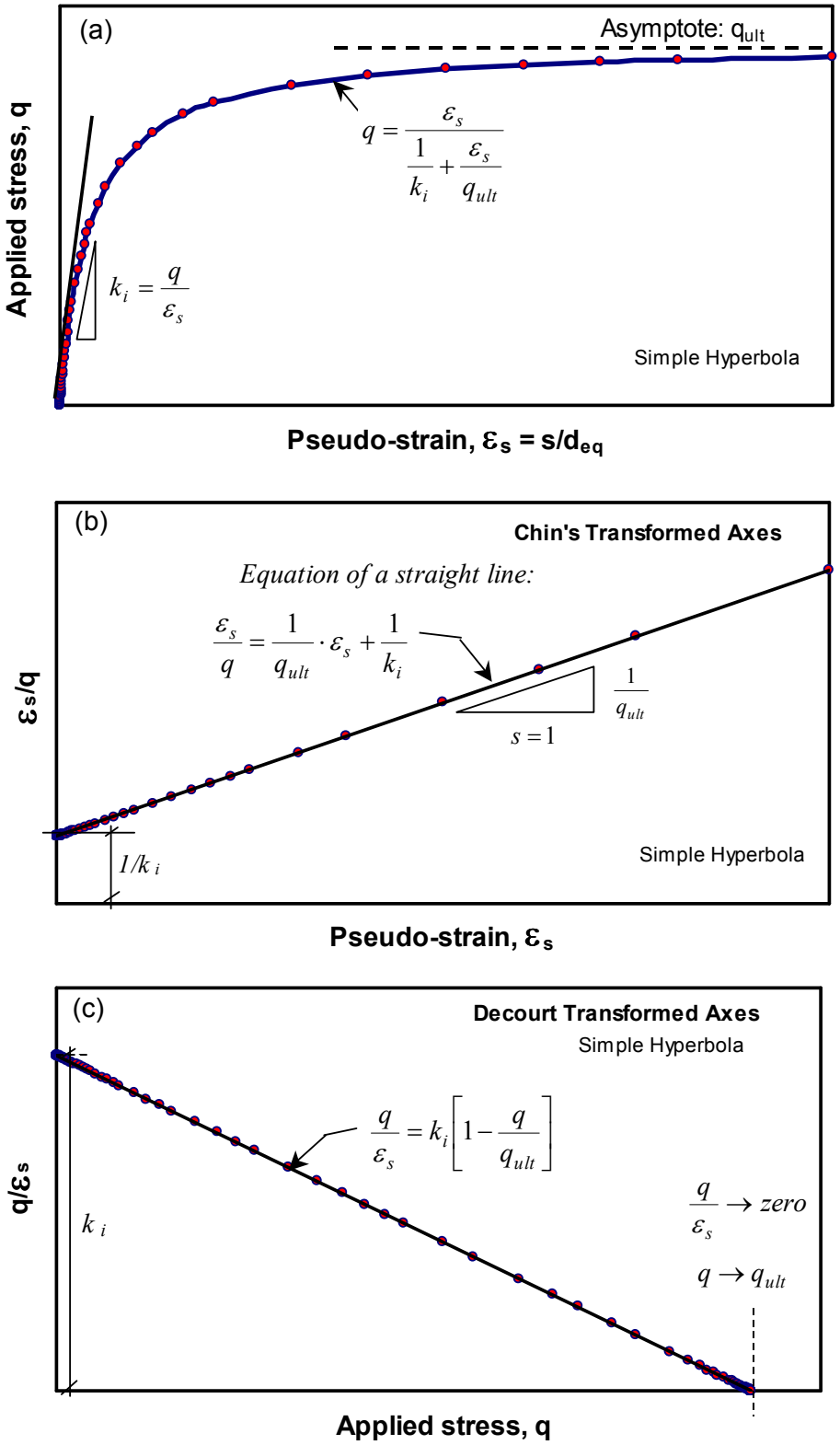


**Figure 2-9.** Load-displacement response (a) plotted on standard axes, (b) per Chin's transformed axes, and (c) per Decourt's zero stiffness procedure

### *2.2.2 Assessment of criteria for evaluating bearing capacity from load tests*

The question now is which of these criteria yields the most reasonable and consistent results in defining bearing capacities of shallow foundations. Five criteria (pseudo-strain = 10%, hyperbolic asymptote, zero-stiffness, Brinch Hansen, and De Beer) are applied to evaluate capacities for each of the load tests included in the database and compared with each other.

The Federal University of Rio Grande do Sul of Brazil conducted a comprehensive experimental footing and plate load test program. Load-displacement results from the loading of a 0.4-m square footing are presented in Figure 2-10-a. The load was applied on the footing using a jack and kentledge system in accordance with ASTM D 1194-72 (Consoli et al., 1998). The maximum applied stress was 489-kPa. Figure 2-10-b shows the applied stress q plotted versus the pseudo-strain $\varepsilon_s$ for the footing. According to s/d = 10% criterion, the bearing capacity is 400-kPa. The hyperbolic asymptote (equivalent to infinite footing displacement) was interpreted to be 568-kPa based on Figure 2-11-a. While the zero-stiffness bearing capacities were the least conservative capacity evaluated at 656 kPa as shown in Figure 2-11-b. Neither De Beer's method (Figure 2-11-c) nor Brinch Hansen method could be applied to the stress-displacement data. Appendix A contains stress-displacement graphs plotted on normal and transformed axes for all 29 footings included in the database. Interpreted capacities using the various criteria are presented in Table 2-2.

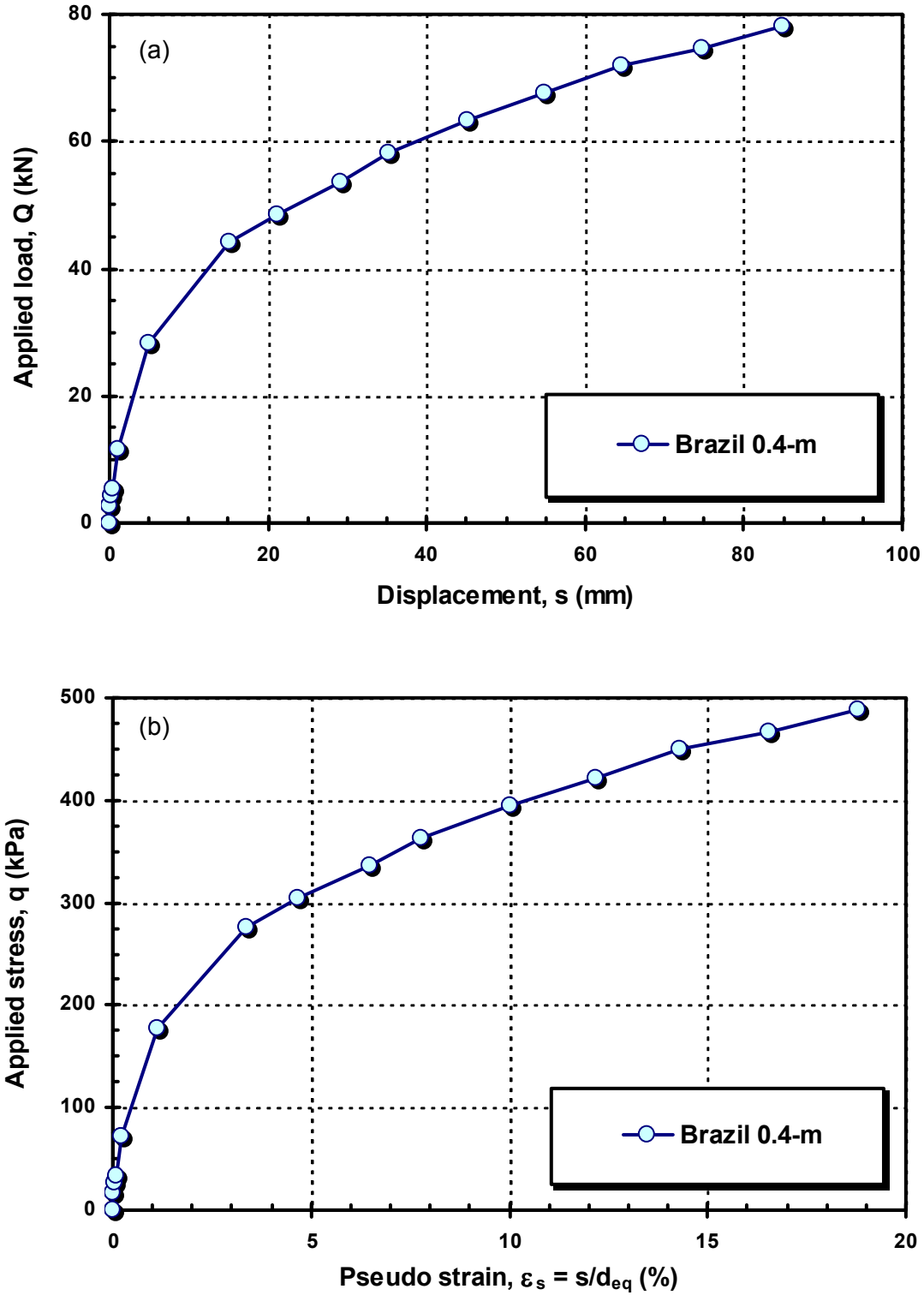


**Figure 2-10.** (a) Load versus displacement curves, (b) Stress versus pseudo-strain curves from the load tests on a 0.4-m square footing resting on a silty sand residuum at Rio Grande do Sul, Brazil (Consoli et al., 1998)

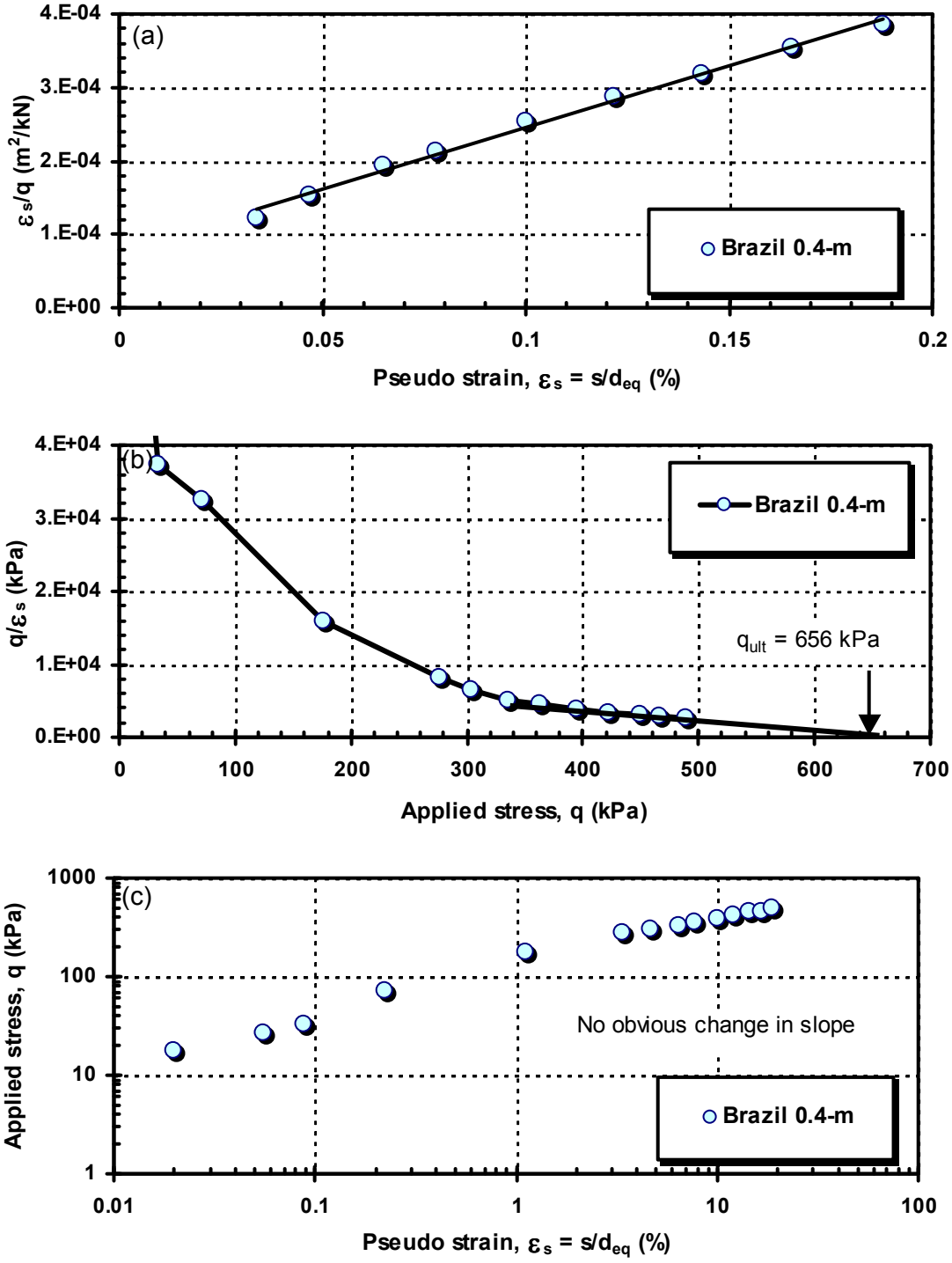


**Figure 2-11.** Load-displacement response plotted per: (a) Chin's transformed axes, (b) Decourt's transformed axes, and (c) De Beer's transformed axes

**Table 2-2.** Interpreted capacities of footings in database using different criteria

| Site | Test | Bearing Capacity (kPa) | | | | | |
|---|---|---|---|---|---|---|---|
| | | Maximum Measured | s/d = 10 % | Hyperbolic Asymptote | Zero Stiffness | De Beer | Brinch Hansen |
| Bangkok, Thailand | BK-1 | 130 | 141* | 149 | 160 | ------- | ------- |
| | BK-2 | 154 | 173* | 187 | 190 | ------- | ------- |
| | BK-3 | 158 | 185* | 207 | 207 | ------- | ------- |
| | BK-4 | 156 | 194* | 194 | 194 | ------- | ------- |
| | BK-5 | 197 | 224* | 245 | 250 | ------- | ------- |
| Belfast, Ireland | BL-1 | 96 | 99* | 100 | 115 | 77 | 96 |
| Bothkennar, UK | BO-1 | 133 | 135* | 160 | 207 | 100 | 126 |
| Cowden, UK | CO-1 | 835 | 709 | 913 | 1000 | ------- | ------- |
| | CO-2 | 886 | 760 | 949 | 1100 | ------- | ------- |
| Fargo, USA | FA-1 | 228 | 242* | 251 | 250 | 180 | 220 |
| Federal University of Rio Grande do Sul, Brazil | BR-1 | 489 | 400 | 464 | 656 | 220 | 420 |
| | BR-2 | 432 | 400 | 294 | 570 | ------- | 400 |
| | BR-3 | 268 | 279* | 251 | 390 | ------- | 245 |
| Greenfield, Portugal | GR-1 | 1004 | 1016* | 2106 | 1950 | ------- | ------ |
| Haga, Norway | HA-1 | 378 | ------ | 380 | 378 | 280 | 378 |
| | HA-2 | 350 | ------ | 350 | 350 | 290 | 344 |
| Labenne, France | LA-1 | 918 | 750 | 1090 | 1054 | ------ | ------ |
| Shellhaven, UK | SN-1 | 79 | 81-85* | 82-86 | 87-95 | 60 | 79 |
| Texas A & M, USA | TX-1 | 1781 | 1600 | 2000 | 2300 | 1400 | ------ |
| | TX-2 | 1464 | 1404* | 1481 | 1870 | 1000 | ------ |
| | TX-3 | 1128 | 1197* | 1600 | 1536 | ------ | ------ |
| | TX-4 | 1139 | 1212* | 1235 | 1445 | ------ | ------ |
| | TX-5 | 989 | 1005* | 1073 | 1450 | ------ | ------ |
| Tornhill, Sweden | TL-1 | 914 | 1095* | 1353 | 1520 | 900 | 900 |
| | TL-2 | 1348 | 1358* | 1667 | 1700 | 980 | 1150 |
| | TL-3 | 700 | 777* | 817 | 850 | ------ | 675 |
| Vagverket, Sweden | VT-1 | 722 | 460 | 1120 | 1700 | ------ | ------ |
| | VT-2 | 400 | 375 | 571 | 560 | ------ | ------ |
| Vattahammar, Sweden | VR-1 | 1702 | 1170 | 2100 | 2300 | ------ | ------ |
| | VR-2 | 770 | 870* | 909 | 1000 | ------ | ------ |

*Data extrapolated using the hyperbolic function

It should be noted that the LPC criterion could be used in only 40% of the cases included in the database because the maximum recorded $s/d_{eq}$ ratios were smaller than 0.1. For load tests where the maximum $s/d_{eq} < 0.1$, data were extrapolated using Equation 2-1 of a regular hyperbola to find the stress equivalent to $s/d_{eq} = 0.1$ as indicated in Table 2-2. Although the maximum-recorded stress is included in the comparison, it should be noted that in many cases, the loading test was terminated due to limitations in the loading frame reaction, tilting, safety, or other complications. Therefore, the maximum-recorded stress is somewhat an arbitrary value. Bearing capacities extrapolated using Decourt's zero-stiffness approach were the most ambiguous. The use of Chin's hyperbolic extrapolation created fewer ambiguities and therefore appeared to be the most useful and objective. De Beer's log-log method could only be applied to 8 cases because of limited displacements. Similarly, the Brinch Hansen criterion could only be used in 11 case histories.

Figure 2-12 shows comparisons between the various interpreted bearing capacities. Figure 2-12-a compares the LPC and hyperbolic interpreted bearing capacities. As expected, the hyperbolic interpreted bearing capacity, or asymptote, is consistently higher than the LPC, with $q_{LPC}/q_{hyp} = 0.73$. Similarly, the zero-stiffness interpreted capacities are consistently higher than the than the LPC, with $q_{LPC}/q_{zs} = 0.66$, according to Figure 2-12-b. Figure 2-12-c shows relatively good agreement between the hyperbolic and zero-stiffness extrapolated bearing capacities with the zero-stiffness method yielding somewhat higher results. Figure 2-12-d shows the hyperbolically extrapolated bearing capacities are in average 24% higher than the measured applied stress. This emphasizes that physical failure is never reached, as suggested by Decourt (1999). Compared to the

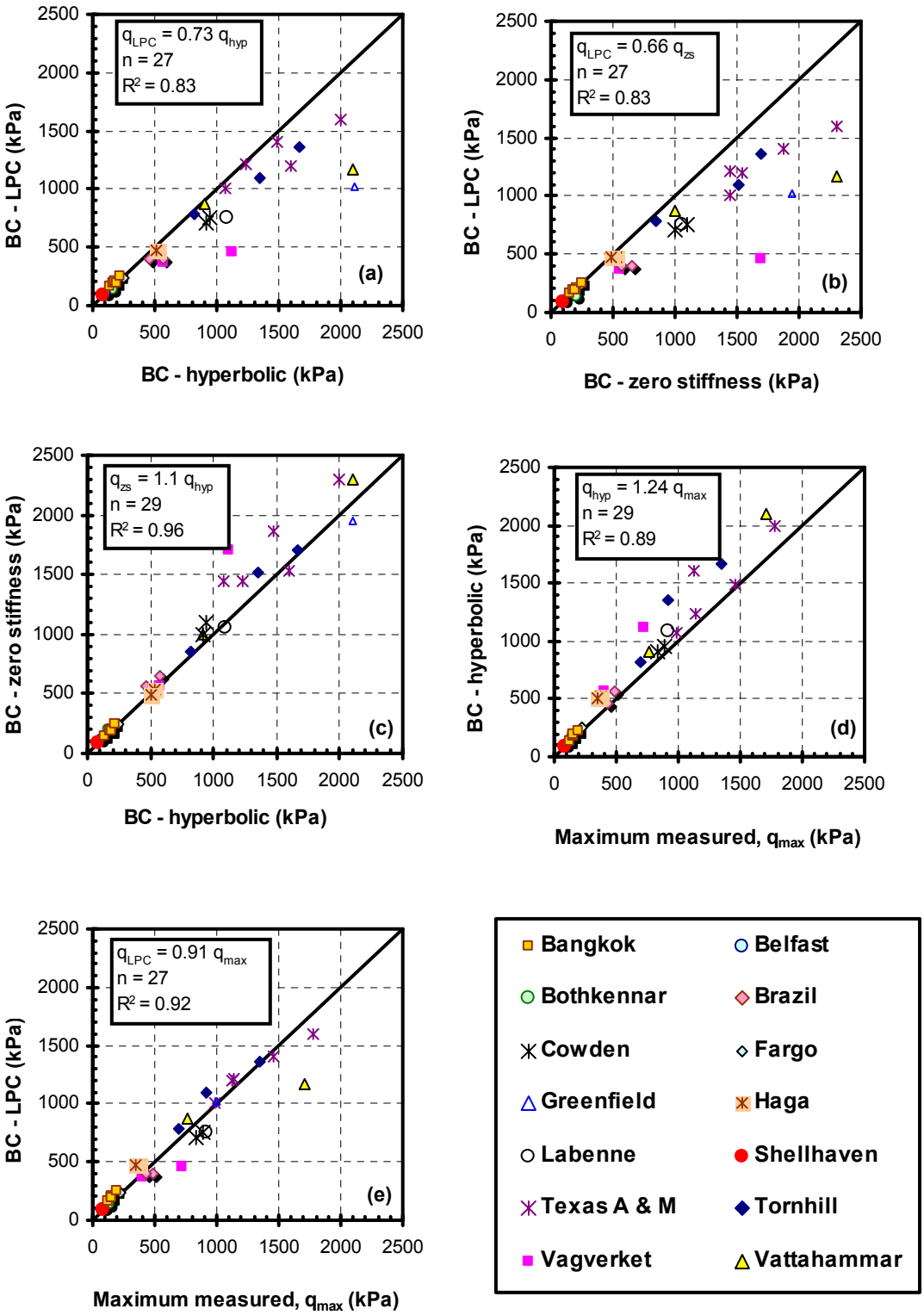


**Figure 2-12.** Comparative summary of interpreted bearing capacities of 30 footings: (a) LPC versus hyperbolic; (b) zero-stiffness versus hyperbolic; (c) LPC versus zero-stiffness; (d) hyperbolic versus maximum measured; (e) LPC versus maximum measured.

maximum applied stress, the LPC interpreted capacities are more conservative, excluding data where the stresses equivalent to $s/d_{eq}$ of 10% are extrapolated (refer to Table 2-2).

## 2.3 Analytical solution for bearing capacity of strip surface footings

The problem of bearing capacity of shallow footings has been studied for over a century and has led to the development of varied solutions. As discussed earlier, full-scale load test are the most definitive means for determining bearing capacity. Numerical analysis comes second to experimental procedures in versatility and reliability. It enables the user to properly model the site conditions (e.g., anisotropy, heterogeneity, variation of properties with depth, boundaries). In addition, the effects of changing the various parameters (e.g., groundwater table, footing dimensions, loading direction, boundary conditions) can be investigated. However, numerical methods require specialized software and modeling expertise, thereby making their use generally restricted to research and/or complex projects. On the other hand, empirical methods are characterized by simplicity but are usually limited in their applicability to specific test types (e.g. CPT: Schmertmann, 1978; pressuremeter: Briaud, 1995). Conversely, analytical methods (e.g. limit equilibrium: Craig and Pariti, 1978; limit plasticity: Meyerhof, 1951; cavity expansion: Vesić, 1975) are more versatile, thus making them more widely used in combination with a number of laboratory and in-situ tests. In this section, the classical analytical solutions for the bearing capacity of shallow footings are discussed.

The bearing capacity of a shallow, vertically loaded, strip footing resting on a homogeneous medium is classically determined using the Terzaghi (1943) superposition method:

$$q_{ult} = cN_c + \frac{1}{2}B\gamma * N_\gamma + \sigma'_{vo}N_q \quad \text{.....(2-4)}$$

where $q_{ult}$ = ultimate stress underneath the footing, c = effective cohesion intercept for drained behavior (c') or the undrained shear strength ($c_u = s_u$) for undrained loading, B = foundation width, $\gamma$*= effective or total unit weight depending on the ground water level, $\sigma_{vo}$' is the effective overburden stress at the foundation level, and $N_c$, $N_\gamma$, $N_q$ are dimensionless bearing capacity factors. Plastic failure zones for surface strip footings are presented in Figure 2-13.

A proper assessment of the bearing factors $N_c$, $N_q$, and $N_\gamma$ is essential for the correct evaluation of bearing capacity. Hence, available bearing capacity factors $N_c$, $N_q$, and $N_\gamma$ determined using analytical, numerical, and statistical methods were reviewed from published sources. The various solutions for the bearing factors $N_c$, $N_q$, $N_\gamma$ (rough footing soil interface) and $N_\gamma$ (smooth footing soil interface) are plotted in Figures 2-14, 2-15, 2-16, and 2-17, listed respectively. References for the bearing factors $N_c$, $N_q$, and $N_\gamma$ are summarized in Tables E-1, E-3, and E-4. The bearing capacity factor $N_c$ is particularly used when computing the bearing capacity of footings resting on clays and silts under undrained loading conditions "$\phi$' = 0". Figure 2-18 shows the bearing capacity factor $N_c$

under undrained loading conditions for various modes of loading. A selection of solutions for $N_c$ of strip footings under undrained loading conditions is also provided in Table E-4.

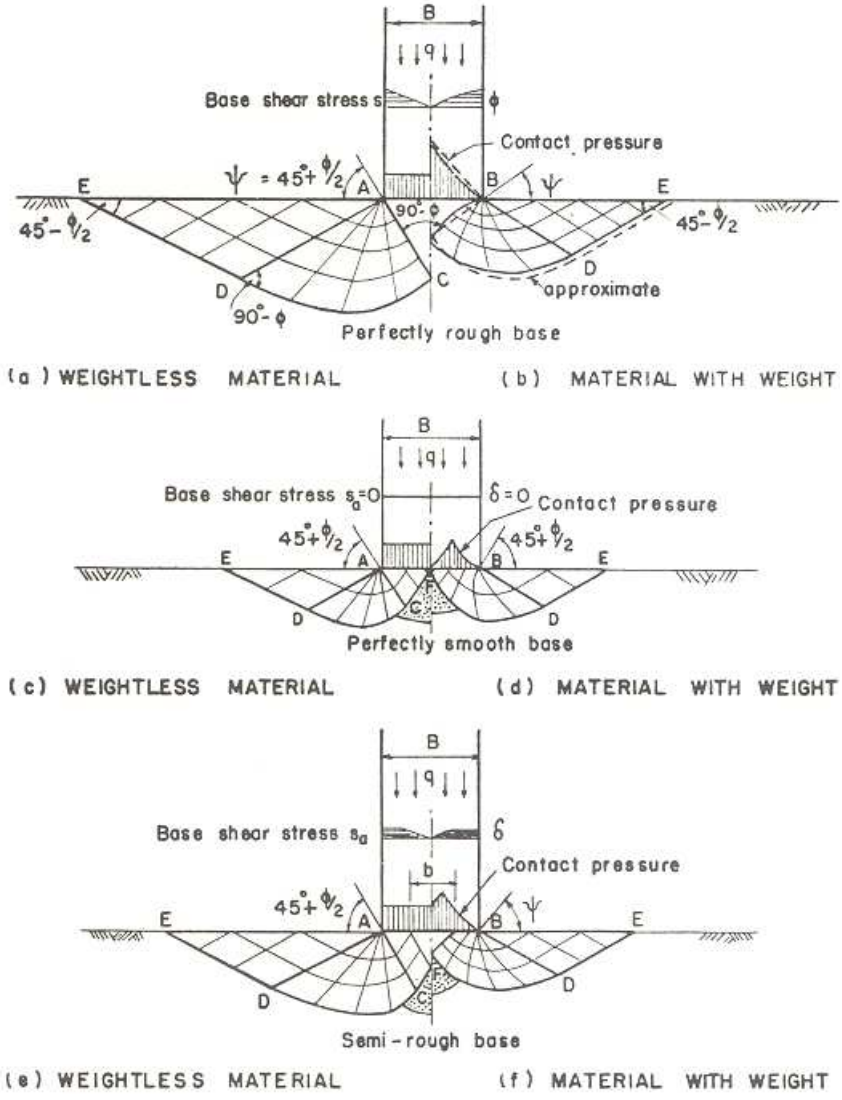


**Figure 2-13.** Plastic zones for surface strip foundations (Meyerhof, 1982a)

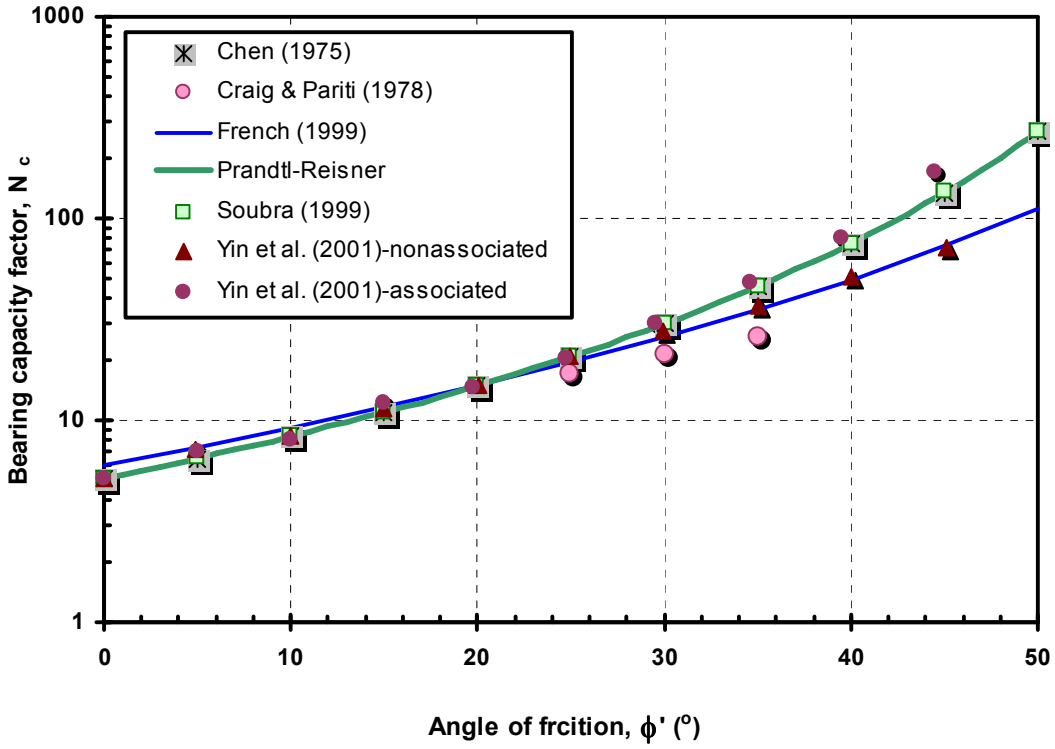


**Figure 2-14.** Variation of the bearing factor $N_c$ with friction angle ϕ' for strip footings

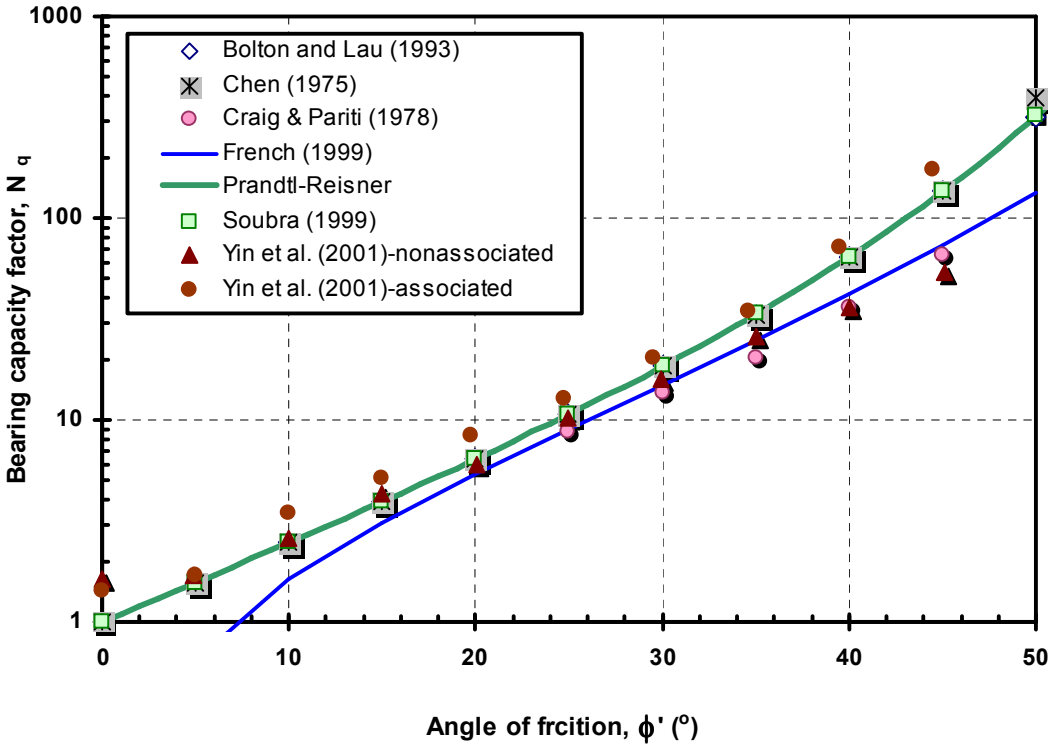


**Figure 2-15.** Variation of the bearing factor $N_q$ with friction angle ϕ' for strip footings

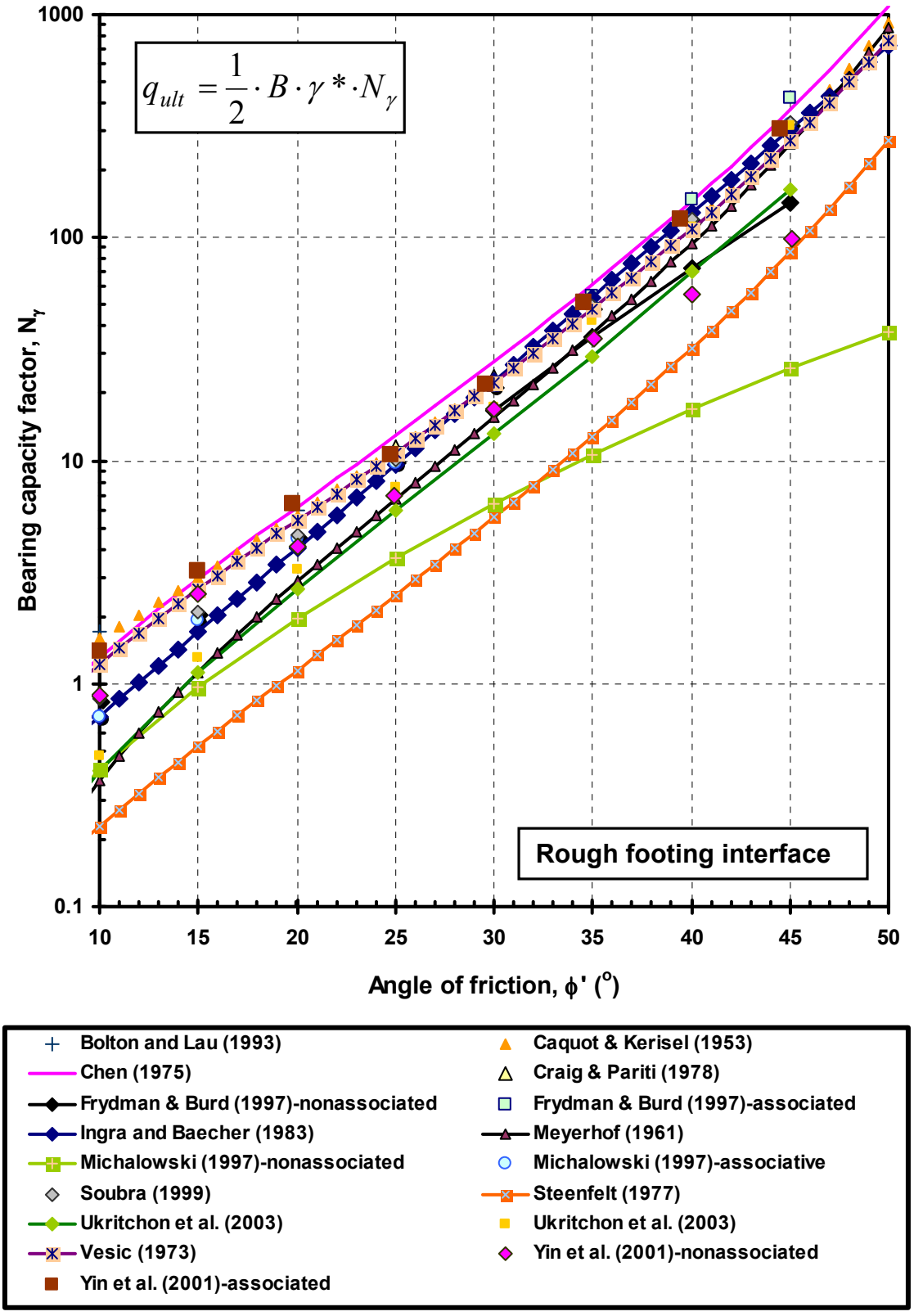


**Figure 2-16.** Variation of the bearing factor $N_\gamma$ with friction angle ϕ' for rough strip footings

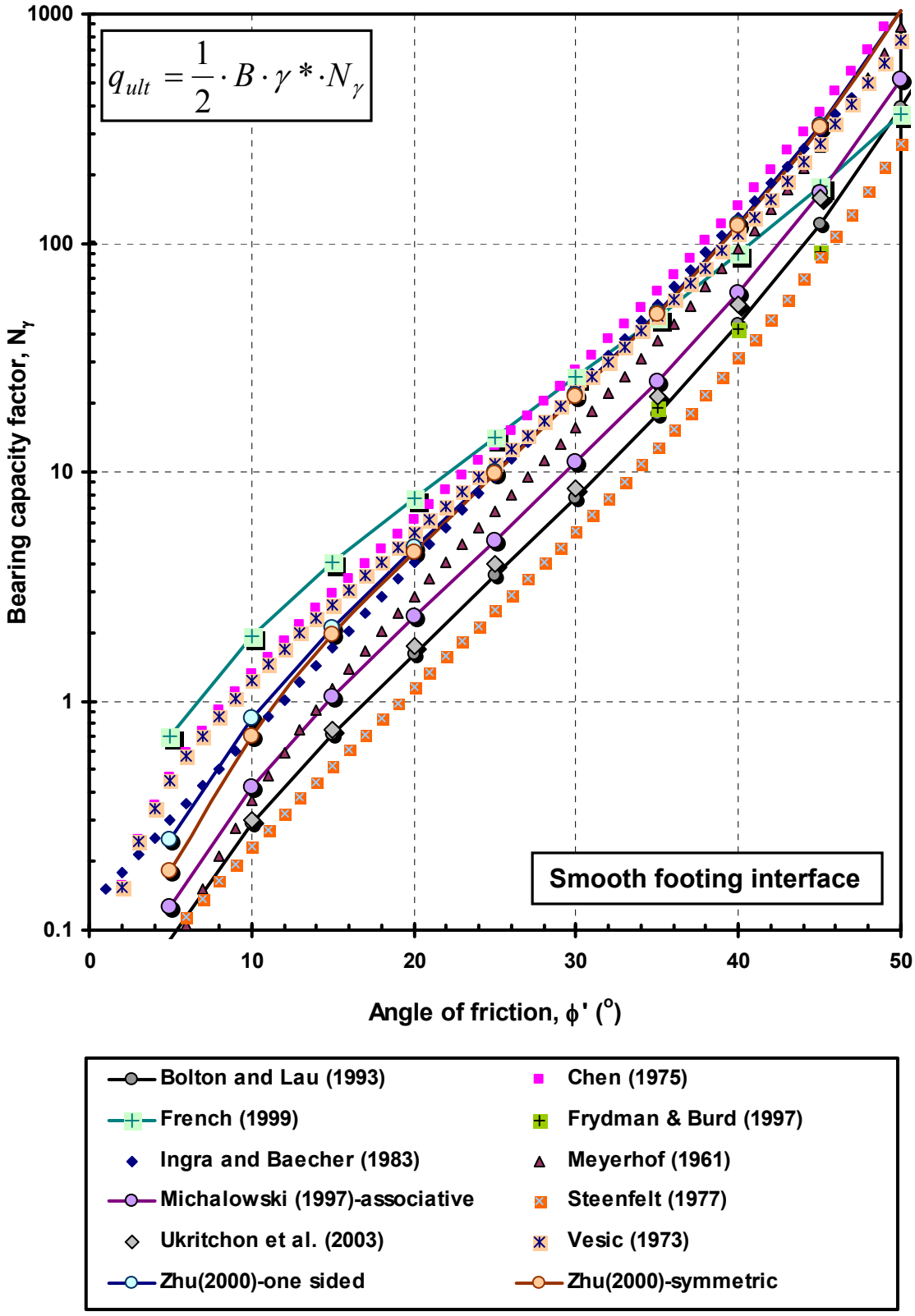


**Figure 2-17.** Variation of the bearing factor $N_\gamma$ with friction angle ϕ' for smooth strip footings

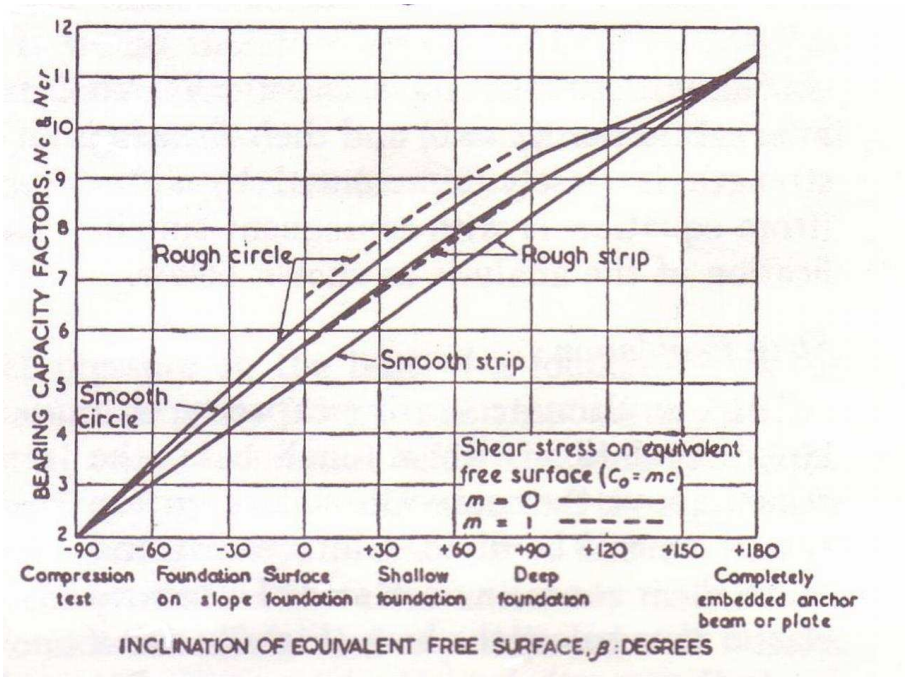


**Figure 2-18.** Variation of the bearing factor $N_c$ with the angle of plastification (β) for strip and circular footings (Meyerhof, 1982b)

In general, there is relatively good agreement between the different methods for calculating $N_c$ and $N_q$. On the other hand, there is considerable variation in $N_\gamma$ as shown in Figures 2-16 and 2-17 depending on the surface roughness of the footing base and the angle of dilatancy (associative or non-associative flow). Several researchers (e.g. Vesić, 1973; Chen, 1975; Chen and McCarron, 1991) have acknowledged the high differences among solutions in the values of $N_\gamma$ compared to $N_c$ and $N_q$.

## 2.4 Generalized bearing capacity equation for shallow footings

The preceding section deals with plane strain problems that are appropriate for long continuous strip footings. Yet the vast majority of footings are square or rectangular, or occasionally circular. Although the effect of footing embedment is accounted for by the

third term of Equation 2-4, poor agreement was found between observed and predicted bearing capacities for footings of different embedment depths (e.g. Fellenius, 2002). This was attributed to the increase of soil strength with depth, which is common in soils (French, 1999).

Accordingly, a generalized formula for calculating the bearing capacity of vertically-loaded shallow footings of any given shape, at any embedment depth is represented by (Vesić, 1973):

$$q_{ult} = c \cdot N_c \cdot \zeta_{cs} \cdot \zeta_{cd} + \frac{1}{2} \cdot B \cdot \gamma^{*} \cdot N_\gamma \cdot \zeta_{\gamma s} \cdot \zeta_{\gamma d} + \sigma_{vo}' \cdot N_q \cdot \zeta_{qs} \cdot \zeta_{qd} \quad \text{.....(2-5)}$$

Appropriate shape and embedment correction factors are given in Tables E-4 and E-5, respectively. Figure 2-19 shows relevant footing dimensions.

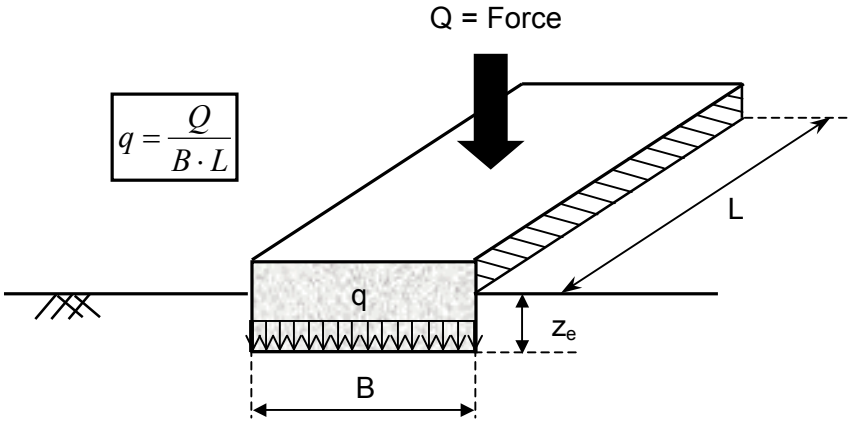


**Figure 2-19.** Footing geometry definitions for bearing capacity factor computations

For shallow foundations, the overburden stress $\sigma_{vo}$' is small making the third term of Equation E-5 generally negligible. Therefore, Equation 2-5 reduces to:

$$q_{ult} = c \cdot N_c \cdot \zeta_{cs} \cdot \zeta_{cd} + \frac{1}{2} \cdot B \cdot \gamma^* \cdot N_\gamma \cdot \zeta_{\gamma s} \cdot \zeta_{\gamma d} \quad \text{(2-6)}$$

Although it is hard to determine drainage conditions accurately in the field, loading is often assumed to take place under either fully undrained or drained conditions, depending on the permeability of the foundation soil and rate of applied loading.

For undrained loading of shallow foundations generally applicable to short-term loadings of clays and silts, Equation 2-6 reduces to:

$$q_{ult} = c \cdot N_c \cdot \zeta_{cs} \cdot \zeta_{cd} \quad \text{(2-7)}$$

where $N_c$, $\zeta_{cs}$, $\zeta_{cd}$ can be calculated using the appropriate charts or equations. The bearing factor ($N_c$, $\zeta_{cs}$, $\zeta_{cd}$) is taken as 5.14 and 6.14 for strip and circular footings, respectively.

For c = 0, the bearing capacity of shallow foundations in drained loading is generally applied to footings on sands, and long-term loading of footings resting on clays and silts calculated as:

$$q_{ult} = \frac{1}{2} \cdot B \cdot \gamma^* \cdot N_\gamma \cdot \zeta_{\gamma s} \cdot \zeta_{\gamma d} \quad \text{(2-8)}$$

where $N_\gamma$, $\zeta_{\gamma s}$, $\zeta_{\gamma d}$ can be determined from the aforementioned equations. For strip footings, bearing factors can be obtained from Figures 2-16 and 2-17. The effect of footing shape can be accounted for using modifying factors listed in Table E-4.

## 2.5 Summary

This chapter provides a review of methods for interpreting bearing capacity from load-displacement measurements obtained from full-scale records or plate load tests. Five criteria for defining bearing capacities are reviewed (Brinch Hansen, De Beer, LPC/10%, Decourt zero-stiffness, hyperbolic). A database of case histories of full-scale load tests was compiled to assess the different criteria. The database consists of 29 footing/plate load tests from 14 different sites. Bearing capacities were evaluated using the five criteria and compared in Table 2-2. It was shown that the hyperbolic criterion is the most objective means for determining bearing capacity from full-scale load tests.

In the latter part of this chapter, analytical bearing capacity solutions for surface strip footings are reviewed. A proper evaluation of the bearing capacity factors $N_c$, $N_q$, $N_\gamma$ is essential for predicting the load-displacement behavior of footings. Bearing capacity factors are summarized in Figures 2-14 through 2-17. The uncertainty associated with the values of $N_\gamma$ is highest compared to $N_c$ and $N_q$. Correction factors accounting for footing shape and embedment depth are reviewed in Appendix E.

# CHAPTER III

# SHALLOW FOUNDATION DISPLACEMENTS

## 3.1 Introduction

The successful design of foundations must ensure that the superstructure does not suffer from excessive displacements. Hence, the reasonable assessment of foundation displacements at working stress levels is of great importance for geotechnical analysis and design. Analytical methods based on the theory of elasticity offer versatile solutions that can be used with results obtained either from laboratory and/or in-situ tests, or both. In this chapter, types of footing deflections and how they are calculated are discussed. A new unified expression is derived that encompasses prior solutions for circular foundations on finite to infinite layers, homogeneous to non-homogeneous soil stiffness with approximate modifications for foundation rigidity and embedment.

## 3.2 Components of displacement

The primary objective of the geotechnical engineer is to ensure the safety, performance, and economy of the foundation or earth structure. Safety is checked by bearing capacity calculations, discussed in Chapter 2. Displacement analysis is then conducted to ensure satisfactory serviceability at working stress levels that are typically one-third or less of the ultimate bearing capacity. In many cases, displacement rather than bearing capacity

is the controlling design criterion. The amount of allowable displacement is dependent on the type of structure and serviceability requirements. Typically, allowable displacement for office buildings resting on shallow footings is 25-mm. While permissible displacement for bridges, mat foundations and parking garages can be as high as 50-mm. Angular distortion (= ratio of differential displacement to foundation spacing) is typically less than 0.002, to prevent cracking caused by such distortion. Foundation displacement (s) can be calculated as the sum of three components according to (refer to Figure 3-1):

$$s = s_i + s_c + s_s \quad \text{.....(3-1)}$$

where ($s_i$) is the undrained distortion, ($s_c$) is the drained consolidation settlement, and ($s_s$) is secondary compression or creep. Undrained distortion or immediate settlement is the portion of displacement that takes place when the load is first applied. Undrained is a short-term condition at constant volume and generally only associated with soft saturated clays, silts and soils with appreciable fines when the loads are applied relatively quickly and soil permeability is low. In many construction projects, rates of loading are actually rather slow and no immediate distortion is realized. Also, most soils have a natural overconsolidation due to erosion, groundwater changes, aging, desiccation, glaciations, cementation, and/or a combination of these factors. Thus the coefficient of consolidation is relatively high in overconsolidated soils and this permits reasonable drainage, such that no excess porewater pressures result ($\Delta u=0$). However, in the case of soft clays and silts with low permeability, undrained displacements ($s_i$) can occur during the loading of

foundations and these magnitudes are often assessed using elastic solutions with constant volume represented by Poisson's ratio ν = 0.5 (e.g. Foott and Ladd, 1981).

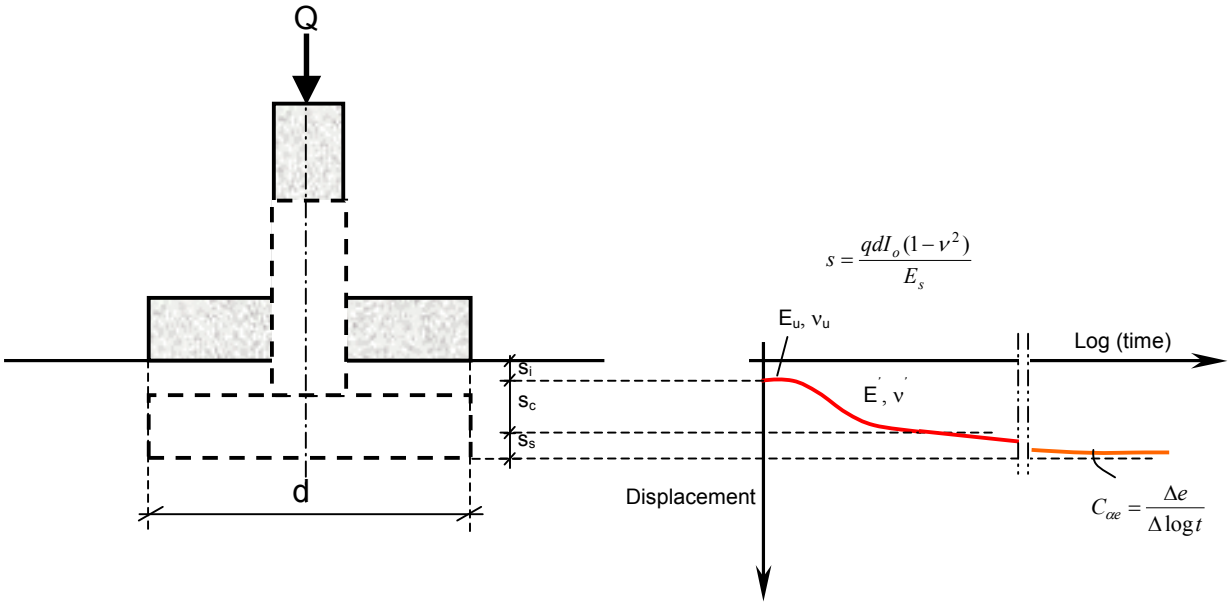


**Figure 3-1.** Schematic of time-displacement beneath a shallow footing

Consolidation settlement ($s_c$) is due to volumetric strains associated with the dissipation of porewater pressure under the applied load (e.g. Leonards, 1976). This is the classical drained settlement corresponding to primary consolidation and conventionally evaluated by e-log $\sigma_v$' results from consolidation tests (e.g. Davis and Poulos, 1968; Mesri and Rokhsar, 1974). Displacements occurring due to drained primary consolidation are termed "settlement" and these occur for all foundations on all types of soils. In lieu of e-log $\sigma_v$' analyses, a constrained modulus (D') approach or elastic modulus (E') can be used since elasticity theory is used to calculate stresses for all approaches (e.g. Fellenius, 2002; Mayne and Poulos, 1999).

Secondary compression or creep settlement ($s_s$) is caused by long-term shear and volumetric strains due to the compression of the soil skeleton after the dissipation of the excess porewater pressures (Mesri and Godlewski, 1977; Eide and Andersen, 1984). These secondary displacements are usually of special concern in soft organic soils, especially large fill loadings that stress the soils beyond the natural preconsolidation.

The relative importance of the settlement components depends on soil type and the nature of structure supported by the foundation. Undrained distortion is of great importance when a load is suddenly applied on saturated fine-grained soils such as clay or silt. Consolidation drained settlement should be checked for foundations resting on all soil types. Secondary settlement or creep should be calculated for all foundations resting on soft, organic fine-grained soils (Holtz, 1991). Some methods also include creep calculations for sands (e.g. Schmertmann, 1970).

## 3.3 Displacement computations using elastic theory

The magnitudes of drained and undrained displacements can be evaluated expeditiously and practically using displacement influence factors and the theory of elasticity (e.g. Harr, 1966; Milovic, 1992). The vertical displacement at the center of a flexible circular foundation resting on an elastic medium (Figure 3-2) is expressed by:

$$s = \frac{qdI_o(1-\nu^2)}{E_{so}} \quad \text{.....(3-2)}$$

where s = foundation displacement, q = stress applied by the footing, d = foundation diameter = 2a, a = foundation radius, $E_{so}$ = equivalent elastic soil Young's modulus beneath foundation base, ν = soil Poisson's ratio, and $I_o$ = surface displacement influence factor that depends on layer thickness, compressible/rigid base interface roughness, and stiffness variation with depth. For example, for a flexible circular footing resting on a homogeneous elastic half-space, $I_o$=1, while for a rigid footing under the same conditions, $I_o$=π/4.

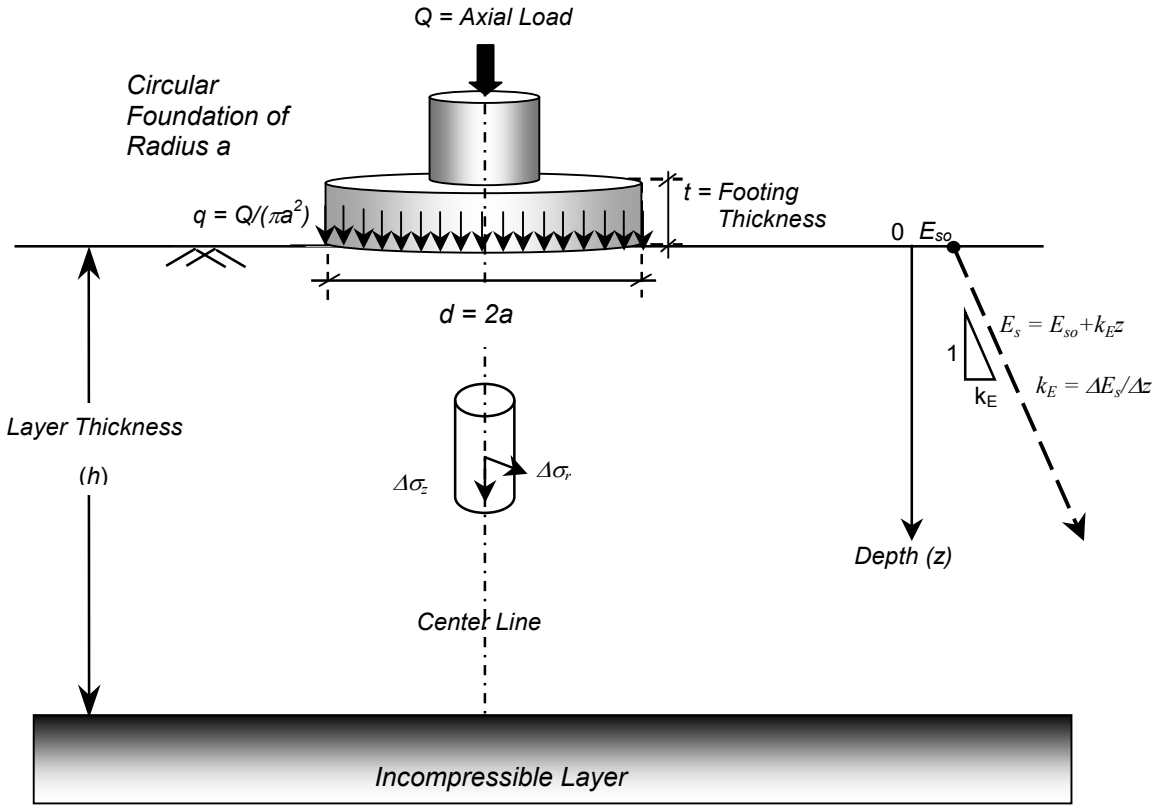


**Figure 3-2.** Schematic diagram of a uniformly loaded circular foundation resting on a compressible Gibson soil layer underlain by a rigid incompressible base

For a given footing, the applied stress (q) and footing diameter (d) are known. The geotechnical engineer needs to identify proper values for the displacement influence factor ($I_o$), equivalent soil modulus ($E_s$), and Poisson's ratio ($\nu$). A discussion of these parameters follows.

### ***3.3.1 Displacement influence factors***

A great number of numerical and analytical solutions are available for the displacement influence factors needed for evaluating the magnitude of displacements beneath shallow foundations. Poulos & Davis (1974) and Milovic (1992) offer compilations of solutions for evaluating displacement influence factors for footings of various shapes (strip, circular, square, rectangular), load distribution (uniform, parabolic, triangular), foundation roughness, Poisson's ratio, soil homogeneity (constant soil modulus or varying with depth), depth to incompressible layer beneath the footing, multilayers, drainage conditions, and foundation stiffness, as well as other variables.

Rigorous solutions for a shallow foundation resting on a compressible, homogenous soil layer underlain by a rigid base are given in graphical form (e.g. Poulos, 1967; Ueshita and Meyerhof, 1968; Brown, 1969a). A closed-form expression for a footing resting on a soil with stiffness linearly increasing with depth (Gibson, 1967) is given only for undrained loading ($\nu$=0.5). To resolve drained loading cases with $\nu' < 0.5$, finite element solutions were developed for estimating the displacement influence factors for non-homogeneous cases (e.g. Carrier and Christian, 1973; Boswell and Scott, 1975). Finite element solutions for layered soil profiles are also given (e.g. Stark and Booker, 1997).

Table 3-1 summarizes a number of available displacement influence factor solutions. The solutions are listed chronologically.

**Table 3-1.** Summary of displacement influence factors under shallow footings

| Footing flexibility | Soil layer thickness | Soil homogeneity | Reference |
|---|---|---|---|
| Flexible | Semi-infinite | Homogeneous | Boussinesq (1885) |
| Flexible | Finite | Homogeneous | Harr (1966) |
| Rigid | Semi-infinite | "Gibson" | Gibson (1967)* |
| Rigid | Finite | Homogeneous | Poulos (1968) |
| Flexible | Finite/Smooth | Homogeneous | Ueshita and Meyerhof (1968) |
| Flexible | Finite/Rough | Homogeneous | Ueshita and Meyerhof (1968) |
| Flexible | Finite to semi-infinite | Homogeneous | Giroud (1972) |
| Rigid | Semi-infinite | "Gibson" | Carrier and Christian (1973) |
| Flexible and rigid | Finite to semi-infinite | Variable | Poulos & Davis (1974) |
| Variable | Semi-infinite | "Gibson" | Boswell and Scott (1975) |
| Flexible | Finite | "Gibson" | Brown and Gibson (1979) |
| Flexible | Finite | Homogeneous | Milovic (1992) |
| Flexible | Semi-infinite | Non-homogeneous | Stark and Booker (1997) |
| Flexible/rigid | Finite to semi-infinite | Homogeneous/"Gibson" | Mayne and Poulos (1999) |

* undrained loading $\nu_u = 0.5$

The various displacement influence factors are generally given in either chart or tabular forms or singular equations, or alternatively provided within compiled computer programs. It is often times confusing which solution is more suitable for a specific problem. A comparable number of graphs, tables, and equations also exist for square, rectangular, and strip footings. As so many separate solutions exist to address the footing displacement problem, it is of interest to have a single generalized approach that can address the important variables. Mayne and Poulos (1999) provided a simple means to obtain approximate displacement influence factors for homogeneous and Gibson soil profiles using a spreadsheet program to numerically integrate the strains beneath the

center of a uniformly loaded flexible footing. They showed that available solutions are quite similar, though these solutions typically seem very different.

The author has improved this approach to obtain closed-form displacement influence factors for circular footings resting on finite to infinite layers of soil having homogenous to "Gibson" soil stiffness profiles, with approximate modifier terms to account for foundation rigidity and embedment.

Figure 3-2 depicts the geometry and nomenclature for an axially loaded circular footing resting on an elastic soil medium. Equation 3-2 can be re-written to define the displacement influence factor $I_o$ as a dimensionless parameter:

$$I_o = \frac{s \cdot E_s}{q \cdot d \cdot \left(1 - \nu^2\right)} \quad \text{.....(3-3)}$$

For $E_s/q = 1$ and $\nu = 0$, the displacement influence factor becomes the pseudo-strain s/d beneath a footing of diameter d and can be calculated as the integration of strains from z* = 0 to z* = h/d, according to:

$$I_o = \frac{s}{d} = \int_0^{h/d} \varepsilon_z dz^* \quad \text{.....(3-4)}$$

where z* = z/d = z/(2a) = normalized depth, and $\varepsilon_z$ = vertical strain. For circular footings, the vertical strain is obtained based on Hooke's law in cylindrical coordinates:

$$\varepsilon_z = \frac{1}{E_s}\left[\Delta\sigma_z - 2\nu\Delta\sigma_r\right] \quad \text{(3-5)}$$

where $\Delta\sigma_z$ = change in vertical stress at depth z beneath the foundation base, $\Delta\sigma_r$ = change in radial stress at depth z, and $\nu$ = soil Poisson's ratio. The change in vertical stress $\Delta\sigma_z$ and radial stress $\Delta\sigma_r$ at the centerline of a footing resting on an infinite half-space is determined based on the integration of surface point loads adopting a simplified Boussinesq solution over a circular area (e.g., Poulos and Davis, 1974):

$$\left(\Delta\sigma_z/q\right) = 1 - \frac{1}{\left[1+\left(a/z\right)^2\right]^{1.5}} \quad \text{(3-6)}$$

$$\left(\Delta\sigma_r/q\right) = \frac{1}{2} + \nu - \frac{(1+\nu)}{\left[\left(a/z\right)^2+1\right]^{0.5}} + \frac{1}{2\cdot\left[\left(a/z\right)^2+1\right]^{1.5}} \quad \text{(3-7)}$$

In geotechnical engineering practice, it is usual to consider only the change in vertical stress ($\Delta\sigma_z$) when computing displacements, particularly for drained primary consolidation. Note that the use of e-log $\sigma_v$' curves from one-dimensional consolidation is commonplace and this procedure relies solely on vertical stress increases (e.g. Holtz and Kovacs, 1981; Terzaghi et al., 1996). Thus, in our simplified evaluation discussed herein the change in radial stresses due to the applied load is neglected in all subsequent analyses. Equation 3-6 gives the change in vertical stress beneath the centerline of a flexible plate resting on an infinite half-space.

Is it logical to use the same formula to calculate the change in vertical stress $\Delta\sigma_z$ for a plate resting on an elastic medium of finite thickness? Based on the theory of elasticity, the stresses developed in a finite layer resting on a rigid base are higher than the stresses developed in a soil layer of infinite thickness (e.g. Giroud, 1970; Milovic, 1992). Accordingly, the change in vertical stress ($\Delta\sigma_z$) is underestimated using Equation 3-6 under a uniformly loaded plate resting on an elastic medium of finite thickness. The increase in stresses caused by the finite layer thickness decreases as h/d ratio increases (Milovic, 1992). Results are shown in Figure 3-3, where the vertical stress influence factor $i_z = \Delta\sigma_z / q$ is plotted for a number of h/d ratios. From a practical standpoint, Boussinesq's solution gives a reasonably accurate approximation for h/d > 1.

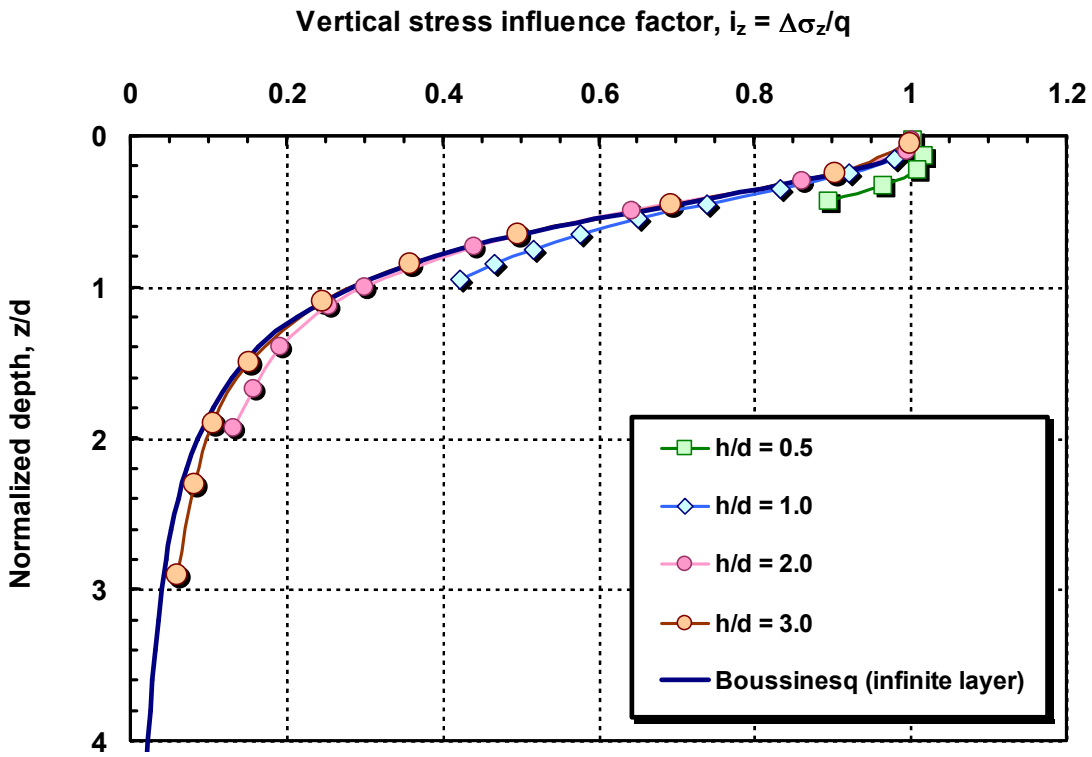


**Figure 3-3.** Effect of finite layer thickness (h) to footing diameter (d) ratio on stress distribution within the compressible soil layer beneath the footing center (modified after Milovic, 1992)

Combining equations 3-4 through 3-7 (for the uniaxial case), a generalized formulation for calculating the displacement influence factor is obtained:

$$I_o = \int_0^{h/d} \frac{\Delta\sigma_z}{E_s} dz^* \quad \text{.....(3-8)}$$

### *3.3.1.1 Homogenous soil profile*

The case of a shallow foundation resting on a homogenous soil stratum ($E_s$ constant with depth) is considered first. Integrating Equation 3-8 between $z^*=0$ and $z^*=h/d$, the displacement influence factor is evaluated as:

$$I_h = \left(1 + h^* - \frac{2 \cdot h^{*2} + 1}{\sqrt{4 \cdot h^{*2} + 1}}\right) \quad \text{.....(3-9)}$$

where $h^*$ = layer thickness factor = h/d. Figure 3-4 shows the variation of the displacement influence factor for a homogeneous soil profile $I_h$ with the normalized layer thickness factor $h^*$. Equation 3-9 is compared to the displacement influence factors reported by Harr (1966) with very good agreement. The difference between the two solutions is less than 10 %.

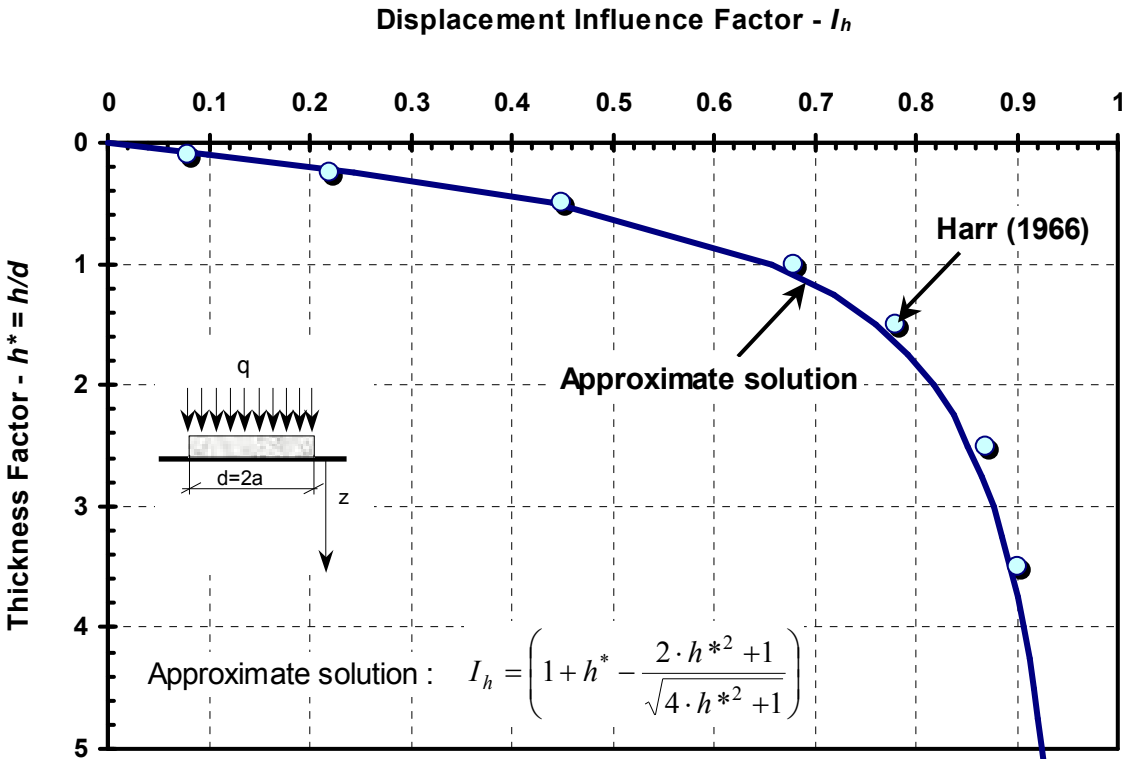


**Figure 3-4.** Displacement influence factors for a flexible circular footing over a homogenous soil of finite thickness (approximate method versus Harr (1966) solution)

Figure 3-5 compares the displacement influence factors from Equation 3-9 to the rigorous mathematical solutions given by Ueshita and Meyerhof (1968) that fully consider the equations of equilibrium and compatibility, kinematics, and complex integrals for a circular footing resting on a finite soil layer underlain by a rigid base with smooth interface. The effect of Poisson's ratio is accounted for by multiplying the factors from Equation 3-9 by $(1-\nu^2)$. The errors between the approximate and exact methods are less than 10 % for h/d > 0.5. Errors are slightly higher for h/d < 0.5 and decrease as h/d approaches infinity. This can be attributed to neglecting the change in radial stresses in addition to the approximation implied by using the simple Boussinesq stress equations applicable for an infinite half space.

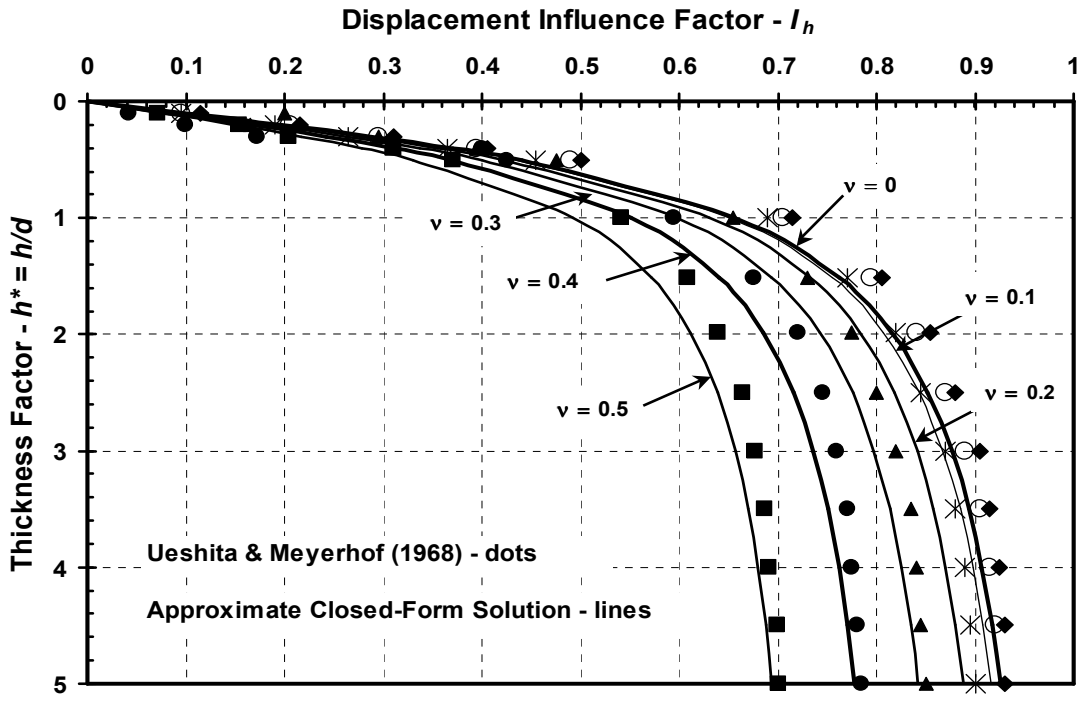


**Figure 3-5.** Displacement influence factors for a flexible circular footing over a homogenous soil of finite thickness (approximate method versus rigorous solution of Ueshita and Meyerhof, 1968)

Milovic (1992) analyzed the problem of a vertically loaded flexible footing resting on an elastic layer of finite thickness underlain by a rigid base. Figure 3-6 shows the approximate displacement influence factors (modified for the Poisson's ratio effect) compared to Milovic's (1992) numerical solution, with fairly good agreement. The error typically decreases as the (h/d) ratio increases with an average error of 10%.

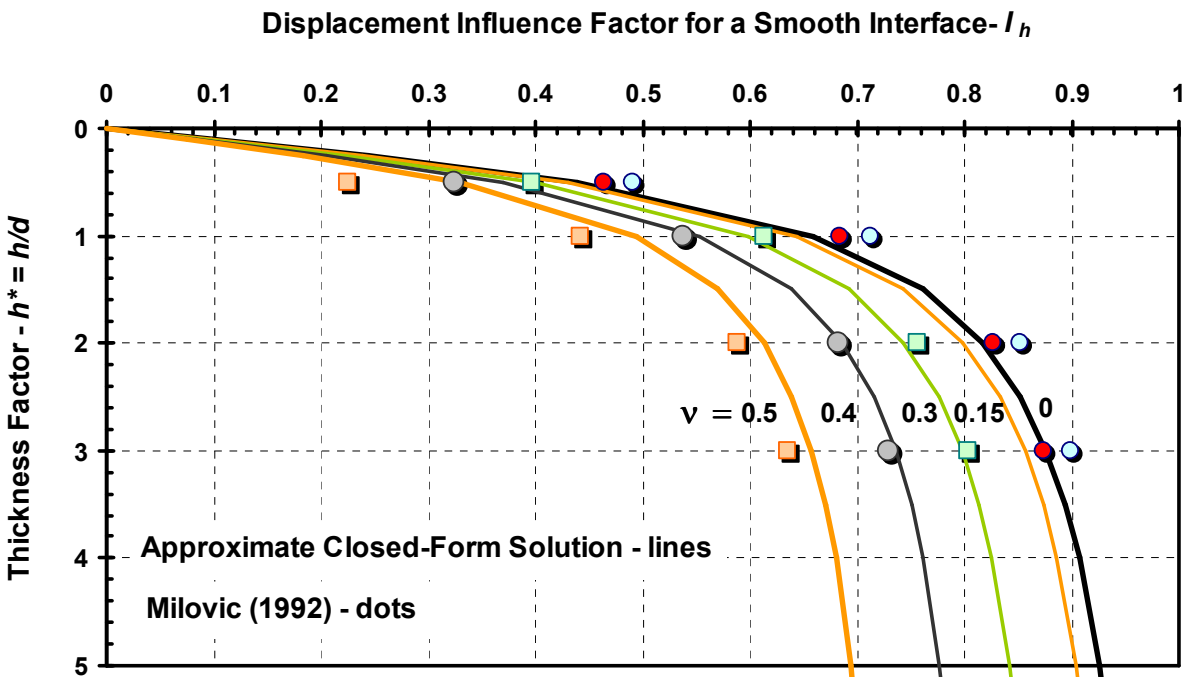


**Figure 3-6.** Displacement influence factors for a flexible circular footing over a homogenous soil of finite thickness (approximate method versus numerical solution of Milovic, 1992)

### *3.3.1.2 Non-homogeneous "Gibson" type soil profile*

In natural soil deposits, the variation of soil moduli with depth may assume any of a number of possible scenarios. Since many soils exhibit stiffness increasing with depth because of the increase in overburden stress, the displacement influence factor ($I_o$) will be evaluated for a Gibson type soil. The variation of elastic modulus for a generalized Gibson soil is expressed by:

$$E_s = E_{so} + k_E z \quad \text{.....(3-10)}$$

where $E_{so}$ = Young's modulus of elasticity directly underneath the foundation base and $k_E$ = linear rate of increase of elastic modulus with depth = $\Delta E_s/\Delta z$. The suggested method

adopts the simplifying hypothesis for a Boussinesq stress distribution beneath a uniformly loaded footing resting on an elastic half space.

Burland et al. (1977) investigated the factors influencing the distribution of the change in vertical stresses and concluded that Boussinesq stress equations yield reasonable results for vertical changes in most cases. However, such a simplification would lead to high inaccuracies for the cases of a stiff layer underlain by a more compressible one and for cross-anisotropic soils. The accuracy of this assumption is confirmed by comparing the approximate solution with other more rigorous solutions (e.g. Scott and Boswell, 1975; Carrier and Christian, 1973).

Using Mathcad, the displacement influence factor was determined using Equations 3-6 and 3-8 with soil modulus increasing with depth according to Equation 3-10. The solution was simplified to this form:

$$I_G = \beta\left[\ln\left[\frac{2\beta + 2h^*}{2\beta\left[2h^* + \sqrt{4h^{*2}+1}\right]}\right] + \frac{2\beta}{4\beta^2+1} - \frac{2\beta - 2h^*}{(4\beta^2+1)\sqrt{4h^{*2}+1}} + \frac{8\beta^3}{(4\beta^2+1)^{1.5}} \cdot \left[\sinh^{-1}\left(\frac{1}{2\beta}\right) - \sinh^{-1}\left(\frac{1-4\beta h^*}{2\beta + 2h^*}\right)\right]\right] \quad \text{.....(3-11)}$$

where $\beta = E_{so}/(k_E d)$ = normalized Gibson modulus ratio and h* = thickness factor = h/d. Figure 3-7 shows the variation of the displacement influence factor ($I_G$) versus ($\beta$) for a Gibson type soil ($\nu = 0$). The results are compared to the approximate solution derived by Mayne and Poulos (1999) using numerical integration and excellent agreement is

found between the two methods. As ($k_E$) tends to zero and β tends to infinity, Equation 3-11 reduces to:

$$I_{G(\beta\to\infty)} = I_h = \left(1 + h^* - \frac{2\cdot h^{*2}+1}{\sqrt{4\cdot h^{*2}+1}}\right) \quad \text{(3-12)}$$

Which is identical to for the influence factor for homogeneous case represented by Equation 3-9. Equation 3-11 is then solved for the case of an infinite half-space (h* tends to infinity) yielding:

$$I_G = \beta\left[\ln\left(\frac{1}{4\beta}\right) + \frac{2\beta+1}{(4\beta^2+1)} + \frac{8\beta^3}{(4\beta^2+1)^{1.5}}\left(\sinh^{-1}(2\beta) + \sinh^{-1}\frac{1}{2\beta}\right)\right] \quad \text{(3-13)}$$

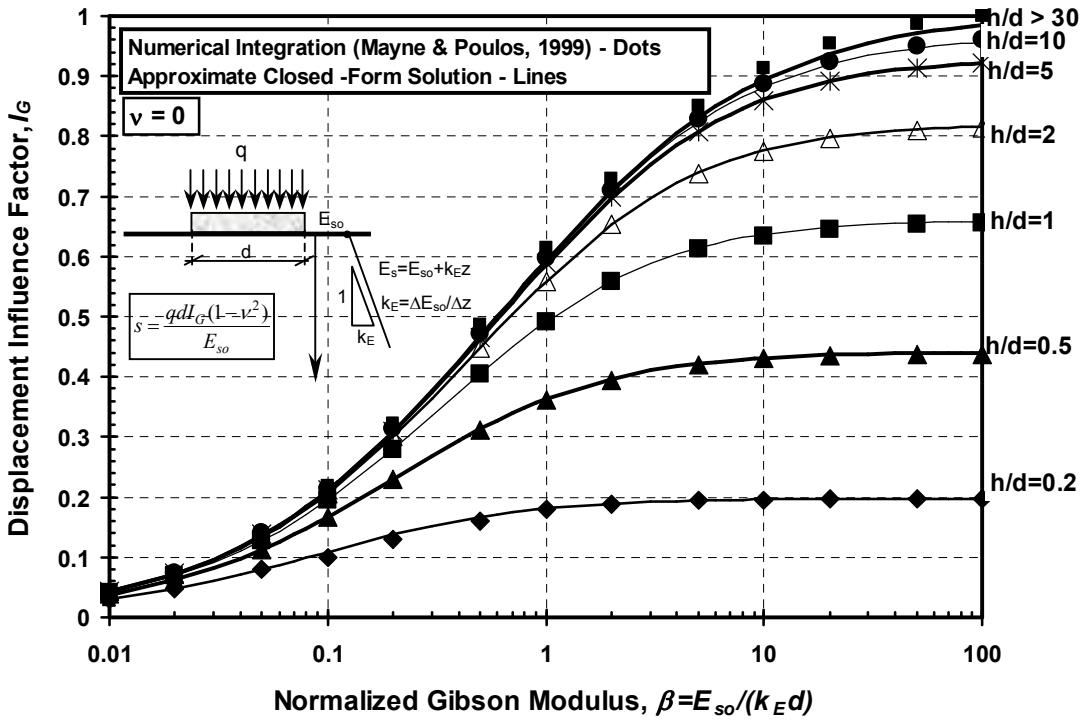


**Figure 3-7.** Displacement influence factors for a flexible circular footing over a Gibson type soil profile (ν = 0)

For a homogenous infinite half-space and $\nu = 0$, the displacement influence factor ($I_G$) approaches 1 according to the theory of elasticity. The equations deduced so far are valid for calculating the displacement influence factor for a perfectly flexible foundation. Influence factors computed using Equation 3-13 are compared to Boswell and Scott (1975) finite element solution for a flexible footing resting on a semi-infinite half space. Figure 3-8 shows Boswell and Scott (1975) parameter (n) for describing the variation of soil modulus with depth and how it is interrelated to the Gibson parameter ($\beta$). The homogeneous soil profile is represented by $n = 1$ (as $\beta$ tends to infinity). Boswell and Scott (1975) present influence factors for computing mean displacement and differential displacement between footing center and edge. Assuming the mean displacement as the average of center and edge displacements, the displacement influence factors under the footing centerline is computed. The approximate influence factor given by Equation 3-13 ($\nu = 0$) multiplied by ($1-\nu^2$) to account for Poisson's ratio effect are compared to Boswell and Scott (1975) displacement influence factors beneath the footing centerline for a perfectly flexible footing as shown in Figure 3-9. Good agreement is found between the two solutions. Better matches are achieved for the higher values of Poisson's ratio.

### ***3.3.2 Effect of foundation flexibility***

The stress distribution, and associated relevant pattern and magnitudes of displacements underneath a footing, are affected by its flexibility. Solutions for the perfectly flexible and perfectly rigid footing are well known (e.g. Harr, 1966; Poulos and Davis, 1974; Milovic, 1992). The effect of intermediate foundation flexibility has been evaluated using finite element analysis on footings and mats by Brown (1969b).

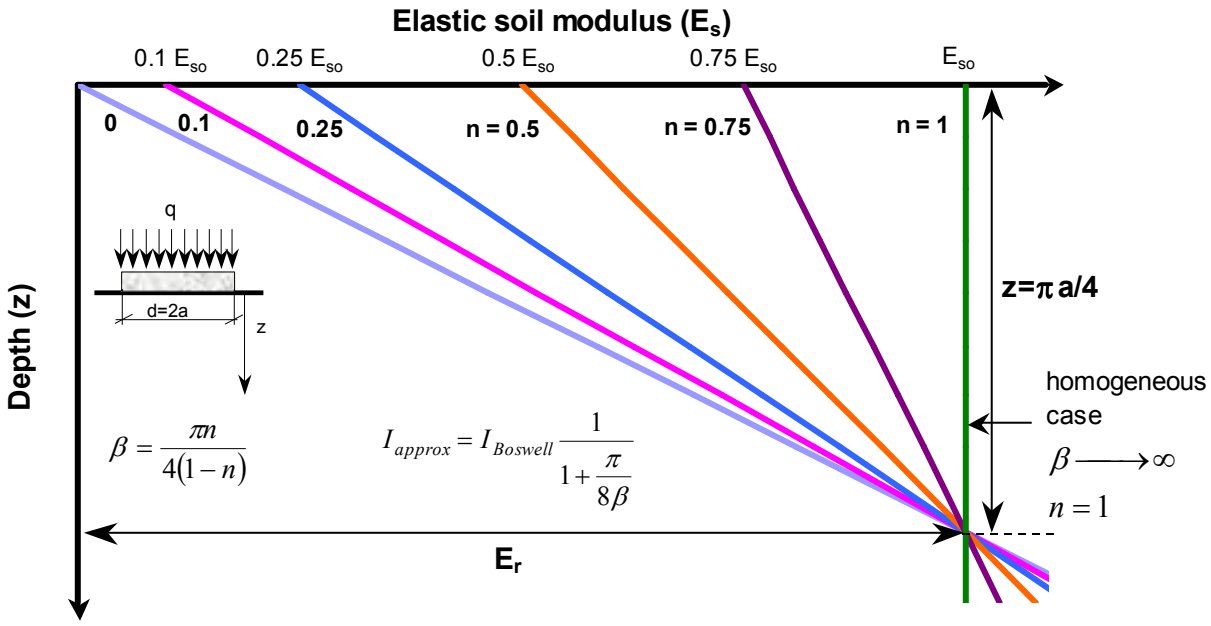


**Figure 3-8.** Variation of elastic modulus with depth according to Scott and Boswell (1975)

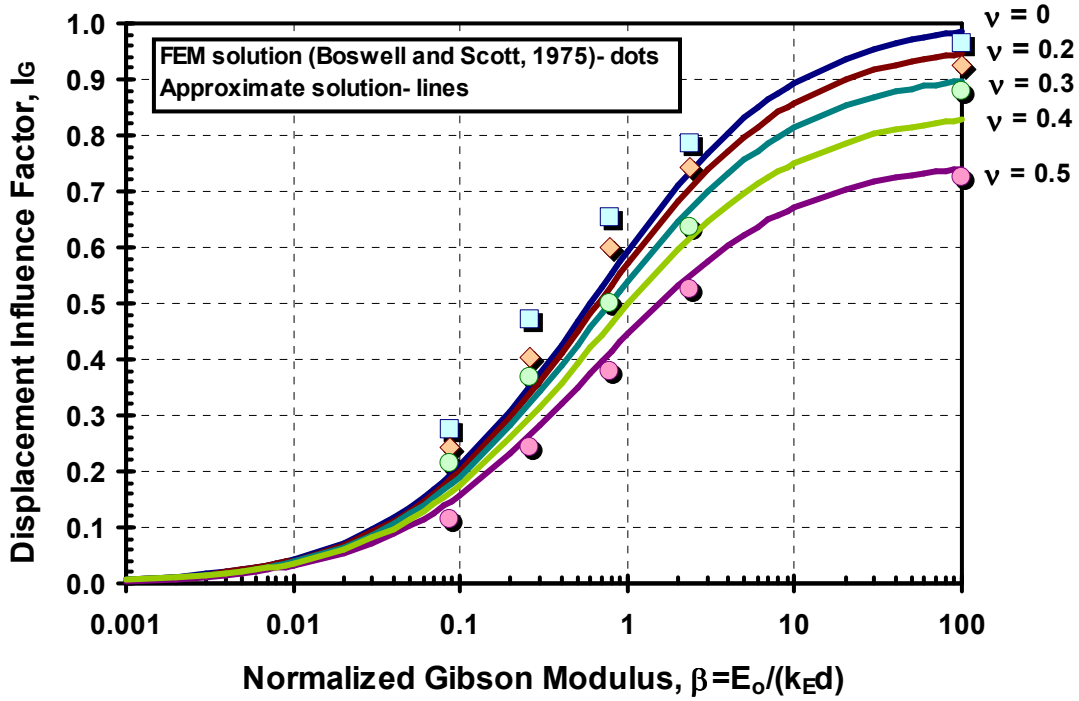


**Figure 3-9.** Displacement influence factors for a flexible circular footing over a Gibson type soil profile for different values of Poisson's ratio (proposed solution versus Boswell and Scott, 1975)

Neglecting the small influence of Poisson's ratios for the foundation and soil materials, a foundation flexibility factor can be expressed as:

$$K_F \approx \frac{E_{foundation}}{E_{soil}} \cdot \left(\frac{t}{a}\right)^3 \quad \text{.....(3-14)}$$

where $K_F$ = foundation flexibility factor; $E_{foundation}$ = modulus of elasticity of the foundation material (e.g. reinforced concrete); $E_{soil} = E_{so} + k_E d$ = average soil modulus beneath the foundation (over a depth equal to twice the foundation diameter d beneath the foundation base); t = foundation thickness, and a = footing radius. Based on the numerical results of Brown (1969b), the foundation flexibility influence factor $I_F$ for an elastic semi-infinite half space can be approximated (Mayne and Poulos, 1999):

$$I_F \approx \frac{\pi}{4} + \frac{1}{4.6 + 10K_F} \quad \text{.....(3-15)}$$

Figure 3-10 shows the variation of the rigidity correction factor with the foundation flexibility factor. For $K_F > 10$, a footing is considered rigid and the flexibility influence factor approaches $\pi/4$. A footing is considered flexible for $K_F < 0.01$ yielding a flexibility influence factor equal to 1. As a matter of fact as the Carrier and Christian solution approaches the homogeneous case with $\beta \longrightarrow \infty$, they recommend correction factors of about 10% increase to correct for the coarseness of their finite element mesh.

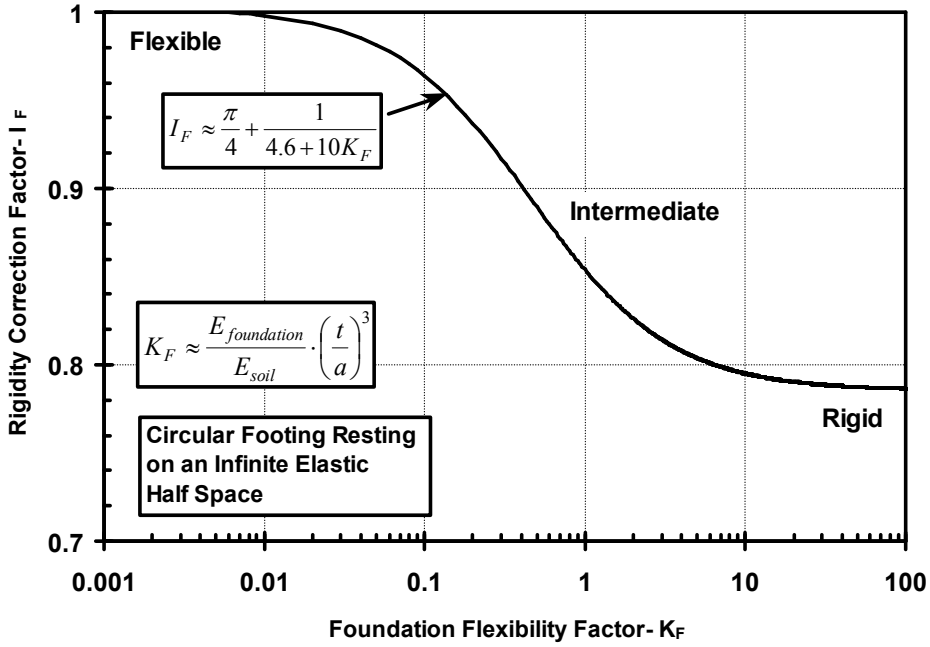


**Figure 3-10.** Rigidity correction factor for shallow foundations (based on Brown, 1969b)

A rigidity influence factor of π/4 is used in combination with Equation 3-9 to obtain the displacement influence factors for rigid footings resting on homogeneous half space. Results are compared to solutions by Poulos (1968) in Figure 3-11. The approximate solution agrees fairly well with Poulos (1968) solution for rigid footings.

The variation of the displacement influence factor $I_G$ resting on a semi-infinite Gibson soil profile is shown in Figure 3-12 for both perfectly flexible and perfectly rigid foundations. Footing rigidity is accounted for by multiplying the displacement influence factors from Equation 3-14 by a rigidity influence factor of π/4. Results are compared to the finite element solutions for a rigid plate published by Carrier and Christian (1973), with good agreement.

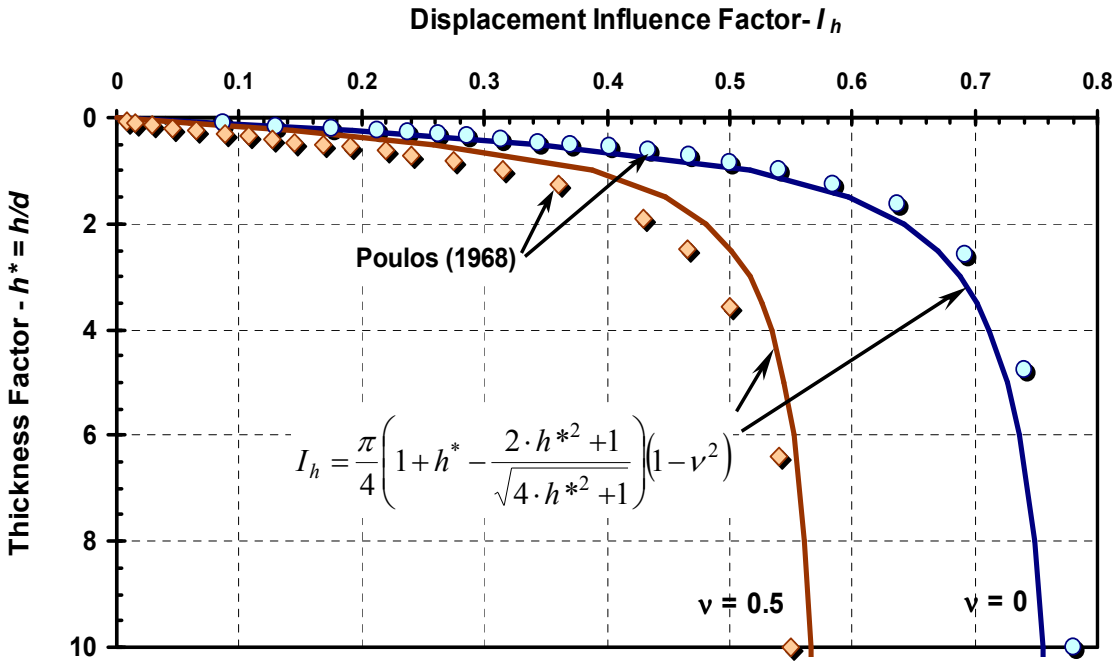


**Figure 3-11.** Displacement influence factors for a rigid circular footing on finite elastic layer (approximate solution versus rigorous solution by Poulos, 1968)

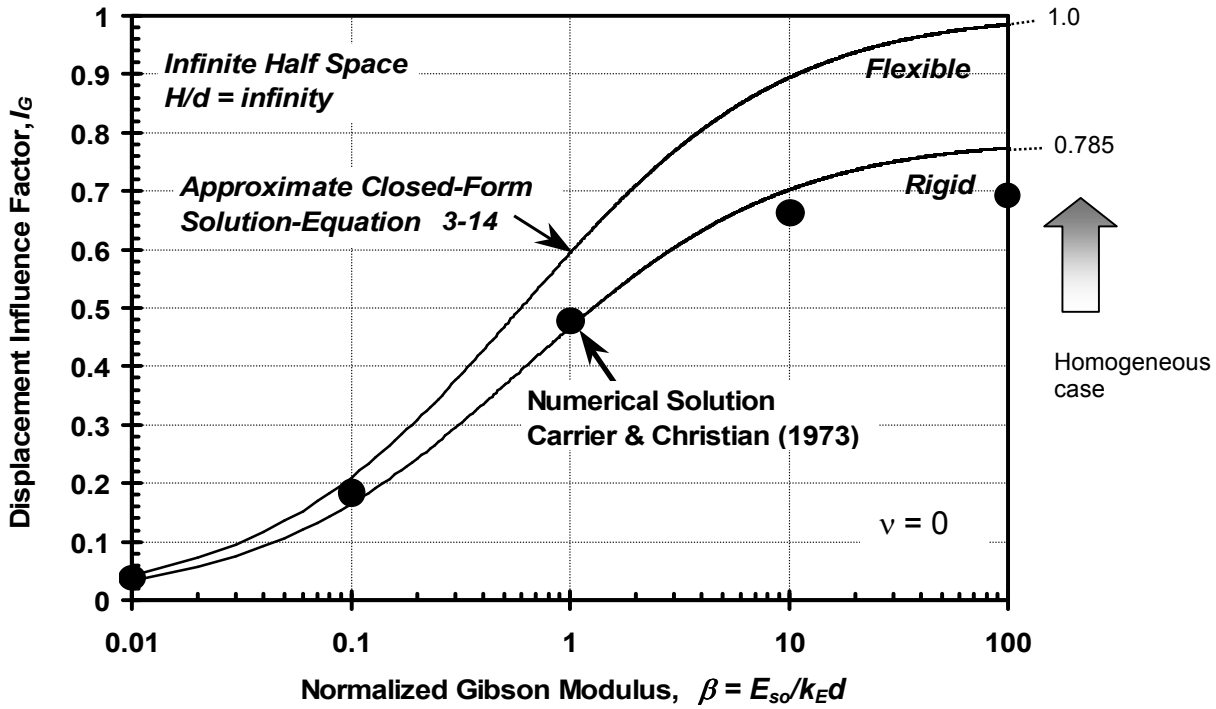


**Figure 3-12.** Displacement influence factors for a circular footing over a semi-infinite Gibson soil profile (proposed method versus numerical solution by Carrier and Christian, 1973)

### *3.3.3 Simplified displacement influence factors*

As Equation 3-11 may appear tedious to some, a simplified formula for estimating the displacement influence factor for a Gibson soil profile ($I_G$) was deduced using curve-fitting techniques:

$$I_G \approx \frac{1}{0.6 \cdot \beta^{-0.8} + \left(\frac{0.23}{h*} + 1\right)^2} \quad \text{.....(3-16)}$$

Influence factors computed from Equations 3-11 and 3-16 are compared in Figure 3-13-a, which shows good agreement between the results computed using both equations. For an infinite half space ($h^*$ tends to infinity ), Equation 3-16 yields:

$$I_G \approx \frac{1}{0.6\beta^{-0.8} + 1} \quad \text{.....(3-17)}$$

Good agreement between equations 3-13 and 3-17, as shown in Figure 3-13-b. As ($\beta$) tends to infinity (homogenous soil profile), Equation 3-16 reduces to:

$$I_G \approx \frac{1}{\left(\frac{0.23}{h^*} + 1\right)^2} \quad \text{.....(3-18)}$$

Good agreement between the solutions given by Equations 3-9 and 3-18, as demonstrated by Figure 3-13-c. Equation 3-17 is in agreement with the numerical solution proposed by Mayne and Poulos (1999).

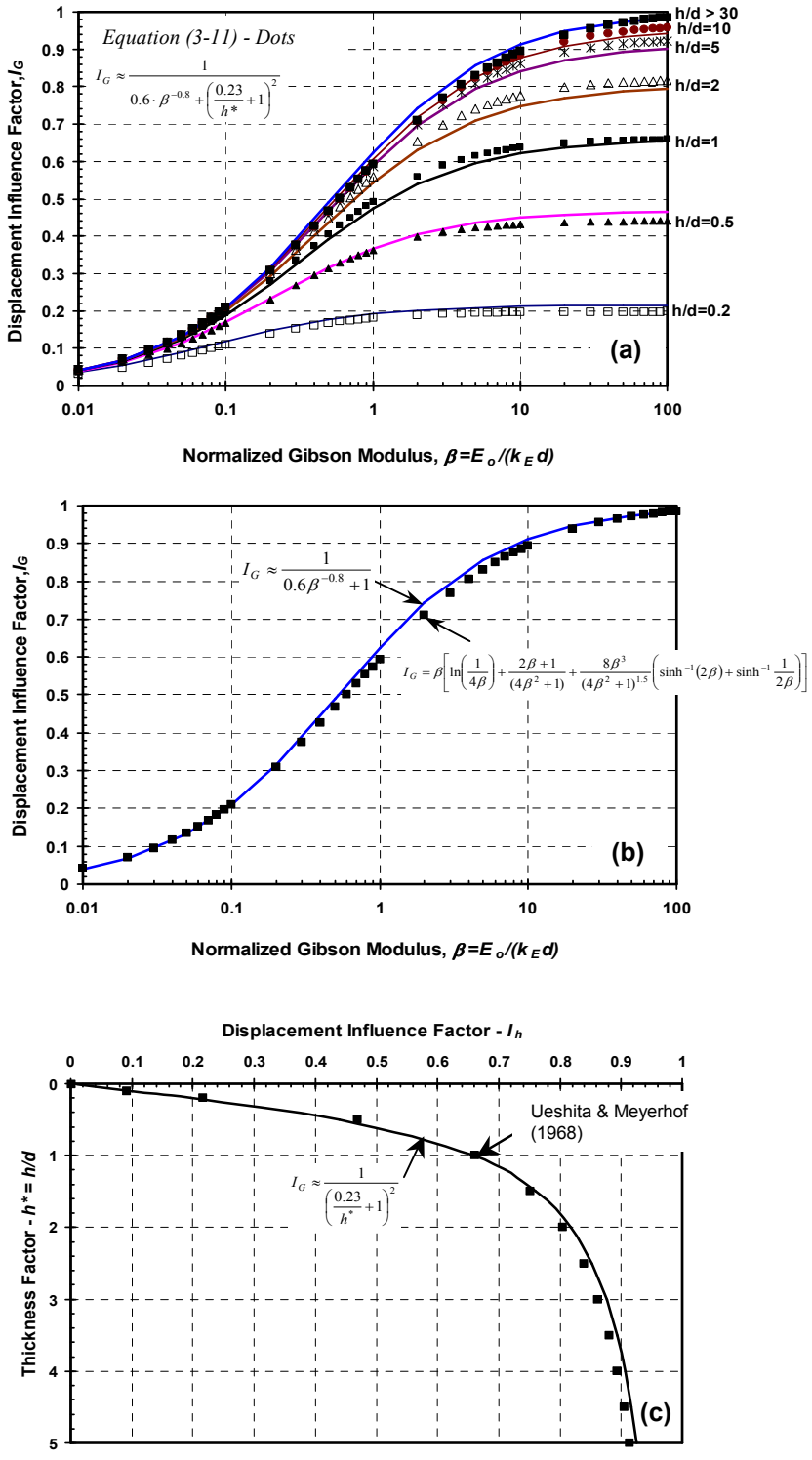


**Figure 3-13.** Evaluation of the accuracy of the simplified equations for the influence factors for: (a) Gibson type soil profile (variable h*); (b) Gibson type soil profile in infinite half space; (c) Homogenous semi-infinite soil layer

## 3.4 Generalized equations for computing displacements beneath circular footings

A general equation for evaluating the displacements beneath the center of circular shallow footings and raft foundations is given by:

$$s_{center} = \frac{q \cdot d \cdot I_G \cdot I_F \cdot I_E \cdot (1-\nu^2)}{E_{so}} \quad \text{.....(3-19)}$$

where $I_G$ is the displacement influence factor per Equation 3-11 or 3-16; $I_F$ is the foundation rigidity correction factor calculated from Equation 3-15; and $I_E$ is a factor accounting for the foundation embedment as determined by Burland (1970) that can be approximated by:

$$I_E \approx 1 - \frac{1}{3.5\exp(1.22\nu - 0.4)\left[\left(d/z_E\right)+1.6\right]} \quad \text{.....(3-20)}$$

where $z_E$ = depth to foundation beneath ground surface. Figure 3-14 shows the effect of embedment on foundation settlement. Generally, embedment influence is seen to be small unless the foundation is embedded at least 5 diameters below grade.

The proposed approximate displacement influence factor solution was shown to compare well with available published solutions where a soil layer is underlain by a stiffer layer. However, the solution is unconservative for the case of a stiff layer underlain by a weaker layer. For this case, it is recommended to use published solutions (e.g. Poulos and Davis, 1974; Milovic, 1992).

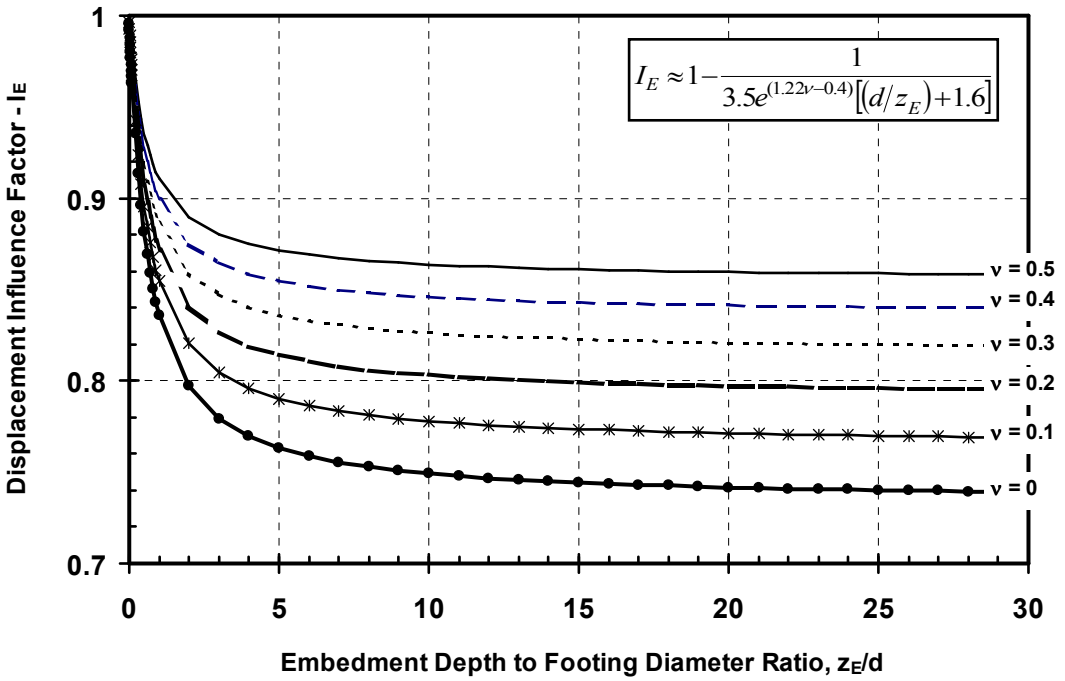


**Figure 3-14.** Effect of embedment on foundation displacement based on numerical results by Burland (1970)

## 3.5 Displacement influence factors for rectangular footing on a homogeneous soil layer

The aforementioned solution was derived for circular footings resting on an elastic compressible layer. The same process can be used to compute displacement influence factors for rectangular footings by numerically integrating strains beneath footing centerline according to:

$$I_o = \int_0^{h/B} \varepsilon_z dz^* \quad \text{.....(3-21)}$$

where h is the depth to incompressible layer, B is the foundation width (smaller footing dimension), z* =z/B is normalized depth, $\varepsilon_z$ is the vertical strain at depth z. Figure 3-15 shows the geometry of the footing considered in the analysis.

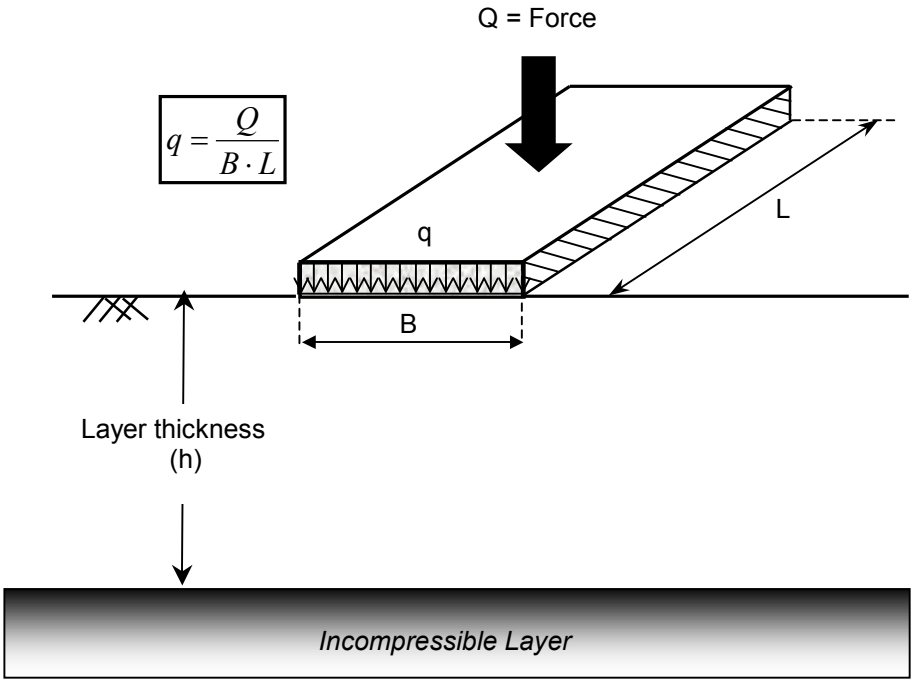


**Figure 3-15.** Geometry of a rectangular footing resting on a compressible soil layer of finite thickness

According to Harr (1966), the vertical stress under the center of a uniformly loaded rectangular area, resting on a semi-infinite half-space at depth z is given by:

$$\sigma_z = \frac{2}{\pi}\frac{m^* n^*}{\sqrt{1+m^{*2}+n^{*2}}}\frac{1+m^{*2}+2n^{*2}}{\left(1+n^{*2}\right)\left(m^{*2}+n^{*2}\right)}+\frac{2}{\pi}\sin^{-1}\left(\frac{m^*}{\sqrt{m^{*2}+n^{*2}}\sqrt{1+n^{*2}}}\right) \quad \text{.....(3-22)}$$

where m* = L/B and n* = 2z/B. Using a spreadsheet, the integral sign of Equation 3-21 is substituted by the summation over small layers:

$$I_o = \sum \Delta I_z \cdot \left(\Delta z / B\right) \quad \text{……...……(3-23)}$$

Displacement influence factors for uniformly loaded rectangular footings are computed for various L/B ratios. Results are compared with Harr (1966) solution as shown in Figure 3-16. As m* = L/B approaches infinity, the rectangular footing becomes a strip footing. The approximate solution is also compared to Milovic (1992) numerically computed displacement influence factors for ν = 0.15, 0.30, and 0.45 in Figures 3-17-a, 3-17-b, and 3-17-c, respectively. The effect of Poisson's ratio is accounted for by multiplying the factors from Equation 3-9 by $(1-\nu^2)$. Good agreement between the two solutions is demonstrated.

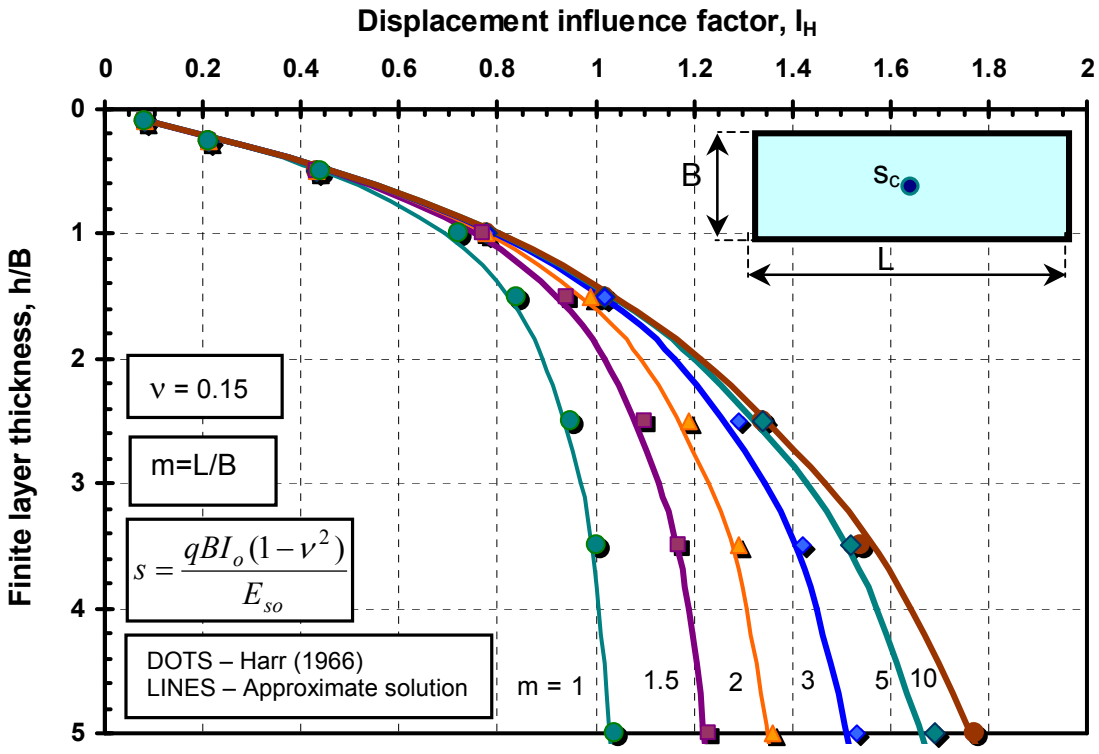


**Figure 3-16.** Displacement influence factors for a flexible rectangular footing over a homogenous soil of finite thickness (approximate method versus Harr (1966) solution)

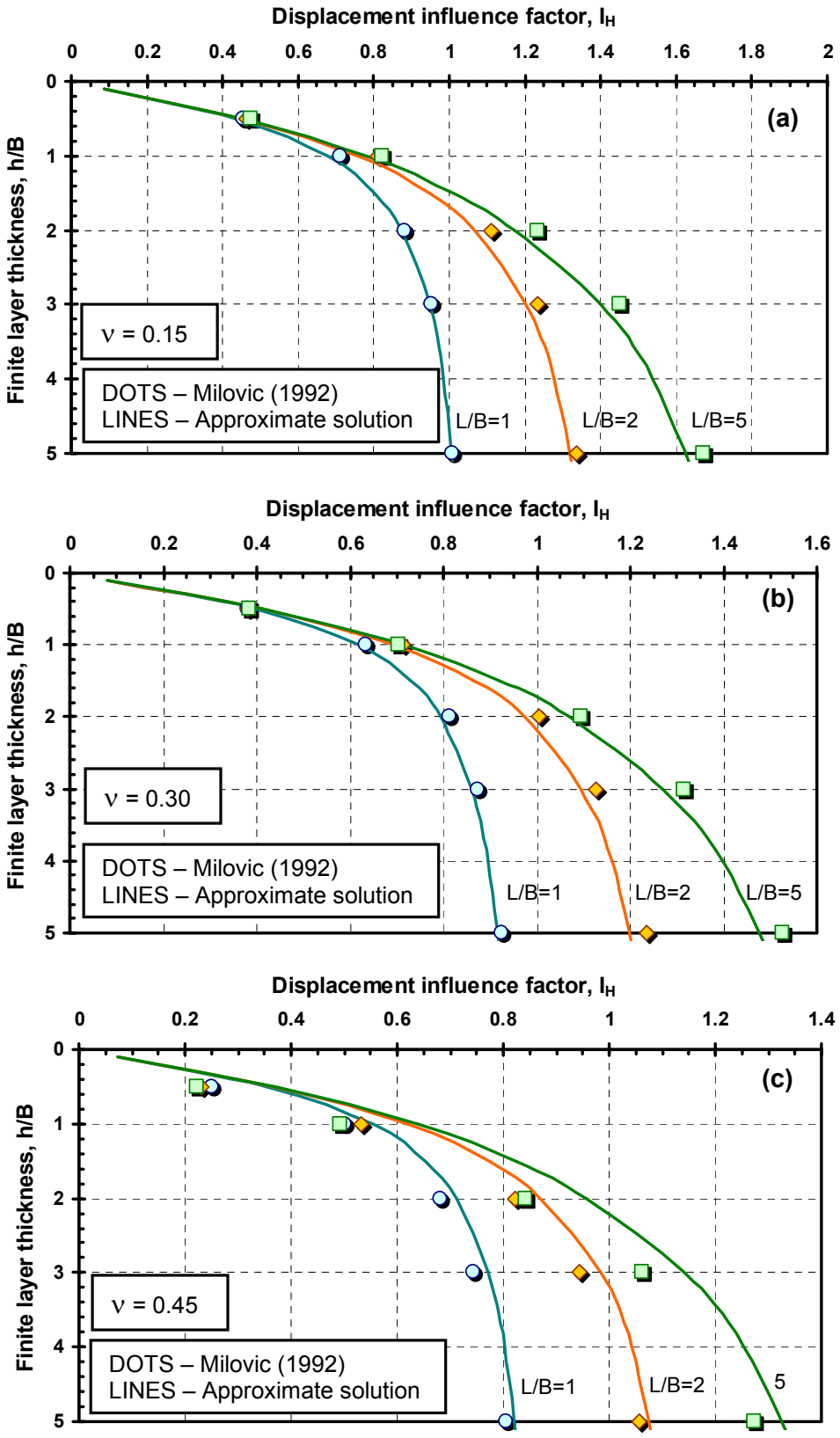


**Figure 3-17.** Displacement influence factors for a flexible rectangular footing over a homogenous soil of finite thickness for: a) ν = 0.15; b) ν = 0.30; and c) ν = 0.45 (approximate method versus Milovic (1992) solution)

## 3.6 Summary

In this chapter, foundation displacement computations using elastic influence factors are reviewed and discussed. A new approximate closed-form solution was derived for use in evaluating the magnitude of displacements at the center of flexible and rigid circular foundations resting on either homogeneous or Gibson soil profiles of finite to infinite depth. Displacements can be calculated with knowledge of soil stiffness beneath the foundation ($E_{so}$), rate of increase of soil stiffness with depth ($k_E$), soil Poisson's ratio ($\nu$), depth to an incompressible layer (h), and foundation diameter (d). The new solution facilitates deflection calculations for shallow footings and raft foundations in a unified approach that compare reasonably with rigorous approaches (e.g. Harr, 1966; Poulos, 1968; Ueshita and Meyerhof 1968), finite element methods (e.g. Carrier and Christian, 1973; Milovic, 1992), and approximate solutions (e.g. Mayne and Poulos, 1999), thereby making it easy to implement by spreadsheet or by commercial mathematical software. The applicability of the method for computing displacement influence factors for rectangular footings is also demonstrated. Approximate displacement influence factors for rectangular footings are compared with Harr (1966) rigorous solution and Milovic (1992) numerical solution with very good agreement. A summary of equations for computing displacements for circular footings using the approximate approach is provided herein:

**Table 3-2.** Summary of equations for computing displacements under circular footings

| | |
|---|---|
| Generalized Equation for computing displacement | $s = \dfrac{q \cdot d \cdot I_G \cdot I_F \cdot I_E \cdot (1-\nu^2)}{E_{so}}$ |
| Generalized displacement influence factor for flexible footings, $I_G$ | $I_G = \beta\left[\ln\left[\dfrac{2\beta + 2h*}{2\beta\left[2h* + \sqrt{4h*^2+1}\right]}\right] + \dfrac{2\beta}{4\beta^2+1} - \dfrac{2\beta - 2h*}{(4\beta^2+1)\sqrt{4h*^2+1}} + \dfrac{8\beta^3}{(4\beta^2+1)^{1.5}} \cdot \left[\sinh^{-1}\left(\dfrac{1}{2\beta}\right) - \sinh^{-1}\left(\dfrac{1-4\beta h*}{2\beta + 2h*}\right)\right]\right]$<br>$I_G \approx \dfrac{1}{0.6 \cdot \beta^{-0.8} + \left(\dfrac{0.23}{h*}+1\right)^2}$ |
| Foundation rigidity influence factor, $I_F$ | $I_F \approx \dfrac{\pi}{4} + \dfrac{1}{4.6 + 10K_F}$ |
| Embedment influence factor, $I_E$ | $I_E \approx 1 - \dfrac{1}{3.5\exp(1.22\nu - 0.4)\left[(d/z_E)+1.6\right]}$ |

Notes:
s= foundation displacement.
q= average applied stress.
d= foundation diameter.
$I_G$= elastic displacement influence factor.
$I_F$= foundation flexibility influence factor.
$I_E$= influence factor for embedment.
ν= soil Poisson's ratio.
$E_{so}$= equivalent elastic soil Young's modulus beneath foundation base.
$\beta = E_{so}/(k_E d)$ = normalized Gibson modulus ratio.
$k_E$ = linear rate of increase of elastic modulus with depth = $\Delta E_s/\Delta z$.
h* = thickness factor = h/d.
$K_F$ = foundation flexibility factor.
$E_{foundation}$ = modulus of elasticity of the foundation material (e.g. reinforced concrete).
$E_{soil}$ = average soil modulus beneath the foundation over a depth z = 2d.
t = foundation thickness.
$z_E$ = depth to foundation base beneath ground surface.

# CHAPTER IV

# SOIL STIFFNESS AT SMALL- TO INTERMEDIATE-TO LARGE- STRAINS

## 4.1 Overview

The stiffness of soils can be quantified using laboratory tests on undisturbed soil specimens, including: oedometer (e.g. Janbu, 1969), triaxial tests (e.g. Lambe, 1968), resonant column testing (e.g. Hardin and Drnevich, 1972), or in the field from in-situ tests including: pressuremeter (Baguelin et al., 1978), flat plate dilatometer (Marchetti, 1980), or by full-scale loading tests of foundations or plates (e.g. Schnaid et al., 1993). Less attractive as an approach, soil stiffness has been indirectly assessed from empirical correlations with in-situ tests such as: cone penetration tests (e.g. Schmertmann, 1970; Mitchell and Gardner, 1975), and standard penetration test (e.g. Schultz and Melzer, 1965; Stroud, 1974).

Of particular interest is the small strain shear modulus ($G_{max} = G_o$) obtained from the shear wave velocity ($G_{max} = \rho_T V_s^2$), where $\rho_T$ is the total mass density and $V_s$ is the shear wave velocity, as it represents a maximum stiffness from which all the moduli can be benchmarked (Burland, 1989). The value of $G_{max}$ is fundamental and applicable to static and dynamic loading, as well as undrained and drained conditions (e.g. Tatsuoka et al., 1997; Lo Presti et al., 1999a, 1999b). Laboratory and field studies show soil stress-strain behavior is non-linear at all strain ranges, even for very small strains (e.g. Jardine et al., 1985). However, linear elasticity still remains the most common means for deformation

analysis. Therefore, the reference stiffness value $G_{max}$ must be reduced to an equivalent modulus, which corresponds to the ambient working load level and appropriate strains. This chapter covers the assessment of soil stiffness at working stress levels for routine design, small strains (nondestructive range), and modulus reduction schemes.

## 4.2 Types of soil stiffness

Soil stiffness can be expressed by a number of interrelated elastic moduli including: shear modulus (G), equivalent Young's modulus (E), bulk modulus (K), or constrained soil modulus (D). Figure 4-1 shows how the different elastic moduli are measured in the laboratory, specifically (E') from triaxial, (D') from one-dimensional consolidation (also termed constrained compression), (K') from hydrostatic compression, and (G') from shear testing. Common shearing modes include direct shear (box), simple shear, and torsional shear. The measured stiffness depends on many factors including: boundary conditions, type and direction of loading, and rate of loading.

As a three-phase geomaterial, soil exists at various states of moisture including: completely dry, partially saturated, or fully saturated. Partially saturated soils are not considered in the current research. For saturated soils, it is standard practice to assume the stress-strain behavior at extreme conditions and to be predominantly either fully-drained or undrained depending on soil type, boundary conditions, and rate of loading. Accordingly, two equivalent elastic soil moduli can be evaluated for these cases: drained (e.g. E') and undrained (e.g. $E_u$) cases.

**Triaxial Compression**

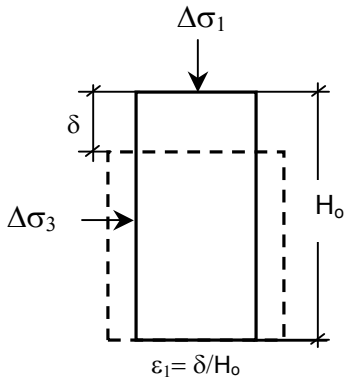


Elastic modulus
$E=(\Delta\sigma_1-\Delta\sigma_3)/\varepsilon$

$$E = 2G(1+\nu)$$

**Constrained Compression**

Oedometer/ consolidometer

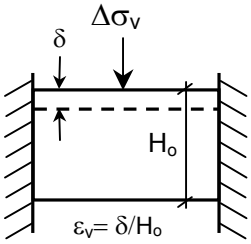


Constrained modulus
$D'=\Delta\sigma_v/\Delta\varepsilon_v$

$$D = \frac{2G(1-\nu)}{(1-2\nu)}$$

**Isotropic Compression**

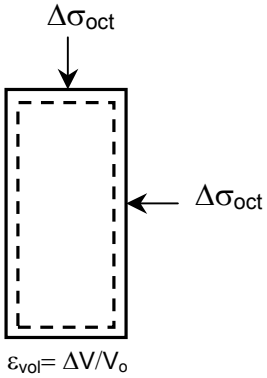


$\Delta\sigma_{oct}$ = change in octahedral stresses
$\Delta\varepsilon_{vol}$ = change in octahedral strains

Bulk modulus
$K'=\Delta\sigma_{oct}/\Delta\varepsilon_{vol}$

$$K = \frac{2G(1+\nu)}{3(1-2\nu)}$$

**Simple Shear**

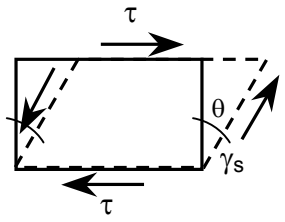


$\gamma_s = \tan\theta$

Shear modulus
$G=\tau/\gamma_s$

$$G = \frac{E}{2(1+\nu)}$$

**Figure 4-1.** Laboratory tests for measuring elastic moduli in the laboratory (modified after Lambe and Whitman, 1979)

Each modulus can be expressed either in terms of a secant modulus $E_{sec}$ $\left[=\frac{\sigma_1-\sigma_3}{\varepsilon_a}\right]$ or tangent modulus $E_{tan}$ $\left[=\frac{d(\sigma_1-\sigma_3)}{d\varepsilon_a}\right]$. Figure 4-2 illustrates the different equivalent elastic moduli that can be measured from a triaxial test. At very small strains, both secant and tangent modulus converge to the small-strain elastic modulus ($E_{max}$) that can also be determined from non-destructive testing. The other elastic moduli can be similarly represented (e.g. $G_{sec}$, $G_{tan}$). Tangential soil modulus is more suitable for numerical modeling as the calculations are performed incrementally. The secant modulus is more suited for analytical solutions. It is also possible to represent an unload-reload modulus, $E_{ur}=\frac{d(\sigma_1-\sigma_3)}{d\varepsilon_a}$ (as depicted in Figure 4-2) which defines a pseudo-elastic response. This is common in one-dimensional oedometer tests in the laboratory and pressuremeter testing in the field.

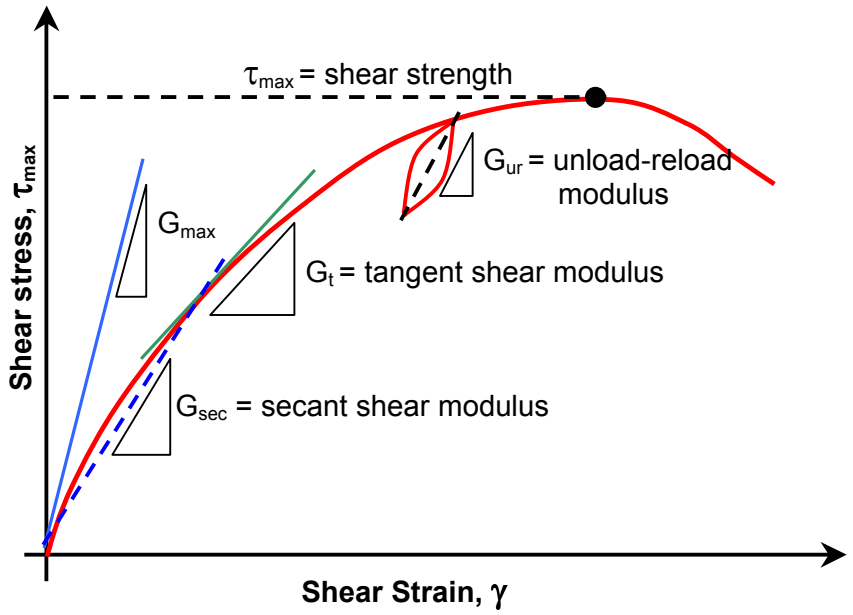


**Figure 4-2.** Definitions of maximum, secant, tangent, and unload-reload shear moduli

## 4.3 Soil stiffness at working stress level

As mentioned in the introduction, soil stiffness can be assessed by laboratory tests on high quality soil samples, directly from select in-situ tests, by back-calculation from full-scale load tests on foundations or plates, or indirectly from in-situ penetration tests. The non-linearity of stiffness with strain and stress level, coupled with different directions of loading and drainage conditions, makes it very difficult for a meaningful cross comparison of the various moduli derived from the different tests, unless a consistent framework and reference stiffness are established. Full-scale instrumented load tests represent the best means for assessing the equivalent soil stiffness, however at great commitment, cost, and time.

Laboratory devices allow for controlled testing the soil at different boundary conditions, strain rates, stress regimes, and controlled drainage. High-quality tube samples are vital for the test results to be meaningful, yet are expensive for soft to firm clays. In many instances, sample disturbance is unavoidable. Special frozen sampling techniques are now available for silts and sands, yet at an extremely high expense.

Hence, it is progressively becoming standard practice to assess stiffness from in-situ tests (e.g. standard penetration test, cone penetration test, flat plate dilatometer, pressuremeter), since data are obtained immediately on site and the variation of stiffness can be ascertained vertically and laterally across the formation. Figure 4-3 illustrates the ranges of shearing strains associated with select in-situ tests. The equivalent soil moduli based on these tests represent the stress-strain response specific to certain stress levels

and drainage conditions. Kohata et al. (1997) noted that soil moduli obtained from conventional laboratory and field tests (except field seismic tests) were too small compared to back-calculated moduli based on full-scale tests. This in turn leads to over-predicting soil deformations.

At very small strains (less than $10^{-4}$%), soils exhibit a very high stiffness represented by the small-strain stiffness ($G_{max}$ or $G_o$), formerly known as the dynamic soil modulus $G_{dyn}$. In fact, the small-strain shear modulus is the key benchmark and establishes the highest soil stiffness achievable to which other moduli can be compared on relative basis. Small-strain stiffness is discussed in greater details in subsequent sections.

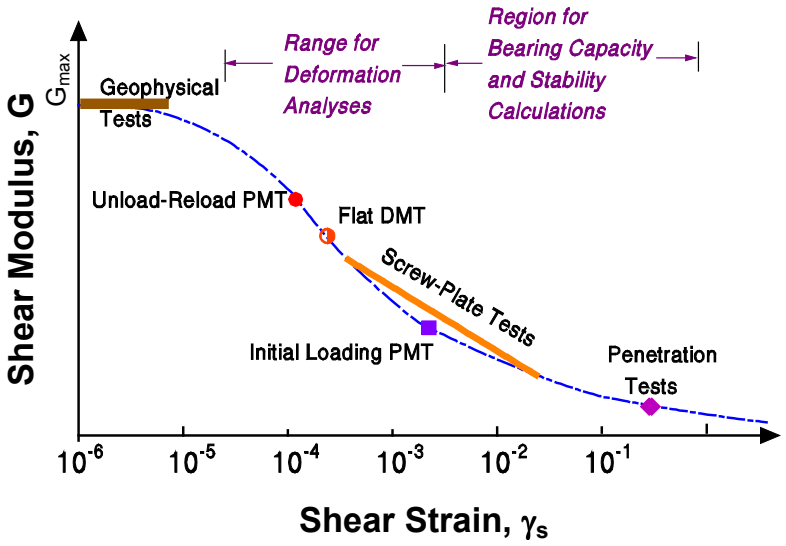


**Figure 4-3.** Variation of modulus with strain level (Mayne and Schneider, 2001)

## 4.4 Soil stiffness at small strain levels

The small-strain shear modulus $G_{max}$ is a fundamental stiffness applicable to all types of geomaterials including clays, silts, sands, gravels, and rocks (Tatsuoka et al., 2001) for

static and dynamic loading (Burland, 1989), and applicable under both drained and undrained loading conditions (Georgiannou et al., 1991; Lo Presti et al., 1996) because excess porewater pressures do not develop at such small strains. The value of $G_{max}$ can be measured using both laboratory and/or in-situ field tests. Laboratory tests include resonant column (e.g. Hardin and Drnevich, 1972); bender elements (e.g. Dyvik and Madshus, 1985); torsional shear apparatus (Teachavorasinskun, et al., 1991); and specially-instrumented triaxial tests with internal local strain measurements (e.g. Jardine et al., 1984). In-situ geophysical tests include the crosshole test (e.g. Hoar & Stokoe, 1978), downhole test (e.g. Woods, 1978; Campanella et al., 1994), spectral analysis of surface waves (e.g. Rix and Leipski, 1991; Stokoe et al, 1994), suspension logger (e.g. Nigbor & Imai, 1994), seismic cone (e.g. Robertson et al, 1986b), and seismic flat dilatometer (e.g. Hepton, 1988). The maximum soil shear modulus can also be estimated empirically from other in-situ and/or laboratory test results (e.g., Hryciw, 1990; Mayne and Rix, 1995; Hegazy and Mayne, 1995), when no direct measurement is available.

Some of the important factors affecting the small-strain stiffness $G_{max}$ are listed in Table 4-1. Figure 4-4 illustrates the various geophysical in-situ and laboratory methods for measuring small strain stiffness. Of particular optimization in geotechnical site characterization, the seismic cone and seismic dilatometer represent efficient means for collecting information about soil stratigraphy, strength, stress history, and shear wave velocity.

**Figure 4-1.** Factors affecting small-strain stiffness $G_{max}$

| Factor | Reference |
|---|---|
| Mean effective stress | Hardin and Drnevich (1972) |
| Void ratio $e_o$ | Hardin and Drnevich (1972) |
| Stress history, OCR | Hardin (1978)<br>Alarcon-Guzman et al. (1989) |
| Rate of loading | Dobry and Vucetic (1987)<br>Lo Presti et al. (1996) |
| Soil plasticity for silts and clays | Vucetic (1994)<br>Lo Presti et al. (1996) |
| Stress anisotropy for sands | Alarcon-Guzman et al. (1989)<br>Yamashita et al. (2003) |
| Creep | Lo Presti et al. (1996) |
| Effective confining stress | Santamarina and Aloufi (1999) |

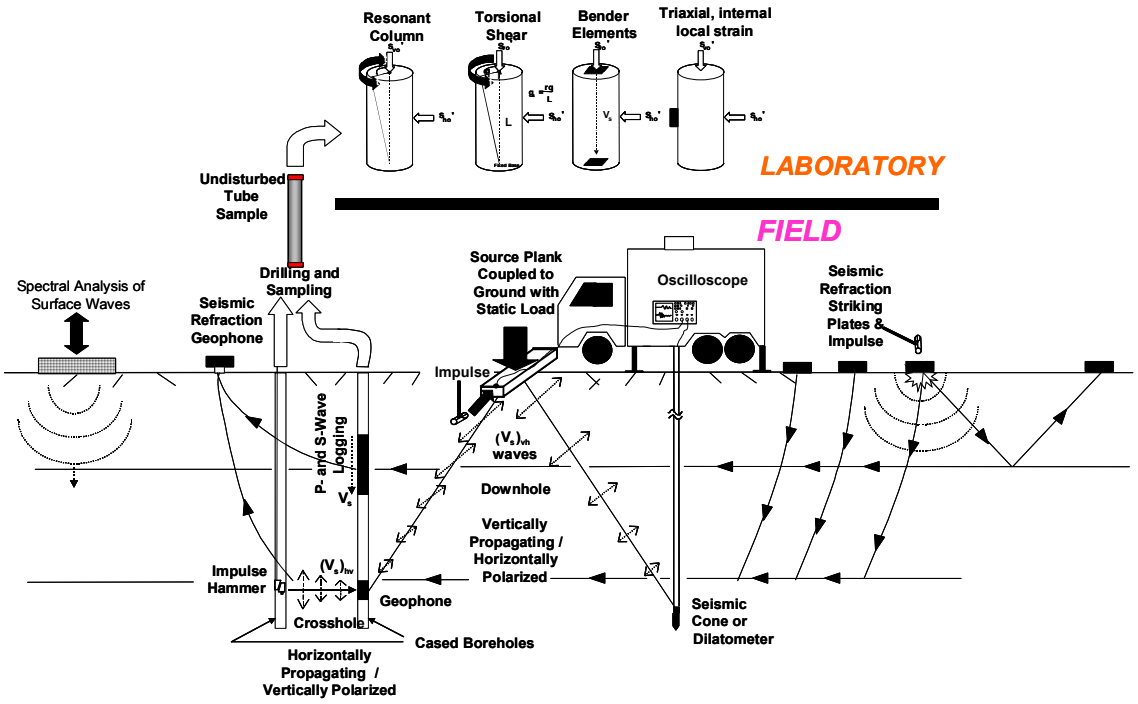


**Figure 4-4.** Schematic diagram of the different methods for measuring the shear wave velocity (Schneider, 2000)

The shear wave velocity $V_s$ is directly related to the maximum shear modulus $G_{max}$:

$$G_{\max} = \rho_t V_s^2 \quad \text{.....(4-1)}$$

where $\rho_t$ is the total soil mass density. An illustrative example of the downhole shear wave velocity measured using the seismic piezocone and corresponding small-strain shear modulus profiles at the Amherst geotechnical test site are shown in Figure 4-5. The Amherst test site consists of a 24-m thick deposit of soft lightly-overconsolidated lacustrine varved clay overlain by a 3-m desiccated crustal layer and 1-m thick clay fill (Lutenegger, et al. 2000; DeGroot and Lutenegger, 2002). The groundwater table lies one meter deep. The mass density, which is also needed for the calculation of overburden stresses, was evaluated making use of an empirical expression obtained by Mayne (2001) from compiled data for many different geomaterials that correlates the shear wave velocity ($V_s$ in m/s), depth (z in meter), and the saturated mass density ($\rho_{sat}$ in gm/cm$^3$):

$$\rho_{sat} = 0.85\log(V_s) - 0.16\log(z) \quad \text{.....(4-2)}$$

In case no direct measurement of the shear wave velocity is available, empirical correlations were developed for estimating either the shear wave velocity or small-strain stiffness $G_{max}$. Hardin (1978) presents a generalized empirical relationship for computing $G_{max}$ determined from wave propagation velocities and cyclic simple shear tests for any soil type as given by:

$$G_{\max} = 1230 \cdot OCR^{k} \cdot \frac{(2.973 - e)}{(1 + e)} \cdot \sigma_o^{0.5} \quad \text{.....(4-3)}$$

Where OCR = overconsolidation ratio, k = empirical parameter varying between 0 for sand and 0.5 for clays with high plasticity, e = void ratio, $\sigma_o = (\sigma_1 + \sigma_2 + \sigma_3)/3$, or the mean principal stress.

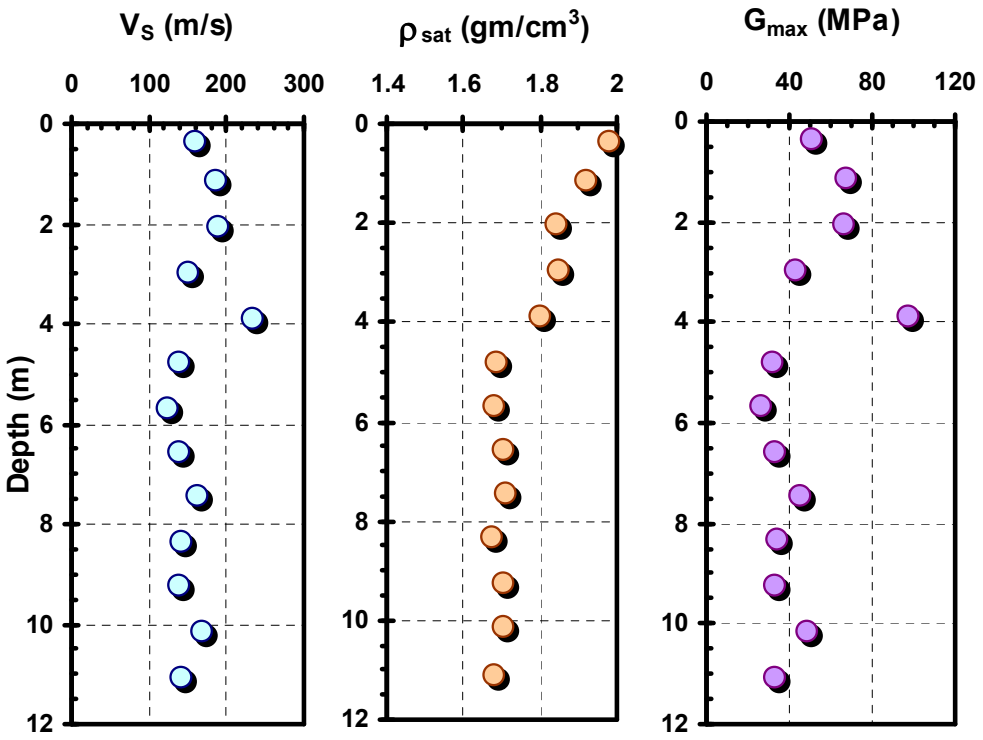


**Figure 4-5.** Downhole shear wave velocity and small-strain shear modulus profiles in varved clay at Amherst from seismic piezocone tests (after Elhakim & Mayne, 2003)

The stress-strain-strength behavior of soil is complex and dependent on many factors including: stress level, direction of loading, anisotropy, rate of loading, and drainage. Therefore, it is challenging to recommend a full set of tests to obtain a characteristic stiffness representing the stress-strain behavior for all possible types of loading.

Nevertheless, the small strain shear modulus $G_{max}$ provides a clear reference value for soil at a specific confining stress and corresponds to strains less than $10^{-6}$ (decimal).

### *4.4.1 Effect of sample disturbance on the small-strain shear modulus*

The effect of sample disturbance on the stress-strain behavior of soil samples has been investigated extensively (e.g. Lacasse et al., 1985; Hight et al., 1992; Tanaka and Tanaka, 1999). In this section, the influence of sample disturbance on the small-strain stiffness measured from laboratory tests is discussed in comparison with in-situ measurement (i.e. crosshole, downhole tests).

Many researchers have compared $G_{max}$ measured using both in-situ and laboratory methods (e.g. Richart, 1977; Kohata et al., 1997; Hight et al., 1997; Landon et al., 2004). The $(G_{max})_{lab}/(G_{max})_{field}$ ratio is indicative of the degree of sample disturbance. This ratio approaches unity for the "undisturbed" soil specimens. Toki et al. (1995) created a database of $(G_{max})_{lab}/(G_{max})_{field}$ ratios from well-documented case studies in Japan, shown in Figure 4-6. The results show the value of $(G_{max})_{lab}/(G_{max})_{field}$ falling within a narrow band between 0.8 and 1.2 for Holocene and Pleistocene clays extracted using thin-walled samplers; and for sands and gravel specimens obtained using in-situ freezing methods. The $(G_{max})_{lab}/(G_{max})_{field}$ ratio exceeds 1 for loose sand recovered using thin-wall samplers and likely densified during sampling , while the ratio is significantly smaller than unity for dense sands extracted using tube samples (Shibuya et al., 2004). Tatsuoka et al. (1997) show the laboratory measured small-strain stiffness $G_{max}$ to be influenced by sampler type, with less disturbance associated large diameter block samplers. The

influence of sample disturbance on the entire stress-strain behavior of soil specimens tested in the laboratory is discussed in detail later in Chapter 5.

Although the above discussion shows that the high quality "undisturbed" soil specimens can yield $G_{max}$ values comparable to in-situ measurements, the field measured shear wave velocity still remains the most definitive and reliable way to determine $G_{max}$. Moreover, in-situ methods allow for measuring the variation of $G_{max}$ both vertically and laterally, which is not achievable using laboratory testing due to cost and time limitations.

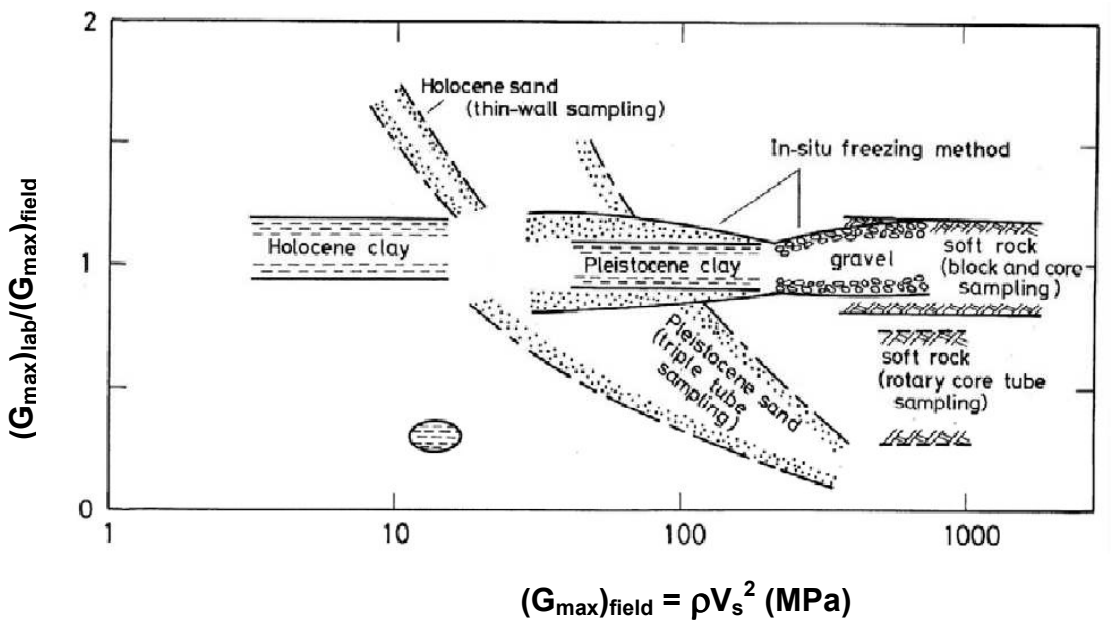


**Figure 4-6.** Ratio of $(G_{max})_{lab}$ measured from laboratory tests to $(G_{max})_{field}$ from geophysical surveys (after Toki et al., 1994)

## 4.5 Reduction of maximum shear modulus with increasing stress/strain levels

For stiffnesses that correspond to intermediate strains, modulus reduction factors $G/G_{max}$ versus the logarithm of the shear strain $\gamma_s$ have been developed, (e.g. Vucetic and Dobry

1991), as shown in Figure 4-7. In particular, these well-known curves apply to dynamic tests at fast loading and thus are influenced by strain rate effects. Their use is restricted to seismic site amplification studies and cyclic behavioral concerns. For static monotonic shear loading, the experimental trends of modulus reduction $G/G_{max}$ with increasing level of shear strain are presented in Figures 4-8-a. The trends are similar to those observed by Hardin & Drnevich (1972), and Vucetic & Dobry (1991) for dynamic tests. These laboratory data are referenced in Table 4-2 and come from static monotonic torsional shear tests on a variety of clays and sands. Solid symbols denote undrained tests (four clays, one sand) while open symbols represent drained test data (three sands, one clay). A similar database of modulus reduction data from triaxial compression tests and plane strain conditions are compiled and presented in Appendix F.

Alternatively, $G/G_{max}$ reductions can be presented in terms of the mobilized shear stress $\tau/\tau_{max}$, as suggested by Fahey and Carter (1993). The $G/G_{max}$ versus $\tau/\tau_{max}$ plots tend to emphasize the intermediate- to large-strain regions, while $G/G_{max}$ versus $\log(\gamma_s)$ curves tend to accentuate the small- to intermediate-strain range. In Figure 4-8-b, the same monotonic torsional shear data are used to show the modulus reduction values $G/G_{max}$ plotted versus the mobilized shear strength $\tau/\tau_{max}$, both on arithmetic scales, where $\tau_{max}$ = shear strength. For undrained loading, $\tau_{max} = s_u$. Surprisingly, all data fall within a relatively narrow band, more so than the more conventional $G/G_{max}$ versus shear strain as those are plotted on semi-log scales. Of additional note, the mobilized strength term may also be considered as the reciprocal of the factor of safety for the problem, or $\tau/\tau_{max} = 1/FS$.

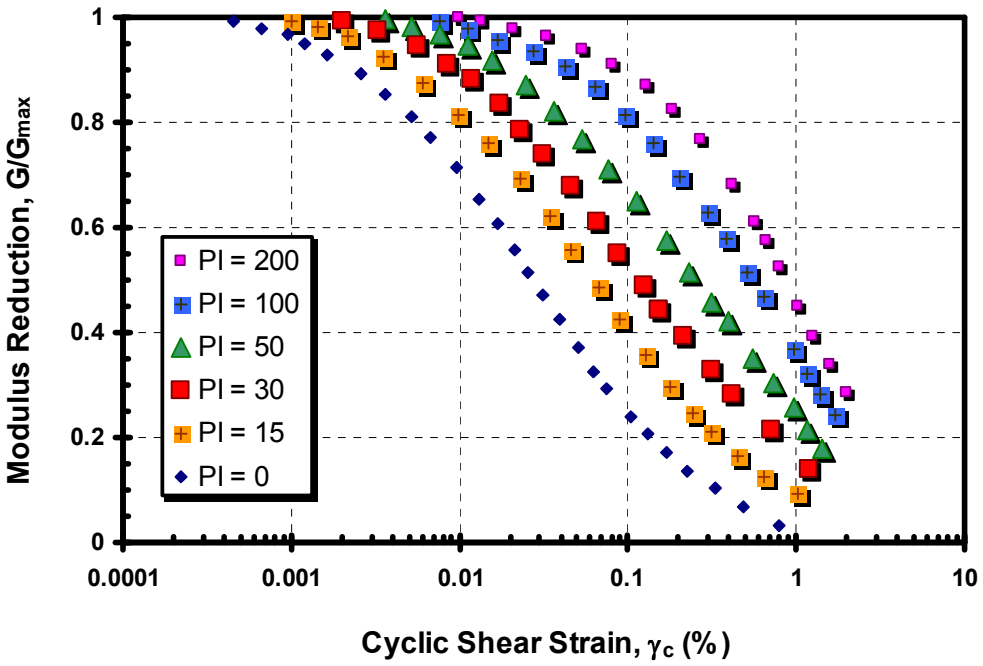


**Figure 4-7.** Modulus reduction with logarithm cyclic shear strain for different values of plasticity index (after Vucetic and Dobry, 1991)

## 4.6 Formulae/methods for non-linear stress-strain representation

A sizeable number of mathematical formulae have been proposed to represent non-linear stress-strain soil response. Since the slope of the stress-strain curve represents a modulus at a certain strain level (or corresponding mobilized stress level), modulus reduction schemes can be implemented into numerical modeling of boundary value problems (e.g. Lee and Salgado, 1999; Zhu and Chang, 2002). Most of the available modulus reduction schemes were created by fitting stress-strain data from a variety of shear tests (triaxial, simple shear, resonant column) over a particular region of interest: small-strains $(\gamma_s \leq 0.001\%)$, intermediate strains $(0.0001\% < \gamma_s < 0.001\%)$, or large strains $(\gamma_s > 0.1\%)$. Thus, many contrived expressions have difficulty in spanning from the very small non-destructive region through working load levels at intermediate strains to failure conditions at high strains that correspond to peak strength and bearing capacity.

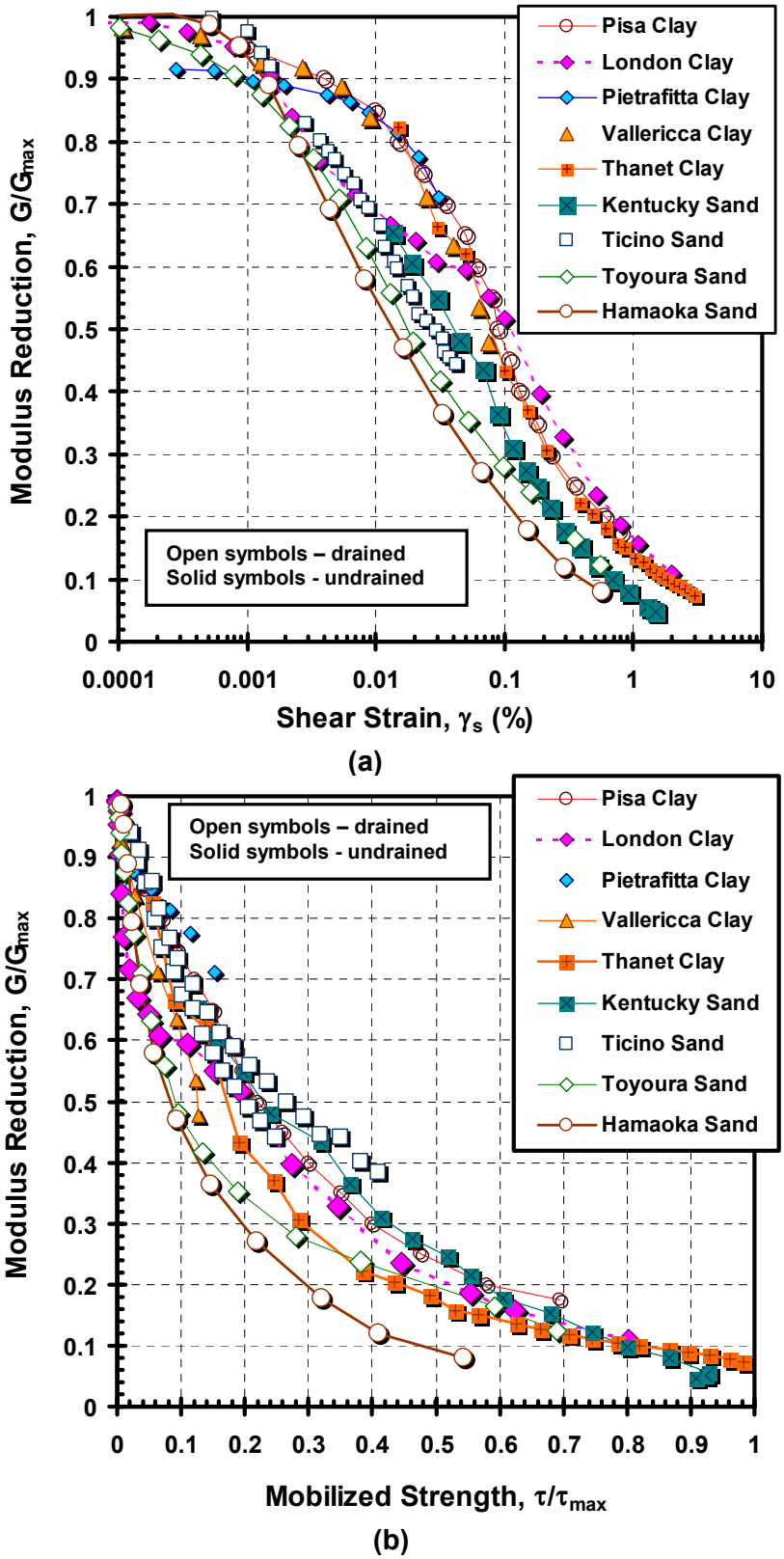


**Figure 4-8.** Modulus reduction data from compiled monotonic torsional shear tests plotted versus: a) logarithmic strain; b) mobilized stress (note: references in Table 4-2)

**Table 4-2.** Reference sources for shear modulus reduction data from static (monotonic) torsional shear tests

| Drainage | Soil Type | Reference | Notes |
|---|---|---|---|
| Undrained | London Clay | Hight et al. (1997) | depth = 57.5 m, $\gamma_b$ = 19.4 kN/m$^3$, $w_n$ = 29.1%, LL = 62.3%, PL = 26.2%, |
| | Pietrafitta Clay | Georgiannou et al. (1991) | $w_n$ = 41.8%, LL = 62 %, PI = 29.6%, |
| | Vallericca Clay | Georgiannou et al. (1991) | $w_n$ = 22-26%, LL = 54%, PI = 26% |
| | Thanet Clay | Hight et al. (1997) | depth = 81 m, $\gamma_b$ = 19.3 kN/m$^3$, $w_n$ = 31.7 %, LL = 102.3%, PL = 37.5%, |
| | Kentucky Clayey Sand | Drnevich & Massarsch (1979) | $w_n$ = 32%, Composition: 11% clay, 31% silt, 49% sand, 8% gravel |
| Drained | Ticino Sand | LoPresti et al. (1993) | $e_o$ = 0.71, $D_{50}$ = 0.54 mm, OCR = 1 and 4 |
| | Toyoura Sand | Teachavorasinskun et al. (1991) | $e_o$ = 0.69, $D_{50}$ = 0.14 mm |
| | Hamaoka Sand | Teachavorasinskun et al. (1991) | $e_o$ = 0.628, $D_{50}$ = 0.237 mm |
| | Pisa Clay | Lo Presti et al. (2003) | LL = 84 %, PL = 33.5 %, $w_n$ = 63%, OCR = 1.75 |

Notes:

$\gamma_b$ = bulk unit weight

$w_n$ = natural water content

LL = liquid limit

PL = plastic limit

PI = plasticity index

$e_o$ = initial void ratio

$D_{50}$ = Sieve diameter equivalent to 50% soil passing

OCR = overconsolidation ratio

Moreover, the representation of post-peak to softened strength values as well as extremely high strains corresponding to residual conditions, may in fact be relevant, but not discussed herein due to full complexities and understanding beyond the current state-of-the-art (Leroueil and Hight, 2003). Efforts here have been restricted to addressing the initial stiffness (i.e. $G_{max}$) and subsequent reductions to intermediate-strains (i.e. $G_{sec}$ and $G_{tan}$), and large-strains at peak strength (i.e. $\tau_{max}$). As such, a suitable modulus reduction model should satisfy several requirements: (1) minimum number of material constants defining stress-strain non-linearity without compromising accuracy; (2) material constants should have a physical meaning; and (3) should be derived easily (Puzrin and Burland, 1996). Furthermore, as the significance of the small-strain stiffness has now become fully recognized, all stress-strain-strength curves should begin at $G_{max}$ (Burland, 1989; Atkinson, 2000; Tatsuoka et al., 2001). A brief overview on the chronological and historical development of the various algorithms follows.

A selected summary of available non-linear stress-strain representation schemes is provided in Table 4-3. The number of non-linear parameters required for the simulation of modulus reduction depends on the particular model formulation. Specific details on each model are given in their corresponding references. Individual appraisals of certain of the existing reduction schemes have been carried out for selected soils by a number of researchers (e.g. Puzrin and Burland, 1996; Lo Presti et al., 1997; Shibuya et al., 2001).

Ramberg-Osgood (1948) is one of the earliest means to represent the non-linear stiffness of soil, requiring three parameters in a power law format. A difficulty with the Ramberg-

Osgood formulation is that the derived shear stresses continue unbounded and the model predicts infinite strength at infinite strain (Burghignoli et al., 1991). Kondner (1963) showed that the stress-strain behavior of clay soils at intermediate- to large- strains could be represented with reasonable accuracy using a simple hyperbola. The initial modulus and strength are the only parameters needed for defining the shape of the stress-strain curve. As such, the strength is bounded by an asymptote, or upper limit. The initial modulus is merely a pseudo-value from the fitting at high-strains however. For sands, the simple hyperbola was insufficient thus modified by Duncan and Chang (1970) to accommodate increased confining stress levels and force a definitive $(\sigma_1-\sigma_3)_f$ measured in laboratory tests with the asymptote, $(\sigma_1-\sigma_3)_{ult}$, given by the hyperbola. Duncan and Chang (1970) were also recognized as the first to incorporate a non-linear stress-strain expression into geotechnical finite element analyses. However, Duncan and Chang (1970) used an initial elastic modulus $E_i$ that is considerably underestimated compared to the small-strain stiffness $E_{max}$ (Lee et al., 2004) thus $E_i$ is a pseudo-initial value. In order to represent resonant column test data at small-strains, Hardin and Drnevich (1972) implemented different modifiers to the hyperbola that permitted $G/G_{max}$ versus log ($\gamma_s$) curves to match small- to intermediate- strains. They also introduced the concept of a reference strain for normalizing the curves, whereby $\gamma_{ref}=\tau_{max}/G_{max}$. The matching and calibration by Hardin and Drnevich applies only to dynamic tests (primarily resonant column) and thus not directly useable in static loading.

**Table 4-3.** List of selected modulus reduction schemes

| Equation | Reference | Notes |
|---|---|---|
| ***Power law fitting model***<br>$\frac{E_t}{E_{\max}} = \frac{1}{1+\alpha \cdot R \cdot y^{R-1}}$<br>where $y = \frac{\varepsilon/\varepsilon_r}{1+\varepsilon/\varepsilon_r}$, $\varepsilon$ is the axial strain at current stress level, $\varepsilon_r$ is a reference strain (= $q_{max}/E_{max}$), α and R are soil parameters obtained from the soil stress strain behavior | Ramberg-Osgood (1948) | ▪ strain hardening algorithm<br>▪ As strains increase, corresponding stresses increase without bound |
| ***Hyperbolic fitting model***<br>$(\sigma_1 - \sigma_3) = \frac{\varepsilon}{1/E_i + \varepsilon/(\sigma_1-\sigma_3)_{\max}}$<br>$\frac{E}{E_i} = \frac{1}{E_i}\cdot\left[\frac{1}{a+b\varepsilon}\right] = 1 - \frac{\sigma_1-\sigma_3}{(\sigma_1-\sigma_3)_{\max}}$<br>a = f(OCR, confining stress, strain rate) | Kondner (1963) | E = equivalent elastic soil modulus<br>$E_i$ = initial modulus<br>a, b = fitting constants |
| ***Parabolic fitting model***<br>$\sigma = \sqrt{\frac{\varepsilon}{a-b\varepsilon}}$ | Brinch Hansen (1963) | a and b are model fitting parameters |
| ***Power law fitting model***<br>$\sigma = \frac{\sqrt{\varepsilon}}{a-b\varepsilon}$ | Brinch Hansen (1963) | a and b are model fitting parameters |
| ***Modified hyperbolic fitting model***<br>$E_t/E_i = (1 - R_f \cdot SL)^2$<br>where $SL = (\sigma_1-\sigma_3)/(\sigma_1-\sigma_3)_f$<br>$R_f = (\sigma_1-\sigma_3)_f/(\sigma_1-\sigma_3)_{ult}$ | Duncan and Chang (1970) | Modified hyperbolic fitting that uses peak strength matching |
| ***Hyperbolic fitting model***<br>$\frac{G}{G_{\max}} = \frac{1}{1+\gamma_h}$<br>$\gamma_h = \frac{\gamma}{\gamma_r}\cdot\left[1 + a\cdot e^{-b(\gamma/\gamma_r)}\right]$<br>where $\gamma$ is the current strain, $\gamma_h$ is the hyperbolic strain, $\gamma_r$ is the reference strain (= $\tau_{max}/G_{max}$), a and b are soil properties | Hardin and Drnevich (1972) | Based on resonant column tests |
| ***Periodic logarithmic fitting model***<br>$\frac{E_s}{s_u} = A + B\cdot\cos\left\{\alpha\left[\log\left(\frac{\varepsilon_a}{C}\right)\right]^{\gamma_x}\right\}$<br>A, B, C, α and $\gamma_x$ determined from triaxial test data | Jardine, et al. (1986) | Implemented for numerical modeling. Requires 5 parameters listed herein plus 2 additional limiting strains |

**Table 4-3.** (continued)

| Equation | Reference | Notes |
|---|---|---|
| ***Modified hyperbolic fitting model***<br>$\frac{G_{\sec}}{G_{\max}} = \frac{\tau_1}{\tau_1 + \gamma \cdot G_{\max}} - \tau_1 \cdot \frac{\frac{\tau_1}{G_{\max}^2}}{\left(\frac{\tau_1}{G_{\max}} + \gamma_{\max}\right)^2} \cdot \frac{1}{\gamma_{\max}^m} \cdot \frac{\gamma^m}{m+1}$<br>where $\tau_1$ and $m$ are positive and real numbers of the modified hyperbolic equations; $G_{sec}$ and $\gamma$ are current secant shear modulus and shear strain, respectively; $\gamma_{max}$ is the maximum shear strain. Hyperbolic model parameters are obtained from:<br>$m \geq 4y_{\max} - 1$ and $\tau_1 = \frac{y_1 \cdot G_{\max}}{\gamma_{\max}}$<br>where $y_1 = \frac{y_{\max} - \frac{1}{2} + \sqrt{\frac{1}{4} - \frac{y_{\max}}{m+1}}}{\frac{m}{m+1} - y_{\max}}$, $y_{\max} = \frac{\tau_{\max}}{G_{\max} \cdot \gamma_{\max}}$ | Prevost and Keane (1990) | Both monotonic & cyclic loading at both low- and high-strains |
| ***Modified hyperbolic fitting model***<br>$Y = Y_{el} + \frac{X - X_{el}}{\frac{1}{C_1(X) + \frac{(X - X_{el})}{C_2(X)}}}$<br>where<br>normalized deviator stress = $Y = \Delta q / \Delta q_{\max}$<br>normalized axial strain = $X = \varepsilon_a / (\varepsilon_a)_r$<br>reference strain = $(\varepsilon_a)_r = \Delta q_{\max} / E_{\max}$<br>$C_1(X)$ and $C_2(X)$ = fitting parameters varying with strain level | Tatsuoka and Shibuya (1992) | Provides good approximation to stress-strain data. However, the required six parameters is too large a number (Shibuya et al., 2001) |
| ***Hyperbolic fitting model***<br>$\frac{G_{\sec}}{G_{\max}} = 1 - f\left(\frac{\tau}{\tau_{\max}}\right)^g$<br>$\frac{G_t}{G_{\max}} = \frac{\left(\frac{G}{G_{\max}}\right)^2}{\left[1 - f(1-g)\left(\frac{\tau}{\tau_{\max}}\right)^g\right]}$<br>where $G_{sec}$ = secant shear modulus at current stress level, $G_t$ = tangent shear modulus at current stress level, $G_t$ = maximum shear modulus, $\tau$ = current shear stress, $\tau_{max}$ = shear strength, f and g = soil parameters describing the non-linear soil behavior | Fahey and Carter (1993) | Modified hyperbolic formulation.<br><br><u>Note</u>:<br>A simple hyperbola obtained for f = 1 and g = 1. |

**Table 4-3.** (continued)

| Equation | Reference | Notes |
|---|---|---|
| ***Modified hyperbola***<br>$\frac{G_{\sec}}{G_{\max}} = \left(1 - \frac{\tau}{\tau_{\max}}\right)^m$<br>With m = 1 for simple hyperbola and m = 2 to 4 for static loading of soils. | Mayne (1994) | Modified hyperbolic formulation. |
| ***Logarithmic fitting model***<br>$\frac{E_{\sec}}{E_{\max}} = 1 - \alpha \cdot \frac{x - x_{th}}{x} \cdot \left[\ln\left(1 + x - x_{th}\right)\right]^R$<br>where:<br>$R = \frac{c(1 + x_L)\ln(1 + x_L)}{x_L(x_L - 1)}$<br>$\alpha = \frac{x_L - 1}{x_L\left[\ln(1 + x_L)\right]^R}$<br>$x_L = \frac{\varepsilon_f E_{\max}}{q_{ult}}$<br>$x_{th} = \frac{\varepsilon_{th}}{\varepsilon_r}$ = normalized threshold strain | Puzrin and Burland (1996; 1998) | Static loading. Several versions (1-, 3-, and 4-parameter) expressions, in addition to a threshold strain. The 1- parameter expression is discussed in more detail in chapter 5. |
| ***Double exponential fitting model***<br>$\frac{E_t}{E_{\max}} = \left[1 - \left(\frac{\Delta q}{\Delta q_{\max}}\right)^m\right]^n$<br>where $E_t$ is the tangent Young's modulus at any stress level, $E_{max}$ is the initial Young's modulus, $\Delta q$ is the increase in deviatoric stress $(=\Delta\sigma_1 - \Delta\sigma_3)$, $\Delta q_{max}$ is the maximum value of $\Delta q$ in compression, $m$ and $n$ are material constants. | Shibuya et al. (1997) | Hybrid of Fahey and Carter (1993) and Mayne (1994) modified hyperbolic expressions. |
| ***Exponential fitting model***<br>$G = \alpha \cdot \gamma^{\beta - 1}$<br>where $\alpha$ and $\beta$ are material constants | Bolton and Whittle (1999) | Power function where stress increases indefinitely beyond the strength of the material |

**Table 4-3.** (continued)

| Equation | Reference | Notes |
|---|---|---|
| ***Hyperbolic fitting model***<br>$\frac{G_s}{G_{\max}} = \left\{1 - f\left[\frac{(q - q_i)}{(q_{\max} - q_i)}\right]^g\right\}\left(\frac{p_o}{p_o^{'}}\right)^{ng}$<br>$\frac{G_t}{G_{\max}} = \frac{(G_s/G_o)^2}{\left[1 - f(1-g)\left(\frac{(q - q_i)}{(q_{\max} - q_i)}\right)^g\right]}\left(\frac{p_o}{p_o^{'}}\right)^{ng}$<br>where $q$ is the deviatoric stress invariant, $q_i$ is the initial deviatoric stress invariant at failure, $q_i$ is the deviatoric stress invariant at failure, $f$, $g$, $n_g$ are material constants, $p_o$ and $p_o$` are the octahedral stress invariants at current and initial stress invariant | Lee and Salgado (1999) | Generalized modified hyperbola for 3-D stresses (extension of Fahey and Carter, 1993) |
| For ε >= $\varepsilon_{th}$, $\frac{E}{E_{\max}} = \frac{1}{1 + \left(\frac{\varepsilon - \varepsilon_{th}}{\varepsilon_r - \varepsilon_{th}}\right)^n}$,<br>$E = E_{\max}$, for ε <= $\varepsilon_{th}$<br>where $\varepsilon_{th}$ is the linear elastic threshold strain, $\varepsilon_r$ is a reference strain equivalent to $E'/E_{\max}$ of 0.5, $n$ is an empirical constant used to change the rate of modulus degradation. | Lehane and Cosgrove (2000) | For Young's modulus of sands |
| ***Modified hyperbolic fitting model***<br>$\frac{E_t}{E_{\max}} = \frac{1 - \left(\frac{\varepsilon_f}{\varepsilon}\right)^r}{1 - \left(\frac{\varepsilon_f}{\varepsilon_{th}}\right)^r}$<br>where ε, $\varepsilon_f$ and $\varepsilon_{th}$ are current strain, strain at failure, and threshold strain, respectively; r is non-linear fitting parameter | Atkinson (2000) | Fitting parameter r is typically in the range of 0.5 to 1.0 |

**Note:** for isotropic elastic geomaterials, E = 2 G (1+ν)

A five-parameter periodic logarithmic function was proposed by Jardine et al. (1986) for use in numerical modeling of foundations, and this was one of the first to span small-, to intermediate-, to large-strains. However, only undrained loading was considered and because of the form chosen, two additional limiting strain parameters were needed to restrict the periodic function, thus a total of seven parameters were needed, many without physical significance.

Later, in order to connect the small-strain stiffness $G_{max}$ to large-strain shear strength, 6 separate fitting parameters (e.g. Tatsuoka and Shibuya, 1992) were introduced to adjust the shape of the hyperbola to fit a wide variety of stress-strain data. However, the parameters have no engineering significance other than curve fitting. A modified hyperbola form with only two parameters has been successfully used for representing laboratory stress-strain data (e.g. Fahey and Carter, 1993; Elhakim and Mayne, 2003; Lee et al., 2004). The modified hyperbola does not meet all the general conditions that should be satisfied by a normalized stress-strain curve outlined by Griffiths & Prevost (1990) and Puzrin & Burland (1996). In addition, the curve fitting parameters do not have a clear physical meaning and are not uniquely defined for a specific set of stress-strain data (Shibuya et al., 2001).

Puzrin and Burland (1996) evaluated seven of the more commonly-used stress-strain functions in light of the mathematical conditions suggested by the authors and additional criteria set by Griffiths & Prevost (1990). The functions included in the study include the original hyperbolic model (Kondner, 1963), and the modified hyperbolic functions

proposed by Hardin and Drnevich (1972), Griffiths and Prevost (1990), and Tatsuoka & Shibuya (1992), as well as the periodic logarithmic function proposed by Jardine et al. (1986). None of these formulations satisfied all the conditions set by Griffiths & Prevost (1990) as well as Puzrin & Burland (1996). A new logarithmic formula was subsequently developed that fulfills all the necessary conditions. The logarithmic function can be fitted to non-linear stress-strain data using one, three, or four parameters, in addition to a threshold strain, depending on the availability of measurements at various strain levels. Even the one-parameter logarithmic function gives good matching with stress-strain data over the entire stress-strain curve. The degree of soil non-linearity is described by the normalized limiting strain ($x_L$), which physically represents the ratio of small-strain modulus $G_{max}$ to the value of shear modulus at peak failure ($G_{min}=\tau_{max}/\gamma_f$), where $\tau_{max}$ is the shear strength and $\gamma_f$ is the shear strain at failure. Thus, the degree of non-linearity is specified by the parameter $x_L$, which has a real and fundamental significance. The derived stress-strain behavior is more non-linear for higher values of $x_L$. The logarithmic function and the normalized limiting stain $x_L$ are discussed in more detail in Chapter 5.

An alternate means to express the physical concept of normalized limiting strain $x_L$ is as the ratio of ($\gamma_f/\gamma_{ref}$) where $\gamma_f$ = strain at failure and $\gamma_{ref}=\tau_{max}/G_{max}$ is the reference strain corresponding to the intersection of the initial small-strain stiffness with the strength of the geomaterial.

## 4.7 Synopsis

In this chapter, different types of soil stiffness associated with mode of loading and strain level are reviewed. The concept of modulus reduction is introduced with the small-strain stiffness $G_{max}$ as the fundamental stiffness, applicable to all geomaterials under both drained and undrained loading conditions for static and dynamic conditions. The various methods for assessing $G_{max}$ from laboratory and in-situ tests are introduced. It is shown that the maximum shear stiffness assessed using in-situ seismic tests provide the most definitive and reliable means for assessing $G_{max}$.

A database of modulus reduction data from static monotonic torsional shear tests is compiled. The trends observed from the database are similar to those observed in dynamic tests. A review of modulus reduction schemes for representing non-linear stress-strain response is presented including hyperbolic, logarithmic, parabolic, and power function. The logarithmic function by Puzrin and Burland (1996, 1998) is found to be the most suitable method for modeling modulus reduction because the parameters have physical meaning and can be easily measured. Of added benefit, only two parameters are needed: the threshold strain $\gamma_{th}$ and the normalized limiting strain $x_L$. The parameter $x_L$ is simply $G_{max}/G_{min}$ where $G_{max} = \rho_T \cdot V_s^2$ and $G_{min} = \tau_{max}/\gamma_f$, where $\tau_{max}$ = shear strength and $\gamma_f$ = strain at failure.

# CHAPTER V

# STRESS-STRAIN RESPONSE OF SOIL REPRESENTED BY LOGARITHMIC FUNCTION

A logarithmic modulus reduction scheme (Puzrin and Burland, 1996, 1998) is adopted to represent the non-linear stress-strain-strength response of soil. Three levels of the model were suggested, using one, three, or four parameters, depending on the availability of test data, in addition to the threshold strain ($\gamma_{th}$). The model has shown high accuracy in reproducing stress-strain behavior of different soils and rocks over the full range of small-to-intermediate-to-high strains. For simplicity in relating the results to simple index properties and in-situ test data, the single-parameter model is applied herein to investigate the factors affecting soil non-linearity. This is achieved by fitting the logarithmic function to laboratory stress-strain data tested in triaxial compression, simple shear, and triaxial extension modes. In all cases, the initial stiffness of the soil is referenced to the in-situ measured small strain shear modulus $G_{max}$.

## 5.1 Logarithmic modulus reduction model

During the modulus reduction phase, the one-parameter logarithmic modulus reduction algorithm (Puzrin and Burland, 1996, 1998) can be formulated in terms of secant modulus $E_s$ and/or tangent modulus $E_t$. These modulus reduction factors are represented, respectively, by equations 5-1-a and 5-1-b:

$$\frac{E_s}{E_{\max}} = 1 - \alpha \cdot \frac{x - x_{th}}{x} \cdot \left[\ln\left(1 + x - x_{th}\right)\right]^R \quad \text{.....(5-1-a)}$$

$$\frac{E_t}{E_{\max}} = 1 - \alpha R \cdot \frac{x - x_{th}}{1 + x - x_{th}} \cdot \left[\ln\left(1 + x - x_{th}\right)\right]^{R-1} - \alpha \cdot \left[\ln\left(1 + x - x_{th}\right)\right]^R \quad \text{.....(5-1-b)}$$

where:

$E_s$, $E_t$, $E_{max}$ = secant, tangent, and small-strain Young's moduli, respectively.

$E_{max} = 2\ G_{max}\ (1+\nu)$

x = normalized strain = $\varepsilon/\varepsilon_r$

$x_{th} = \frac{\varepsilon_{th}}{\varepsilon_r}$ = normalized threshold strain

$\varepsilon_r$ = reference strain = $\frac{q_L - q_o}{E_{\max}}$

$q_{max}$ = deviatoric stress at failure = $\left(\sigma_1 - \sigma_3\right)_{\max}$

$q_o$ = initial deviator stresses = $\sigma'_{vo}\left(1 - K_o\right)$

$\sigma_{vo}$' = effective overburden stress

$K_o$ = at rest earth pressure coefficient

$$R = \left(\frac{1 - x_{th}}{x_L - x_{th}} - \frac{1 - c}{x_L}\right) \cdot \frac{(1 + x_L - x_{th})\ln(1 + x_L - x_{th})}{x_L - 1}$$

$$\alpha = \frac{x_L - 1}{\left(x_L - x_{th}\right) \cdot \left[\ln(1 + x_L - x_{th})\right]^R}$$

$x_L$ = normalized limiting strain = $\frac{\varepsilon_L}{\varepsilon_r}$

$\varepsilon_L$ = limiting strain (defined from Figure 5-1-a)

c = parameter of the logarithmic function (defined in Figure 5-1-b)

Figure 5-1-a and 5-1-b illustrate the definitions of the parameters needed for Equations 5-1-a and 5-1-b. The normalized limiting strain $x_L$ was originally defined (Puzrin and Burland, 1996) as the ratio of the limiting strain $\varepsilon_L$ to the reference strain $\varepsilon_r=q_{max}/E_{max}$ (defined in Figure 5-1-a), $x_L= \varepsilon_L/\varepsilon_r$. For c=1 at peak strength, the limiting strain $\varepsilon_L$ coincides with the failure strain, $\varepsilon_f$ (refer to Figure 5-1-b). In this case, the normalized limiting strain $x_L$ can alternatively be defined as the ratio of the small-strain stiffness ($E_{max}$ or $G_{max}$) to the equivalent corresponding secant modulus at failure ($E_{min}$ or $G_{min}$), thus $x_L= E_{max}/E_{min}$ or $G_{max}/G_{min}$. By definition, the value of the normalized limiting strain $x_L$ can never be less than unity. For $x_L = 1$, the model behaves as a purely linear elastic material.

Figures 5-2-a and 5-2-b show the variation of the intermediate parameters $R$ and $\alpha$ with the normalized limiting strain. Both fitting parameters $R$ and $\alpha$ are always positive (typical ranges for soils: $0.04<R<0.5$; $0.6<\alpha<0.9$). The limiting normalized strain ($x_L$) is the parameter determining the rate of modulus degradation. The value of $R$ is typically less than unity for soils and greater than unity for rocks (Puzrin and Burland, 1996). Figures 5-3-a and 5-3-b show the variation of the secant Young's modulus with the strain level and mobilized strength ($\tau/\tau_{max}$ or $q/q_{max}$) respectively. The normalized limiting strain ($x_L$) was varied between 5 and 80. The stress-strain behavior becomes more non-linear as the normalized limiting strain $x_L$ increases.

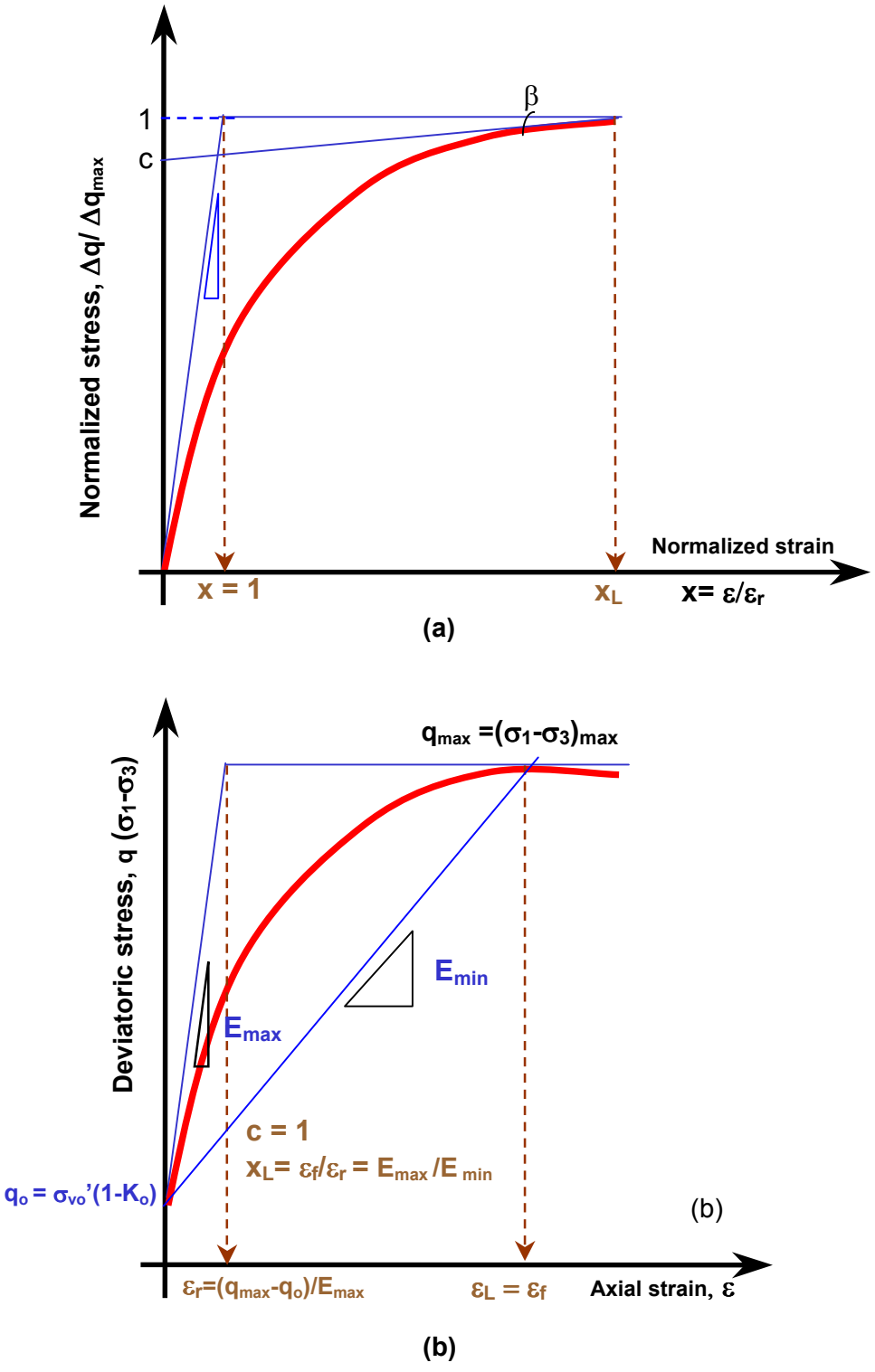


**Figure 5-1** Schematic diagram showing the physical parameters for the logarithmic function: a) generalized form (as defined by Puzrin and Burland, 1996); b) for c=1 at peak strength

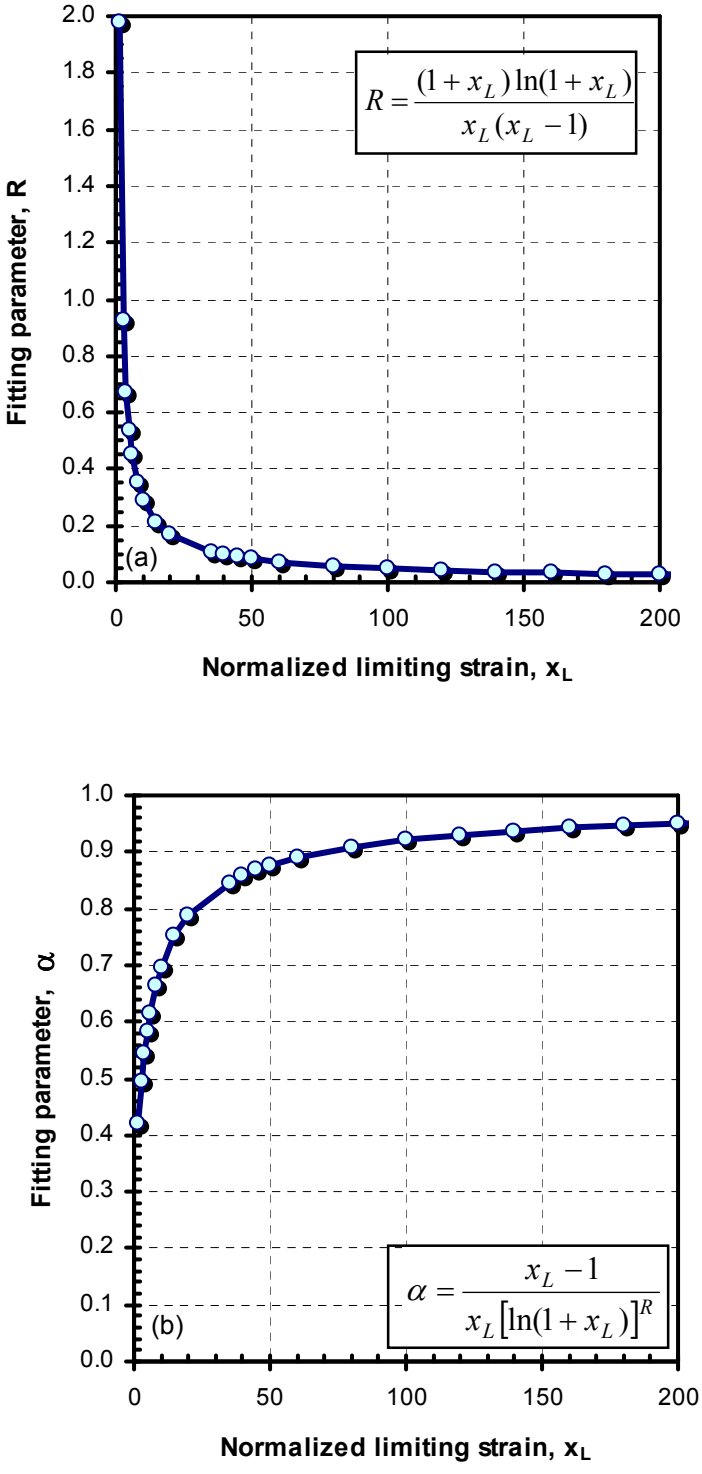


**Figure 5-2** Variation of intermediate parameters R and α with the normalized limiting strain $x_L$

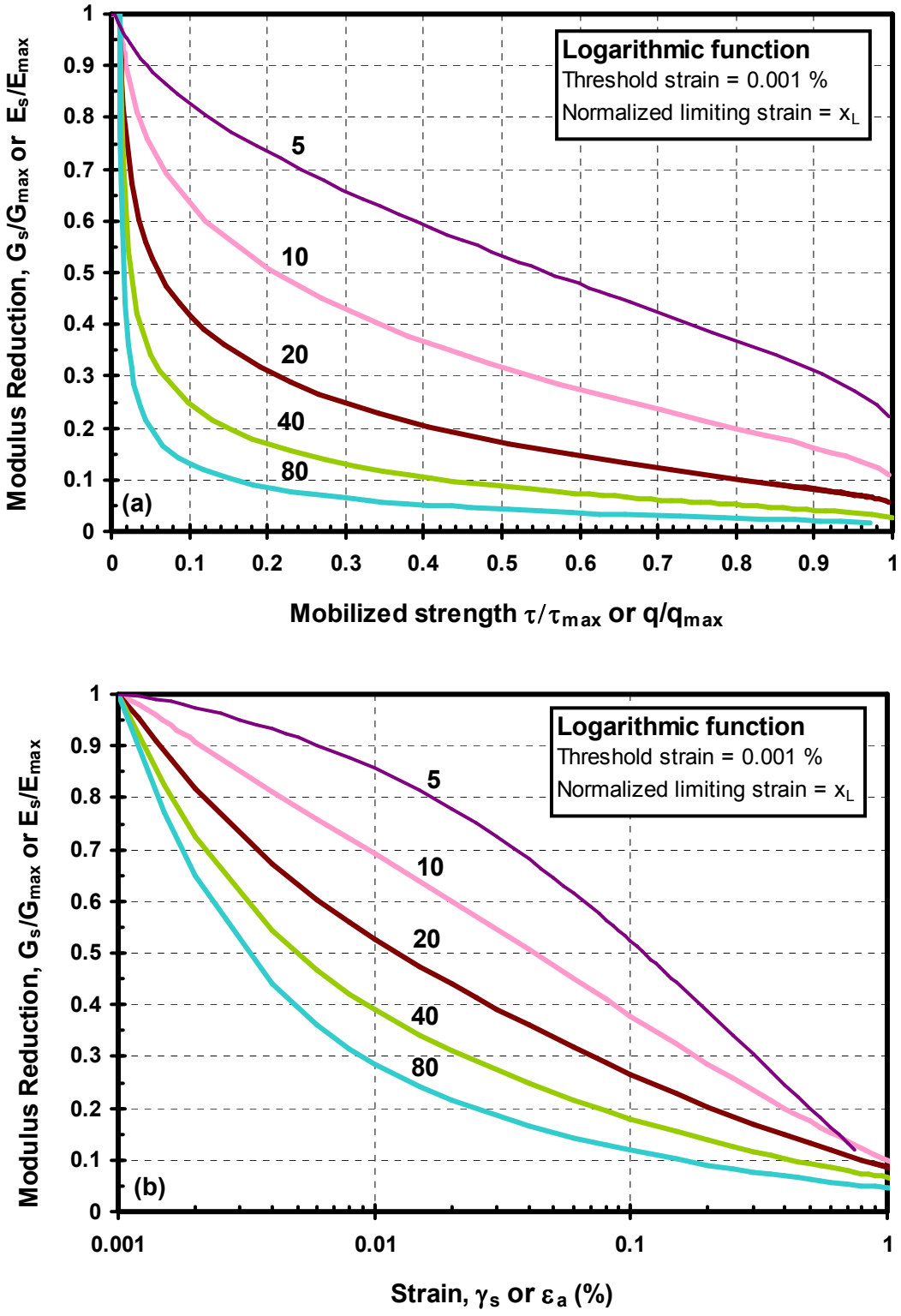


**Figure 5-3.** Variation of soil secant modulus according to the logarithmic function with: (a) mobilized strength (b) strain level.

Generally, non-linear soil behavior is identified and defined by laboratory test data. Soil stress-strain behavior depends on the quality of specimens, types of test, boundary conditions, and rate of loading. How these factors affect the value of the normalized limiting strain $x_L$ is discussed later in this chapter.

## 5.2 Threshold strain

A threshold strain $\gamma_{th}$ can be established below which the stress-strain behavior of soil can be essentially considered linearly elastic (Vucetic and Dobry, 1991; Vucetic, 1994). According to Santamarina et al. (2001), the linear threshold strain separates elastic constant fabric behavior from the degradation regime where soil fabric changes. In other words, soil stiffness is constant at $G_{max}$ for deformations smaller than the threshold strain as illustrated by Figure 5-4. This level of strain depends on several factors including soil type, plasticity, rate of loading, and stress history. Vucetic (1994) created a database for threshold strains measured in a variety of drained and undrained cyclic tests, including simple shear, resonant column, and triaxial tests. A similar database of threshold strains measured in resonant column tests conducted on different soil types was established by Lo Presti et al. (1996). The average $\gamma_{th}$ trends from both databases are plotted in Figure 5-5.

The dynamic threshold strain has received considerably more attention compared to its monotonic equivalent that applies to static loading. A database of monotonic torsional shear test data was compiled and presented in Figure 4-9 in Chapter 4.

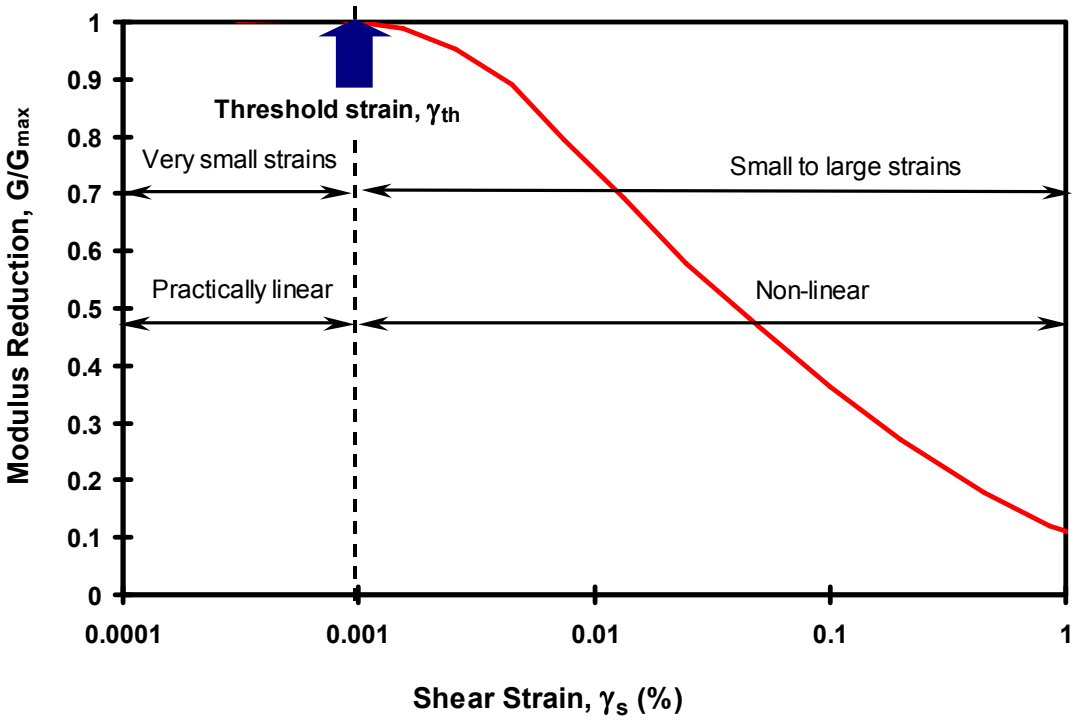


**Figure 5-4.** Reduction of shear modulus with the increase in strain level (modified after Vucetic 1994)

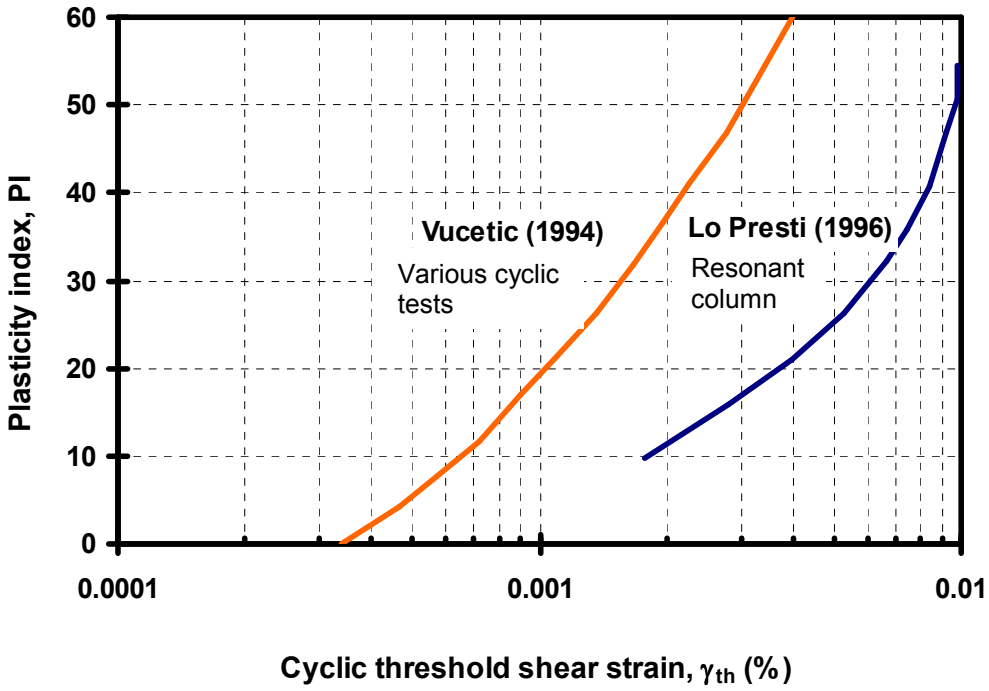


**Figure 5-5.** Effect of plasticity index on the cyclic threshold strain (Vucetic, 1994; Lo Presti, 1996)

Based on the monotonic torsional shear database, the threshold strain varies between 0.0005 % to 0.005 %. Likely, the values of $\gamma_{th}$ are affected by the rate of loading. For data on NSF clay (e.g. Shibuya et al., 1996; Shibuya et al., 1997), Figure 5-6 shows that the threshold strain ($\gamma_{th}$) increases with rate of loading.

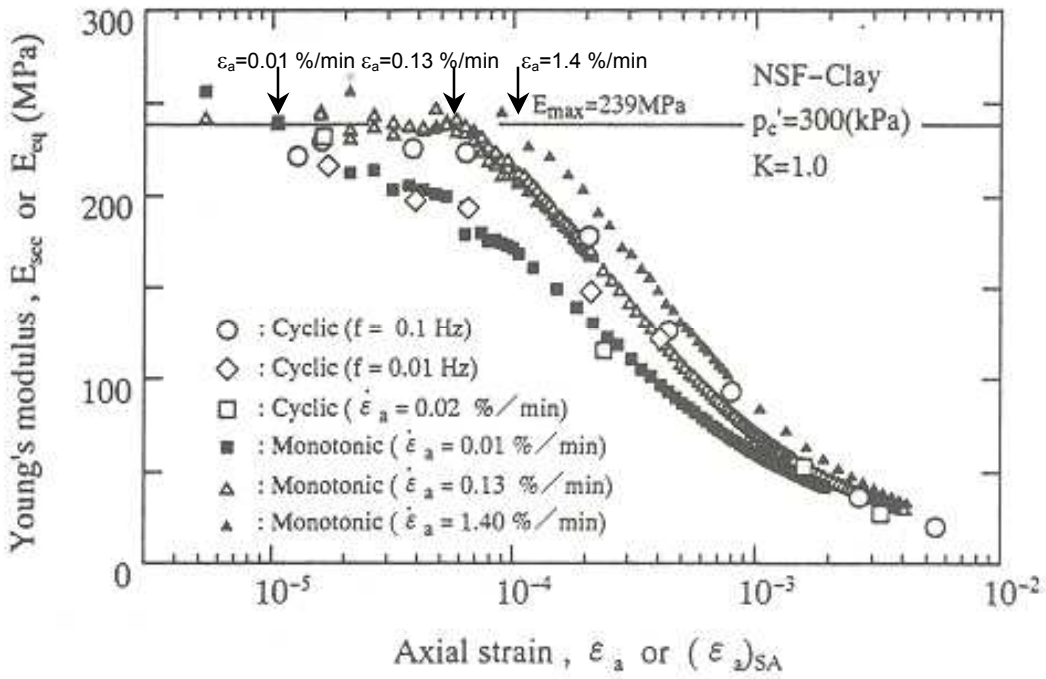


**Figure 5-6.** The effect of the rate of loading on the threshold strain (Shibuya et al., 1996)

## 5.3 Factors affecting soil non-linearity under undrained loading conditions

Several factors affect the degree of non-linearity measured using laboratory tests. These include: sample disturbance, mode of loading, and rate of loading as discussed in the following sections.

### *5.3.1 Sample disturbance*

Generally, it is well-known that sampling disturbance reduces the measured value of preconsolidation in oedometer tests, reduces peak strength values in laboratory shear tests, and lowers the small-strain shear modulus in resonant column tests. Attempts to minimize soil disturbance during extraction have resulted in the development of larger piston-type samplers to produce high quality soil specimens (e.g. Berre et al., 1969; Lefebvre and Poulin, 1979).

The mechanical behavior of soils tested in the laboratory is affected by sample disturbance during tube pushing extraction, sealing, transportation, extrusion, trimming, and mounting the specimen (Tanaka et al., 2001; Hight et al., 1992; Lacasse et al., 1985). This is illustrated by Figure 5-7, which shows the potential sources of error using hypothetical stress paths (Ladd and Lambe, 1963; Baligh et al., 1987, Ladd and DeGroot, 2003). Table 5-1 lists 8 different types of samplers with their main dimensions and features. It should be noted that all the listed samplers (except for Sherbrooke, also known as block samplers) employ tubes for soil extraction. Tanaka (2000) investigated the influence of using the various samplers listed in Table 5-1 on soil disturbance. The effect of sampler type on the measured stress-strain-strength behavior of Ariake clay is presented in Figure 5-8, which shows a hierarchy of curves depending on the level of sample disturbance. As sample disturbance increases, lower soil strengths and higher failure strains are recorded. Tanaka (2000) concluded that the Japanese Standard Fixed

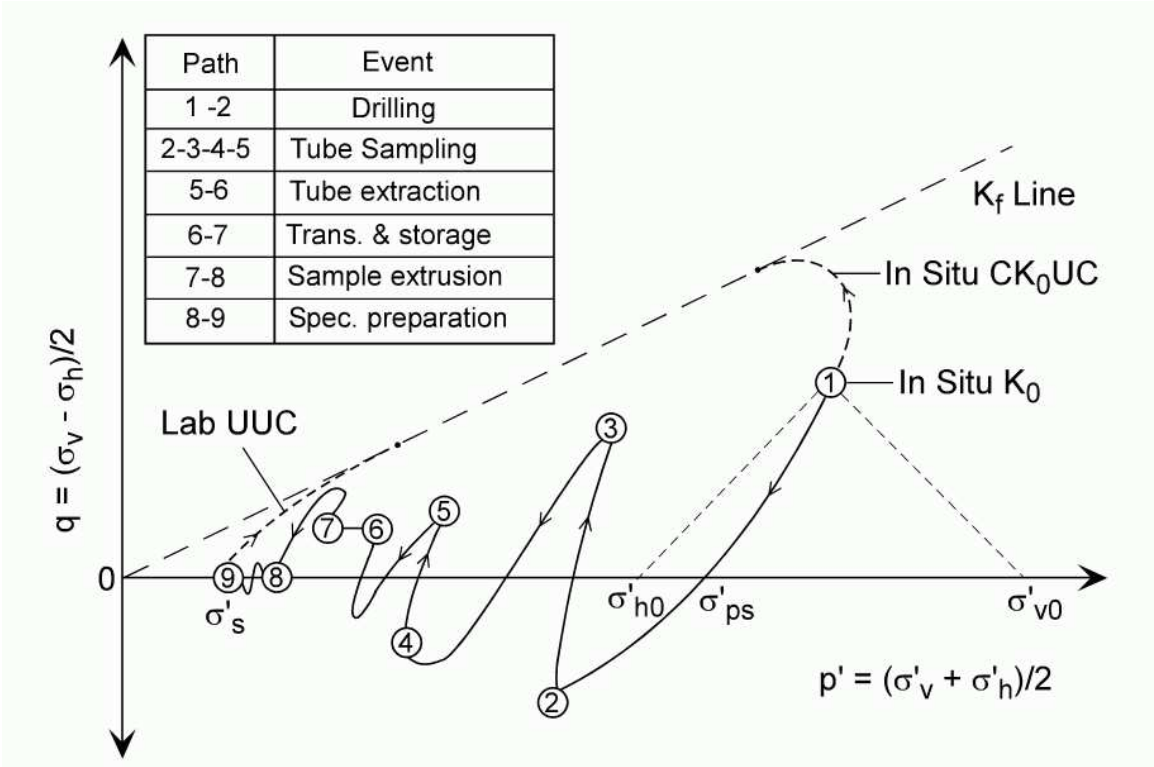


**Figure 5-7.** Hypothetical stress path during tube sampling and specimen preparation of centerline element of low OCR clay (Ladd and DeGroot, 2003)

**Table 5-1.** Main dimensions and features of soil samplers (modified after Tanaka, 2000)

| Sampler | Inside diameter (mm) | Inside diameter (mm) | Sampler length (mm) | Thickness (mm) | Area Ratio (%)** | Piston |
|---|---|---|---|---|---|---|
| JPN | 78 | 75 | 1000 | 1.5 | 7.5 | Yes |
| Laval | 216 | 208 | 660 | 4.0 | 7.3 | No |
| Shelby | 75.3 | 72 | 610 | 1.65 | 8.6 | No |
| NGI54 | 80 | 54 | 768 | 13 | 54.4 | Yes |
| ELE100 | 104.4 | 101 | 500 | 1.7 | 6.4 | Yes |
| Sherbrooke (Block sampler) | N/A*** | 350* | 250* | N/A*** | N/A*** | No |
| NGI95 | 105.6 | 95 | 1000 | 5.3 | 14 | Yes |
| Split-barrel | 51.1 | 34.9 | 450-600 | 8.1 | 112 | No |

* Specimen dimensions

** Area ratio = $\frac{\left(d^2_{external} - d^2_{internal}\right)}{d^2_{internal}}$ (US Army Corps of Engineers, 1996)

*** Sherbrooke sampler employs a special sampling technique that does not require a sampling tube. Refer to Lefebvre and Poulin (1979) for more details

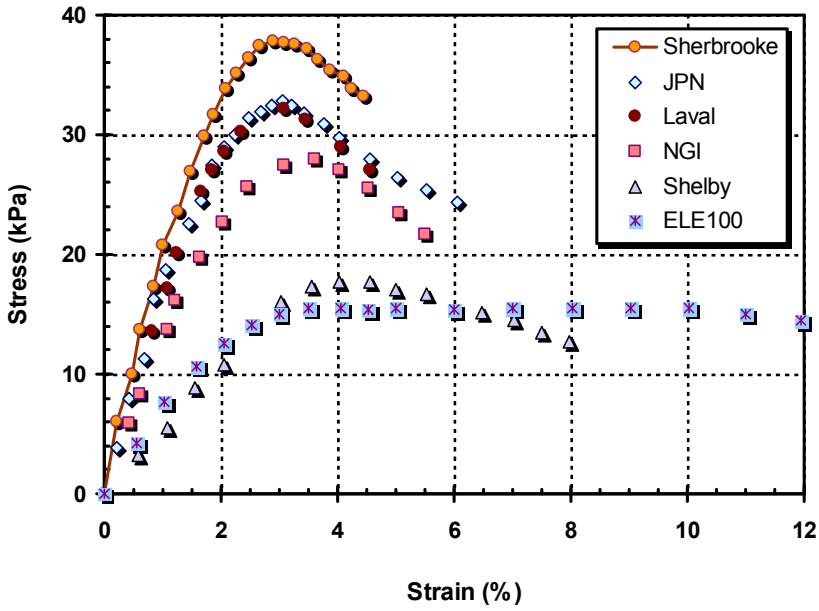


**Figure 5-8.** Effect of sampler type on the unconfined compression stress-strain behavior of Ariake clay from 10-m depth (Tanaka et al., 2000)

piston sampler JPN yielded quality similar to Laval and Sherbrooke samplers except for low plasticity clays. Shelby, NGI, and ELE100 samplers yielded lower quality samples, having lower strengths and larger strains to failure. Note that the influence of sample quality on the small-strain shear modulus $G_{max}$ was covered previously in Chapter 4.

The effect of sample disturbance on the non-linear stress-strain behavior of soils is now quantified by backfitting parameters to selected laboratory test data. Values of the normalized limiting strain ($x_L$) are computed from measured stress-strain data of specimens extracted with different samplers then tested under the same conditions. The selected soils, strength properties, sampler type, test mode and sources of data are listed in Table 5-2. The data contains soils from 5 sites. Tests included in the study were tested under different loading conditions: unconfined compression, $K_o$-consolidated triaxial

**Table 5-2** List of properties of soils used in investigating factors affecting $x_L$

| Site and Depth (m) | Test Type | Sampler Type | $G_{max}$ MPa | $\sigma_{vo}'$ kPa | $K_o$ | $s_u/\sigma_{vo}'$ | $\Delta q_u$ kPa | $\varepsilon_f$ (%) | $\varepsilon_r$ (%) | $x_L$ | Reference |
|---|---|---|---|---|---|---|---|---|---|---|---|
| Ariake | CKoUC | Laval | 4.4 | 35 | 0.45 | 0.48 | 214 | 1.2 | 0.10 | 11 | Tanaka and |
| 8 m | CKoUE | Laval | 4.4 | 35 | 0.45 | 0.29 | 40 | 7.0 | 0.30 | 23 | Tanaka (1999) |
| Ariake | $CK_oUC$ | Sherbrooke | 5.4 | 40 | 0.45 | 0.51 | 20 | 1.25 | 0.12 | 10 | Tanaka & |
| 10 m | $CK_oUC$ | ELE100 | 5.4 | 40 | 0.45 | 0.51 | 20 | 2.3 | 0.12 | 19 | Tanaka (1999); Tatsuoka (2002) |
| Bothkennar | $CK_oUC$ | Laval | 12 | 28.5 | 0.79 | 0.71 | 35 | 1.1 | 0.10 | 11 | Hight et al. |
| 2.7 m | $CK_oUC$ | Sherbrooke | 12 | 28.5 | 0.79 | 0.64 | 31 | 1.5 | 0.09 | 17 | (1992); |
| | $CK_oUC$ | Piston | 12 | 28.5 | 0.79 | 0.62 | 30 | 2.2 | 0.08 | 27 | Hight et al. |
| Bothkennar | CKoUC | Laval | 17 | 48 | 0.60 | 0.52 | 31 | 0.85 | 0.06 | 14 | (1997) |
| 5.3 to 5.4 m | CKoUE | Laval | 17 | 48 | 0.60 | 0.26 | 44 | 1.6 | 0.09 | 19 | |
| Bothkennar | $CK_oUC$ | Laval | 28.4 | 100 | 0.70 | 0.38 | 46 | 1.4 | 0.05 | 26 | |
| 12.6 m | $CK_oUC$ | Piston | 28.4 | 100 | 0.70 | 0.36 | 43 | 2.8 | 0.05 | 55 | |
| Bothkennar | $CK_oUC$ | Laval | 43.4 | 120 | 0.67 | 0.40 | 56 | 1.5 | 0.04 | 34 | |
| 15.3 m | $CK_oUC$ | Piston | 43.4 | 120 | 0.67 | 0.33 | 40 | 2.6 | 0.03 | 85 | |
| Bothkennar | UC | Sherbrooke | 16.7 | 89 | N/A | 0.39 | 69 | 2.5 | 0.14 | 18 | Hight et al. |
| 11 m | UC | ELE100 | 16.7 | 89 | N/A | 0.28 | 50 | 11.5 | 0.10 | 116 | (1997) |
| | | | | | | | | | | | Tanaka (2000) |
| Onsoy | $CK_oUC$ | Sherbrooke | 10.5 | 24 | 0.50 | 0.63 | 14 | 1.0 | 0.05 | 22 | Lacasse et al. |
| 3.2-3.5 m | $CK_oUC$ | NGI95 | 10.5 | 24 | 0.50 | 0.52 | 13 | 1.4 | 0.04 | 32 | (1985) |
| Onsoy | DSS | Sherbrooke | 14.1 | 39 | 0.50 | 0.33 | 13 | 1.5 | 0.09 | 17 | Gillespie et al. |
| 6.2 m | DSS | NGI95 | 14.1 | 39 | 0.50 | 0.35 | 14 | 1.3 | 0.10 | 13 | (1985) |
| San | CKoUC | Piston | 10.7 | 67 | 0.60 | 0.40 | 35 | 1.4 | 0.09 | 16 | Hunt et al. |
| Francisco | DSS | Piston | 10.7 | 67 | 0.60 | 0.27 | 18 | 9.0 | 0.17 | 53 | (2002) |
| 7.3-7.75 m | | | | | | | | | | | Pestana et al. |
| | | | | | | | | | | | (2002) |
| Singapore | CKoUC | JPN | 39 | 210 | 0.66 | 0.38 | 89 | 0.85 | 0.08 | 11 | Tanaka et al. |
| 22 m | CKoUE | JPN | 39 | 210 | 0.66 | 0.33 | 220 | 6.4 | 0.19 | 34 | (2001) |
| | | | | | | | | | | | Watabe (1999) |

Notes:
$CK_oUC$ = $K_o$-consolidated undrained triaxial compression
$CK_oUE$ = $K_o$-consolidated undrained triaxial extension
UC = unconfined compression
DSS = direct simple shear
$G_{max}$ = small-strain shear modulus
$\sigma_{vo}'$ = effective overburden stress
$K_o$ = at rest earth pressure coefficient
$s_u$ = undrained shear strength
$\Delta q_u = (\sigma_1-\sigma_3)_f-(\sigma_1-\sigma_3)_o$
$\varepsilon_f$ = strain at failure
$\varepsilon_r$ = reference strain
$x_L$ = normalized limiting strain

compression, $K_o$-consolidated triaxial extension, and direct simple shear. The stress-strain data are normalized by the deviatoric stress $\Delta q_u = q_{max}-q_o$ and reference strain $\varepsilon_r=\Delta q_u/E_{max}$, respectively. Fitted stress-strain data are presented in Appendix B. The normalized limiting strain $x_L$ was calculated for each test, as shown in Table 5-2. A higher value of $x_L$ indicates a more non-linear stress-strain behavior.

As an example, stress-strain results from $CK_oUC$ tests from Bothkennar (depth = 2.7 m) are presented in Figure 5-9-a. As expected, the stress-strain behavior depends on sample quality. The Laval and Sherbrooke samplers yield better quality samples (higher strengths and smaller failure strains) compared to the Piston sampler. Fitted normalized stress-strain data are plotted in Figure 5-9-b. The normalized limiting strains $x_L$ are 11, 17, and 27 for Laval, Sherbrooke, and Piston samplers, respectively.

Another example is illustrated by the direct simple shear test results from Onsoy (depth = 6.2 m). Specimens extracted using Sherbrooke and NGI95 samplers are compared in Figures 5-10-a and 5-10-b. Raw and fitted normalized stress-strain data are presented in Figures 5-10-a and 5-10-b, respectively. The difference in $x_L$ between the two samples is quite small (within 20 %), which could be within the natural variability of the soil. On the other hand, two specimens from the same site, extracted using the Sherbrooke and NGI95 samplers and tested in $CK_oUC$, demonstrated a larger increase in $x_L$ (about 50 %), as shown in Figures 5-11-a and 5-11-b indicating that different modes of loading are influenced to differing degrees by sample disturbance. Specifically, triaxial compression tests appear much more affected by sample disturbance than simple shear mode.

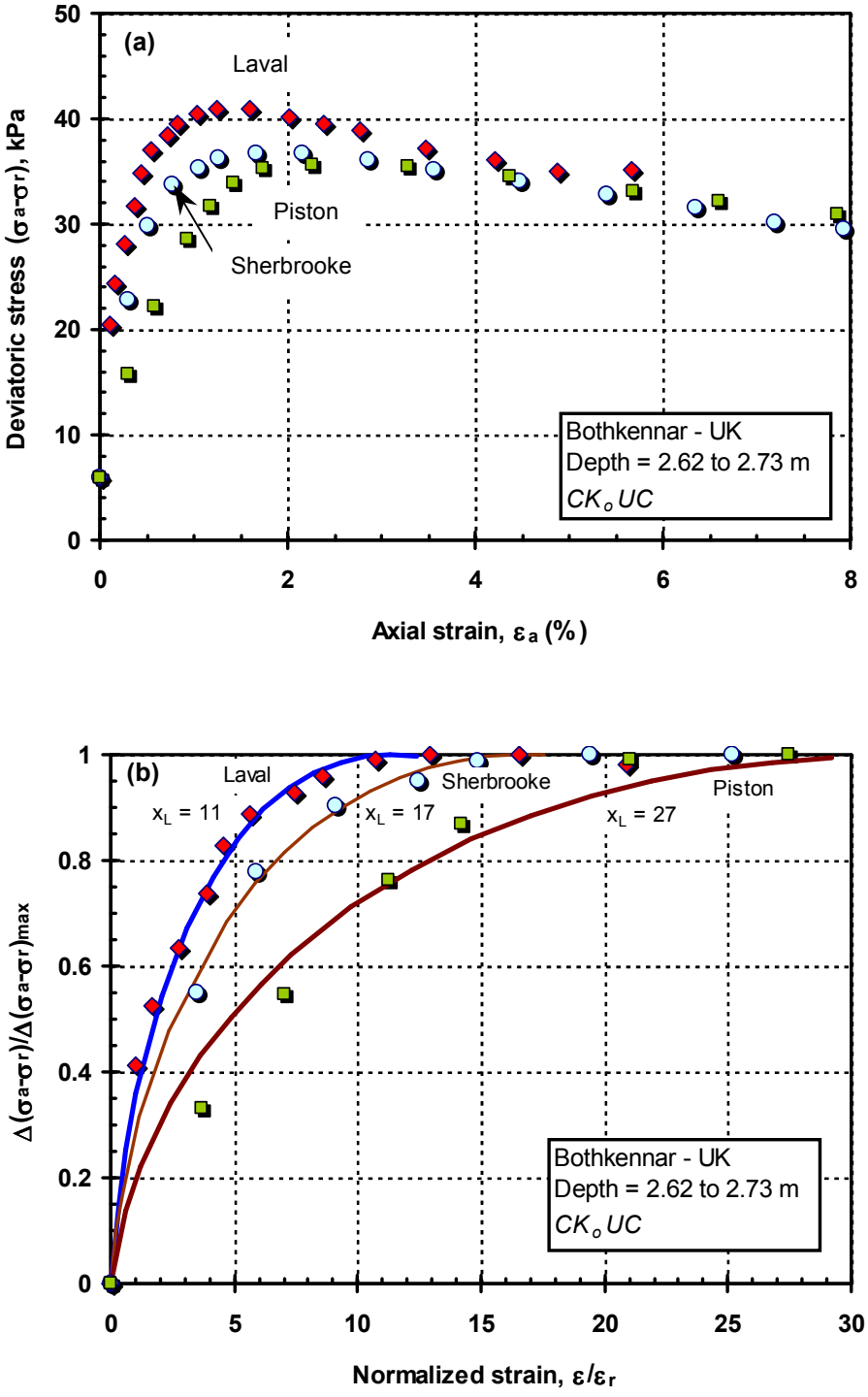


**Figure 5-9.** Effect of sample quality on non-linear stress-strain behavior of Bothkennar clay (2.62-2.73m) under anisotropically consolidated undrained triaxial compression: a) raw stress-strain data (Hight et al., 1992; 1997) b) normalized stress-strain results

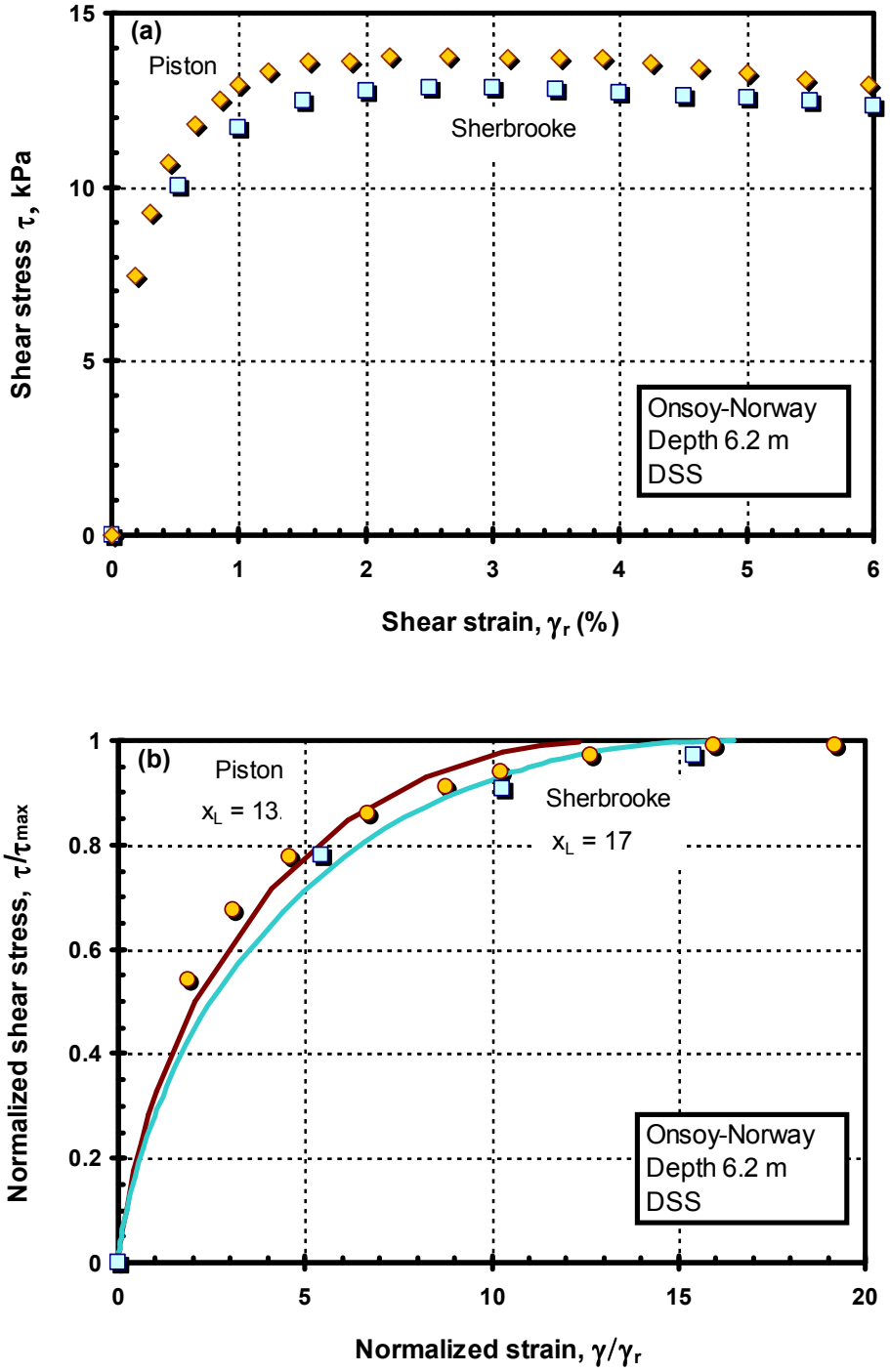


**Figure 5-10.** Effect of sample quality on non-linear stress-strain behavior of Onsoy clay (6.2 m) in direct simple shear: a) raw stress-strain data (Lacasse et al., 1985; Gillespie et al., 1985) b) normalized stress-strain results

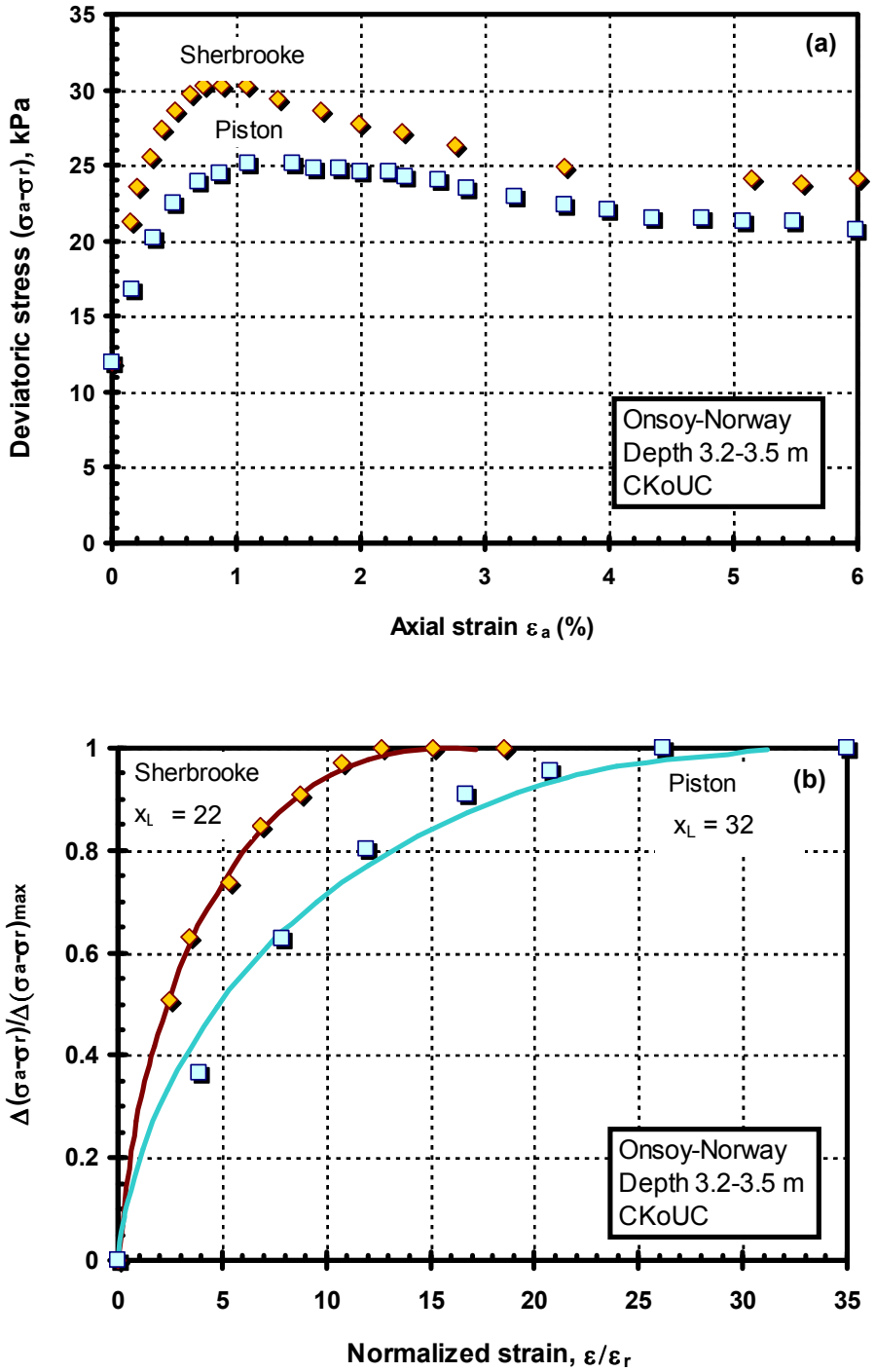


**Figure 5-11.** Effect of sample quality on non-linear stress-strain behavior of Onsoy clay (3.2-3.5 m) under anisotropically consolidated undrained triaxial compression: a) raw stress-strain data (Lacasse et al., 1985; Gillespie et al., 1985) b) normalized stress-strain results

### *5.3.2 Mode of loading*

The undrained strength of soils is not a fundamental property, but depends on several factors including the failure mode, strain rate, stress history, and soil anisotropy, making the undrained strength dependent on test type (Koutsoftas, 1981; Wroth, 1984; Koutsoftas and Ladd, 1985; Kulhawy and Mayne, 1990). The mode of loading affects stress-strain non-linearity and its influence is investigated in this section.

A selection of stress-strain tests on soils tested under different loading conditions was created. Soil properties and test types are listed in Table 5-2. Soils included in the study come from 4 sites (Ariake, Japan; Bothkennar, UK; Onsoy, Norway; and San Francisco, USA). Fitted stress-strain data from the different sites are presented in Appendix B. When comparing the stress-strain behavior of soil specimens under different modes of loading, specimens extracted using samplers of comparable quality were used to provide a common basis.

As an example, raw and normalized stress-strain data from $CK_oUC$ and $CK_oUE$ tests from Singapore (depth 22 m) are compared in Figures 5-12-a and 5-12-b, respectively. Both specimens were extracted using the Japanese sampler JPN, so they were subjected to similar amounts of disturbance. The raw data shows the failure strain in extension ($\varepsilon_f$ = 7.0 %) is approximately 6 times that in compression ($\varepsilon_f$ = 1.2 %). Consequently, $x_L$ in extension is higher than in compression, indicating a more non-linear stress-strain behavior.

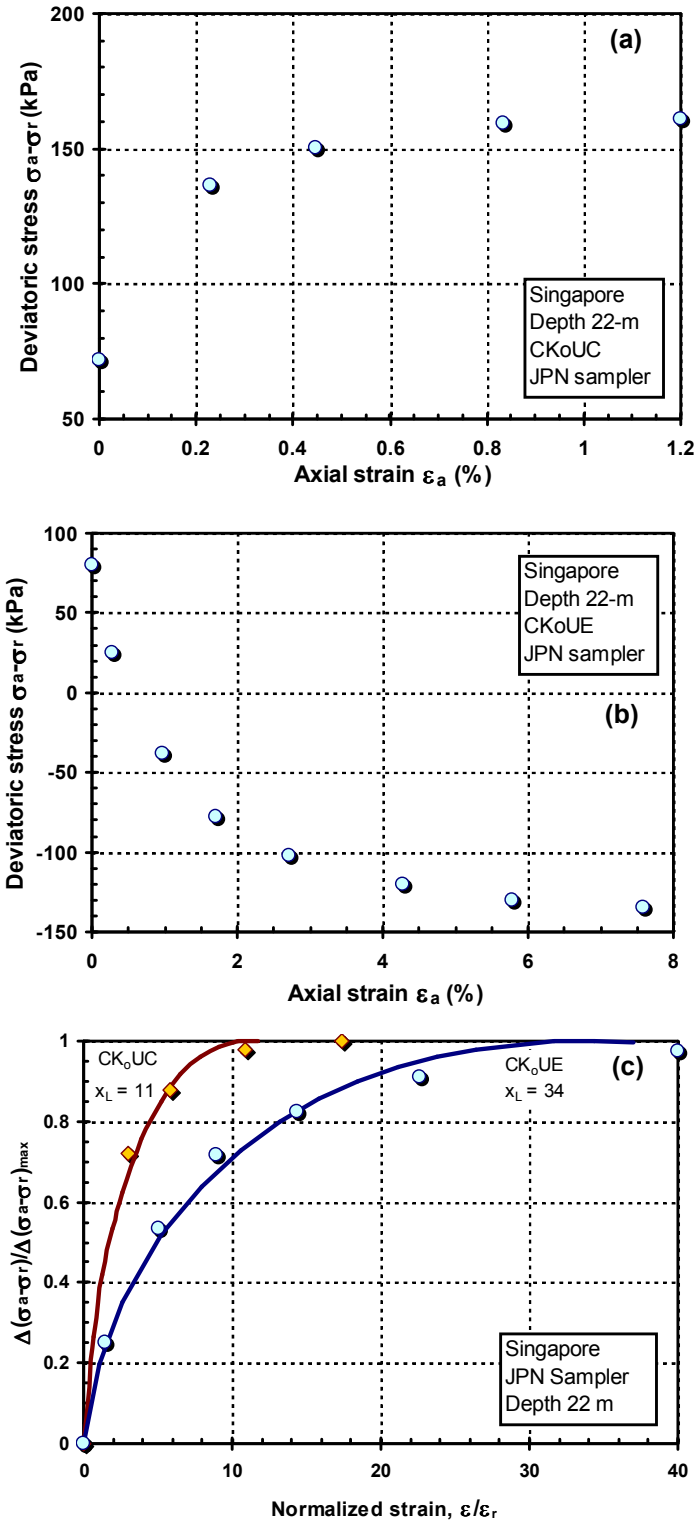


**Figure 5-12.** Effect of shear test mode on non-linear stress-strain behavior of Singapore clay (22 m): a) raw $CK_oUC$ stress-strain data; b) raw $CK_oUE$ stress-strain data (Watabe, 1999; Tanaka et al., 2001); c) normalized stress-strain results

Koutsoftas and Ladd (1985) investigated the effect of the mode of loading on undrained stress-strain behavior of AGS marine clay. The clay was tested at OCR = 1 under $K_o$-consolidated plane strain compression and extension, and direct simple shear conditions, as well as at higher overconsolidation ratios. The normalized shear stress versus strain plots for the different modes are shown in Figure 5-13. The plot also shows the average stress strain response as a dotted line. The average stress-strain behavior is closest to the direct simple shear response. Ladd (1991) suggests using the direct simple shear stress-strain response as a "rational" selection representative of soil behavior. Although it is more accurate to consider the relative contributions of each mode, such sophistication is impractical and unjustifiable given the uncertainties associated with stress-strain and stress history data (Koutsoftas and Ladd, 1985).

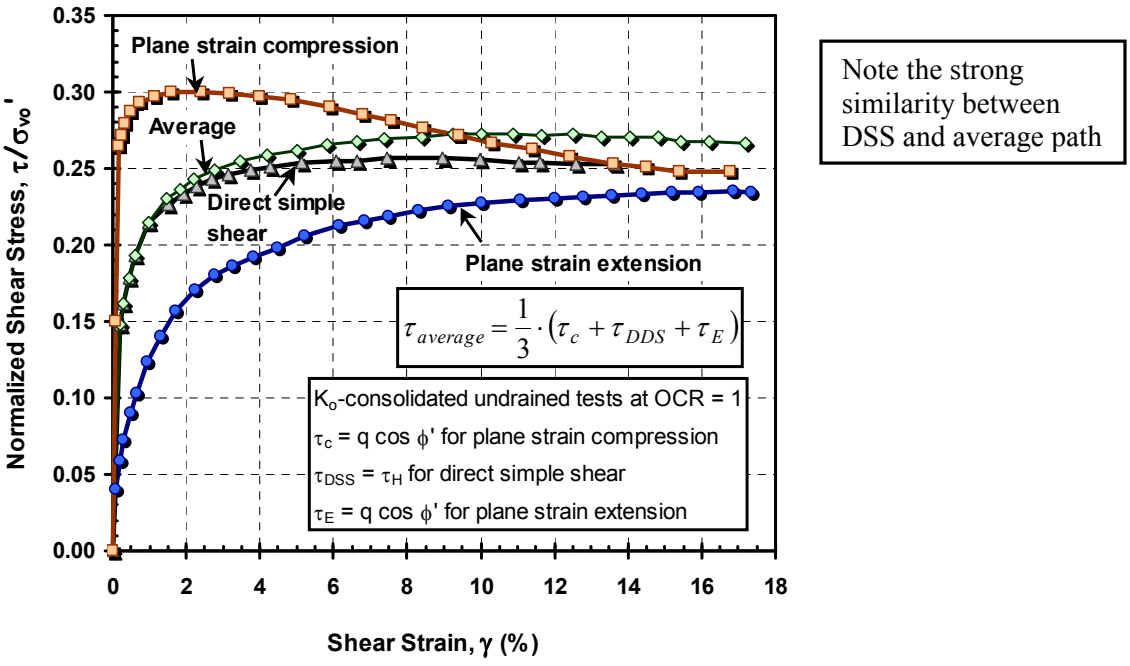


**Figure 5-13.** Normalized stress-strain data for AGS marine clay illustrating the strain compatibility technique (Koutsoftas and Ladd, 1985)

### *5.3.3 Rate of loading*

The normalized limiting strain $x_L$ depends on the values of small-strain stiffness, soil strength, and failure strain. From a practical viewpoint, the small-strain stiffness is hardly influenced by the rate of loading (Leroueil and Marques, 1996; Lo Presti et al., 1996). Figure 5-14 shows small-strain stiffness $G_{max}$ values measured by torsional shear tests performed at different rates of loading on two soils (clay and silty sand). Although the small strain stiffness slightly increases with increasing strain rates, it is acceptable to assume that the small strain stiffness is essentially independent of rate of loading from a practical standpoint (Lo Presti et al., 1996).

The influence of the rate of loading on the undrained strength of soils is well acknowledged (e.g. Hight et al., 1992; Shibuya et al., 1996; Leroueil and Marques, 1996). On the average, the undrained shear strength increases about 10% per logarithmic cycle of strain rate (Kulhawy and Mayne, 1990), as shown in Figure 5-15. The reference value of axial strain rate for measuring the undrained shear strength in laboratory tests is generally taken at 1%/hour.

Sheahan et al. (1996) investigated the influence of varying the rate of loading on the stress-strain behavior of resedimented Boston blue clay by performing a series of 25 $K_o$-consolidated undrained triaxial compression tests at different rates of loading. Samples were consolidated to different overconsolidation ratios (OCR = 1, 2, 4 and 8). For each OCR, the triaxial compression test was performed at 4 different axial strain rates (0.05 %,

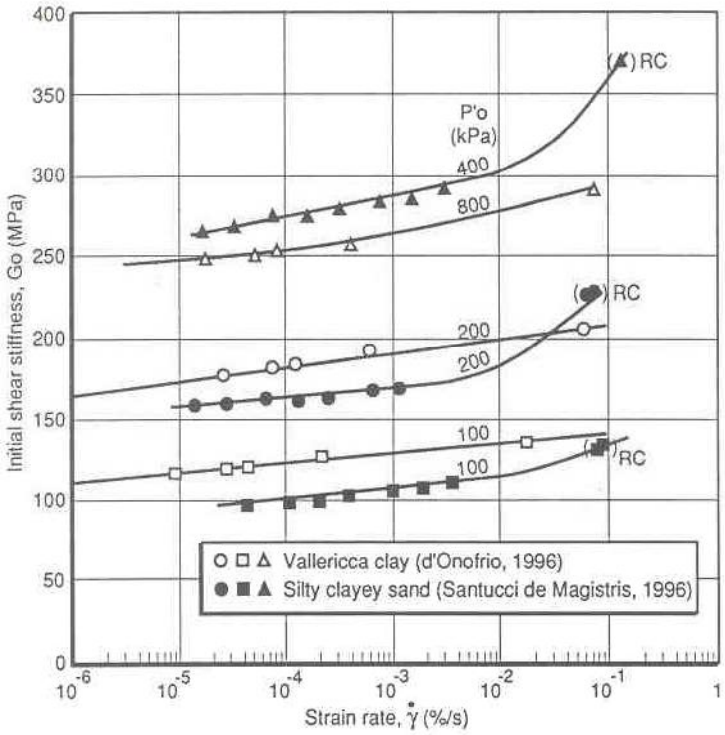


**Figure 5-14.** Effect of strain rate on the small-strain shear modulus $G_{max}$ (Leroueil and Marques, 1996)

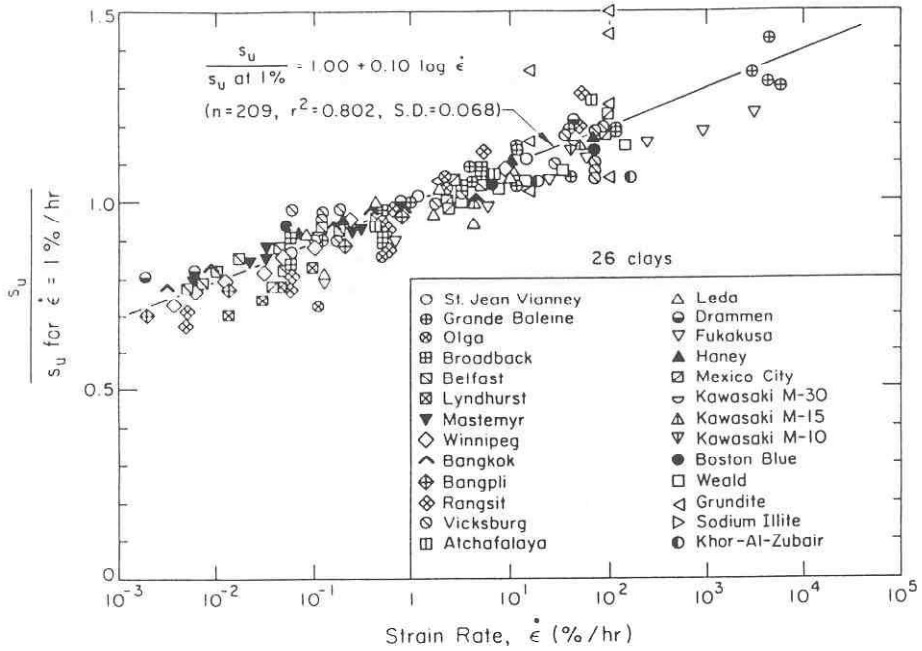


**Figure 5-15.** Effect of strain rate on undrained strength (Kulhawy and Mayne, 1990)

0.5 %, 5 %, and 50 %/h). Results from the study show that the failure strain $\varepsilon_f$ is essentially independent of the strain rate for the different overconsolidation ratios, as shown in Figure 5-16.

The normalized limiting strain $x_L$, describing stress-strain non-linearity, is defined as the ratio of failure to reference strains, where the reference strain [$\varepsilon_r = (q_{max}-q_o)/E_{max}$]. Based on the above discussion, the reference strain increases with rate of loading (due to the increase in strength, $q_{max}$), while the failure strain $\varepsilon_f$ and initial stiffness $E_{max}$ are essentially independent of the strain rate. Accordingly, $x_L$ decreases with strain rate i.e. soil stress-strain behavior becomes less non-linear for higher rates of loading. The dependency of $x_L$ on the rate of loading is demonstrated, graphically, in Figure 5-17.

Results of anisotropically consolidated triaxial compression tests performed on Bothkennar clay at different rates of loading (after Hight et al., 1992) are shown in Figure 5-18-a. The two samples were extracted using Laval samplers from a depth of approximately 5.4-m. Tests were performed using two rates of loading: 0.04%/hour and 0.2 %/hour for tests A and B, respectively. Normalized stress-strain data fitted with a logarithmic function are shown in Figure 5-18-b. Relevant soil properties are presented on the plots. The fitted normalized limiting strain $x_L$ is higher for the lower rate of loading, in agreement with the aforementioned hypothesis.

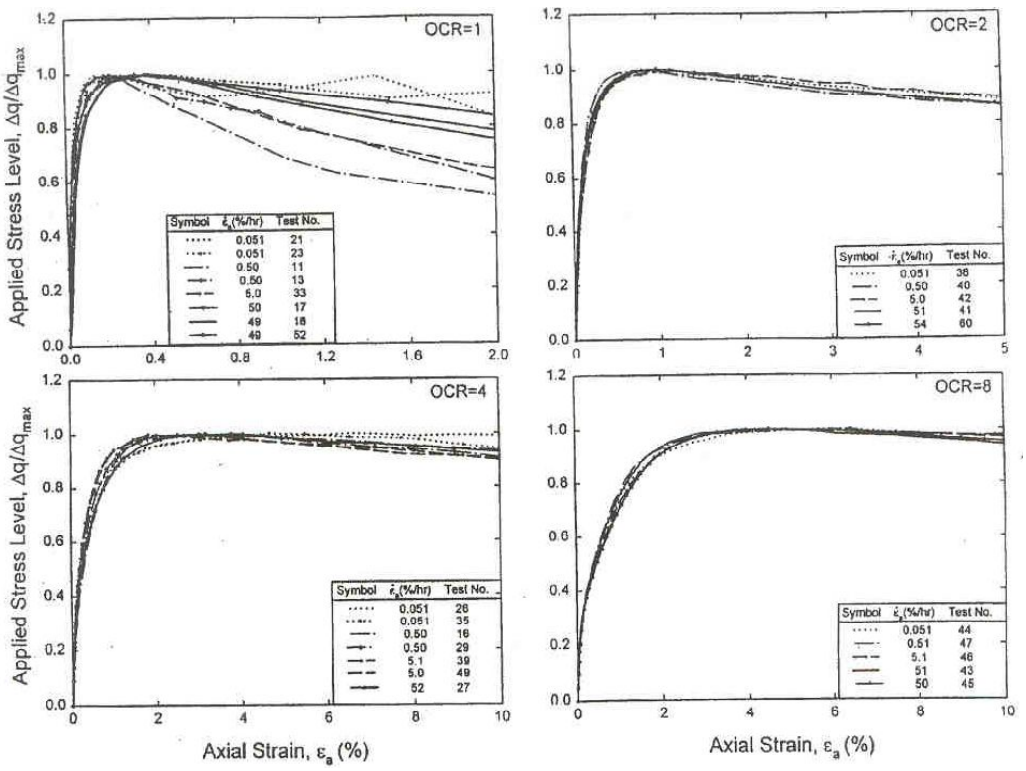


**Figure 5-16.** Applied shear stress level versus strain for $CK_oUC$ tests on resedimented Boston blue clay (Sheahan et al., 1996)

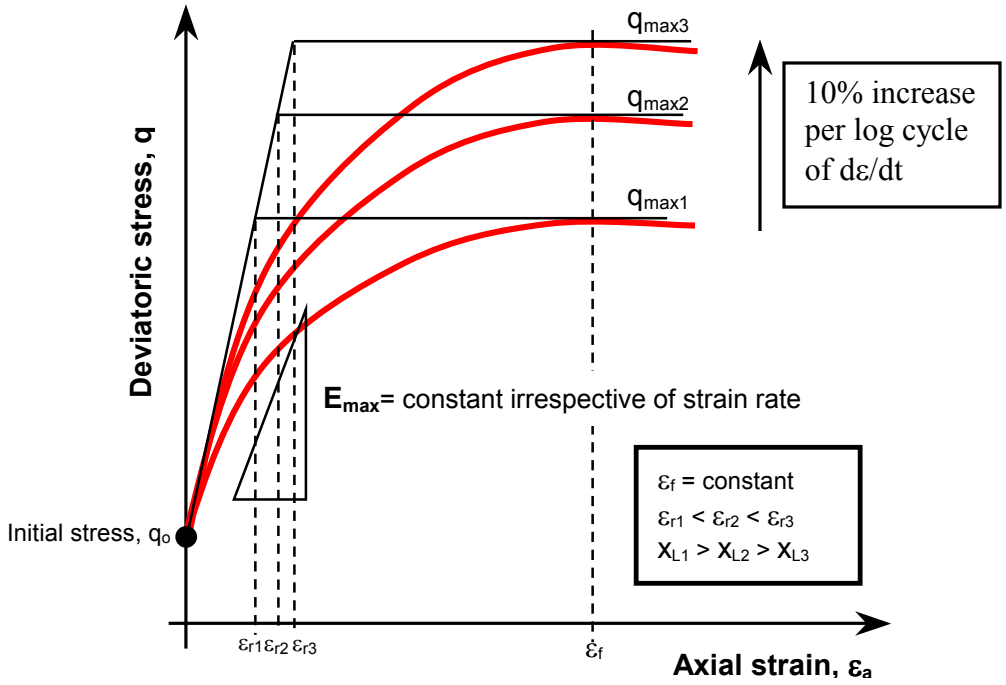


**Figure 5-17.** Schematic diagram illustrating the influence of the rate of loading on the normalized limiting strain $x_L$

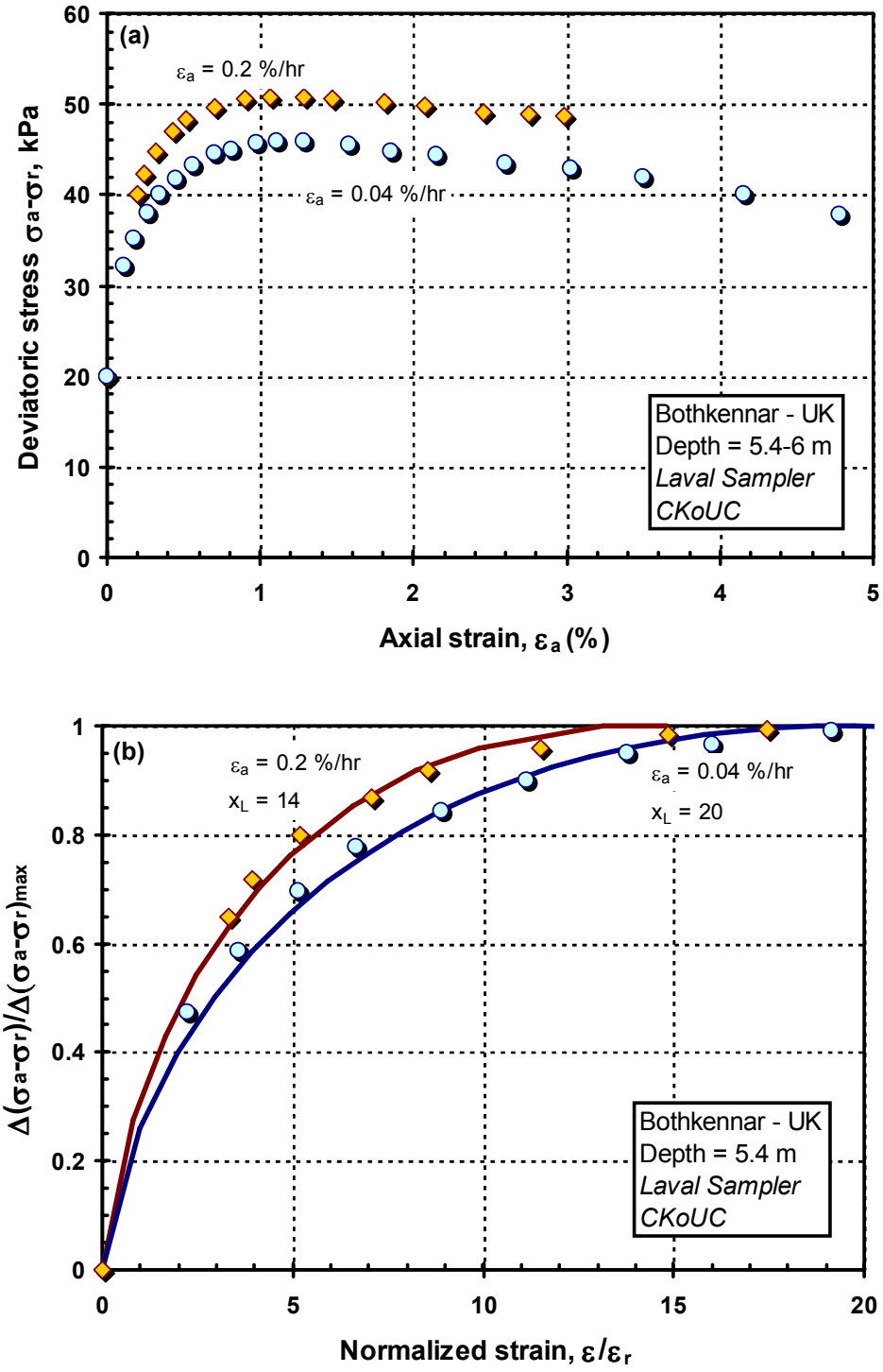


**Figure 5-18.** Influence of the rate of loading on the non-linear stress behavior of anisotropically consolidated undrained compression tests on Bothkennar clay (depth = 5.4-6 m): a) raw stress-strain data (Hight et al., 1992; 1997) b) normalized stress-strain results

## 5.4 Drained loading of cohesionless soils

Due to the cohesionless nature of sands and gravels, it is very difficult to extract "undisturbed" specimens from such soil deposits using conventional thin-walled tube sampling techniques. One method to obtain undisturbed sand or gravel samples is using in-situ ground freezing methods (Adachi, 1989; Mimura, 2003). The procedure is relatively expensive and therefore only employed in special critical projects.

Mimura (2003) performed series of in-situ and laboratory tests on undisturbed sand specimens extracted using the freezing technique. Tests were performed at three sites in Japan: Edo, Natori, and Yodo. The tests included isotropically consolidated drained triaxial compression tests on three "undisturbed" specimens from the three sites. Small-strain shear moduli for three sites are reported by Yamashita et al. (2003). Relevant properties of the three specimens are listed in Table 5-3. Measured angles of friction ranged between $41.9^{o}$ and $44.5^{o}$. Laboratory stress-strain data are fitted using the logarithmic function. The normalized limiting strains $x_L$ are computed for each sand specimen. Raw and fitted stress-strain responses from Edo site are presented in Figure 5-19-a and 5-19-b, respectively. The normalized limiting strain $x_L$ for the Edo sand frozen specimen was found to be 15. Similar plots for the stress-strain response of the frozen sand specimens from Natori and Yodo sites are presented in Figures 5-20 and 5-21, respectively. A normalized limiting strain of 20 was computed for both Natori and Yodo specimens.

**Table 5-3.** Properties of 3 frozen sand specimens tested in isotropically consolidated triaxial drained compression test

| Site Depth (m) | $e_{max}$ | $e_{min}$ | $\sigma_{vo}'$ kPa | $G_{max}$ MPa | $\phi'$ ($^{o}$) | $q_u$ [c] kPa | $\varepsilon_r$ % | $\varepsilon_f$ % | $x_L$ | Reference |
|---|---|---|---|---|---|---|---|---|---|---|
| Edo Sand 3.7 to 3.85 m | 1.227 | 0.812 | 49 | 34 | 41.9 | 186 | 0.23 | 3.4 | 15 | Mimura (2003); Yamashita et al. (2003) |
| Natori Sand 8.1 to 8.25 m | 1.167 | 0.765 | 83.3 | 78 | 44.5 | 395 | 0.21 | 4.2 | 20 | |
| Yodo 8 to 8.15 m | 1.054 | 0.665 | 98 | 62 | 42.4 | 415 | 0.28 | 5.5 | 20 | |

Notes:
$e_{max}$ = maximum void ratio
$e_{min}$ = minimum void ratio
$\sigma_{vo}'$ = effective overburden stress
$G_{max}$ = small-strain shear modulus
$\phi'$ = effective angle of friction
$q_u = (\sigma_1-\sigma_3)_f$
$\varepsilon_f$ = strain at failure
$\varepsilon_r$ = reference strain
$x_L$ = normalized limiting strain

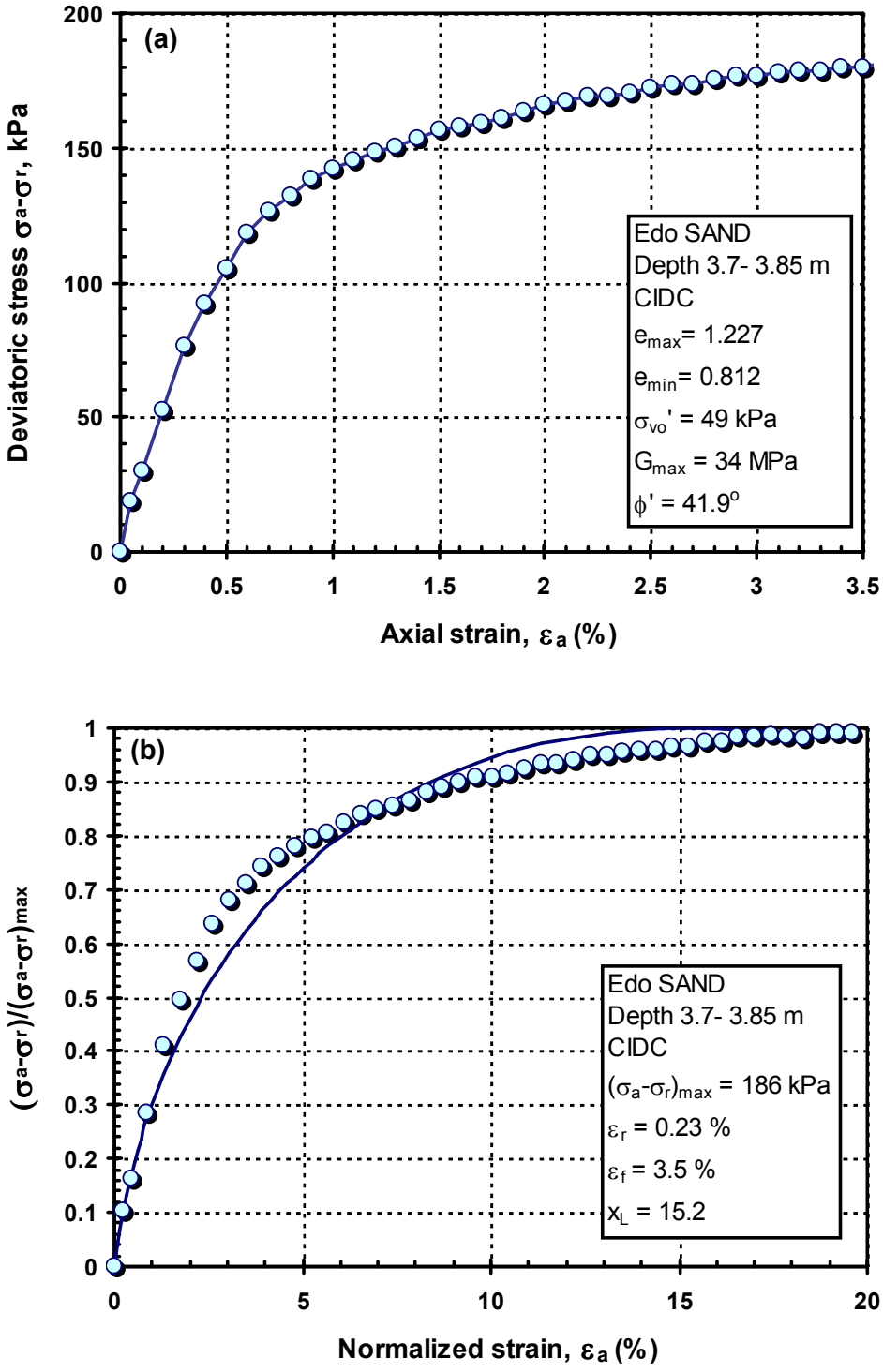


**Figure 5-19.** Normalized stress-strain data from CIDC tests on "undisturbed" frozen Edo sand specimens: a) raw stress-strain data (Mimura, 2003; Yamashita et al., 2003); b) normalized stress-strain results

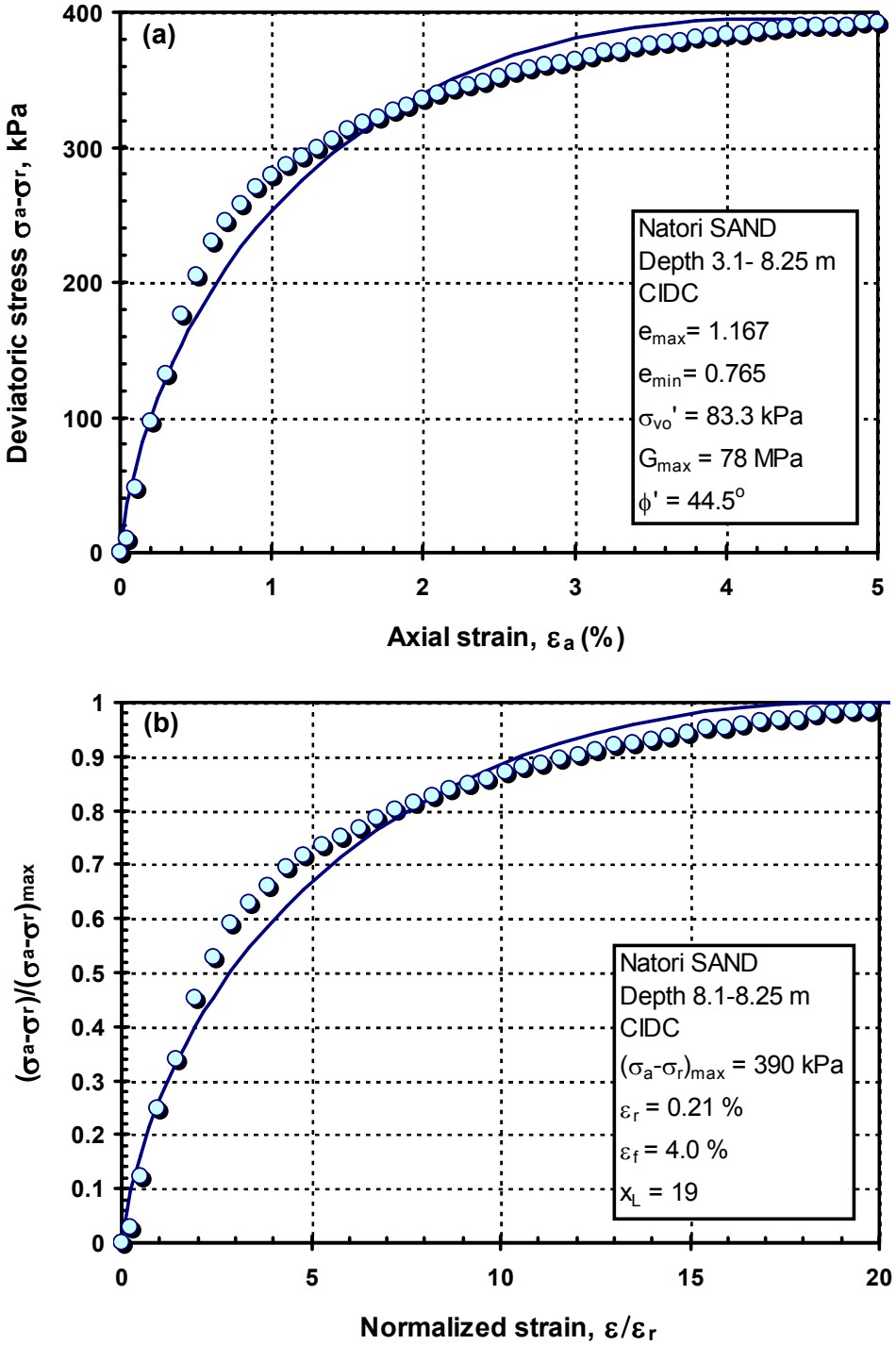


**Figure 5-20.** Normalized stress-strain data from CIDC tests on "undisturbed" frozen Natori sand specimens: a) raw stress-strain data (Mimura, 2003; Yamashita et al., 2003); b) normalized stress-strain results

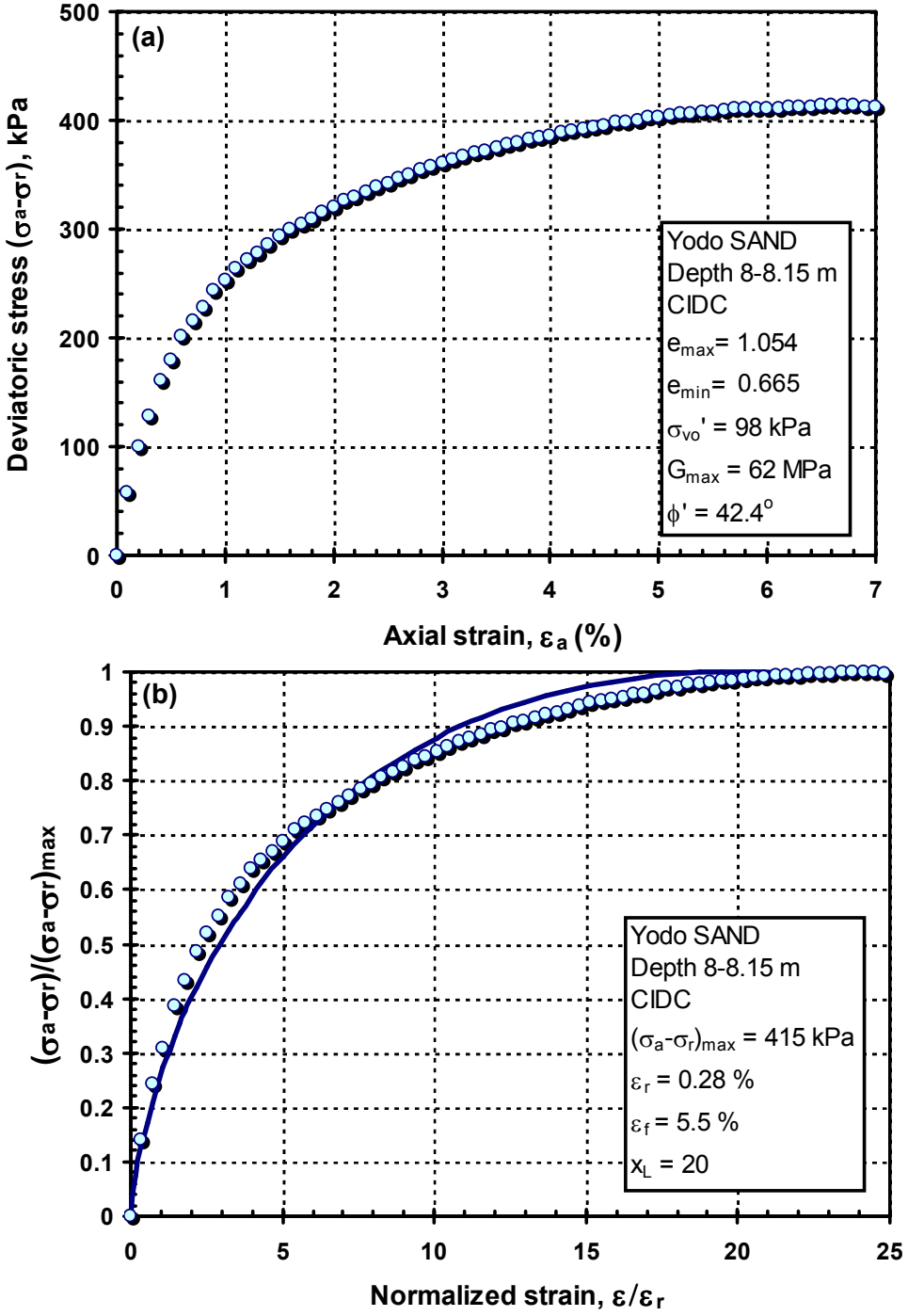


**Figure 5-21.** Normalized stress-strain data from CIDC tests on "undisturbed" frozen Yodo sand specimens: a) raw stress-strain data (Mimura, 2003; Yamashita et al., 2003); b) normalized stress-strain results

## 5.5 Non-linear stress-strain behavior and index soil properties

Due to the difficulty and high cost of obtaining "undisturbed" soils specimens, it would be highly beneficial to correlate soil non-linear stress-strain properties to index soil properties that can be easily determined from in-situ and/or laboratory tests. This section is dedicated to explore such relationships.

### *5.5.1 Clays and silts*

A logical way to obtain the normalized limiting strain $x_L$ ($x_L = \varepsilon_f / \varepsilon_r$) is by estimating the strain at failure $\varepsilon_f$ and normalizing it by the reference strain $\varepsilon_r$. The reference strain is defined as the ratio of the maximum deviatoric stress $q_{max}$ to the maximum Young's modulus $E_{max}$ for triaxial tests. For shear testing, the reference strain is defined as the ratio of shear strength $\tau_{max}$ to the maximum shear modulus $G_{max}$. Small strain soil stiffness can be easily measured from in-situ/laboratory tests as discussed in Chapter 4. Similarly, soil strength can either be measured in the laboratory (e.g. triaxial compression, direct simple shear, triaxial extension) or evaluated from in-situ tests (e.g. cone penetration test CPT, dilatometer DMT, standard penetration test SPT). Accordingly, the reference strain $\varepsilon_r$ can be computed in a straightforward manner.

The strain at failure is typically determined from peak values measured in laboratory tests. Attempts have been made to correlate failure strain to index soil properties (e.g. Koutsoftas, 1981; Koutsoftas and Ladd, 1985; DeGroot et al., 1992; Atkinson, 2000). For example, Koutsoftas (1981) performed a series of undrained shear tests, including triaxial compression, triaxial extension, and direct simple shear under $K_o$-consolidated

specimens of a marine clay. He investigated the influence of shear test type on the soil strength and failure strain. Based on Massachusetts Institute of Technology experience for over three decades, complimented with data from the Norwegian Geotechnical Institute files, DeGroot et al. (1992) created a database of failure strain from direct simple shear tests on 27 normally consolidated soil specimens and found the failure strains to increase with plasticity index as shown in Figure 5-22. To enhance the trend, the database was expanded to 66 data points from more recent studies, presented in Figure 5-23, with references given in Appendix B.

The DSS data on silty Holocene clay showed that strains to failure $\gamma_f$ are essentially independent of the overconsolidation ratio (Koutsoftas and Ladd, 1985). This is shown in Figure 5-24 which shows the failure strain in compression to increase with OCR, whereas the overconsolidation ratio has minimal effect on the strain at failure under direct simple shear conditions. Similarly, direct simple shear data at different overconsolidation ratios show essentially constant shear strains at failure $\gamma_f$ for Amherst varved clay (Bonus, 1995), AGS clay (Koutsoftas, 1981), and James Bay clay (Jamiolkowski et al., 1985). It should be noted that shear strains for triaxial tests were computed as 1.5 times axial strains for comparison with direct simple shear data. Accordingly, the normalized limiting strain can be computed from the small strain stiffness $G_{max}$ (refer to Chapter 4); undrained shear strength $s_u$ (appendix E); and strain to failure (Figure 5-23), by the expression: $x_L = \frac{\gamma_f}{\gamma_r} = \frac{\gamma_f}{(G_{max} / s_u)}$.

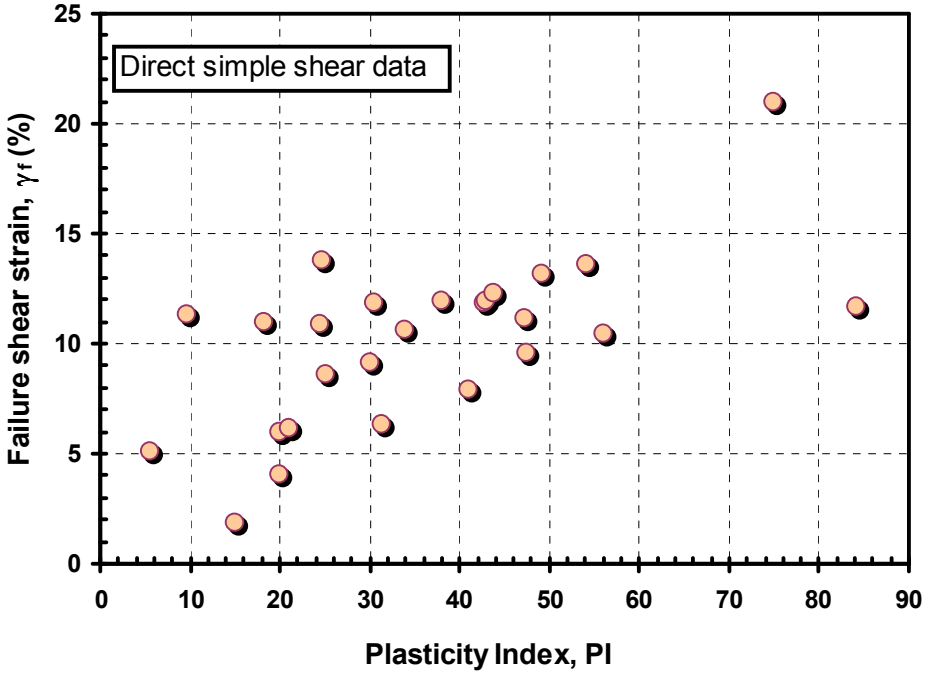


**Figure 5-22.** Relationship between the failure shear strain ($\gamma_f$) and plasticity index (PI) for normally consolidated clays and silts tested in DSS (after DeGroot et al., 1992).

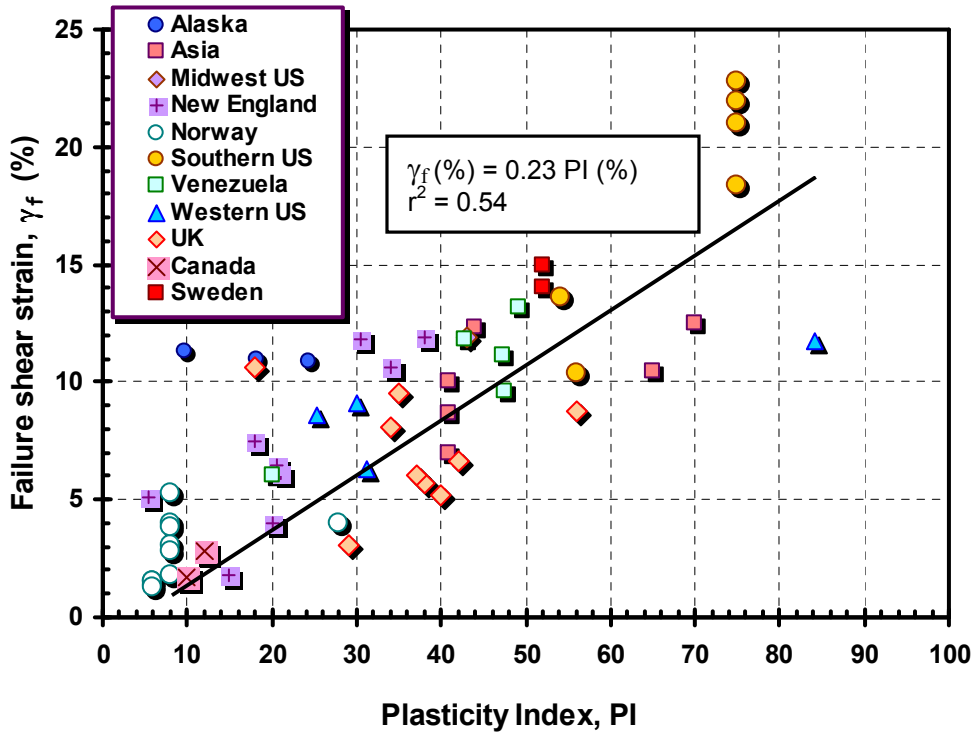


**Figure 5-23.** Expanded relationship between the failure shear strain ($\gamma_f$) and plasticity index (PI) for normally consolidated clays and silts tested in direct simple shear.

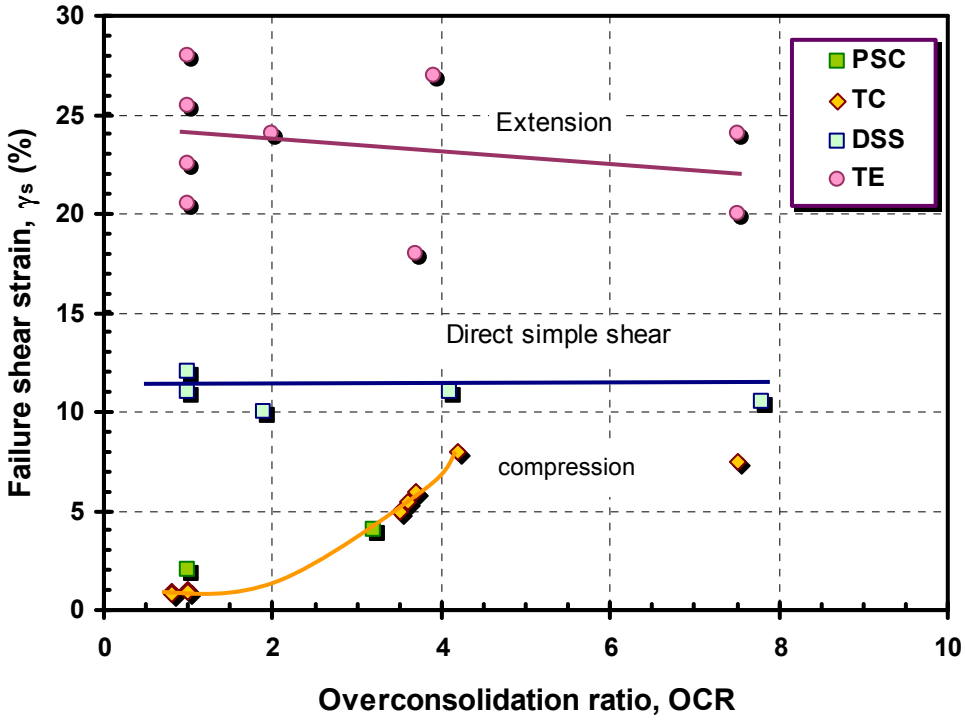


**Figure 5-24.** Effect of overconsolidation ratio on the failure shear strain for Holocene clay under different modes of loading (after Koutsoftas and Ladd, 1985)

### *5.5.2 Sands*

Similar to evaluating the degree of stress-strain non-linearity, the normalized limiting strain $x_L$ can be evaluated knowing the small-strain stiffness $G_{max}$, shear strength $\tau_{max}$, and strain to failure $\gamma_f$. The small-strain stiffness $G_{max}$ can be obtained from basic soil properties using Hardin (1978) correlation. While the shear strength $\tau_{max}$ can be computed as $\sigma_{vo}'\tan(\phi')$, where $\sigma_{vo}'$ and $\phi'$ are the effective overburden stress and angle of internal friction.

In this section, parameters influencing failure strains are reviewed. Marachi et al. (1981) investigated the influence of confining stresses and sand initial void ratio on failure strains of Monterey sand No. 20 (uniformly graded predominantly rounded to subrounded quartz) tested under triaxial and plain strain compression. It was shown that failure strains decrease with sand initial void ratio i.e. denser sands exhibit smaller failure strains. On the other hand, higher failure strains were measured for tests performed under higher confining stresses. This is shown in Figure 5-25. Similar results were found for the influence of relative density on failure strains in studies by Al-Hussaini (1973) and Holubec & D'Appolonia (1973). Figure 5-26 shows the variation of failure strains with relative density for different sands and beads.

In addition, relative density was found to influence the degree of non-linearity in the stress-strain behavior of sand (e.g. Lee, 1999; Lee and Salgado, 2000; Lee et al., 2004). For clean Ottawa sand, Lee (1999) found the soil modulus to reduce at a faster rate for loose sands compared to dense sands in drained triaxial compression, as shown in Figure 5-27. The data are fitted using the logarithmic function with the normalized limiting strain $x_L$ = 12 and 35 for relative densities $D_R$ of 63% and 27%, respectively. Lee et al. (2004) quantify the influence of relative density and silt content on the degree of stress-strain non-linearity of sands.

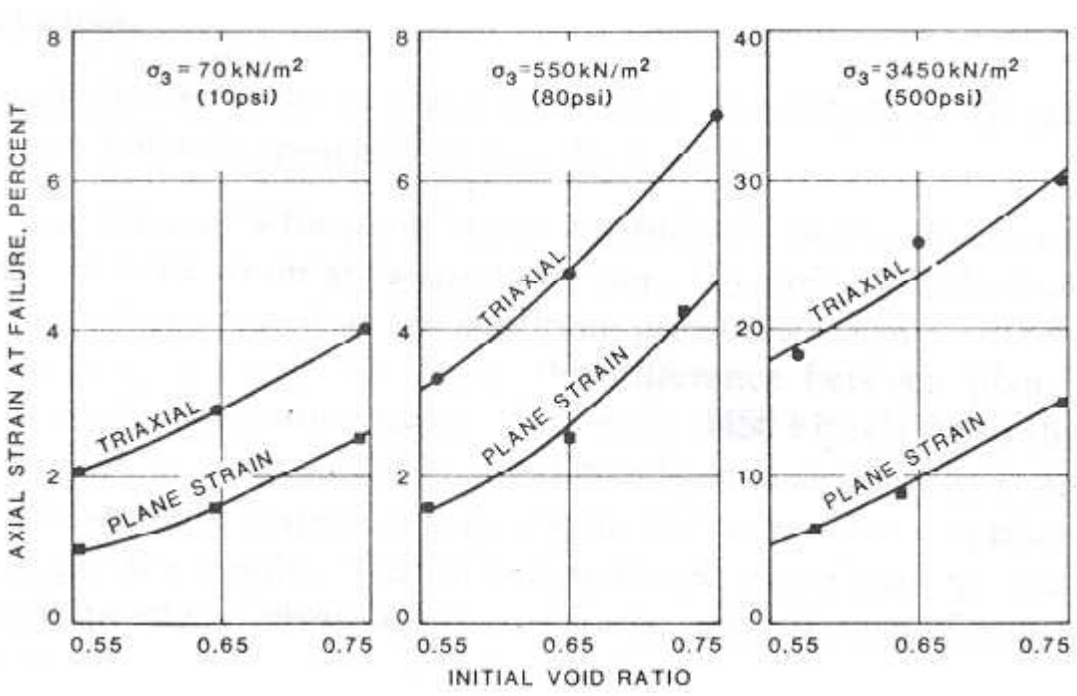


**Figure 5-25.** Axial failure strains for plane strain and triaxial compression tests on Monterey sand No. 20 (Marachi et al., 1981).

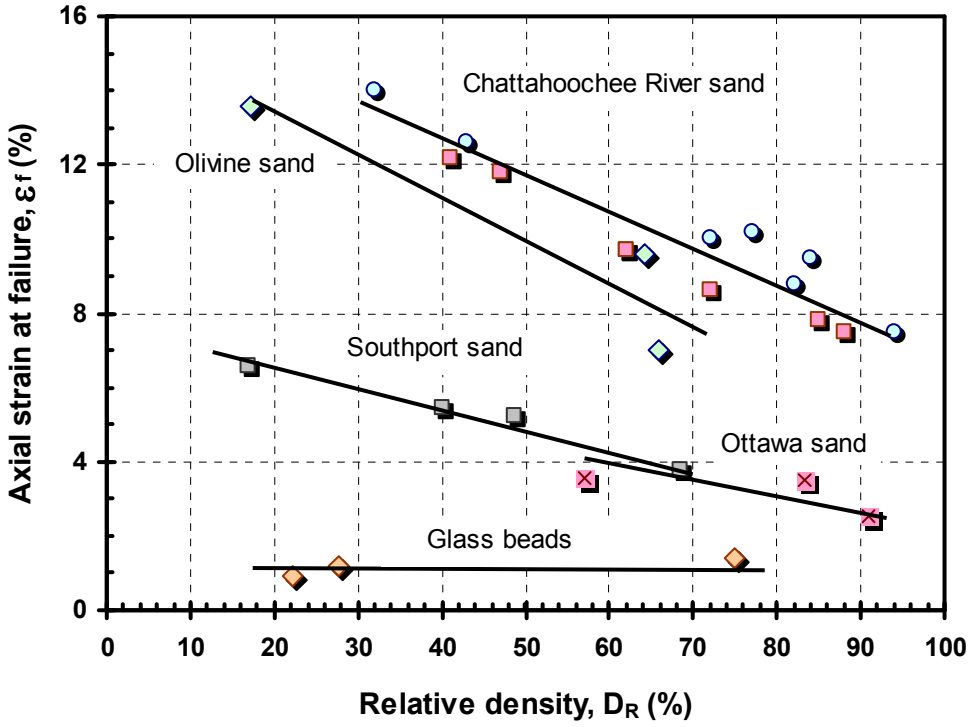


**Figure 5-26.** Variation of axial failure strains with relative density for different sands and beads (data from Al-Hussaini, 1973 and Holubec & D'Appolonia, 1973).

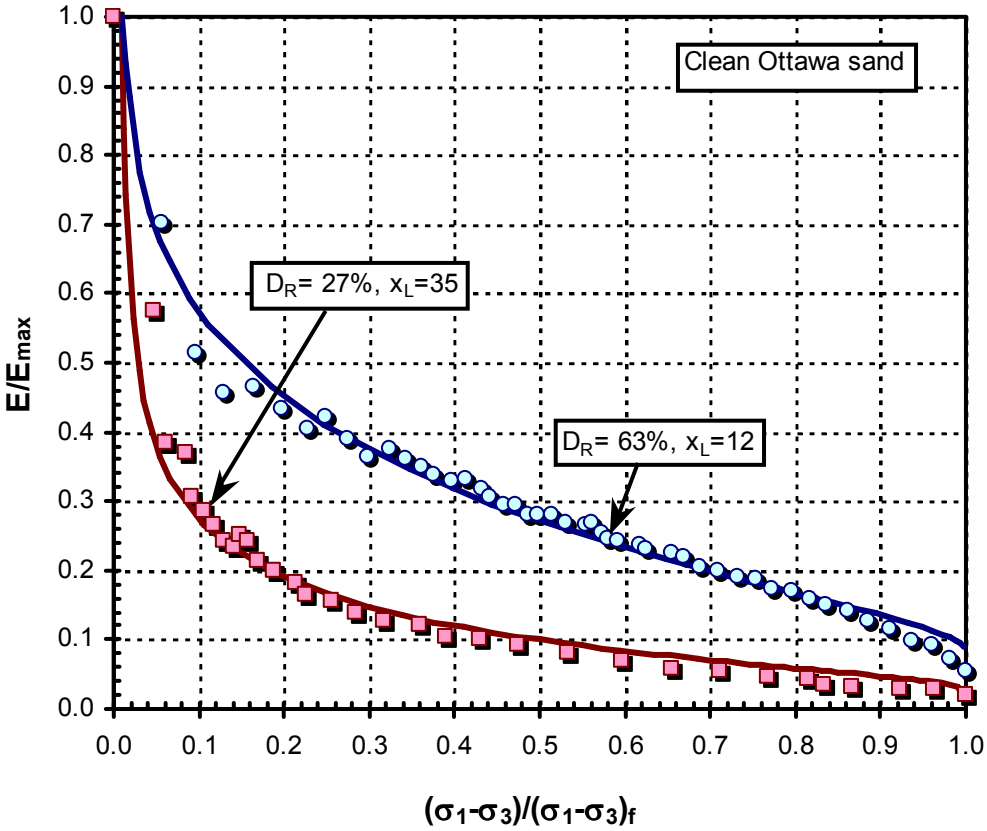


**Figure 5-27.** Effect of the relative density of sand on the rate of modulus reduction of clean sands in triaxial compression (laboratory data after Lee et al., 2004)

## 5.6 Summary and conclusions

The logarithmic function (Puzrin and Burland, 1996; 1998) provides a logical and convenient means to represent the stress-strain response of geomaterials. The function requires 2 input parameters: threshold strain $\gamma_{th}$ and normalized limiting strain $x_L$. The threshold strain $\gamma_{th}$ was shown to vary between 0.0005% and 0.005% based on a database of monotonic torsional shear test data. Several factors that affect the value of the normalized limiting strain $x_L$ are investigated. These factors include: sample disturbance, mode of loading, and loading rate. A database of the undrained stress-strain response of

clays extracted using different samplers and loaded under different modes of loading was created. Analysis of the stress-strain data shows that the degree of non-linearity increases with sample disturbance. The degree of non-linearity is also dependent on the mode of loading (compression, direct simple shear, extension), with triaxial compression as the stiffest. It was also shown that stress-strain non-linearity increases with slower rates of loading.

Based on Massachusetts Institute of Technology experience for over three decades DeGroot et al. (1992), the failure shear strain $\gamma_f$ in undrained direct simple shear is correlated to plasticity index for fine-grained soils. Failure strains in the drained loading of sands were shown to vary with initial void ratio, relative density, and confining stress. Knowledge of the maximum shear modulus $G_{max}$ and shear strength $\tau_{max}$ enables the computation of the normalized limiting strain $x_L$ according to $x_L = \frac{\gamma_f}{\gamma_r} = \frac{\gamma_f}{\left(G_{\max} / s_u\right)}$.

# CHAPTER VI

# LOGARITHMIC NON-LINEAR ELASTIC PLASTIC MODEL

## 6.1 Introduction

Constitutive models vary in the degree of complexity and their ability to accurately represent material behavior. Models that require a larger number of parameters usually better represent the behavior, however, obtaining input parameters can be quite expensive and difficult – if not impossible– for application on real projects. Linear elasticity is the simplest available constitutive model with the minimum number of parameters, making it the most widely used method for computing foundation displacements (see Figure 6-1). Despite its broad applicability, soil behavior under loading is neither linear nor elastic. Therefore, linear elastic-plastic models were developed and formulated (e.g. Drucker-Prager, Mohr-Coulomb). Such models are good for representing soil failure by plasticity; however, soil deformations remain linear up to failure, which is unrealistic.

Non-linear elastic-plastic and pseudo-plastic models have been developed to better represent actual stress-strain behavior (e.g. Jardine et al., 1986; Fahey and Carter, 1993; Viana da Fonseca and Sousa, 2002; Lee and Salgado, 2002). However, available non-linear models either involve a large number of parameters, e.g. MIT E-3 with 15 parameters (Whittle, 1993) or lack in physical meaning, e.g. the 33 parameters associated with the endochronic theory (Bazant, 1978).

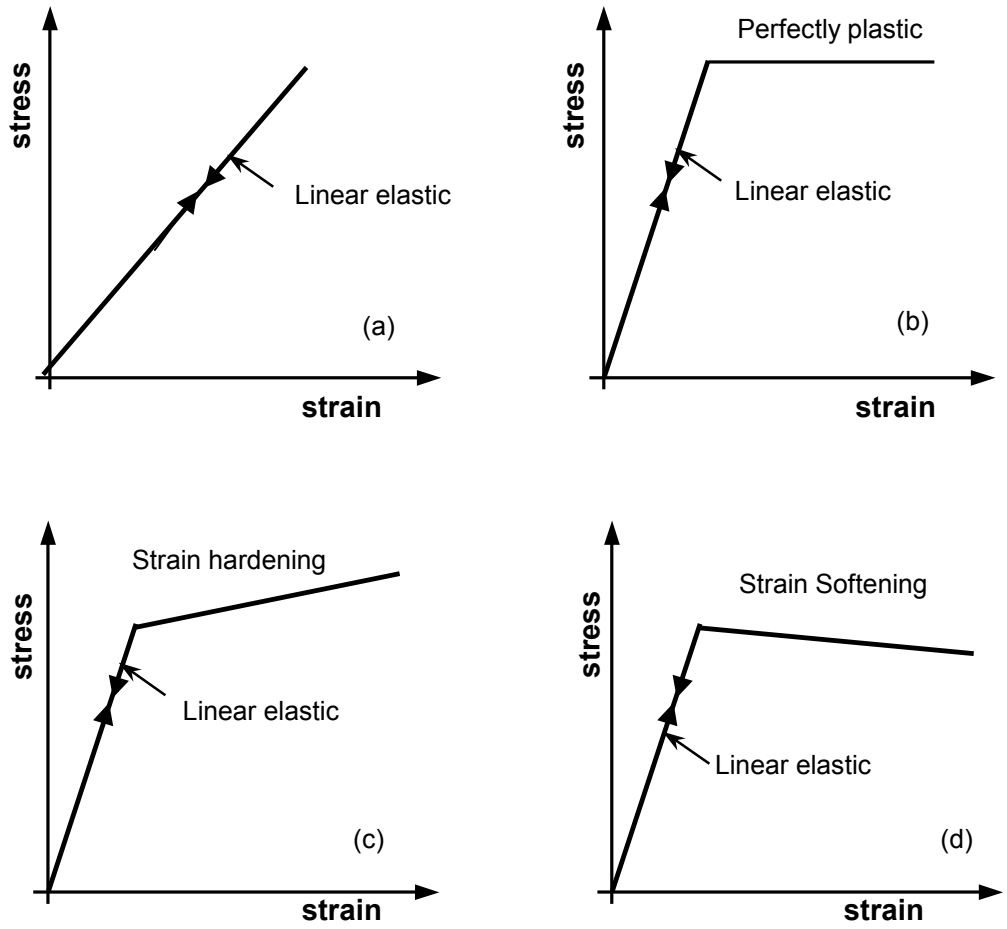


**Figure 6-1.** (a) Linear elastic model; (b) linear elastic perfectly plastic model; (c) linear elastic strain hardening model; (d) linear elastic strain softening model

A balance between a reasonable number of soil constants and the realistic determination of input parameter values by laboratory and/or field methods is desired by the geotechnical profession (Barbour and Krahn, 2004). The logarithmic modulus degradation model proposed by Puzrin and Burland (1996; 1998) and presented in Chapter 5, overcomes both problems.

In this chapter, the logarithmic expression is incorporated into a non-linear elastic model in three-dimensional stress space. The shear modulus is maintained constant at $G = G_{max}$ below a specified threshold strain $\gamma_{th}$. As the elements deform beyond the threshold strain yet below the yield surface, the shear modulus decreases with an increase in stress level. The logarithmic non-linear elastic model is verified by comparing the stress-strain behavior of boundary value problems to the behavior of a linear elastic-plastic Drucker-Prager model. An excellent agreement was found between the stress-strain behavior for simulations of the triaxial compression test. However, disagreement was found when modeling the load-displacement behavior of shallow circular footings, as will be discussed subsequently in the chapter. Therefore, a more complex logarithmic non-linear elastic-plastic model LOGNEP was implemented. When stresses reach the yield surface, the stress-strain behavior is no longer defined by elasticity. A flow rule defines the plastic stress-strain relationship by means of a plastic potential function. The flow is known as associated if the plastic potential function is equal to the failure criterion. If the plastic potential function is different from the failure, flow is known as non-associated. Both the associated and non-associated potentials are incorporated in the LOGNEP model. After failure, soil can soften or harden or act as perfectly plastic. The suggested model is developed to be perfectly plastic and calibrated versus the Drucker-Prager model for the case of $x_L$ of 1, which is equivalent to linear elasticity.

## 6.2 Logarithmic non-linear elastic stress-strain model for numerical analysis

A constitutive law describes the stress-strain relationship a body undergoes when loaded. For elastic materials, the state of stress is only a function of the state of strains. When an

elastic body is loaded then unloaded to its initial state of stress, it does not maintain any permanent deformations (Desai and Siriwardane, 1984). Elastic behavior can be either linear or nonlinear as shown in Figure 6-2. Hooke's law is the simplest representation of linear elastic behavior between stress $\sigma_{ij}$ and strain $\varepsilon_{ij}$.

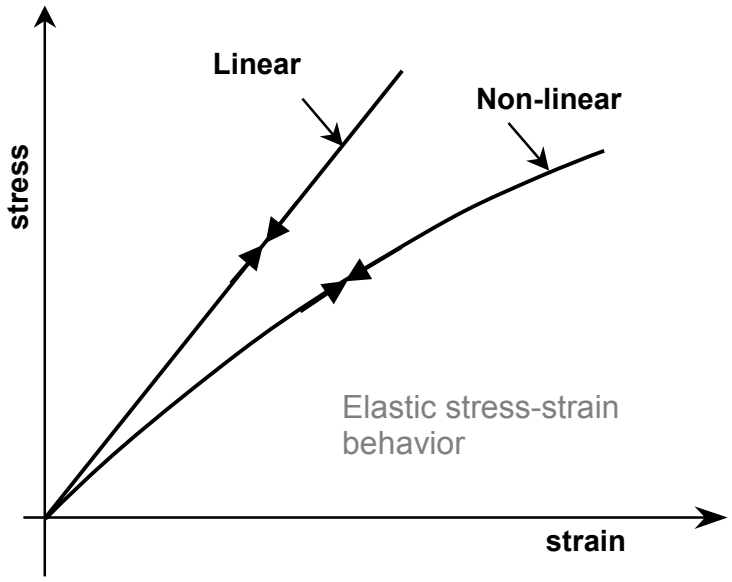


**Figure 6-2.** Linear and non-linear elastic stress-strain relationship

Reducing the shear modulus with the increase in strain/stress level simulates non-linearity in an equivalent elastic domain. As discussed in Chapter 4, soil stiffness can be expressed in terms of the shear modulus (G), Young's modulus (E), bulk modulus (K), and Poisson's ratio (ν). It is more convenient to use the shear modulus (G) and bulk modulus (K) for numerical modeling purposes (Itasca Consulting Group Inc.-a, 2001). The shear stiffness (G) can be expressed either by tangent value ($G_t$) or secant ($G_{sec}$)

moduli. For numerical modeling, it is more convenient to use the tangent modulus because the analysis is performed incrementally, whereas in closed-form analytical elastic solutions, a secant modulus is more appropriate.

The secant and tangent shear moduli both reduce with an increase in the octahedral strain invariant $\gamma_{oct}$ using the logarithmic function according to Equations 6-1-a and 6-1-b, respectively:

$$\frac{G_{\text{sec}}}{G_{\max}} = 1 - \alpha \cdot \frac{x - x_{th}}{x} \cdot \left[\ln\left(1 + x - x_{th}\right)\right]^{R} \quad \text{.....(6-1-a)}$$

$$\frac{G_t}{G_{\max}} = 1 - \alpha R \cdot \frac{x - x_{th}}{1 + x - x_{th}} \cdot \left[\ln\left(1 + x - x_{th}\right)\right]^{R-1} - \alpha \cdot \left[\ln\left(1 + x - x_{th}\right)\right]^{R-1} \quad \text{.....(6-1-b)}$$

where:

$G_{sec}$, $G_t$, $G_{max}$= secant, tangent, and initial shear moduli respectively.

$x = \frac{\gamma_{oct}}{\gamma_r}$ = normalized octahedral strain

$\gamma_{oct} = \sqrt{\frac{1}{6}\left[\left(\varepsilon_{11} - \varepsilon_{22}\right)^2 + \left(\varepsilon_{22} - \varepsilon_{33}\right)^2 + \left(\varepsilon_{11} - \varepsilon_{33}\right)^2\right] + \varepsilon_{12}^2}$ (refer to Figure 6-3)

$\gamma_r$ = reference shear strain = $\frac{\tau_{\max} - \tau_o}{G_{\max}}$

$\tau_{max}$ = shear strength

$\tau_o$ = initial shear stress

$$R = \left( \frac{1 - x_{th}}{x_L - x_{th}} \right) \cdot \frac{(1 + x_L - x_{th}) \ln(1 + x_L - x_{th})}{x_L - 1}$$

$$\alpha = \frac{x_L - 1}{(x_L - x_{th}) \cdot [\ln(1 + x_L - x_{th})]^R}$$

$x_L$ = normalized limiting strain = $\frac{\gamma_f}{\gamma_r}$

$\gamma_f$ = shear strain at failure.

$x_{th} = \frac{\gamma_{th}}{\gamma_r}$ = normalized threshold shear strain

$\gamma_{th}$ = elastic threshold strain

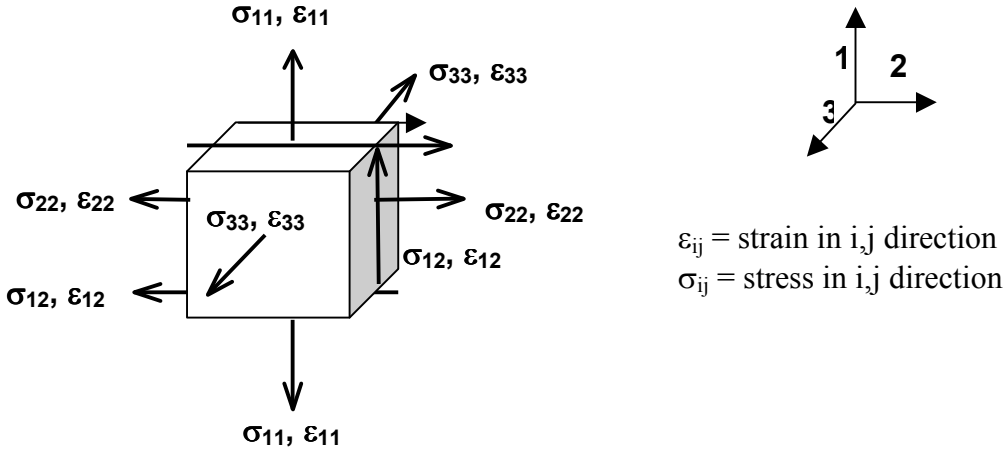


**Figure 6-3.** Stress and strain components in a soil element

### ***6.2.1 Variation of bulk modulus and Poisson's ratio with strain level***

The shear (G) and bulk (K) moduli are interrelated through Poisson's ratio ν. Accordingly, as the shear modulus (G) reduces in a non-linear manner, either the bulk

modulus or Poisson's ratio will vary with the strain/stress level. Therefore, when implementing a non-linear elastic model, either the bulk modulus or Poisson's ratio needs to adjust with the variation in shear modulus (Fahey and Carter, 1993). If Poisson's ratio $\nu$ = constant, then the bulk modulus $K_t$ varies according to equation 6-2-a:

$$K_t = \frac{2G_t(1+\nu)}{3(1-2\nu)} \quad \text{.....(6-2-a)}$$

Alternatively, if $K_t$ = constant, then Poisson's ratio $\nu$ varies according to equation 6-2-b:

$$\nu = \frac{3K_t - 2G_t}{2 \cdot (G_t + 3K_t)} \quad \text{.....(6-2-b)}$$

Later, both approaches will be investigated to show that either approach can be used effectively, as they give similar results.

### ***6.2.2 Poisson's ratio and drainage type***

For undrained loading of an isotropic elastic material, it is well established that Poisson's ratio $\nu_u = 0.5$, corresponding to no volume change ($\Delta V = 0$). This is fine in closed-form analytics that do not account for bulk modulus, yet equivalent to an infinite bulk modulus in numerical simulations, causing instabilities. Therefore, an initial value of Poisson's ratio of 0.495 is applied and $\nu$ is allowed to vary according to Equation 6-2-b, keeping

the bulk modulus constant. Near failure states, as the shear modulus approaches zero, Poisson's ratio approaches 0.5 as the bulk modulus approaches infinity.

Conventionally, strain measurements during laboratory triaxial tests have been obtained externally to the specimen. External measurements reflect problems associated with stress non-uniformity, seating errors, end effects, and capping problems. Poisson's ratios ($\nu = -\varepsilon_v/\varepsilon_h$) computed from these flawed measurements indicated that $\nu$ varies between 0.25 to 0.45. With the introduction of internal measurement devices, more accurate strain measurements became available (Tatsuoka and Shibuya, 1992; Lo Presti, 1994; Jamiolkowski et al., 1994). Lehane and Cosgrove (2000) created a database of Poisson's ratio with the axial strain level computed from triaxial compression tests with internal strain measurements, shown in Figure 6-4. The database shows Poisson's ratio for the small strain elastic range to vary between 0.12 and 0.30 with an average value of 0.20. The increase in Poisson's ratio with strain indicates the onset of plastic deformations according to Lehane and Cosgrove (2000). Therefore, it was decided to adopt an initial Poisson's ratio of 0.20 for all the drained analyses. The influence of varying either Poisson's ratio $\nu$ or bulk modulus K with the increase in stress/strain levels is investigated later in the chapter.

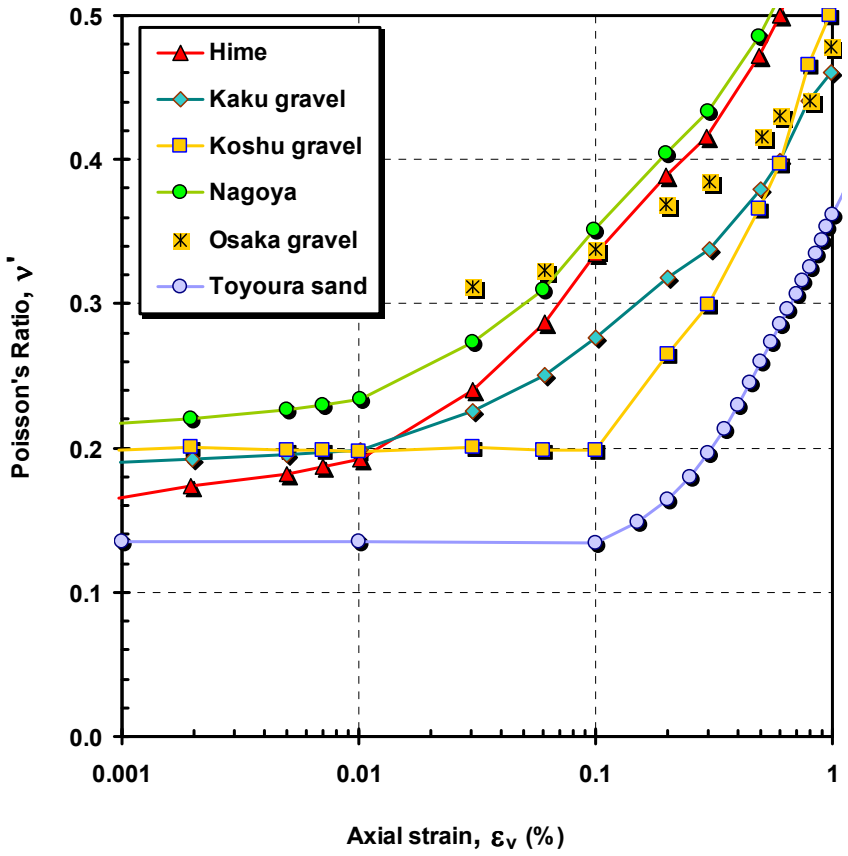


**Figure 6-4.** Poisson's ratio ν' in drained compression tests plotted versus axial strain $\varepsilon_v$ (Lehane and Cosgrove, 2000)

## 6.3 Verification of the logarithmic non-linear elastic model

In order to validate the logarithmic non-linear elastic model, it was incorporated into a numerical analysis software package. FLAC (Fast Lagrangian Analysis of Continua) is a two-dimensional finite difference program for modeling the behavior of structures resting on soils, rocks, or other materials that undergo plastic flow (Itasca Consulting Group Inc., 2001). It has 10 well-known built-in constitutive models, including linear elastic, Drucker-Prager, Mohr-Coulomb, and Modified Cam-Clay. However, there are no built-in constitutive models that account for non-linear stress-strain-strength response of soils that begin at the fundamental initial tangent shear modulus $G_{max}$. FLAC enables users to

encode their own models using FISH, a programming language embedded in FLAC. The logarithmic non-linear elastic model was incorporated into FLAC as a user-defined constitutive model using a special subroutine written by the author in FISH language. The model is initially validated by comparison with the built-in Drucker-Prager model for a normalized limiting strain $x_L = 1$ which is equivalent to the linear elastic-plastic model. The influence of varying the normalized limiting strain $x_L$ on the stress-displacement behavior under shallow footings is investigated. FLAC version 4.0 is used in all subsequent analyses.

### *6.3.1 Simulated triaxial compression test*

As an initial check, the behavior of a cylindrical soil specimen tested in triaxial compression was simulated. The specimen was consolidated under both isotropic and anisotropic stress state conditions.

Due to symmetry, only half the problem is modeled. Horizontal displacements were restricted at the axis of symmetry. No restrictions were imposed on the other vertical boundary. Vertical displacements were constrained on the top and bottom boundaries to model the rigid plates compressing the specimen. Vertical stresses were applied to the top and bottom of the specimen, while horizontal stresses were imposed on the vertical boundary other than the symmetry line. Applying a constant displacement incrementally on the top and bottom boundaries replicated vertical loading. Specimen size was chosen so that the height to diameter h/d ratio was 2. Figure 6-5 shows a schematic diagram of

the mesh used for the analysis with the appropriate boundary conditions. The simulation running time depends on the grid size and displacement increment. It is desirable to minimize the running time without compromising the accuracy of the solution. Therefore, a number of simulations were performed using different mesh sizes to eliminate the effects of mesh-size dependence. A 20 x 80 grid was the smallest grid size to overcome mesh dependency. Similarly, several analyses were performed using different loading increments to determine the maximum loading rate that can be used without compromising accuracy. By trial and error, the maximum applied displacement increment was found to be $2 \times 10^{-8}$ m/step. Figure 6-6 shows the FLAC grid used in the simulations of the triaxial compression test.

Numerical instabilities in the simulations of the triaxial compression tests took place as the shear modulus approached zero. It was therefore decided to set a minimum value for the tangent shear modulus of 1 kPa, which was found to provide numerical stability and therefore used henceforth.

The logarithmic non-linear elastic model was used to reproduce undrained loading in triaxial compression ($\nu_u = 0.495$). For a preliminary check, the simulated stress-strain behavior is compared to results obtained using FLAC with its built in Drucker-Prager linear elastic-plastic model. Listed in Table 6-1 are the soil properties used for the simulation as case 1, where the normalized limiting strain $x_L$ equals 1 for equivalent linear elastic behavior. For $x_L = 1$, the value of the fitting parameter R approaches

infinity because of singularity. As this value causes instability to the solution, a close value, $x_L = 1.01$, was used for the linear elastic case.

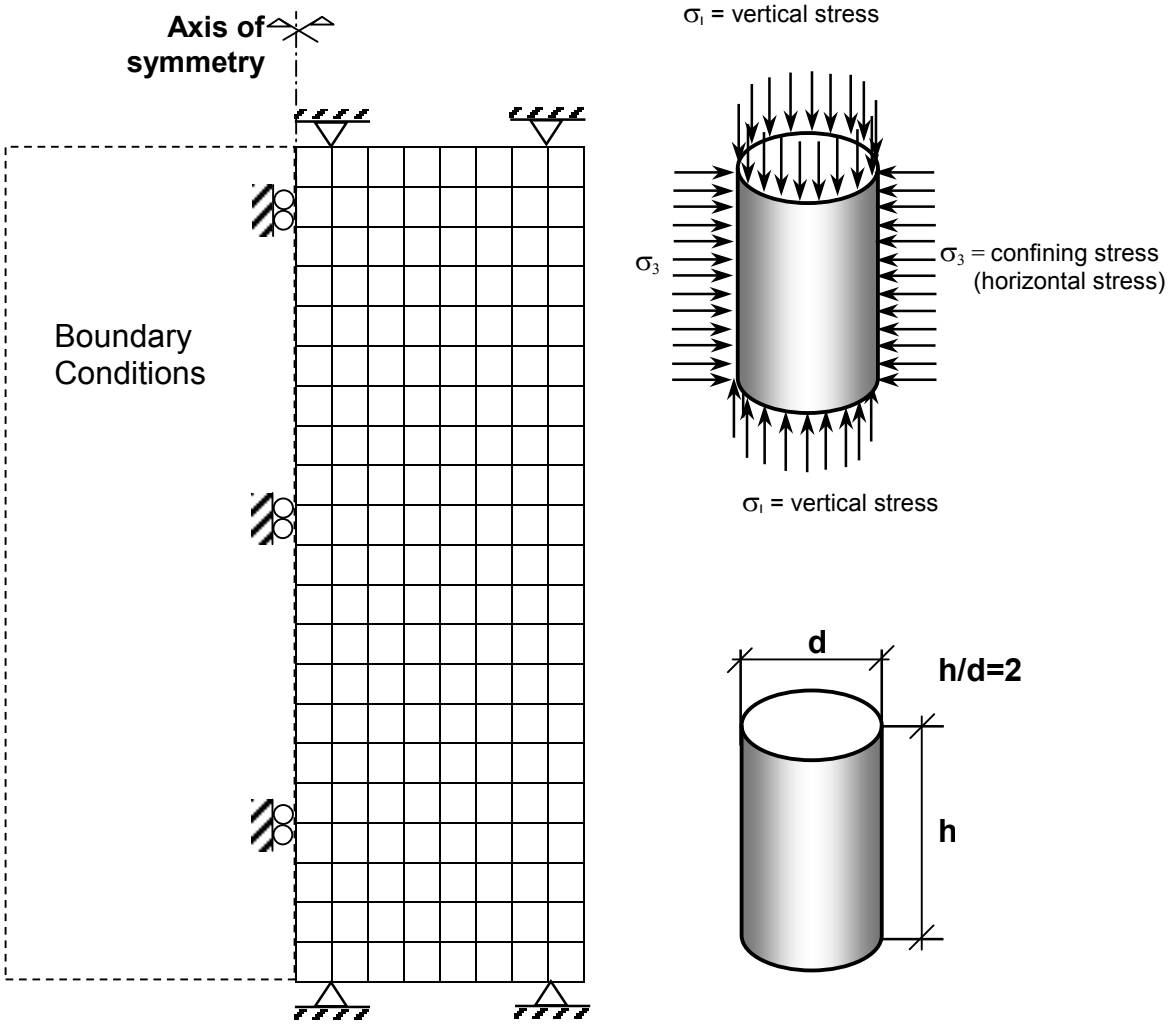


**Figure 6-5.** Example finite difference mesh with boundary conditions used for the analysis of an anisotropically consolidated triaxial compression sand specimen

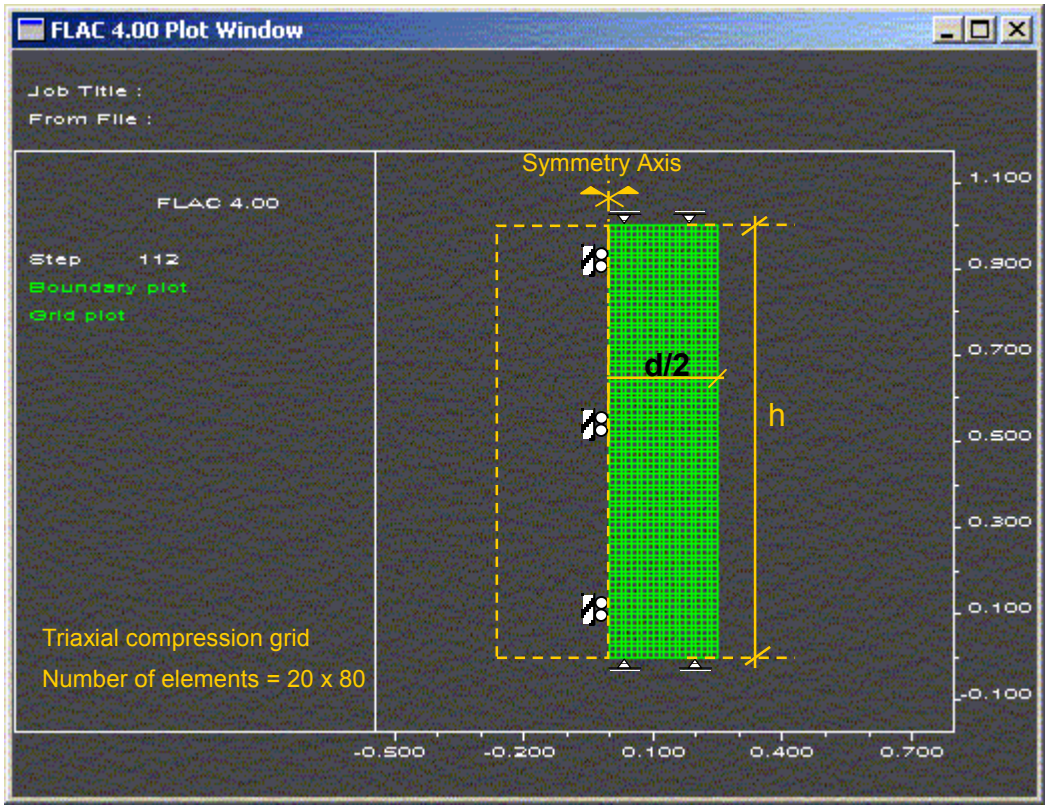


**Figure 6-6.** Finite difference grid used for the simulation of triaxial compression test

**Table 6-1.** List of soil properties used in simulations

| Case number | 1 | 2 | 3 | 4 | 5 |
|---|---|---|---|---|---|
| Initial shear modulus, $G_{max}$ (MPa) | 100 | 100 | 100 | 100 | 100 |
| Initial Poisson's ratio, $\nu_o$ | 0.495 | 0.495 | 0.495 | 0.2 | 0.2 |
| Angle of friction, $\phi'$ ($^o$) | 0 | 0 | 0 | 20 | 30 |
| Dilation angle, $\psi'$ ($^o$) | 0 | 0 | 0 | 0 | 0 |
| Cohesion intercept, c' (kPa) | 0 | 0 | 0 | 10 | 0 |
| Initial confining stress, $\sigma_3$ (kPa) | 50 | 50 | 50 | 100 | 100 |
| Initial confining stress, $\sigma_3$ (kPa) | 100 | 100 | 100 | 100 | 100 |
| Undrained shear strength, $s_u$ (kPa) | 100 | 100 | 100 | N/A | N/A |
| Threshold strain, $\gamma_{th}$ (%) *For non-linear model only* | 0.001 | 0.001 | 0.001 | 0.001 | 0.001 |
| Normalized limiting strain, $x_L$ *For non-linear model only* | 1.01 | 20 | 50 | 10 | 30 |

Generated stress-strain curves are presented in Figure 6-7. An excellent match was found between the stress-strain curves obtained using the two models. The effect of varying the normalized limiting strain $x_L$ on the stress-strain behavior is illustrated by conducting simulations where all soil parameters are kept the same except for the normalized limiting strain $x_L$ (case numbers 1, 2 and 3 listed in Table 6-1), as shown in Figure 6-8.

The next step is investigating the effect of varying either the bulk modulus or Poisson's ratio on the stress-strain behavior in triaxial compression tests in drained loading. Stress-strain results from simulated drained triaxial compression tests are given in Figures 6-9-a and 6-9-b. Both tests depict the behavior of cylindrical soil specimens under drained conditions (assuming Poisson's ratio $\nu = 0.2$). Soil properties used in the analyses are listed as case numbers 4 and 5. Cases 4 and 5 simulate the stress- strain behavior under isotropically consolidated conditions ($K_o = 1$).

As shown in Figure 6-9-a, a slightly softer stress-strain behavior is observed when the bulk modulus softens with the increase in strain level. Similarly, the stress-strain behavior of test 5 is slightly softer for the case when the bulk modulus is allowed to soften compared to maintaining it constant. Comparable results are reported by Fahey and Carter (1993) on modeling pressuremeter response in sands. Allowing the bulk and shear moduli to decrease with strain level simultaneously leads to numerical instabilities at high strains because both moduli approach zero close to failure. As the difference in the stress-strain behavior is quite small between varying Poisson's ratio or bulk modulus, for all practical purposes, it was decided to perform the analysis keeping the bulk modulus constant to ensure numerical stability.

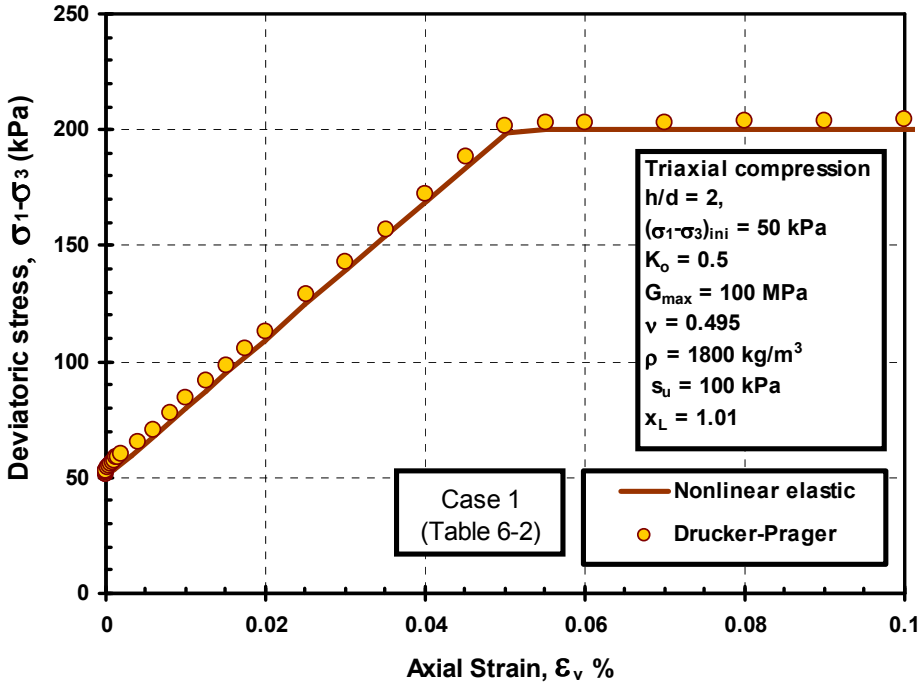


**Figure 6-7.** Verification of the logarithmic non-linear elastic model by comparison of stress-strain data simulated by Drucker-Prager and logarithmic nonlinear elastic models (case 1 in Table 6-1)

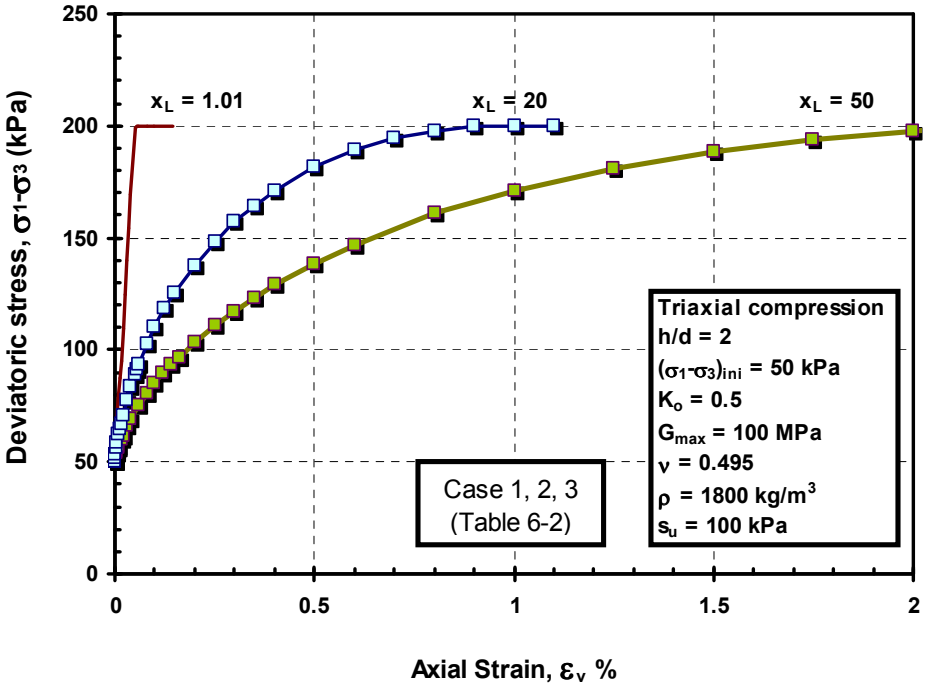


**Figure 6-8.** Effect of the normalized limiting strain $x_L$ on the non-linear stress-strain behavior of soil in triaxial compression (cases 1, 2, and 3 in Table 6-1)

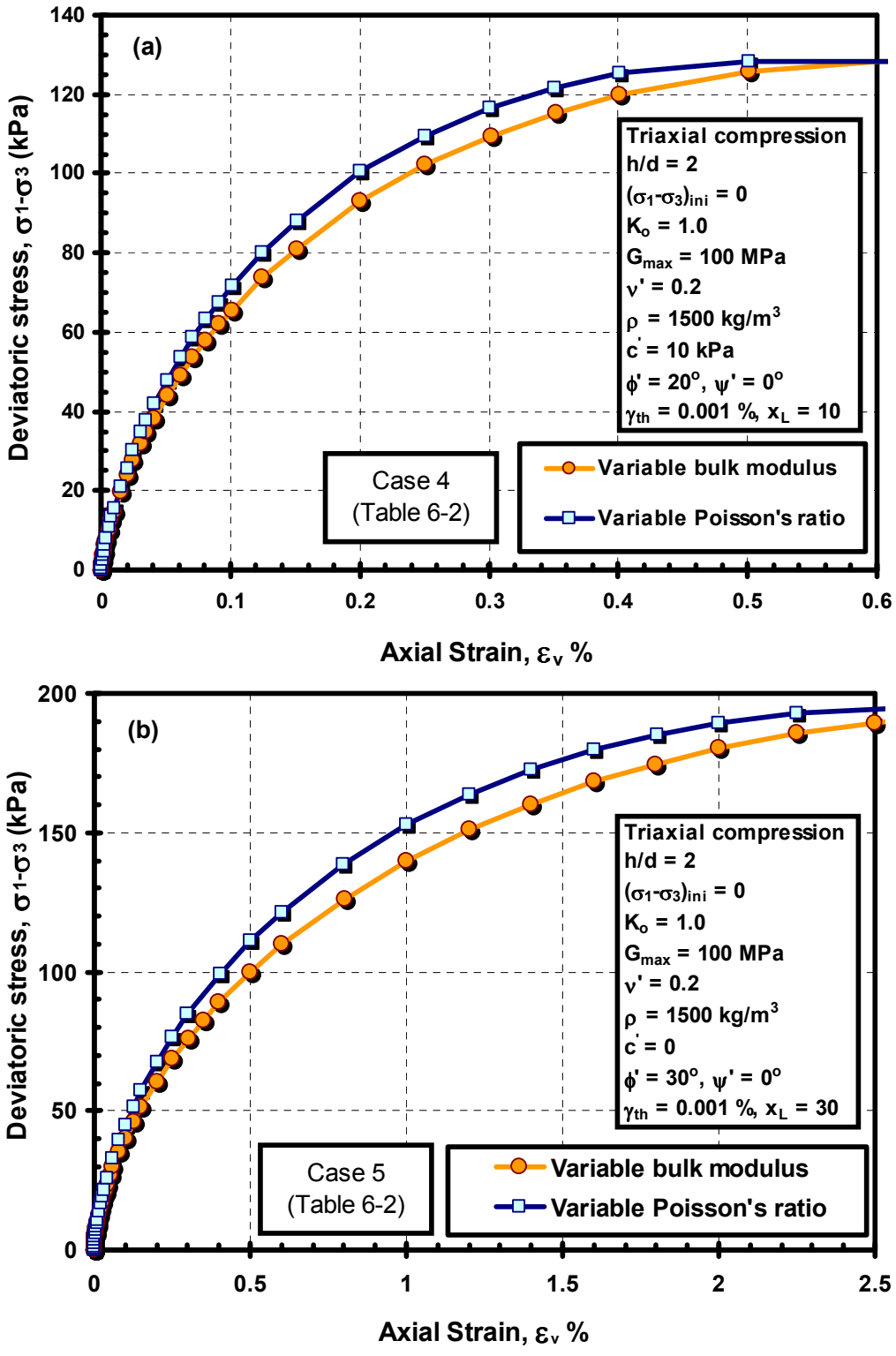


**Figure 6-9.** Effect of varying Poisson's ratio versus varying bulk modulus on the stress-strain behavior of isotropically consolidated triaxial compression drained tests for soils with normalized limiting strains of: (a) $x_L$= 10, (b) $x_L$= 30.

#### *6.3.1.1 Effect of threshold strain on simulated stress-strain response*

The value of the threshold strain $\gamma_{th}$ measured from both static and dynamic tests are discussed in Chapter 5. Based on a database of monotonic torsional shear tests presented in Figure 4-9-a, the threshold strain is found to vary between 0.0005 % to 0.005 %. The effect of using a threshold strain on the numerical simulations of triaxial compression stress-strain data was examined using soil properties from case 4 are given in Table 6-1. The stress-strain behavior of an anisotropically consolidated triaxial test is simulated in two cases using a threshold strain of zero and 0.001 %. Figure 6-10-a compares the simulated stress-strain behavior for the two values of the threshold strain in the intermediate- to high-strain range. Virtually, there is no difference between the two plots. In Figure 6-10-b, the small- to intermediate- strain range is accentuated. There is no appreciable difference between the stress-strain plots except for very small strains (less than 0.02 %), where the soil behavior appears slightly softer when no threshold strain is used. For the purposes of this study, the difference in the stress-strain behavior can be considered small. It was therefore decided to keep the threshold strain constant at $10^{-3}$ % for all further analyses. It should be noted that Lehane (2000) adopted $\varepsilon_{th} = 10^{-3}$% when modeling shallow footings. Other researchers modeling the non-linear response of soils under static loading did not include the effect of the threshold strain such as Fahey and Carter (1993) on the pressuremeter; Lee & Salgado (1999) on piles; Lee & Salgado (2002) on shallow footings; Viana da Fonseca & Sousa on footing (2002); and Zhu & Chang on piles (2002).

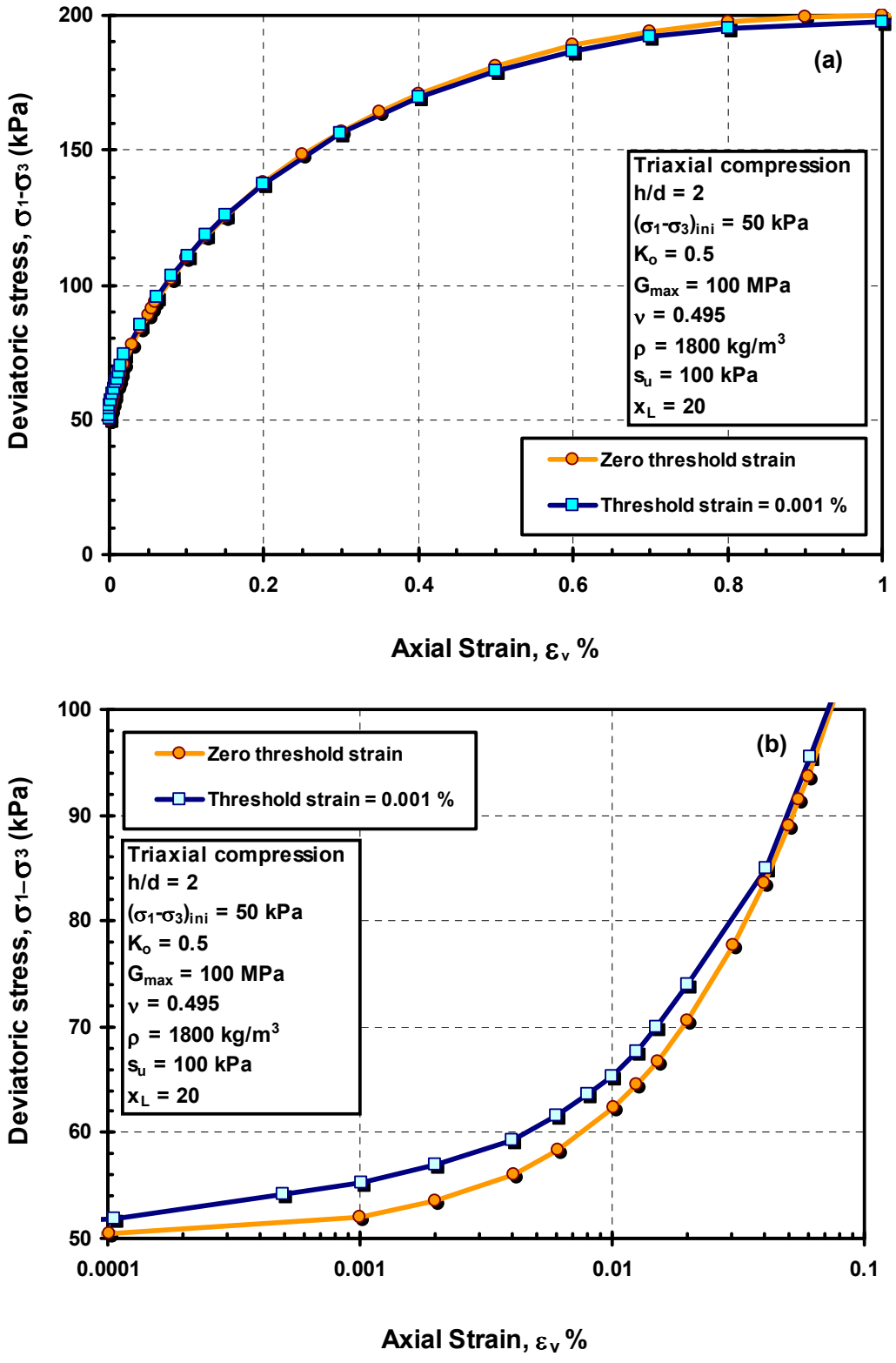


**Figure 6-10.** Effect of a threshold strain $\gamma_{th}$ on the simulated stress-strain behavior of an anisotropically consolidated compression triaxial test: (a) overall behavior (case 4, Table 6-1); (b) small strain range

### *6.3.2 Simulated stress displacement response vertically loaded circular footing*

The logarithmic non-linear elastic model is validated for the case of a circular footing resting on a homogeneous soil layer. A schematic diagram illustrating the boundary conditions is shown in Figure 6-11. Due to the symmetric nature of the problem, only half the footing and underlying soil are modeled. Rollers that restrict the horizontal movement were positioned at the centerline and the other vertical boundary. Allowing vertical movement at the other vertical boundary was adopted to avoid overestimating the load (Frydman and Burd, 1997). Hinges, preventing vertical and horizontal motion, were placed at the bottom boundary. A smooth footing-soil interface was replicated by imposing no restraint on the horizontal movement at the nodal contacts between the footing and underlying soil layer. Applying uniform vertical displacements on a portion of the upper horizontal boundary simulates a rigid footing. The average stress underneath the footing is calculated as the summation of vertical forces at the nodes at the base of the footing, divided by the footing area. The footing displacement is taken equal to the vertical displacement applied to the footing. A non-uniform grid was used in the footing analysis to use a smaller number of elements, decrease the computer running time for each simulation. Similar to the triaxial test, several grid sizes and loading increments were trial tested before deciding on the optimum grid size and loading increment.

A 65 x 65 biased mesh, shown in Figure 6-12, is the smallest mesh size that can be used for modeling circular footings under undrained loading without compromising the solution accuracy. The mesh used for modeling the undrained loading of strip footings is

shown in Chapter 7. Meshes used for modeling the drained loading of circular and strip footings are presented in Chapter 8. A biased mesh was used because more elements can be placed in regions with anticipated higher stress changes, i.e. closer to the loaded area.

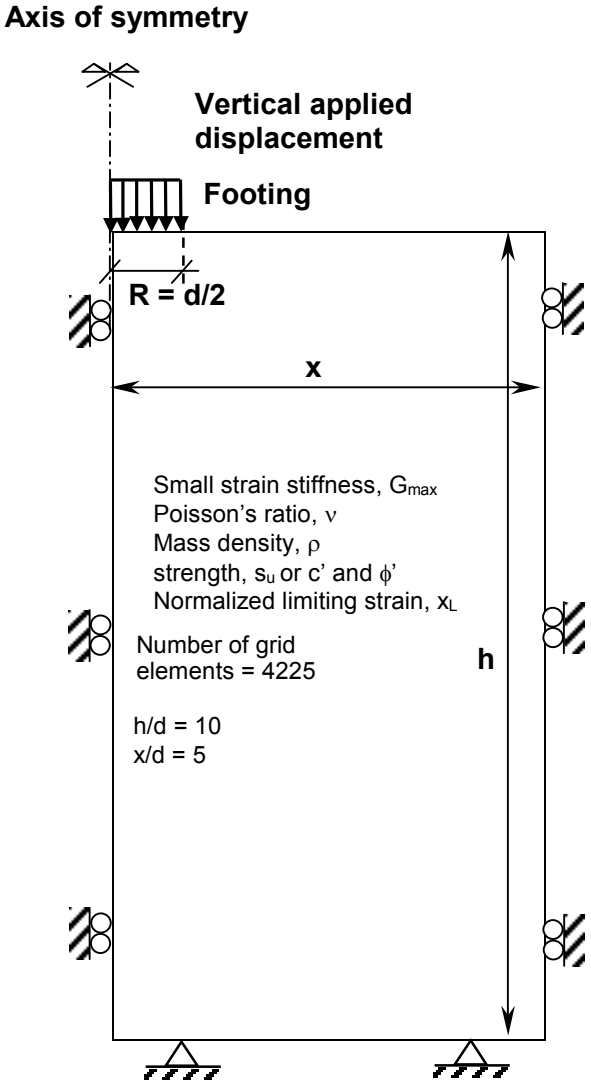


**Figure 6-11.** Schematic diagram illustrating the mesh size and boundary conditions applied for the analysis of a circular shallow footing resting on a homogeneous, isotropic soil layer

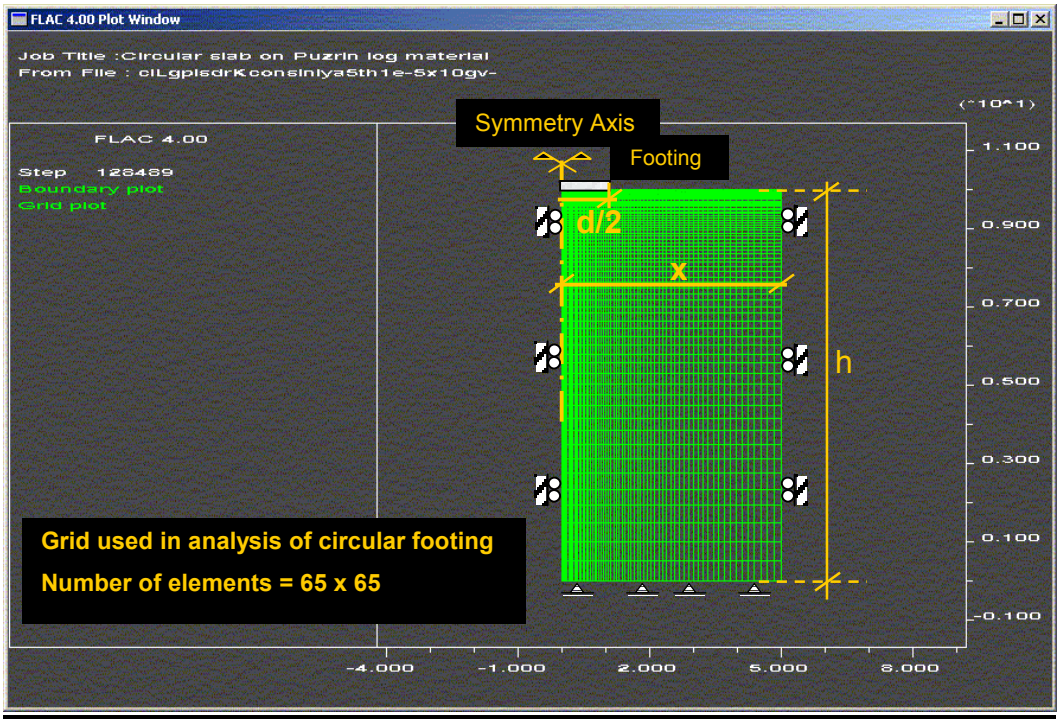


**Figure 6-12.** Finite difference grid for modeling a circular smooth rigid shallow footing resting on a homogeneous semi-infinite half space

Analyses of a 1-m diameter rigid, circular footing with smooth interface resting on a homogenous infinite half space were performed. For linear elastic solutions, the influence zone beneath a footing is traditionally taken as twice the footing width (Schmertmann, 1970). Jardine et al. (1986) have shown that computed displacements beneath a footing, using non-linear stress-strain soil response, reduce at a faster rate compared to linear elastic solutions. Therefore, it is considered acceptable to have a soil layer thickness to footing diameter ratio h/d = 10. The effect of having a lateral boundary is also minimized, by having the ratio of the distance from the footing centerline to the lateral boundary to the footing diameter x/d equal 5. These h/d and x/d ratios are comparable or more conservative in minimizing boundary effects on footing behavior in

comparison to similar numerical simulations (e.g. Carrier and Christian, 1973; Jardine et al., 1986; Frydman and Burd, 1997; Griffiths et al., 2002).

Soil properties, listed as case number 1 in Table 6-1, were used to model the stress-displacement behavior beneath the footing centerline. Results are compared to stress-displacement behavior using the conventional Drucker-Prager linear elastic-plastic model in Figure 6-13.

An excellent match is found between the stress-displacement curves up to 65% of the Drucker-Prager failure stress. The discrepancy at higher stresses is attributed to the different normality assumptions associated with each model (Detournay, 2003). In plasticity, normality defines the direction of the plastic strain vector through a flow rule, to which the incremental strain vectors are perpendicular (Desai and Siriwardane, 1984). Therefore, it was decided to further model the behavior with a more complex approach using a non-linear elastic-plastic formulation, as discussed subsequently.

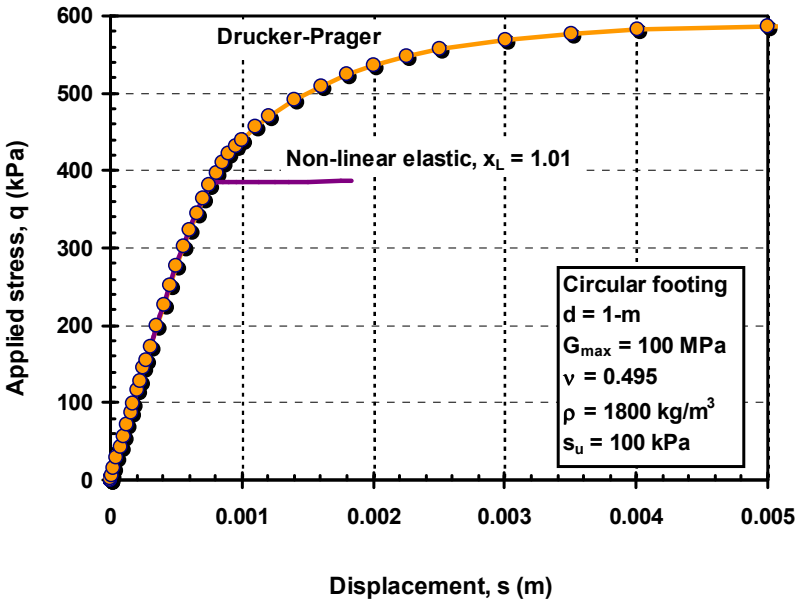


**Figure 6-13.** Comparison of load-displacement curves obtained from FLAC analyses using both the logarithmic nonlinear elastic model versus linear elastic-plastic Drucker-Prager model (case number 1, Table 6-1)

## 6.4 Yield criterion and plasticity

The deformations discussed so far are elastic and recoverable. Irrecoverable deformations are known as inelastic or plastic. If both elastic and plastic deformations take place, behavior is known as elastic-plastic. There are two main requirements needed to describe material plastic behavior under mechanical loading: 1) the yield or failure criterion, and 2) post-yield behavior. These two aspects will be discussed in details in the following sections.

### *6.4.1 Yield criterion*

The yield criterion defines the onset of plasticity or the end of elastic relationship. For elastic-plastic materials, the material follows elastic theory until failure and then deforms

under constant shear stress in the plastic range. This criterion can be expressed mathematically as follows:

F < 0 for the elastic range……..…..…….(6-3)

F = 0 for plastic range…….……..……..(6-4)

The failure surface F is represented by the Drucker-Prager failure envelope shown in Figure 6-14. The Drucker-Prager failure criterion was chosen for the model not the Mohr-Coulomb because the latter does not account for the effects of intermediate principal stresses (Desai and Siriwardane, 1984). The failure envelope $F^s$ is defined between points A and B by (Itasca-c, 2001):

$$F^s = \sqrt{J_{2D}} - q_\phi \cdot J_1 - k_\phi \quad \text{……...…….…..…..(6-5)}$$

The tensile yield function defines the envelope $F^t$ between points B and C according to:

$$F^t = J_1 - \sigma^t \quad \text{…….……(6-6)}$$

where:

$q_\phi$ = material property for frictional resistance (defined later in the chapter).

$k_\phi$ = material property from cohesion intercept (defined later in the chapter).

$\sigma^t$ = tensile strength of the material (zero for soils).

$J_1 = \sigma_1 + \sigma_2 + \sigma_3$.

$$J_{2D} = \frac{1}{6}\left[(\sigma_{11} - \sigma_{22})^2 + (\sigma_{22} - \sigma_{33})^2 + (\sigma_{11} - \sigma_{33})^2 + \sigma_{12}^2\right]$$

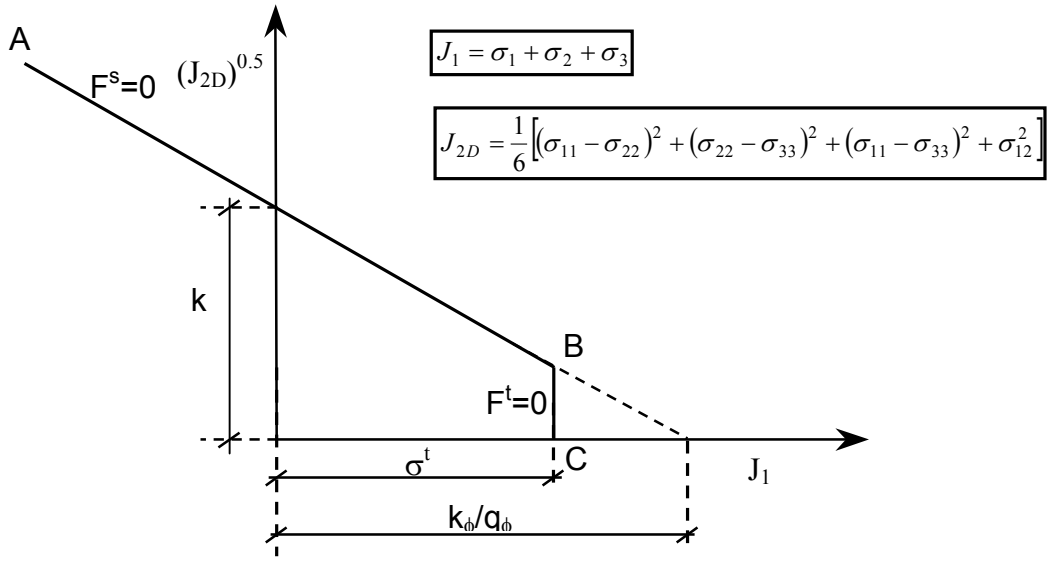


**Figure 6-14.** Drucker-Prager failure criterion (Itasca, 2001-c)

When the state of stress reaches the yield surface for a perfectly plastic material, the stress follows the yield surface during loading. If the stress decreases and falls inside the yield surface, this is known as unloading. When yield is reached, the stress-strain behavior is controlled by plasticity. Therefore, post-yield stress-strain behavior needs to be defined. This is illustrated in Figure 6-15.

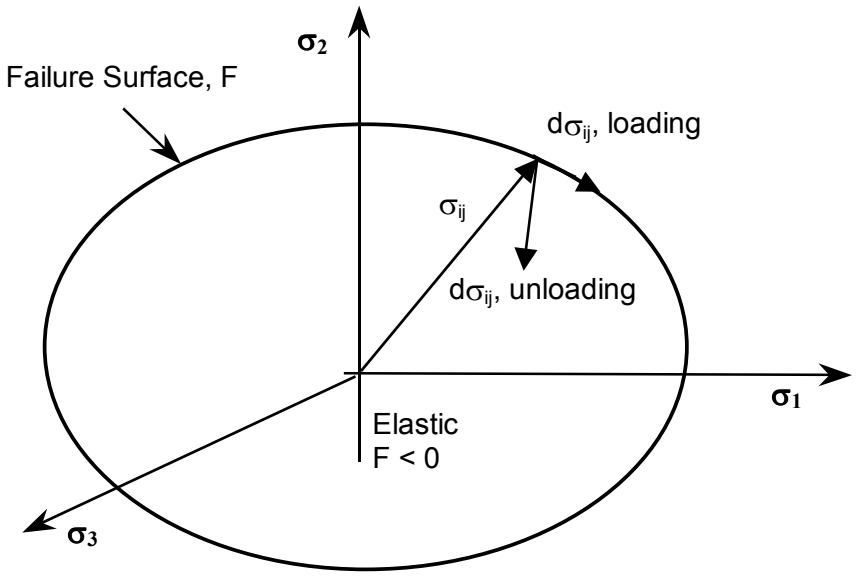


**Figure 6-15.** State of stresses for an elastic-perfectly plastic material (after Lee, 1999)

### *6.4.2 Post-yield stress-strain relationship*

When failure is reached, plastic behavior can be modeled as either perfectly plastic or strain hardening/softening (refer to Figure 6-1). The model considered is perfectly plastic with a yield surface constant and independent of the state of stress. The stress state is not allowed to move outside the yield surface.

The total incremental strain can be expressed as the sum of elastic and plastic strain increments as given by:

$$d\varepsilon_{ij} = d\varepsilon_{ij}^{e} + d\varepsilon_{ij}^{p} \quad \text{.....(6-7)}$$

where $d\varepsilon_{ij}$, $d\varepsilon_{ij}^{e}$, and $d\varepsilon_{ij}^{p}$ are the total, elastic, and plastic strain increments, respectively. The elastic strain component is calculated using Hooke's law in

incremental form. A flow rule is what defines the relationship between the plastic strain increment and the current state of stress for a yielded material undergoing loading. The magnitude and direction of plastic strain increment are determined according to:

$$d\varepsilon_{ij}^{p} = d\lambda \frac{\delta g'}{\delta \sigma_{ij}} \quad \text{.....(6-8)}$$

where $d\lambda$ is a positive scalar proportionality constant, $g'$ is the plastic potential function. If the potential and yield functions are equal, the flow is called associated. Otherwise, the flow is non-associated. According to Equation 6-8, the plastic strain is normal to the surface of the potential function $g'$ in the stress space at the current state of stress $\sigma_{ij}$. This is known as the normality condition. For a perfectly plastic behavior, the work done by the stress increment $d\sigma_{ij}$ and strain increment $d\varepsilon_{ij}$ is equal to zero because the stress $\sigma_{ij}$ remains constant after failure is reached.

In non-linear elastic models, large strains are generated simulating the onset of plasticity. When a non-linear elastic model is used in combination with a plastic flow model, both elastic and plastic strains are computed. After failure is reached, plastic strains are computed using plasticity theory. However, large elastic pseudo-plastic strains are also calculated. This results in computing large plastic strains twice. Therefore, the true elastic strains should be computed instead of large pseudo -plastic elastic strains after failure is reached. This is achieved by using the maximum shear modulus $G_{max}$ in elastic strain computation after plasticity is reached, as demonstrated by Fahey and Carter (1993). The constitutive model LOGNEP is presented in Appendix G.

## 6.5 Determination of Drucker-Prager model parameters

The Drucker-Prager criterion is represented by a cone in the principal stress space with its axis along $\sigma_1 = \sigma_2 = \sigma_3$ and apex at $\sigma_1 = \sigma_2 = \sigma_3 = k_\phi/q_\phi$, (refer to Figure 6-16-a). The Mohr-Coulomb criterion is viewed as a pyramid with an irregular hexagonal base in the same space. They both share the same axis $\sigma_1 = \sigma_2 = \sigma_3$ with an apex at $\sigma_1 = \sigma_2 = \sigma_3 = c' \cot \phi$, as shown in Figure 6-15-b (Itasca-c, 2001). The Drucker-Prager parameters can be adjusted so the cone circumscribes the hexagonal pyramid yielding (Mizuno and Chen, 1980; Chen and Liu, 1990):

$$q_\phi = \frac{6}{\sqrt{3} \cdot (3 - \sin\phi')} \cdot \sin\phi' \quad \text{.....(6-9)}$$

$$k_\phi = \frac{6}{\sqrt{3} \cdot (3 - \sin\phi')} \cdot c' \cdot \cos\phi' \quad \text{.....(6-10)}$$

Equations 6-9 and 6-10 are used in matching conventional triaxial compression (Desai and Siriwardane, 1984). If the Drucker-Prager parameters are adjusted so a cone inscribes the hexagonal pyramid, the following interrelationships are obtained (Chen and Mizuno, 1980):

$$q_\phi = \frac{6}{\sqrt{3} \cdot (3 + \sin\phi')} \cdot \sin\phi' \quad \text{.....(6-11)}$$

$$k_\phi = \frac{6}{\sqrt{3} \cdot (3 + \sin\phi')} \cdot c' \cdot \cos\phi' \quad \text{.....(6-12)}$$

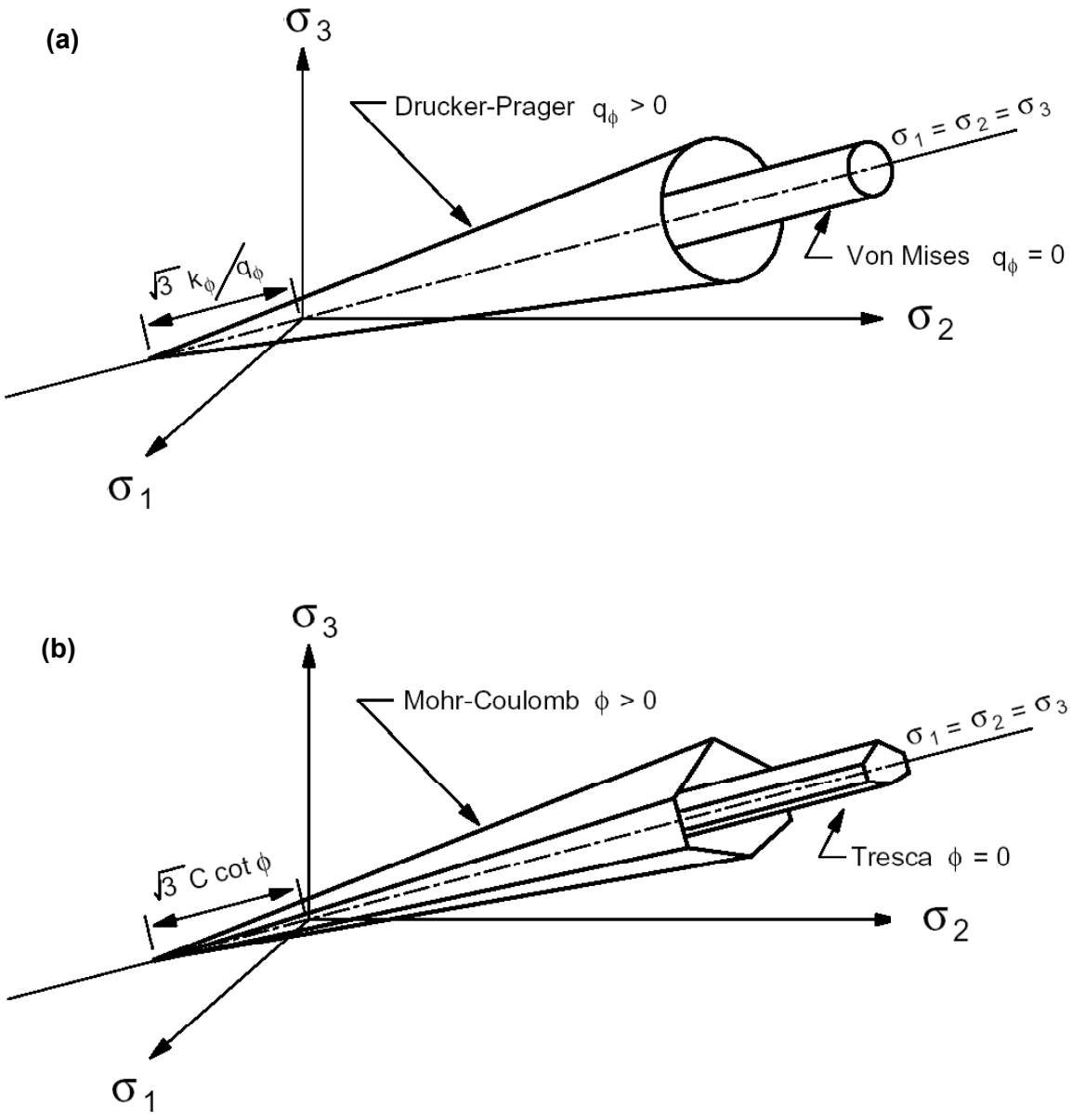


**Figure 6-16.** (a) Drucker-Prager and von Mises yield surfaces in principal stress space; (b) Mohr-Coulomb and Tresca yield surfaces in principal stress space (Itasca, 2001-c)

When modeling a circular footing under undrained loading conditions "$\phi = 0$", Equations 6-9 and 6-10 yield identical results to Equations 6-11 and 6-12:

$$q_\phi = 0 \quad \text{.....(6-13)}$$

$$k_\phi = \frac{2}{\sqrt{3}} \cdot c_u \quad \text{.....(6-14)}$$

where $c_u = s_u$ = undrained shear strength. The use of equations 6-13 and 6-14 in computing parameters for modeling the undrained loading of circular footings will be shown to match analytical results in Chapter 7. For modeling circular footings under drained loading conditions, the problem is more complex because Equations 6-9 and 6-10 (compression) yield results that are quite different from Equations 6-11 and 6-12 (extension). For spread footing foundations and embankments under vertical loading, a combination of triaxial compression (TC), direct simple shear (DSS), and triaxial extension (TE) best represents soil behavior along the failure surface (Kulhawy and Mayne, 1990; Ladd, 1991). Therefore, it is suitable to use different strength modes depending on the directional loading conditions. For simplicity, the average of the different strengths can be used for bearing capacity purposes involving shallow spread footings (Larsson, 1980; Aas et al., 1986; Ladd, 1991). The validity of this assumption will be shown in Chapter 8.

For the plane strain case ($\varepsilon_{33} = 0$), the Mohr-Coulomb parameters (c' and $\phi$') were related to Drucker-Prager parameters ($k_\phi$ and $q_\phi$) (Drucker and Prager, 1952; Mizuno and Chen, 1980):

$$q_\phi = \frac{\tan\phi'}{\sqrt{9 + 12\tan^2\phi'}} \quad \text{.....(6-15)}$$

$$k_\phi = \frac{3 \cdot c'}{\sqrt{9 + 12\tan^2\phi'}} \quad \text{.....(6-16)}$$

Equations 6-15 and 6-16 were successfully used to compute Drucker-Prager parameters for modeling strip footings under both undrained and drained loading conditions, as will be shown in Chapters 7 and 8.

## 6.6 Verification of the non-linear elastic-plastic formulation (LOGNEP)

The logarithmic non-linear elastic plastic model *LOGNEP* was calibrated versus results using the FLAC built-in elastic-plastic Drucker-Prager model. Both models are based on octahedral stress and strain invariants and use the same yield surface and flow rules. Accordingly, both models should yield the same failure stress and same stress-strain behavior for linear analysis. Full linearity is achieved in the *LOGNEP model* when a normalized limiting strain $x_L$ of 1.01 is used. Simulations of anisotropically consolidated undrained triaxial tests were conducted to check the logarithmic nonlinear elastic plastic model *LOGNEP* versus the built-in linear elastic plastic Drucker-Prager model. The same boundary conditions and grid shown in Figures 6-5 and 6-6 were used for the

simulation. The test was simulated using the soil properties of case number 1 listed in Table 6-2. An excellent match was found between the stress-strain curves obtained using both methods, as shown in Figure 6-17.

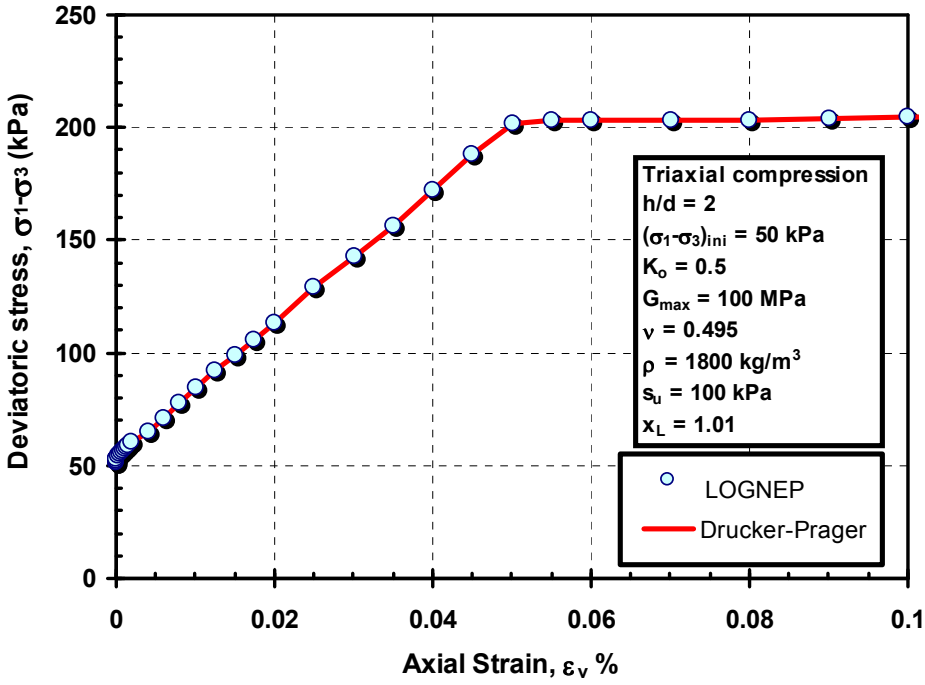


**Figure 6-17.** *LOGNEP* model verification versus the Drucker-Prager linear elastic plastic built-in model for a triaxial test simulation

The *LOGNEP* model was also calibrated for the case of the vertical loading of a shallow, smooth, circular footing resting on a homogenous soil layer. The boundary conditions and grid used in the analysis are shown in Figures 6-10 and 6-11. Soil properties used in modeling the footing response are listed as case number 1 in Table 6-1. The stress at failure for both the *LOGNEP* model and Drucker-Prager are identical.

The generated load-displacement curve is shown in Figure 6-18. The influence of stress-strain non-linearity is explored by varying the normalized limiting strain $x_L$. Simulations of the behavior of vertically loaded circular footings are conducted where all soil parameters are kept the same except for the normalized limiting strain $x_L$ (case numbers 2 and 3 listed in Table 6-1). The simulated stress-displacement responses are shown in Figure 6-19. The linear elastic plastic model ($x_L$ = 1.01) generates the stiffest response. As expected, the stress-displacement response becomes softer as $x_L$ increases. Figures 6-20-a and 6-20-b show the vertical displacement contours within the soil mass for $x_L$ = 1.01 and 50, respectively, for a load factor of 0.75. Displacements close to the edge of the soil mass are nil, confirming that the mesh used in the analysis is of sufficient size to eliminate boundary effects. Figures 6-21-a and 6-21-b show the variation of footing displacement s under the footing centerline relative to the displacement at ground surface $s_G$ for load factors ($q/q_{ult}$) of 0.2, 0.35 and 0.5. It is observed that the displacements diminish faster with depth for a non-linear elastic material ($x_L$ = 20, 50) compared to linear elastic plastic one ($x_L$ = 1.01). This observation agrees with similar findings by Jardine et al. (1986).

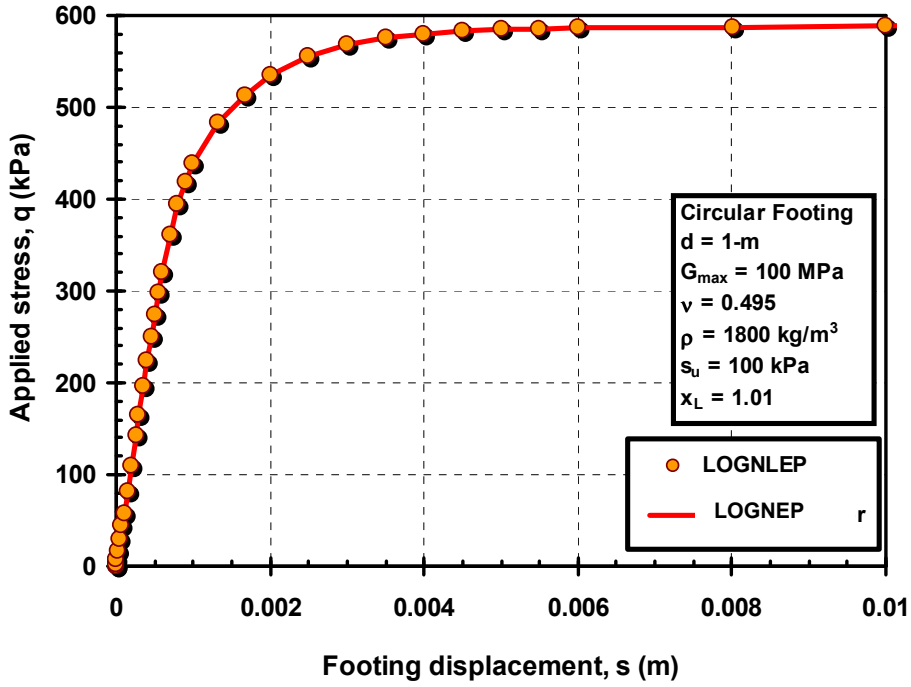


**Figure 6-18.** *LOGNEP* model verification for a 1-m diameter footing resting on a semi-infinite half space (undrained loading)

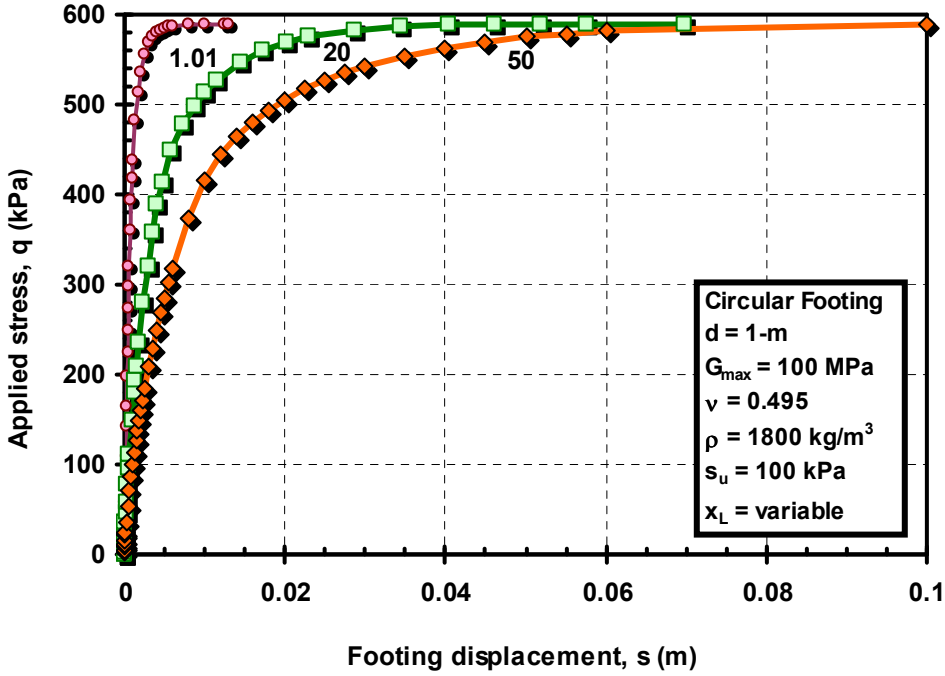


**Figure 6-19.** Effect of the normalized limiting strain $x_L$ on the stress-displacement response of vertically loaded circular footings under undrained loading conditions

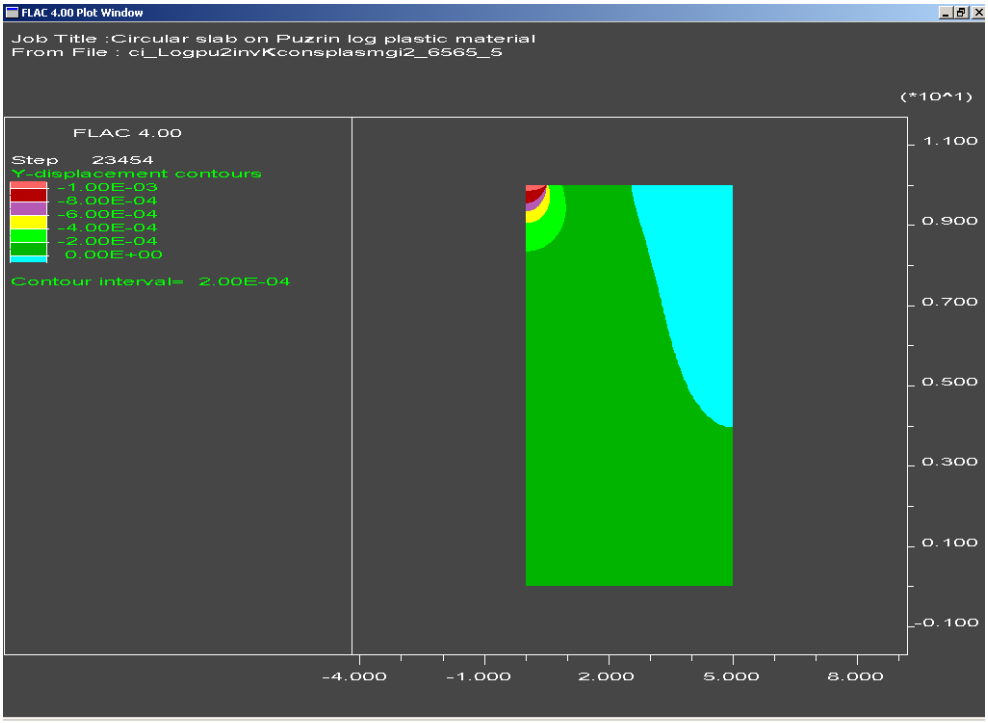


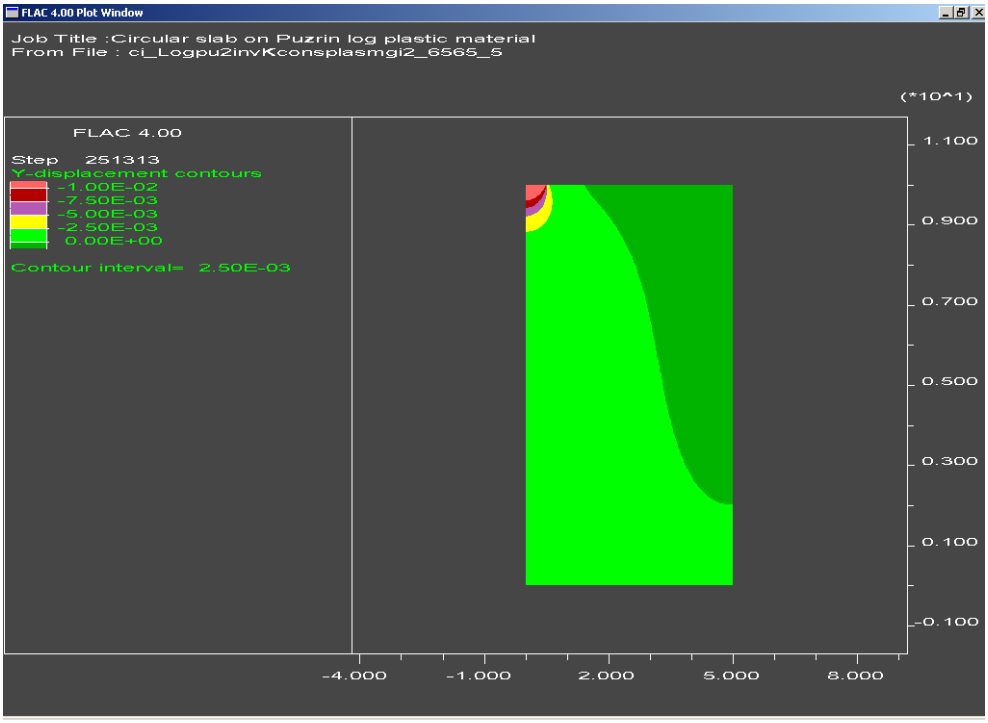


**Figure 6-20.** Contours of vertical displacement (in meters) due to the loading of rigid, circular footing under undrained loading conditions for a load factor of 0.2 for (a) $x_L$ = 1.01; and (b) $x_L$ = 50 (load factor = 0.75)

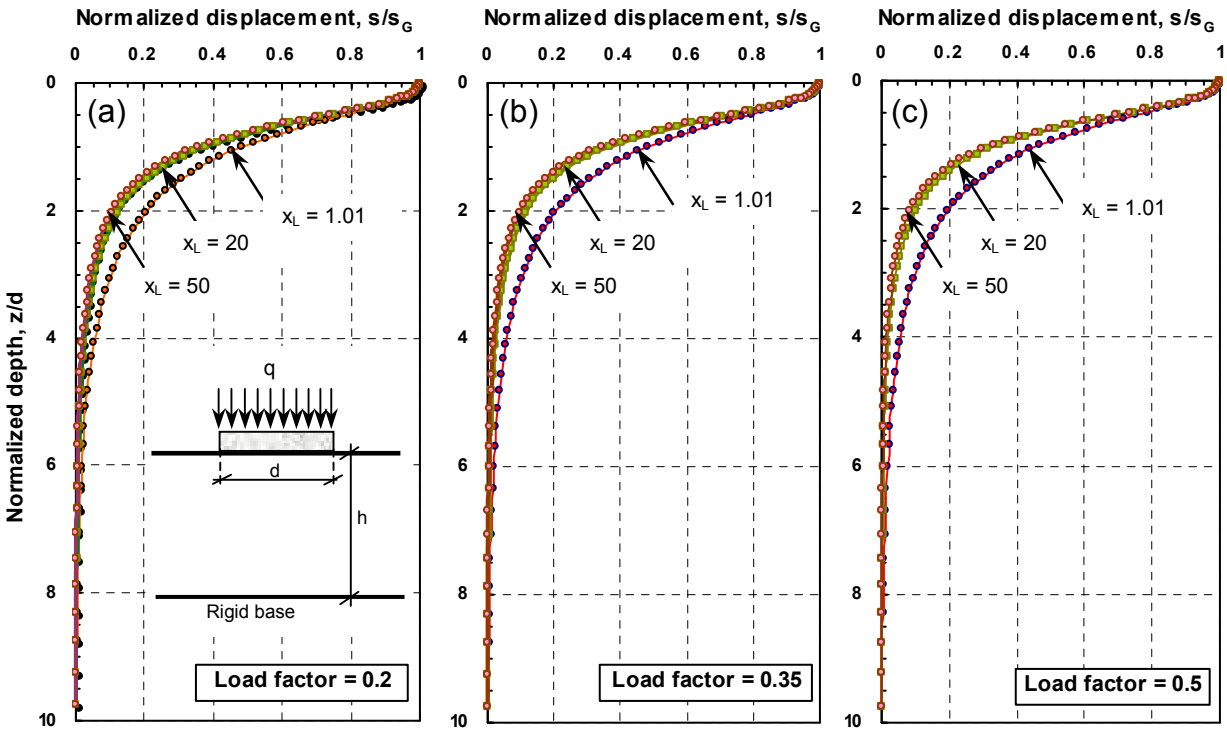


**Figure 6-21.** Effect of the normalized limiting strain $x_L$ on the displacement distribution beneath the centerline of vertically loaded circular footings under undrained loading conditions for load factors $q/q_{ult}$ (a) 0.2; (b) 0.35; and (c) 0.5

## 6.7 Synopsis

Geomaterial behavior is described using constitutive models that vary in their complexity and accuracy in representing mechanical behavior. First, a logarithmic non-linear elastic model was introduced and calibrated for triaxial compression tests and shallow footing load tests, by comparison with the linear elastic Drucker-Prager model. Excellent agreement of stress-strain curves from triaxial compression simulations, under both isotropic and anisotropic conditions, was found using both models. However, there was poor agreement in the load-displacement curve when modeling the shallow footings at

high stress levels. This was attributed to the different coaxiality criteria associated with each model. It was, therefore, decided to add a plastic component to the model to match the well-established Drucker-Prager model. The modified form gave a logarithmic non-linear elastic-plastic LOGNEP model. When the LOGNEP was calibrated versus the Drucker-Prager model under both triaxial compression conditions and shallow footing simulations tests, excellent agreement was found between both models. The influence of varying the normalized limiting strain $x_L$ on the stress-displacement behavior beneath the footing and displacement distribution are investigated.

# CHAPTER VII

# UNDRAINED DISPLACEMENT RESPONSE OF SHALLOW FOUNDATIONS

## 7.1 Overview

Numerical simulations are conducted of footings resting on soil exhibiting non-linear stress-strain-strength behavior under undrained conditions. The logarithmic non-linear elastic perfectly plastic *LOGNEP* model was formulated and incorporated into the numerical modeling software FLAC (Fast Lagrangian Analysis of Continua) as a user-defined constitutive model, presented in Chapter 6. Input soil parameters required by the model are: (1) initial shear modulus, $G_{max}$, (2) non-linear modulus reduction parameter, $x_L$, (3) Poisson's ratio, $\nu$; (4) strength defined by either effective stress parameters (cohesion intercept c', angle of internal friction $\phi$', and angle of dilation $\psi$), or undrained shear strength, $s_u$; and (5) mass density $\rho$. The degree of material non-linearity is controlled by the normalized limiting strain $x_L$, as discussed in previous chapters. As undrained loading is addressed here, the relevant failure state is represented by the undrained shear strength, $s_u$.

The detailed numerical modeling of any geotechnical problem requires special finite element or finite difference software, which is typically expensive and involves special user skills and modeling experiences.

It would be valuable to directly relate the non-linear behavior of a soil element to the overall non-linear behavior of the structure/foundation resting on the soil medium, as shown in Figure 7-1. That is, there is an observed parallelism between the non-linear

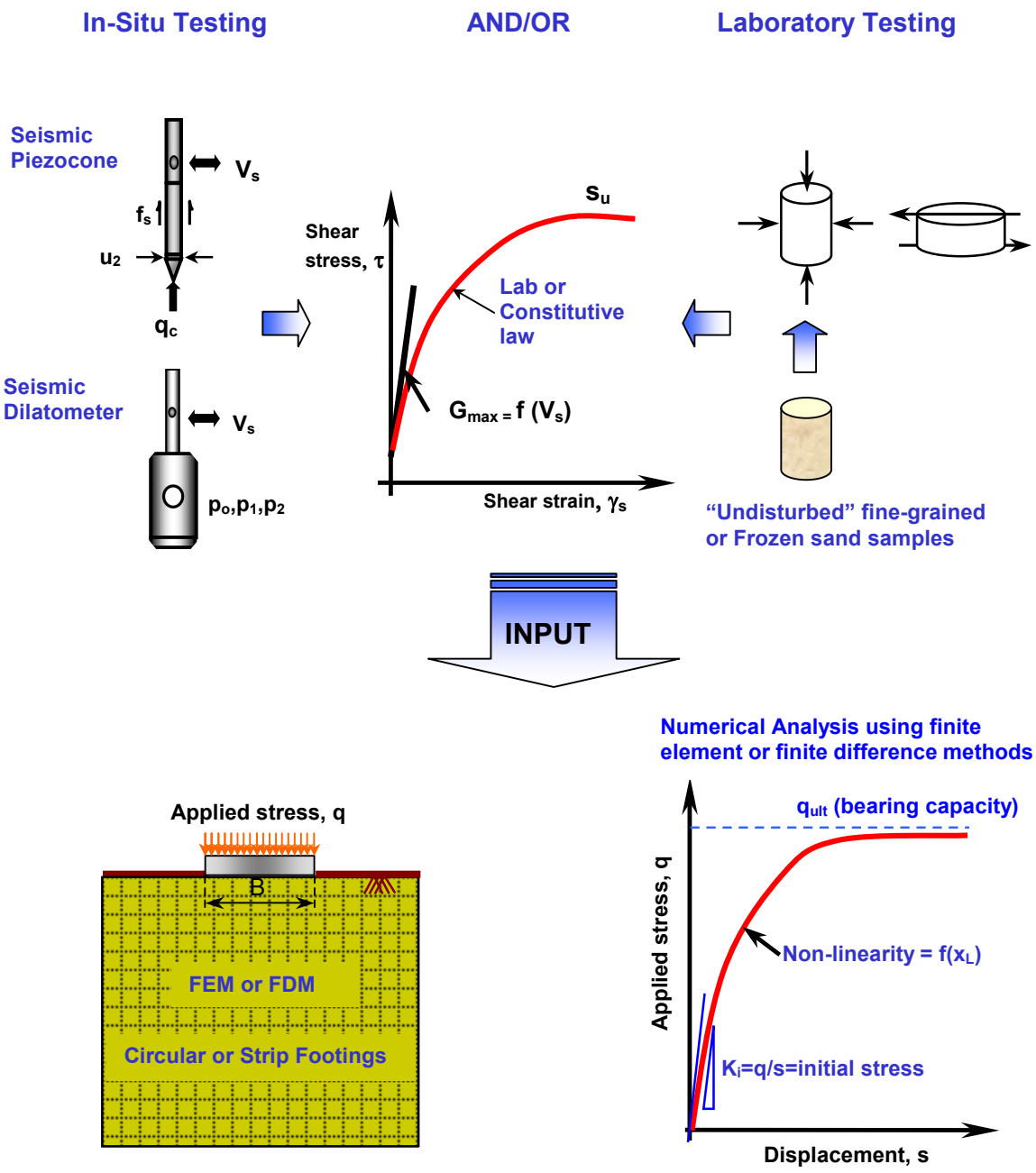


**Figure 7-1.** Schematic diagram illustrating the purpose of the current study of relating soil behavior on the element level to the overall behavior of a soil mass under loading

stress-strain-strength of a soil element and the complete non-linear load-displacement-capacity response of a footing, supported by thousands or millions of soil elements. How can one scale up the "representative" single soil element behavior to mimic an equivalent foundation system? The current research is focused on the FLAC numerical modeling of a rigid, smooth, shallow footing, subjected to vertical loading, resting on a homogeneous deep soil profile.

Attempts have been made to directly relate the behavior of a soil element to the performance of an integrated soil mass under loading. Atkinson (2000) proposed an upward scaling factor of three relating the stress-strain behavior of a triaxial compression specimen to the overall load-displacement curve beneath the centerline of a footing resting on the same medium. However, this scaling factor was based on two small model chamber plate load tests resting on carbonate and silica sands, where the triaxial compression stress-strain data were synthetically simulated. Tatsuoka et al. (2001) conceptually proposed a parallelism between the stress-strain behavior of a single soil element and the load-displacement behavior of foundations. Lehane and Fahey (2002) presented an approach for computing displacements underneath circular footings resting on sand at working stress levels. The method accounts for the non-linear behavior of soil stiffness with strain/stress levels, and density dependence, but assumes Boussinesq's stress distributions underneath the footing.

In this chapter, a parametric study of the different soil and footing properties affecting the stress-displacement response of shallow footings was performed. Parameters considered

in the study include: a) initial soil stresses (mass soil density $\rho$ and at rest earth pressure coefficient $K_o$); b) footing width; c) undrained shear strength; d) small-strain stiffness $G_{max}$; and e) normalized limiting strain $x_L$.

## 7.2 Initial in-situ stresses

The grid and boundary conditions used for modeling the footing/soil system are the same as presented in figures 6-11 and 6-12. Soil is assumed to behave according to the logarithmic elastic plastic *LOGNEP* model. Initial stresses within the soil mass are generated before any load is applied to the footing.

At any site, initial soil stresses exist before any construction work is started. It is important to replicate the in-situ stress conditions because they could influence any subsequent analysis. Although there could be an infinite number of initial stress profiles, the problem is limited by maintaining equilibrium and not violating yield conditions when using a plastic constitutive model. The vertical overburden stress at any depth z within the soil mass is computed as the summation of vertical stress $\sigma_{vo} = (\Sigma\ \rho_i g\ \Delta z_i)$, where g is the gravitational acceleration, $\rho_i$ is the soil mass density, and $\Delta z_i$ is the soil layer thickness. For a homogeneous soil profile, the vertical overburden stress can be calculated as ($\rho$gz), where z is the depth measured from the ground surface. Effective stresses are simulated by replacing $\rho$ with ($\rho - \rho_w$), where $\rho_w$ is the soil mass density. Horizontal stresses are not as easily computed. In many cases, the horizontal stress $\sigma_{ho}$'

is determined by the at rest coefficient $K_o$, where $K_o = \sigma_{ho}'/\sigma_{vo}'$ (e.g., Mayne and Kulhawy, 1982).

A number of simulations were conducted where the soil mass density and the at-rest earth pressure coefficient $K_o$ were varied to investigate their effect on the load-displacement behavior of footings. After initial stresses are generated within the grid, soil is assigned the proper constitutive model, i.e. *LOGNEP*. The footing is loaded by the incremental application of vertical displacements to the grid points representing the footing. The applied stress is computed as the average applied load divided by the area of the footing.

The simulated load-displacement results are presented in Figures 7-2-a through 7-2-c. Figure 7-2-a illustrates the effect of the at-rest earth pressure coefficient $K_o$ on the stress-displacement response of vertically loaded footing resting on a linear elastic plastic soil ($x_L$ = 1) medium. Simulations were performed for $K_o$ of 0.5 and 1.0. The effect of varying $K_o$ is small. The influence of varying $K_o$ was further investigated for $x_L$ = 50, where $K_o$ was varied between 0.4 and 2.1. No appreciable effect for $K_o$ can be found, as shown in Figure 7-2-b. Similarly, the effect of varying the soil mass density $\rho$ is shown in Figure 7-2-c, where $\rho$ is varied between 1800 kg/m$^3$ (total) and 800 kg/m$^3$ (submerged). There is no significant influence for $\rho$ on the stress-displacement footing response.

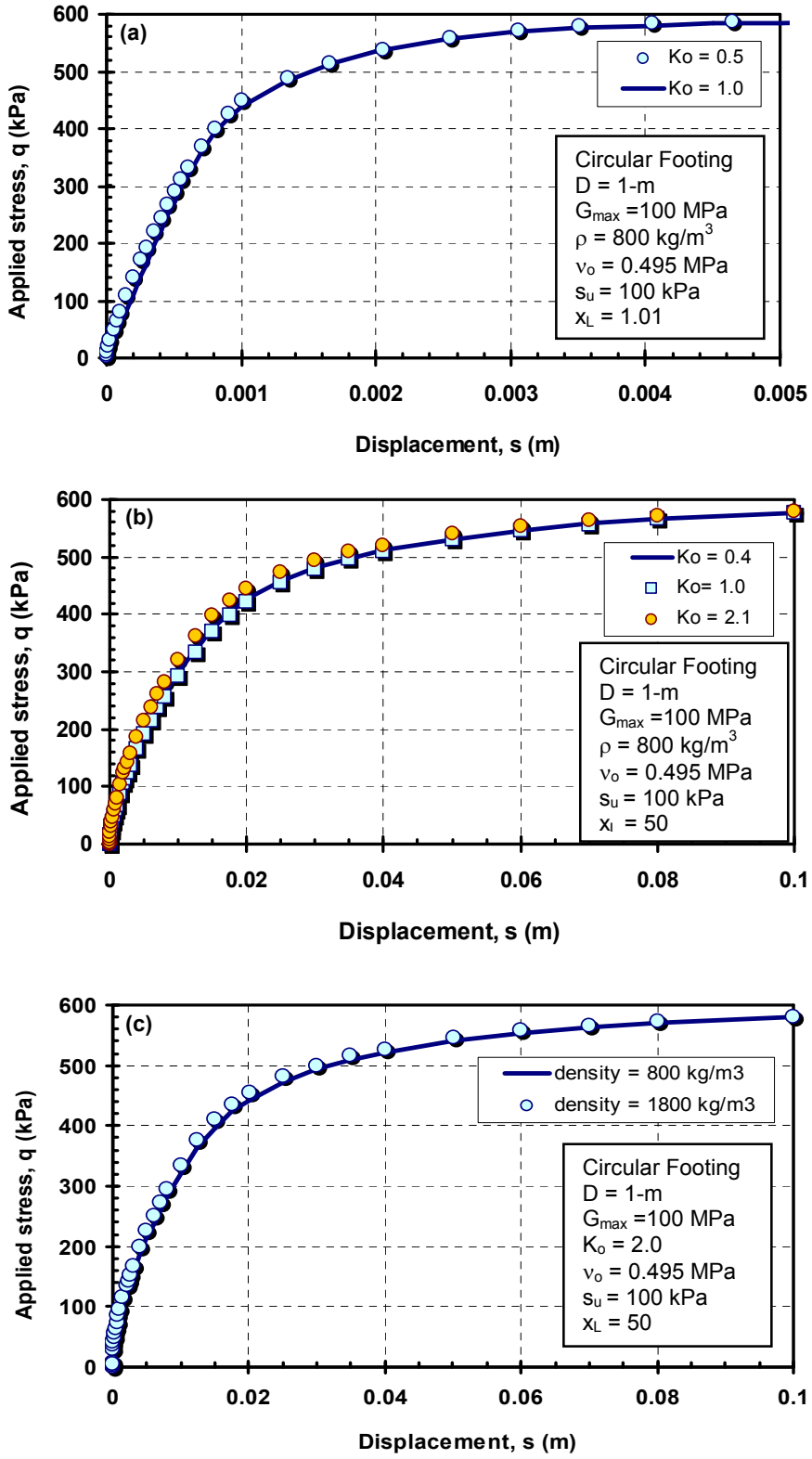


**Figure 7-2.** Effect of initial stresses on the stress-displacement response of circular: (a) varying $K_o$ for linear elastic plastic soil; (b) varying $K_o$ for non-linear elastic plastic soil ($x_L = 50$); (c) varying soil mass density for $x_L = 50$.

## 7.3 Parameters affecting footing stress-displacement response

The effect of varying the input soil and footing properties on the stress-displacement response of circular footings is explored in this section. The non-linear LOGNEP model is used for the simulations. Parameters considered in the study include: (a) footing diameter d; (b) undrained shear strength $s_u$; (c) small-strain shear modulus $G_{max}$; and (d) the normalized limiting strain $x_L$ representing varying degrees of stress-strain non-linearity. The different parameters included in the study are listed in Table 7-1.

In all the simulations, soil is considered fully saturated ($\gamma_{total}$ = 18 kN/m$^3$, $\gamma_{sub}$ = 8 kN/m$^3$) and the at-rest earth pressure coefficient $K_o$ was maintained constant at 1. Undrained loading conditions are simulated by using a Poisson's ratio $\nu_u$ of 0.495. Simulations are denoted using five part alphanumeric acronyms, according to Table 7-1. The first letter of the test name indicates the footing shape: Ci for circular footings and St for strip footings. Subsequent numbers denote the footing width B, undrained shear strength $s_u$, the maximum shear modulus $G_{max}$, and the normalized limiting strain $x_L$, respectively. For example, simulation Ci-1-1-2-10 corresponding to a 0.5-m diameter footing resting on a clay soil that is subjected to undrained loading conditions, where the clay has an undrained shear strength $s_u$ of 50 kPa, small-strain shear modulus $G_{max}$ of 50 MPa, and normalized limiting strain $x_L$ of 10.

In cases Ci-1-1-2-5 through Ci-3-1-2-200, the undrained shear strength and maximum shear modulus were kept constant, while the footing diameter was varied. Simulations using six different values of normalized limiting strains $x_L$ ranging between 5 and 200

**Table 7-1.** Notations for naming footing simulations using *LOGNEP* model

| Parameter | Notation | Value/Meaning |
|---|---|---|
| Footing shape | Ci | Circular |
| | St | Strip |
| Footing width, B | 1 | 0.5 m |
| | 2 | 1 m |
| | 3 | 2 m |
| Undrained shear strength, $s_u$ | 1 | 50 kPa |
| | 2 | 100 kPa |
| | 3 | 200 kPa |
| Maximum shear modulus, $G_{max}$ | 1 | 50 MPa |
| | 2 | 100 MPa |
| | 3 | 200 MPa |
| Normalized limiting strain, $x_L$ | 1 | 1.01 |
| | 5 | 5 |
| | 10 | 10 |
| | 30 | 30 |
| | 50 | 50 |
| | 100 | 100 |
| | 200 | 200 |

Note: Acronym defining case number given by alphanumerical code: Ci/St-B-$s_u$-$G_{max}$-$x_L$

(highly non-linear). The calculated stress-displacement curves underneath the footing centerlines are plotted in Figures 7-3. As expected, the average stress underneath the footing remains constant (same constitutive model and shear strength), while displacements increase with the footing size because the influence zone beneath the footing increases with size (Poulos and Davis, 1974). The bearing capacity factor $N_c$ computed from the analyses is 6, approximately within 2% from Vesic (1975) solution of 6.14.

In simulations Ci-2-1-1-5 through Ci-2-2-1-200, a 1-m rigid circular footing with smooth interface is analyzed. The small-strain shear modulus $G_{max}$ is kept constant at 100 MPa for all analyses. Three values for the undrained shear strength ($s_u$ = 50, 100, 200 kPa) are used in the simulations. The normalized limiting strain $x_L$ is varied between 5 and 200. The applied stress-displacement curves from the simulations are presented in Figure 7-4. As anticipated, the stress at failure varies with shear strength. The resulting stress-displacement curves are dependent on both the undrained strength $s_u$, and the normalized limiting strain $x_L$.

Another set of simulations (Ci-2-2-1-5 through Ci-2-2-2-200) was performed to examine the effect of changing the small-strain stiffness $G_{max}$. The footing diameter, undrained shear strength and Poisson's ratio were kept constant for all the simulations. The normalized limiting strain $x_L$ was varied between 5 and 200. Figure 7-5 shows the stress-displacement curves from all the simulations. As the value of the small-strain stiffness $G_{max}$ becomes higher, the stress-displacement footing behavior becomes stiffer.

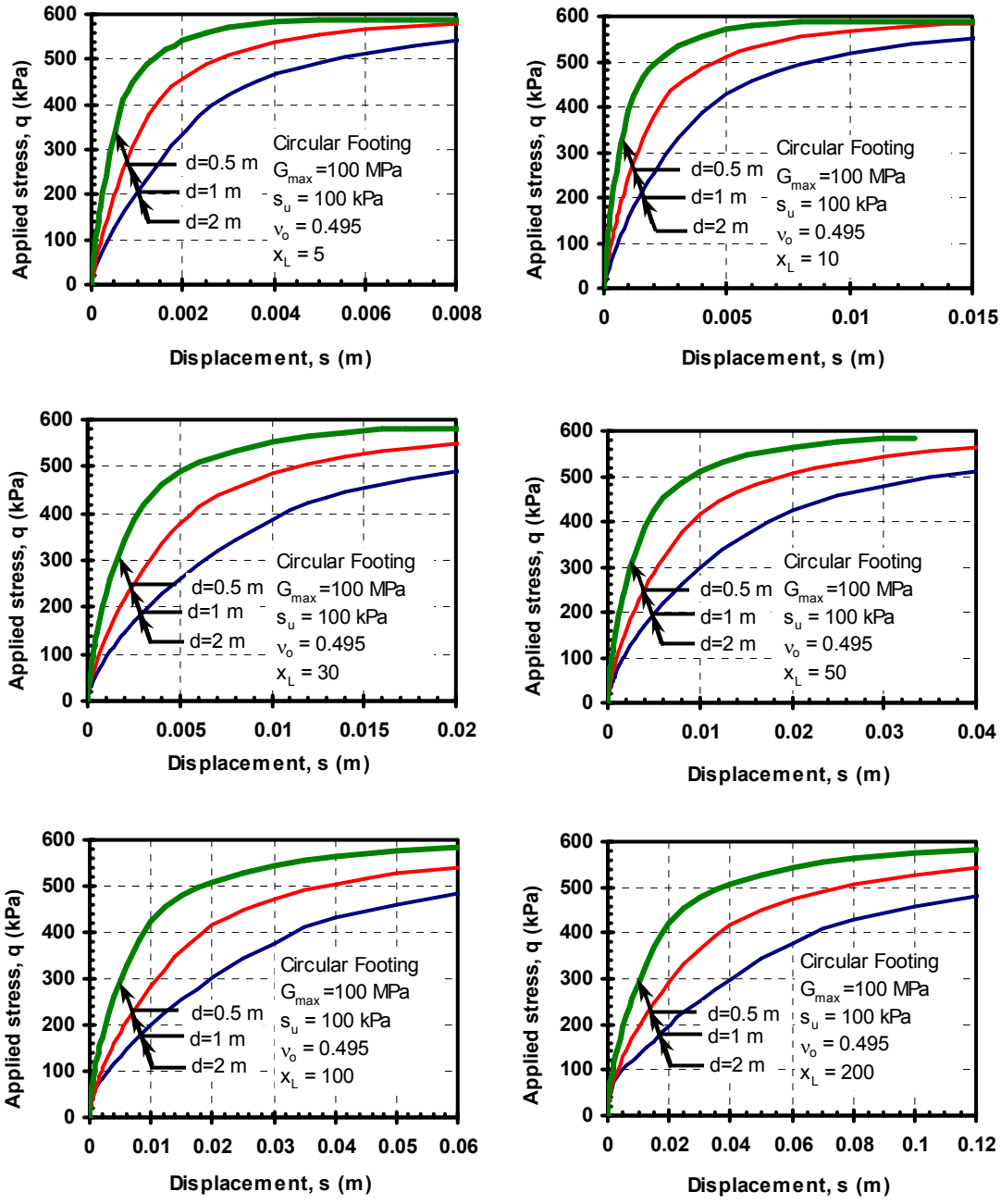


**Figure 7-3.** The effect of footing size on the stress-displacement behavior of a circular footing resting on homogeneous clay (cases Ci-1-1-1-5 through Ci-3-1-1-200)

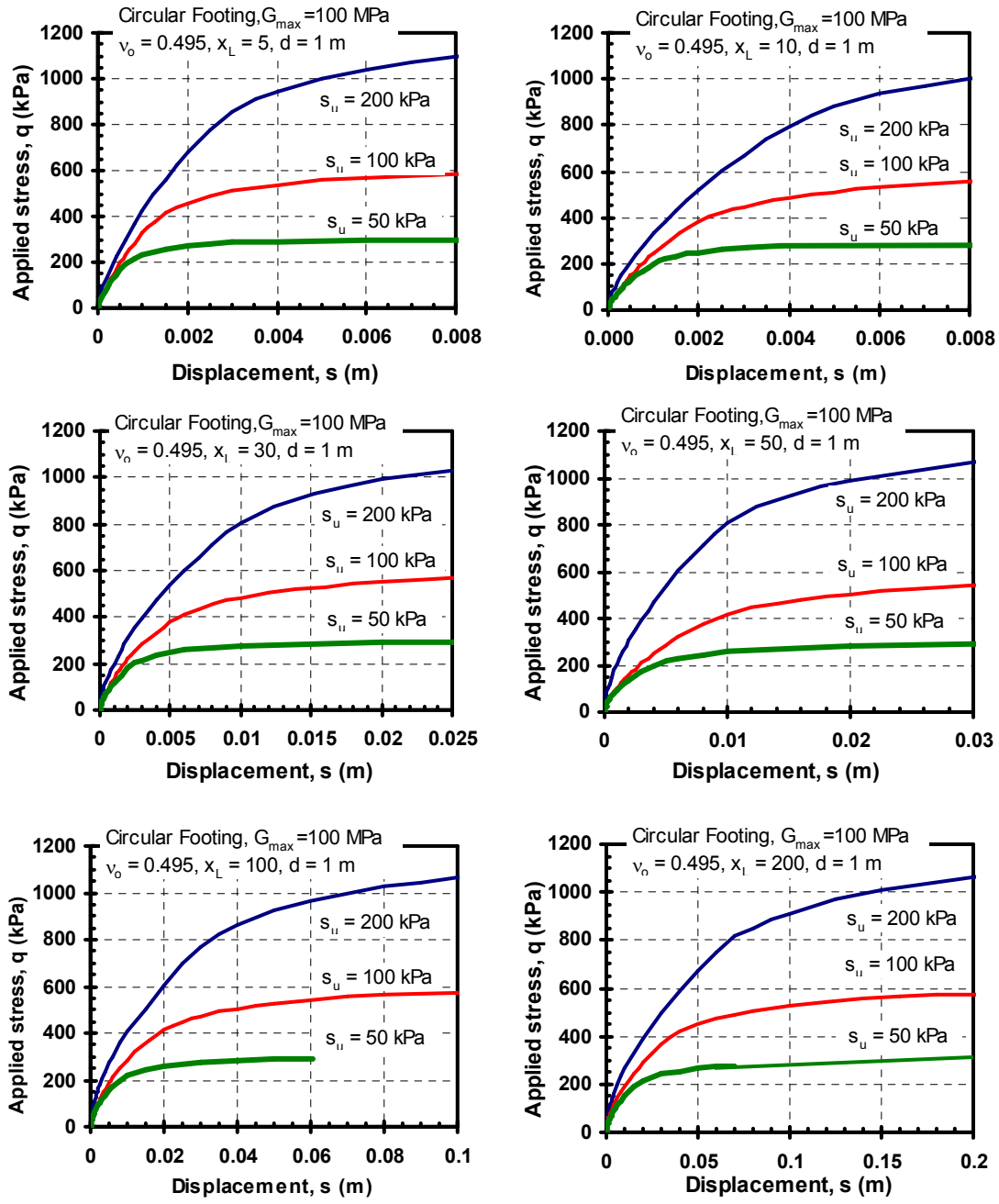


**Figure 7-4.** The effect of soil strength on the stress-displacement behavior of a circular footing resting on homogeneous clay (cases Ci-2-1-1-5 through Ci-2-2-1-200)

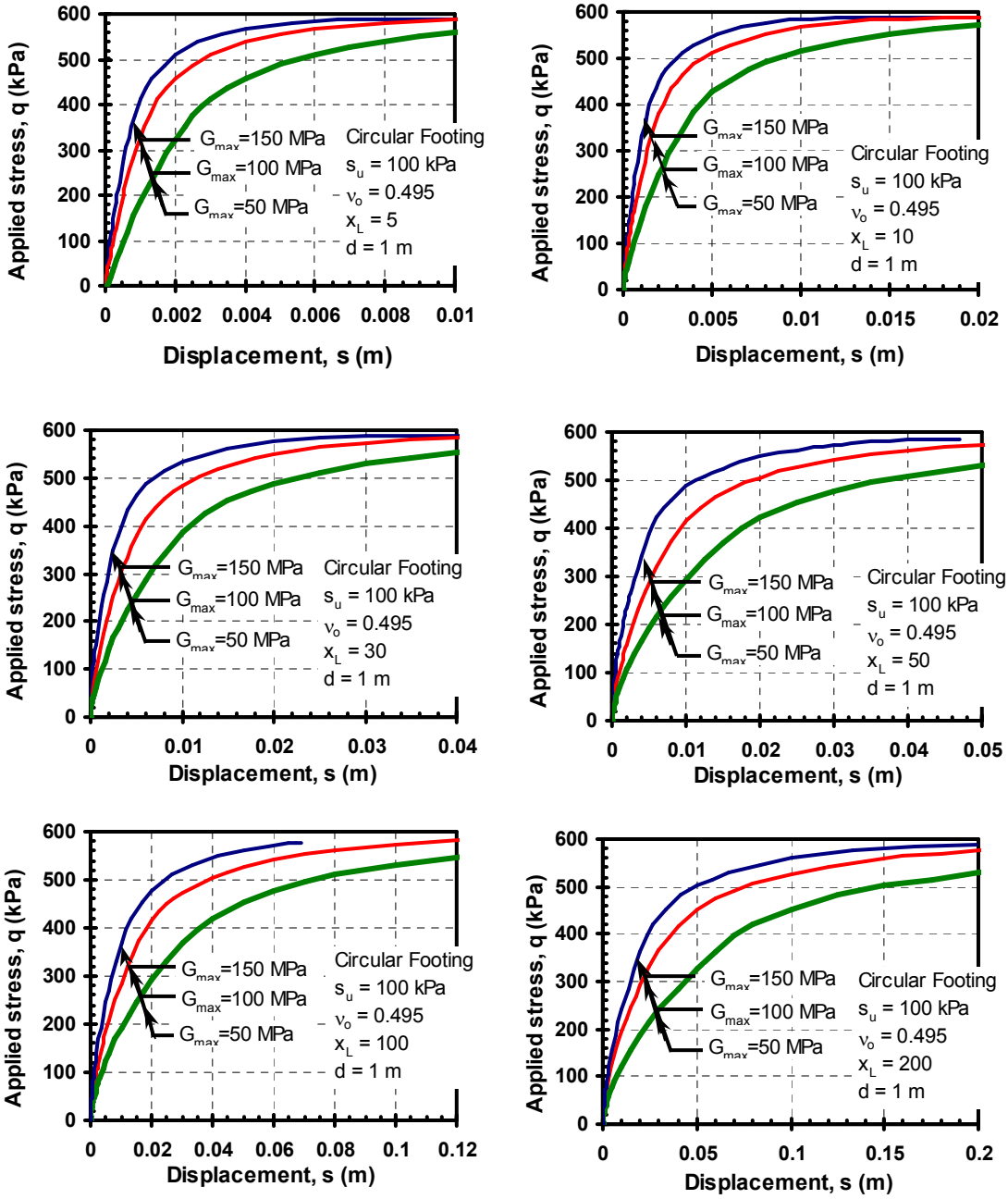


**Figure 7-5.** The effect of small-strain stiffness on the stress-displacement behavior of a circular footing resting on homogeneous clay (cases Ci-2-2-1-5 through Ci-2-2-2-200)

Based on the numerical simulations, the stress-displacement response of vertically loaded circular footings under undrained conditions depends on footing diameter d, undrained shear strength $s_u$, small-strain stiffness $G_{max}$, and degree of non-linearity defined by the normalized limiting strain $x_L$. As mentioned earlier, one objective of this study is to scale up the behavior of a single soil element to the overall behavior of a footing. Therefore, normalizing the results can help minimize the factors influencing the stress-displacement response. A new normalization scheme is introduced and verified in the coming section.

## 7.4 Proposed stress-displacement normalization scheme

Load-displacement curves for shallow or deep foundations are typically plotted as applied load (Q) versus the displacement (s), or alternatively as applied stress (q) versus pseudo-strain (s/B), where s is the displacement of the foundation and B is the foundation width or its equivalent diameter (e.g., Berardi and Lancellota, 1994; Briaud and Jeanjean, 1994; Hight and Higgins, 1995; Consoli et al., 1998; Atkinson, 2000). Although this normalization scheme is simple and convenient to use, it is merely an approximate "averaged" strain in definition. It was, therefore, decided to normalize the data using a new scheme that accounts for soil elastic properties (shear modulus, G and Poisson's ratio, ν), bearing capacity ($Q_{ult}$ or $q_{ult}$), and footing diameter or width (B). Accordingly, the following normalization, which accounts for these factors, is used:

$$X = s/s_r \quad \text{(7-1-a)}$$

$$Y = q/q_{ult} \quad \text{(7-1-b)}$$

$$s_r = q_{ult}/K_i \quad \text{(7-1-c)}$$

where X is the normalized displacement, s is the vertical displacement, $s_r$ is a vertical reference displacement (function of soil elastic properties, bearing capacity, and footing width), Y is the normalized stress, q is the vertical applied stress, $q_{ult}$ is the peak stress (i.e. bearing capacity), and $K_i$ is the initial stiffness of the soil-footing system. The definitions of the various parameters used in the analysis are illustrated in Figure 7-6-a and 7-6-b.

This type of normalization scheme has been previously used for developing non-linear modulus degradation formulae based on fitting laboratory stress-strain data (e.g. Hardin and Drnevich, 1972; Puzrin and Burland, 1996).

As discussed in Chapter 2, bearing capacity is not particularly well defined from actual footing load tests. It was therefore decided to compute the peak stress or bearing capacity $q_{ult}$ as the hyperbolic extrapolated asymptote, for consistency. The initial stiffness of the footing-soil system is calculated from the theory of elasticity according to:

$$K_i = \frac{q_{ult}}{s_r} = \frac{E_{\max}}{B \cdot I} \quad \text{.....(7-2)}$$

where B is the foundation width (or equivalent diameter for non-circular footings), $E_{max}$ $\left[= 2 \cdot G_{\max} \cdot (1+\nu)\right]$ is the maximum Young's modulus, I is an influence factor depending on the footing rigidity, layer thickness, and Poisson's ratio. For example, I=1 for a flexible circular footing resting on a semi-infinite elastic medium with homogeneous modulus having $\nu = 0$. Therefore, the reference displacement is defined by:

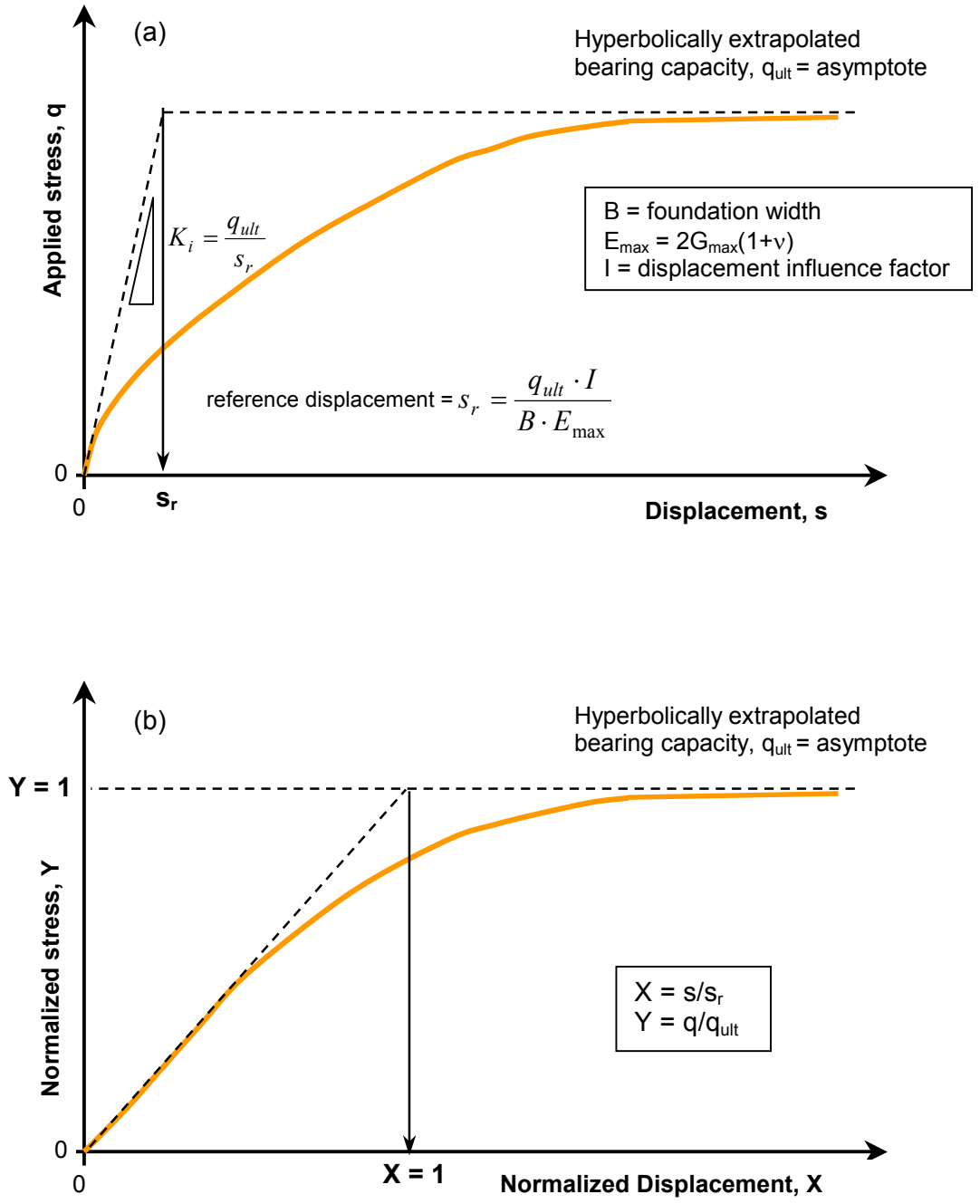


**Figure 7-6.** Illustration of parameters used in the normalization of foundation load-displacement response

$$s_r = \frac{q_{ult} \cdot I \cdot B}{E_{\max}} \quad \text{.....(7-3)}$$

The displacement influence factors for rigid circular shallow footings resting on a deep homogeneous soil profile, under both undrained and drained conditions, are computed according to the solutions presented in Chapter 3. The factors for rigid circular footings are 0.60 and 0.75 for undrained ($\nu$ = 0.5) and drained ($\nu$ = 0.2) cases, respectively, according to Equations 3-13 and 3-15. For strip footings, the influence factors are 1.31 and 1.90 for undrained ($\nu$ = 0.5) and drained ($\nu$ = 0.2) analyses, respectively, according to Milovic (1993).

## 7.5 Verification of the proposed normalization scheme

The effect of using the proposed normalization scheme on the representation of the load-displacement response under circular footings is investigated in this section.

### *7.5.1 Circular footing resting on linear elastic-plastic medium*

It was decided to simulate the behavior of circular rigid footings resting on a linear elastic-plastic Drucker-Prager medium. In these simulations, the footing width, soil undrained shear strength and shear modulus were varied. Both simulated "raw" and normalized stress-displacement response curves are plotted for comparison.

Table 7-2 shows the input soil properties and footing dimensions used in the study. In simulations 1 through 7, a 1-m diameter footing resting on a soil having undrained shear strength $s_u$ of 20 kPa is used. The equivalent shear modulus G is varied between 0.2 MPa

and 100 MPa. In simulation 8, a 2-m diameter footing resting on a soil with undrained shear strength $s_u$ and equivalent shear modulus G of 100 kPa and 10 MPa, respectively, is modeled. All simulations are undrained ($\nu_u = 0.495$). Figure 7-7-a shows the stress-displacement results for simulations 1 through 8. The large variability in the stress-displacement response is obvious.

**Table 7-2.** Soil properties and footing dimensions used in the analysis of circular rigid footings resting on homogeneous Drucker-Prager linear elastic-plastic model

| Simulation case number | Footing diameter, d (m) | Undrained shear Strength, $s_u$ (kPa) | Shear modulus, G (MPa) | Rigidity index $G/s_u$ |
|---|---|---|---|---|
| 1 | 1 | 20 | 0.2 | 10 |
| 2 | 1 | 20 | 0.4 | 20 |
| 3 | 1 | 20 | 1 | 50 |
| 4 | 1 | 20 | 2 | 100 |
| 5 | 1 | 20 | 10 | 500 |
| 6 | 1 | 20 | 20 | 1000 |
| 7 | 1 | 40 | 5 | 125 |
| 8 | 2 | 100 | 10 | 100 |

The simulation results are re-plotted in normalized form as $q/q_{ult}$ versus s/d shown in Figure 7-7-b. The normalization of the vertical applied stress q by the bearing capacity $q_{ult}$ caused all the curves to flatten to a common $q/q_{ult}$ ratio approaching unity at large displacements. However, there are still significant differences in the normalized displacement curves using the pseudo-strain parameter, s/d. Figure 7-7-c shows the fully normalized results plotted as $q/q_{ult}$ versus $s/s_r$. The proposed normalization scheme causes all the stress-displacement curves to collapse onto a single line, regardless of soil properties and/or footing dimensions. Thus, the procedure appears reasonable as a means of dimensional analysis to allow comparisons of results and rational normalization.

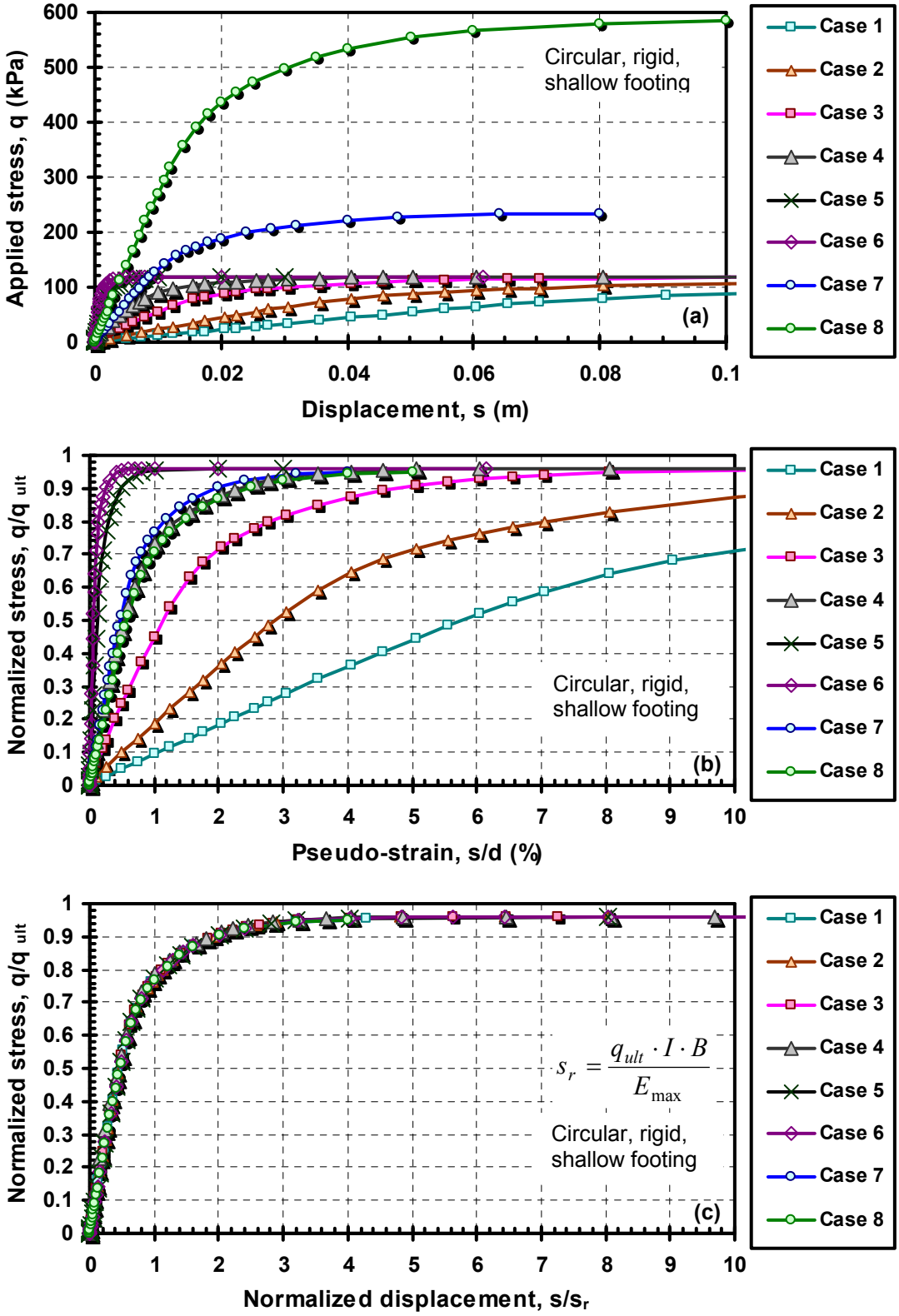


**Figure 7-7.** FLAC simulations of circular footing for undrained cases on linear elastic-plastic clay as given in Table 7-2: a) "raw" q versus s plot, b) $q/q_{ult}$ versus pseudo-strain s/d plot, c) Normalized $q/q_{ult}$ versus $s/s_r$ plot

### *7.5.2 Circular footing resting on non-linear elastic-plastic medium*

It has been shown that there is a unique stress-displacement relationship for linear elastic-plastic soil models. In this section, the proposed normalization scheme is applied to the simulated stress-displacement responses presented in Figures 7-3 through 7-5. The normalized stress-displacement plots are presented in Figures 7-8 through 7-10.

Figure 7-8 demonstrates how the proposed normalization scheme makes the stress-displacement response independent of the footing size represented by the diameter. Similarly, Figure 7-9 and 7-10 show that the normalized stress-displacement response is independent of the value of the undrained shear strength and the small-strain stiffness $G_{max}$, respectively. Accordingly, normalized stress-displacement response become only a function of the normalized limiting strain $x_L$.

Figure 7-11-a summarizes all the normalized stress-displacement response plots from the vertical loading for a smooth, circular footings resting on a homogeneous soil layer, under undrained loading conditions. The curves are only a function of the normalized limiting strain $x_L$. Normalized stress-strain curves depicting the behavior of a single element are shown in Figure 7-11-b for different values of the normalized limiting strain $x_L$. Parallelism between the overall stress-displacement behavior of a footing and the stress-strain response of a single soil element is noticed and is further investigated in Chapter 9.

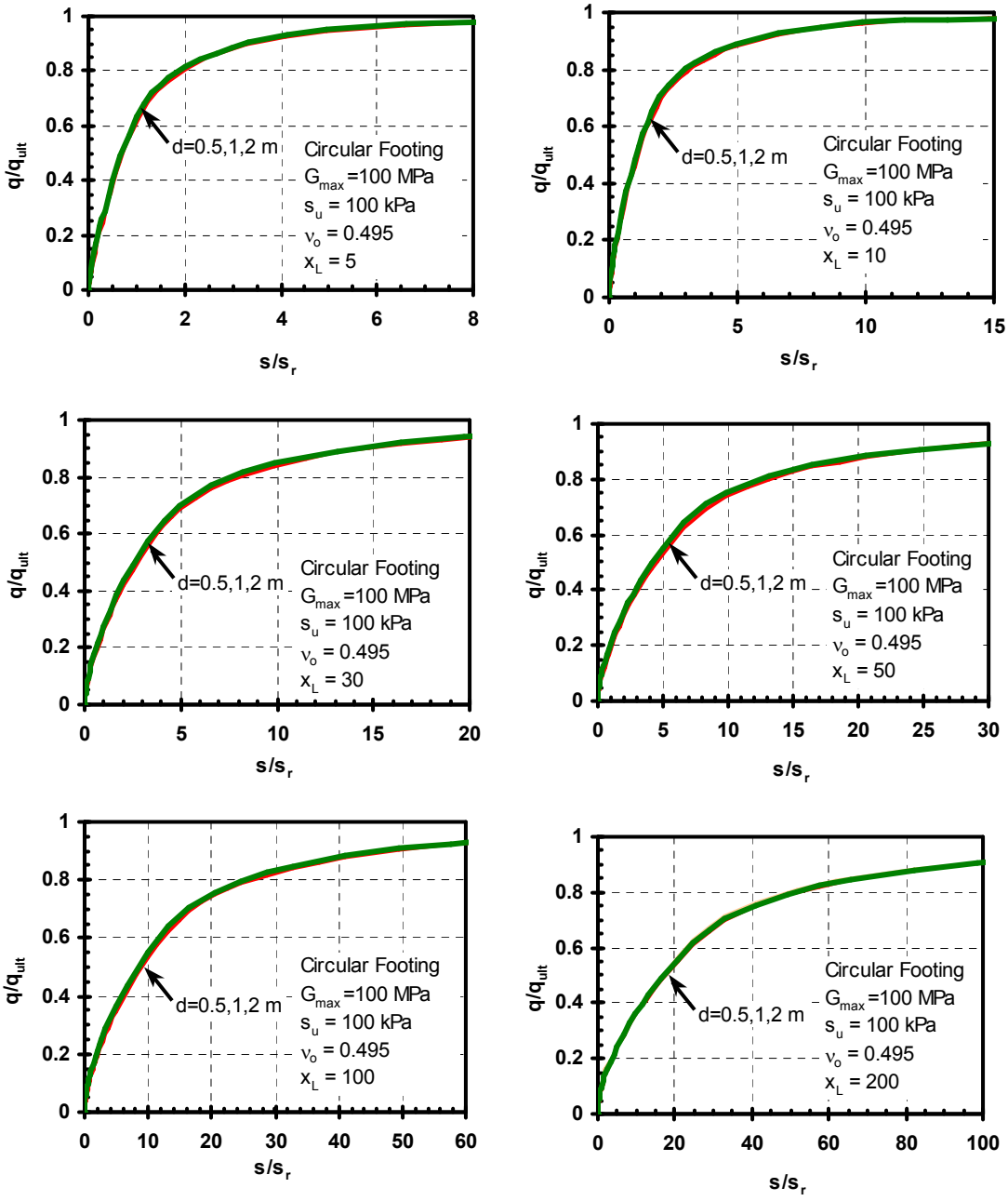


**Figure 7-8.** Stress-displacement curves underneath the centerline of a circular footing on homogeneous clay (cases Ci-1-1-1-5 through Ci-3-1-1-200) plotted in normalized form (cases varying the footing size)

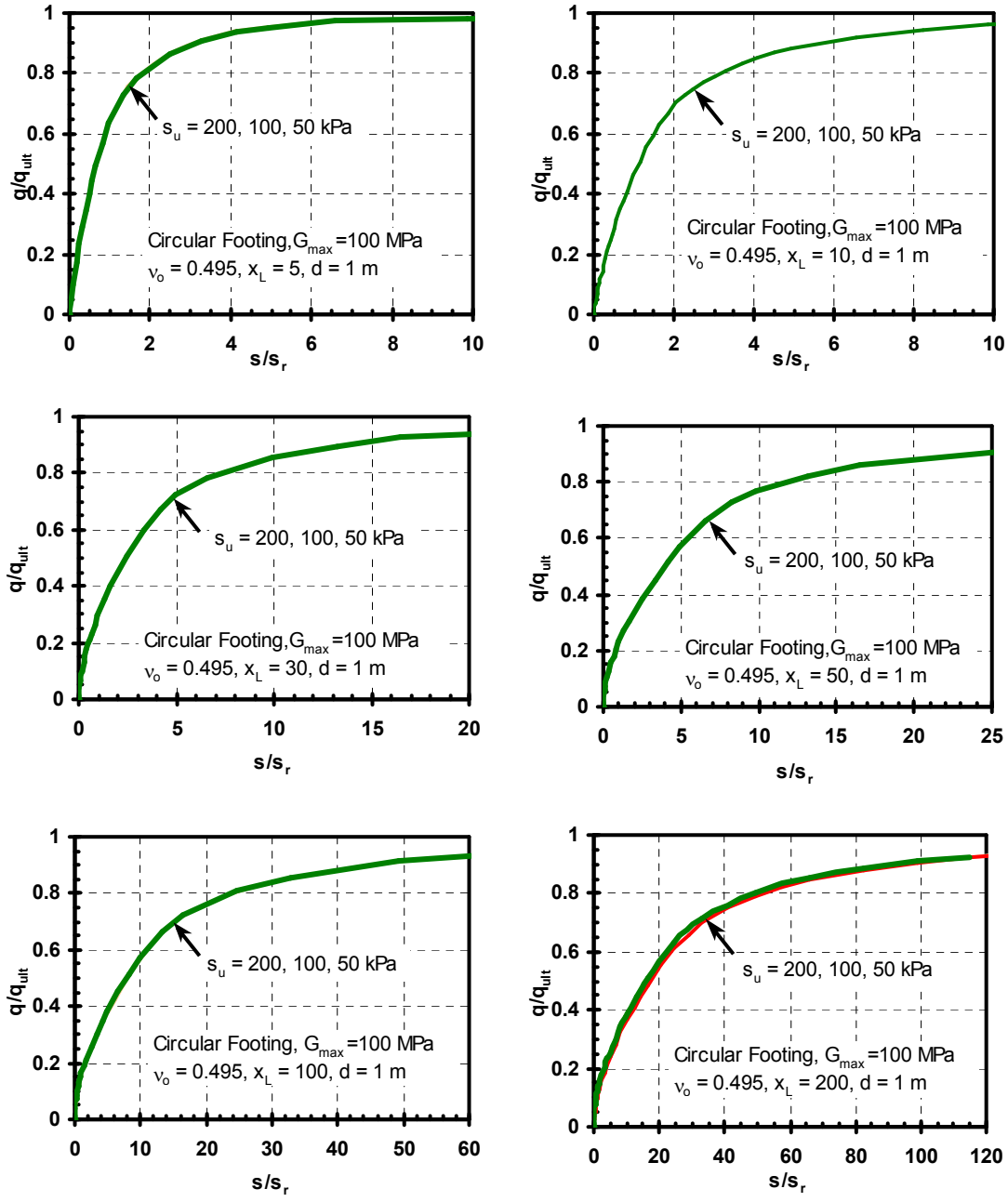


**Figure 7-9.** Stress-displacement curves underneath the centerline of a circular footing on homogeneous clay (cases Ci-2-1-1-5 through Ci-2-2-1-200) plotted in normalized form (cases varying the undrained shear strength)

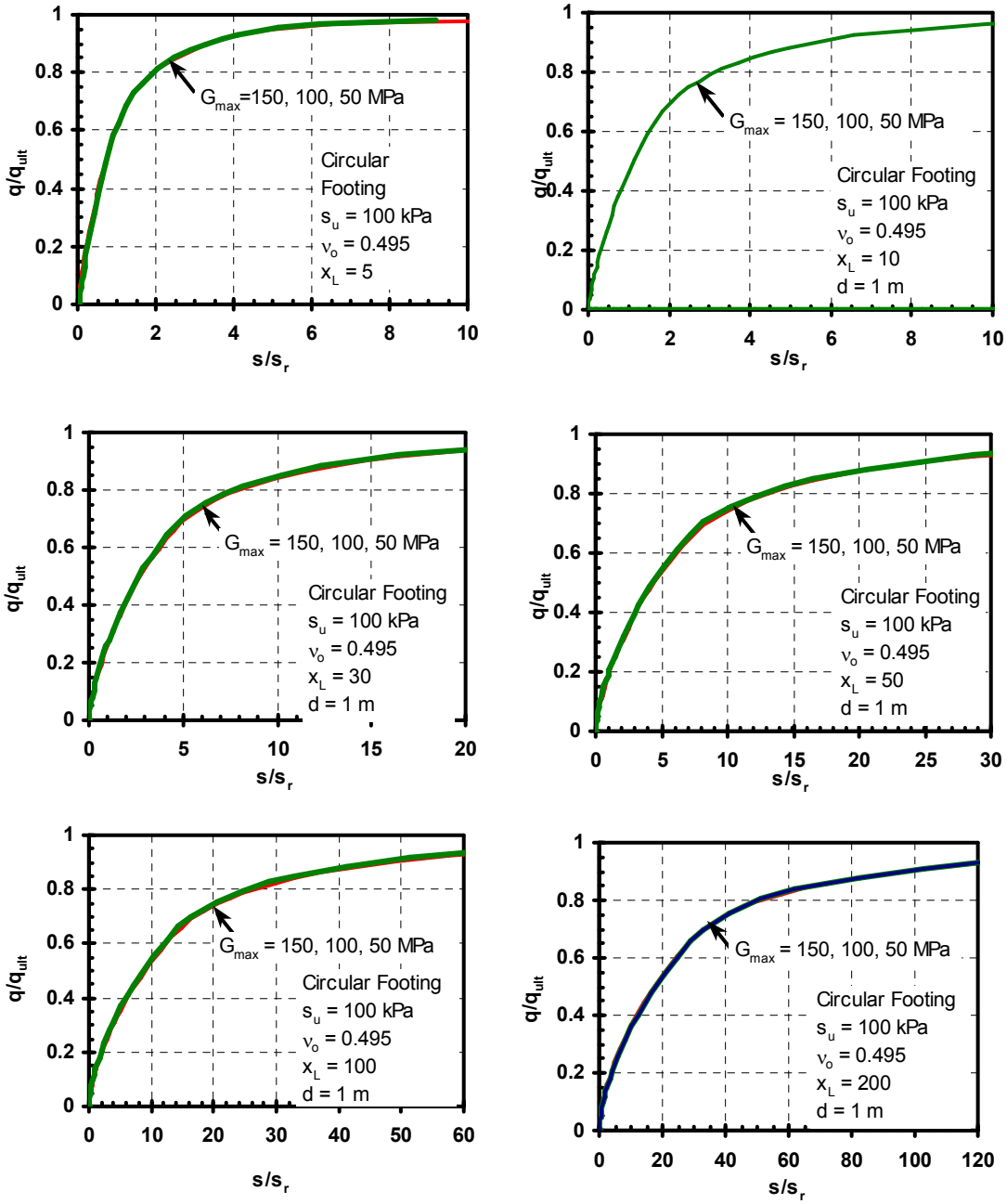


**Figure 7-10.** Stress-displacement curves underneath the centerline of a circular footing on homogeneous clay (cases Ci-2-2-1-5 through Ci-2-2-2-200) plotted in normalized form (cases varying the small-strain stiffness)

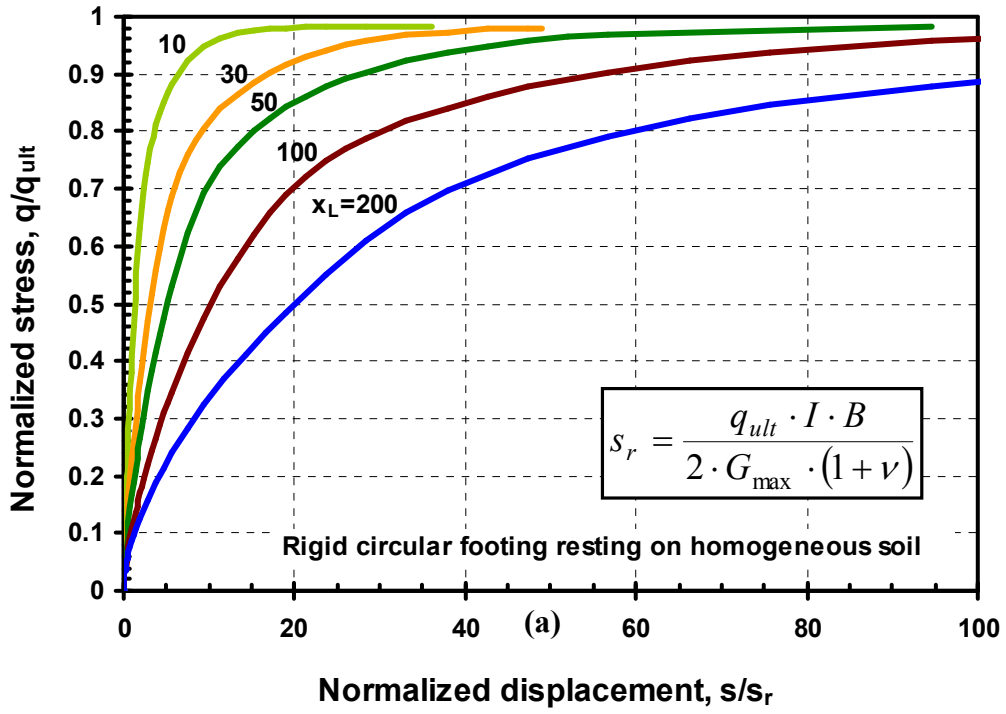


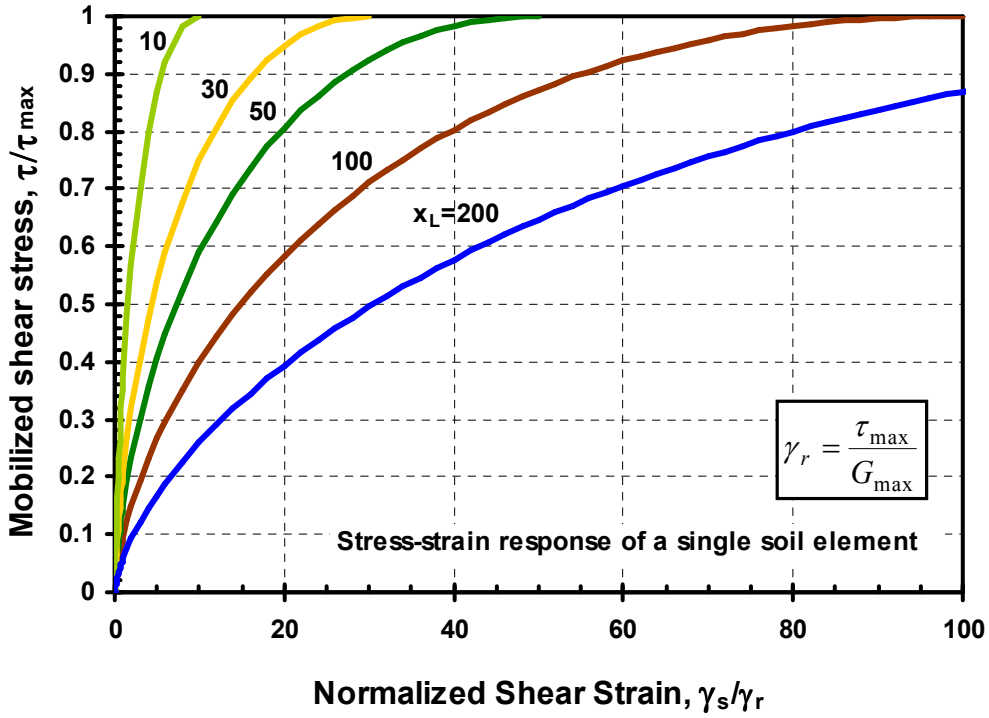


**(b)**

**Figure 7-11.** a) Normalized stress-displacement curves for a circular, rigid, footing resting on a homogenous non-linear elastic plastic clay layer for undrained loading conditions; b) normalized stress-strain response for a single soil element

### *7.5.3 Strip/continuous footings resting on non-linear elastic-plastic medium*

The analysis of a shallow strip footing resting on a soil layer can be solved as a plane strain problem when the footing width is considerably smaller compared to its length (B/L < 0.2). A rigid strip footing resting on a thick clay layer that is fully saturated ($\gamma_{total}$ = 18 kN/m$^3$, $\gamma_{sub}$ = 8 kN/m$^3$) is now simulated using the LOGNEP model to obtain the load-displacement behavior under undrained loading conditions ($\nu_u$ = 0.495). Due to the symmetric nature of the problem, only half the footing and underlying soil are input. Rollers that restrict the horizontal movement were positioned at the centerline and vertical boundary. Hinges, preventing vertical and horizontal motion, were placed at the bottom boundary. A smooth footing-soil interface was replicated by imposing no restraint on the horizontal movement at the nodal contacts between the footing and underlying soil layer. The boundary conditions are shown in Figure 7-12. Applying uniform vertical displacements on a portion of the upper horizontal boundary simulates a rigid footing. The average stress beneath the footing is calculated as the summation of vertical forces at the nodes at the base of the footing, divided by the footing width. The footing displacement is taken equal to the vertical displacement applied to the footing. A non-uniform grid was chosen for the footing analysis to use a smaller number of elements, decreasing the computer running time for each simulation. The smallest size mesh to overcome mesh dependency consisted of 4225 elements (65 x 65 biased mesh), shown in Figure 7-12.

The aim of the study is to find a unique load-displacement relationship for the non-linear behavior of the strip footing. First, a number of runs were performed where the footing

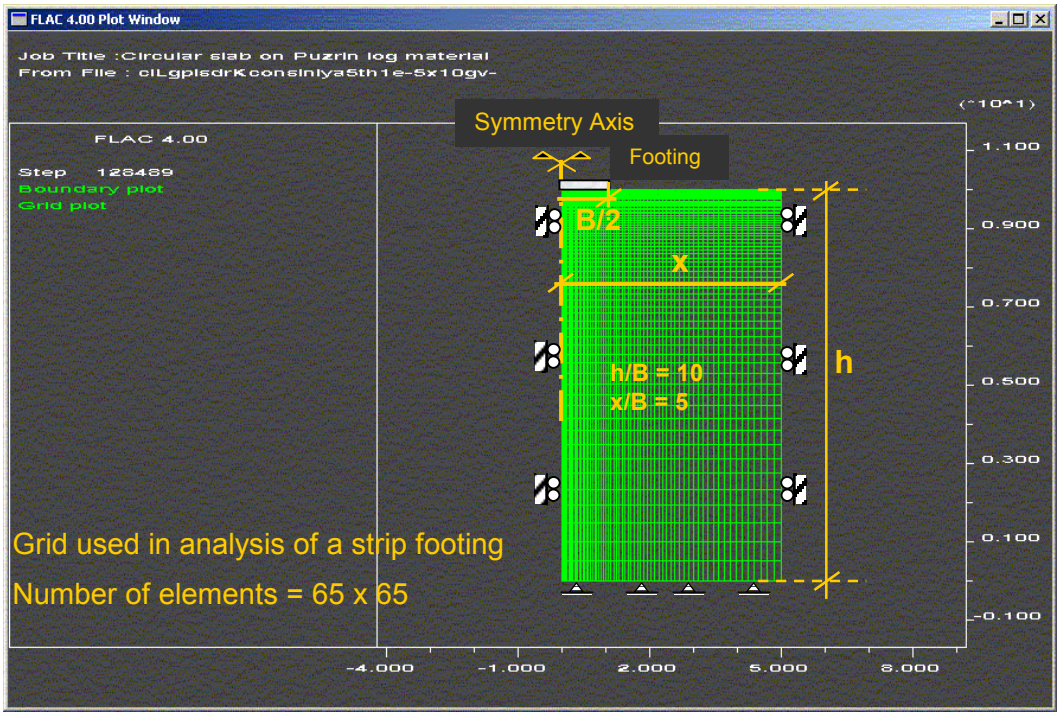


**Figure 7-12.** Finite difference grid for modeling a rigid strip footing resting on a homogeneous clay layer

width B, maximum shear modulus $G_{max}$, and undrained shear strength $s_u$ were varied, maintaining the normalized limiting strain $x_L$ constant to verify the suggested normalization produces results are dependent only on the normalized limiting strain $x_L$. Simulations were performed for $x_L$ values of 10 and 50.

The "raw" simulated stress-displacement curves are presented in Figure 7-13-a and 7-13-b. The bearing capacity factor $N_c$ computed from the analyses is 5.14, which is in excellent agreement with the Prandtl's wedge solution ($N_c$ = 5.14) that is derived in a Mohr-Coulomb failure criterion. The load-displacement curves are dependent on footing size B, maximum shear modulus $G_{max}$, and undrained shear strength $s_u$. However, when results are properly normalized, they all collapse onto a single line representative of a

normalized limiting strain $x_L$ = 10, as shown in Figures 7-13-c and 7-13-d. Normalized stress-displacement curves for a plethora of normalized limiting strains $x_L$ (10, 30, 50, 100, 200) are presented in Figure 7-13. As the value of the normalized limiting strain increases, the stress-displacement behavior becomes more non-linear.

## 7.6 Summary and conclusions

The non-linear elastic plastic *LOGNEP* model was used to simulate the stress-displacement behavior under the centerline of vertically loaded rigid footings under undrained loading. The effects of varying the overburden stresses $\sigma_{vo}$ and at rest earth pressure coefficient $K_o$ on the stress-displacement behavior under footings were found to have small influences on the stress-displacement behavior of shallow footings. Factors controlling the footing behavior under vertical loading are: maximum shear modulus ($G_{max}$), Poisson's ratio ($\nu$), undrained shear strength ($s_u$), normalized limiting strain ($x_L$), footing shape (circular or strip), and footing width (d or B). A new normalization scheme is suggested that accounts for the effect of the soil properties ($G_{max}$, $\nu$, $s_u$) and footing size (d or B). Applied stresses are normalized with respect to the ultimate bearing capacity ($q_{ult}$) while displacements are normalized by a reference displacement ($s_r=q_{ult}/K_i$), where ($K_i$) is the initial stiffness of the footing-soil system. Subsequently, the normalized stress-displacement behavior is dependent on the footing shape and the normalized limiting strain $x_L$ that represents the degree of non-linearity in the soil stress-strain-strength behavior. Figures7-11-a and 7-14 show the unique stress-displacement relationship for circular and strip footings, respectively, under undrained conditions for differing degrees of non-linearity.

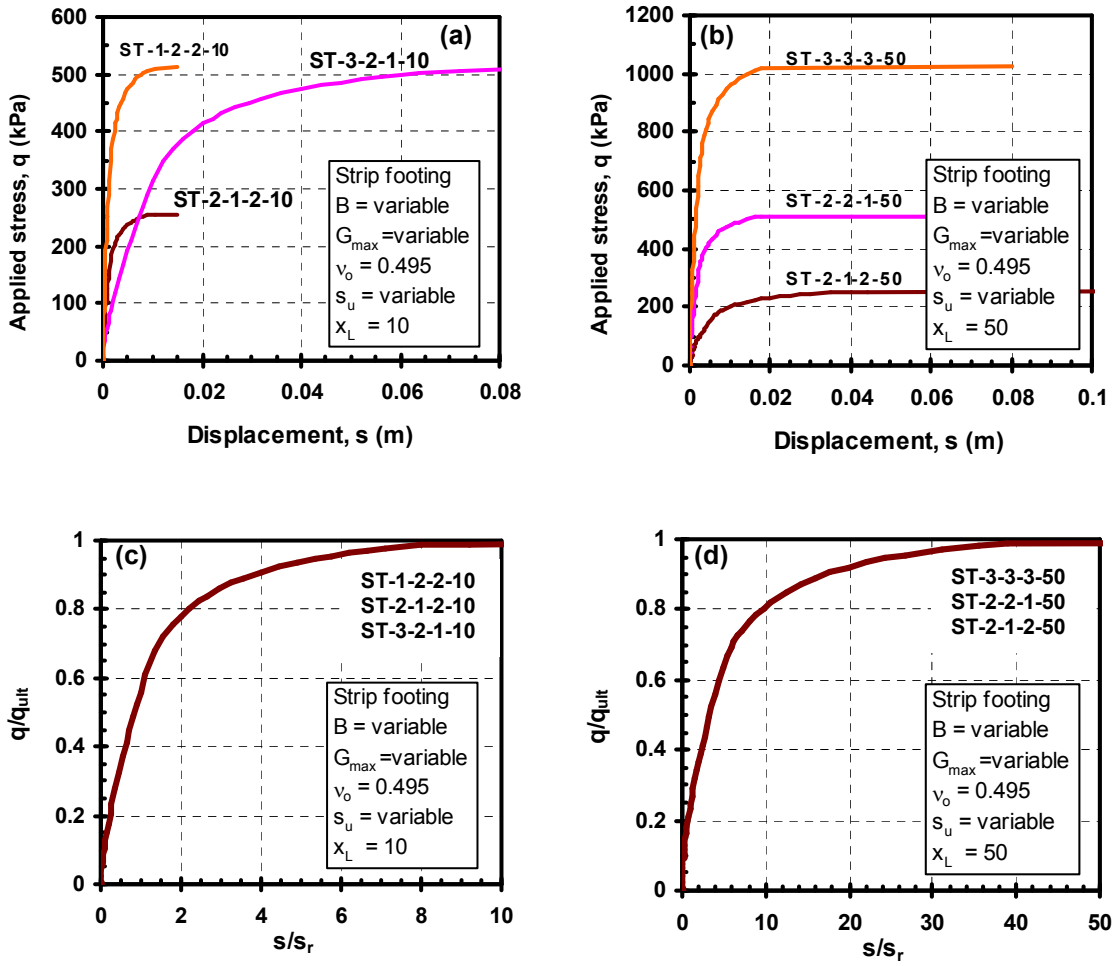


**Figure 7-13.** FLAC simulations of strip footing for undrained cases on non-linear elastic plastic LOGNEP clay: a) simulated "raw" stress-displacement curves for $x_L$ = 10; b) simulated "raw" stress-displacement curves for $x_L$ = 50; c) normalized stress-displacement curves for $x_L$ = 10; and d) normalized stress-displacement curves $x_L$ = 50

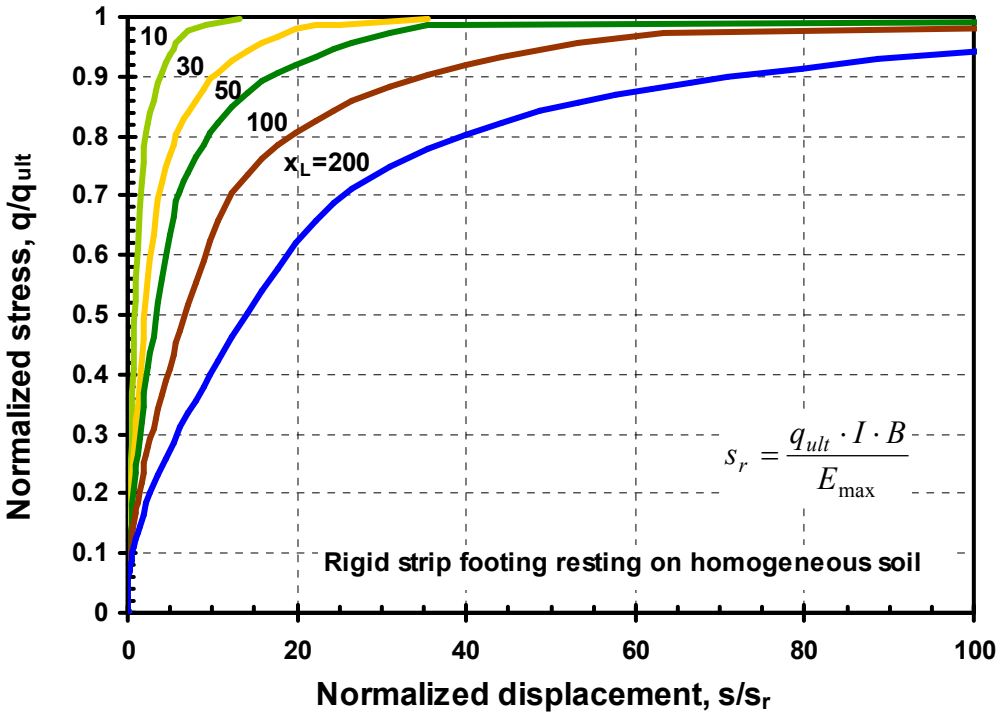


**Figure 7-14.** Normalized stress-displacement curves for a rigid, smooth, strip footing resting on a homogenous clay layer under undrained loading conditions

# CHAPTER VIII

# DRAINED LOADING OF RIGID SHALLOW FOUNDATIONS

## 8.1 Overview

The drained stress-displacement response of rigid shallow footings on homogeneous soil is numerically investigated using the logarithmic nonlinear elastic perfectly plastic *LOGNEP* model. Input soil parameters required by the model include: soil density $\rho$; initial shear modulus $G_{max}$ and normalized limiting strain $x_L$, Poisson's ratio $\nu$; and drained strength envelope defined by: cohesion intercept c', angle of internal friction $\phi$', and angle of dilation $\psi$. The analyses herein address shallow circular and strip footings situated at the ground surface, resting on purely cohesionless soil ($\phi$', c' = 0), with non-associated flow ($\psi = 0$).

## 8.2 Modeling the drained stress-displacement response of circular footings

First, the biased mesh used to model the undrained stress-displacement response beneath circular footings presented earlier in Chapters 6 and 7 was used for simulating drained stress-strain footing response. However, the solution was found not to be numerically stable. Similar observations were made by Erickson & Drescher (2002) and Yin et al. (2001) when modeling footings resting on purely cohesionless soils (c' = 0). The use of an unbiased mesh with square elements provided better stability for analyzing the footings. Due to symmetry, only half the problem is modeled. Several mesh sizes were

tested to ensure the solution is independent of mesh size. A 50x50 mesh, shown in Figure 8-1, has been used because it provided accurate results with minimum number of elements. The ratio of depth to rigid base to footing radius (h/R) is 10. The ratio of the distance between the symmetry line to the non-symmetry vertical boundary to footing radius (x/R) is 10. Horizontal displacements are restricted along both the symmetry and non-symmetry vertical boundaries. Both vertical and horizontal displacements are restricted at the horizontal lower boundary.

Vertical stresses were computed assuming the soil is fully saturated ($\gamma_{sat}$ = 18 kN/m$^3$). The at-rest earth pressure coefficient $K_o$ is assumed equal to unity. The footing is loaded by the incremental application of vertical displacements to the grid points representing the footing. Horizontal displacements are permitted at these nodal locations simulating a smooth footing/soil interface. The applied stress is computed as the average applied load divided by the area of the footing.

A series of simulations has been conducted to investigate parameters influencing the drained stress-displacement response of vertically loaded footings. In the numerical study, the footing shape is varied (circular and strip). The following parameters have been varied to explore their effect on footing response: footing width B, small-strain shear modulus $G_{max}$, angle of internal friction $\phi$', and normalized limiting strain $x_L$. Only purely cohesionless materials (c' = 0) with non-associated flow (angle of dilation $\psi = 0^o$) are considered in this study. Simulations are denoted using a five part alphanumeric acronyms (similar to Table 7-1). The first letter of the test name indicates the footing

shape: circular Ci or strip St. Subsequent numbers denote the footing with B, angle of internal friction $\phi$', the maximum shear modulus $G_{max}$, and the normalized limiting strain $x_L$, respectively. For example simulation Ci-1-2-2-10 is of a 0.5-m diameter footing, angle of internal friction $\phi$' of 30$^o$, small-strain shear modulus $G_{max}$ of 50 MPa, and normalized limiting strain $x_L$ of 10. Soil properties and footing dimensions used in the simulations are listed in Table 8-1.

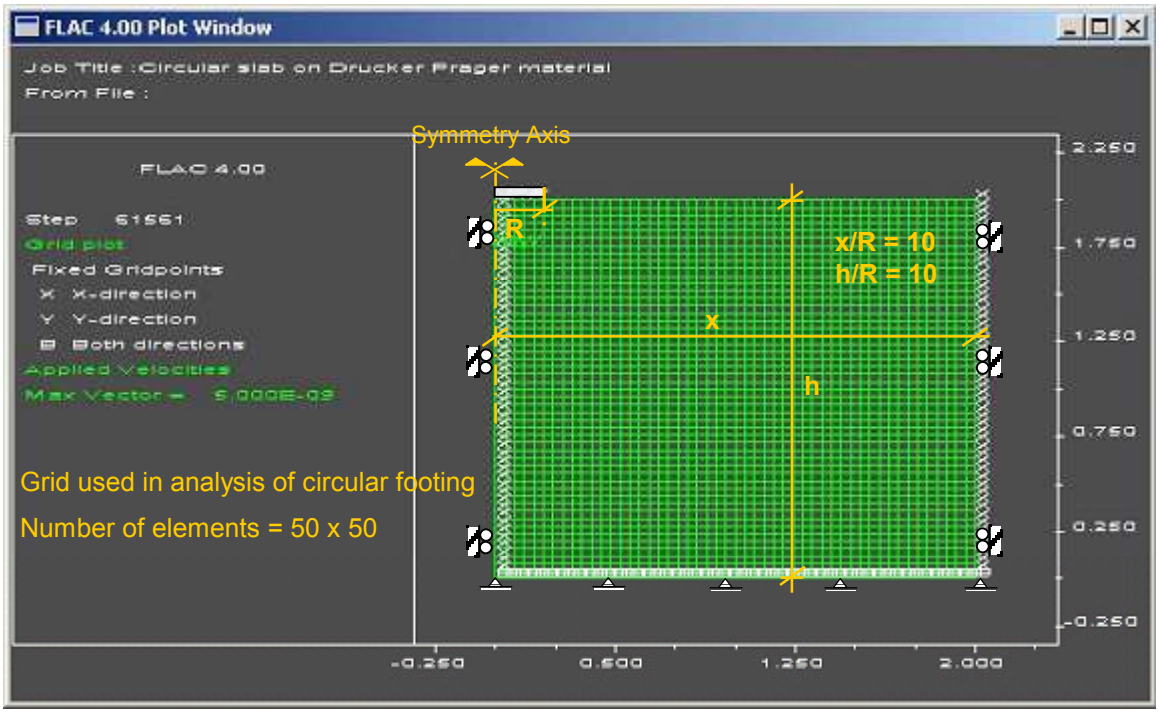


**Figure 8-1.** Uniform 50x50 square element mesh for modeling shallow footings under drained loading conditions

For purely frictional materials, very shallow soil elements behave linearly elastic up to failure, irrespective of the value of the normalized limiting strain $x_L$ due to the very low effective confining stresses. This problem can be overcome by applying an overburden

surcharge stress to the ground surface (e.g. Lehane and Fahey, 2002). Alternatively, assigning the soil a cohesion intercept (c'> 0) would do likewise (Erickson and Drescher, 2002). However, it is safer from a design standpoint to neglect the contributions of cohesion intercept and surcharge stress to footing stability. Alternatively, the problem has been solved by neglecting the threshold strain when modeling surface footings resting on purely cohesionless soil ($\phi$', c'= 0). Other researchers modeling the non-linear stress-strain response of footings did not take the threshold strain into consideration e.g. Fahey and Carter (1993); Lee and Salgado (2002); and Viana da Fonseca & Sousa (2002).

### *8.2.1 Normalized drained stress-displacement response of circular footings*

Figure 8-2-a shows the stress-displacement response under a circular footing resting on a cohesionless soil for $\phi' = 30^o$ and $x_L = 30$. Simulations have been performed for three values of the small-strain shear modulus $G_{max}$= 50, 100, 200 MPa. Three footing diameters have been used 0.5-m, 1.0-m, and 2.0-m. Similarly, Figures 8-2-b and 8-2-c show the stress-displacement response for ($\phi' = 35^o$, $x_L = 50$) and ($\phi' = 40^o$, $x_L = 100$), respectively. As expected, the stress-displacement response in all cases is dependent on the small-strain stiffness $G_{max}$ and footing diameter d. By normalizing footing displacement by a reference displacement $s/s_r$ and applied stress by bearing capacity $q/q_{ult}$, all curves collapse onto a single line as shown in Figures 8-3-a through 8-3-c.

**Table 8-1.** Notations for naming footing simulations using *LOGNEP* model

| Parameter | Notation | Value/Meaning |
|---|---|---|
| Footing shape | Ci | circular |
| | St | strip |
| Footing width, B | 1 | 0.5 m |
| | 2 | 1 m |
| | 3 | 2 m |
| Angle of internal friction, $\phi$' | 1 | $30^o$ |
| | 2 | $35^o$ |
| | 3 | $40^o$ |
| Maximum shear modulus, $G_{max}$ | 1 | 50 MPa |
| | 2 | 100 MPa |
| | 3 | 200 MPa |
| Normalized limiting strain, $x_L$ | 10 | 10 |
| | 30 | 30 |
| | 50 | 50 |
| | 100 | 100 |

**Notes:**

1. Acronym defining case number given by alphanumerical code: Ci/St-B-$\phi$'-$G_{max}$-$x_L$
2. Angle of dilation $\psi = 0^o$
3. Cohesion intercept c' = 0

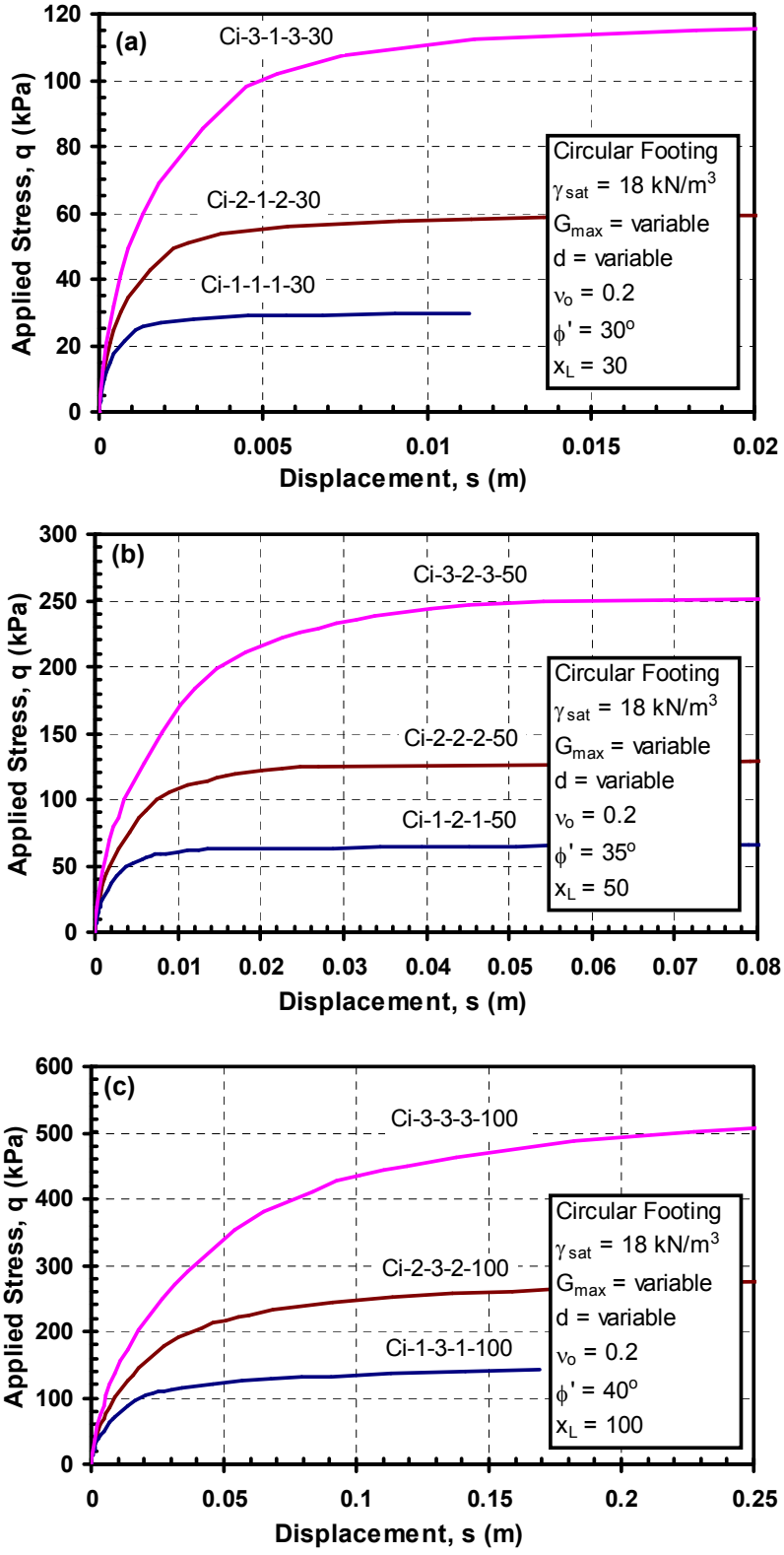


**Figure 8-2.** Simulated stress-displacement curves representing vertical displacements beneath circular rigid footings under drained loading conditions: a) $\phi' = 30^o$, $x_L = 30$; c) $\phi' = 35^o$, $x_L = 50$; d) $\phi' = 40^o$, $x_L = 100$.

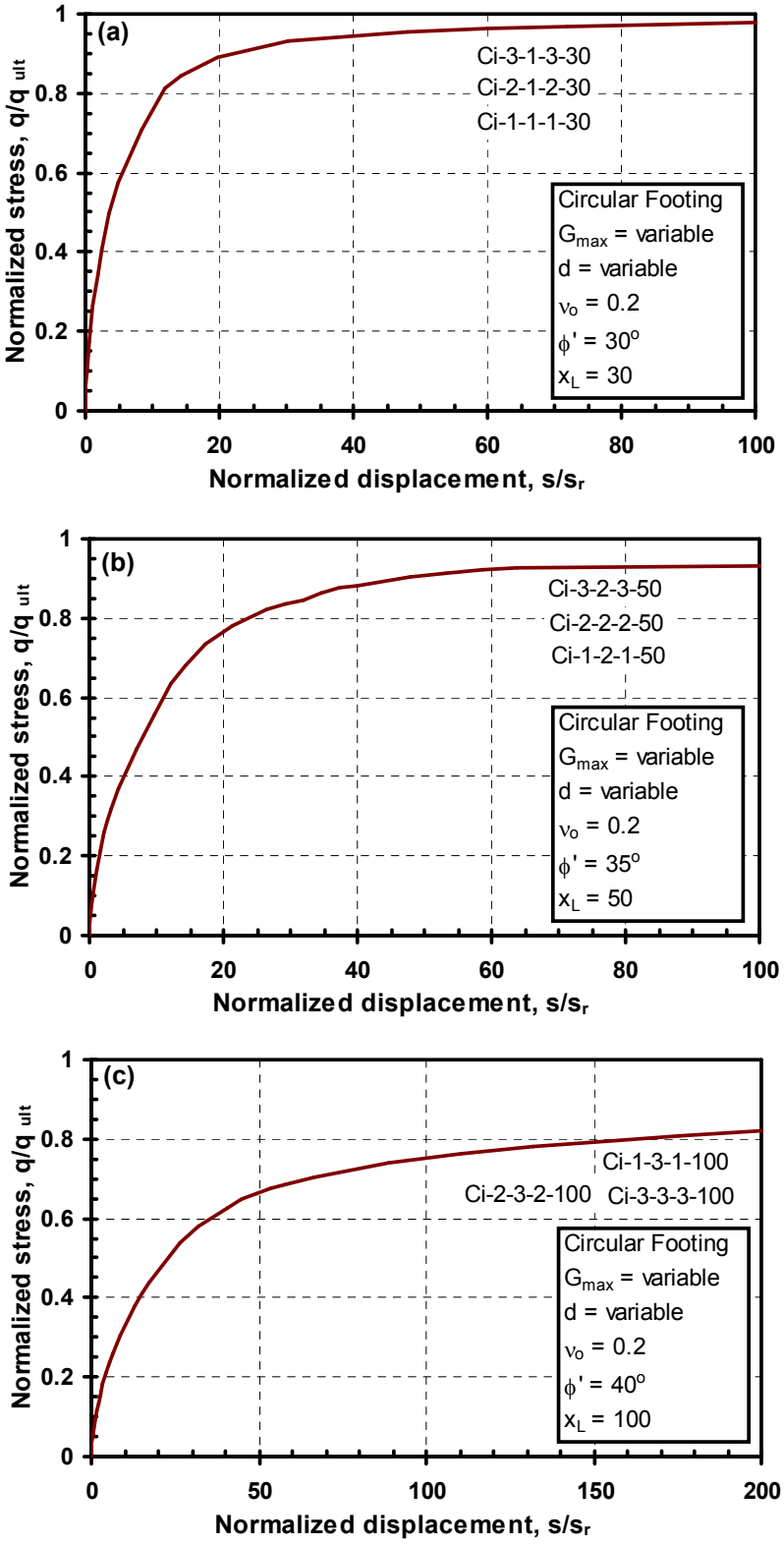


**Figure 8-3.** Normalized simulated stress-displacement curves representing vertical displacements beneath circular rigid footings under drained loading conditions: a) $\phi' = 30^o$, $x_L = 30$; b) $\phi' = 35^o$, $x_L = 50$; c) $\phi' = 40^o$, $x_L = 100$.

### *8.2.2 Bearing capacity factors for circular surface footings*

The bearing capacity of a vertically-loaded foundation resting on a homogeneous half-space is classically determined using the Terzaghi (1943) superposition method:

$$q_{ult} = cN_c + \frac{1}{2}B\gamma^* N_\gamma + \sigma'_{vo}N_q \quad \text{.....(8-1)}$$

where $q_{ult}$ = ultimate stress beneath the footing, c = effective cohesion intercept for drained behavior (c') or the undrained shear strength ($c_u = s_u$) for undrained loading, B = foundation width, $\gamma^*$= effective or total unit weight depending on the groundwater level, $\sigma_{vo}'$ is the effective overburden stress at the foundation level, and $N_c$, $N_\gamma$, $N_q$ are dimensionless bearing capacity factors.

An accurate assessment of the bearing capacity factors $N_c$, $N_q$, and $N_\gamma$ is essential for the correct evaluation of bearing capacity. In general, there is relatively good agreement between the different methods for calculating $N_c$ and $N_q$, while the variation is much higher for the factor $N_\gamma$ (Vesić, 1973; Chen, 1975; Chen and McCarron, 1991). A shallow footing resting directly on the surface of cohesionless soil (c'=0) has essentially zero surface surcharge ($\sigma_{vo}' = 0$). Therefore, equation (8-1) reduces simply to (e.g. Ingra and Baecher, 1983):

$$q_{ult} = \frac{1}{2}\cdot B\cdot\gamma^*\cdot N_\gamma \cdot \zeta_{\gamma s} \quad \text{.....(8-2)}$$

where $\zeta_{\gamma s}$ is footing shape correction factor (refer to Appendix E). The bearing capacity factors $N_\gamma$ for the different friction angles are backfigured from the current numerical analyses via Equation 8-2. The computed values of $N_\gamma$ are compared to values reported in the literature in Table 8-2. Present computations provide results close to those reported previously in the literature. Erickson and Drescher (2002) numerically computed the bearing capacity factor $N_\gamma$ for different values of $\phi'$ and $\psi$. Results reported in Table 8-2 are for a non-associated flow with $\psi = 0$. It should be noted that Erickson & Drescher (2002) mention that their reported factors may have been overestimated because of the grid coarseness. Using a finer mesh, Erickson & Drescher (2002) found a 10% drop in $N_\gamma$ for $\phi' = \psi = 35^o$.

**Table 8-2.** Summary of $N_\gamma$ values for smooth circular footings for non-associative flow

| $\phi'$ ($^o$) | This research | Erickson & Drescher (2002) | Bolton & Lau (1993) |
|---|---|---|---|
| 20 | 1.5 | 1.5 | 1.3 |
| 30 | 6.7 | ---- | 7.1 |
| 35 | 15.0 | 17.0 | 18.2 |
| 40 | 36.5 | 43.0 | 51.0 |

**Notes:**
1. Angle of dilation $\psi = 0^o$
2. Cohesion intercept c' = 0

### *8.2.3 Generalized drained stress-displacement response of circular footings*

A series of simulations has been performed to investigate the effect of varying the normalized limiting strain $x_L$ on the footing stress-displacement response for ($\phi' = 30^o$, $35^o$, and $40^o$). The simulations have been conducted for $x_L$ = 10, 30, 50, and 100. The footing width and small-strain stiffness $G_{max}$ have been maintained constant at 1-m and 100 MPa, respectively. The normalized stress-displacement footing responses, for $\phi' = 30^o$, $35^o$, and $40^o$, are presented in Figures 8-4, 8-5, and 8-6, respectively.

The stress-displacement curves show some fluctuations that become more obvious for higher friction angles $\phi$'. The curves presented in this chapter have been adjusted for minor instabilities. Yin et al. (2001) noticed similar behavior when modeling strip footing resting on soil with non-associative flow ($\psi = 0$). De Borst and Vermeer (1984) noted numerical instabilities occurred when modeling a footing resting on soil with non-associative flow ($\psi < \phi$'). The instabilities increased as the flow became more non-associative with the difference between the angle of internal friction $\phi$' and $\psi$ increasing. Solutions for the case of $\psi = 0^o$ could not be obtained. The FLAC manual acknowledges the persistence of fluctuations in the load and velocity fields for materials with high friction angles and low dilatancy (Itasca-d, 2001).

As the stress-strain behavior becomes more non-linear ($x_L$ increases), the displacement necessary to reach failure also increases. With the increase in values of the normalized limiting strain $x_L$ and the angle of internal friction $\phi$', the displacement to failure can become unrealistically high, as illustrated in Figure 8-7 which shows the stress-displacement behavior beneath a 1-m circular footing ($\phi' = 40^o$, $x_L = 50$). The simulation was allowed to run up to a displacement of 1-m (which is unreasonably high but was performed for illustrative purposes). As discussed in Chapter 2, it is common practice to take the bearing capacity as the stress corresponding to a pseudo-strain s/d of 10 %. The bearing capacity interpreted based on a specific value of s/d is dependent on the soil stiffness. Although this is suitable for use at a specific site (constant stiffness, footing size), a more consistent approach is needed that accounts for soil elastic properties in

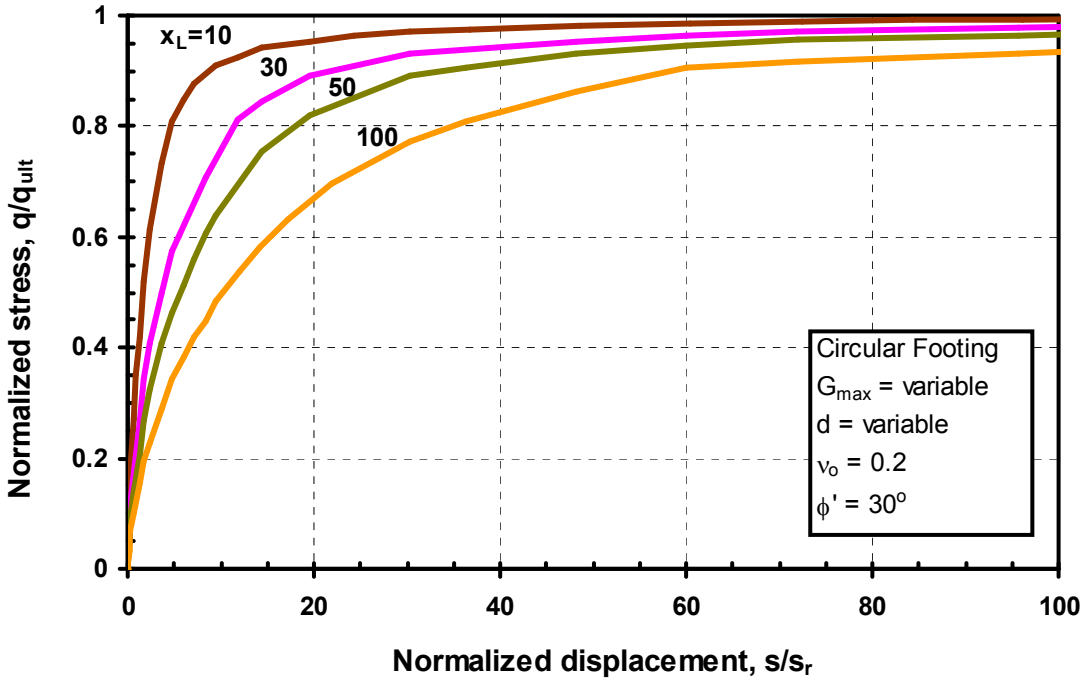


**Figure 8-4.** Normalized stress-displacement curves for a smooth, rigid, circular footing resting on non-linear elastic plastic LOGNEP soil ($\phi$' = 30°, $\psi$ = 0°)

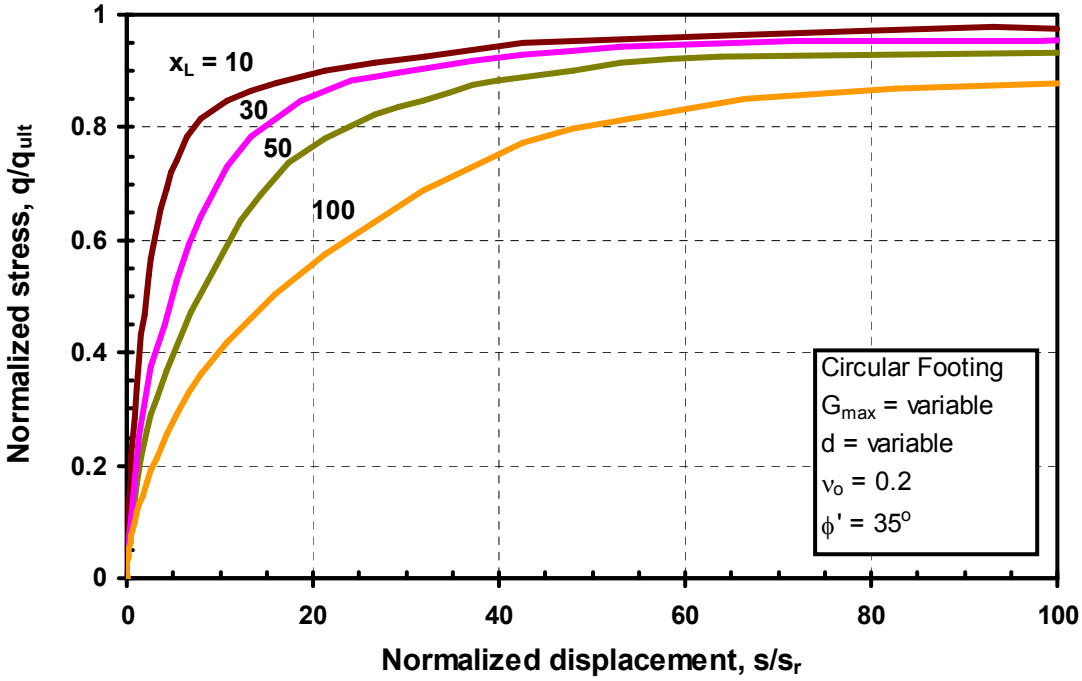


**Figure 8-5.** Normalized stress-displacement curves for a smooth, rigid, circular footing resting on non-linear elastic plastic LOGNEP soil ($\phi$' = 35°, $\psi$ = 0°)

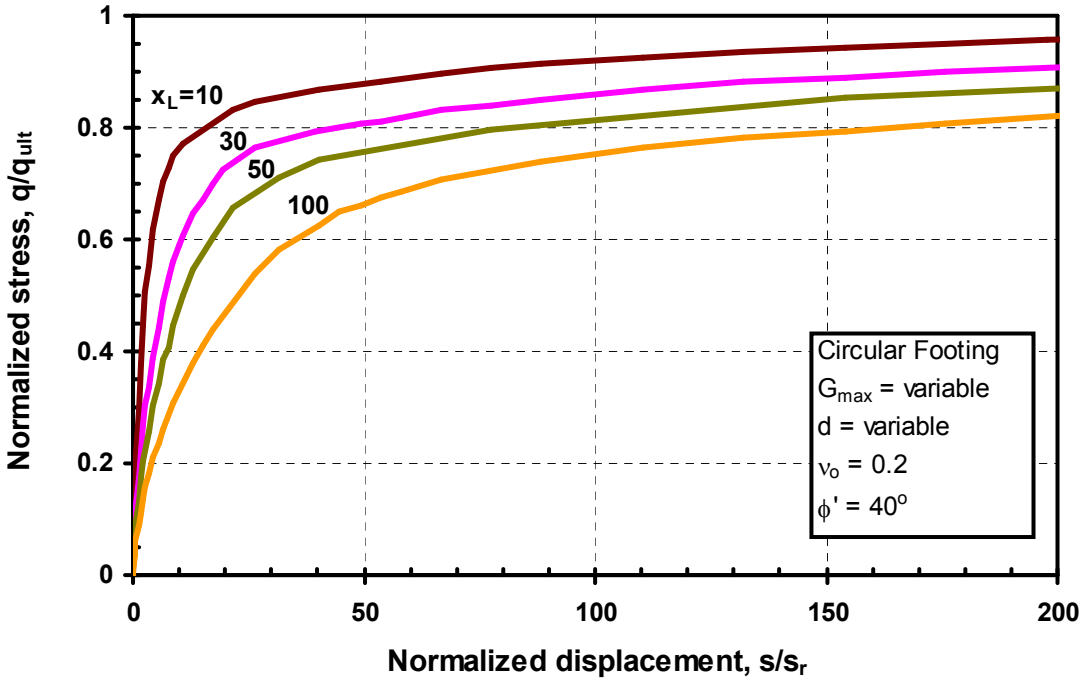


**Figure 8-6.** Normalized stress-displacement curves for a smooth, rigid, circular footing resting on nonlinear elastic plastic LOGNEP soil ($\phi' = 40^o$, $\psi = 0^o$)

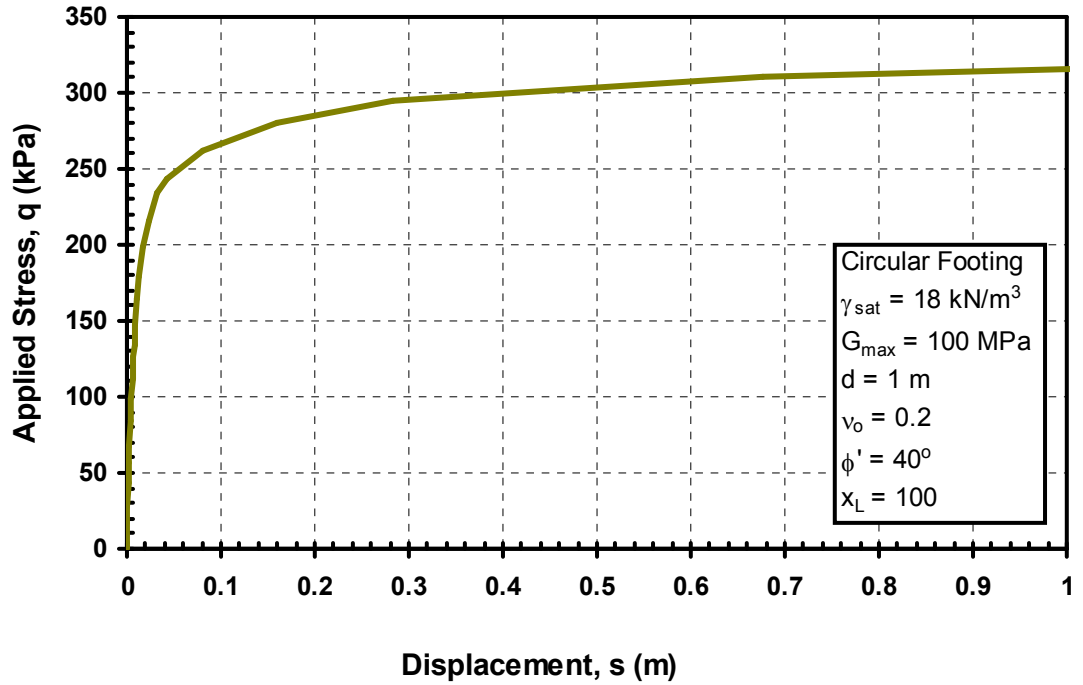


**Figure 8-7.** Simulated stress-displacement underneath a 1-m diameter smooth, rigid footing ($\phi'=40^o$, $x_L=50$).

addition to footing dimensions. It was decided to cut off the graphs at a normalized displacement ($s/s_r$) of 100, even though stresses continued higher.

## 8.3 Modeling the drained stress-displacement response of strip footings

The strip footing is modeled similar to the circular footing discussed previously in this chapter, shown in Figure 8-1, but using plane strain conditions instead of the axisymmetric case. The applied stress is computed as the average applied load divided by the footing width. Displacements are calculated as the average displacement of the grid points underneath the footing.

### *8.3.1 Normalized drained stress-displacement response of strip footings*

Similar to the drained loading of vertically loaded circular footings, a parametric study was performed to investigate factors influencing the stress-displacement response of strip footings. The study included varying the footing width B, maximum shear modulus $G_{max}$, normalized limiting strain $x_L$, and internal friction angle $\phi$'. Simulated stress-displacement footings responses are shown in Figure 8-8. Figure 8-8-a shows the drained stress-displacement response under a strip footing resting on a soil having an angle of internal friction $\phi' = 30^o$ and $x_L = 30$. Simulations have been performed for three values of the small-strain shear modulus $G_{max}$= 50, 100, 200 MPa. Three footing diameters have been used 0.5-m, 1.0-m, and 2.0-m. Similarly, Figures 8-8-b and 8-8-c show the stress-displacement response for ($\phi' = 35^o$, $x_L = 50$); and ($\phi' = 40^o$, $x_L = 100$), respectively. By normalizing footing displacement by a reference displacement $s/s_r$ and applied stress by bearing capacity $q/q_{ult}$, all curves collapse onto a single line as shown in Figures 8-9-a

through 8-9-c. As anticipated, the stress-displacement behavior varies with the footing width B, small-strain shear modulus $G_{max}$, normalized limiting strain $x_L$ and angle of internal friction $\phi$'.

### *8.3.2 Bearing capacity factors for strip footing*

Equation 8-2 was used to backfigure the bearing capacity factor $N_\gamma$ equivalent to the values of the angle of friction $\phi$'. Results are compared to other values reported in literature as shown in Figure 8-10. There is a large variation in results depending on method of analysis and associative/non-associative flow. For $\phi' = 20^o$, the bearing factor ($N_\gamma$) varied between 1.15 (Steenfelt, 1977) and 7.74 (French, 1999), while the factor ranged between 16.96 (Michalowski, 1997) and 145.2 (Chen, 1975). The factors computed in the current study are in close agreement with values computed by Michalowski (1997) for a smooth, strip footing with a non-associative flow ($\psi=0^o$) using a kinematical approach of limit analysis (multi-block mechanism).

### *8.3.3 Generalized stress-displacement curves of strip footings*

Similar to circular footings, a number of simulations of load tests of strip footings resting on homogeneous soil profile under drained loading ($\nu_o$=0.2) were conducted to generate normalized stress-displacement curves characteristic of the different angles of friction angles: $\phi' = 30^o$, $35^o$, and $40^o$. The simulations were performed using normalized limiting strains $x_L$ of 10, 30, 50, and 100. The normalized stress-displacement results are presented in Figures 8-11 through 8-13 for $\phi' = 30^o$, $35^o$, and $40^o$, respectively.

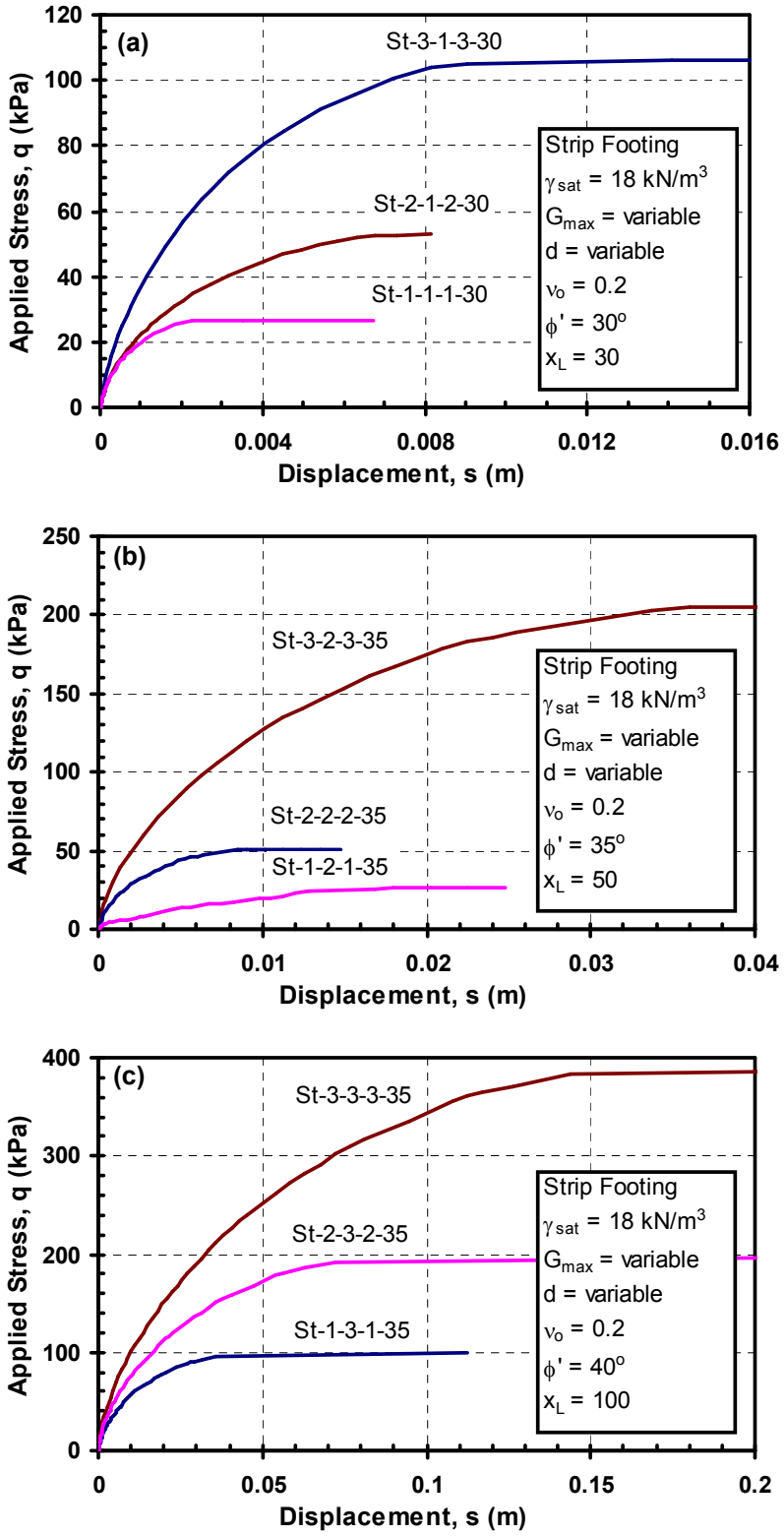


**Figure 8-8.** Simulated stress-displacement curves representing vertical displacements beneath rigid strip footings under drained loading conditions: a) $\phi' = 30^o$, $x_L = 30$; b) $\phi' = 35^o$, $x_L = 50$; c) $\phi' = 40^o$, $x_L = 100$.

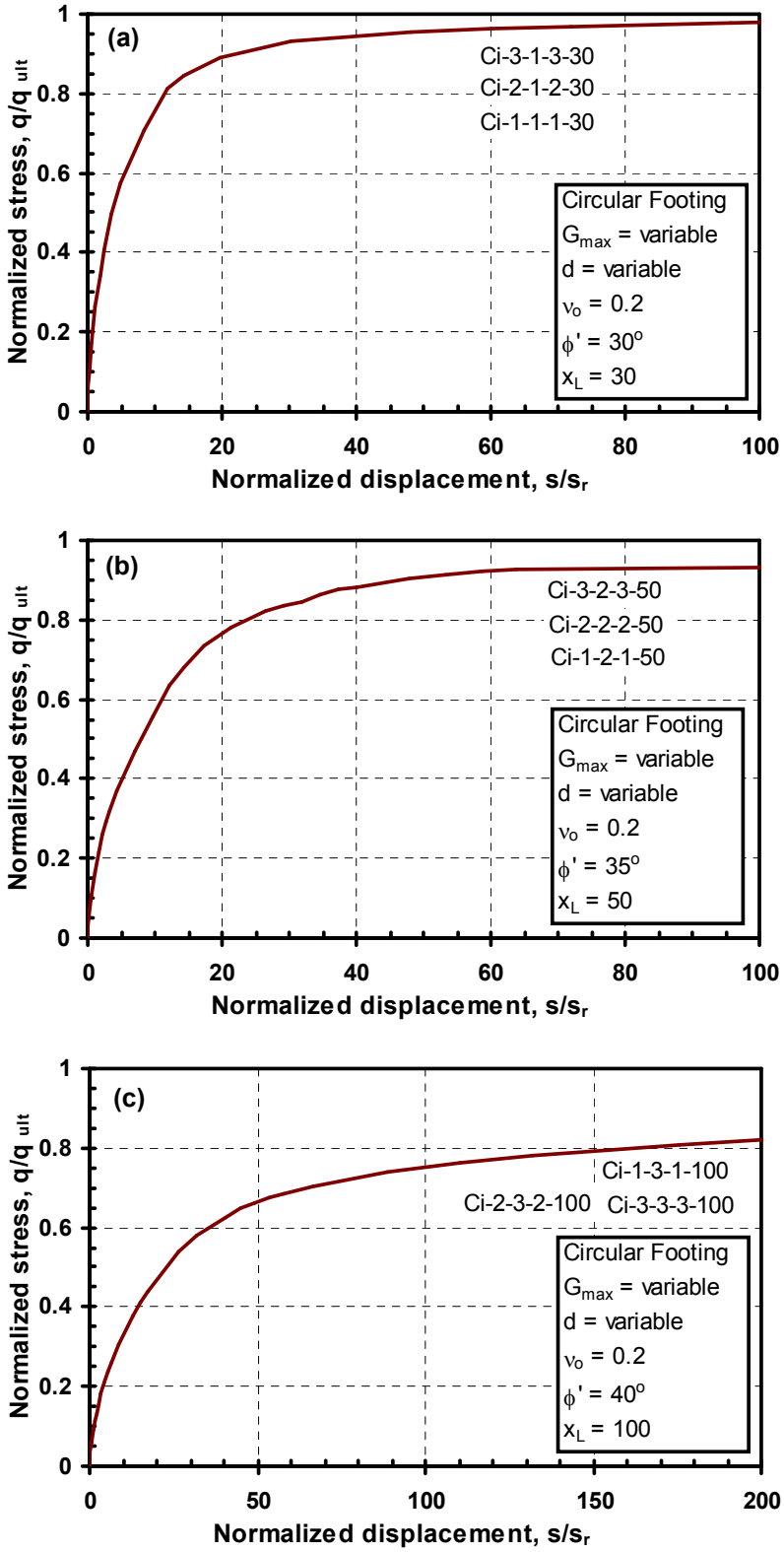


**Figure 8-9.** Normalized simulated stress-displacement curves representing vertical displacements beneath rigid strip footings under drained loading conditions: a) $\phi' = 30^o$, $x_L = 30$; b) $\phi' = 35^o$, $x_L = 50$; c) $\phi' = 40^o$, $x_L = 100$.

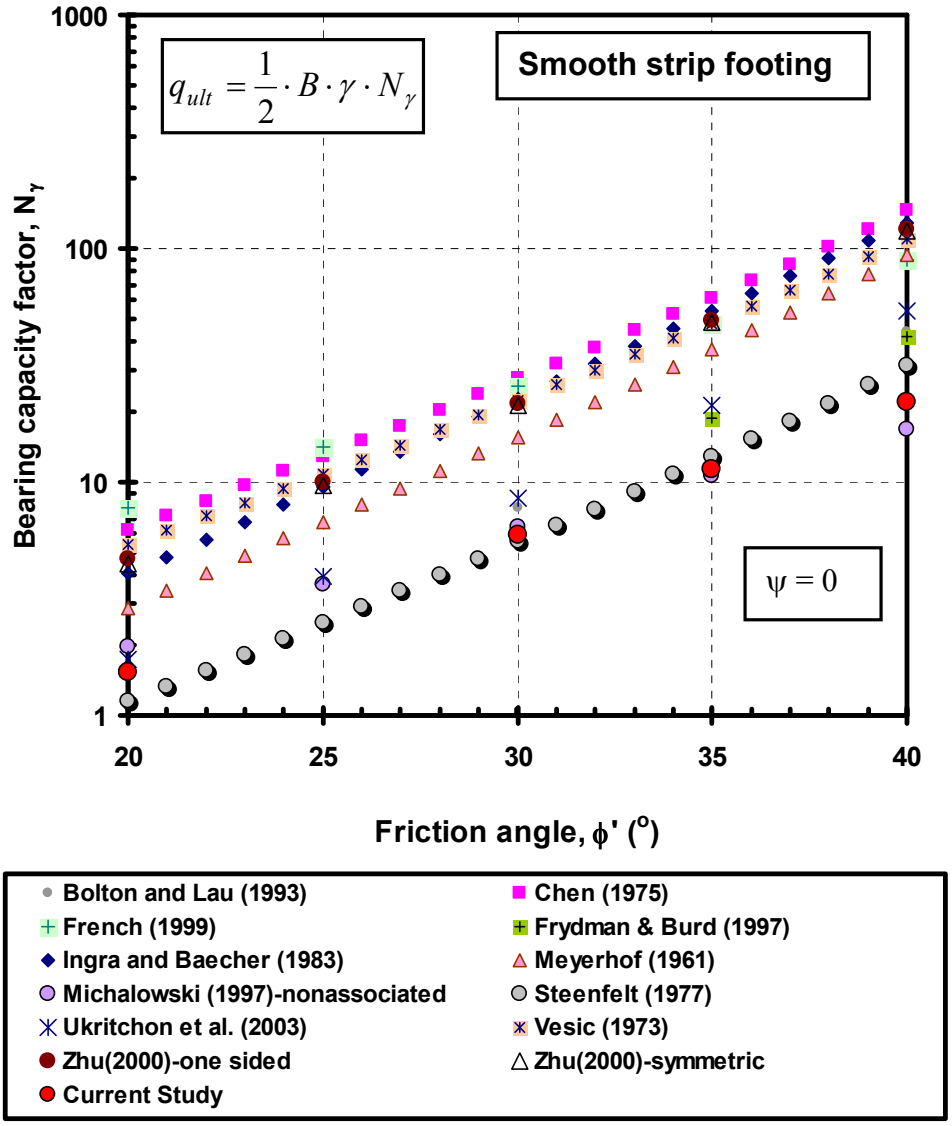


**Figure 8-10.** Comparison of the bearing capacity factor $N_\gamma$ computed from the current study and other studies from literature for smooth strip footings

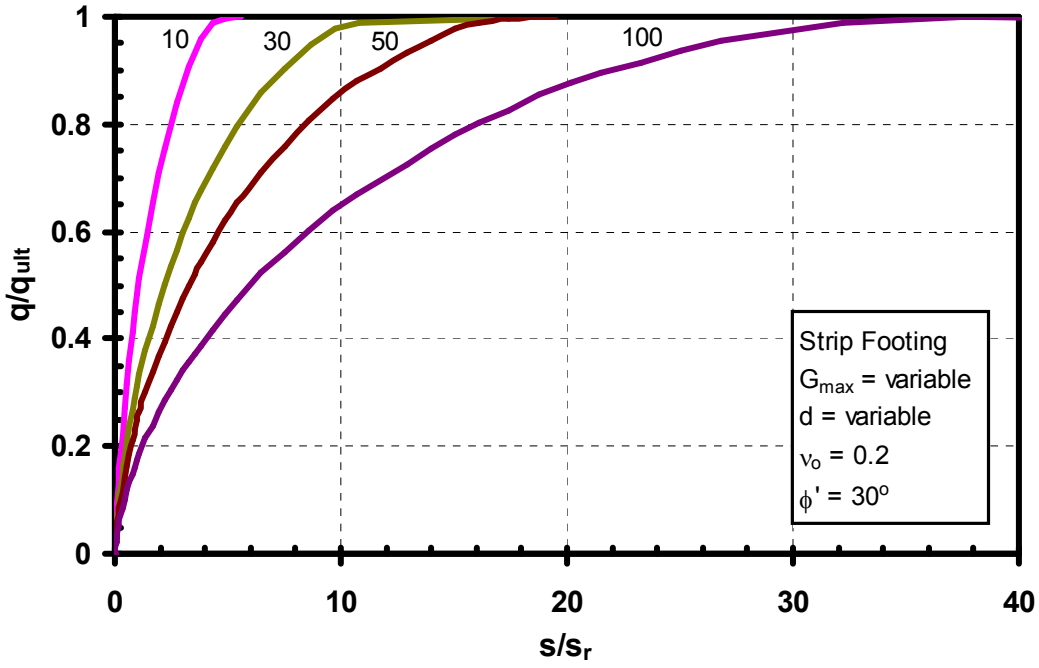


**Figure 8-11.** Normalized stress-displacement curves for a smooth, rigid, strip footing resting on nonlinear elastic plastic LOGNEP soil ($\phi' = 30^o$, $\psi = 0^o$)

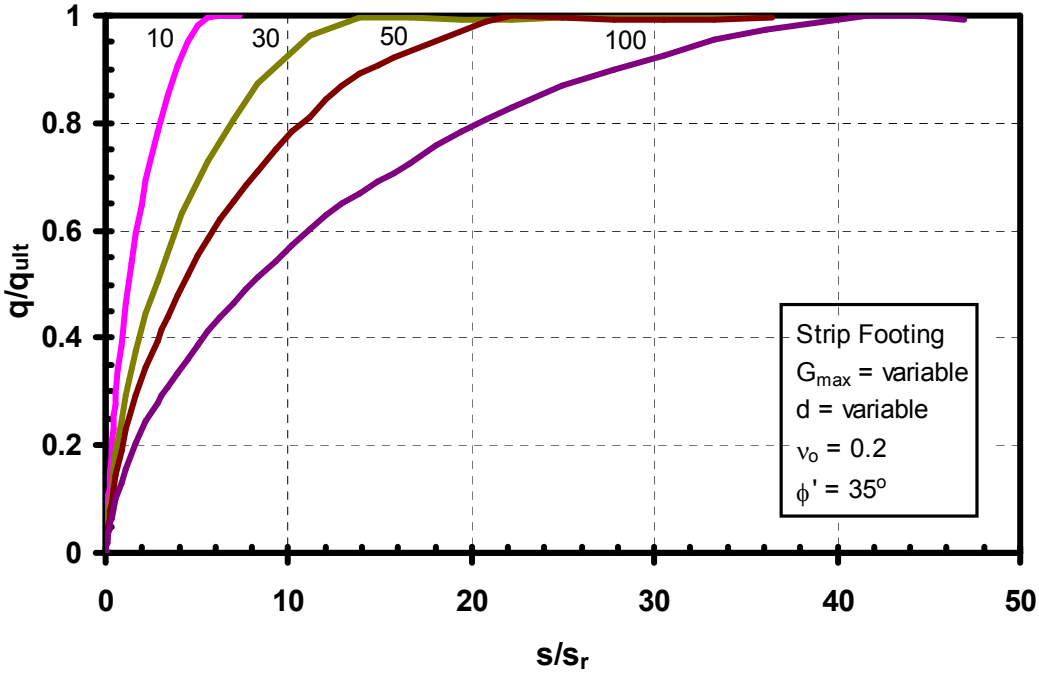


**Figure 8-12.** Normalized stress-displacement curves for a smooth, rigid, strip footing resting on nonlinear elastic plastic LOGNEP soil ($\phi' = 35^o$, $\psi = 0^o$)

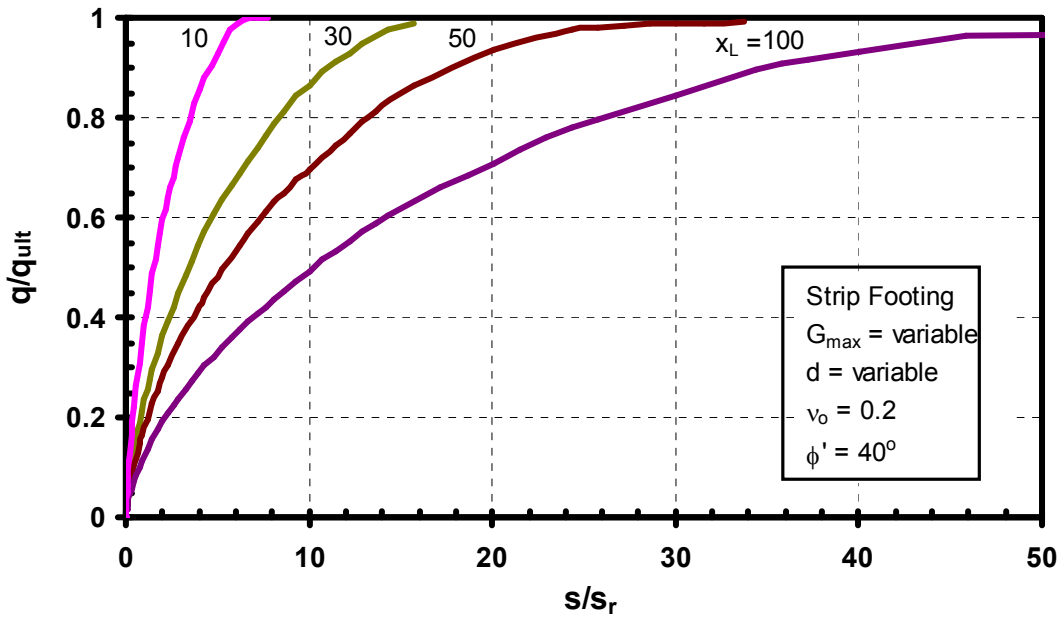


**Figure 8-13.** Normalized stress-displacement curves for a smooth, rigid, strip footing resting on nonlinear elastic plastic LOGNEP soil ($\phi' = 40^o$, $\psi = 0^o$)

## 8.4 Summary and conclusions

This chapter deals with the stress-displacement behavior of smooth, rigid, surface footings subjected to vertical loading under drained loading conditions. Two types of surface footings were considered: circular and strip. The computed bearing capacity factors $N_\gamma$ for circular foundations were found in good agreement with values reported by Erickson and Drescher (2002), as shown in Table 8-2. For strip footings, the bearing capacity factors $N_\gamma$ agreed well with factors reported by Michalowski (1997), as presented in Figure 8-10.

Normalizing the applied stresses by bearing capacity $q_{ult}$ and displacements by reference displacement $s_r$ was shown to work for both circular and strip footings. The "raw" simulated stress-displacement curves under vertically loaded footings depend on the

angle of internal friction $\phi$', maximum shear modulus $G_{max}$, footing shape (circular or strip) and dimensions (d or B), and the normalized limiting strain $x_L$. With proper normalization, stress-displacement curves were generated that are only dependent on the normalized limiting strain $x_L$ and the angle of internal friction $\phi$'. General normalized stress-displacement curves for circular footings are presented in Figures 8-4 through 8-6 for $\phi' = 30^o$, $35^o$, and $40^o$, respectively. Similar curves were produced for vertically loaded strip footings as presented in Figures 8-11 through 8-13.

# CHAPTER IX

## APPROXIMATE EQUIVALENT NON-LINEAR ELASTIC CLOSED-FORM SOLUTION FOR FOOTING DISPLACEMENTS

Normalized stress-displacement curves were presented graphically for the behavior of circular and strip footings under both undrained and drained loading conditions in Chapters 7 and 8, respectively. Results were presented in graphical form. It would be convenient to have a closed-form solution that enables designers to directly produce stress-displacement curves using spreadsheet programs or commercial mathematical software.

An approximate closed-form solution is proposed within an elastic continuum framework. The footing-soil system is represented by an elastic continuum with an average equivalent stiffness K. The system stiffness starts at an initial value $K_i$ (corresponding to the small-strain shear modulus $G_{max}$). The footing bearing capacity $q_{ult}$ is computed analytically using appropriate bearing capacity factors presented in Chapters 7 and 8. A modulus reduction scheme is used to degrade the footing-soil stiffness $K_i$ until failure is reached. Beginning at the maximum equivalent stiffness $K_i$, it is reduced as a function of the normalized applied stress $q/q_{ult}$, where q and $q_{ult}$ are the average applied stress and bearing capacity, respectively.

## 9.1 Approximate equivalent elastic closed-form solution for footing displacement

Footing displacements are computed within an elastic continuum framework (e.g. Poulos, 1967; Ueshita and Meyerhof, 1968; Brown, 1969a), according to:

$$s = \frac{q}{K} \quad \text{.....(9-1)}$$

where s = foundation displacement, q = applied stress acting beneath the foundation, $K = E_s / BI$ = representative footing-soil system stiffness, where $E_s$ = equivalent elastic Young's modulus, and I = surface displacement influence factor that depends Poisson's ratio, foundation rigidity, layer thickness, interface roughness, and soil stiffness variation with depth. This equation can be modified to account for soil non-linearity by substituting $K_i.r_f$ instead of the representative footing-soil system stiffness K according to:

$$s = \frac{q}{K_i \cdot r_f} \quad \text{.....(9-2)}$$

where $K_i$ is initial stiffness of the footing-soil system $\left[K_i = E_{\max} / BI\right]$, where $E_{max}$ is the maximum Young's modulus and $r_f$ is a modulus reduction factor as a function of the normalized applied stress ($q/q_{ult}$). Equation 9-2 will be formulated in terms of normalized stress ($q/q_{ult}$) and normalized displacement ($s/s_r$), according to:

$$\frac{s}{s_r} = \frac{(q/q_{ult})}{\left(K_i \cdot \frac{s_r}{q_{ult}}\right) \cdot r_f} \quad \text{.....(9-3)}$$

where $s_r$ is the reference displacement computed as $s_r = q_{ult} / K_i$ and $q_{ult}$ is the ultimate bearing capacity. Given that $K_i = q_{ult} / s_r$ (refer to Equation 7-2), Equation (9-3) reduces to:

$$\frac{s}{s_r} = \frac{(q/q_{ult})}{r_f} \quad \text{.....(9-4)}$$

It is now necessary to choose a mathematical expression for modulus reduction that begins at the small-strain stiffness and allows the modulus to diminish with the increase in stress level. It is also advantageous to choose a simple formulation suitable for simplified analytical solutions (Mayne, 2003). Therefore the modified hyperbola (Fahey and Carter, 1993; Fahey et al., 1994; Fahey, 1998) was chosen for modulus reduction:

$$r_f = \left[1 - f^* \left[\frac{q}{q_{ult}}\right]^{g^*}\right] \quad \text{.....(9-5)}$$

where $f^*$ and $g^*$ are empirical fitting parameters that distort the shape of the hyperbolic function. The modified hyperbola was used to fit stress-displacement data for footings on sand by Mayne & Poulos (2001) and for a footing on clayey silt by Mayne (2003).

Equation 9-5 reduces to a regular hyperbola for $f^* = 1$ and $g^* = 1$. The rate of modulus reduction decreases at initial loading for $g^* > 1$. While the modulus reduces more rapidly when the value of $g^*$ is less than 1. For $f^* = 1$, failure is never reached. The value of $f^*$ must be set below 1 for failure to be reached at a finite displacement. Values of $f^*$ greater than 1 are meaningless (Fahey, 2001). Figure 9-1 shows the effects of varying the fitting parameters $f^*$ and $g^*$. The $f^*$ parameter is essentially the same as the $R_f$ parameter in Duncan-Chang hyperbola to reduce the hyperbolic asymptote to the measured failure/peak value. Duncan and Chang (1970) recommended $R_f \sim 0.9$. Lee and Salgado (2004) reported $R_f$ values varying between 0.86 and 0.99 for drained triaxial compression tests on sand samples with different silt contents and relative densities.

It should be noted that the normalized applied stress is the reciprocal of the factor of safety $\left[FS = 1/\left(q/q_{ult}\right)\right]$. Therefore, the reciprocal of the factor of safety can be substituted instead of the normalized stress ($q/q_{ult}$), allowing for simpler estimates of the equivalent soil modulus for deformation analyses following stability calculations.

### ***9.1.1 Undrained loading of circular and strip footings***

Figure 9-2 shows the hyperbolic function fitted to the normalized simulated stress displacement curves beneath rigid, circular footings under undrained loading conditions, for different values of the normalized limiting strain $x_L$. The model fitting parameters (f* and g*) are listed in Table 9-1.

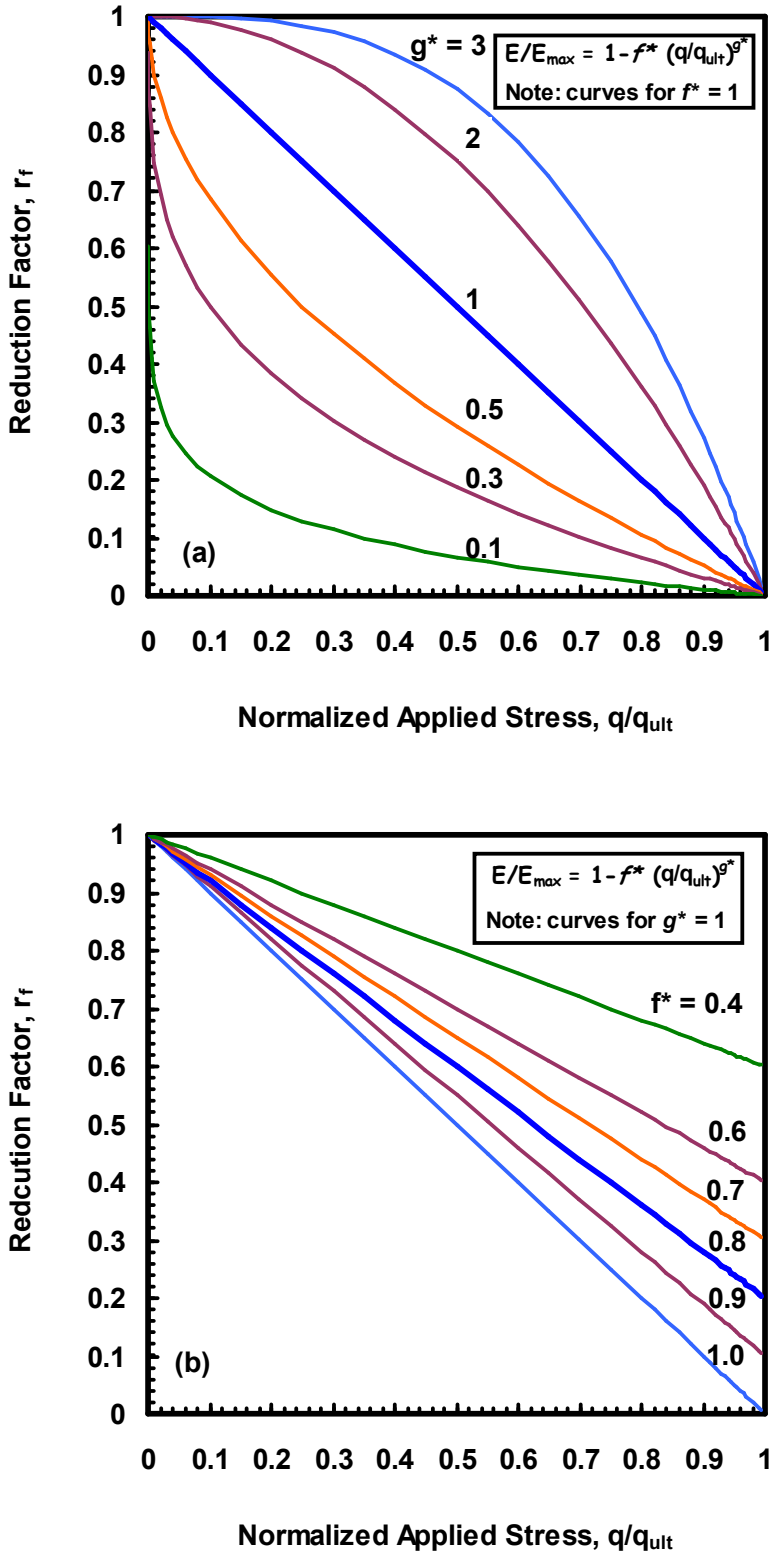


**Figure 9-1.** The effect of varying the fitting parameters f and g on the modulus reduction factor $R_f$: (a) $f^* = 1$ and $g^*$ variable; (b) $f^*$ variable and $g^* = 1$

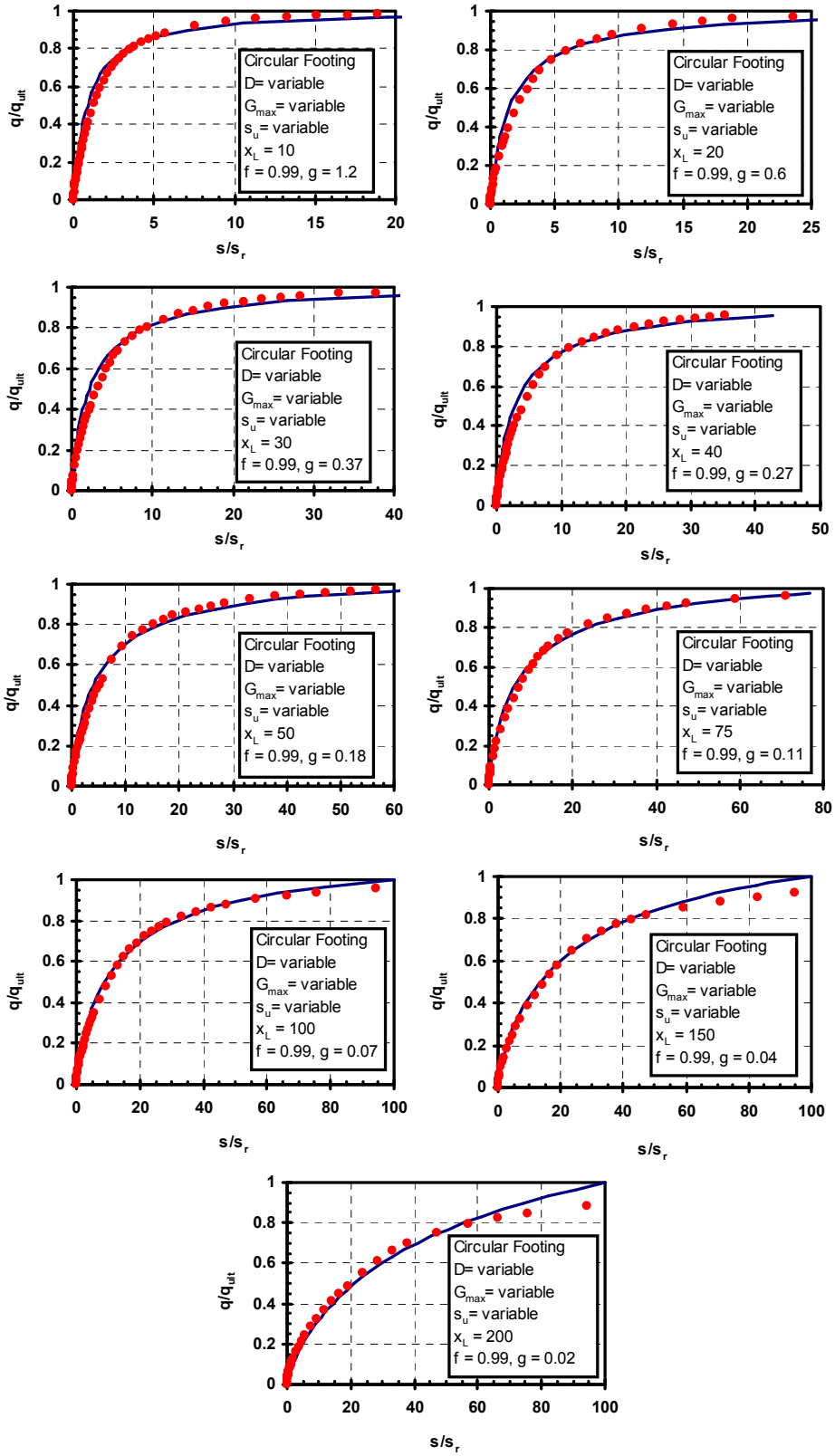


**Figure 9-2.** Fitted non-linear hyperbolic functions to normalized simulated stress-displacement curves under rigid circular footings under undrained loading

Similarly, modified hyperbolas were fitted to the normalized stress-displacement curves beneath strip footings under undrained loading conditions, as shown in Figure 9-3. The fitting parameters are listed in Table 9-1. The value of f* was maintained at 0.99 for all values of the normalized limiting strain.

As the degree of soil non-linearity increases (higher values of $x_L$), the value of the fitting parameter g* (controlling the rate at which the modulus reduces) decreases, indicating an increase in the displacement to failure. The variation of the fitting parameter g* with the normalized limiting strain $x_L$, for both circular and strip footings, is plotted in Figure 9-4, for the undrained loading cases. The dots shown in the Figure represent the results given in Table 9-1. As an approximation, the non-linear parameters g* and $x_L$ are interrelated by:

$$x_L \approx \frac{1}{\left(0.07g^* + 0.0024\right)^{0.95}} \text{ (circular footing)}\ldots\ldots\ldots

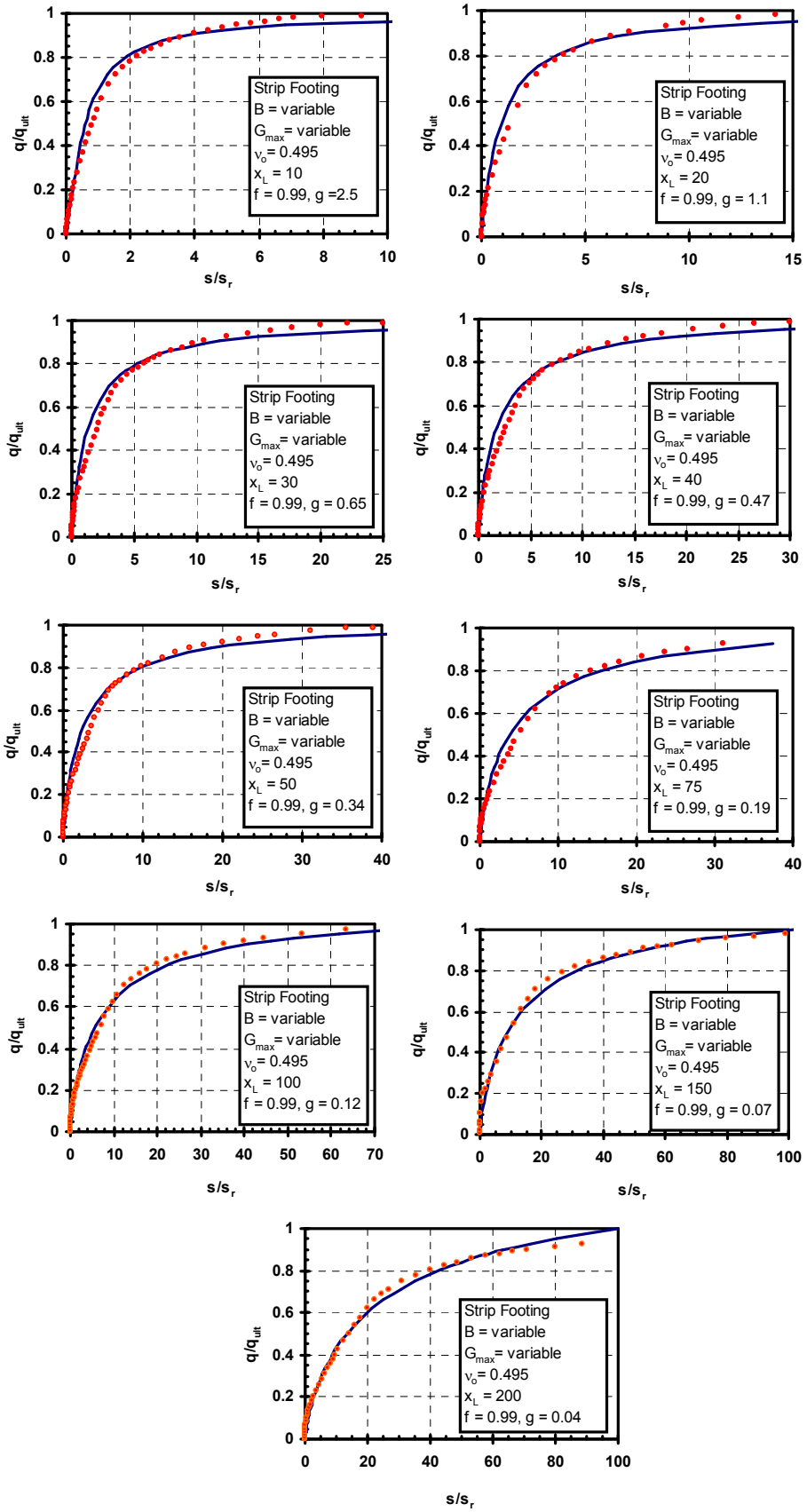


**Figure 9-3.** Fitted non-linear hyperbolic functions to normalized simulated stress-displacement curves under rigid strip footings under undrained loading

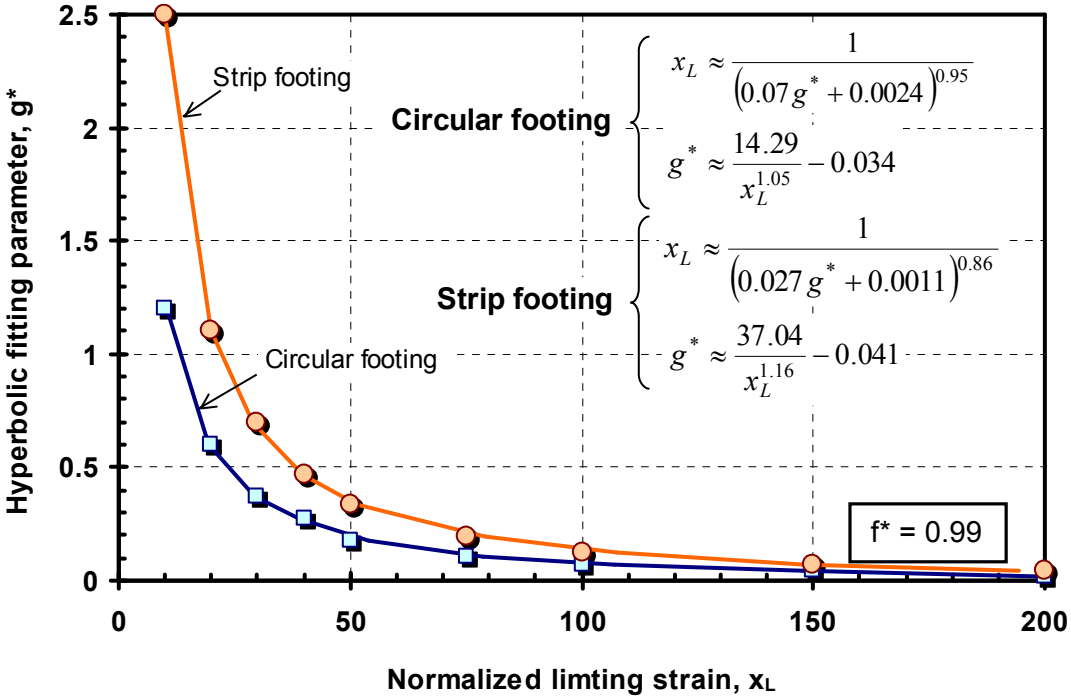


**Figure 9-4.** Variation of the hyperbolic fitting parameter g* (defining the overall non-linear stress-displacement behavior of shallow foundations) with the normalized limiting strain $x_L$ (defining the representative non-linear stress-strain behavior of a single soil element) under undrained loading conditions

**Table 9-1.** Fitting parameters (f* and g*) under rigid footings in undrained loading

| Normalized limiting Strain $x_L$ | Circular footing | | Strip footing | |
|---|---|---|---|---|
| | g* | $R^2$ | g* | $R^2$ |
| 10 | 1.20 | 0.93 | 2.5 | 0.87 |
| 20 | 0.60 | 0.97 | 1.1 | 0.94 |
| 30 | 0.37 | 0.98 | 0.65 | 0.94 |
| 40 | 0.27 | 0.99 | 0.47 | 0.91 |
| 50 | 0.18 | 0.97 | 0.34 | 0.95 |
| 75 | 0.11 | 0.99 | 0.19 | 0.99 |
| 100 | 0.07 | 0.95 | 0.12 | 0.99 |
| 150 | 0.04 | 0.93 | 0.07 | 0.99 |
| 200 | 0.02 | 0.96 | 0.04 | 0.96 |

Note: f* = 0.99

### *9.1.2 Drained loading of circular and strip footings*

The modified hyperbolic function was fitted to normalized stress displacement results obtained from drained loading simulations presented in Chapter 8. Figures 9-5 through 9-7 show the fitted curves for rigid, circular footings under drained loading conditions for friction angles of $30^o$, $35^o$, and $40^o$, respectively. The fitting parameters are summarized in Table 9-2. Similarly, normalized stress displacement behavior under strip footings were fitted with the hyperbolic function, as shown in Figures 9-8 through 9-10 for friction angles $30^o$, $35^o$, and $40^o$, respectively. Fitting parameters f* and g* are presented numerically in Table 9-2. The value of the fitting parameter g* decreases as non-linearity (expressed by $x_L$) increases, while the value of f* increases because the displacement to failure increases. The variation of g* with the normalized limiting strain $x_L$ for circular footings under drained loading is presented in Figure 9-11 as dots. Approximate close-form solutions are given by:

$\phi' = 30^o$: $x_L \approx \dfrac{1}{0.11g^* + 0.003}$, f*=0.99……..…….…….(9-8-a)

$\phi' = 30^o$: $g^* \approx \dfrac{9.09}{x_L} - 0.03$, f*=0.99……..……..……(9-8-b)

$\phi' = 35^o$: $x_L \approx \dfrac{1}{\left(0.51g^* + 0.086\right)^2}$, f*=0.99…….……..….(9-9-a)

$\phi' = 35^o$: $g^* \approx \dfrac{1.96}{\sqrt{x_L}} - 0.17$, f*=0.99……...……..….(9-9-b)

$\phi' = 40^o$: $x_L \approx \dfrac{1}{\left(0.5g^*\right)^{1.1}}$, f*=1.00……..….(9-10-a)

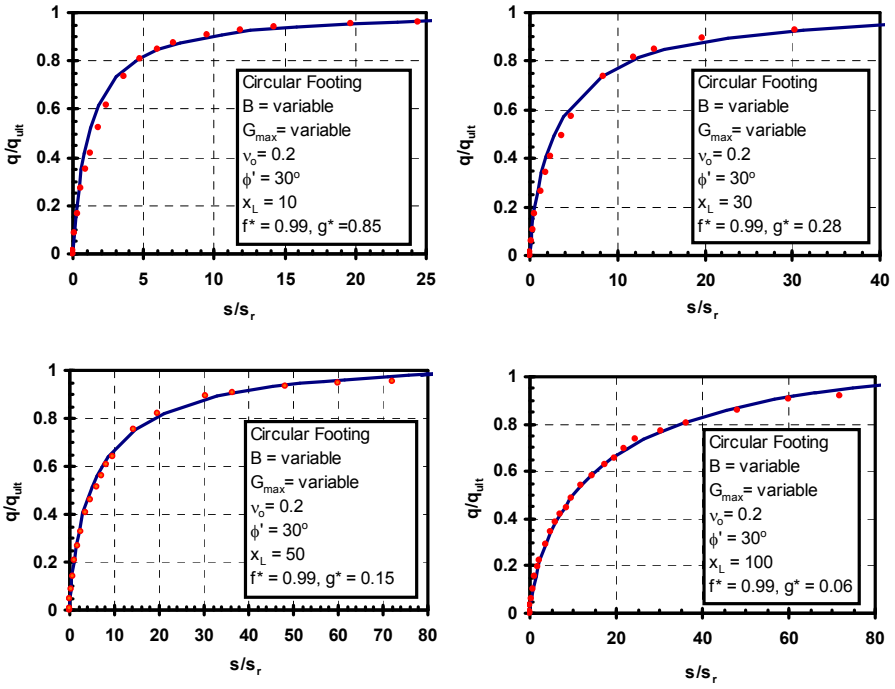


**Figure 9-5.** Fitted non-linear hyperbolic function to normalized simulated stress-displacement curves under rigid, circular footings under drained loading ($\phi' = 30^o$)

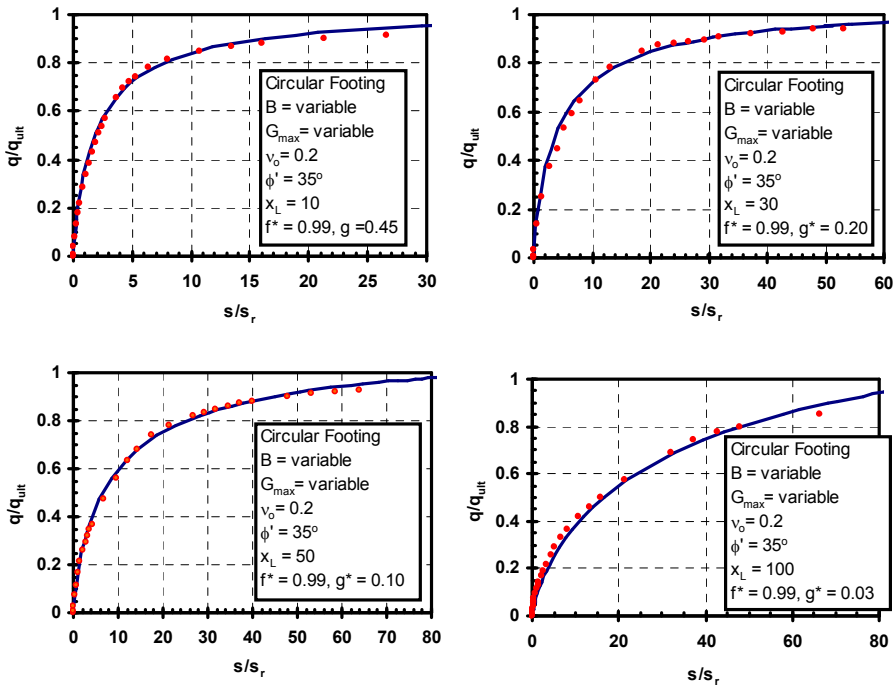


**Figure 9-6.** Fitted non-linear hyperbolic function to normalized simulated stress-displacement curves under rigid, circular footings under drained loading ($\phi' = 35^o$)

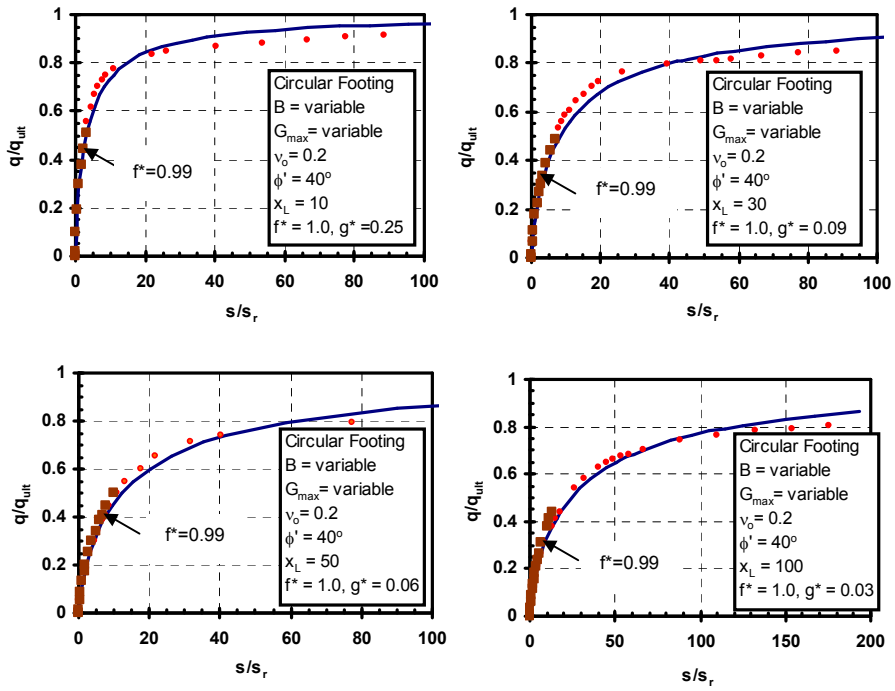


**Figure 9-7.** Fitted non-linear hyperbolic function to normalized simulated stress-displacement curves under rigid, circular footings under drained loading ($\phi' = 40^o$)

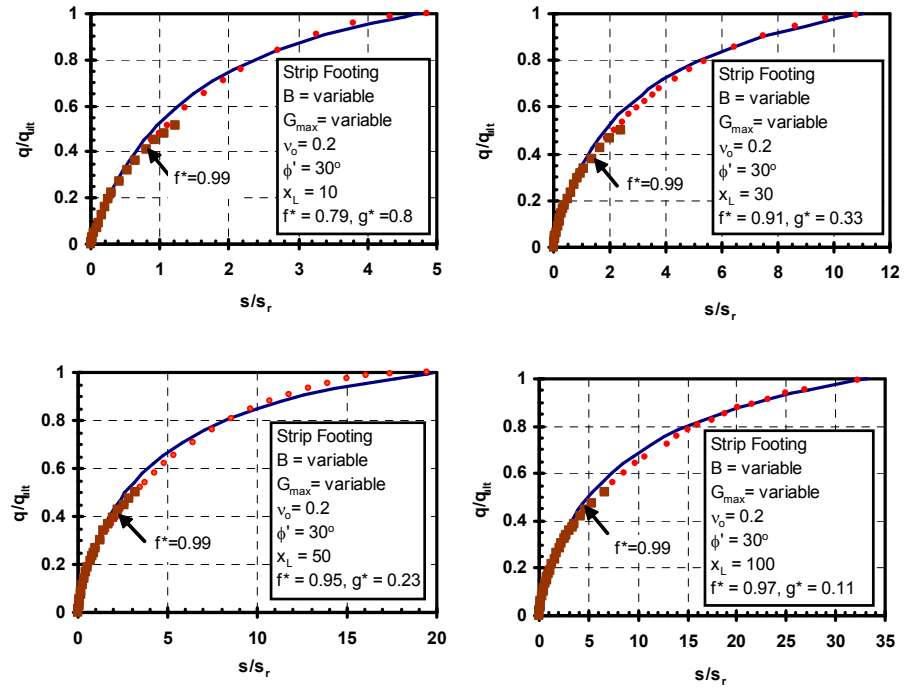


**Figure 9-8.** Fitted non-linear hyperbolic function to normalized simulated stress-displacement curves under rigid, strip footings under drained loading ($\phi' = 30^o$)

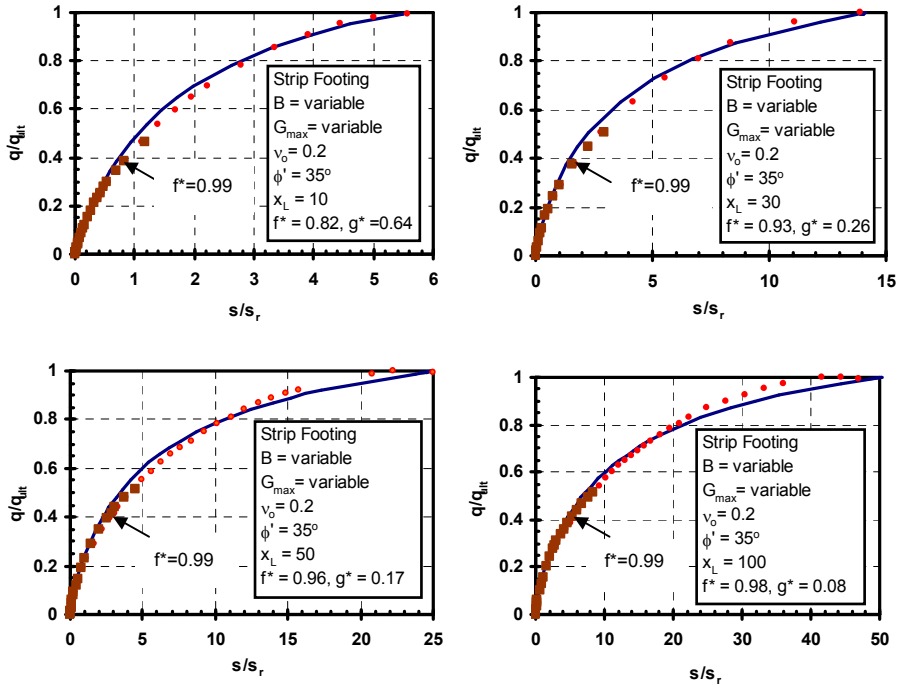


**Figure 9-9.** Fitted non-linear hyperbolic function to normalized simulated stress-displacement curves under rigid, strip footings under drained loading ($\phi' = 35^o$)

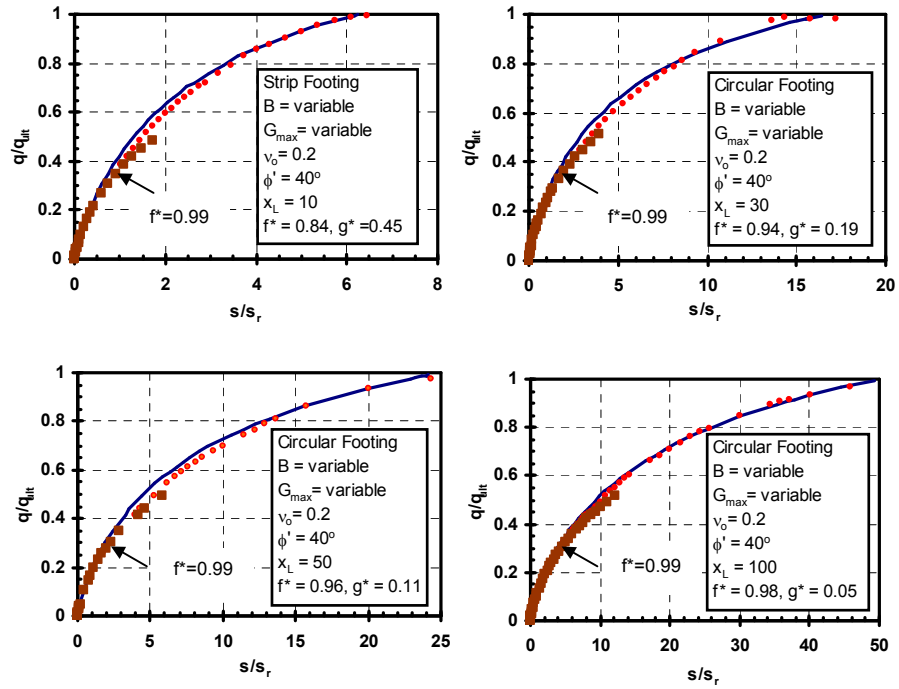


**Figure 9-10.** Fitted non-linear hyperbolic function to normalized simulated stress-displacement curves under rigid, strip footings under drained loading ($\phi' = 40^o$)

**Table 9-2.** Fitting parameters (f* and g*) under rigid footings in drained loading

| Angle of friction | Normalized limiting strain, $x_L$ | Circular footing | | | Strip footing | | |
|---|---|---|---|---|---|---|---|
| | | f* | g* | $R^2$ | f* | g* | $R^2$ |
| 30 | 10 | 0.99 | 0.70 | 0.97 | 0.79 | 0.80 | 0.99 |
| | 30 | 0.99 | 0.28 | 0.97 | 0.91 | 0.33 | 0.99 |
| | 50 | 0.99 | 0.20 | 0.95 | 0.95 | 0.23 | 0.98 |
| | 100 | 0.99 | 0.09 | 0.92 | 0.97 | 0.11 | 0.99 |
| 35 | 10 | 0.99 | 0.45 | 0.96 | 0.82 | 0.64 | 0.99 |
| | 30 | 0.99 | 0.20 | 0.98 | 0.93 | 0.26 | 0.99 |
| | 50 | 0.99 | 0.10 | 0.99 | 0.96 | 0.17 | 0.95 |
| | 100 | 0.99 | 0.05 | 0.99 | 0.98 | 0.08 | 0.96 |
| 40 | 10 | 1.00 | 0.25 | 0.98 | 0.84 | 0.45 | 0.99 |
| | 30 | 1.00 | 0.09 | 0.98 | 0.94 | 0.19 | 0.99 |
| | 50 | 1.00 | 0.06 | 0.98 | 0.96 | 0.11 | 0.99 |
| | 100 | 1.00 | 0.03 | 0.98 | 0.98 | 0.05 | 0.99 |

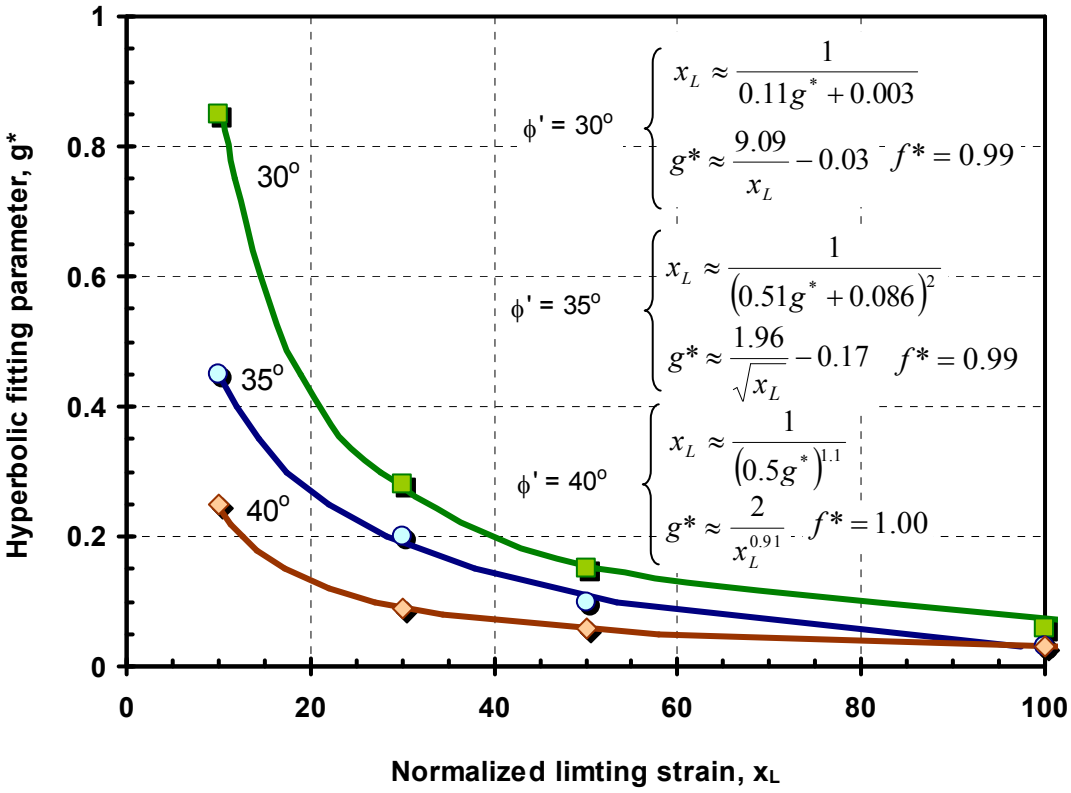


**Figure 9-11.** Variation of the hyperbolic fitting parameter g* (defining the overall non-linear stress-displacement behavior of shallow foundations) with the normalized limiting strain $x_L$ (defining the representative non-linear stress-strain behavior of a single soil element) for circular footings under drained loading conditions

$\phi' = 40^o$: $g^* \approx \frac{2}{x_L^{0.91}}$, f*=1.00……..……..….(9-10-b)

Similarly, the variation of the fitting parameter g* with the normalized limiting strain $x_L$ for strip footings under drained loading is presented graphically in Figure 9-12. The values of the fitting parameters f* and g* are listed in Table 9-2. Approximate closed-form solutions interrelating g* and $x_L$ are given by:

$\phi' = 30^o$: $x_L \approx \frac{1}{(0.23g^* + 0.014)^{1.43}}$ ……..……..…..…….…….(9-11-a)

$\phi' = 30^o$: $g^* \approx \frac{4.35}{x_L^{0.7}} - 0.06$ ..……..……..…..……..….(9-11-b)

$\phi' = 35^o$: $x_L \approx \frac{1}{(0.29g^* + 0.017)^{1.43}}$ ……..……..…..…….…….(9-12-a)

$\phi' = 35^o$: $g^* \approx \frac{3.45}{x_L^{0.7}} - 0.06$ ……..…..…….……..……..…….(9-12-b)

$\phi' = 40^o$: $x_L \approx \frac{1}{(0.4g^* + 0.02)^{1.43}}$ ……..……..…..…….…….(9-13-a)

$\phi' = 40^o$: $g^* \approx \frac{2.5}{x_L^{0.7}} - 0.05$ ……..……..……..…….....….(9-13-b)

$\phi' = 30^o, 35^o, 40^o$: $f^* \approx 0.99 - \frac{3.5 - 0.046\phi'}{x_L}$ ……..……...…(9-14)

Figure 9-12 compares the computed and approximate values of the fitting parameters g* computed using Equations 9-11-a through 9-13-b, with good agreement. The value of f*

varied with both $x_L$ and $\phi$' according to Equation 9-14. The accuracy of Equation 9-14 is demonstrated in Figure 9-13.

It is worth noting that although the value of f* was not maintained constant at 0.99 for the drained stress-displacement response of both circular and strip footings under drained loading conditions, using f* of 0.99 yield good agreement with the simulated stress-displacement response in the working stress level up to a load factor of 2. This is illustrated by the dotted lines shown in Figures 9-7 through 9-10.

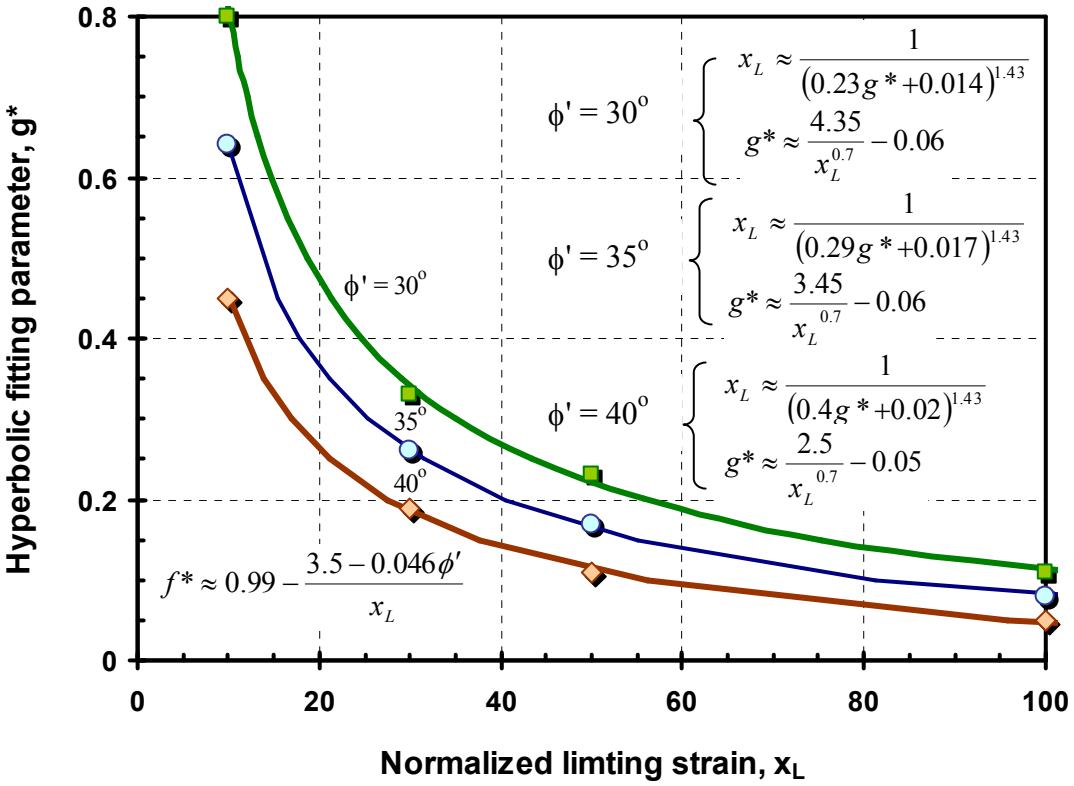


**Figure 9-12.** Variation of the hyperbolic fitting parameter g* (defining the overall nonlinear stress-displacement behavior of shallow foundations) with the normalized limiting strain $x_L$ (defining the representative nonlinear stress-strain behavior of a single soil element) for strip footings under drained loading conditions

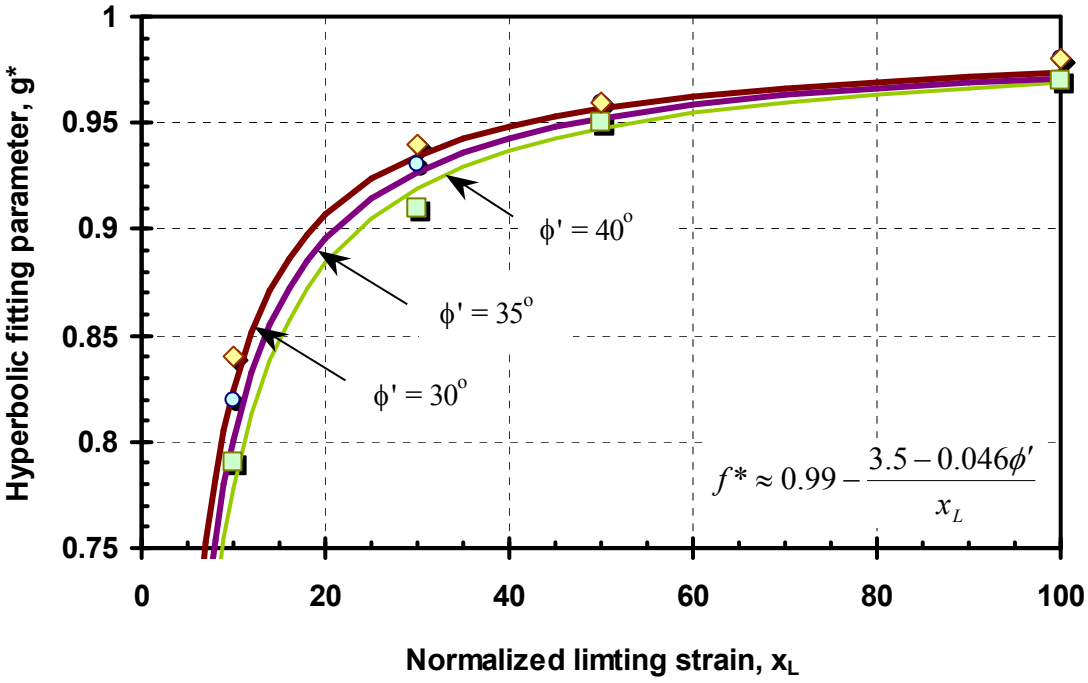


**Figure 9-13.** Variation of the hyperbolic fitting parameter f* with the normalized limiting strain $x_L$ for strip footings under drained loading conditions

## 9.2 Summary and conclusions

An approximate closed-form solution within a non-linear elastic framework is proposed to simplify displacement computations. The closed-form solution assumes an equivalent average soil/footing stiffness, which starts at a value corresponding to the small strain stiffness $E_{max}$. This "global" modulus reduces with the increase in stress level represented by $q/q_{ult}$, where $q_{ult}$ is determined by bearing capacity. A modified hyperbola (Fahey and Carter, 1993; Fahey et al., 1994; Fahey, 1998) was used as a simple means to express the modulus reduction.

The modified hyperbola is fitted to the normalized stress-displacement curves obtained from the simulated loading of circular and strip footings, under both undrained and

drained loading conditions. The fitting parameters of the modified hyperbola (describing the overall behavior of the footing) are matched with the corresponding normalized limiting strain $x_L$ (defining the non-linear behavior of the soil element).

It should be noted that the normalized applied stress is the reciprocal of the factor of safety $\left[FS = 1/\left(q/q_{ult}\right)\right]$. Therefore, the reciprocal of the factor of safety can be substituted instead of the normalized stress ($q/q_{ult}$), allowing for simpler calculations of non-linear stress-displacement curves for routine design (Mayne, 2003).

# CHAPTER X

# CALIBRATION OF CLOSED-FORM SOLUTION USING FOOTING LOAD DISPLACEMENT RESPONSE DATA

In this chapter, a database of footing load tests is used to calibrate the closed-form model presented in Chapter 9. The database comprises shallow footings on soils under both undrained and drained loading conditions. All analyses start at the fundamental small strain stiffness $G_{max}$. In most of the case studies, $G_{max}$ values are available from in-situ measurements. When measurements are unavailable, other soil parameters were used to provide an estimate of $G_{max}$. Modified hyperbolae were fitted to the normalized load test data and average normalized limiting strains $x_L$ were backcalculated using relationships presented in Chapter 9.

## 10.1 Model calibration based on footing load tests

Load test data are classified into 2 categories depending on prevalent drainage conditions during loading, i.e. undrained versus drained. Generally, undrained loading is associated with footings situated on fine-grained soils (clays), whereas drained loading corresponds to foundations on sands.

### *10.1.1 Undrained loading*

The database of undrained loading cases consists of 9 full-scale loading tests from 6 sites (Brand et al., 1972; Schnaid et al., 1993; Bowey and Wood, 1994; Jardine et al., 1995;

Lehane, 2003; Powell and Butcher, 2003), one case study failure (Nordlund and Deere, 1972), and 8 model footing tests (Kinner and Ladd, 1973; Stallebrass and Taylor, 1997). Table 10-1 summarizes soil types, footing dimensions, and groundwater table elevations relative to the footing. Soil profiles include 6 natural soil deposits (varying from soft clays to stiff overconsolidated clays and glacial tills), 7 model tests on reconstituted Boston blue clay, and 1 centrifuge test on remolded Speswhite kaolin. Footing shapes include circular, square, and rectangular. The foundation sizes varied widely, ranging from very small 0.06-m model circular footings to large unexpected failures of mat foundations (66.5 by 15.9 m).

The small strain stiffness is a required input for the proposed nonlinear model. It can be measured using either field measurements (e.g. crosshole test, downhole test, spectral analysis of surface waves, seismic piezocone/dilatometer) or laboratory tests (resonant column, torsional shear apparatus, bender elements, or specially instrumented triaxial tests with internal local strain measurements), as discussed in Chapter 4. Measured values of $G_{max}$ were available for most sites. Otherwise, $G_{max}$ was evaluated empirically from correlative relationships with other in-situ and/or laboratory test results (e.g., Larsson and Mulabdić, 1991; Mayne and Rix, 1995; Hegazy and Mayne, 1995).

Index soil properties and small-strain stiffness $G_{max}$ at each site are reported in Table 10-2. Soils ranged from normally to lightly overconsolidated (e.g. Bothkennar and Shellhaven) to overconsolidated (e.g. kaolin) with an overconsolidation ratio of 8.5.

**Table 10-1.** Database of footing load tests under undrained loading conditions

| Site | Soil Type | GWT below foundation level (m) | Dimensions B x L (mxm) | L/B | Test type | Bearing capacity $q_{ult}$ (kPa)[a] | Reference |
|---|---|---|---|---|---|---|---|
| Bangkok, Thailand | soft clay | 0 | 1.05 x 1.05 | 1 | Full-scale | 154 | Brand et al. (1972) Shibuya & Tamrakar (1999) |
| | | | 0.9 x 0.9 | 1 | | 187 | |
| | | | 0.75 x 0.75 | 1 | | 207 | |
| | | | 0.675 x 0.675 | 1 | | 194 | |
| | | | 0.6 x 0.6 | 1 | | 245 | |
| Belfast, Ireland | soft clayey silt | 0 | 2 x 2 | 1 | Full-scale | 100 | Lehane (2003) |
| Boston Blue Clay, USA | reconstituted soft clay | 0 | 0.0159 x 0.127 | 8 | Model tests | 472[b] | Kinner and Ladd (1973) |
| | | | 0.0159 x 0.127 | 8 | | 428[c] | |
| | | | 0.0159 x 0.127 | 8 | | 379[d] | |
| Bothkennar, UK | soft clay | 0.2 | 2.2 x 2.2 | 1 | Full-scale | 150 | Hight et al. (1997) Jardine et al. (1995) |
| Cowden, UK | glacial till | 0 | 0.865 x 0.865 | 1 | Plate load test | 1600 | Powell & Butcher |
| Fargo, USA (Grain Elevator) | silty clay (sand layer 4.5 to 6m) | 2.2 | 66.5 x 15.9 | 4.2 | Actual failure | 244 | Nordlund and Deere (1972) |
| Speswhite Kaolin | reconstituted clay | 0.026-0.052 | 0.06 x 0.06 | 1 | Model centrifuge | 373 | Stallebrass and Taylor (1997) |
| Shellhaven, UK | soft clay | 0.75 | 5 x 14 | 2.8 | Full-scale | 86 | Schnaid et al. (1993) |

[a] Bearing capacities computed using the hyperbolic asymptote presented in Chapter 2.
[b] Number of tests =2, OCR = 1.
[c] Number of tests =2, OCR = 2.
[d] Number of tests =3, OCR = 4.

Soil rigidity is represented by the ratio of Young's modulus to compressive strength, $E/q_{max}$ (Atkinson, 2000), where $q_{\max} = (\sigma_a - \sigma_r)_{\max} = 2 \cdot s_u$. Young's modulus E can be defined at different strain levels. In this section, the maximum Young's modulus $[E_{\max} = 2G_{\max}(1+\nu)]$ is used to describe soil rigidity. The undrained shear strengths reported in Table 10-2 are backcalculated from the load tests using the hyperbolic extrapolated bearing capacity $q_{ult}$, where $q_{ult} = N_c\ s_u$ with the appropriate bearing capacity factors ($N_c$= 6.14 for all cases except for tests on Boston blue clay, Fargo and Shellhaven that were analyzed as strip footings with $N_c$ = 5.14). The maximum rigidity $E_{max}/q_{max}$ for the natural clays varied between 611 and 1885. The reconstituted kaolin had a much higher $E_{max}/q_{max}$ ratio of 5000, as reported by Atkinson (2000). There is generally good agreement between the computed $E_{max}/q_{max}$ in comparison to worldwide data for a number of different materials summarized by Tatsuoka and Shibuya (1992), shown in Figure 10-1. Data from the current study are plotted as solid symbols. Atkinson (2000) showed $E_{max}/q_{max}$ varying between 5000 (reconstituted kaolin deposit) and 1000 (stiff soils).

The rigidity index $I_r$ is defined as the ratio of the shear modulus to the undrained shear strength $I_R = G/s_u$ (e.g. Vesic 1972). For undrained loading ($\nu$=0.5), the maximum rigidity index $G_{max}/s_u$ relates to the maximum soil rigidity $E_{max}/q_{max}$ according to:

$$G_{\max} / s_u = \frac{2}{3} \cdot E_{\max} / q_{\max}$$

**Table 10-2.** Soil properties in the vicinity of the footings in the database

| Site | PL (%) | LL (%) | $w_c$ (%) | OCR | $G_{max}$ MPa | Operational $s_u$ kPa | $E_{max}/q_{max}$ | Reference |
|---|---|---|---|---|---|---|---|---|
| Bangkok, Thailand | 35 | 90 | 80 | 1-2 | 12[a] | 25-40 | 900-1440 | Brand et al. (1972) Shibuya & Tamrakar (1999) |
| Belfast, Ireland | 22-37 | 41-74 | 40-60 | 1.5-2 | 10[a] | 16.3 | 920 | Lehane (2003) |
| Boston Blue Clay | 39-43 | 18-22 | 100[g] | 1-4 | 46[b] | 74-92 | 750-935 | Kinner and Ladd (1973) |
| Bothkennar, UK | 24-35 | 50-78 | 45-70 | 1.5 | 14[a] | 24.4 | 800 | Hight et al. (1997) Jardine et al. (1995) |
| Cowden, UK | 10-15 | 36-40 | 15-20 | 2-5 | 100[c] | 172 | 873 | Powell & Butcher |
| Fargo, USA (Grain elevator) | 29-43 | 80-112 | 21-74 | 1.2-2 | 50[d] | 40 | 1885 | Nordlund and Deere (1972) |
| Speswhite Kaolin | 31-38 | 53-69 | N/A | 8.5 | 117[e] | 35 | 5000 | Stallebrass & Taylor (1997) Almeida & Parry (1988) Esquivel & Silva (2000) |
| Shellhaven, UK | 26-41 | 70-117 | 40-120 | 1.2-2.1 | 7-11.5[f] | 14 | 960 | Schnaid et al. (1993) |

[a] Downhole test

[b] $G_{max}$ estimated from index soil properties using Weiler (1988) relationship.

[c] Average value based on downhole, crosshole, Rayleigh wave test results reported by Powell and Butcher (2003)

[d] $G_{max}$ estimated from vane shear test results (correlation by Larsson and Mulabdić, 1991).

[e] $E^u_{\max} \big/ q_f$ = 5000 (Atkinson, 2000).

[f] Field measurements of $G_{max}$ available from 3-10 m (Hight and Higgins, 1995). Above 3 m, $G_{max}$ is computed based on piezocone data (Mayne and Rix, 1993).

[g] Water content before consolidation.

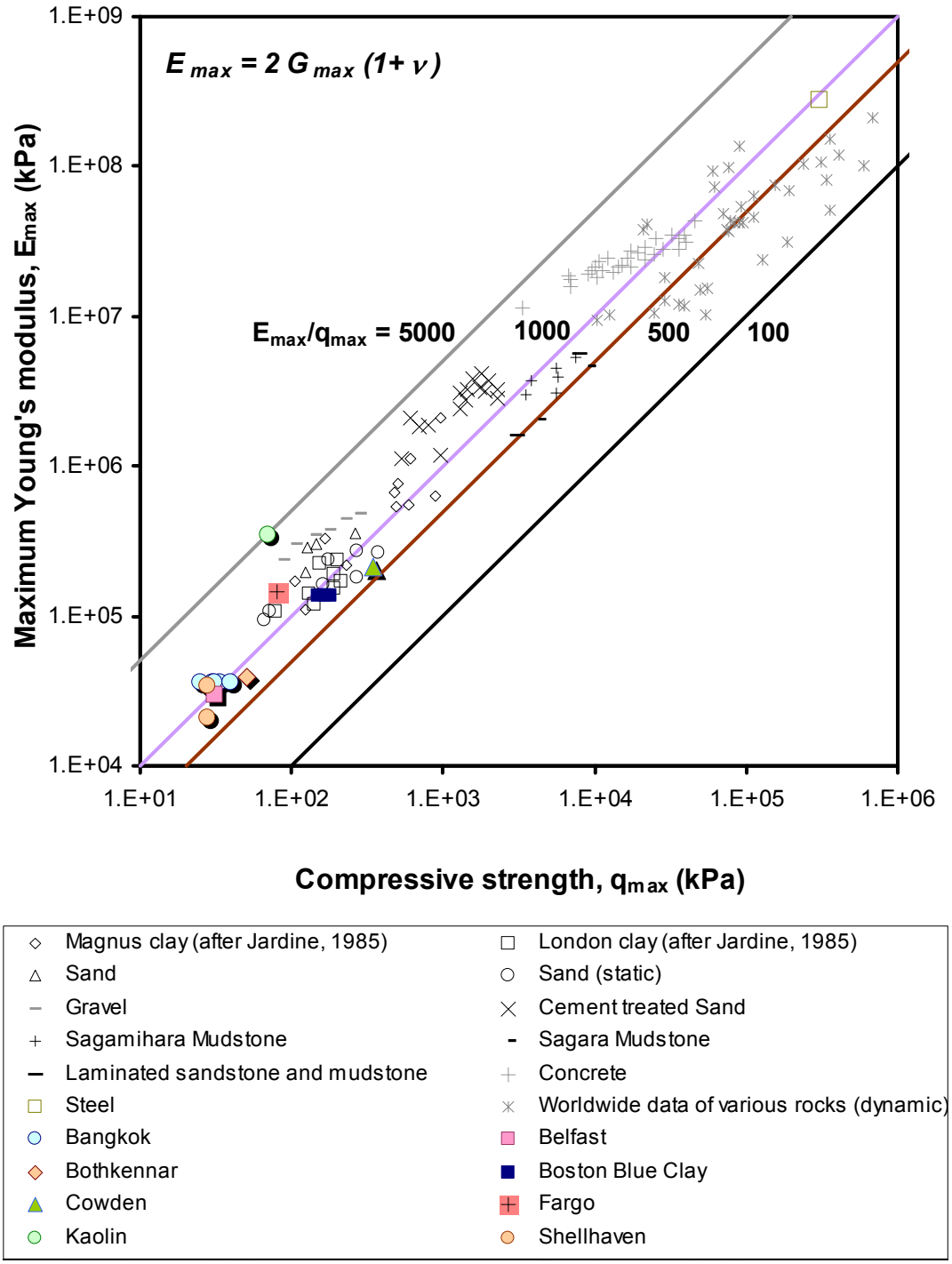


**Figure 10-1.** Relationship between the maximum Young's modulus $E_{max}$ and compressive strength $q_{max}$ for a wide range of materials compared to values used in current study (modified after Tatsuoka and Shibuya, 1992)

#### *10.1.1.1 Non-linear soil properties computed from footing load tests*

For each of the case studies, applied stresses q were normalized by the bearing capacity $q_{ult}$ to provide a mobilized resistance, $q/q_{ult}$. Footing displacements were normalized with respect to the reference displacement $s_r$. The reference displacement value $s_r$ is the displacement intersect of the projected value of the initial elastic soil-foundation stiffness $K_i = E_{max} / B \cdot I$ with bearing capacity $q_{ult}$, or $s_r = q_{ult} \cdot d \cdot I / E_{max}$. Bearing capacities were evaluated by fitting hyperbolae to stress-displacement curves, as presented in Chapter 2. The determination of the initial overall stiffness of the soil-footing system is outlined in more detail in Chapter 9. Computed values of $K_i$ varied between 8.7 MN/m$^3$ (Fargo grain elevator: 66.5 m x 15.9 m) and 10.6 GN/m$^3$ (model centrifuge circular footing). The wide range in the value of $K_i$ reflects the broad variation in footing sizes included in the database, since $K_i$ is inversely proportional with footing width. The values of the reference displacement $s_r$ ranged between 0.02 mm and 28 mm for the kaolin model footing and Fargo grain elevator, respectively. The reference displacement depends on footing size, resulting in a wide range of values. The ratio of the maximum to minimum reference displacements is 1400. Normalizing the reference displacement $s_r$ with respect to footing width resulted in a narrower range of ($s_r$/B) values ranging between $3.4 \times 10^{-4}$ and $4.8 \times 10^{-3}$, with a ratio of maximum to minimum of 14.

**Table 10-3.** Database of footing load test data for undrained loading conditions

| Site | Dimension B x L (m x m) | Bearing capacity $q_{ult}$ (kPa)[a] | Initial stiffness $K_i$ ($MN/m^3$) | Ref displ. $s_r$ (mm) | $s_r/B$ | Fitting parameter g* | Normal limiting strain $x_L$ | Ref. strain $\gamma_r$ (%) | Failure Strain $\gamma_f$ (%) |
|---|---|---|---|---|---|---|---|---|---|
| Bangkok, Thailand | 1.05 x 1.05 | 154 | 65 | 2.4 | $2.3x10^{-3}$ | 0.25 | 41 | 0.21 | 8.6 |
| | 0.9 x 0.9 | 187 | 67 | 2.8 | $3.3x10^{-3}$ | 0.26 | 40 | 0.25 | 10.2 |
| | 0.75 x 0.75 | 207 | 68 | 3.0 | $3.8x10^{-3}$ | 0.36 | 34 | 0.28 | 9.5 |
| | 0.675 x 0.675 | 194 | 67 | 2.9 | $4.0x10^{-3}$ | 0.32 | 30 | 0.26 | 7.9 |
| | 0.6 x 0.6 | 245 | 76 | 3.2 | $4.8x10^{-3}$ | 0.40 | 28 | 0.33 | 9.3 |
| Belfast, Ireland | 2 x 2 | 100 | 25 | 4.0 | $2.0x10^{-3}$ | 0.22 | 46 | 0.16 | 7.5 |
| Boston Blue Clay, USA | 0.016 x 0.13 | 472 | 7559 | 0.062 | $3.9x10^{-3}$ | 1.0 | 22 | 0.20 | 4.3 |
| | 0.016 x 0.13 | 428 | 7559 | 0.057 | $3.6x10^{-3}$ | 1.2 | 19 | 0.18 | 3.4 |
| | 0.016 x 0.13 | 379 | 7559 | 0.05 | $3.2x10^{-3}$ | 0.52 | 37 | 0.16 | 5.9 |
| Bothkennar, UK | 2.2 x 2.2 | 150 | 30.8 | 4.9 | $2.0x10^{-4}$ | 0.4 | 28 | 0.17 | 4.9 |
| Cowden, UK | 0.865 x 0.865 | 1602 | 630 | 2.5 | $2.9x10^{-3}$ | 0.25 | 41 | 0.17 | 7 |
| Fargo, USA (Grain elevator) | 66.5 x 15.9 | 244 | 8.7 | 29 | $7.7x10^{-4}$ | 1.1 | 20 | 0.1 | 2 |
| Kaolin | 0.06 x 0.06 | 373 | 10590 | 0.02 | $3.4x10^{-4}$ | 0.03 | 170 | 0.03 | 5.1 |
| Shellhaven, UK | 5 x 14 | 86 | 10 | 8.8 | $9.3x10^{-4}$ | 0.6 | 33 | 0.19 | 6.1 |

Notes:

- $q_{ult}$ is defined by the hyperbolic asymptote, as discussed in Chapter 2.
- $s_r$ =reference displacement, introduced in Chapter 7.
- $K_i$ is the initial soil-footing stiffness computed according to Equation 7-2.
- Reference displacement $s_r$ is calculated according to Equation 7-1-c.
- B is the footing equivalent diameter circle ( except for Boston Blue Clay and Fargo that are analyzed as strip footing, with B taken as the footing width.
- The hyperbolic fitting parameter f* = 0.99 for all the case studies.
- The normalized limiting strain $x_L$ is back-calculated from the fitting parameter g* according to Equation 9-6

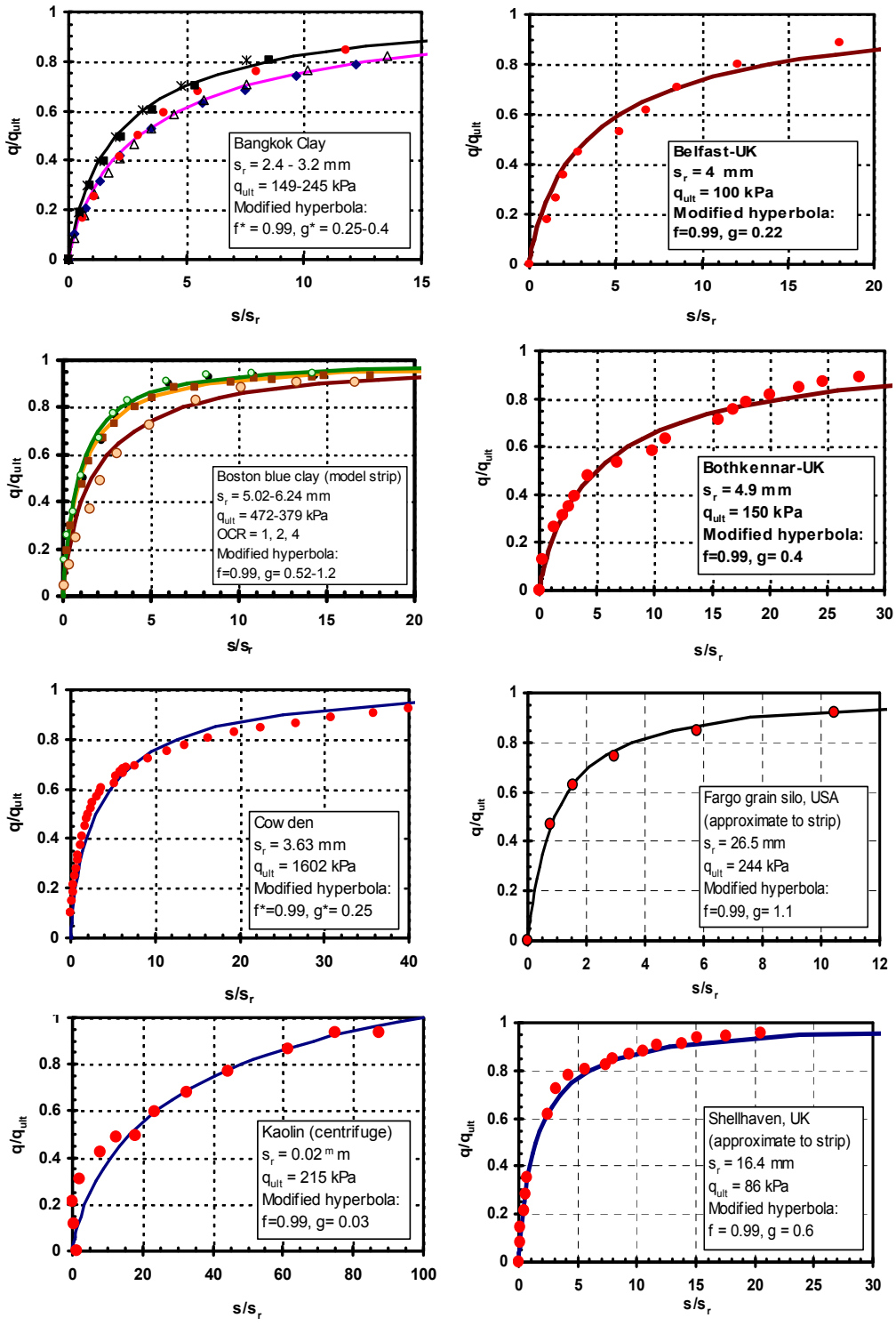


**Figure 10-2.** Fitted hyperbolic functions and normalized stress-displacement curves under shallow footings for undrained loading conditions

Modified hyperbolae were fitted to the normalized stress-displacement curves. Data are presented in Table 10-3. The fitting parameter f* is maintained constant and equal to 0.99, in agreement with statistical fitting of simulated stress-displacement results for all natural soil deposits.

It should be noted that the fitting parameter f* mainly influences the displacement needed to reach failure and has small influence on the working stress region, which is the stress level of concern of engineers. The fitting parameter g* was varied to match the data. The lower values of g* indicate higher degrees of nonlinear stress-displacement behavior. The values of g* and corresponding normalized limiting strain $x_L$ are listed in Table 10-3. All the footings were analyzed as circular except for Boston Blue Clay, Fargo, and Shellhaven. These footings are rectangular in shape with L/B ratio greater or equal to 2.8, and therefore were considered as strip. Values of g* ranged between 1.1 (Fargo) and 0.03 (kaolin), with the corresponding $x_L$ varying between 19 and 170. These values are within the range of 10 to 200 reported by Atkinson (2000).

Using the backcalculated value of the normalized limiting strain $x_L$ and the reference strain $\gamma_r$ ($=s_u/G_{max}$), the average strain to failure $\gamma_f$ of a representative soil element is computed. The respective values for each case are reported in Table 10-3. The computed strains to failure ranged between 2% and 10.2%. The backcalculated strains to failure are plotted versus the representative plasticity index at each site as shown in Figure 10-3. The backcalculated failure strains compare well with failure strains measured in direct simple shear tests presented on the same plot. There is a relatively

good match between the two data sets, except for Fargo. This discrepancy can be attributed to the fact that there is no measured small-strain stiffness and presence of a sand layer approximately 5-m below ground surface. Also, the top soil layer was highly cracked (Nordlund and Deere, 1972).

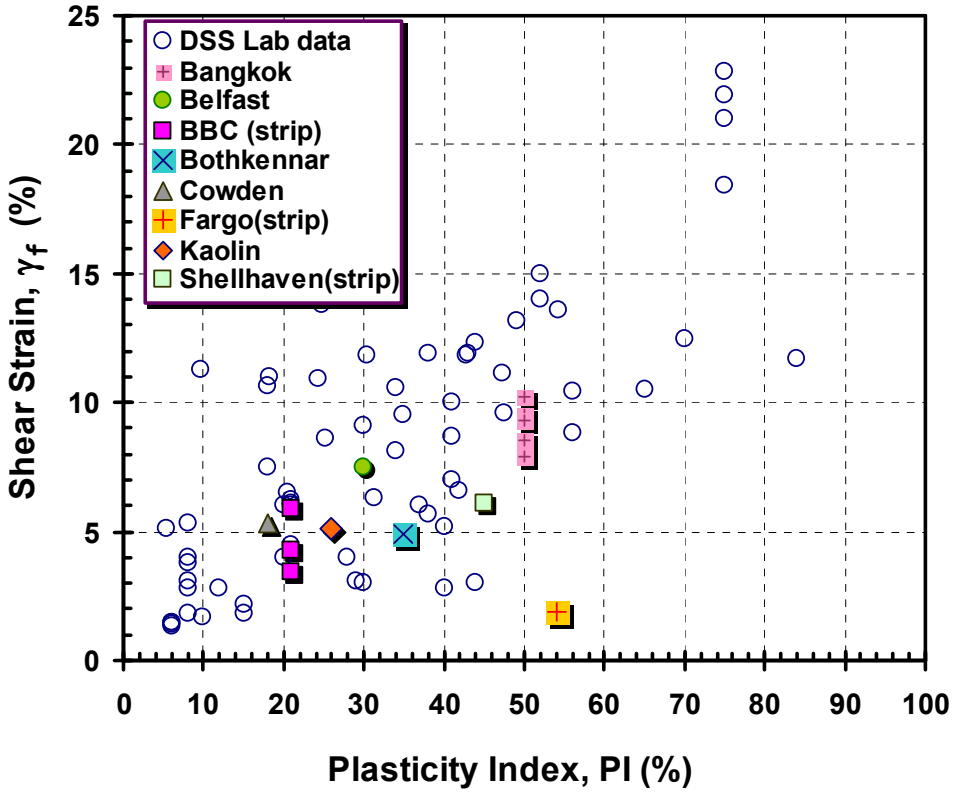


**Figure 10-3.** Comparison of backcalculated failure strains from footing load tests versus failure strains in direct simple shear under undrained loading conditions

### *10.1.2 Drained loading*

In this section, load-displacement data from footing load tests under drained conditions are analyzed. The database consists of 6 footings resting on sand (Briaud and Jeanjean, 1994; Amar et al, 1994), 2 footings on silt (Larsson, 1997), and 5 footings, slowly loaded,

on sandy silty clay till (Larsson, 2001). All eleven tests were performed at four different sites. Table 10-4 summarizes the soil information, footing dimensions, and location of groundwater table relative to the footing. All the footings included in the database are square, with plan sizes varying between 0.5 m x 0.5 m and 3 m x 3 m. The reported bearing capacities are hyperbolic asymptotes. Additional details about determining the bearing capacities of footings are in Chapter 2. The interpreted bearing capacities varied between 571 and 2000 kPa. In comparison with Table 10-1, drained bearing capacities are generally greater than undrained bearing capacity cases.

Due to the high permeability of sands, the footing load tests at the sand sites are considered fully drained. For the Tornhill and Vagverket sites, the rate of loading was conducted slow enough to ensure that the excess porewater pressures, monitored using piezometers, dissipated before the load was increased at each step (Larsson, 1997; Larsson, 2001).

Relevant soil properties are listed in Table 10-5. Soils in the database include sands (Labenne; Texas A and M), sandy silty clay till (Tornhill), and silt (Vagverket). The bulk unit weights varied between 15.5 kN/m$^3$ and 21 kN/m$^3$. Angles of internal friction varied between 30$^o$ and 35$^o$. The small-strain shear modulus was either measured using in-situ methods (crosshole test or seismic cone penetrometer) or evaluated indirectly from cone penetration data. The values of $G_{max}$ ranged from 28 MPa (Vagverket) and 116 MPa (Tornhill).

**Table 10-4.** Database of footing load test data under drained loading conditions

| Site | Soil Type | GWT below foundation level (m) | Dimensions B x L (m x m) | Test type | Bearing capacity $q_{ult}$ (kPa) | Reference |
|---|---|---|---|---|---|---|
| Labenne, France | dune sand | 3 | 0.7 x 0.7 | Full-scale | 1090 | Amar et al (1994) |
| Texas A & M, USA | Eocene deltaic Sand | 4.9 | 1 x 1 | Full-scale | 2000 | Briaud and Gibbens (1999) |
| | | | 1.5 x 1.5 | | 1481 | |
| | | | 2.5 x 2.5 | | 1600 | |
| | | | 3 x 3 | | 1235 | |
| | | | 3 x 3 | | 1073 | |
| Tornhill, Sweden | Sandy silty clay till | 0.2 | 0.5 x 0.5 | Full-scale | 1353 | Larsson (2001) |
| | | | 1 x 1 | | 1667 | |
| | | | 2 x 2 | | 817 | |
| Vagverket , Sweden | Silt | variable | 0.5 x 0.5 | Full-scale | 1120 | Larsson (1997) |
| | | | 1 x 1 | | 571 | |

* B/L =1 for all footings.

**Table 10-5.** Soil properties in the vicinity of the footings in the database of drained loading of shallow footings

| Site | PL (%) | LL (%) | $w_c$ (%) | $\phi'$ (degree) | $\gamma$ KN/m$^3$ | $G_{max}$ MPa | Reference |
|---|---|---|---|---|---|---|---|
| Labenne | N/A | N/A | 5 | 35 | 16 | 30[a] | Amar et al (1994) Jardine and Lehane (1993) |
| Texas A&M | N/A | N/A | 5 | 32[d] | 15.5 | 95-107[b] | Briaud and Gibbens (1999) |
| Tornhill | 10-38 | 20-45 | 10-23 | 30 | 21 | 107-116[c] | Larsson (2001) |
| Vagverket | 18-24 | 30 | 30 | 35 | 19-20 | 28[c] | Larsson (1997) |

[a] $G_{max}$ estimated from cone penetration test reported by Jardine and Lehane (1993) using Mayne and Hegazy (1996)

[b] Shear wave velocities measured using the cross hole method

[c] Shear wave velocities measured using the seismic cone penetrometer

[d] Based on the borehole shear test (Briaud and Gibbens, 1999)

### *10.1.2.1 Non-linear soil properties computed from drained footing load tests*

The normalized stress-displacement curves ($q/q_{ult}$ versus $s/s_r$) were plotted for all the case studies, as shown in Figure 10-4. All relevant parameters ($q_{ult}$, $K_i$, $s_r$, $s_r/B$) are listed in Table 10-6. The maximum global stiffness $K_i$ varied between 85 MN/m$^3$ and 355 MN/m$^3$. Reference displacements $s_r$ varied between 3.5 mm and 13 mm.

Modified hyperbolae were fitted to the normalized stress-displacement curves, shown in Figure 10-6. The hyperbolic fitting parameter f* was maintained at 0.99 for all the case studies. The fitting parameter g* was varied to best match the normalized data. The values of g* ranged from 0.05 (Vagverket) up to 0.45 (Texas A and M – 3 m), with an average of 0.22. The corresponding non-linear parameter $x_L$ varied between 15 and 80 with an average of 39.

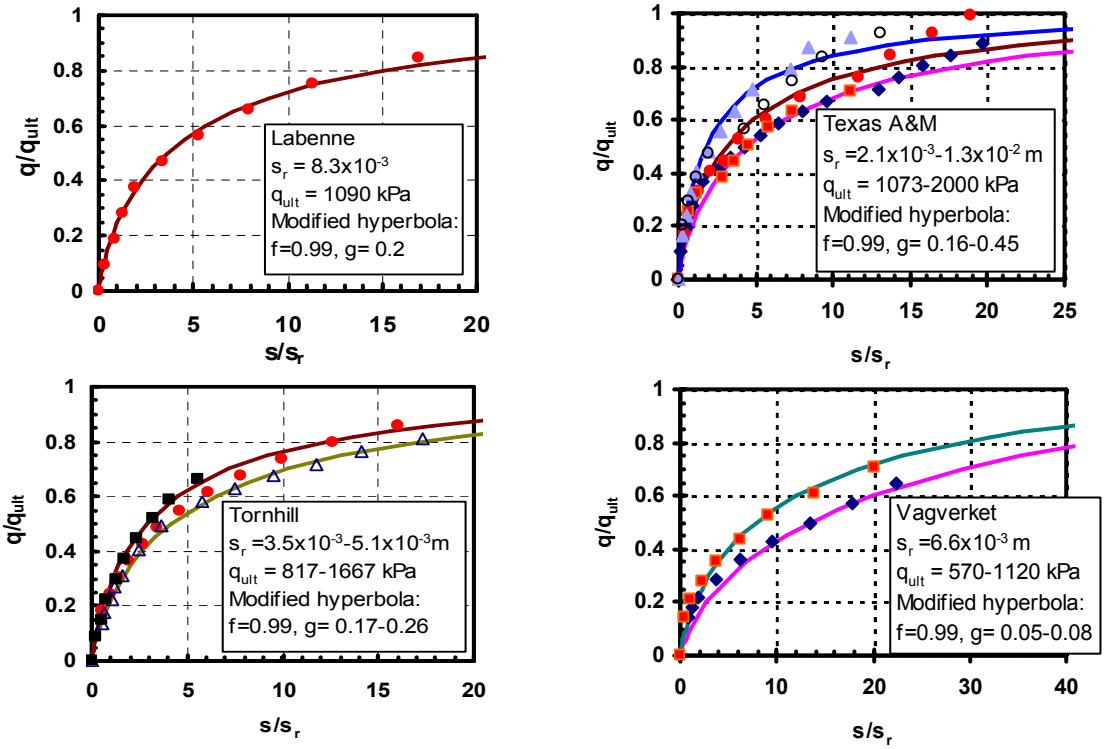


**Figure 10-4.** Fitted hyperbolic functions fitted to normalized stress-displacement curves under shallow footings under drained loading conditions

**Table 10-6.** Database of footing load test data under drained loading conditions

| Site | Dimensions B x L * (m x m) | Bearing capacity $q_{ult}$ (kPa) | Initial stiffness $K_i$ ($MN/m^3$) | Ref. displ. (mm) | Normalized reference displacement $s_r/B$ | Fitting parameter, g * | Normal. limiting strain, $x_L$ |
|---|---|---|---|---|---|---|---|
| Labenne, France | 0.7 x 0.7 | 1090 | 131 | 8.3 | $1.2x10^{-2}$ | 0.2 | 28 |
| Texas A & M, USA | 1 x 1 | 2000 | 271 | 7.4 | $7.4x10^{-3}$ | 0.16 | 44 |
| | 1.5 x 1.5 | 1481 | 214 | 6.9 | $4.6x10^{-3}$ | 0.24 | 29 |
| | 2.5 x 2.5 | 1600 | 131 | 12 | $4.9x10^{-3}$ | 0.18 | 39 |
| | 3 x 3 | 1235 | 97 | 13 | $4.3x10^{-3}$ | 0.45 | 15 |
| | 3 x 3 | 1073 | 97 | 11 | $7.4x10^{-3}$ | 0.39 | 17 |
| Tornhill, Sweden | 0.5 x 0.5 | 1353 | 355 | 7.4 | $7.4x10^{-3}$ | 0.26 | 31 |
| | 1 x 1 | 1667 | 329 | 5.1 | $5.1x10^{-3}$ | 0.18 | 44 |
| | 2 x 2 | 817 | 237 | 3.5 | $1.7x10^{-3}$ | 0.23 | 34 |
| Vagverket, Sweden | 0.5 x 0.5 | 1120 | 169 | 6.6 | $1.3x10^{-2}$ | 0.05 | 80 |
| | 1 x 1 | 571 | 85 | 6.7 | $6.7x10^{-3}$ | 0.08 | 62 |

Notes:

- $q_{ult}$ is defined by the hyperbolic asymptote, as discussed in Chapter 2.
- $K_i$ is the initial soil-footing stiffness computed according to Equation 7-2.
- Reference displacement $s_r$ is calculated according to Equation 7-1-c.
- B is the equivalent diameter circle.
- The hyperbolic fitting parameter f* = 0.99 for all the case studies.
- The normalized limiting strain $x_L$ is back-calculated from the fitting parameter g* according to Equation 9-6

## 10.2 Summary and conclusions

In this Chapter, the closed-form analytical solution was applied to 14 footings under undrained loading conditions and 11 footings under drained loading. The applied stresses were normalized by the hyperbolic extrapolated bearing capacity $q_{ult}$. Displacements are normalized by reference displacement ($s_r = K_i/q_{ult}$). The normalized limiting strains were back-calculated to best fit the normalized stress-displacement data ($q/q_{ult}$ versus $s/s_r$).

For the database of undrained loading, soil stress histories varied from normally consolidated (OCR = 1-2) to overconsolidated (OCR = 8.5). The normalized data were fitted with modified hyperbolae starting at $K_i$ according to the method outlined in Chapter 9. The fitting parameter f* was maintained constant at 0.99, while the fitting parameter g* was varied to fit the data, ranging between 1.1 and 0.03. The corresponding normalized limiting strains were computed. The lowest $x_L$ of 19 and highest of 170 corresponded to the model strip footing tests on Boston Blue Clay and Speswhite remolded kaolin, respectively. Failure strains backcalculated for the case studies compare well with the direct simple shear failure strains suggested by DeGroot et al. (1992).

The soils in the drained loading database contained sands, silty sand clay till, and clay. The angles of internal friction varied between $30^o$ and $35^o$. Due to the high permeability of sands, the footing load tests in the sand sites are considered fully drained. For the Tornhill and Vagverket sites, the rate of loading was slow enough to ensure pore water

pressures, monitored using piezometers, dissipate before the load is increased (Larsson, 1997; Larsson, 2001). Thus these too were drained loading tests.

Stress-displacement data were normalized and plotted as $q/q_{ult}$ versus $s/s_r$. Modified hyperbolae were fitted to the normalized stress-displacement curves. The hyperbolic fitting parameter f* was maintained at 0.99 for all the case studies. The fitting parameter g* was varied to fit the normalized data. The values of g* ranged between 0.05 (Vagverket) and 0.45 (Texas A & M – 3 m), with an average of 0.22. The corresponding nonlinear parameter $x_L$ varied between 15 and 80 with an average of 39.

# CHAPTER XI

# CONCLUSIONS AND RECOMMENDATIONS

## 11.1 Conclusions

A parametric study was performed to model the stress-displacement behavior of vertically loaded shallow footings starting from the fundamental small-strain stiffness $G_{max}$ up to failure. A generalized schematic diagram of the stress-displacement curve of a vertically loaded footing is presented in Figure 11-1. The initial slope of the stress-displacement curve is defined by the soil-footing stiffness obtained from classical continuum theory $K_i$ [$= \frac{2 \cdot G_{max} \cdot (1+\nu)}{B \cdot I}$], where $G_{max}$ = small-strain shear modulus, $\nu$ = Poisson's ratio, B = footing width, and I = displacement influence factor.

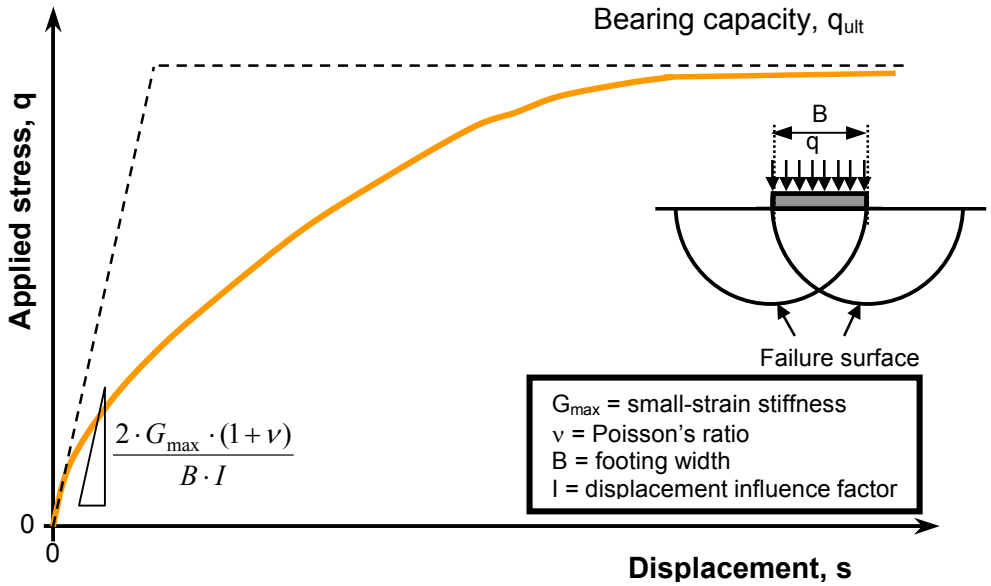


**Figure 11-1.** Schematic diagram of a "typical" stress-displacement curve of a vertically loaded shallow footing

Failure is defined by the bearing capacity defined by classical limit plasticity solutions where $q_{ult}$ [= $N_c s_u$ (undrained loading) or $0.5\gamma^* N_\gamma B$ (drained loading)]. The two regions are connected by a non-linear modulus reduction scheme and used to develop a closed-form approach for practical use. The different parts comprising the stress-displacement footing response were explored in the dissertation. A new analytical non-linear elastic method is proposed to simulate footing behavior. The main findings of the study are outlined herein.

Bearing capacity can be defined conceptually as the ultimate stress $q_{ult}$ when the footing approaches infinite settlement. However, full-scale load tests may not always reach this plateau due to constraints of performance and/or equipment limitations. The hyperbolic asymptote provides a consistent and rational method for evaluating bearing capacity from full-scale load test results. These extrapolated values represent upper limit values that are suitable for comparative purposes. Although full-scale load tests are the most definitive means to determine bearing capacity, they are very expensive and time consuming. Analytical solutions based on limit plasticity theory are more commonly used for obtaining bearing capacity $q_{ult}$.

A realistic evaluation of foundation displacement at working stress levels ($q_{all} = \frac{q_{ult}}{FS}$) is essential to guarantee the structural soundness and serviceability of a structure. Analytical methods based on the theory of elasticity offer versatile solutions that can be used with soil properties measured laboratory and/or in-situ tests. Displacement influence factors provide expedient means to compute foundation displacements. These

factors depend on the footing shape, soil layer thickness, compressible/rigid base interface roughness, stiffness variation with depth, and footing rigidity. A large number of numerical and rigorous solutions are available for specific cases. Most of these solutions are presented either graphically or in tabular format or as equations, making them appear very different from each other, although they are quite similar. Based on Boussinesq's stress distribution, an approximate closed-form solution was derived for use in evaluating the magnitude of displacement at the center of circular flexible footings resting on either homogeneous or Gibson soil profiles of finite to infinite depth. Approximate correction factors are used to account for footing rigidity and depth of embedment. The new solution facilitates deflection calculations for shallow footings and raft foundations in a unified approach that compares reasonably well with other solutions (e.g. Harr, 1966; Poulos, 1968; Ueshita and Meyerhof 1968; Carrier and Christian, 1973; Scott and Boswell, 1975; Milovic, 1992, Mayne and Poulos, 1999). The applicability of this approach is demonstrated for use in rectangular footings is demonstrated, with good comparisons with available rigorous solution Harr (1966) and numerical solution Milovic (1992).

The small-strain shear modulus $G_{max}$ is a fundamental soil property that is applicable to both monotonic static and dynamic loading conditions, as well to both drained and undrained loading. Yet, $G_{max}$ is too stiff for direct use in computing foundation displacements. For dynamic tests, modulus reduction curves [$G/G_{max}$ versus $\log(\gamma)$] have been developed to calculate the shear modulus at a given strain level (e.g. Vucetic and Dobry 1991). A database of static torsional shear tests was created to explore modulus

reduction trends under monotonic loading. The trends are similar to those observed for dynamic tests, yet the more fundamental monotonic tests are not governed by the high strain rate effects influencing data from resonant column and cyclic triaxial tests.

A large number of mathematical formulae have been derived to simulate modulus reduction with increased strain (or stress) levels. A review of modulus reduction schemes for representing non-linear stress-strain response was performed including hyperbolic, logarithmic, parabolic, and power function. The logarithmic modulus reduction scheme (Puzrin and Burland, 1996; 1998) was found to be the most suitable method because the parameters have physical meaning and can be easily measured.

The degree of stress-strain non-linearity represented by a logarithmic function is expressed by the normalized limiting strain $x_L = \gamma_f/\gamma_r$, where $\gamma_f$ is the failure shear strain and $\gamma_r$ is a reference strain computed as $\tau_{max}/G_{max}$. The degree of stress-strain non-linearity increases for higher values of $x_L$. The influence of sample disturbance, mode and rate of loading on the degree of stress non-linearity were reviewed by fitting $x_L$ values to available laboratory test data.

The normalized limiting strain $x_L$ can be computed knowing the small-strain stiffness $G_{max}$, strength $\tau_{max}$, and failure strain $\gamma_f$. The small-strain stiffness $G_{max}$ can either be measured from in-situ tests (e.g. seismic piezocone) or using empirical correlations (e.g. Hardin, 1978). Similarly, soil strength can either be measured in the laboratory (e.g. triaxial compression, direct simple shear, triaxial extension) or evaluated from in-situ

tests (e.g. cone penetration test CPT, dilatometer DMT, standard penetration test SPT). Accordingly, the reference strain $\varepsilon_r$ can be computed in a straightforward manner. Due to the difficulty of obtaining "undisturbed" soil specimens, it would be beneficial to estimate the strain at failure $\gamma_f$.

The logarithmic modulus reduction scheme is incorporated into a non-linear elastic plastic model in three-dimensional stress space. The shear modulus is maintained constant at $G = G_{max}$ below a specified threshold strain $\gamma_{th}$. The degree of soil non-linearity is defined by the normalized limiting strain $x_L$. When a yield surface is reached, soil becomes perfectly plastic where the stress-strain relationship is defined by a flow rule. The model was formulated to allow the representation of both associated and non-associated flow. The logarithmic non-linear elastic plastic model LOGNEP was encoded using FISH language in the finite difference program FLAC. For $x_L = 1$, the simulated LOGNEP stress-strain response becomes linear elastic plastic. Accordingly, the LOGNEP model was verified versus the FLAC built-in Drucker-Prager model for $x_L = 1$, with excellent agreement. LOGNEP has the advantage of defining the degree of non-linearity using the normalized limiting strain $x_L$ which is easily calculated from soil properties.

One of the objectives of this research is to probe the parallelism between the behavior of a single soil element and the overall stress-displacement of shallow footings. Typically, soil stress-strain response can be described as partially-saturated, fully-undrained, or fully-drained. In the current research, only completely undrained ($\nu=0.5$) and drained

($\nu$=0.2) stress-strain responses were considered. For the undrained footing response to vertical loading, displacements were found to be controlled by the small-strain shear modulus $G_{max}$, normalized limiting strain $x_L$, undrained shear strength $s_u$, and footing width B or diameter d. A new normalization scheme was introduced to account for the effects of the small-strain shear modulus $G_{max}$, undrained shear strength $s_u$, and footing width B or diameter d. Applied stresses are normalized with respect to the ultimate bearing capacity $q_{ult}$ while displacements are normalized by a reference displacement ($s_r=q_{ult}/K_i$), where $K_i$ is the initial stiffness of the footing-soil system. The normalized simulated stress-displacement data are reduced to functions of the normalized limiting strain $x_L$. The validity of the normalization scheme was verified for both circular and strip footings. Generalized stress-displacement curves were generated to simulate the response of vertically loaded circular and strip footings for different values of the normalized limiting strain $x_L$. Similarly, the stress-displacement response of circular and strip footings -under drained conditions- was simulated using LOGNEP for different soil properties. Generalized stress-displacement response curves were generated for $\phi'= 30^o$, $35^o$, and $40^o$, for both circular and strip footing subjected to vertical loading.

An approximate closed-form solution was introduced to simulate the stress-displacement response of vertically loaded footings within an elastic framework. The proposed method deals with the footing-soil system as an elastic medium with an average modulus K. The soil-footing stiffness starts at an initial stiffness $K_i$ (equivalent to the small-strain shear modulus $G_{max}$). This "global" modulus reduces with the increase in applied stress level represented by $q/q_{ult}$, where $q_{ult}$ is determined by bearing capacity. A modified hyperbola

(Fahey and Carter, 1993; Fahey et al., 1994; Fahey, 1998) was used as simple means to reduce $K_i$ with the applied stress level q. The modified hyperbola was fitted to normalized stress-displacement response data simulated using the LOGNEP model. The hyperbolic fitting parameters f* and g* (describing the stress-displacement response of the footing) were matched to the normalized limiting strain $x_L$ (describing the stress-strain behavior of a soil element). It should be noted that the normalized applied stress $q/q_{ult}$ is the reciprocal of the factor of safety, allowing for simpler computations of non-linear stress-displacement response in routine design.

The approximate closed-form solution was calibrated using a database of stress-displacement response data of full-scale footing and plate load tests, model plate tests, and centrifuge model load tests. The database incorporated data from undrained and drained loading conditions. Soils included in the database comprise clays, silts and sands. The small-strain shear modulus $G_{max}$ was measured using in-situ and/or laboratory tests for most of the case studies. When no actual measurements were available, $G_{max}$ was evaluated using index soil properties. The fitting parameter f* was maintained constant at 0.99, for both undrained and drained loading conditions. For undrained loading, the fitting parameter g* varied between 1.1 and 0.03, with equivalent normalized limiting strain $x_L$ varying between 19 and 170. Corresponding backfigured failure strains $\gamma_f$ were computed and found to compare well with the direct simple shear failure strains compiled by DeGroot (1992) further expanded database as presented in Chapter 5. For drained loading, the fitting parameter g* varied between 0.05 and 0.45 with corresponding $x_L$ values of 80 and 15.

## 11.2 Proposed closed-form method for computing footing displacements

1. Calculate bearing capacity ($q_{ult}$) according to:

   - Undrained loading: $q_{ult} = N_c^* \cdot s_u$, where $N_c^*$ = 5.14 and 6.00 for shallow strip and square/circular footings, respectively; and $s_u$ is the undrained shear strength.
   - Drained loading: $q_{ult} = 0.5 \cdot B \cdot \gamma^* \cdot N_\gamma^*$, where B = footing width, $\gamma^*$ = effective or total unit weight depending on groundwater level, $N_\gamma^*$ = bearing capacity factors ($\psi = 0^o$, c=0) given in Table 11-1.

**Table 11-1.** Summary of $N_\gamma$ values for smooth circular and strip footings

| $\phi'$ ($^O$) | Circular Footing | Strip Footing |
|---|---|---|
| 20 | 1.5 | 1.5 |
| 30 | 6.7 | 5.9 |
| 35 | 15.0 | 11.4 |
| 40 | 36.5 | 22.1 |

Notes:
1. Angle of dilation $\psi = 0^o$
2. Cohesion intercept c' = 0

2. Compute the initial "global" soil-footing stiffness ($K_i$):

$$K_i = \frac{2 \cdot G_{\max} \cdot (1+\nu)}{B \cdot I_h \cdot I_F \cdot I_E} \quad \text{.....(11-1)}$$

where $G_{max}$ = small-strain shear modulus, $\nu$ = Poisson's ratio = 0.5 and 0.2 for undrained and drained loading, respectively; B = footing width, $I_h$ = displacement influence factor, $I_F$ = foundation flexibility influence factor, and $I_E$ = influence

factor for embedment. For circular footings, the influence factors can be computed as shown in Table 11-2. The influence displacement factors for strip footings are 1.31 and 1.90 for undrained loading (ν=0.5) and drained (ν=0.2) analyses, respectively, according to Milovic (1992).

**Table 11-2.** Summary of equations for computing displacements under circular footings

| | |
|---|---|
| Generalized Equation for computing displacement | $s = \frac{q \cdot d \cdot I_h \cdot I_F \cdot I_E \cdot (1-\nu^2)}{E_s}$ |
| Displacement influence factor for flexible footings on homogeneous soil profile, $I_G$ | $I_h = \left(1 + h^* - \frac{2 \cdot h^{*2} + 1}{\sqrt{4 \cdot h^{*2} + 1}}\right)$ |
| Foundation rigidity influence factor, $I_F$ | $I_F \approx \frac{\pi}{4} + \frac{1}{4.6 + 10K_F}$ |
| Embedment influence factor, $I_E$ | $I_E \approx 1 - \frac{1}{3.5\exp(1.22\nu - 0.4)\left[(d/z_E) + 1.6\right]}$ |
| Notes:<br>s= foundation displacement.<br>q= average applied stress.<br>d= foundation diameter.<br>$I_h$= elastic displacement influence factor for a flexible footing on a homogeneous soil layer.<br>$I_F$= foundation flexibility influence factor.<br>$I_E$= influence factor for embedment.<br>ν= soil Poisson's ratio.<br>$E_{so}$= equivalent elastic soil Young's modulus beneath foundation base.<br>h* = thickness factor = h/d.<br>$K_F$ = foundation flexibility factor.<br>$E_{foundation}$ = modulus of elasticity of the foundation material (e.g. reinforced concrete).<br>$E_{soil}$ = average soil modulus beneath the foundation over a depth z = 2d.<br>t = foundation thickness.<br>$z_E$ = depth to foundation base beneath ground surface. | |

3. Evaluate the normalized limiting strain $x_L = \frac{G_{\max}}{G_{\min}}$ defining the degree of stress-strain non-linearity where $G_{\max} = \rho_T \cdot V_s^2$ and $G_{\min} = \frac{\tau_{\max}}{\gamma_f}$. The shear wave velocity $V_s$, shear strength $\tau_{max}$, and shear strain at failure $\gamma_f$ can be obtained from laboratory and/or in-situ tests:

- High-quality "undisturbed" soil specimens are essential for all laboratory tests. The shear wave velocity $V_s$ can be measured from resonant column, bender elements, torsional shear apparatus, and specially instrumented triaxial tests with internal local strain measurements. Strength and strain to failure are measured from direct simple shear, triaxial and/or plane strain compression and extension tests.
- The shear wave velocity $V_s$ is measured from in-situ geophysical tests (e.g. crosshole test, downhole test, spectral analysis of surface waves). Shear strength $\tau_{max}$ evaluated from in-situ tests (e.g. CPTu, DMT). The seismic piezocone and dilatometer provide expedient and economic means for determining both $G_{max}$ and $\tau_{max}$. For clays under undrained loading, shear strain at failure $\gamma_f$ can be estimated using DeGroot et al. (1992) database showing $\gamma_f$ increases with plasticity index. For drained loading of sands, it was shown that the failure strain $\gamma_f$ depends on the confining stress, relative density, and degree of particle angularity.

4. Based on the value of the normalized limiting strain $x_L$, footing type, and drainage type, appropriate modulus reduction factor ($r_f = G/G_{max}$) are presented in Table (11-3).
5. Evaluate the stress-displacement response of the footing according to:

$$s = \frac{q \cdot B \cdot I}{2 \cdot G_{\max} \cdot (1+\nu) \cdot r_f} \quad \text{.....(11-2)}$$

**Table 11-3.** Formulae for computing modulus reduction factor $r_f$

| Footing shape | Drainage | Reduction factor, $r_f$ |
|---|---|---|
| Circular | Undrained | $r_f = 1 - 0.99\left(\frac{q}{q_{ult}}\right)^{\left(\frac{14.29}{x_L^{1.05}} - 0.034\right)}$ |
| | Drained $\phi' = 30^o$ | $r_f = 1 - 0.99\left(\frac{q}{q_{ult}}\right)^{\left(\frac{9.09}{x_L} - 0.03\right)}$ |
| | Drained $\phi' = 35^o$ | $r_f = 1 - 0.99\left(\frac{q}{q_{ult}}\right)^{\left(\frac{1.96}{x_L} - 0.17\right)}$ |
| | Drained $\phi' = 40^o$ | $r_f = 1 - \left(\frac{q}{q_{ult}}\right)^{\left(\frac{2.00}{x_L^{0.91}}\right)}$ |
| Strip | Undrained | $r_f = 1 - 0.99\left(\frac{q}{q_{ult}}\right)^{\left(\frac{37.04}{x_L^{1.16}} - 0.041\right)}$ |
| | Drained $\phi' = 30^o$ | $r_f = 1 - (0.99 - \frac{2.12}{x_L}) \cdot \left(\frac{q}{q_{ult}}\right)^{\left(\frac{4.35}{x_L^{0.7}} - 0.06\right)}$ |
| | Drained $\phi' = 35^o$ | $r_f = 1 - (0.99 - \frac{1.89}{x_L}) \cdot \left(\frac{q}{q_{ult}}\right)^{\left(\frac{3.45}{x_L^{0.7}} - 0.06\right)}$ |
| | Drained $\phi' = 40^o$ | $r_f = 1 - (0.99 - \frac{1.66}{x_L}) \cdot \left(\frac{q}{q_{ult}}\right)^{\left(\frac{2.50}{x_L^{0.7}} - 0.05\right)}$ |

## 11.3 Simplified closed-form method for computing footing displacements

Generally, geotechnical engineers are interested in estimating footing displacements in the working stress region (factor of safety greater than 3). For factors of safety between 2 and 10, a simplified formula was developed to calculate footing displacements under circular footings according to ($2 < FS < 10$):

$$\frac{s}{s_r} = \frac{\theta \cdot \left(\frac{G_{\max}}{G_{\min}}\right)^{0.85}}{FS^{1.6}} \quad \text{.....(11-3)}$$

where:

s = footing displacement.

$s_r$ = reference displacement = $\frac{q_{ult} \cdot I_h \cdot I_F \cdot I_E}{d \cdot G_{\max} \cdot (1+\upsilon)}$.

$I_h$, $I_F$, $I_E$ = displacement, footing flexibility and embedment influence factors, respectively (refer to Table 11-2).

$G_{max}$ = representative small-strain shear modulus = $\rho_T^2 \cdot V_s^2$.

$\rho_T$= representative total soil mass density.

$V_s$ = representative shear wave velocity.

$G_{min}$ = minimum secant shear modulus = $\frac{\tau_{\max}}{\gamma_f}$.

$\tau_{max}$ = representative soil strength.

$\gamma_f$ = representative failure strain.

$\nu$ = Poisson's ratio.

$\theta$ = constant dependent on drainage type and friction angle according to Table (11-4).

q = applied stress.

$q_{ult}$ = ultimate bearing capacity.

**Table 11-4.** Values of constant θ

| Friction angle, ϕ' ($^o$) | θ |
|---|---|
| Undrained "ϕ = 0$^o$" | 0.58 |
| Drained, 30$^o$ | 0.56 |
| Drained, 35$^o$ | 0.75 |
| Drained, 40$^o$ | 1.06 |

The accuracy of Equation 11-3 in representing the normalized displacement of circular footings is demonstrated in Figures 11-2 and 11-3, which show the variation of the normalized displacement $s/s_r$ with factor of safety $q/q_{ult}$ for different degrees of non-linearity. Simulated results are presented as dots while the approximate closed-form solution is shown as solid lines. Good match is found between the simulated and closed-form solutions.

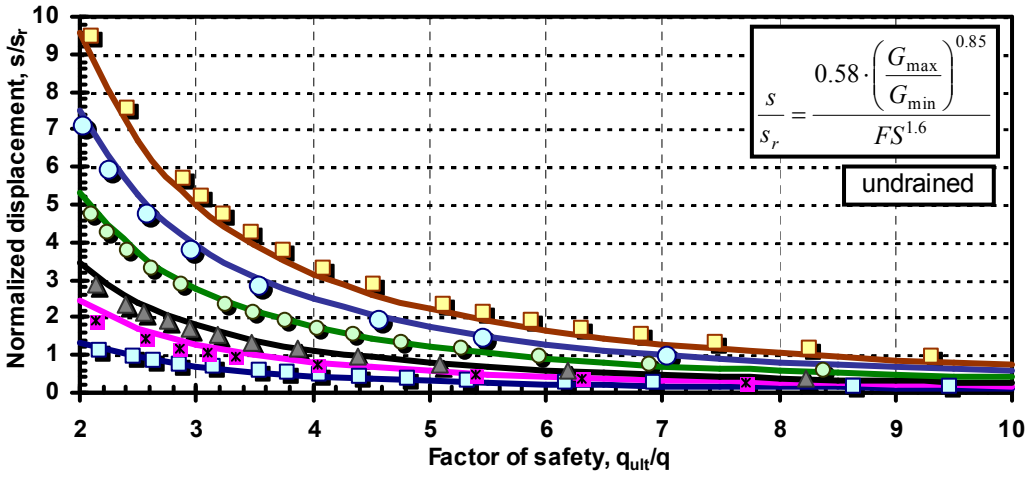


**Figure 11-2.** Variation of the normalized footing displacement ($s/s_r$) with factor of safety for different normalized limiting strains for undrained loading of circular footings

Alternatively, Equation 11-2 can be reformatted to calculate displacement (s) as a function of applied stress (q) according to:

$$s \approx \frac{d \cdot I_h \cdot I_F \cdot I_E}{2 \cdot G_{\max}^{0.15} \cdot G_{\min}^{0.85} \cdot (1+\nu)} \cdot \theta \cdot \frac{q^{1.6}}{q_{ult}^{0.6}} \quad \text{.....(11-3)}$$

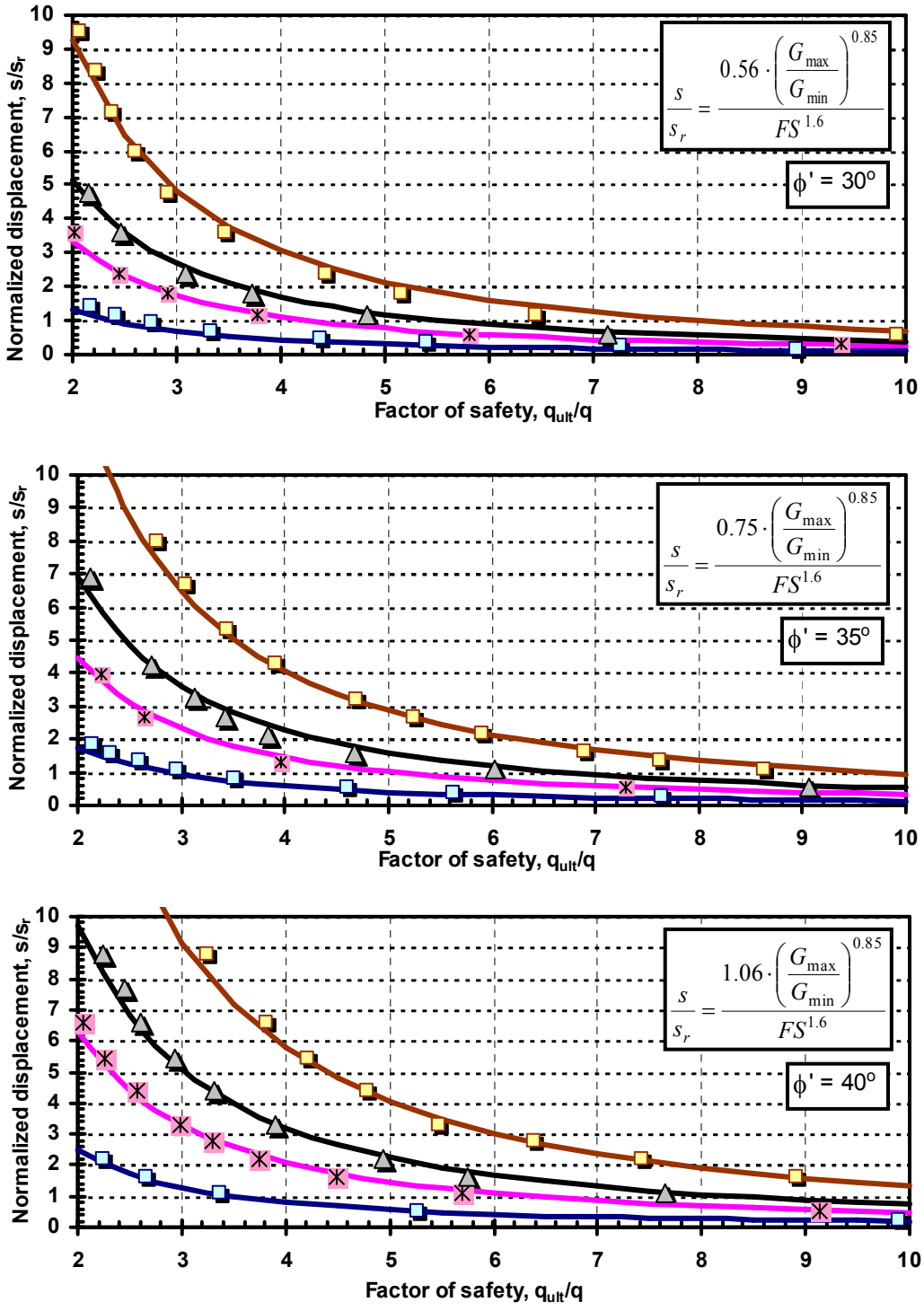


**Figure 11-3.** Variation of the normalized footing displacement ($s/s_r$) with factor of safety for different normalized limiting strains for drained loading of circular footings for f' = 30°, 35°, 40°

## 11.4 Recommendations for future research

The current study proposed numerical and analytical solutions to the small-strain stiffness $G_{max}$ in modeling non-linear response of shallow footings. It would be highly desirable to explore the applicability of the same procedure for use with deep foundations under both drained and undrained conditions.

The non-linearity of the soil stress-strain response was defined using small-strain soil properties ($G_{max}$, $\gamma_{th}$) and high-strain levels ($s_u$ or $\tau_{max}$). The possibility of measuring a soil modulus at an intermediate stress level would improve the degree of accuracy of defining the degree of stress-strain non-linearity. An intermediate soil modulus can be obtained using the research dilatometer (e.g. Campanella et al., 1985) and/or the pressuremeter (e.g. Mayne, 2001).

# APPENDIX A

## SHALLOW FOUNDATION LOAD-DISPLACEMENT DATABASE

A database of 29 load tests on footings and large plates was compiled to examine the different criteria to determine bearing capacity. The full set of data is from 14 test sites, as presented in Table A-1. The case histories include a wide range of surface foundations varying from 0.4-m square footings (Federal University of Rio Grande do Sul, Brazil) to large unexpected failures of mat foundations 66.5 x 15.9 m (Fargo, USA). Soil types range from soft to stiff clays to silts and sands.

**Table A-1.** Database of load test data on shallow footings

| *Site* | *Soil Type* | *GWT (m)* | *Foundation dimensions B x L (m x m)* | *Test No.* | *Drainage Conditions during loading* | *Reference:* |
|---|---|---|---|---|---|---|
| Bangkok, Thailand | Soft clay | 0 | 1.05 x 1.05 | BK-1 | Undrained | Brand et al. (1972) |
| | | | 0.9 x 0.9 | BK-2 | | |
| | | | 0.75 x 0.75 | BK-3 | | |
| | | | 0.675 x 0.675 | BK-4 | | |
| | | | 0.6 x 0.6 | BK-5 | | |
| Belfast, Ireland | Soft clayey silt | 0 | 2 x 2 | BL-1 | Undrained | Lehane (2003) |
| Bothkennar, UK | Soft marine to estuarine clay | 0.2 | 2.2 x 2.2 | BO-1 | Undrained | Hight et al. (1997) Jardine et al. (1995) |
| Cowden, UK | Glacial till | 1[a] | 0.865 x 0.865 | CO-1 | Undrained | Marsland & Powell (1980) |
| | | | 0.865 x 0.865 | CO-2 | | |
| Fargo, USA (Grain Elevator) | Silty clay (sand layer 4.5 to 6m) | 2.2 | 66.5 x 15.9 | FO-1 | Undrained | Nordlund and Deere (1972) |
| Federal University of Rio Grande do Sul, Brazil | Silty sand residuum | 4 | 0.4 x 0.4 | BR-1 | Partially Saturated | Consoli et al. (1998) |
| | | | 0.7 x 0.7 | BR-2 | | |
| Greenfield, Portugal | Silty sand to silty clayey | variable | 1.2 x 1.2 (Circular) | GR-1 | Partially Saturated | Viana da Fonseca (2001) |
| Haga, Norway | Medium stiff OC clay | > 8 | 1 x 1 | HA-1 | Undrained | Andersen and Stenhamar (1982) |
| | | | 1 x 1 | HA-2 | | |
| Labenne, France | Dune sand | 3 | 0.7 x 0.7 | LA-1 | Drained | Amar, et al |
| Shellhaven, UK | Soft clay | 0.75 | 5 x 14 | SN-1 | Undrained | Schnaid et al. |
| Texas A & M, USA | Eocene deltaic sand | 4.9 | 1 x 1 | TX-1 | Drained | Briaud and Gibbens (1999) |
| | | | 1.5 x 1.5 | TX-2 | | |
| | | | 2.5 x 2.5 | TX-3 | | |
| | | | 3 x 3 | TX-4 | | |
| | | | 3 x 3 | TX-5 | | |
| Tornhill, Sweden | Clay till | 0.2 | 0.5 x 0.5 | TL-1 | Drained | Larsson (1997) |
| | | | 1 x 1 | TL-2 | | |
| | | | 2 x 2 | TL-3 | | |
| Vagverket, Sweden | Silt | 0.2 | 0.5 x 0.5 | VT-1 | Drained | Larsson (1997) |
| | | | 1 x 1 | VT-2 | | |
| Vattahammar, Sweden | Silt to clayey silt | 12.65 | 0.5 x 0.5 | VR-1 | Drained | Larsson (1997) |
| | | | 1 x 1 | VR-2 | | |

Notes:

[a] Underdrainage to lower chalk layer. Ground water table is not fully hydrostatic.

GWT = groundwater table *below foundation level*

B = footing width

L = footing length

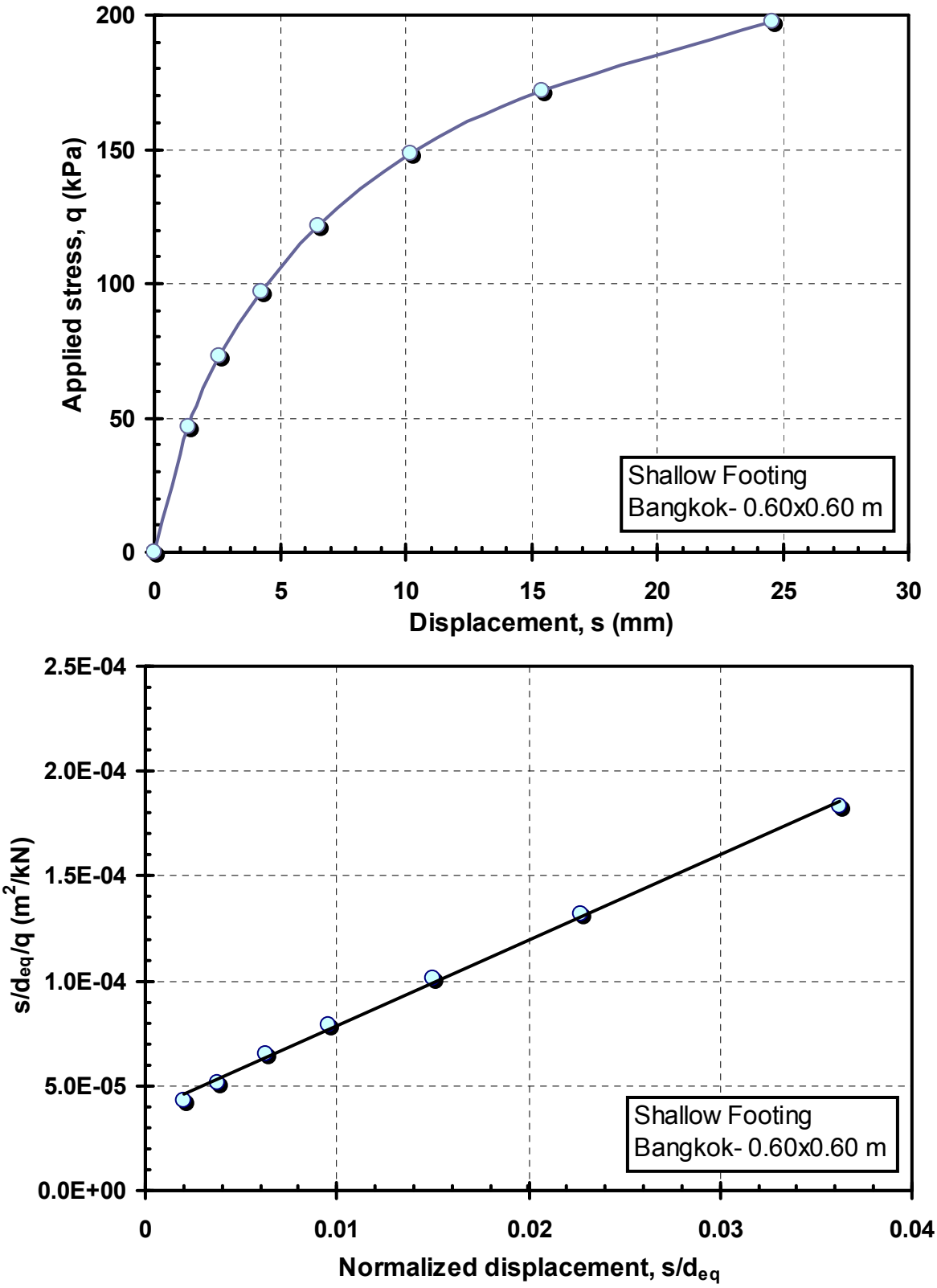


**Figure A-1.** Footing stress-displacement response plotted on (a) standard axes, (b) per Chin's transformed axes, (raw data from Brand et al., 1972)

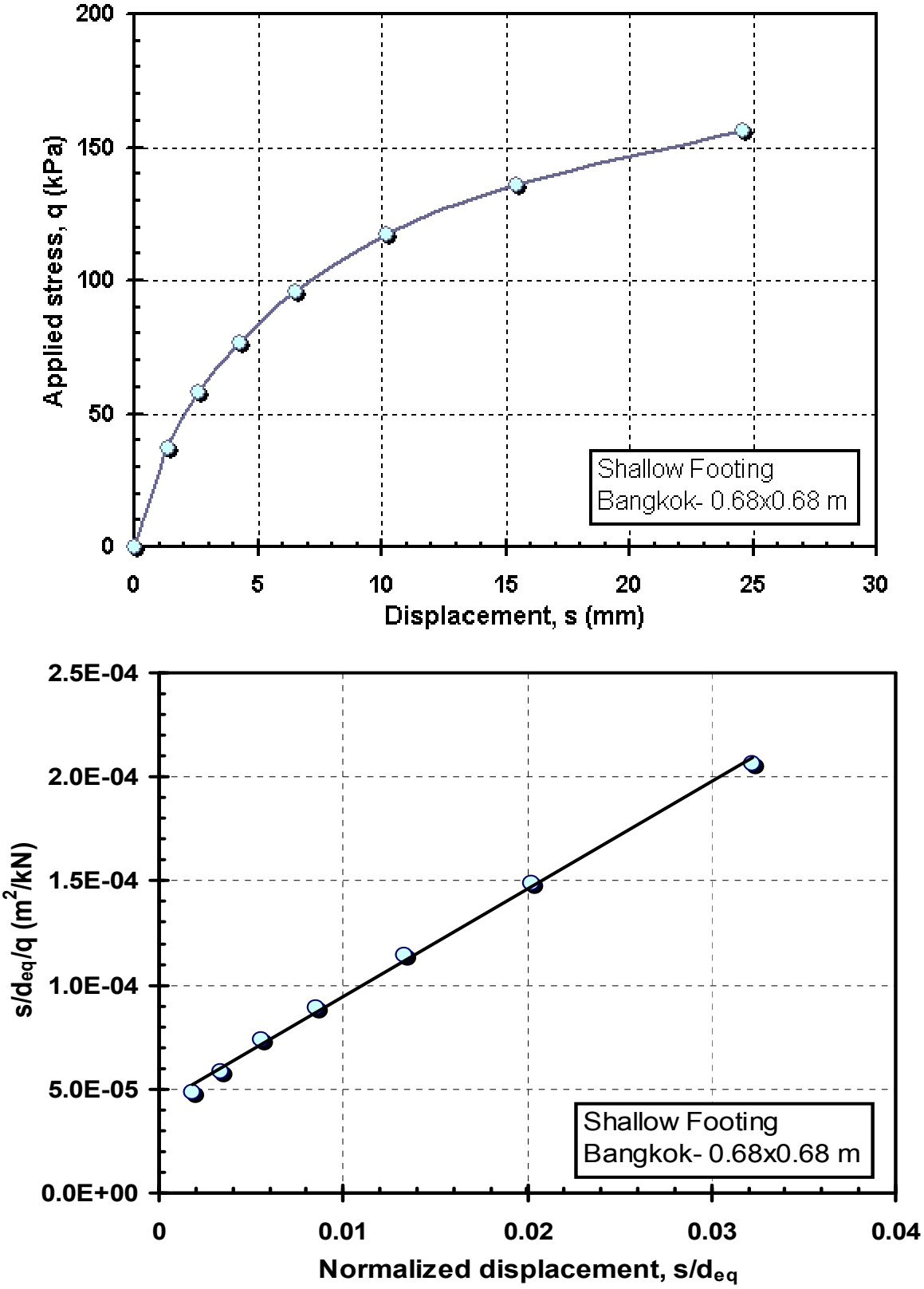


**Figure A-2.** Footing stress-displacement response plotted on (a) standard axes, (b) per Chin's transformed axes (raw data from Brand et al., 1972)

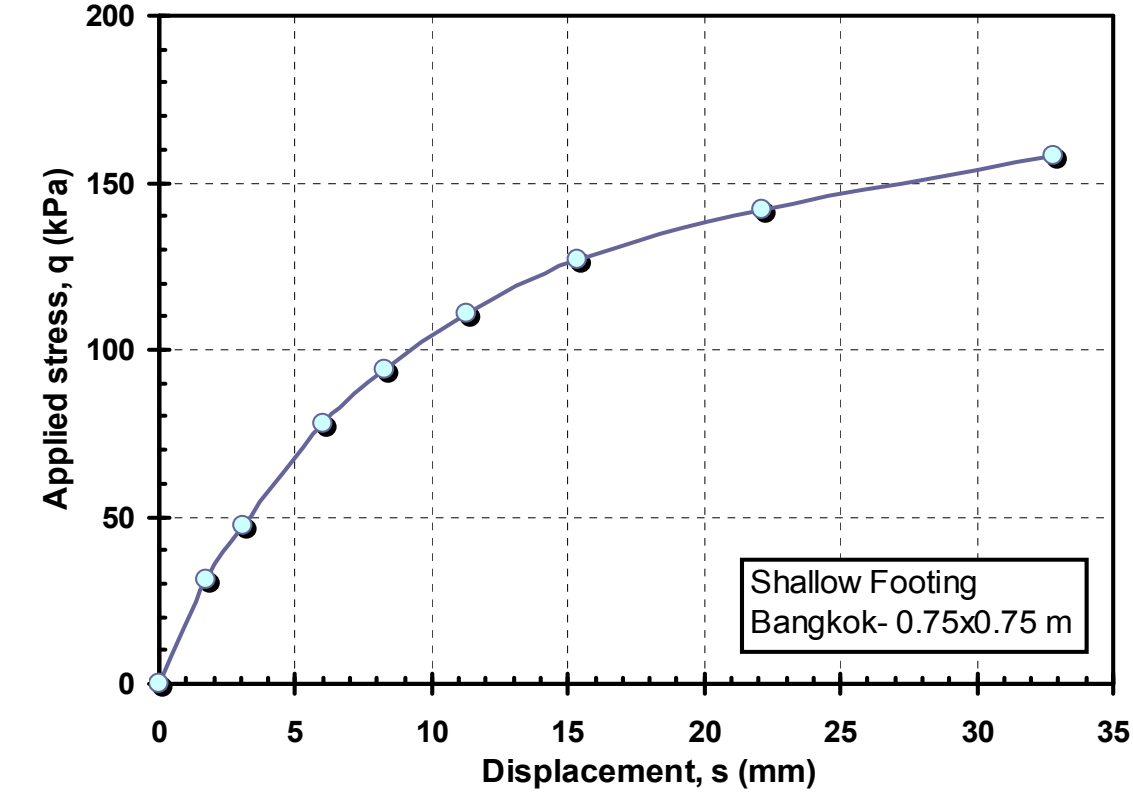


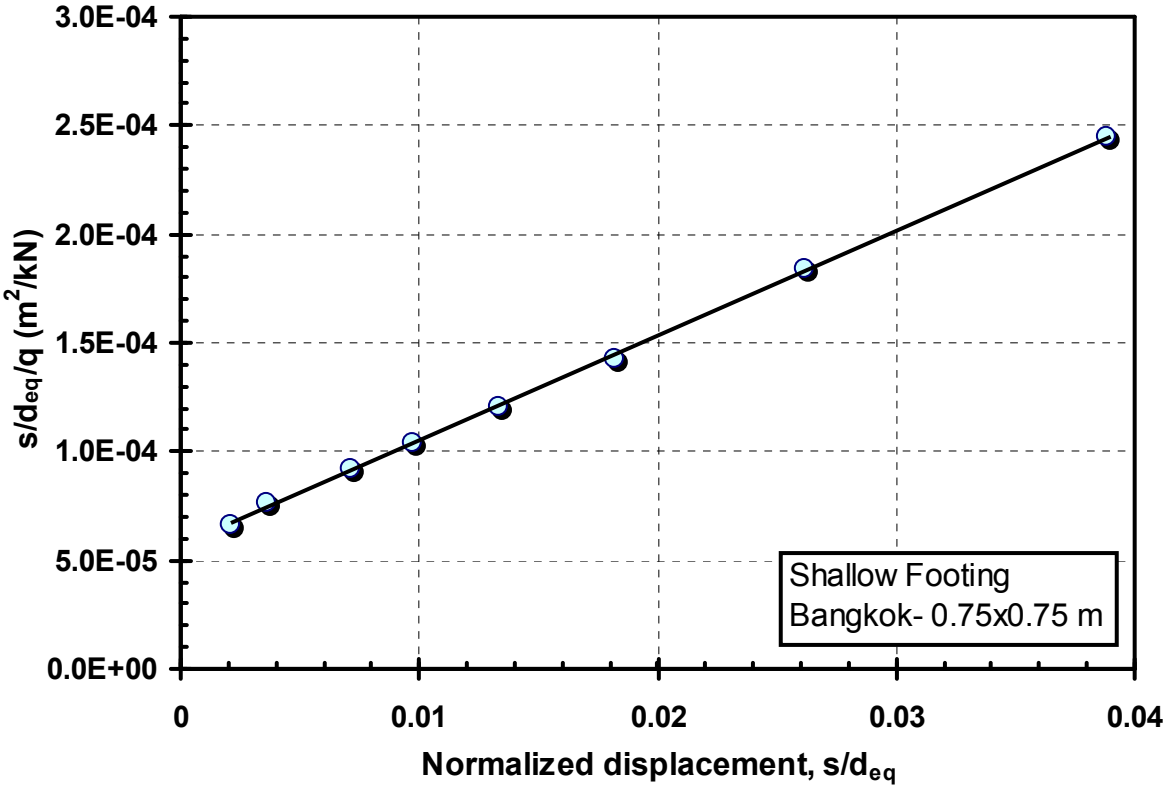


**Figure A-3.** Footing stress-displacement response plotted on (a) standard axes, (b) per Chin's transformed axes, and (c) per De Beer's transformed axes (raw data from Brand et al., 1972)

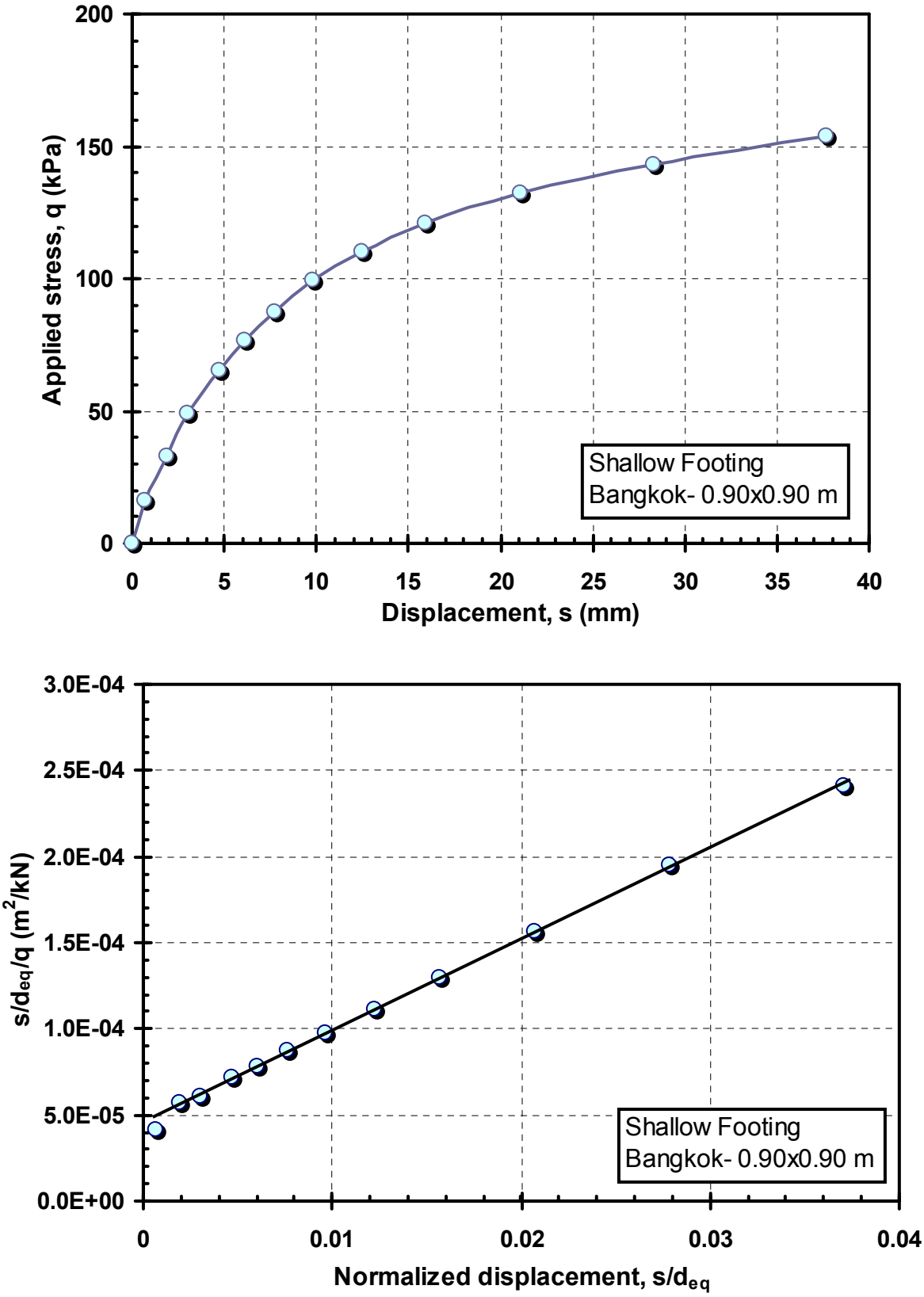


**Figure A-4.** Footing stress-displacement response plotted on (a) standard axes, (b) per Chin's transformed axes (raw data from Brand et al., 1972)

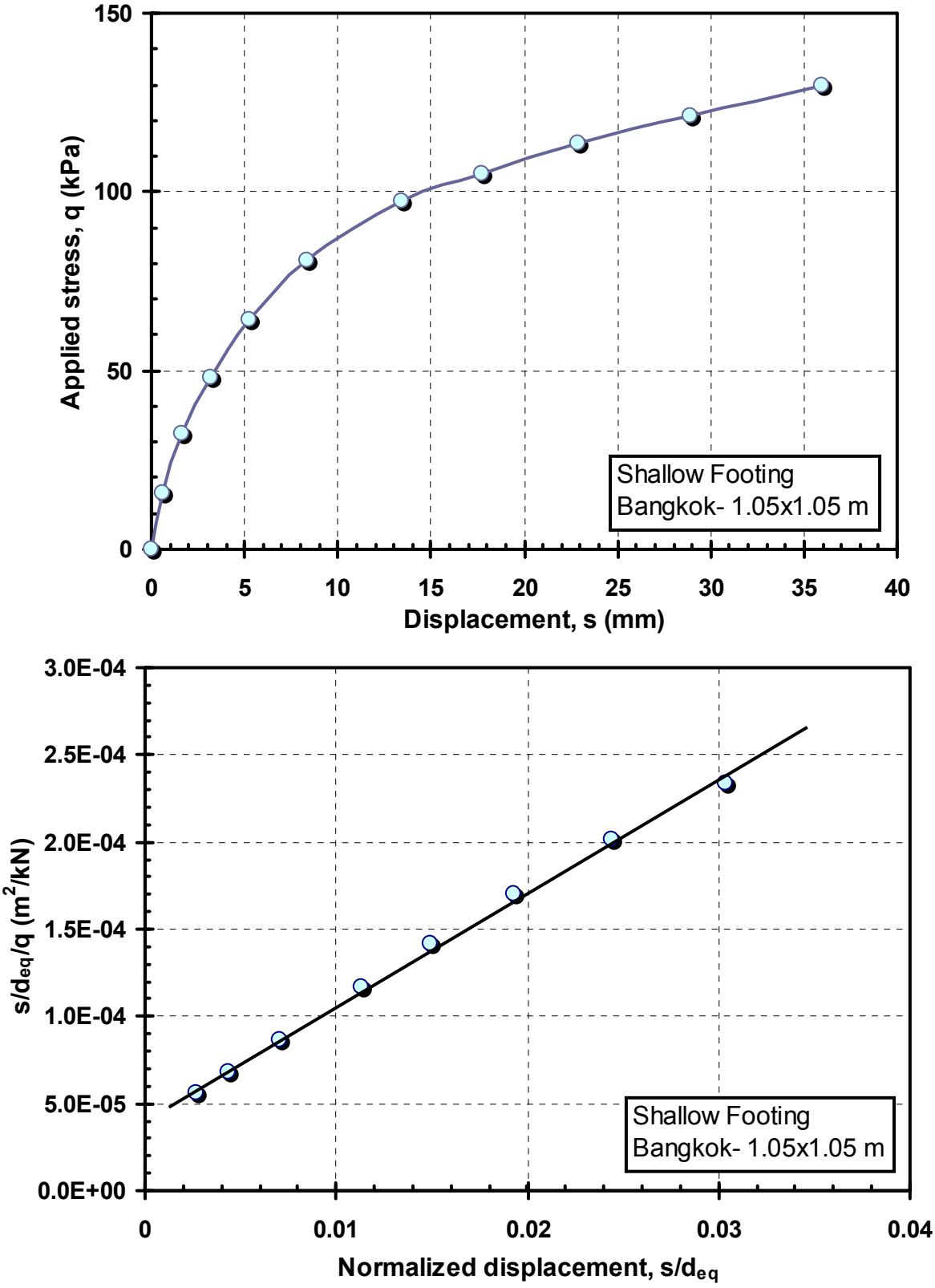


**Figure A-5.** Footing stress-displacement response plotted on (a) standard axes, (b) per Chin's transformed axes (raw data from Brand et al., 1972)

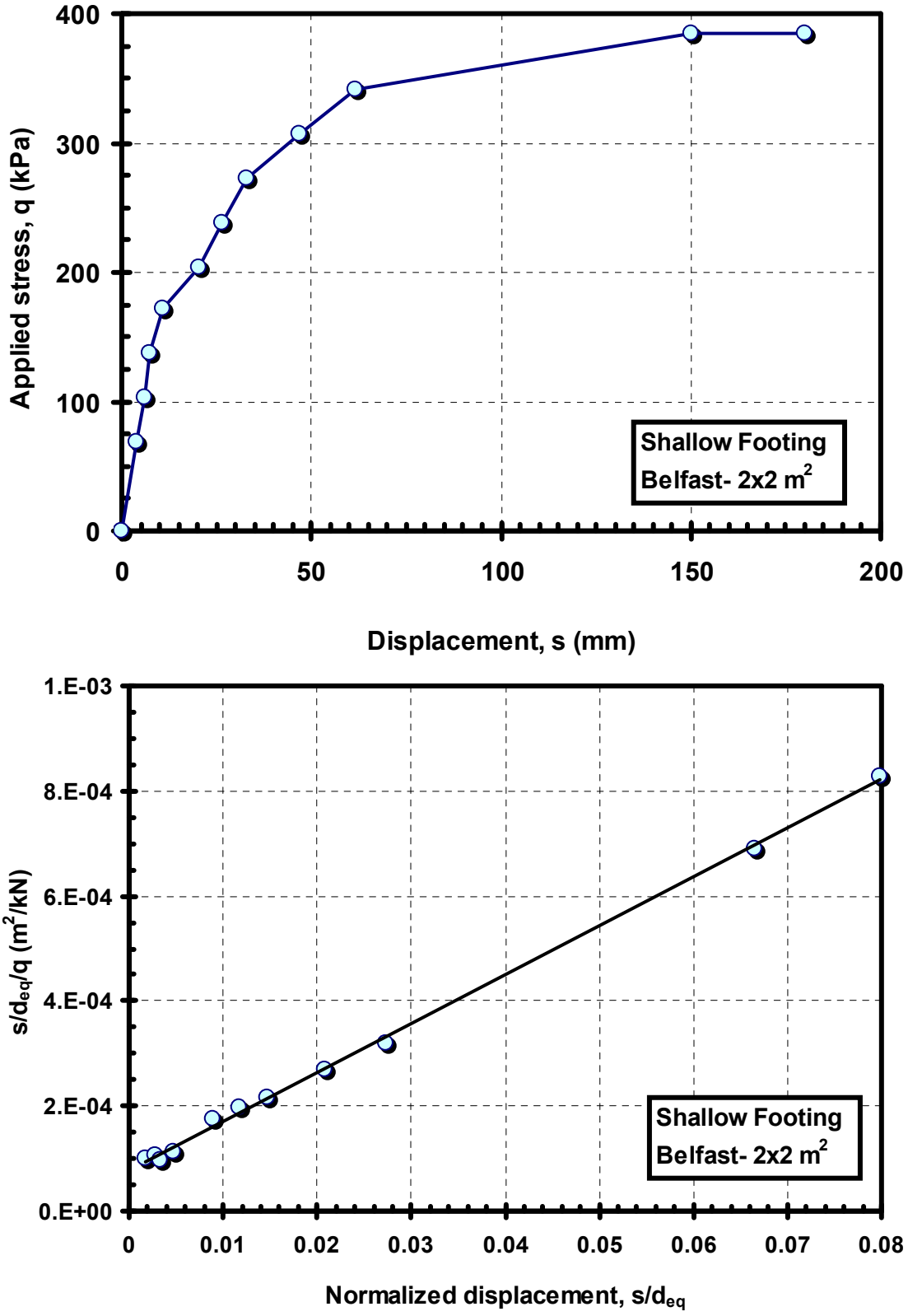


**Figure A-6.** Footing stress-displacement response plotted on (a) standard axes, (b) per Chin's transformed axes (raw data from Lehane, 2003)

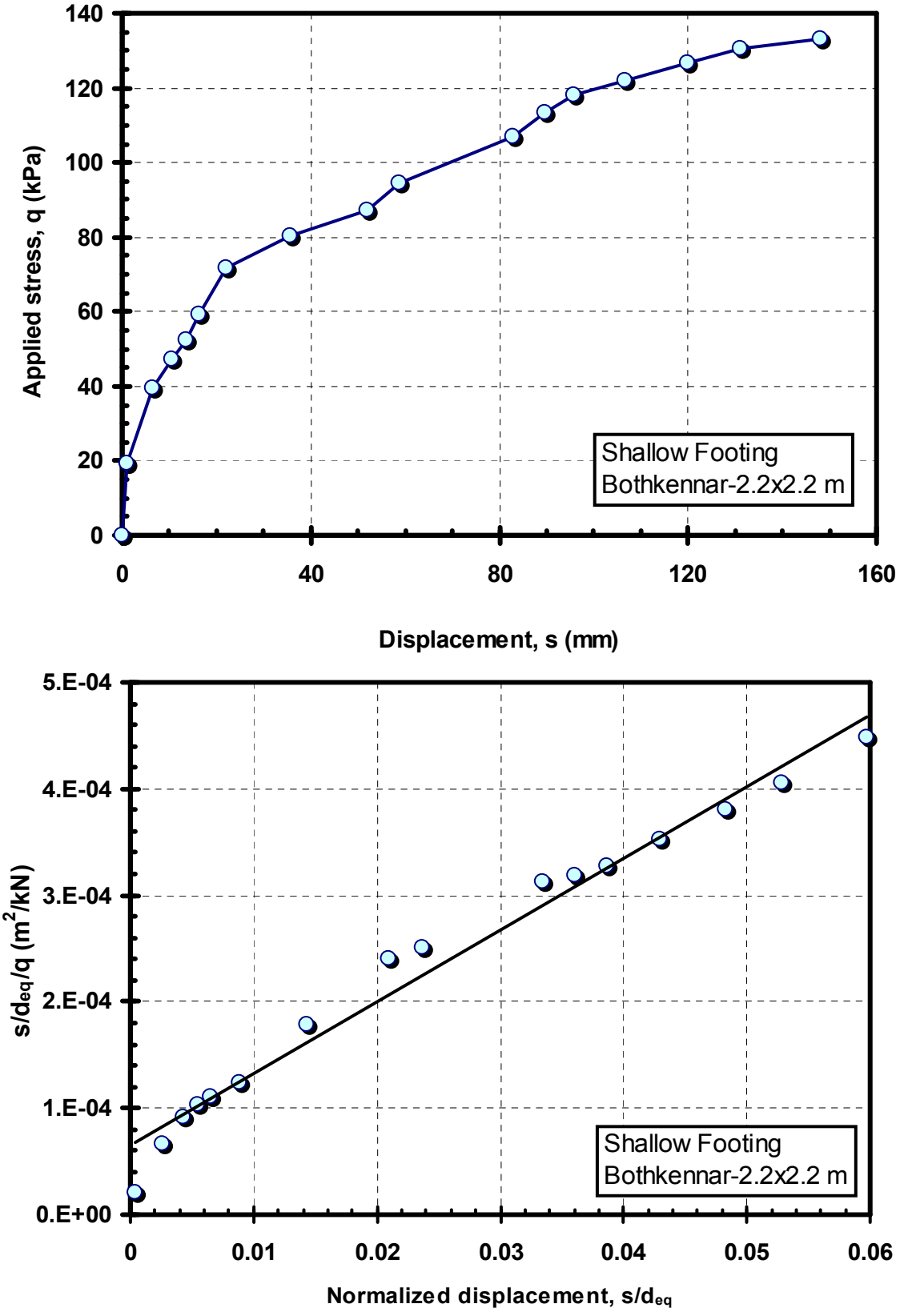


**Figure A-7.** Footing stress-displacement response plotted on (a) standard axes, (b) per Chin's transformed axes (raw data from Hight et al., 1997; Jardine et al. 1995)

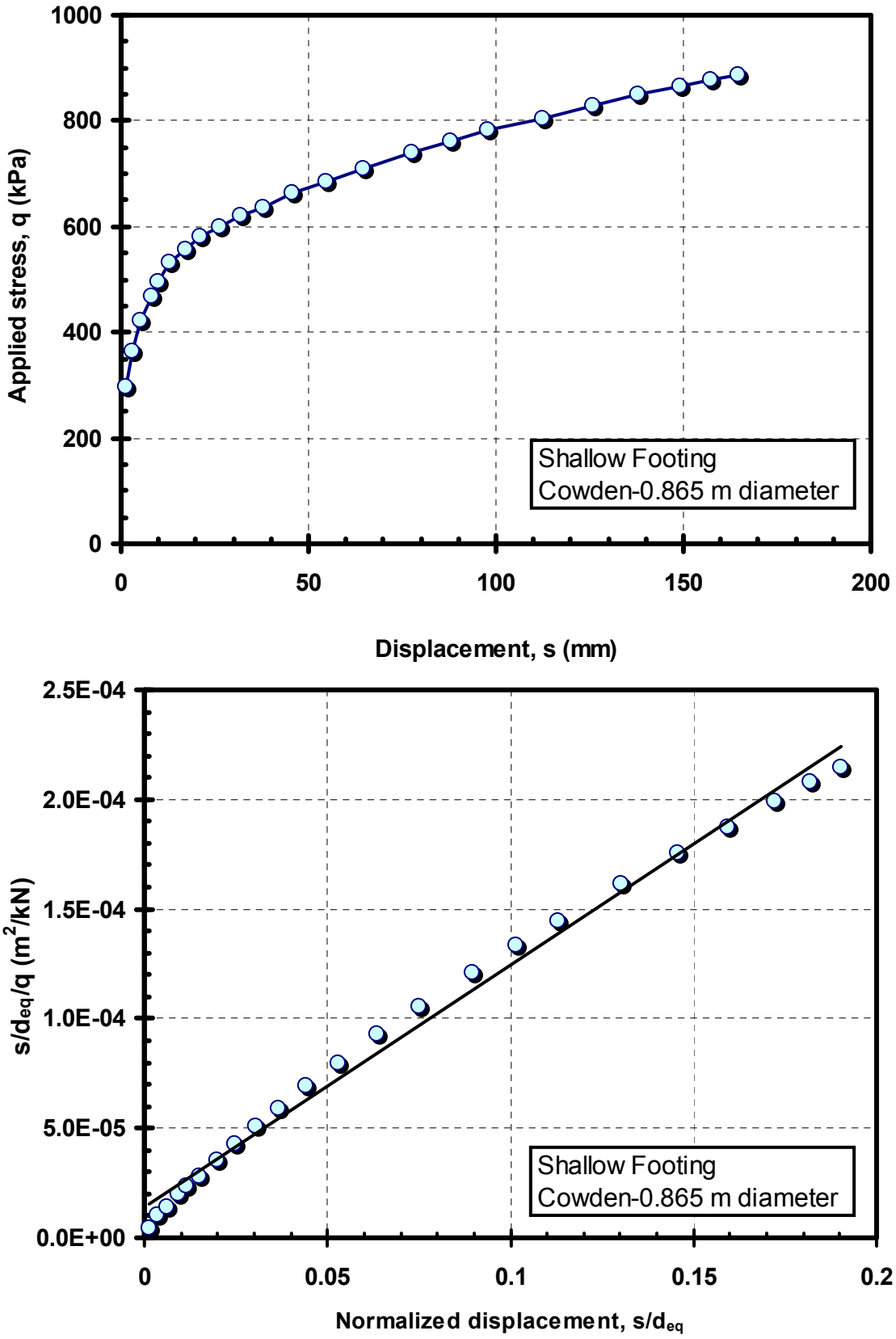


**Figure A-8.** Footing stress-displacement response plotted on (a) standard axes, (b) per Chin's transformed axes (raw data from Marsland and Powell, 1980)

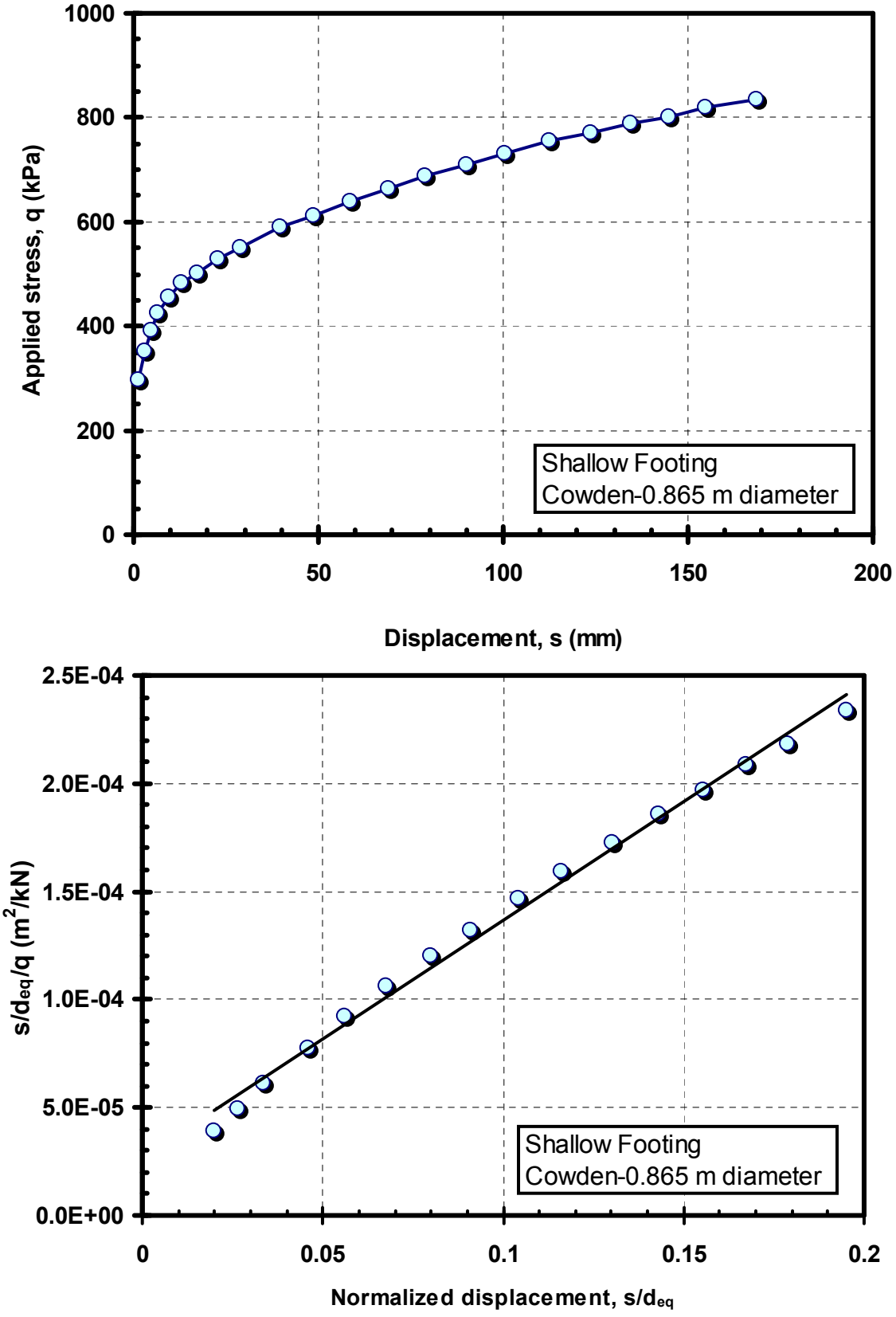


**Figure A-9.** Footing stress-displacement response plotted on (a) standard axes, (b) per Chin's transformed axes (raw data from Marsland and Powell, 1980)

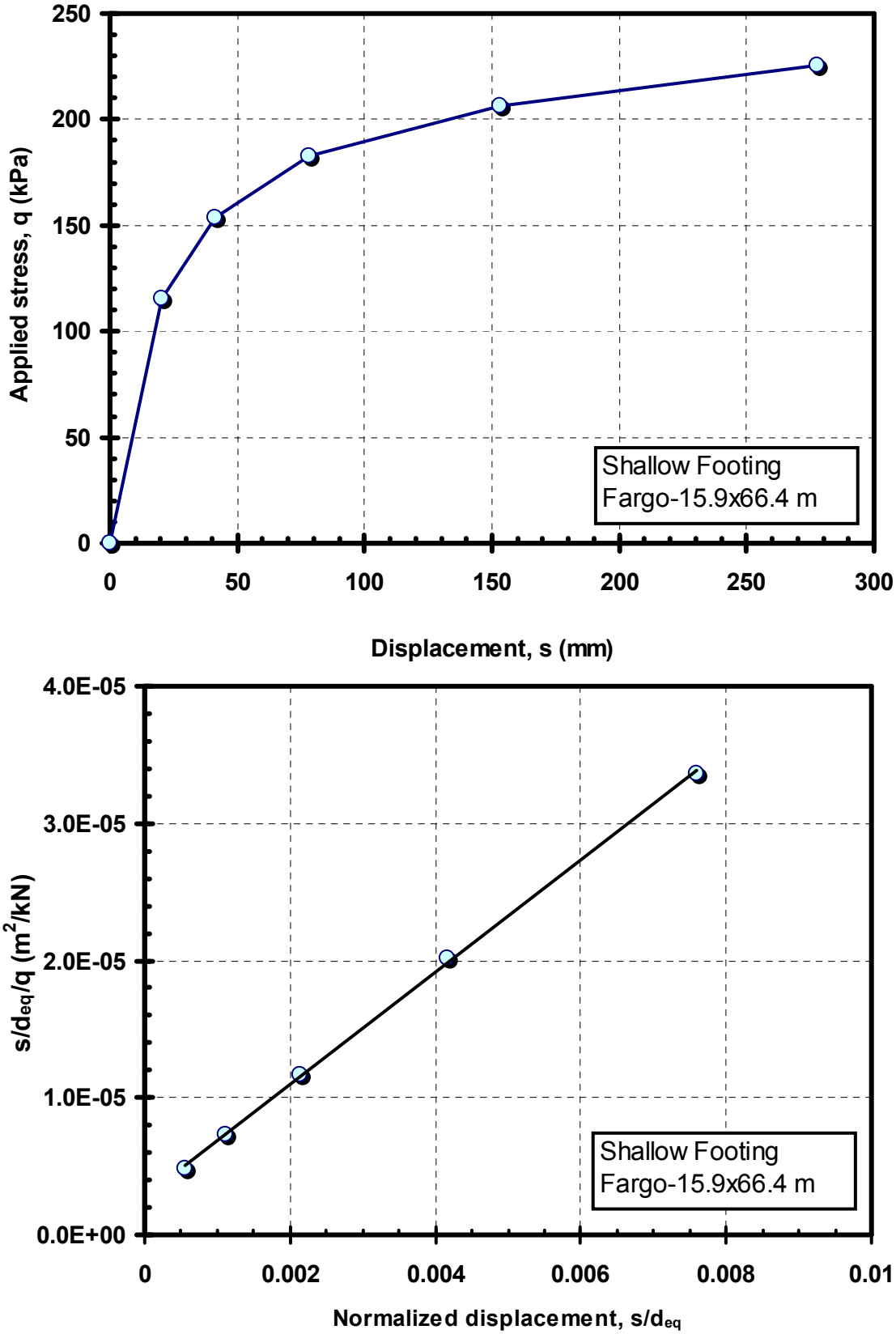


**Figure A-10.** Footing stress-displacement response plotted on (a) standard axes, (b) per Chin's transformed axes (raw data from Nordlund and Deere, 1972)

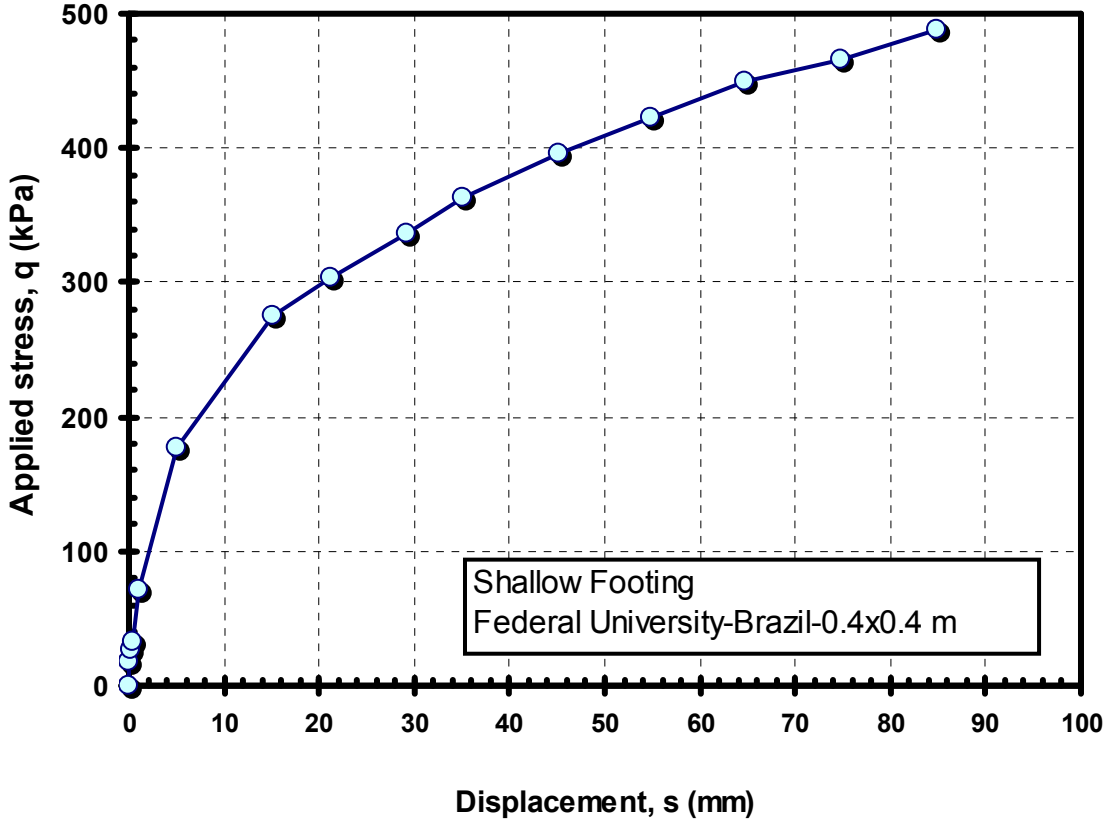


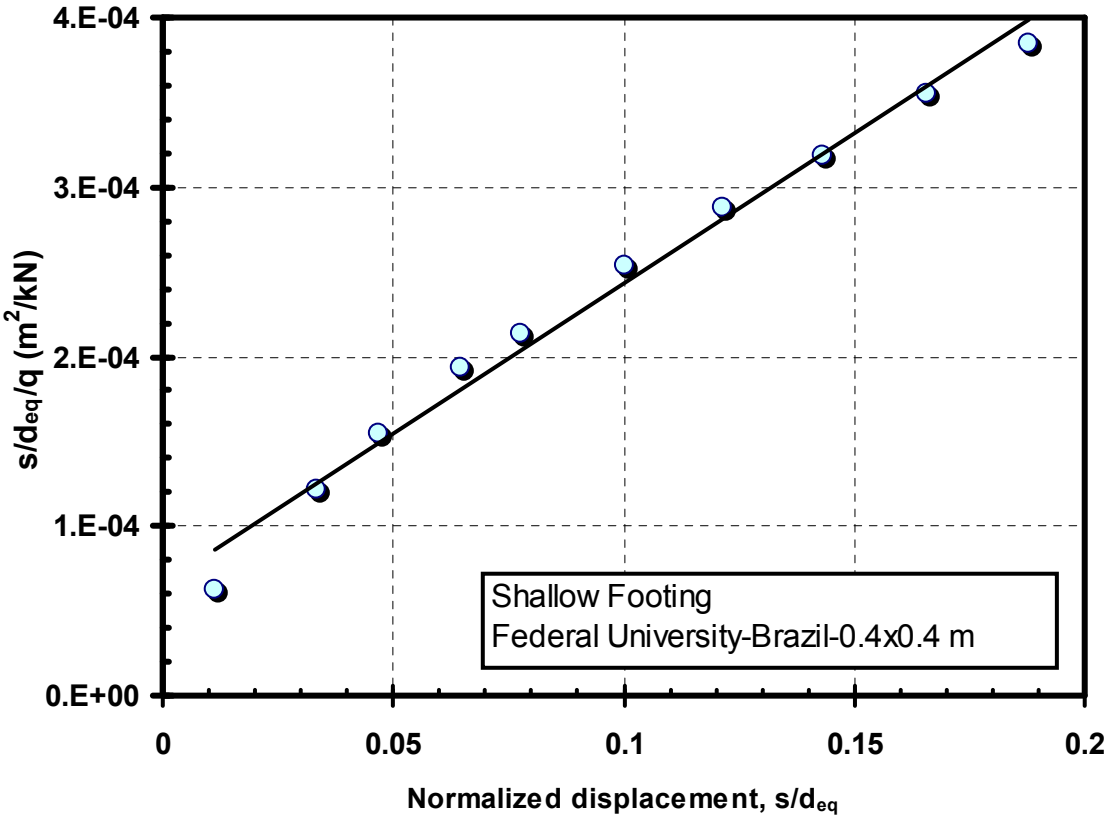


**Figure A-11.** Footing stress-displacement response plotted on (a) standard axes, (b) per Chin's transformed axes (raw data from Consoli et al., 1998)

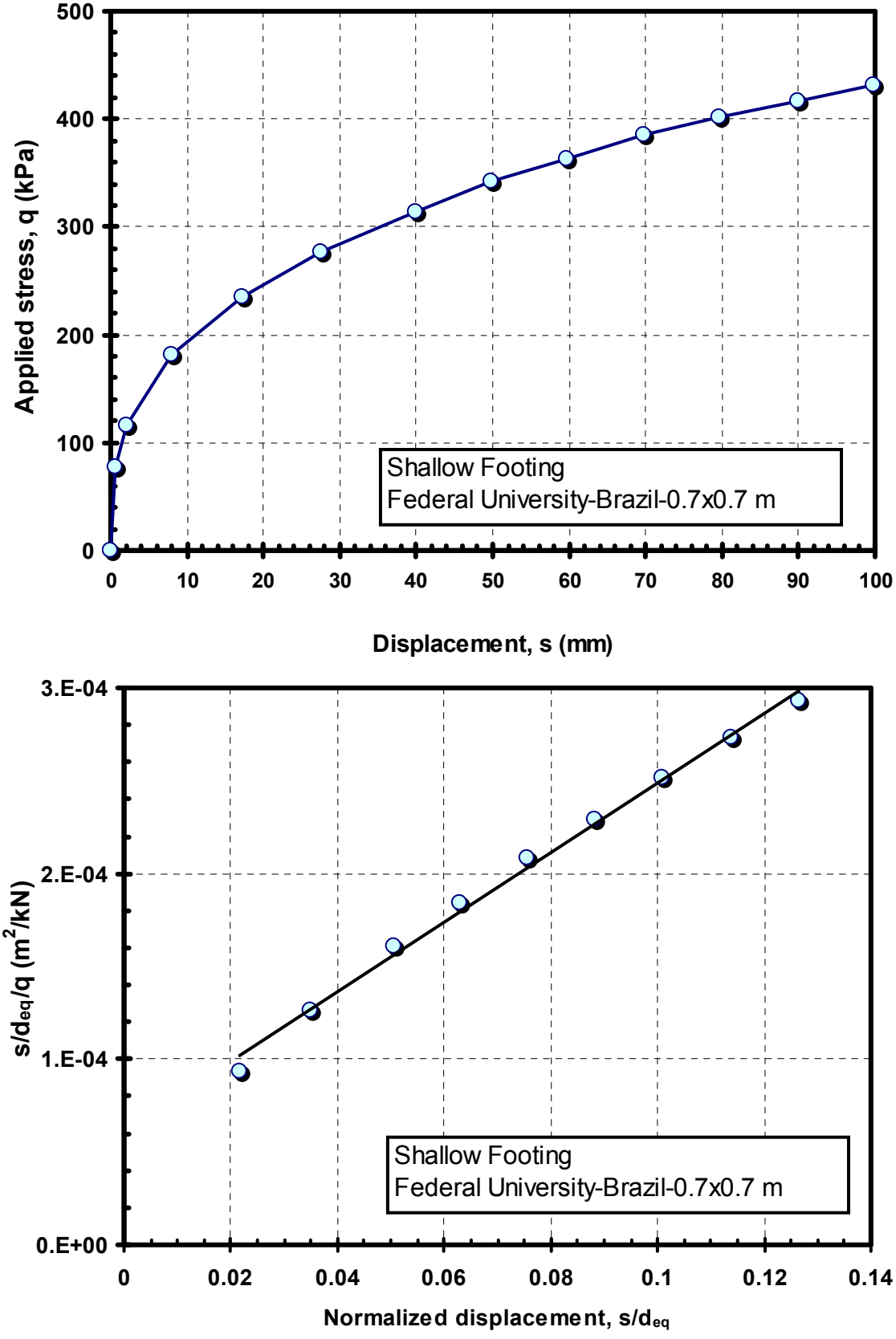


**Figure A-12.** Footing stress-displacement response plotted on (a) standard axes, (b) per Chin's transformed axes (raw data from Consoli et al., 1998)

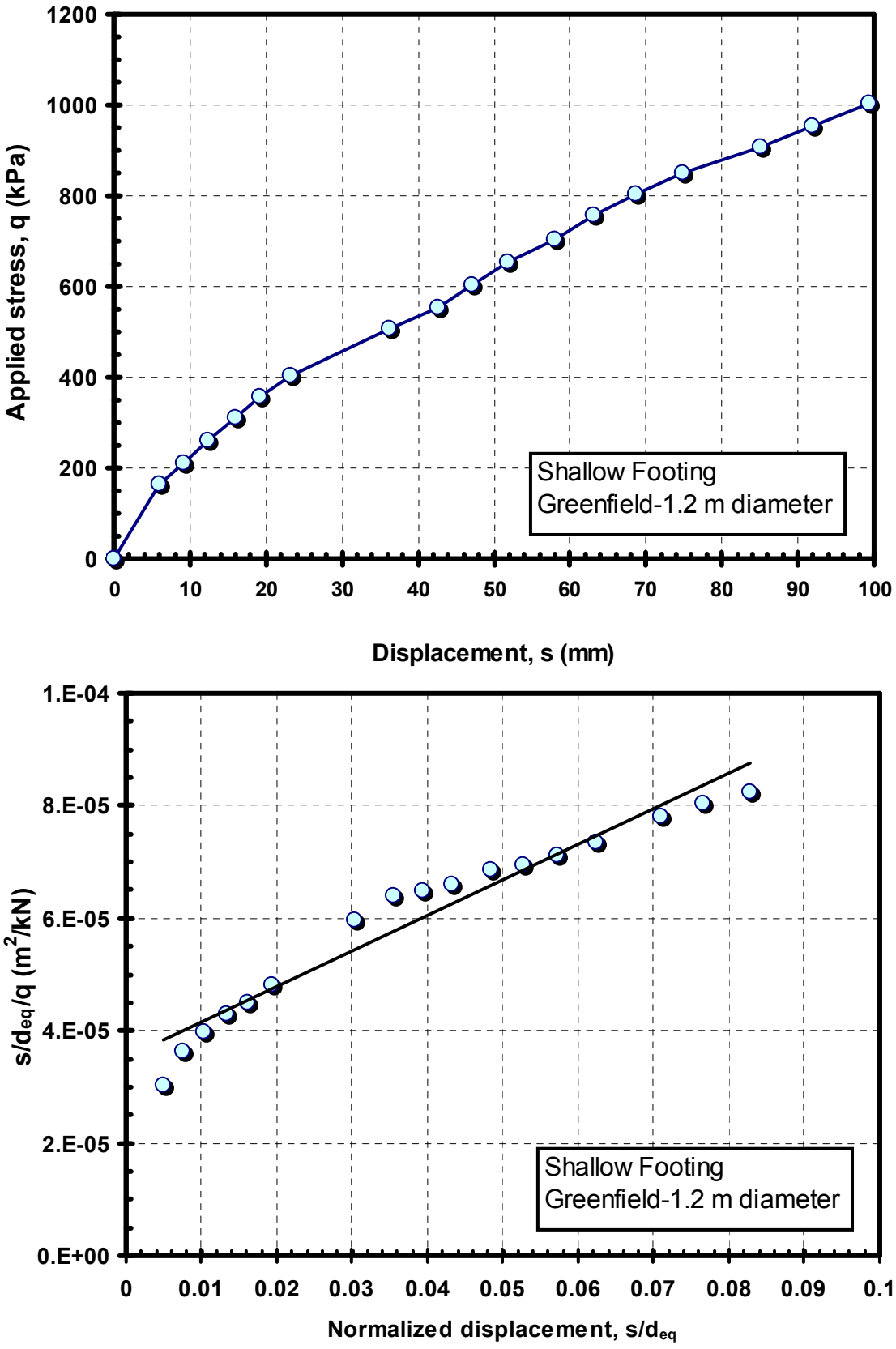


**Figure A-13.** Footing stress-displacement response plotted on (a) standard axes, (b) per Chin's transformed axes (raw data from Viana da Fonseca, 2001)

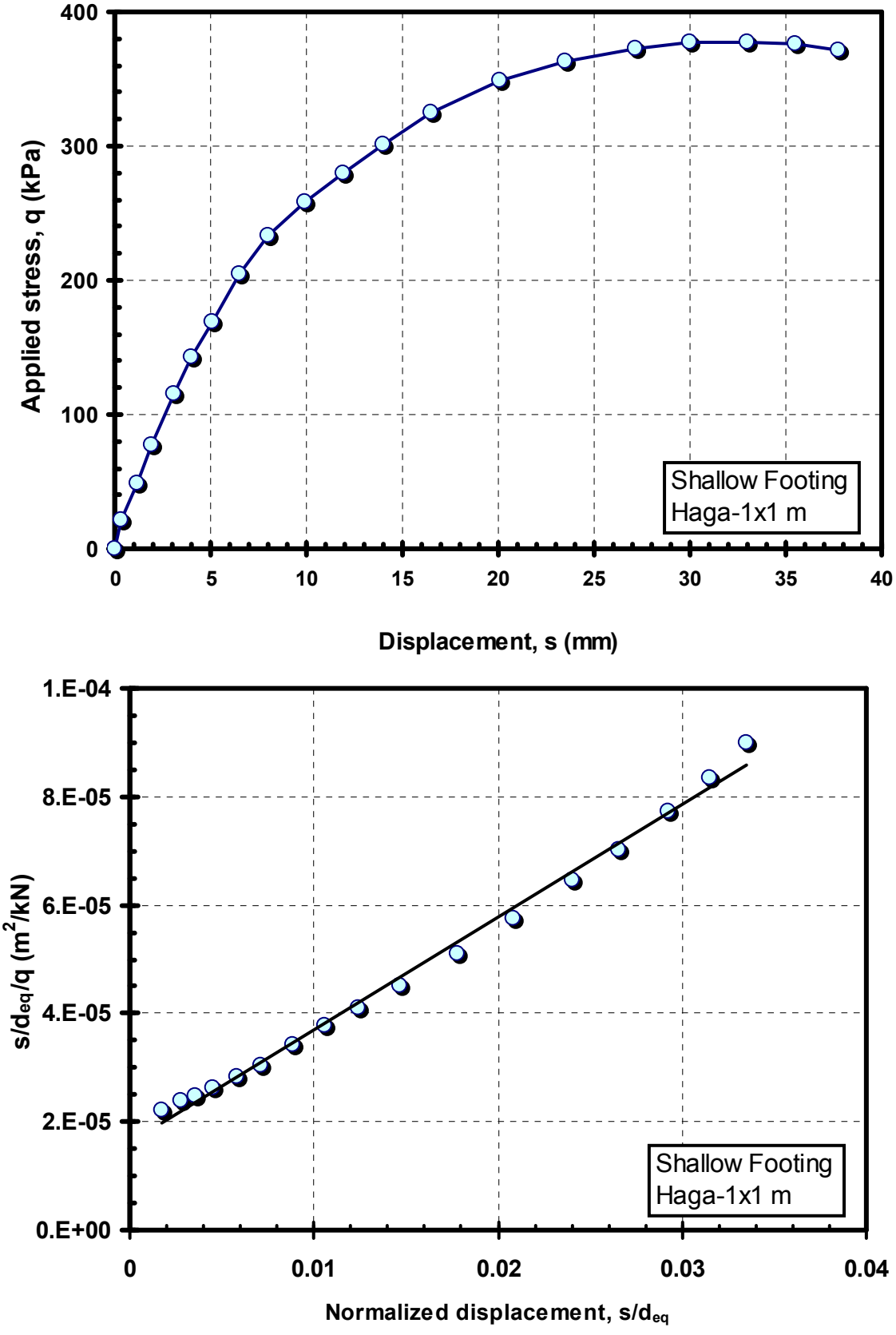


**Figure A-14.** Footing stress-displacement response plotted on (a) standard axes, (b) per Chin's transformed axes (raw data from Andersen and Stenhamar, 1982)

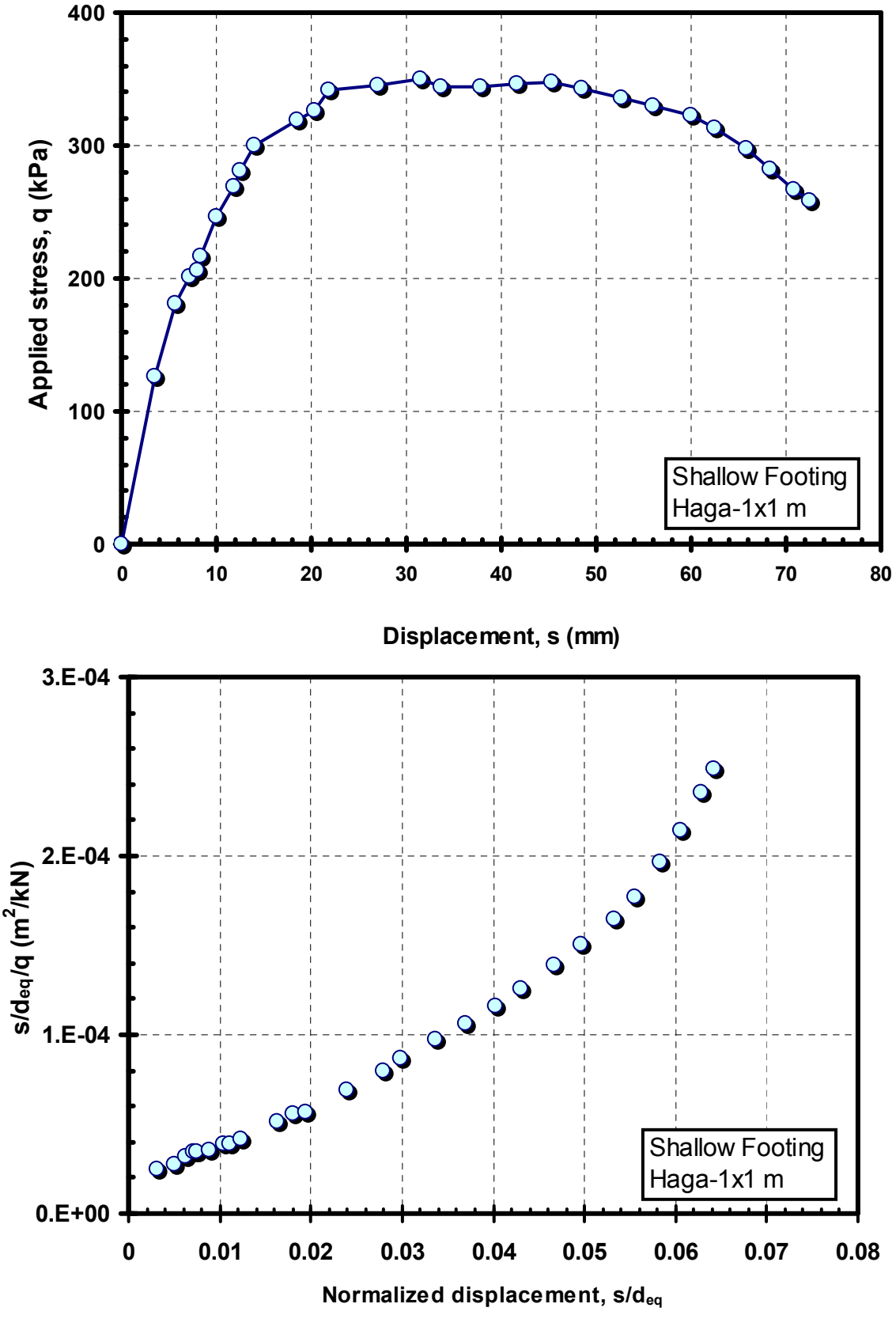


**Figure A-15.** Footing stress-displacement response plotted on (a) standard axes, (b) per Chin's transformed axes (raw data from Andersen and Stenhamar, 1982)

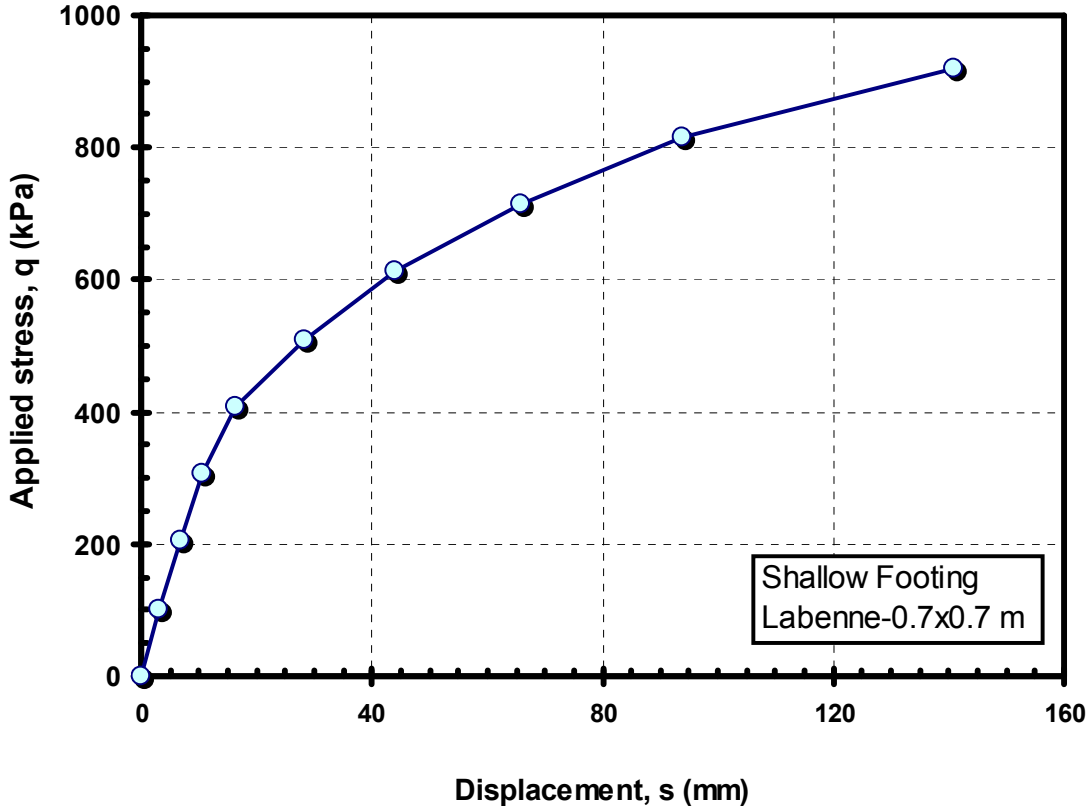


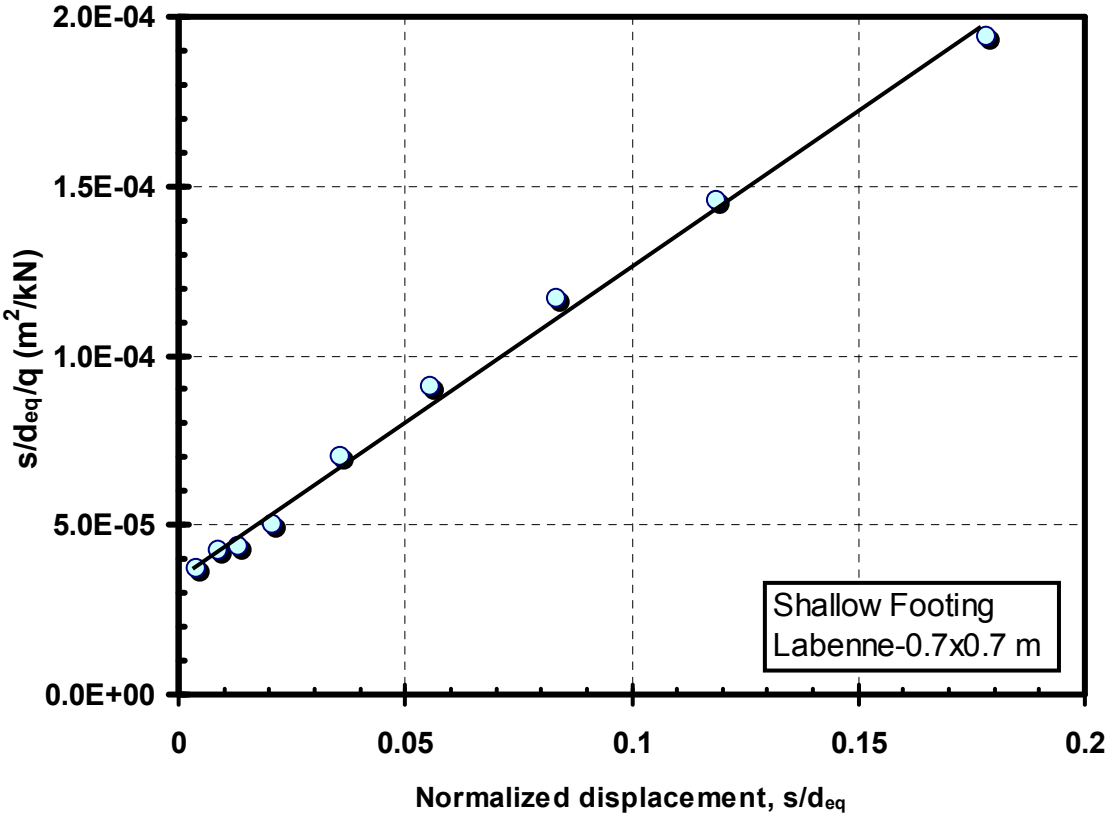


**Figure A-16.** Footing stress-displacement response plotted on (a) standard axes, (b) per Chin's transformed axes (raw data from Amar, et al., 1994)

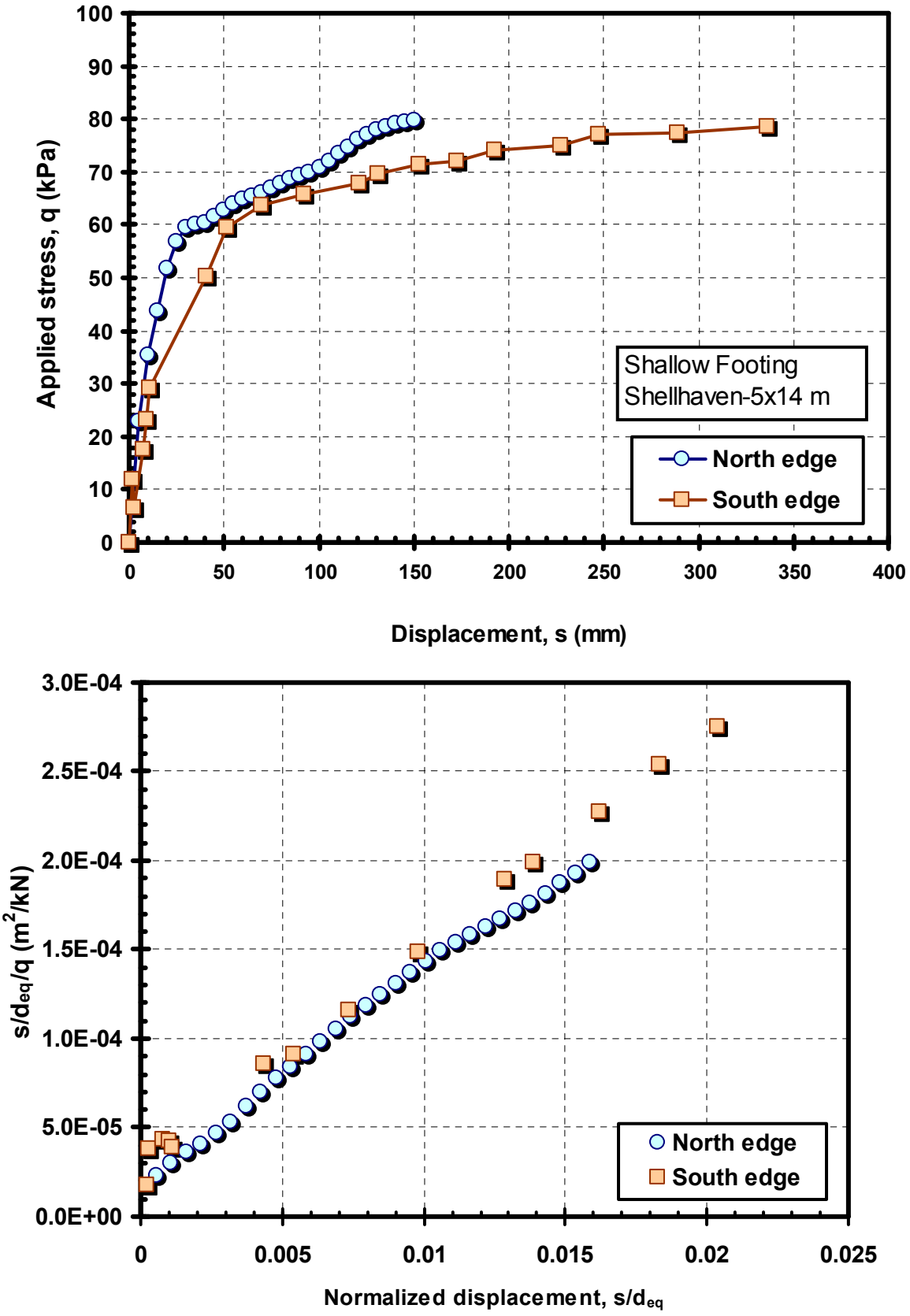


**Figure A-17.** Footing stress-displacement response plotted on (a) standard axes, (b) per Chin's transformed axes (raw data from Schnaid et al., 1993)

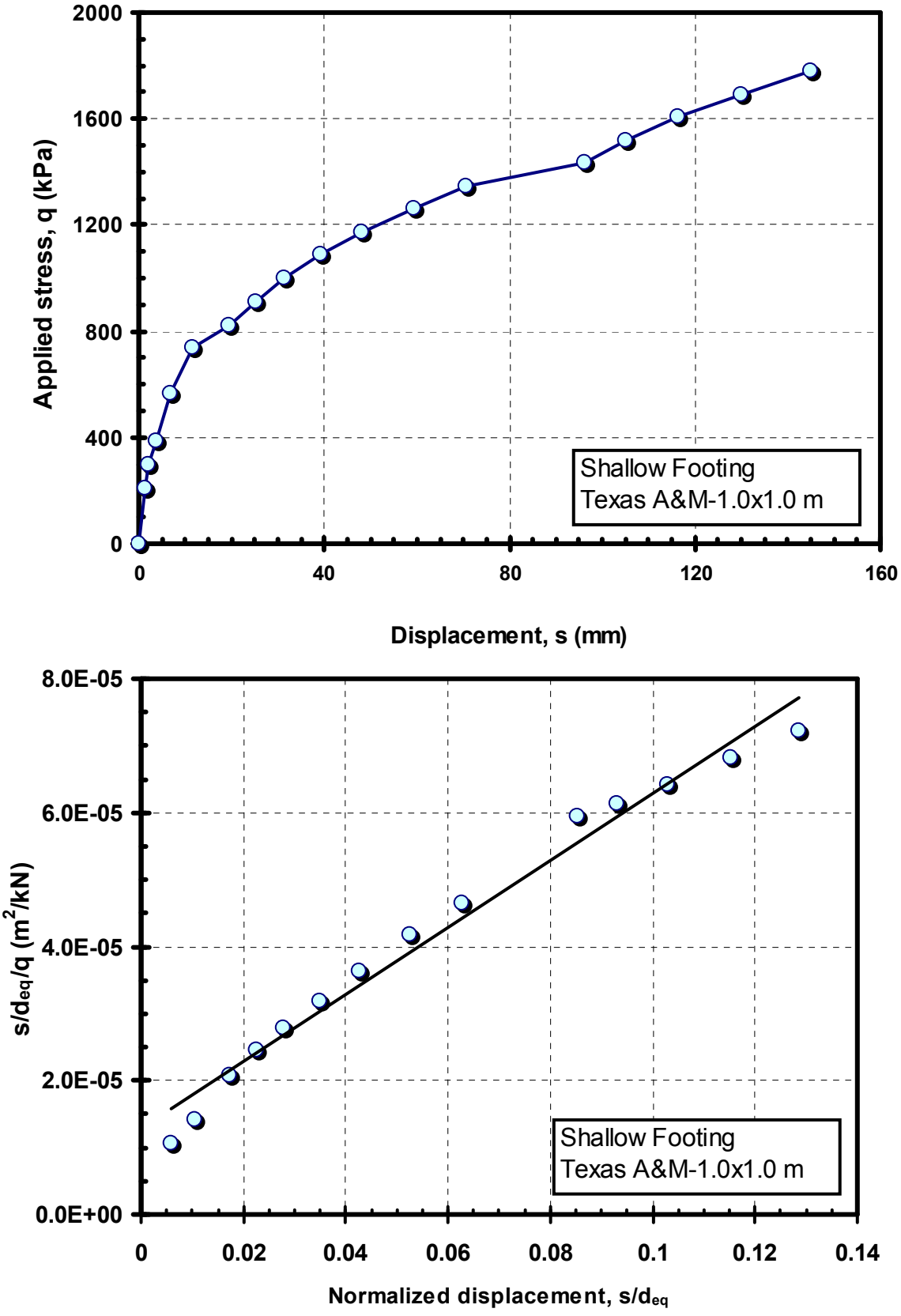


**Figure A-18.** Footing stress-displacement response plotted on (a) standard axes, (b) per Chin's transformed axes (raw data from Briaud and Gibbens, 1999)

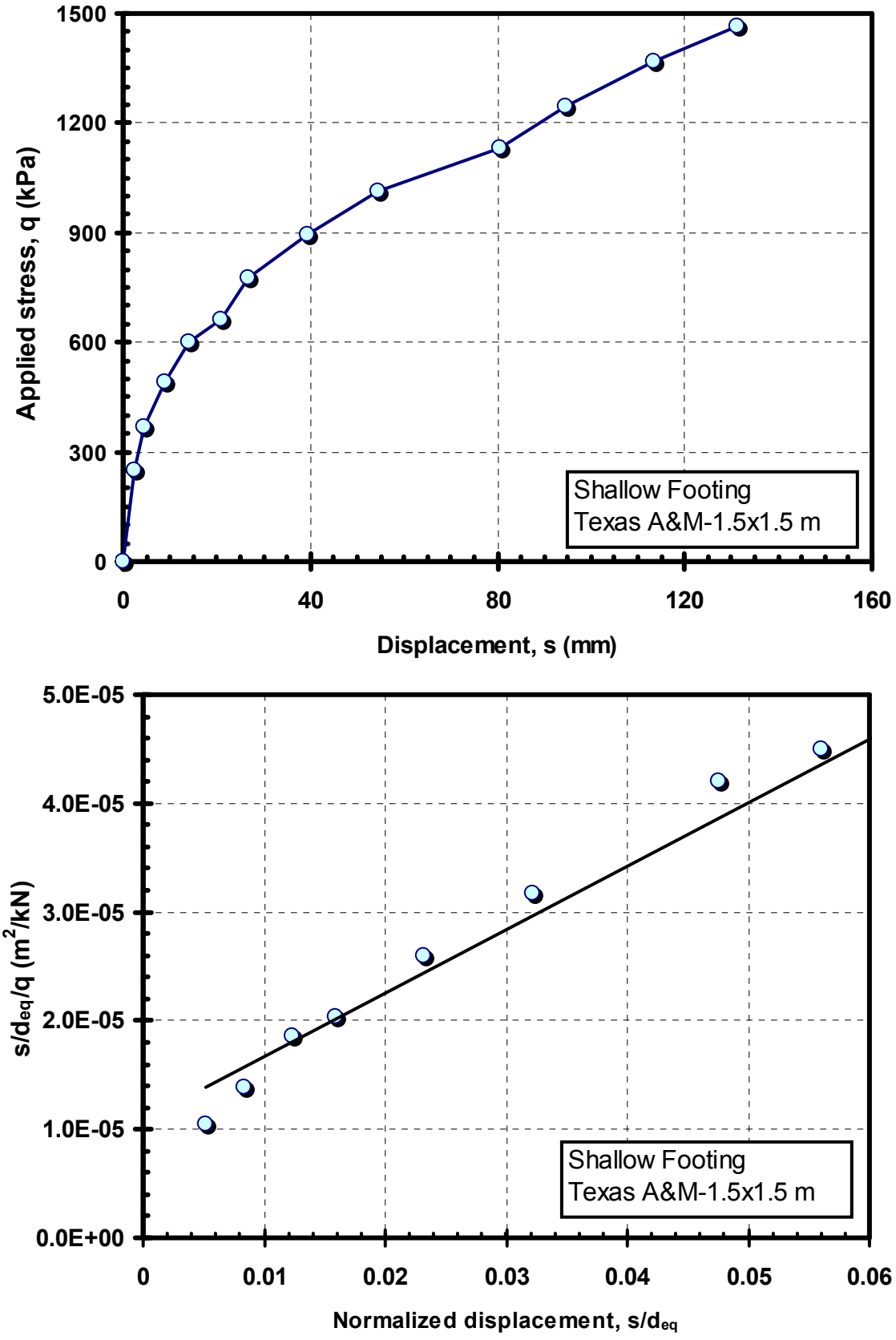


**Figure A-19.** Footing stress-displacement response plotted on (a) standard axes, (b) per Chin's transformed axes (raw data from Briaud and Gibbens, 1999)

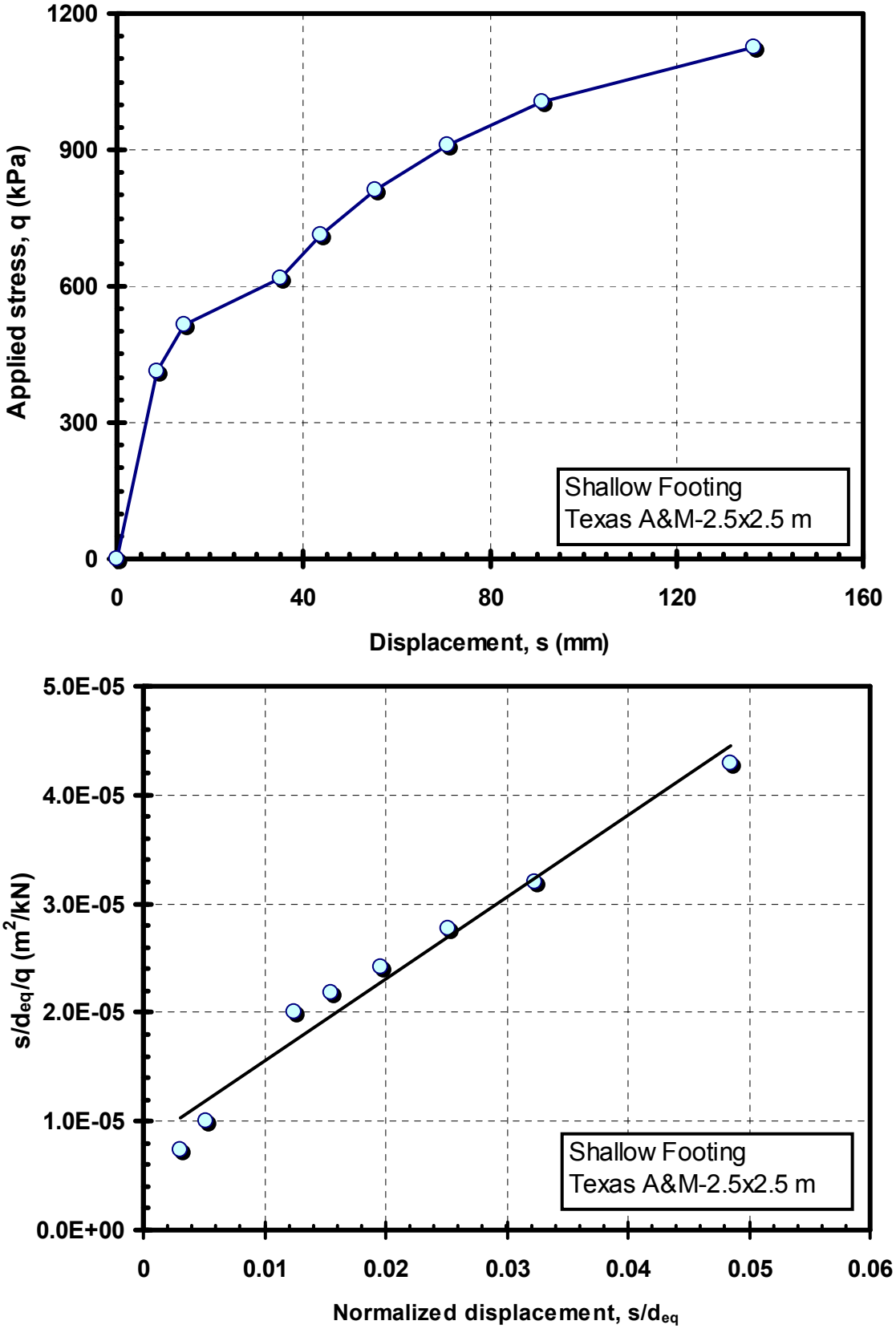


**Figure A-20.** Footing stress-displacement response plotted on (a) standard axes, (b) per Chin's transformed axes (raw data from Briaud and Gibbens, 1999)

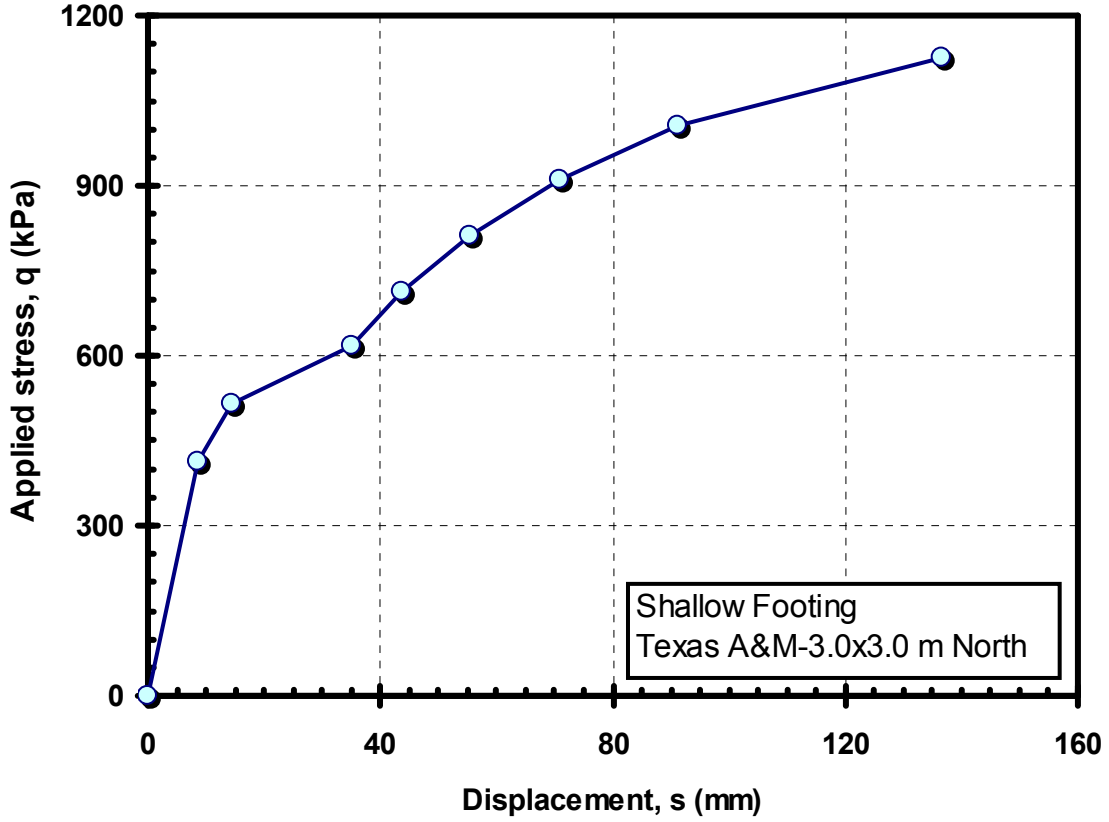


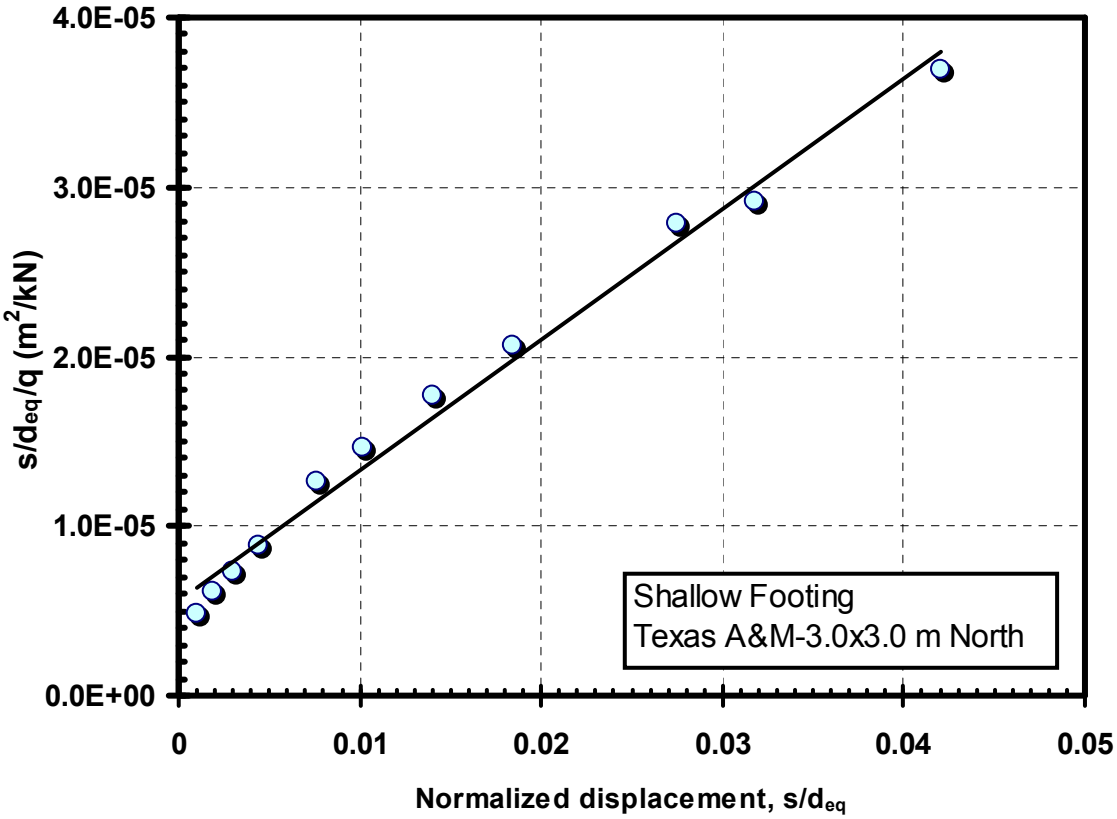


**Figure A-21.** Footing stress-displacement response plotted on (a) standard axes, (b) per Chin's transformed axes (raw data from Briaud and Gibbens, 1999)

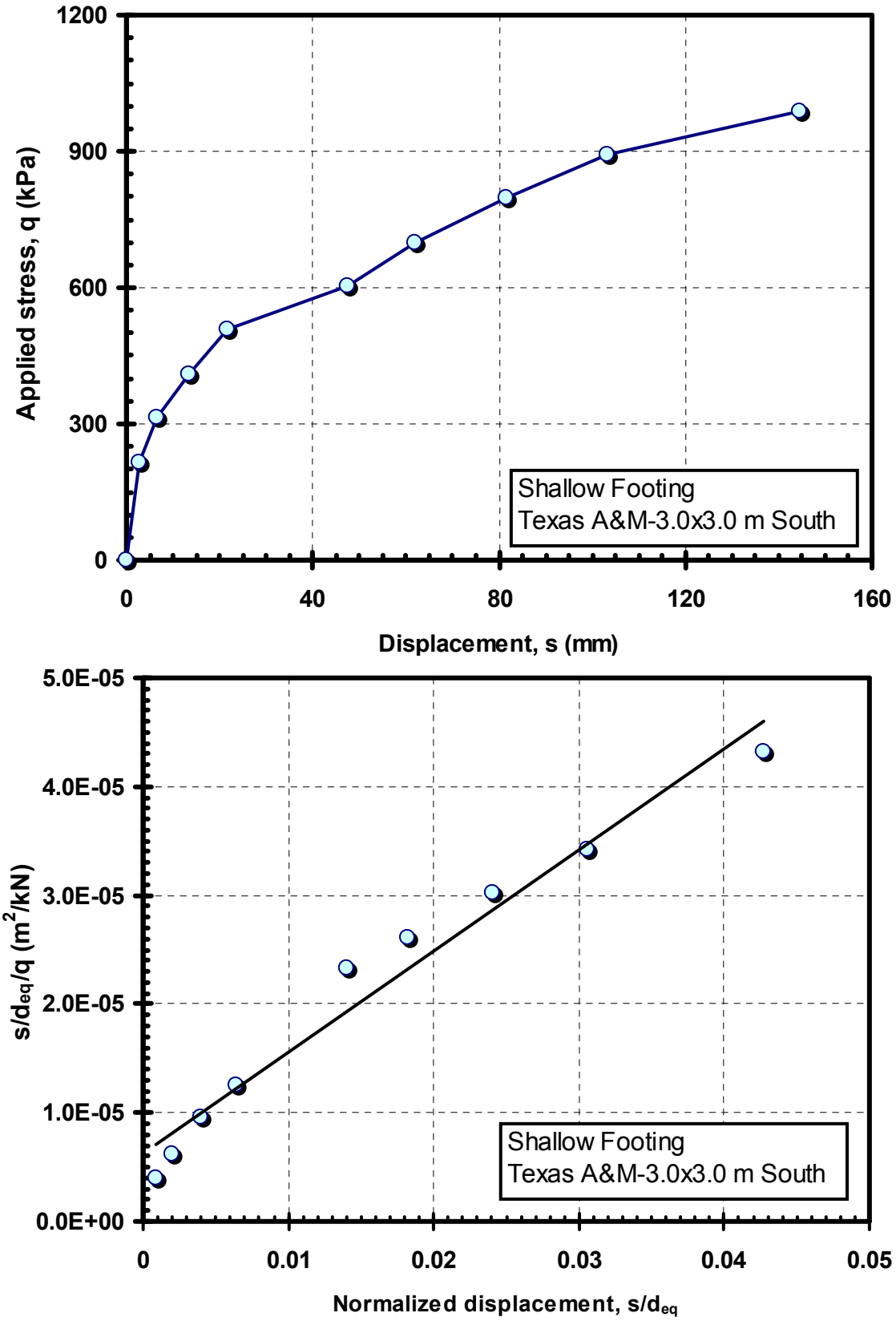


**Figure A-22.** Footing stress-displacement response plotted on (a) standard axes, (b) per Chin's transformed axes (raw data from Briaud and Gibbens, 1999)

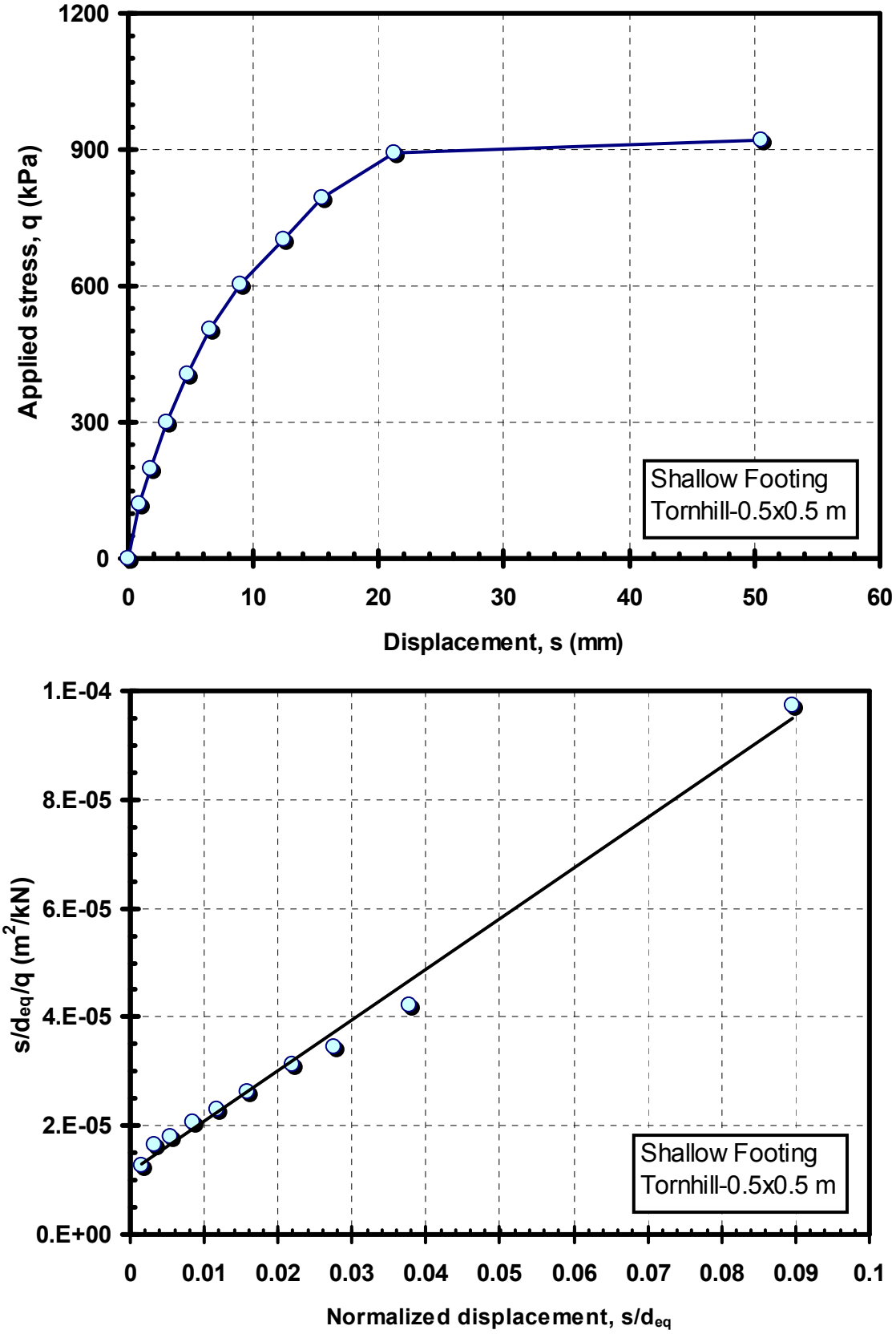


**Figure A-23.** Footing stress-displacement response plotted on (a) standard axes, (b) per Chin's transformed axes (raw data from Larrson, 1997)

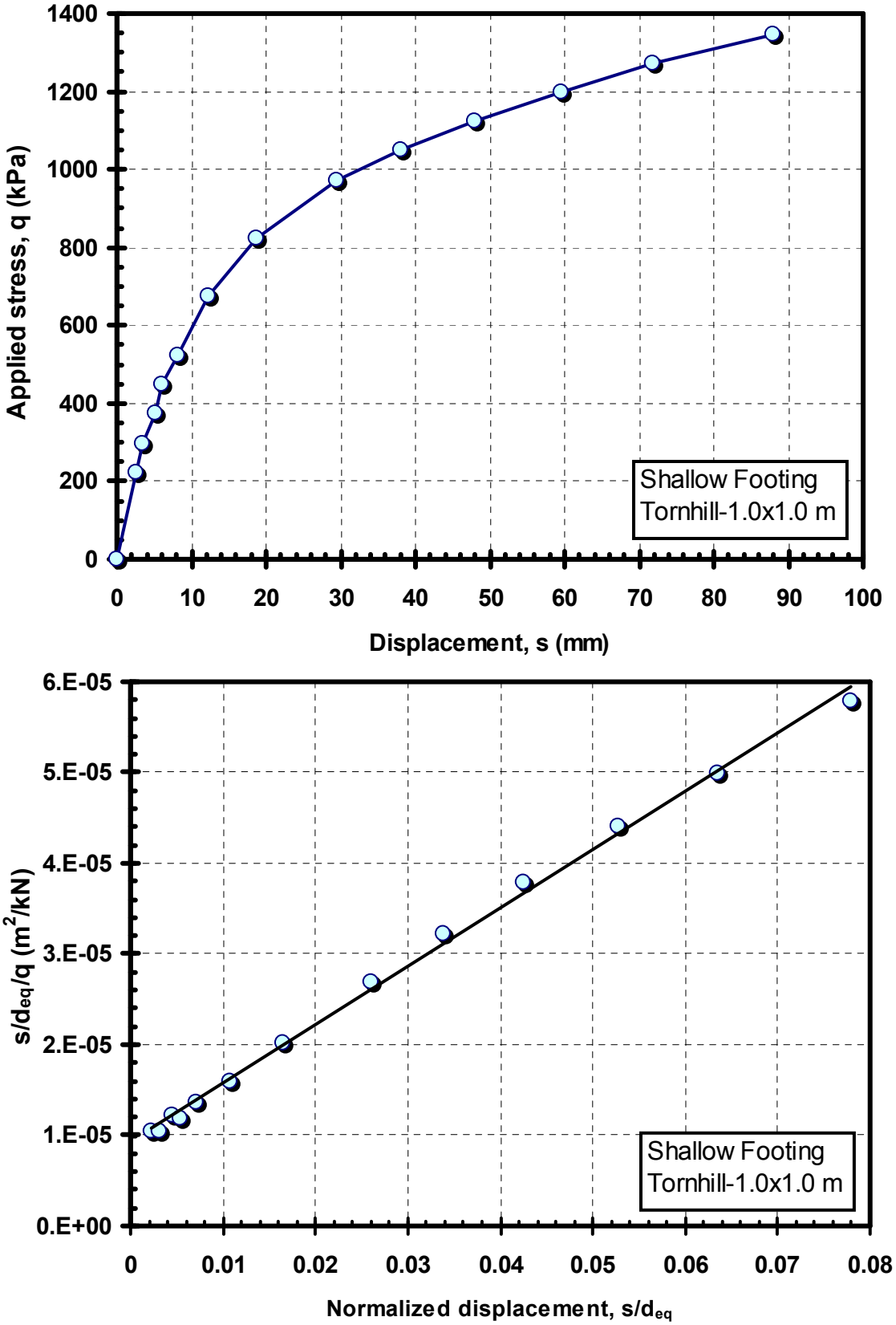


**Figure A-24.** Footing stress-displacement response plotted on (a) standard axes, (b) per Chin's transformed axes (raw data from Larsson, 1997)

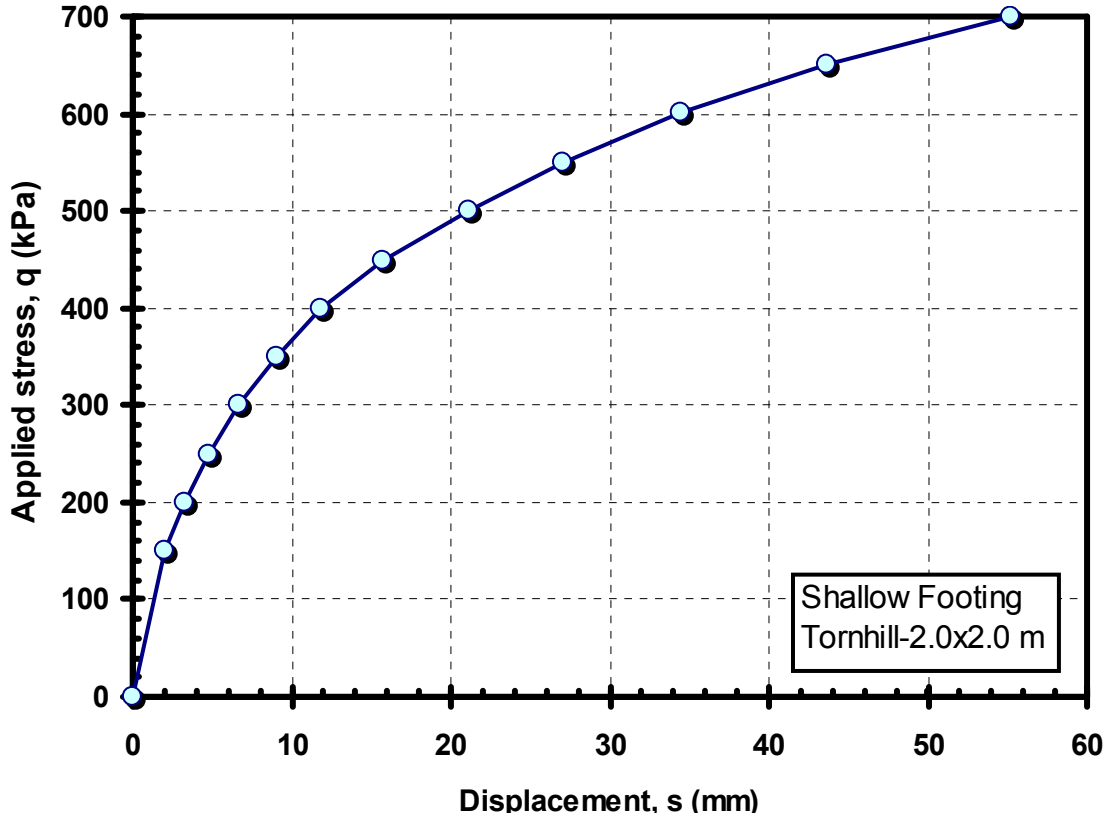


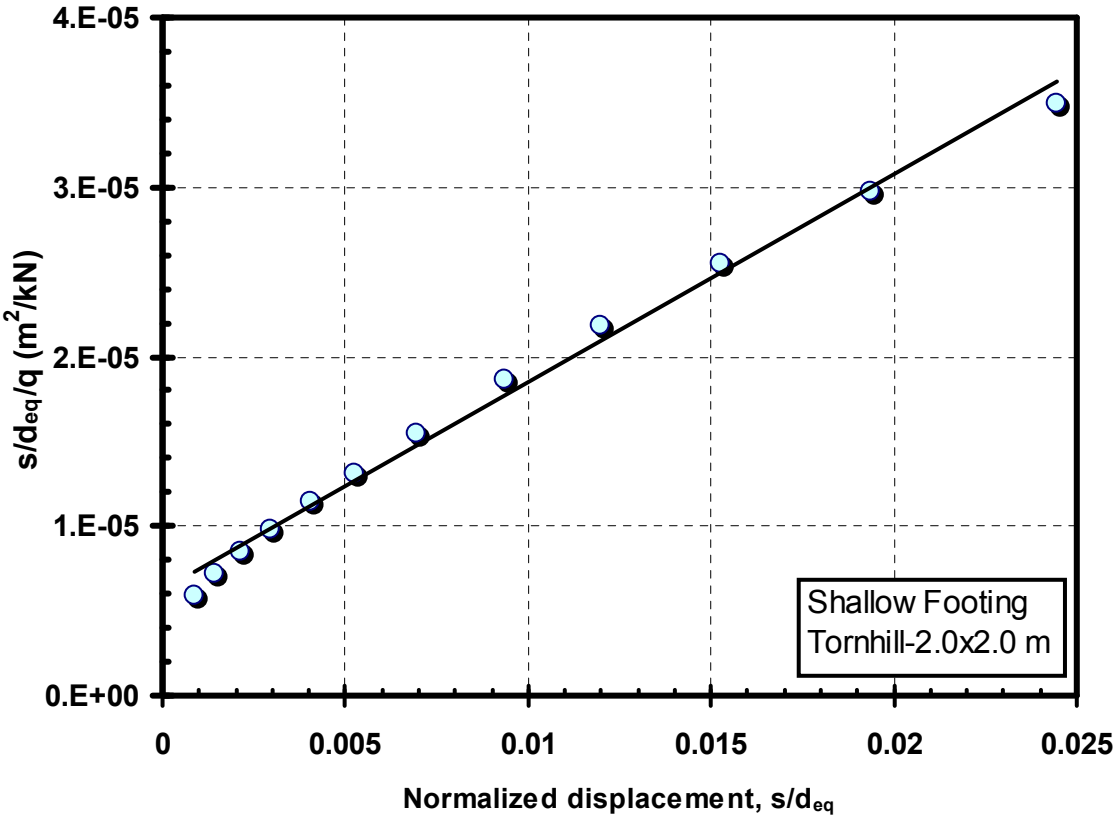


**Figure A-25.** Footing stress-displacement response plotted on (a) standard axes, (b) per Chin's transformed axes (raw data from Larsson, 1997)

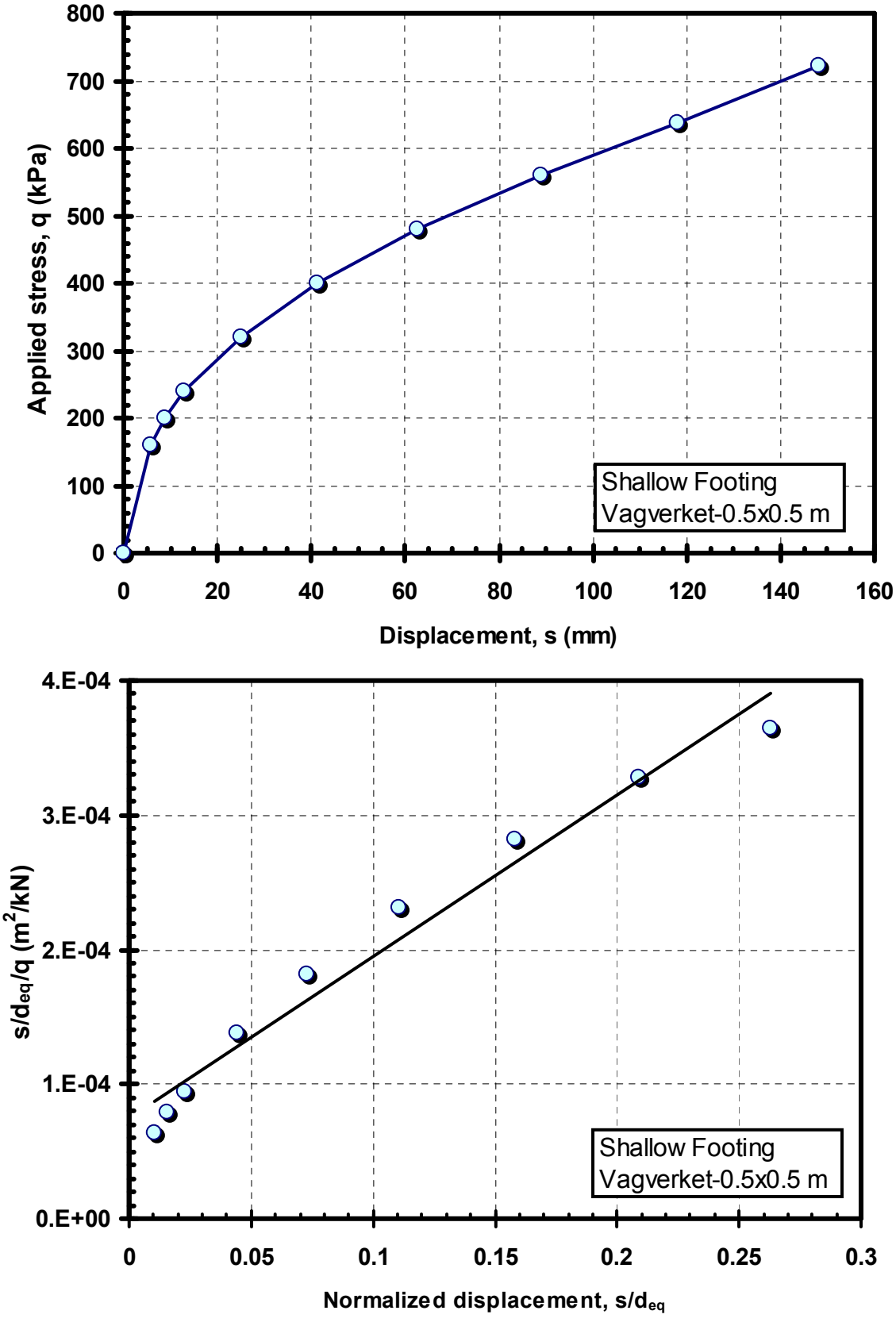


**Figure A-26.** Footing stress-displacement response plotted on (a) standard axes, (b) per Chin's transformed axes (raw data from Larsson, 1997)

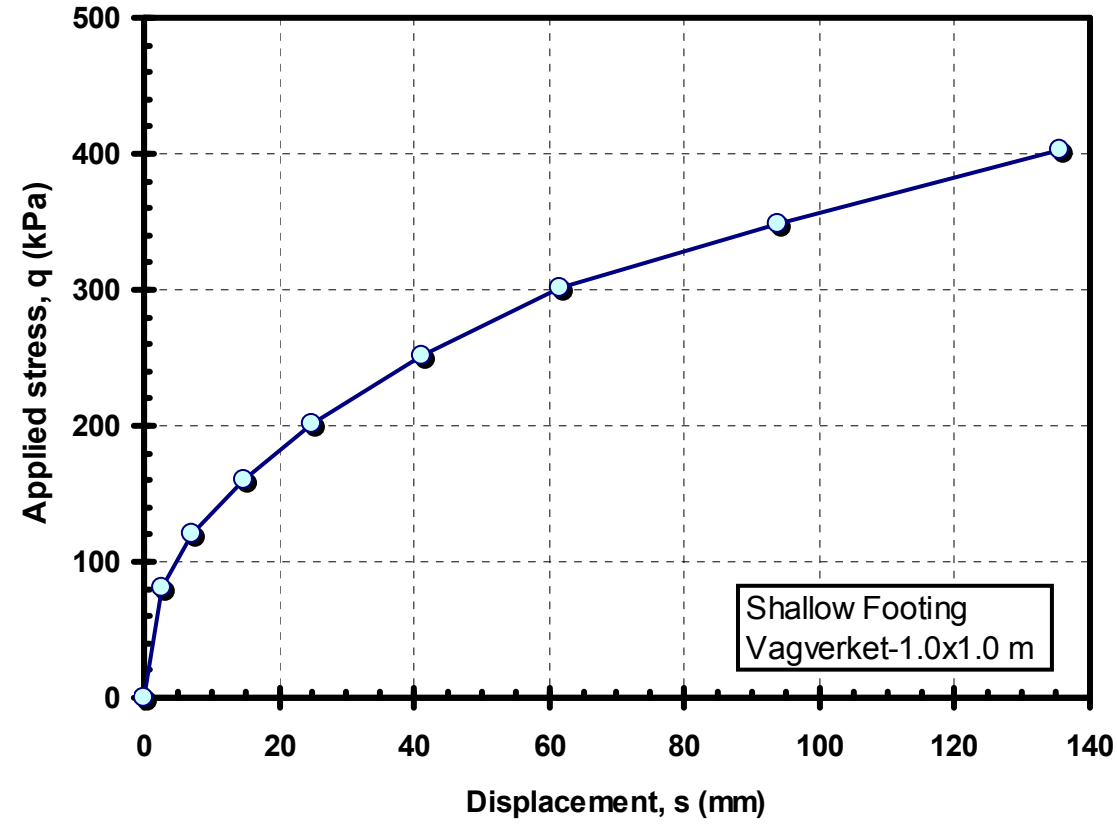


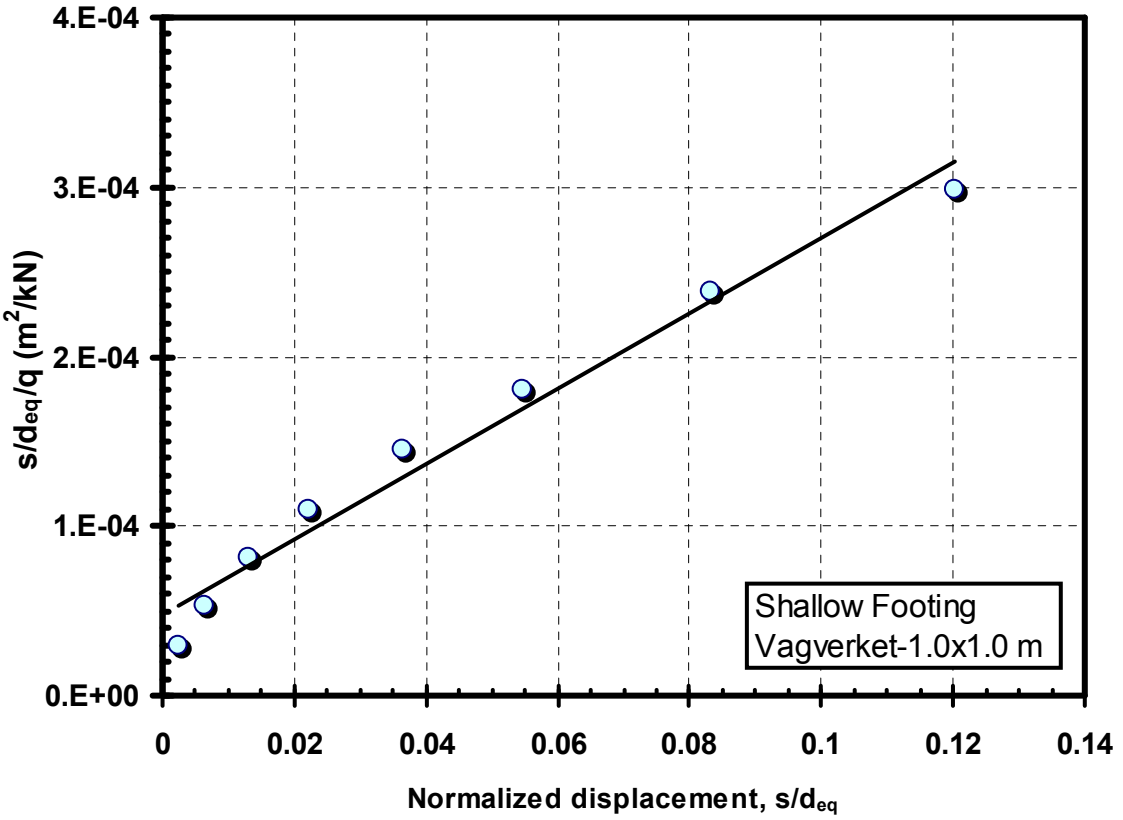


**Figure A-27.** Footing stress-displacement response plotted on (a) standard axes, (b) per Chin's transformed axes (raw data from Larsson, 1997)

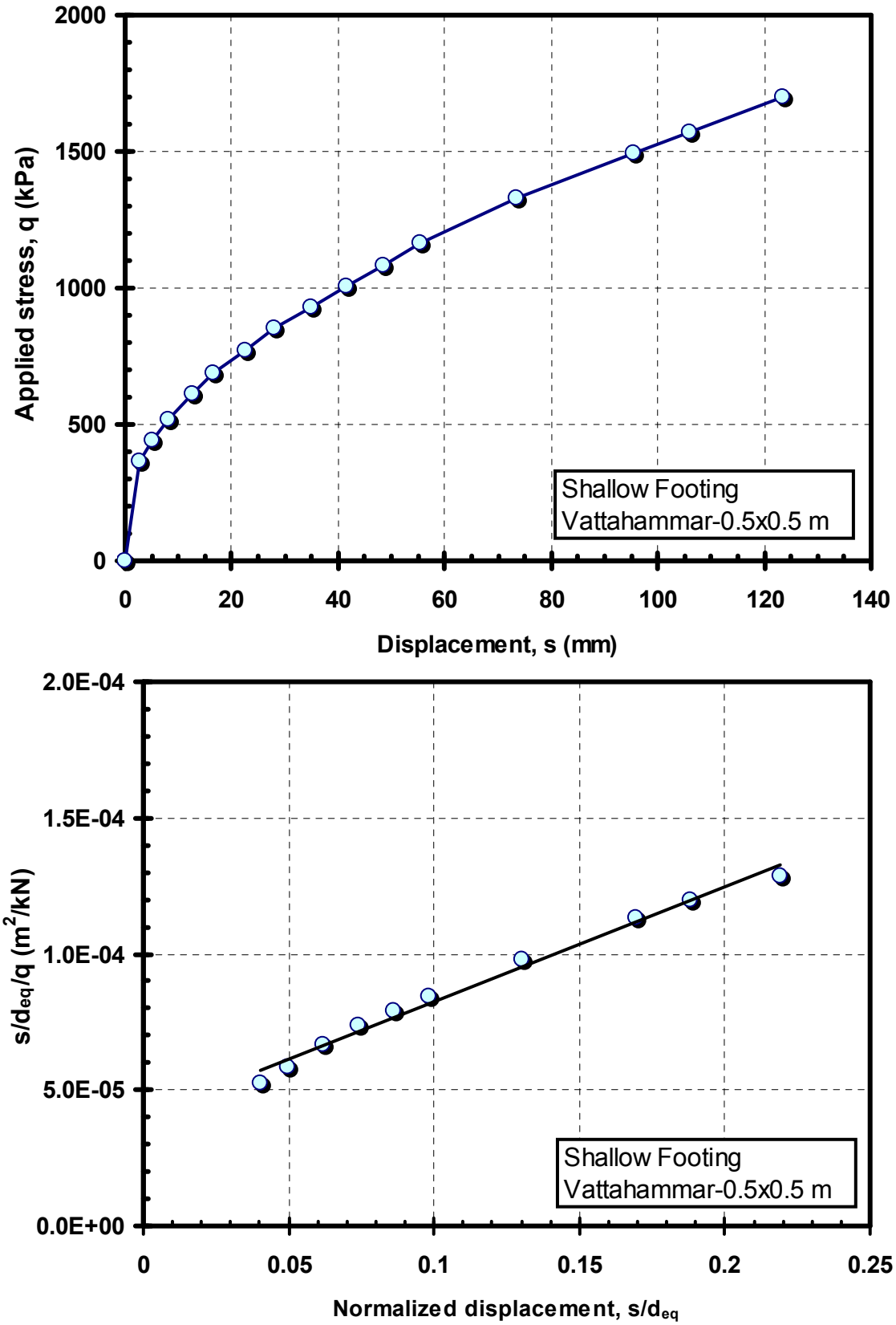


**Figure A-28.** Footing stress-displacement response plotted on (a) standard axes, (b) per Chin's transformed axes (raw data from Larsson, 1997)

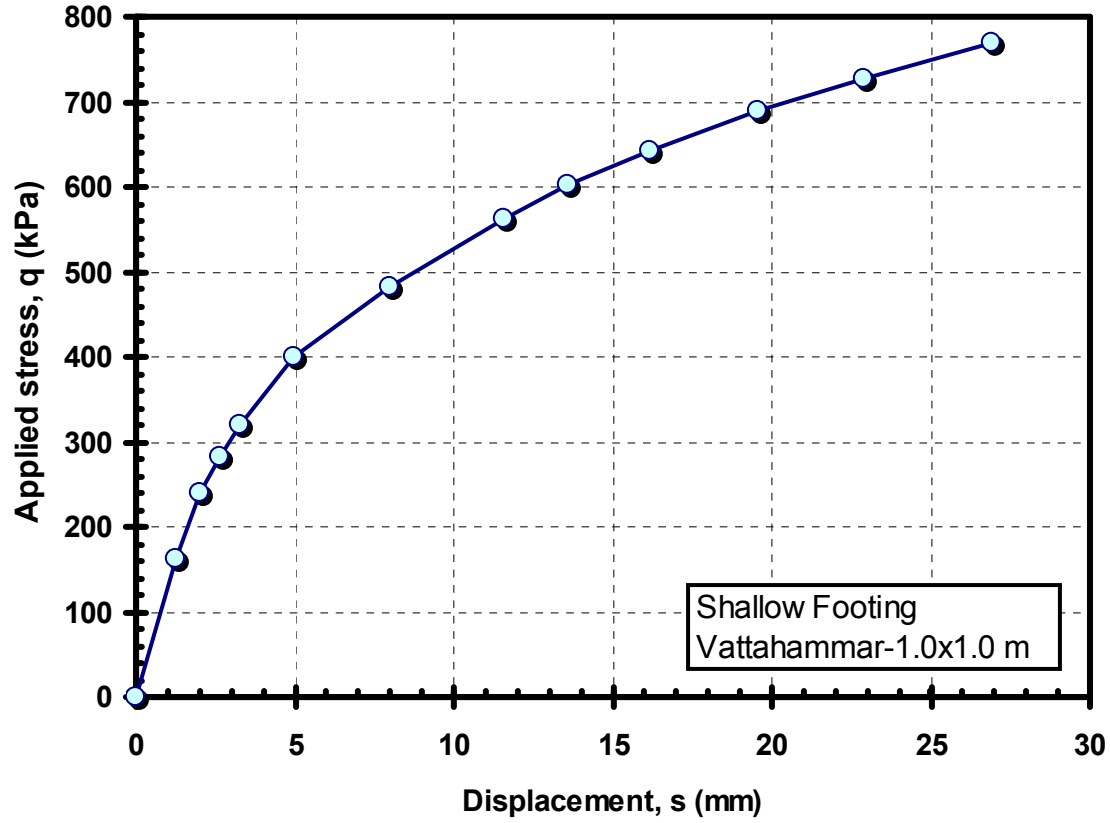


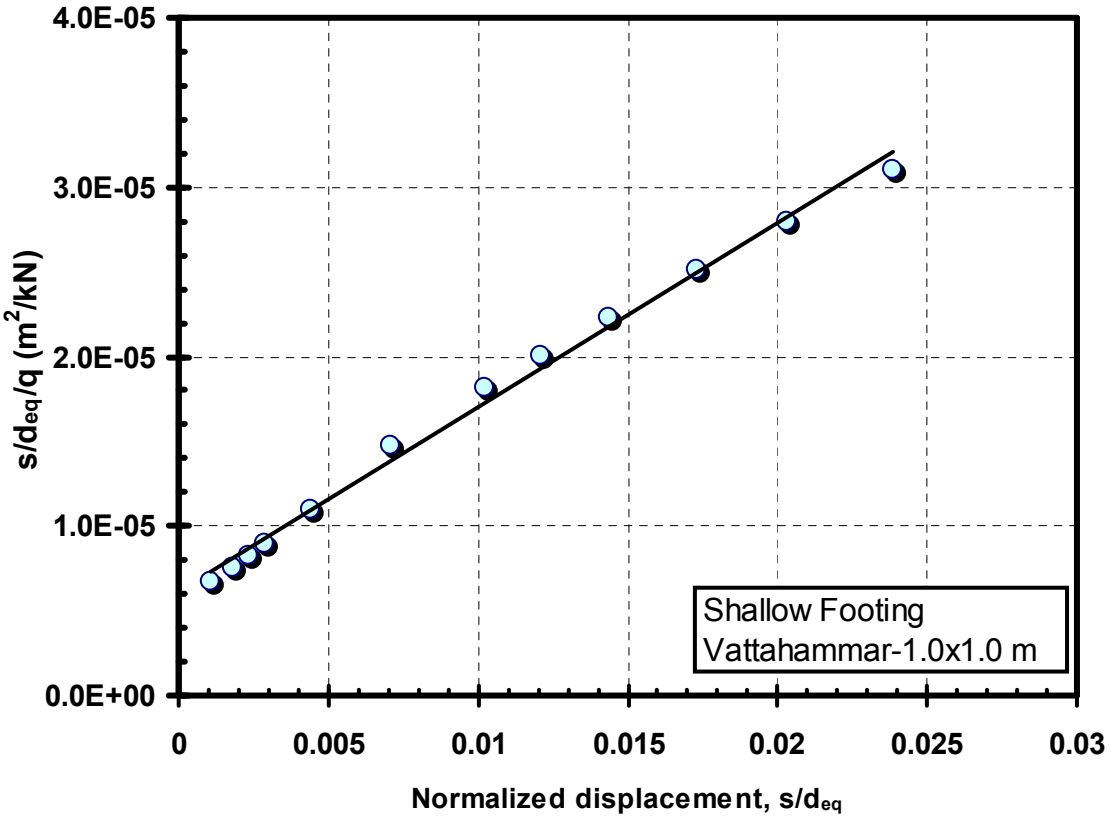


**Figure A-29.** Footing stress-displacement response plotted on (a) standard axes, (b) per Chin's transformed axes (raw data from Larsson, 1997)

# APPENDIX B

## LABORATORY STRESS-STRAIN DATA FOR CALIBRATION OF LOGARITHMIC FITTING FUNCTION

This appendix contains undrained laboratory stress-strain curves used to calibrate the non-linear stress-strain response of clays and silts. Soils included in the calibration are listed in Table B-1. The table includes: site location, test type, sampler type, small-strain stiffness $G_{max}$, effective overburden stress $\sigma_{vo}'$, at rest earth pressure coefficient, normalized shear strength $s_u/ \sigma_{vo}'$, $\Delta q_u = (\sigma_1-\sigma_3)_{max}$, failure strain $\varepsilon_f$ (%), reference strain $\varepsilon_r$ (%), normalized limiting strain $x_L$, and relevant references. The database includes stress-strain response data from unconfined compression tests, $K_o$-consolidated compression tests, direct simple shear tests and $K_o$-consolidated extension tests. Table B-2 lists the references for direct simple shear failure strains, plastic limit, liquid limit, and plasticity indices for data presented in Chapter V. Soils included in the database have plasticity indices ranging from 6% and 84.1%. The stress-strain data presented in Table B-1 are plotted in Figures B-1 through B-40.

**Table B-1.** List of properties of soils used in investigating factors affecting $x_L$

| Site and Depth (m) | Test Type | Sampler Type | $G_{max}$ MPa | $\sigma_{vo}'$ kPa | $K_o$ | $s_u/\sigma_{vo}'$ | $\Delta q_u$ kPa | $\varepsilon_f$ (%) | $\varepsilon_r$ (%) | $x_L$ | Figure | Reference |
|---|---|---|---|---|---|---|---|---|---|---|---|---|
| Ariake-8 m | $CK_oUC$ | Laval | 4.4 | 35 | 0.45 | 0.48 | 214 | 1.20 | 0.11 | 11 | B-1 | Tanaka & Tanaka (1999) |
| Ariake-8 m | $CK_oUE$ | Laval | 4.4 | 35 | 0.45 | 0.29 | 40 | 7.00 | 0.30 | 23 | B-2 | |
| Ariake-10 m | $CK_oUC$ | Sherbrooke | 5.4 | 40 | 0.45 | 0.51 | 20 | 1.25 | 0.12 | 10.4 | B-3 | Tanaka & Tanaka (1999); Tatsuoka (2002) |
| Ariake-10 m | $CK_oUC$ | ELE100 | 5.4 | 40 | 0.45 | 0.51 | 20 | 2.30 | 0.12 | 19.0 | B-4 | |
| BKK1-5.6 m | $CK_oUC$ | Laval | 9.4 | 57 | 0.70 | 0.34 | 38 | 1.60 | 0.14 | 11.4 | B-5 | Shibuya & Tamrakar(1999) |
| BKK1-9.6 m | $CK_oUC$ | Laval | 10.9 | 85 | 0.74 | 0.40 | 44 | 2.00 | 0.13 | 15.4 | B-6 | |
| BKK1-13.6 m | $CK_oUC$ | Laval | 17.2 | 133 | 0.74 | 0.33 | 53 | 1.50 | 0.10 | 15.0 | B-7 | |
| BKK1-17.2 m | $CK_oUC$ | Laval | 51.8 | 174 | 0.53 | 0.39 | 61 | 0.50 | 0.04 | 12.5 | B-8 | |
| BKK2-5.3 m | $CK_oUC$ | Laval | 9.0 | 35 | 0.54 | 0.76 | 37 | 0.70 | 0.14 | 5.0 | B-9 | Shibuya et al. (2000) |
| BKK2-7.3 m | $CK_oUC$ | Laval | 9.0 | 50 | 0.40 | 0.53 | 23 | 0.80 | 0.09 | 9.0 | B-10 | Shibuya et al. (2000) |
| BKK2-9.3 m | $CK_oUC$ | Laval | 10.0 | 70 | 0.37 | 0.46 | 20 | 0.70 | 0.07 | 10.0 | B-11 | Shibuya et al. (2000) |
| BKK2-11.3 m | $CK_oUC$ | Laval | 18.0 | 97 | 0.44 | 0.40 | 23 | 0.65 | 0.04 | 15.5 | B-12 | Shibuya et al. (2000) |
| BKK2-13.3 m | $CK_oUC$ | Laval | 23.0 | 143 | 0.51 | 0.34 | 26 | 0.65 | 0.04 | 15.5 | B-13 | Shibuya et al. (2000) |
| BOK-2.62 m | $CK_oUC$ | Laval | 12.0 | 28.5 | 0.79 | 0.72 | 35 | 1.10 | 0.10 | 11.0 | B-14 | Hight et al. (1992); Hight et al. (1997) |
| BOK -2.67 m | $CK_oUC$ | Sherbrooke | 12.0 | 28.5 | 0.79 | 0.64 | 31 | 1.50 | 0.09 | 16.7 | B-15 | |
| BOK -2.73 m | $CK_oUC$ | Piston | 12.0 | 28.5 | 0.79 | 0.63 | 30 | 2.70 | 0.08 | 33.8 | B-16 | |
| BOK -5.3 m | $CK_oUE$ | Laval | 17.0 | 48 | 0.60 | 0.26 | 44 | 1.60 | 0.09 | 18.7 | B-17 | |
| BOK -5.4 m | $CK_oUC$ | Laval | 17.0 | 48 | 0.60 | 0.52 | 31 | 0.85 | 0.06 | 14.0 | B-18 | |
| BOK –6.0 m | $CK_oUC$ | Laval | 17.0 | 53 | 0.60 | 0.43 | 26 | 1.00 | 0.051 | 19.6 | B-19 | |
| BOK -7.89m | $CK_oUC$ | Laval | 20.3 | 67 | 0.58 | 0.58 | 32 | 1.15 | 0.05 | 23.0 | B-20 | |
| BOK -12.57m | $CK_oUC$ | Piston | 28.4 | 100 | 0.70 | 0.36 | 43 | 2.80 | 0.050 | 56.0 | B-21 | |
| BOK -12.61m | $CK_oUC$ | Laval | 28.4 | 100 | 0.70 | 0.38 | 46 | 1.40 | 0.054 | 27.7 | B-22 | |
| BOK -15.35m | $CK_oUC$ | Laval | 43.4 | 120 | 0.67 | 0.40 | 56 | 1.50 | 0.04 | 36 | B-23 | |
| BOK -15.26m | $CK_oUC$ | Piston | 43.4 | 120 | 0.67 | 0.33 | 40 | 2.60 | 0.03 | 85 | B-24 | |
| BOK -11 m | UC | Sherbrooke | 16.7 | 89 | N/A | 0.39 | 69 | 2.50 | 0.14 | 17.9 | B-25 | Hight et al. (1997) Tanaka (2000) |
| BOK -11 m | UC | ELE100 | 16.7 | 89 | N/A | 0.28 | 50 | 11.5 | 0.10 | 115 | B-26 | |
| LIE -16m | $CK_oUC$ | Sherbrooke | 78.0 | 136 | 0.50 | 0.37 | 32 | 0.40 | 0.014 | 29.6 | B-27 | Lunne and Lacasse (1999) Tanaka (2000) |
| LOU -12 m | $CK_oUC$ | Laval | 26.0 | 92 | 0.89 | 0.46 | 113 | 1.20 | 0.14 | 8.6 | B-28 | Tanaka et al. (2001) |
| Onsoy-3.2 m | $CK_oUC$ | Sherbrooke | 10.5 | 24 | 0.41 | 0.63 | 14 | 1.00 | 0.046 | 19.3 | B-29 | Lacasse et al. (1985) Gillespie et al. (1985) |
| Onsoy-3.5 m | $CK_oUC$ | NGI95 | 10.5 | 24 | 0.51 | 0.52 | 13 | 1.35 | 0.043 | 31.4 | B-30 | |
| Onsoy-6.2 m | DSS | Sherbrooke | 14.1 | 35 | N/A | 0.36 | 13 | 1.55 | 0.09 | 17.2 | B-31 | |
| Onsoy-6.2 m | DSS | NGI95 | 14.1 | 35 | N/A | 0.38 | 14 | 1.30 | 0.096 | 13.5 | B-32 | |
| SF -7.3 m | DSS | Piston | 10.7 | 67 | N/A | 0.27 | 18 | 6.0* | 0.17* | 35.5 | B-33 | Hunt et al. (2002) Pestana et al. (2002) |
| SF -7.75 m | $CK_oUC$ | Piston | 10.7 | 67 | 0.62 | 0.40 | 28 | 1.20 | 0.09 | 14 | B-34 | |
| SF -12.4 m | $CK_oUC$ | Piston | 14.8 | 105 | 0.62 | 0.35 | 22 | 1.62 | 0.05 | 32 | B-35 | |
| SF -23.25 m | $CK_oUC$ | Piston | 25.5 | 178 | 0.62 | 0.33 | 27 | 1.20 | 0.04 | 33.6 | B-36 | |
| SNG -20 m | $CK_oUC$ | JPN | 29.0 | 196 | 0.29 | 0.68 | 52 | 0.75 | 0.06 | 12.7 | B-37 | Tanaka et al. (2001) Watabe (1999) |
| SNG -22 m | $CK_oUC$ | JPN | 39.0 | 210 | 0.66 | 0.38 | 89 | 0.85 | 0.08 | 11 | B-38 | |
| SNG -22 m | $CK_oUE$ | JPN | 39.0 | 210 | 0.62 | 0.33 | 220 | 6.40 | 0.19 | 34 | B-39 | |
| YAM -29.5m | $CK_oUC$ | JPN | 43.0 | 250 | 0.50 | 0.79 | 253 | 1.10 | 0.20 | 5.4 | B-40 | Tanaka et al. (2001) |

Notes:
$CK_oUC$ = $K_o$-consolidated undrained triaxial compression
$CK_oUE$ = $K_o$-consolidated undrained triaxial extension
UC = unconfined compression
DSS = direct simple shear
$G_{max}$ = small-strain shear modulus
$\sigma_{vo}'$ = effective overburden stress
$K_o$ = at rest earth pressure coefficient
$s_u$ = undrained shear strength
$\Delta q_u = (\sigma_1-\sigma_3)_f-(\sigma_1-\sigma_3)_o$
$\varepsilon_f$ = strain at failure
$\varepsilon_r$ = reference strain
$x_L$ = normalized limiting strain
*shear strain $\gamma$

BKK1 = Bangkok (AIT)
BKK1 = Bangkok (NNH)
BOK = Bothkennar
LIE = Lierstranda
LOU= Louiseville
SF = San Francisco
SNG = Singapore
YAM = Yamashita

**Table B-2.** List of soil properties used in direct simple shear failure strain database

| Location | OCR | $w_n$ (%) | LL (%) | PI (%) | $\gamma_f$ (%) | Reference |
|---|---|---|---|---|---|---|
| Higher Harrison Bay, Alaska | 1 | N/A | N/A | 9.7 | 11.3 | Yin (1985)* |
| Lower Harrison Bay, Alaska | 1 | N/A | N/A | 18.3 | 11.0 | Yin (1985)* |
| Smith Bay W, Alaska | 1 | N/A | N/A | 24.4 | 10.9 | Young (1986)* |
| Smith Bay T, Alaska | 1 | N/A | N/A | 24.8 | 13.8 | Young (1986)* |
| Bangkok (CH), Thailand | 1 | 48.6 | 65 | 41.0 | 8.7 | Ladd and Edgers (1972)* |
| Bangkok (CH), Thailand | 1 | 52.2 | 65 | 41.0 | 7.0 | Ladd and Edgers (1972)* |
| Bangkok (CH), Thailand | 1 | 52.2 | 65 | 41.0 | 10.0 | Ladd and Edgers (1972)* |
| Bombay, India | 1 | N/A | N/A | 43.9 | 12.3 | MIT (1982)* |
| Ariake, Japan | 1 | 130 | 110 | 65.0 | 10.5 | Tang et al. (1994) |
| Ariake, Japan | 1 | 140 | 120 | 70.0 | 12.5 | Tang et al. (1994) |
| Omaha, Midwest | 1 | N/A | N/A | 43.0 | 11.9 | MIT (1985)* |
| Franklin NH, New England | 1 | N/A | N/A | 5.5 | 5.1 | MIT (1983)* |
| Portsmouth, New England | 1 | N/A | N/A | 15.0 | 1.6 | Ladd and Edgers (1972)* |
| Portland, New England | 1 | N/A | N/A | 20.0 | 4.0 | Ladd and Edgers (1972)* |
| Boston, New England | 1 | N/A | N/A | 21.0 | 6.1 | Ladd and Edgers (1972)* |
| Draw 7 Mass, New England | 1 | N/A | N/A | 30.5 | 11.8 | MIT (1987)* |
| Maine, New England | 1 | N/A | N/A | 34.0 | 10.6 | Ladd and Edgers (1972)* |
| New Jersey, New England | 1 | 32 | 36 | 18.0 | 7.5 | Koutsoftas (1970) |
| AGS, New England | 1 | N/A | N/A | 38.0 | 11.9 | Koutsoftas and Ladd (1970) |
| Connecticut Valley, New England | 1 | N/A | N/A | 20.5 | 6.5 | Lacasse et al. (1972)* |
| James Bay`B-2, Canada | 3 | 40 | 31 | 12.0 | 2.81 | Lefebvre et al. (1988) |
| James Bay`B-6, Canada | 1.45 | 42.4 | 31 | 10.0 | 1.69 | Lefebvre et al. (1988) |
| Linkoping, Sweden | 1 | 90 | 80 | 52.0 | 15.0 | Larsson (1977) |
| Linkoping, Sweden | 1 | 90 | 80 | 52.0 | 14.0 | Larsson (1977) |
| Ellingsrud, Norway | 1.3 | 37 | 27 | 6.0 | 1.5 | Lacasse et al. (1985) |
| Ellingsrud, Norway | 1.3 | 36 | 27 | 6.0 | 1.4 | Lacasse et al. (1985) |
| Ellingsrud, Norway | 1.3 | 39 | 27 | 6.0 | 1.5 | Lacasse et al. (1985) |
| Ellingsrud, Norway | 1.3 | 35 | 27 | 6.0 | 1.3 | Lacasse et al. (1985) |
| Manglerud, Norway | 1 | 34.6 | 27 | 8.0 | 4.0 | Bjerrum and Landva (1966) |
| Manglerud, Norway | 1 | 34.6 | 27 | 8.0 | 3.1 | Bjerrum and Landva (1966) |
| Manglerud, Norway | 1 | 34.3 | 27 | 8.0 | 5.3 | Bjerrum and Landva (1966) |
| Manglerud, Norway | 1 | 35.6 | 27 | 8.0 | 3.8 | Bjerrum and Landva (1966) |
| Emmerstad, Norway | 1.2 | 44 | 28 | 8.0 | 2.8 | Lacasse et al. (1985) |
| Emmerstad, Norway | 1.2 | 44 | 28 | 8.0 | 1.8 | Lacasse et al. (1985) |
| Drammen, Norway | 1 | 50 | 55 | 28.0 | 4.0 | Dyvik et al. (1987) |
| Haga, Norway | 1 | N/A | N/A | 15.0 | 2.2 | Lacasse and Vucetic (1970) |
| Onsoy, Norway | 2.3 | 64 | 58 | 30.0 | 3.0 | Lacasse et al. (1985) |
| Onsoy, Norway | 1.5 | 70 | 70 | 40.0 | 2.8 | Lacasse et al. (1985) |

**Table B-2.** (continued)

| Location | OCR | $w_n$ (%) | LL (%) | PI (%) | $\gamma_f$ (%) | Reference |
|---|---|---|---|---|---|---|
| Onsoy, Norway | 1.5 | 71 | 70 | 44.0 | 3.0 | Lacasse et al. (1985) |
| Cowden, UK | | N/A | N/A | 18.0 | 10.67 | Atkinson et al. (1991) |
| Bothkennar, UK | 1.5 | N/A | 61 | 34.0 | 8.1 | Hight (2003) |
| Bothkennar, UK | 1.5 | N/A | 69 | 35.0 | 9.5 | Hight (2003) |
| Bothkennar, UK | 1.5 | N/A | 73 | 38.0 | 5.7 | Hight (2003) |
| Bothkennar, UK | 1.5 | N/A | 72 | 40.0 | 5.2 | Hight (2003) |
| Bothkennar, UK | 1.5 | N/A | 68 | 37.0 | 6.0 | Hight (2003) |
| Bothkennar, UK | 1.5 | N/A | 73 | 38.0 | 5.7 | Hight (2003) |
| Bothkennar, UK | 1.5 | N/A | 58 | 29.0 | 3.1 | Hight (2003) |
| Empire, LA, Southern USA | N/A | N/A | N/A | 54.2 | 13.6 | Azzouz and Baligh (1984) |
| Alabama, Southern USA | N/A | N/A | N/A | 56.0 | 10.4 | MIT (1988)* |
| Atchafalaya, LA, Southern USA | 1 | N/A | N/A | 75.0 | 21.0 | Williams (1973)* |
| Atchafalaya, LA, Southern USA | 1 | 72 | 95 | 75.0 | 18.4 | Ladd and Edgers (1972)* |
| Atchafalaya, LA, Southern USA | 1 | 72.6 | 95 | 75.0 | 22.8 | Ladd and Edgers (1972)* |
| Atchafalaya, LA, Southern USA | 1 | 76.3 | 95 | 75.0 | 21.9 | Ladd and Edgers (1972)* |
| Tuy Cariaco, Venezuela | 1 | N/A | N/A | 20.0 | 6.0 | Mishu et al. (1982)* |
| Orinoco, Venezuela | 1 | N/A | N/A | 42.8 | 11.8 | Ladd et al. (1980)* |
| Orinoco, Venezuela | 1 | N/A | N/A | 47.3 | 11.1 | Ladd et al. (1980)* |
| North of Paria, Venezuela | 1 | N/A | N/A | 47.5 | 9.6 | Mishu et al. (1982)* |
| Tuy Cariaco, Venezuela | 1 | N/A | N/A | 49.1 | 13.2 | Mishu et al. (1982)* |
| San Francisco, Western USA | 1 | N/A | N/A | 25.2 | 8.6 | MIT (1985)* |
| Great Salt Lake, Western USA | 1 | N/A | N/A | 30.0 | 9.1 | MIT (1987)* |
| Great Salt Lake, Western USA | 1 | N/A | N/A | 31.3 | 6.3 | MIT (1985)* |
| Klamath Falls, Western USA | 1 | N/A | N/A | 84.1 | 11.7 | MIT (1986)* |
| Boston, Eastern USA | 1 | 37 | 41 | 21.0 | 6.0 | Ladd and Edgers (1972)* |
| Boston, Eastern USA | 1 | 37 | 41 | 21.0 | 4.5 | Ladd and Edgers (1972)* |
| Boston, Eastern USA | 1 | 37 | 41 | 21.0 | 6.2 | Ladd and Edgers (1972)* |

* DeGroot et al. (1992)

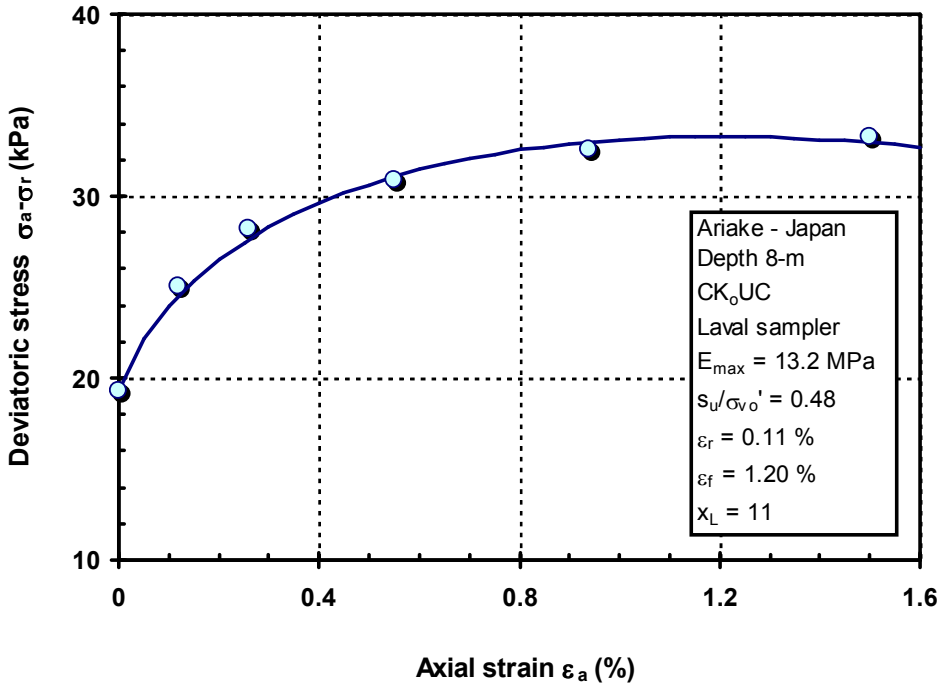


**Figure B-1.** Logarithmic function fitted to stress-strain data from $CK_oUC$ test on a Laval clay sample from Ariake-Japan, depth = 8-m (Tanaka and Tanaka, 1999)

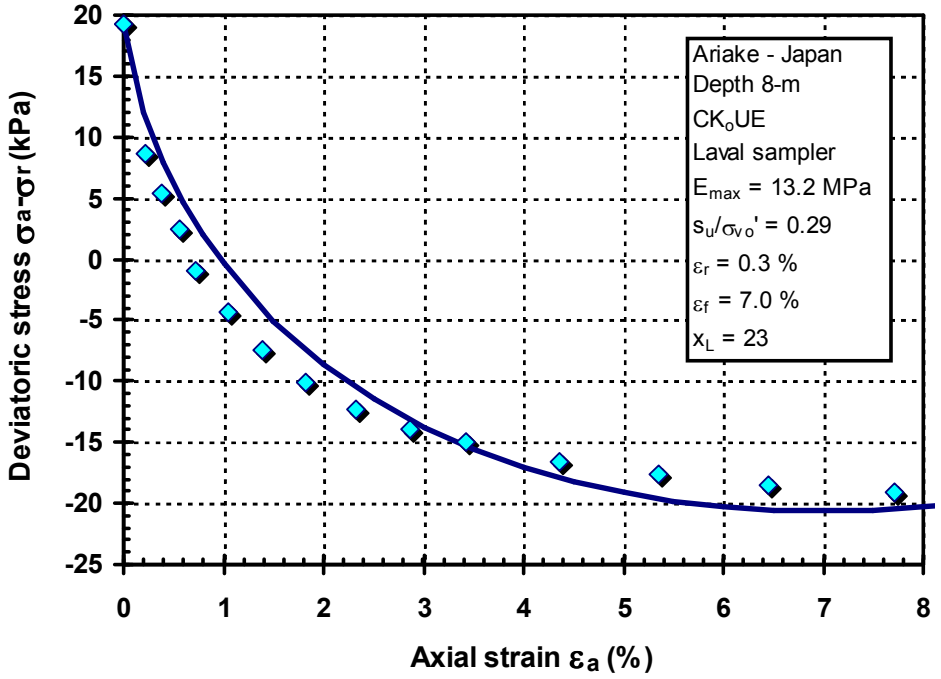


**Figure B-2.** Logarithmic function fitted to stress-strain data from $CK_oUE$ test on a Laval clay sample from Ariake-Japan, depth = 8-m (Tanaka and Tanaka, 1999)

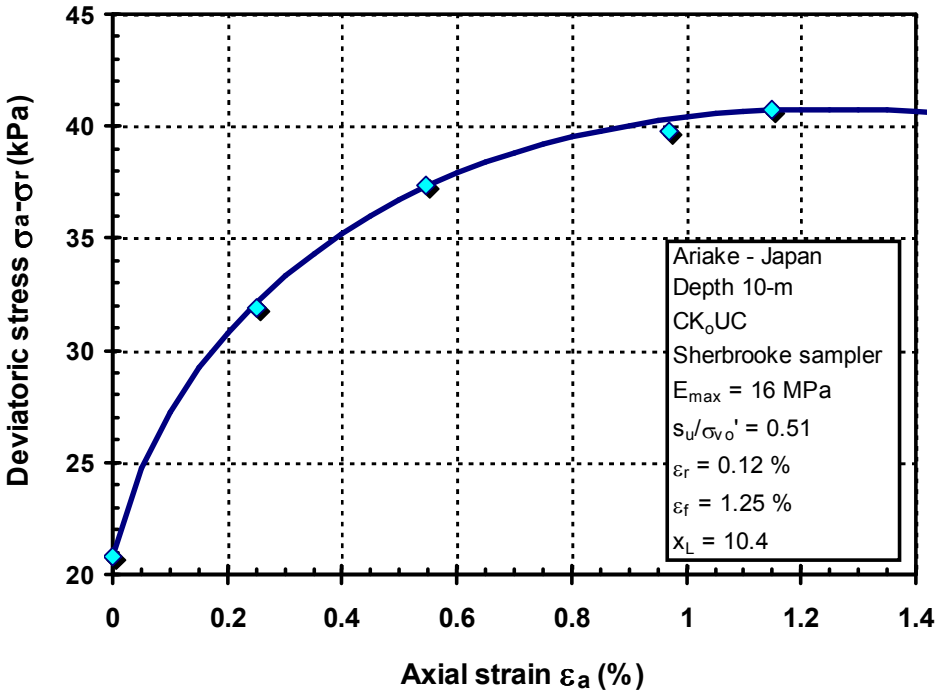


**Figure B-3.** Logarithmic function fitted to stress-strain data from $CK_oUC$ test on a Sherbrooke clay sample from Ariake-Japan, depth = 10-m (Tanaka and Tanaka, 1999; Tatsuoka, 2002)

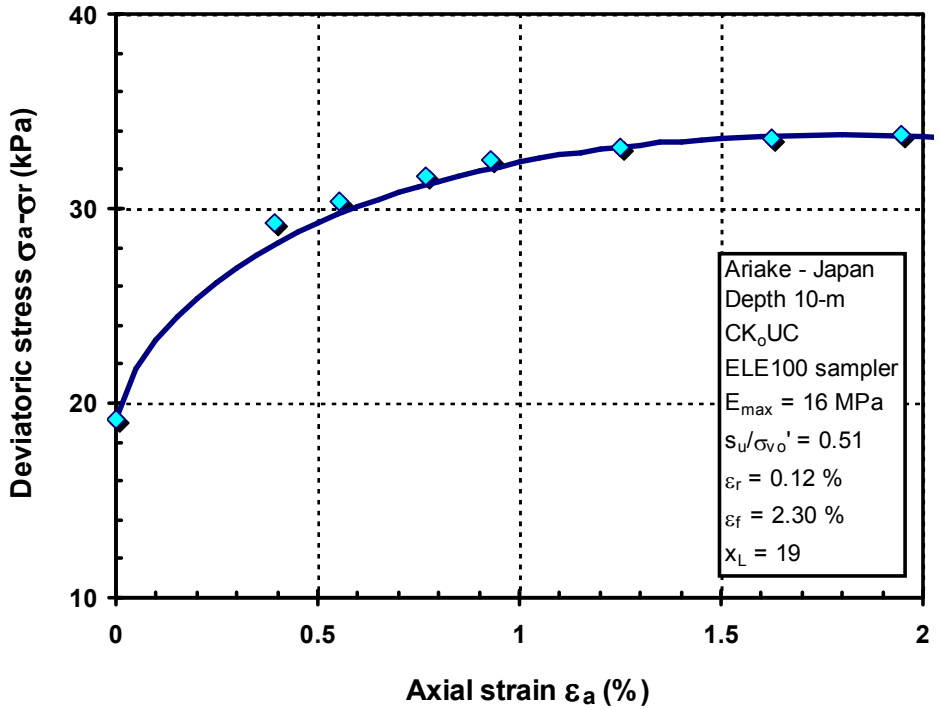


**Figure B-4** Logarithmic function fitted to stress-strain data from $CK_oUC$ test on an ELE100 clay sample from Ariake-Japan, depth = 10-m (Tanaka and Tanaka, 1999; Tatsuoka, 2002)

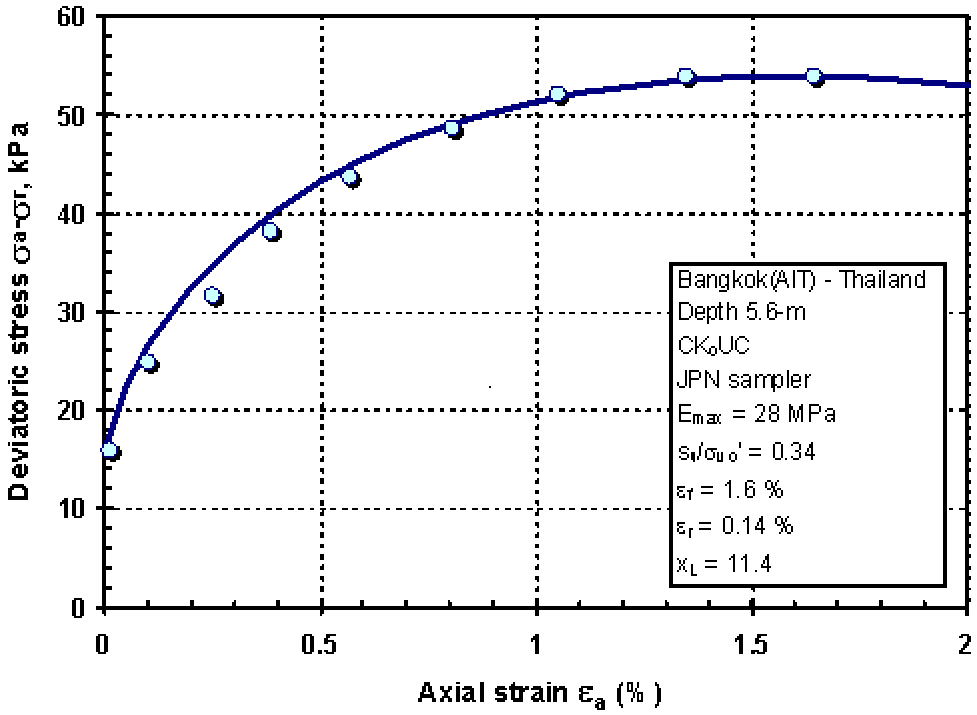


**Figure B-5.** Logarithmic function fitted to stress-strain data from $CK_oUC$ test on a JPN clay sample from Bangkok (AIT)-Thailand, depth =5.6-m (Shibuya and Tamrakar, 1999)

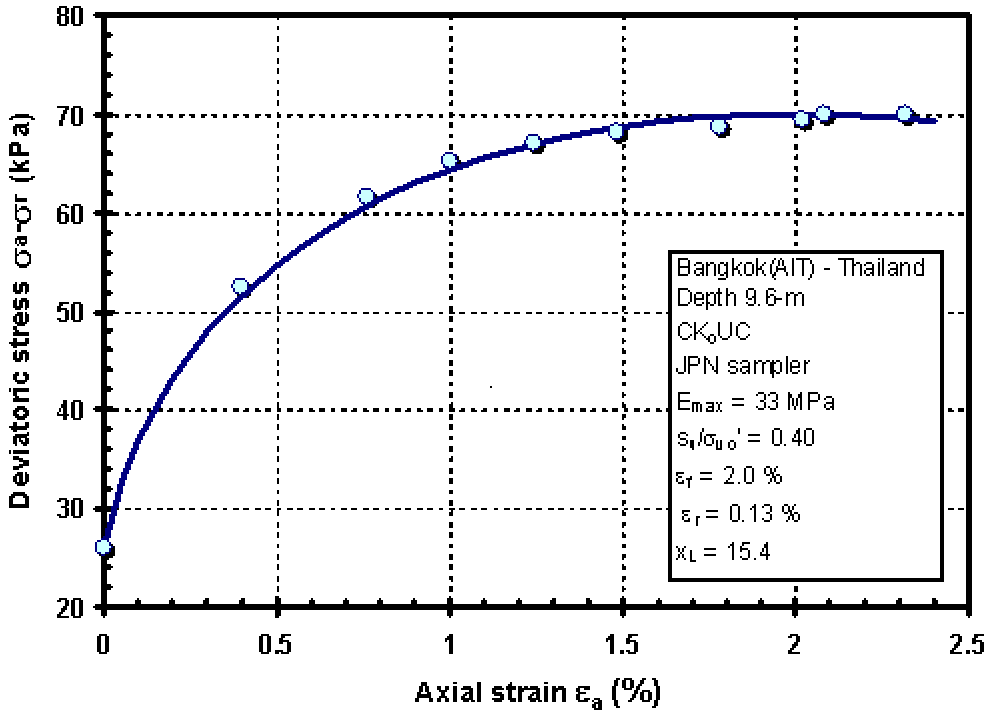


**Figure B-6.** Logarithmic function fitted to stress-strain data from $CK_oUC$ test on a JPN clay sample from Bangkok (AIT)-Thailand, depth = 9.6-m (Shibuya and Tamrakar, 1999)

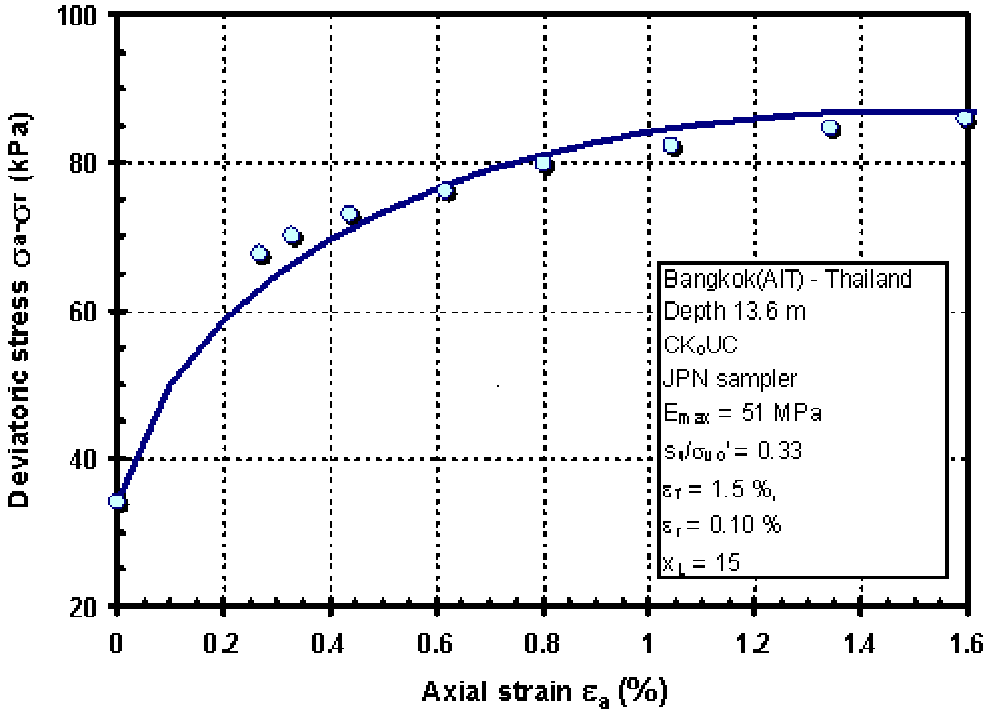


**Figure B-7** Logarithmic function fitted to stress-strain data from $CK_oUC$ test on a JPN clay sample from Bangkok-Thailand, depth = 13.6-m (Shibuya and Tamrakar, 1999)

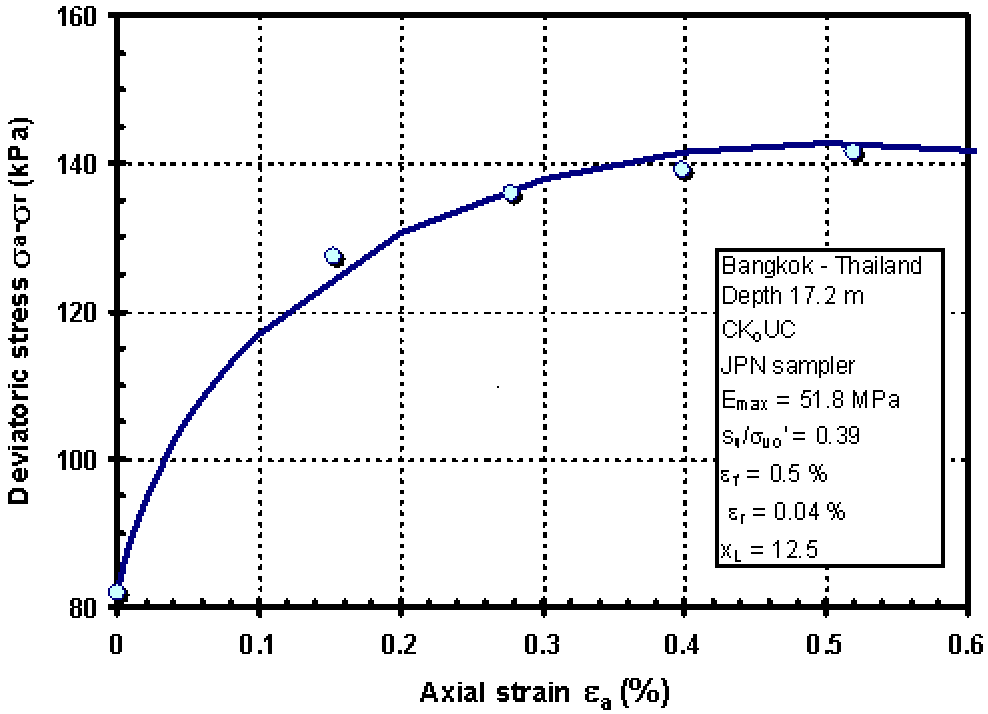


**Figure B-8.** Logarithmic function fitted to stress-strain data from $CK_oUC$ test on a JPN clay from Bangkok-Thailand, depth = 17.2-m (Shibuya and Tamrakar, 1999)

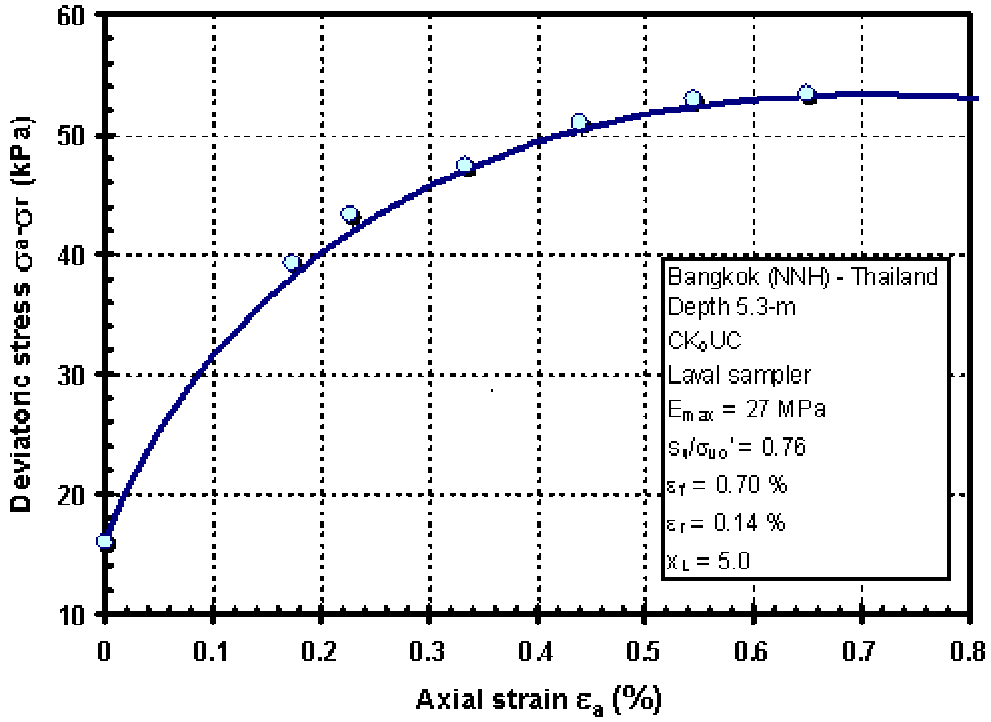


**Figure B-9** Logarithmic function fitted to stress-strain data from $CK_oUC$ test on a Laval clay sample from Bangkok (NNH)-Thailand, depth = 5.3-m (Shibuya et al., 2000)

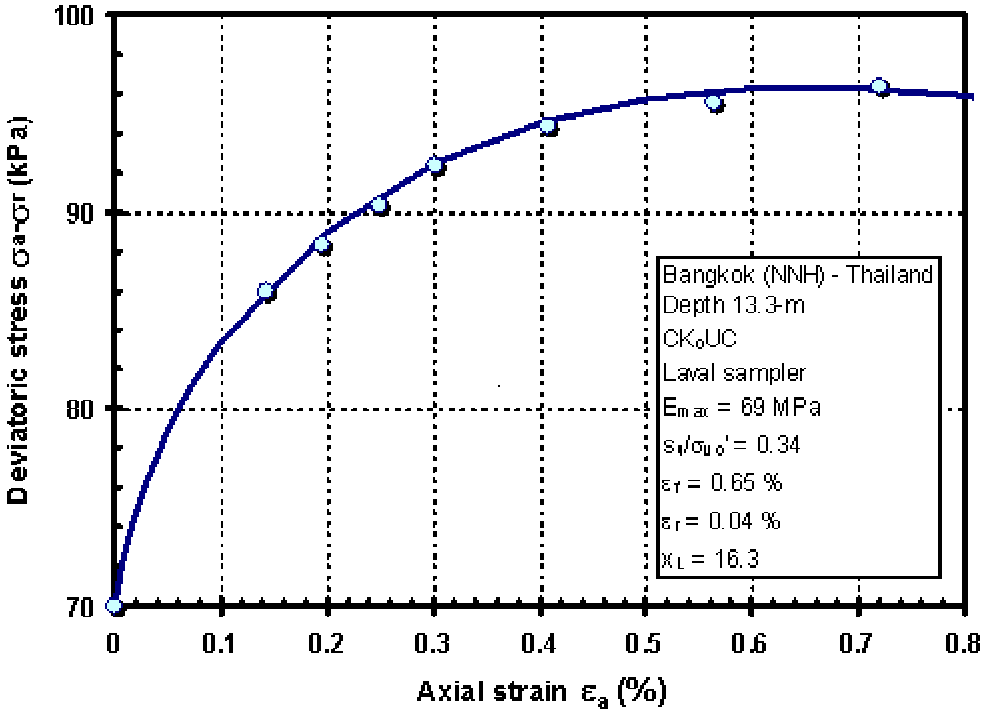


**Figure B-10.** Logarithmic function fitted to stress-strain data from $CK_oUC$ test on a Laval clay sample from Bangkok (NNH)-Thailand, depth = 7.3-m (Shibuya et al., 2000)

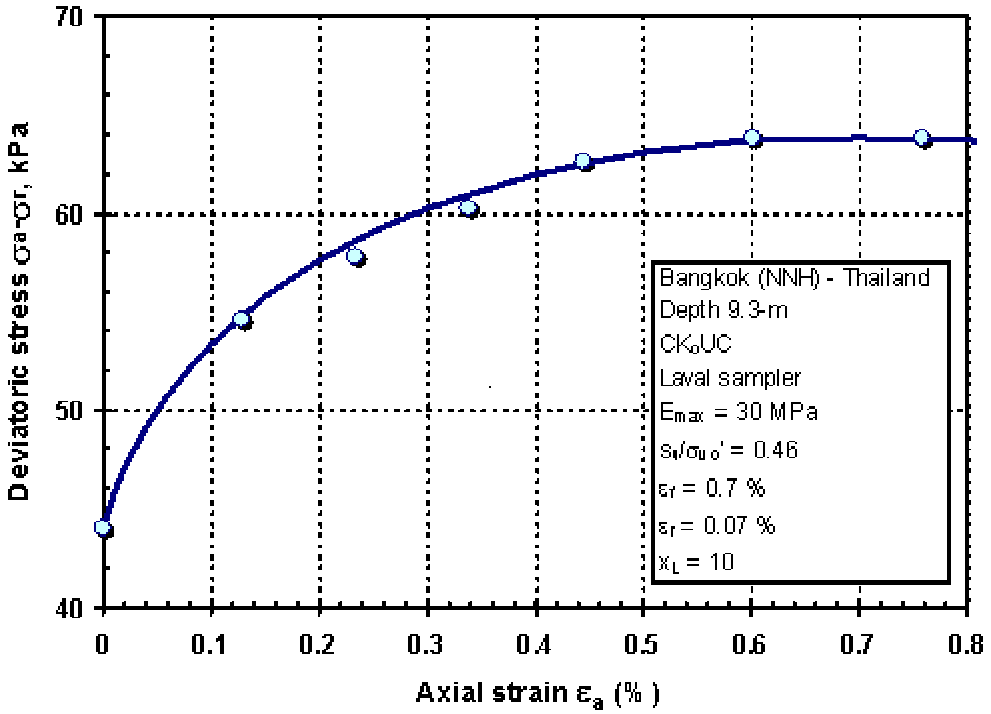


**Figure B-11.** Logarithmic function fitted to stress-strain data from $CK_oUC$ test on a Laval clay sample from Bangkok (NNH)-Thailand, depth = 9.3-m (Shibuya et al., 2000)

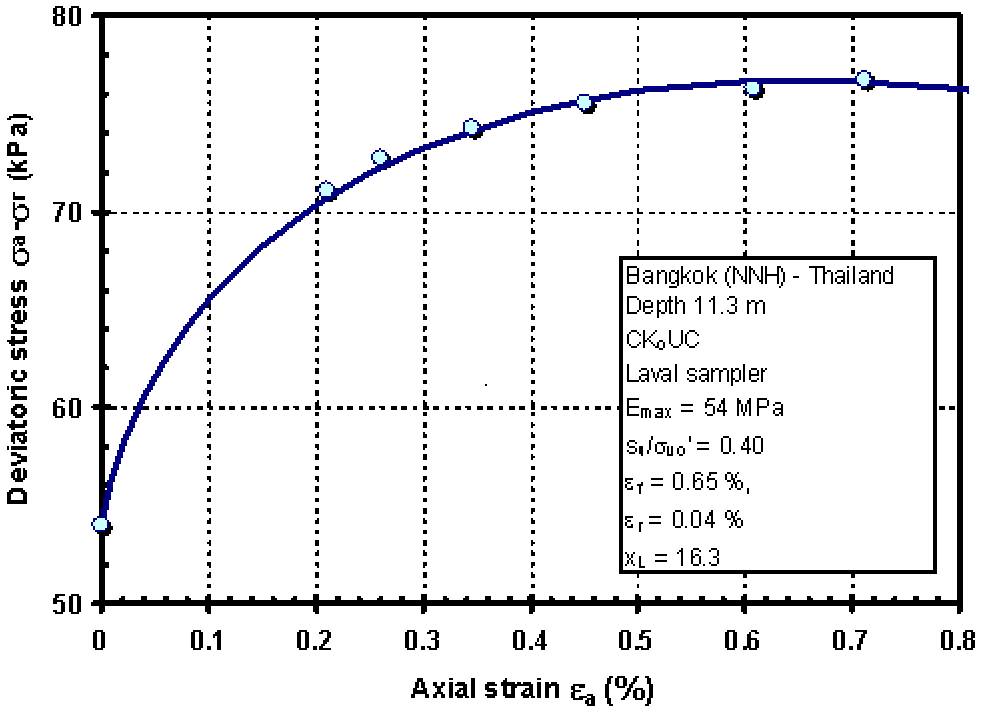


**Figure B-12.** Logarithmic function fitted to stress-strain data from $CK_oUC$ test on a Laval clay sample from Bangkok (NNH)-Thailand, depth = 11.3-m (Shibuya et al., 2000)

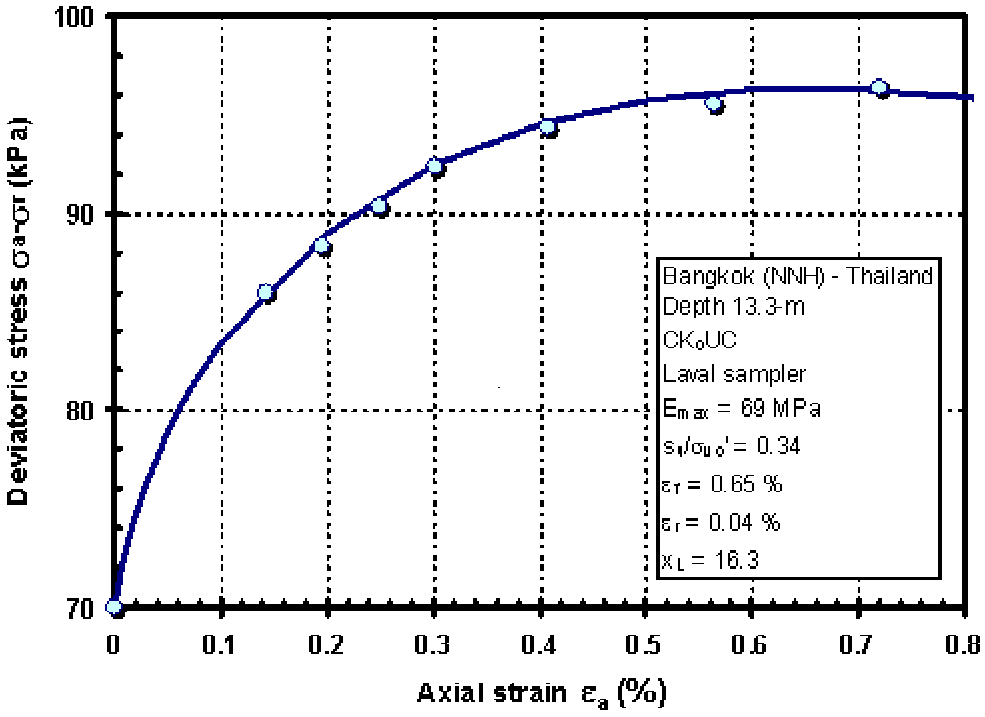


**Figure B-13.** Logarithmic function fitted to stress-strain data from $CK_oUC$ test on a Laval clay sample from Bangkok (NNH)-Thailand, depth = 13.3-m (Shibuya et al., 2000)

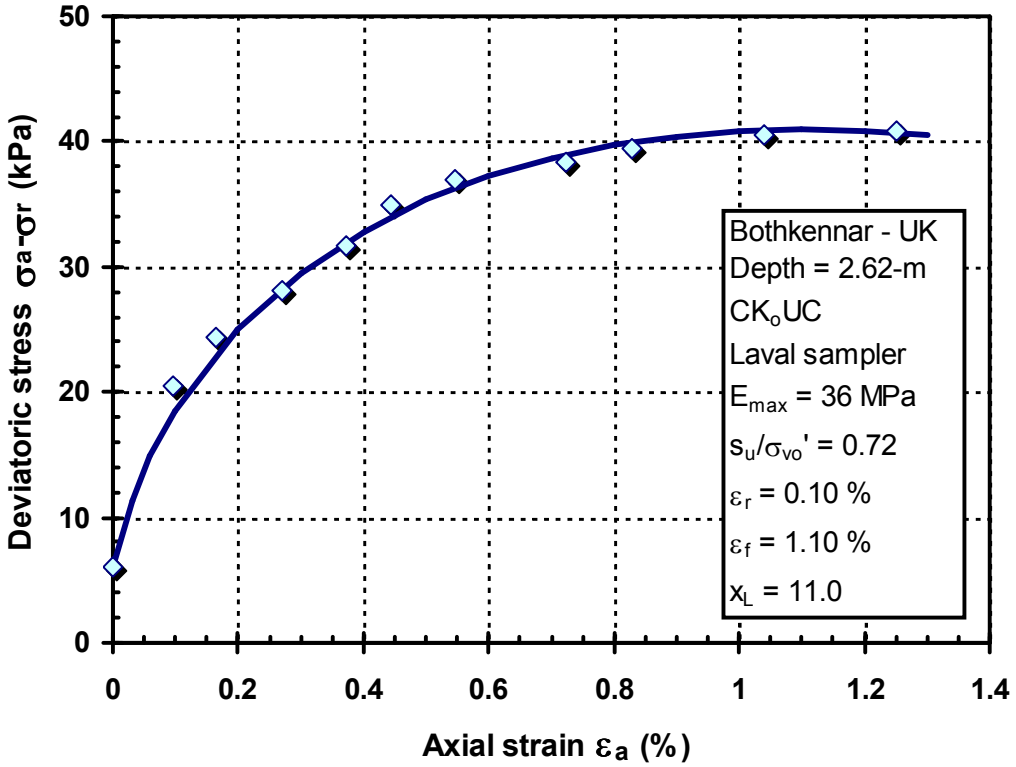


**Figure B-14.** Logarithmic function fitted to stress-strain data from $CK_oUC$ test on a Laval sample from Bothkennar-UK, depth = 2.62-m (Hight et al., 1992; 1997)

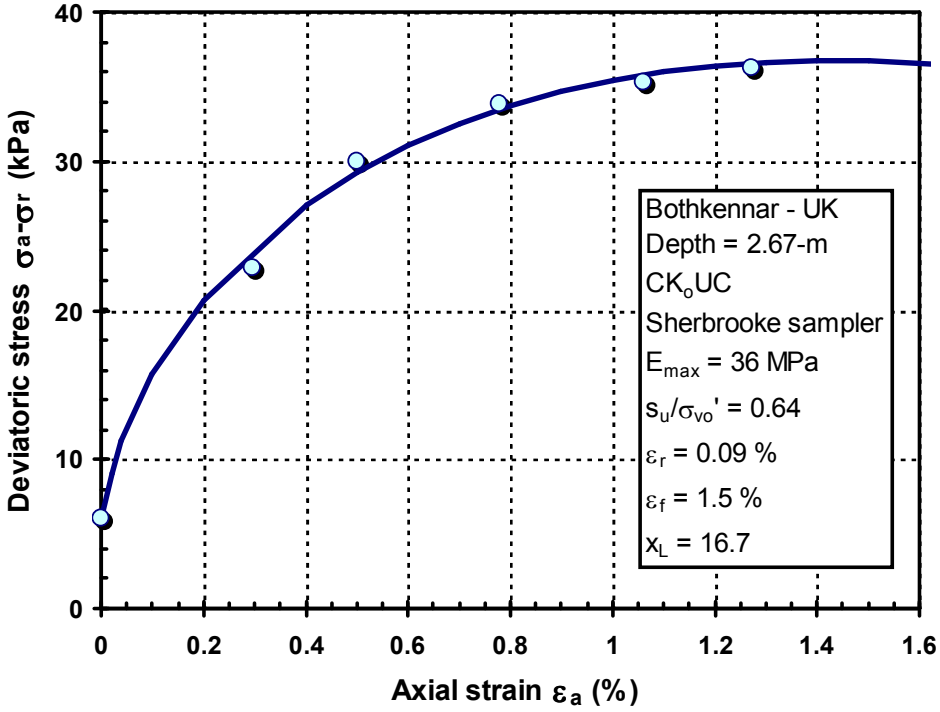


**Figure B-15.** Logarithmic function fitted to stress-strain data from $CK_oUC$ test on a Sherbrooke clay sample from Bothkennar-UK, depth = 2.67-m (Hight et al., 1992; 1997)

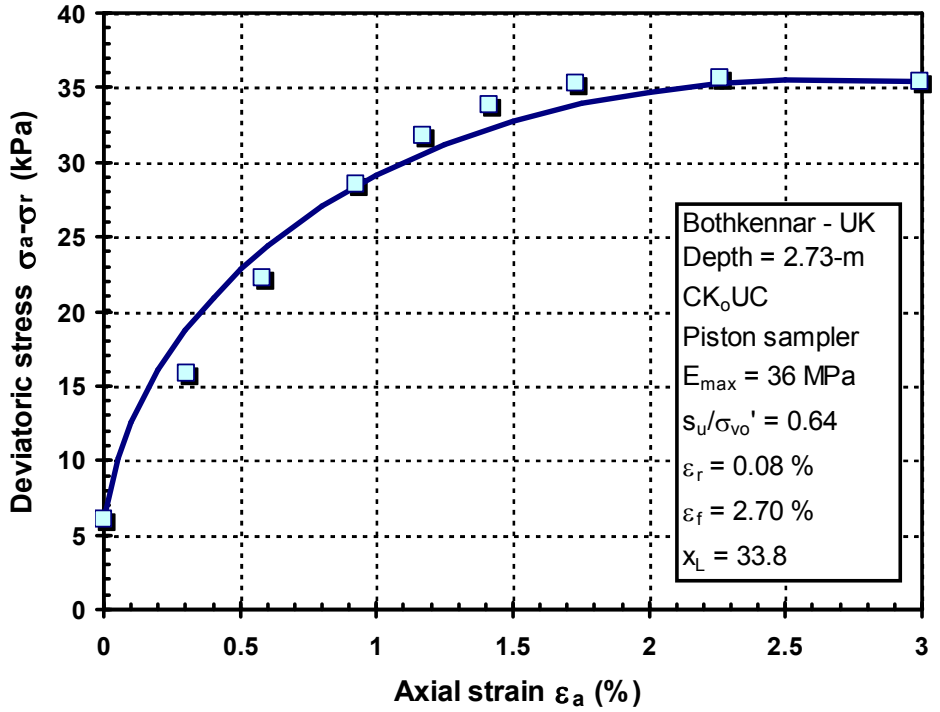


**Figure B-16.** Logarithmic function fitted to stress-strain data from $CK_oUC$ test on a piston clay sample from Bothkennar-UK, depth = 2.73-m (Hight et al., 1992; 1997)

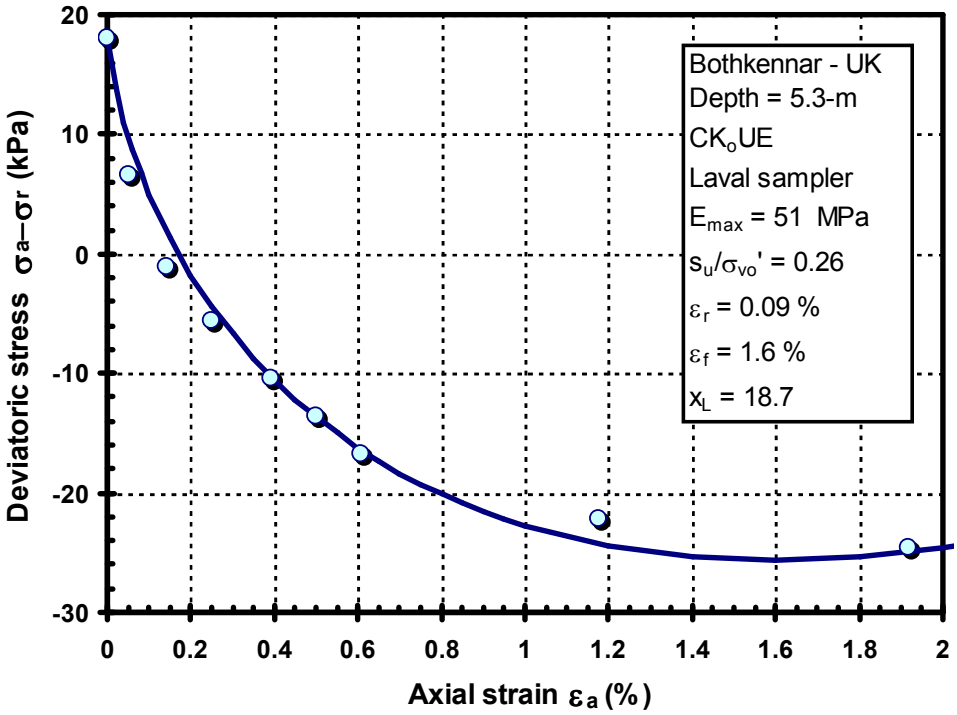


**Figure B-17.** Logarithmic function fitted to stress-strain data from $CK_oUC$ test on a Laval clay sample from Bothkennar-UK, depth = 5.3-m (Hight et al., 1992; 1997)

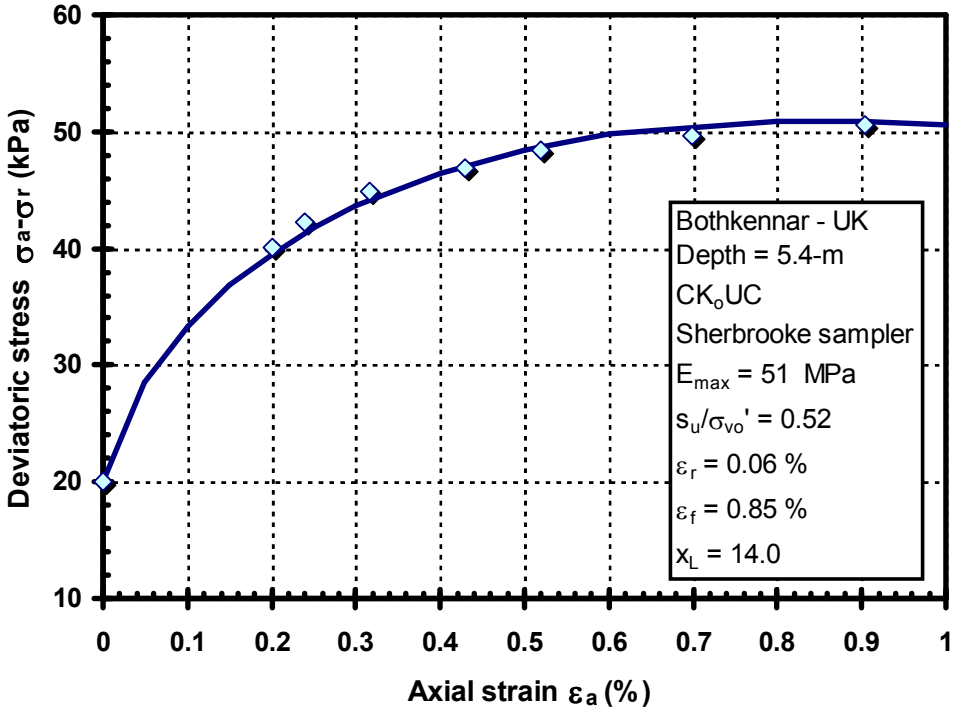


**Figure B-18.** Logarithmic function fitted to stress-strain data from $CK_oUC$ test on a Sherbrooke clay sample from Bothkennar-UK, depth = 5.4-m (Hight et al., 1992; 1997)

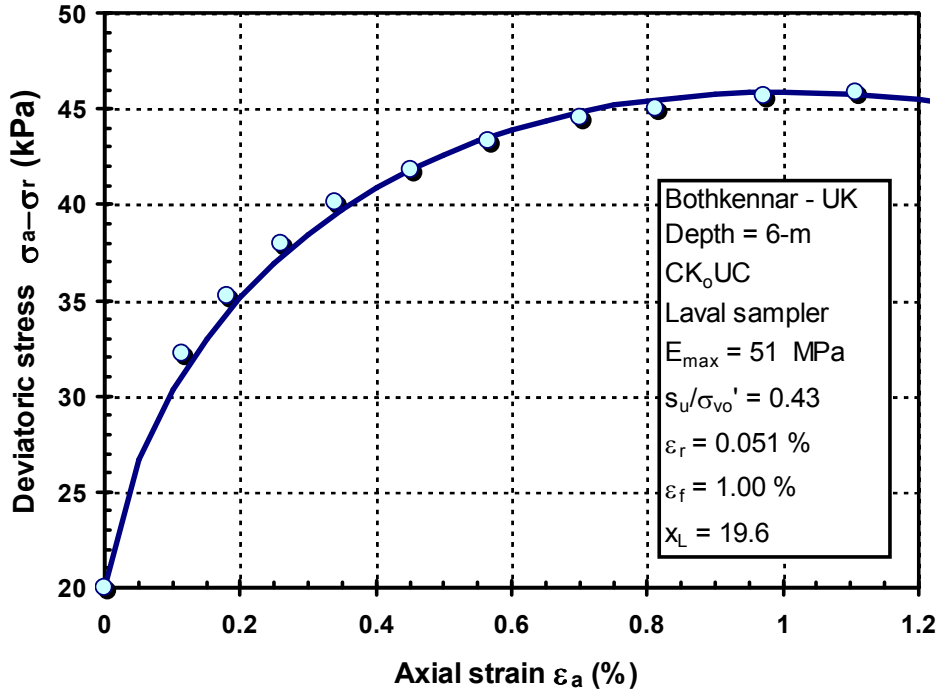


**Figure B-19.** Logarithmic function fitted to stress-strain data from $CK_oUC$ test on a Laval clay sample from Laval-UK, depth = 7.9-m (Hight et al., 1992; 1997)

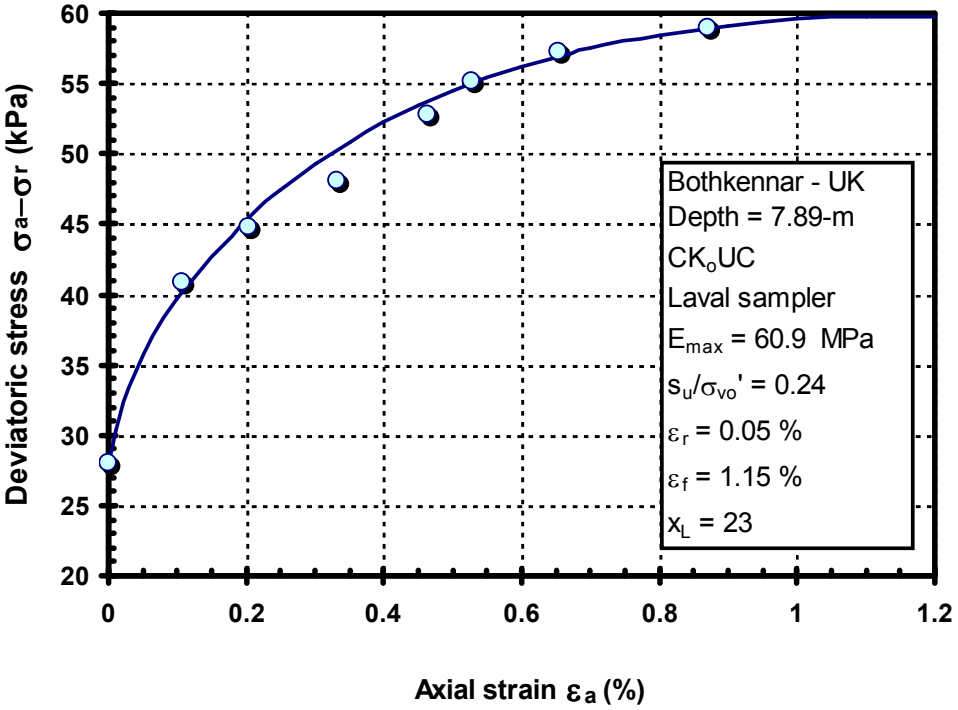


**Figure B-20.** Logarithmic function fitted to stress-strain data from $CK_oUC$ test on a Laval clay sample from Bothkennar-UK, depth = 7.9-m (Hight et al., 1992; 1997)

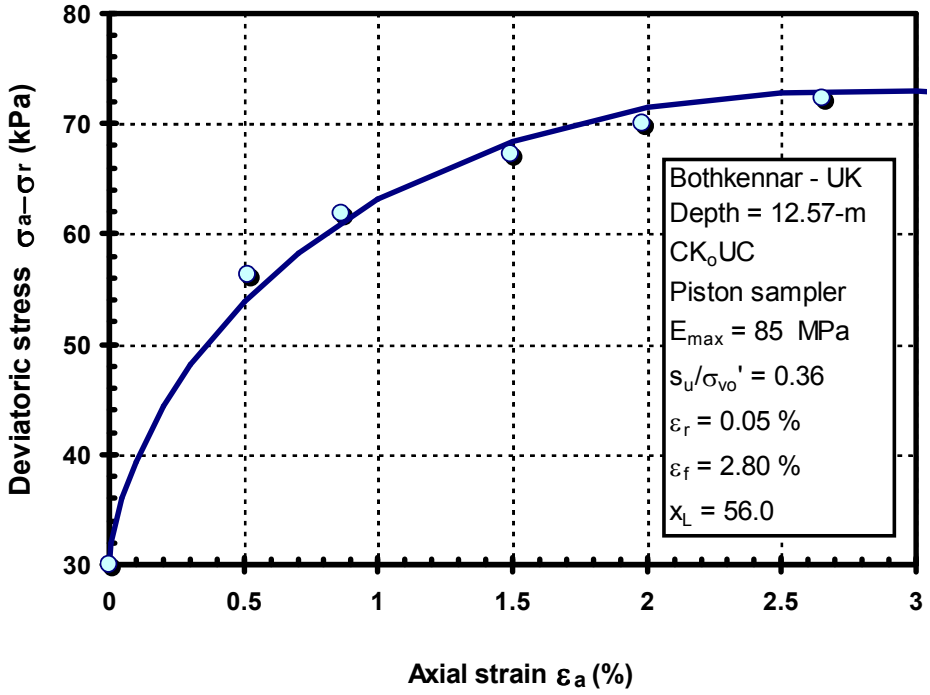


**Figure B-21.** Logarithmic function fitted to stress-strain data from $CK_oUC$ test on a Laval clay sample from Bothkennar-UK, depth = 12.57-m (Hight et al., 1992; 1997)

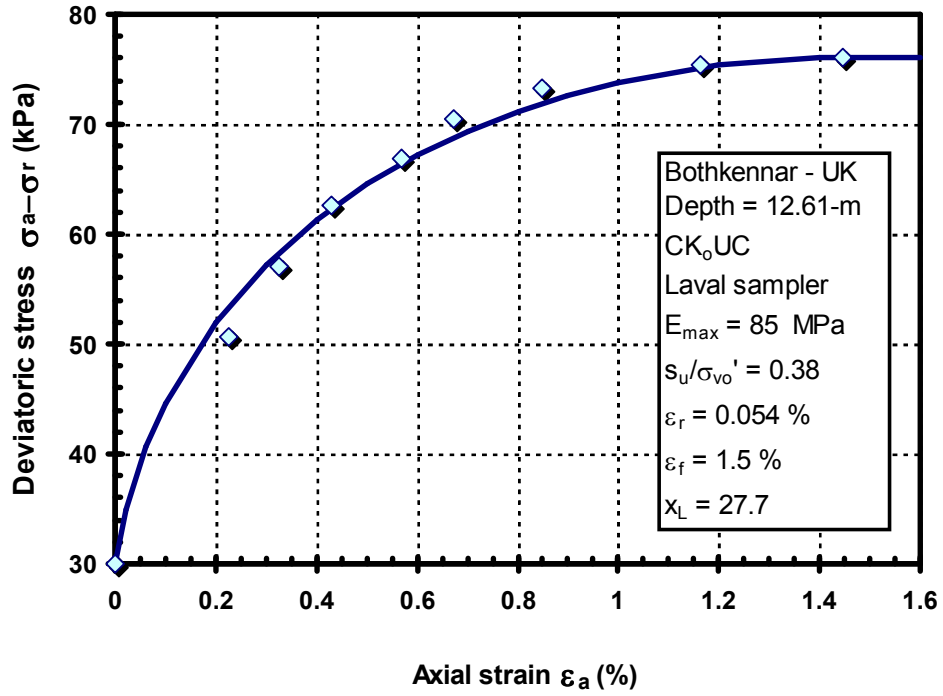


**Figure B-22.** Logarithmic function fitted to stress-strain data from $CK_oUC$ test on a Laval clay sample from Bothkennar-UK, depth = 12.61-m (Hight et al., 1992; 1997)

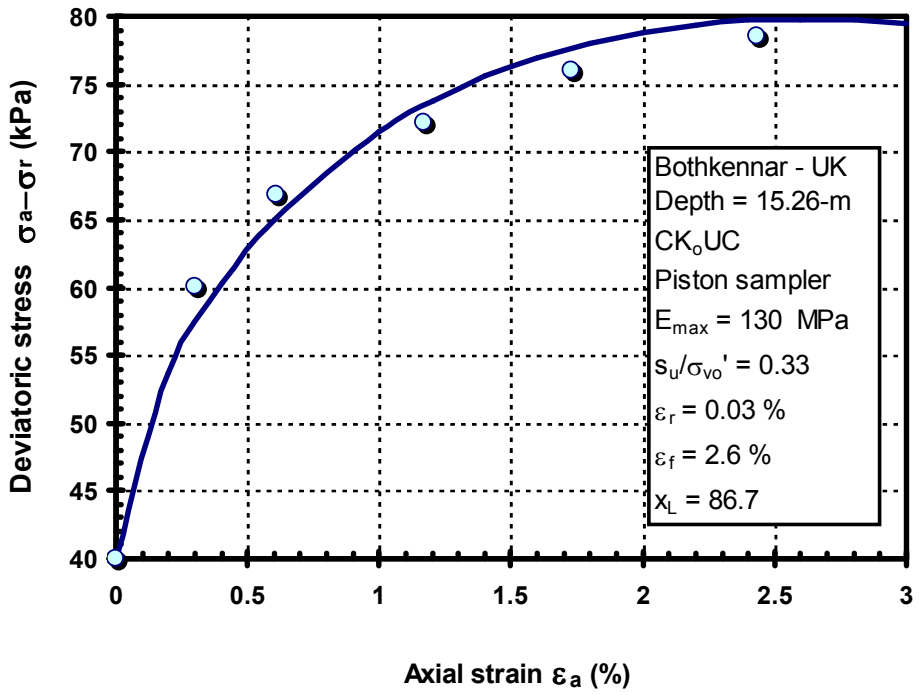


**Figure B-23.** Logarithmic function fitted to stress-strain data from $CK_oUC$ test on a piston clay sample from Bothkennar-UK, depth = 15.26-m (Hight et al., 1992; 1997)

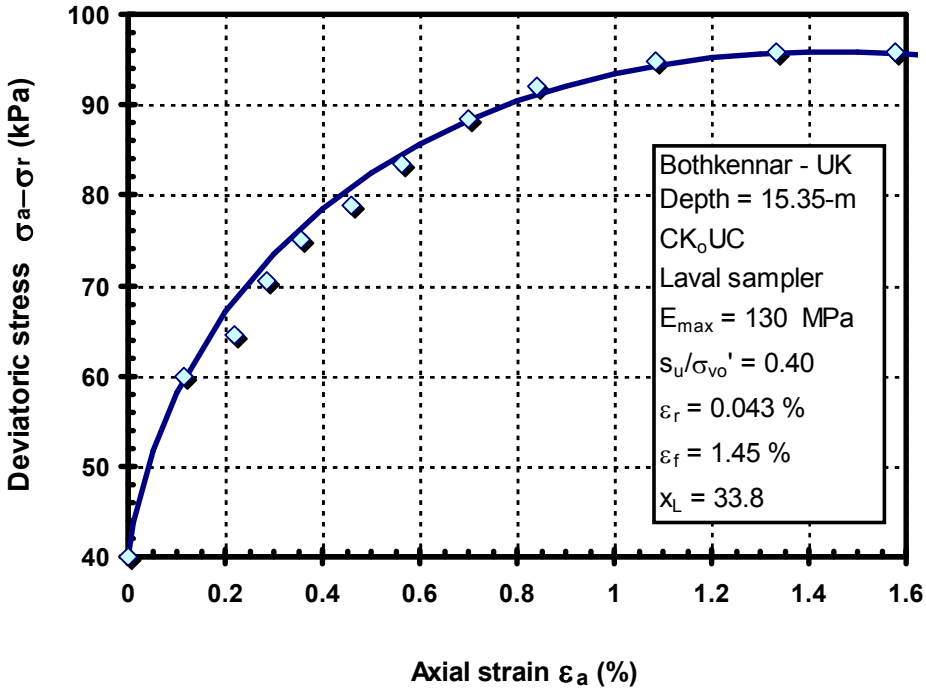


**Figure B-24.** Logarithmic function fitted to stress-strain data from $CK_oUC$ test on a Laval clay sample from Bothkennar-UK, depth = 15.35-m (Hight et al., 1992; 1997)

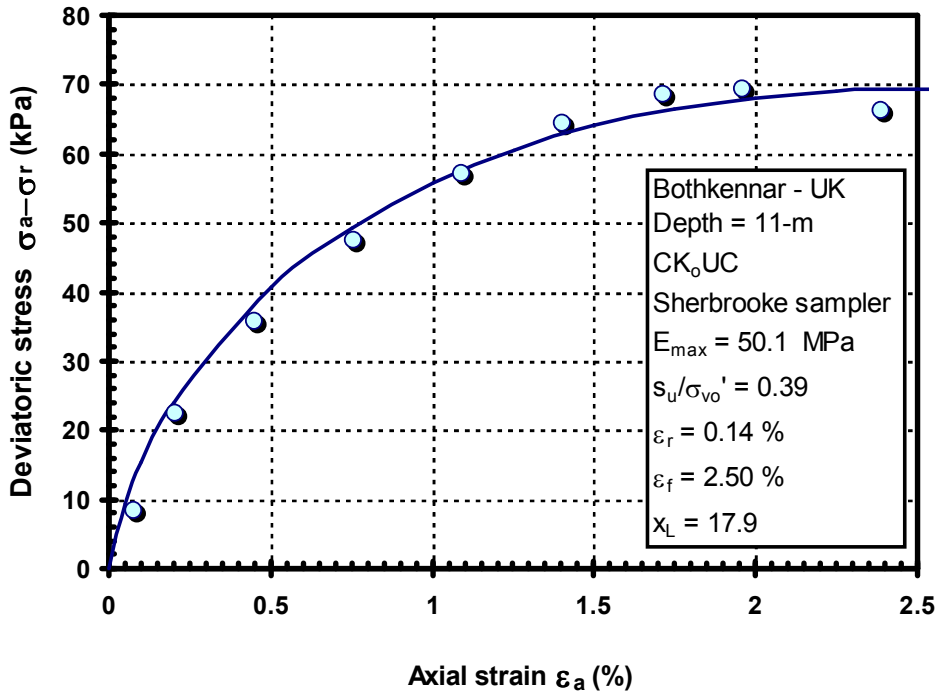


**Figure B-25.** Logarithmic function fitted to stress-strain data from UC test on a Sherbrooke clay sample from Bothkennar-UK, depth = 11-m (Hight et al., 1997; Tanaka, 2000)

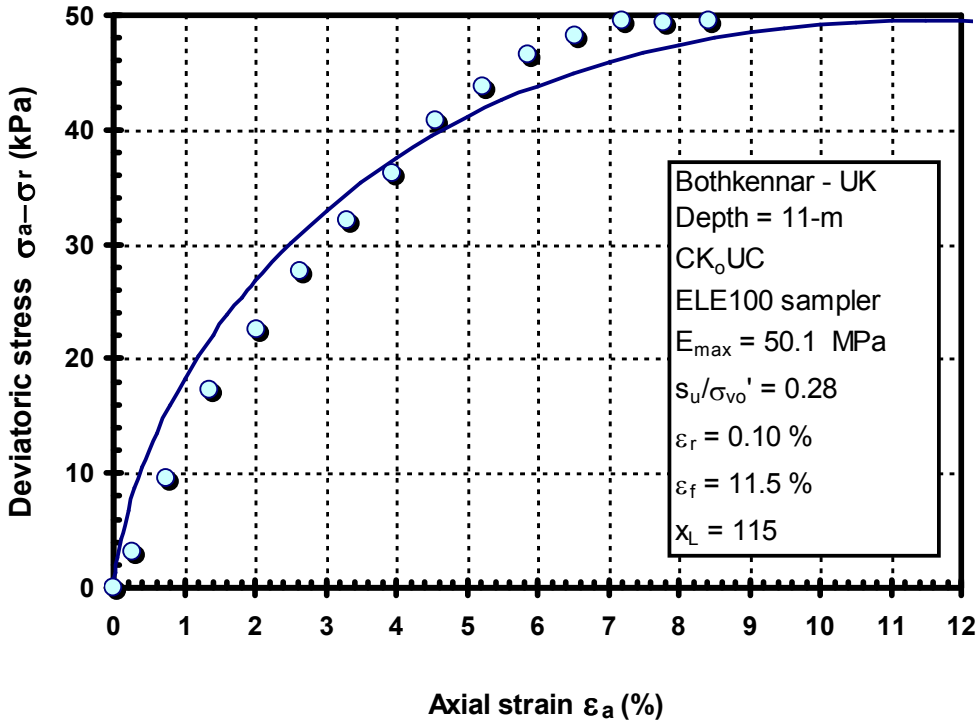


**Figure B-26.** Logarithmic function fitted to stress-strain data from UC test on an ELE100 clay sample from Bothkennar-UK, depth = 11-m (Hight et al., 1997; Tanaka, 2000)

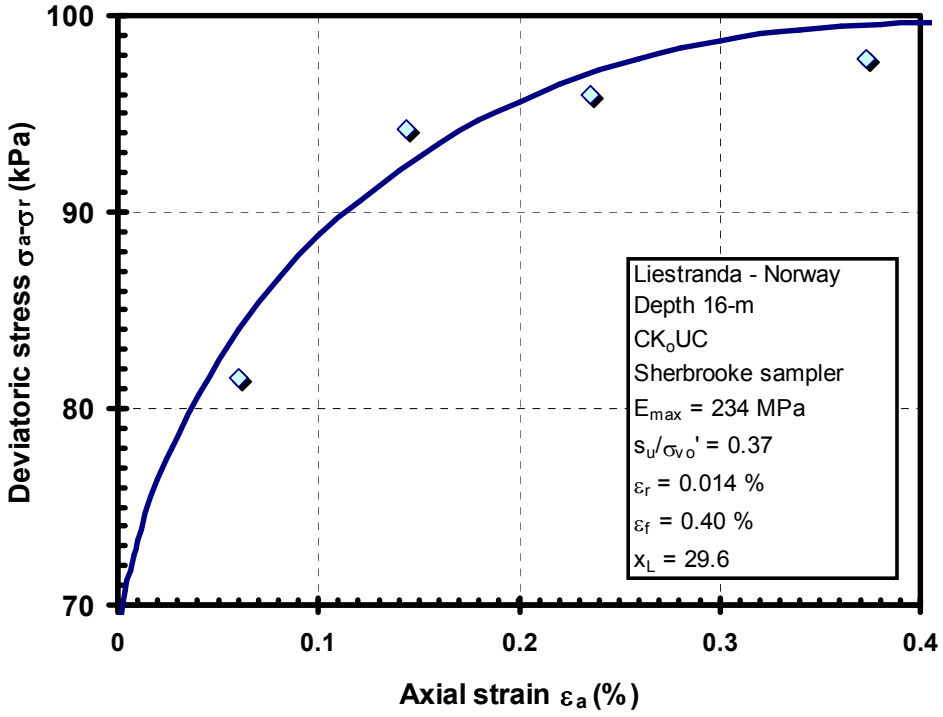


**Figure B-27.** Logarithmic function fitted to stress-strain data from $CK_oUC$ test on a Sherbrooke clay sample from Liestranda-Norway, depth = 16-m (Lunne and Lacasse, 1999; Tanaka, 2000)

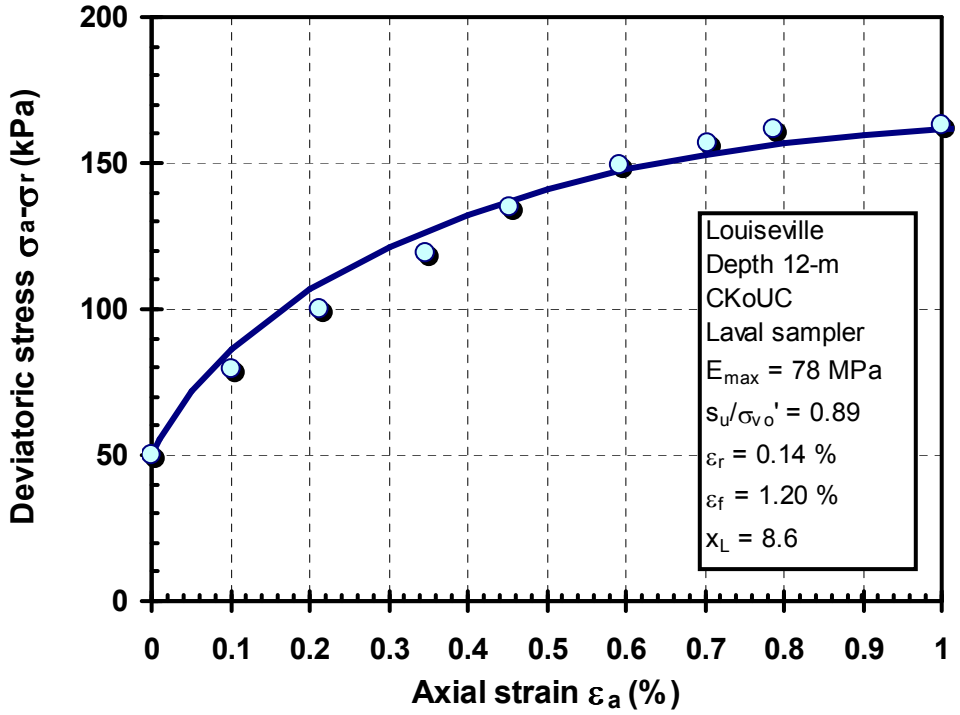


**Figure B-28.** Logarithmic function fitted to stress-strain data from $CK_oUC$ test on a Sherbrooke clay sample from Louisville-Canada, depth = 12-m (Tanaka et al., 2001)

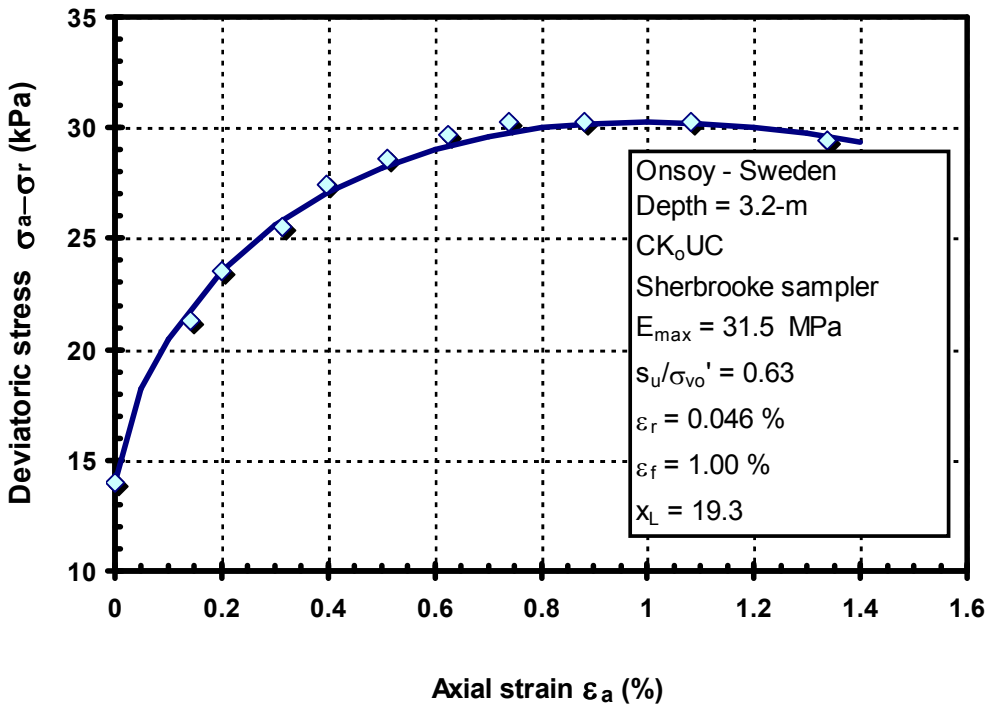


**Figure B-29.** Logarithmic function fitted to stress-strain data from $CK_oUC$ test on a Sherbrooke clay sample from Onsoy, depth = 3.2-m (Lacasse et al., 1985; Gillespie et al., 1985)

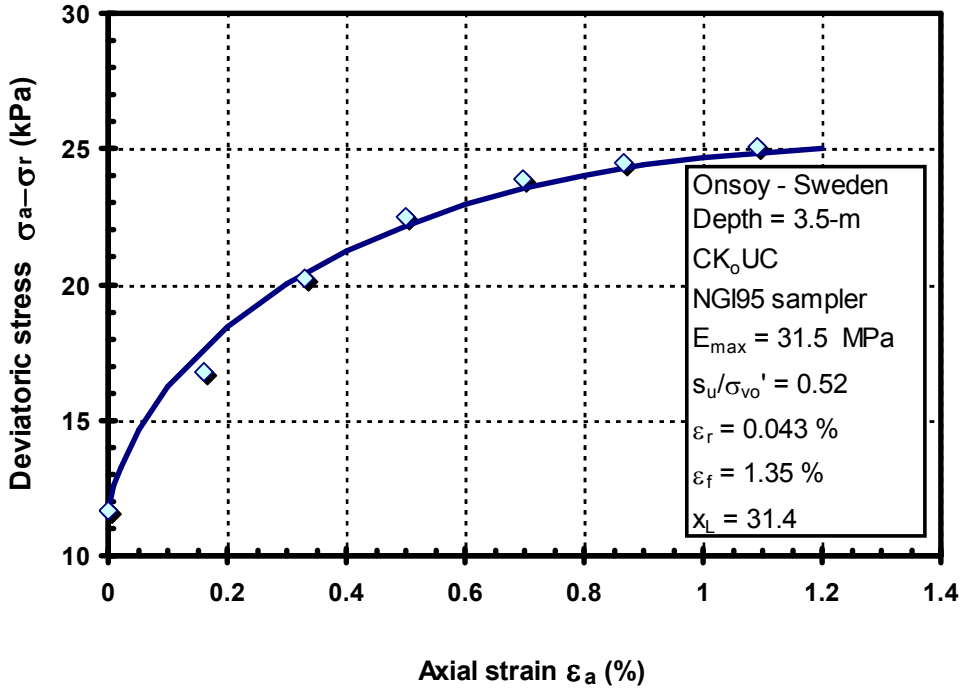


**Figure B-30.** Logarithmic function fitted to stress-strain data from $CK_oUC$ test on a piston clay sample from Onsoy-Norway, depth = 3.5-m (Lacasse et al., 1985; Gillespie et al., 1985)

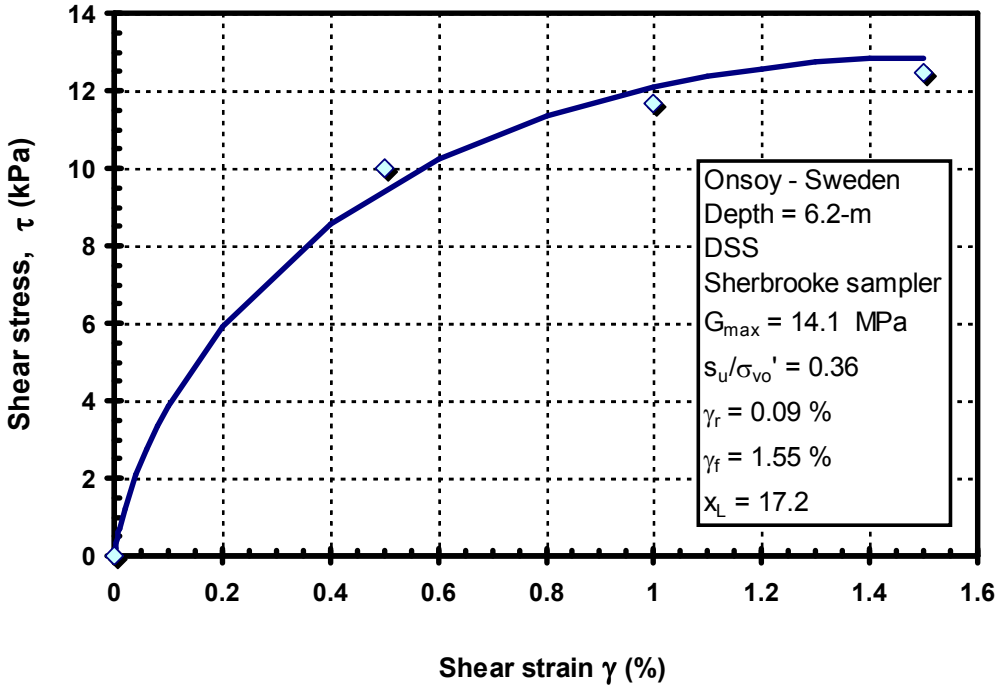


**Figure B-31.** Logarithmic function fitted to stress-strain data from DSS test on a Sherbrooke clay sample from Onsoy-Norway, depth= 6.2-m (Lacasse et al., 1985; Gillespie et al., 1985)

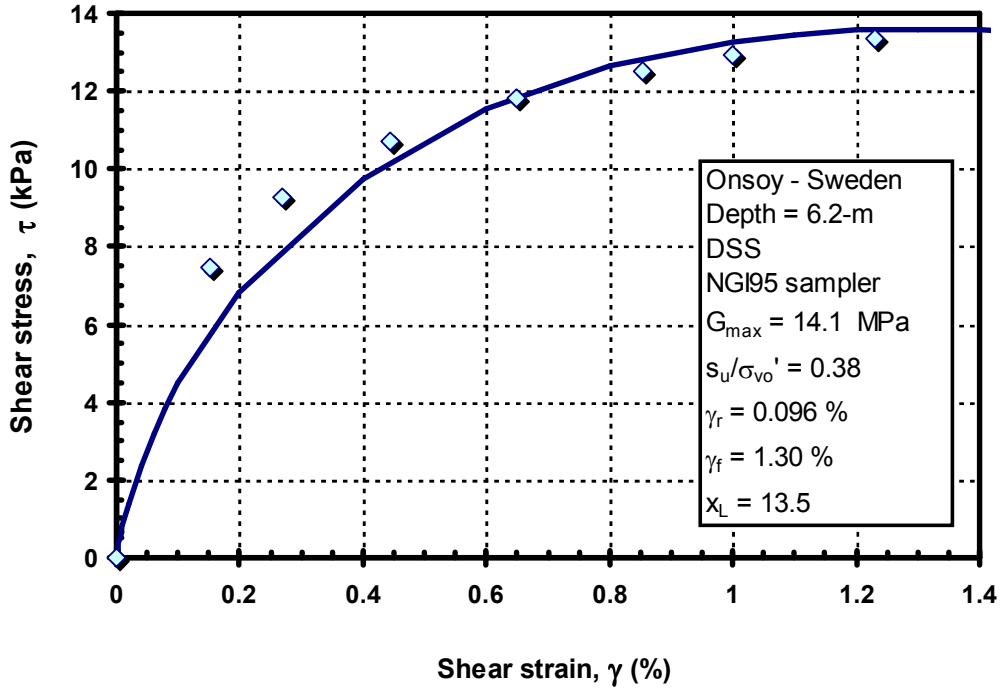


**Figure B-32.** Logarithmic function fitted to stress-strain data from DSS test on a NGI95 piston clay sample from Onsoy-Norway, depth= 6.2-m (Lacasse et al., 1985; Gillespie et al., 1985)

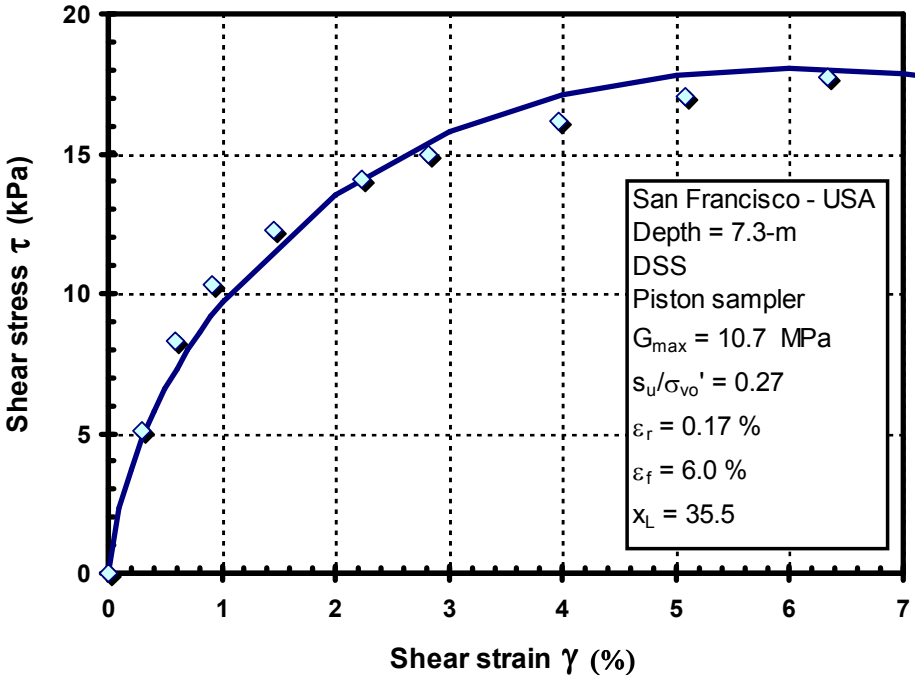


**Figure B-33.** Logarithmic function fitted to stress-strain data from DSS test on a piston clay sample from San Francisco-USA, depth= 7.3-m (Hunt et al., 2002; Pestana et al., 2002)

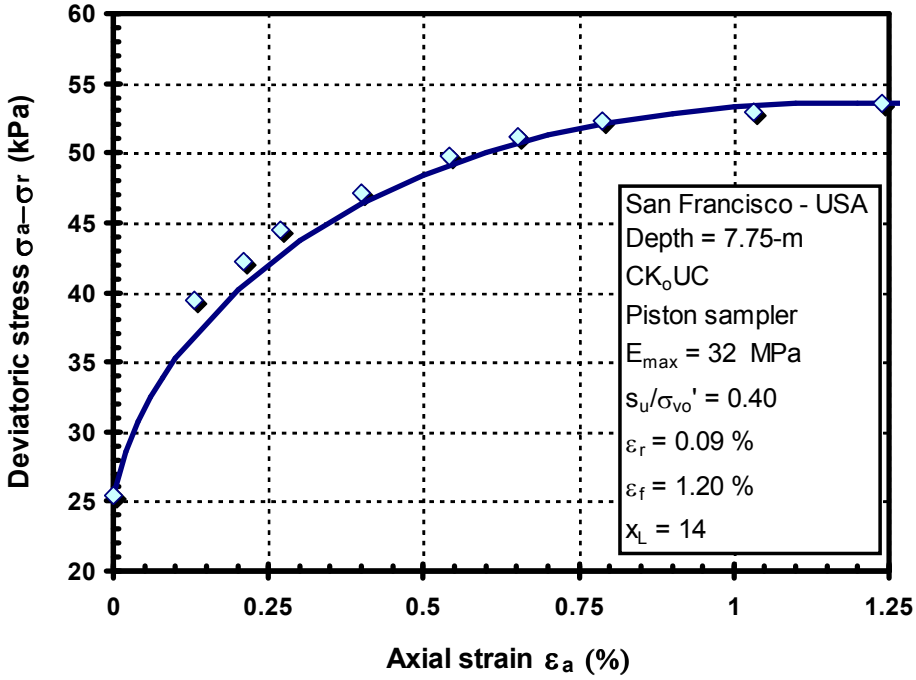


**Figure B-34.** Logarithmic function fitted to stress-strain data from $CK_oUC$ test on a piston clay sample from San Francisco-USA, depth= 7.75-m (Hunt et al., 2002; Pestana et al., 2002)

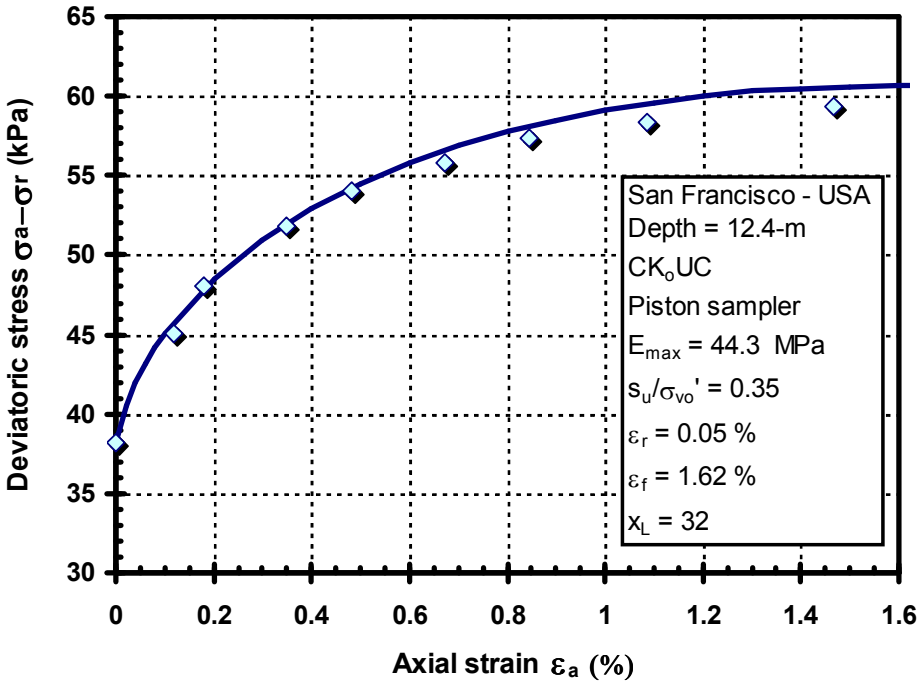


**Figure B-35.** Logarithmic function fitted to stress-strain data from $CK_oUC$ test on a piston clay sample from San Francisco-USA, depth= 12.4-m (Hunt et al., 2002; Pestana et al., 2002)

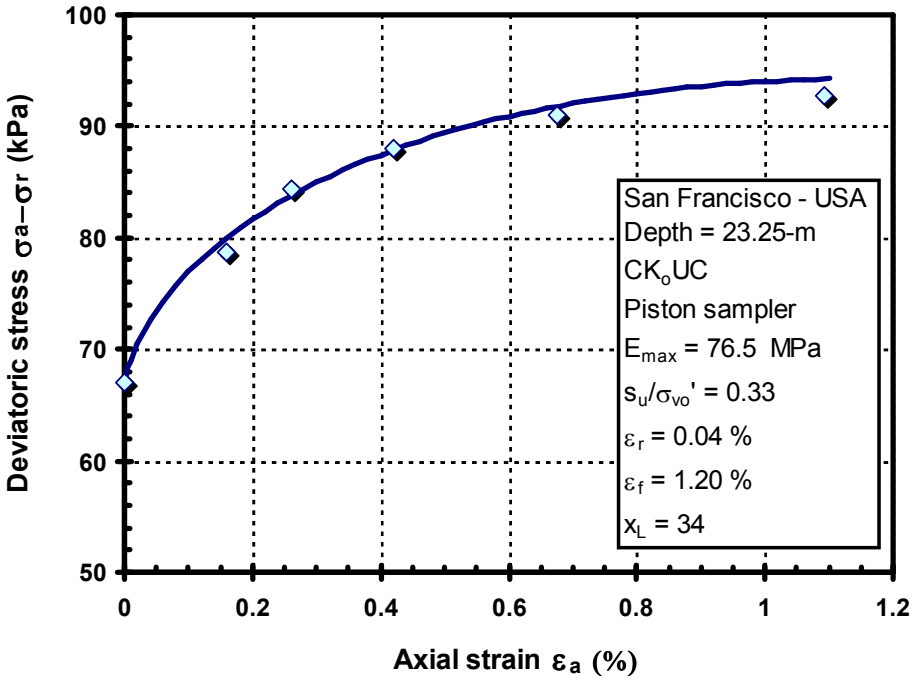


**Figure B-36.** Logarithmic function fitted to stress-strain data from $CK_oUC$ test on a piston clay sample from San Francisco-USA, depth= 23.25-m (Hunt et al., 2002; Pestana et al., 2002)

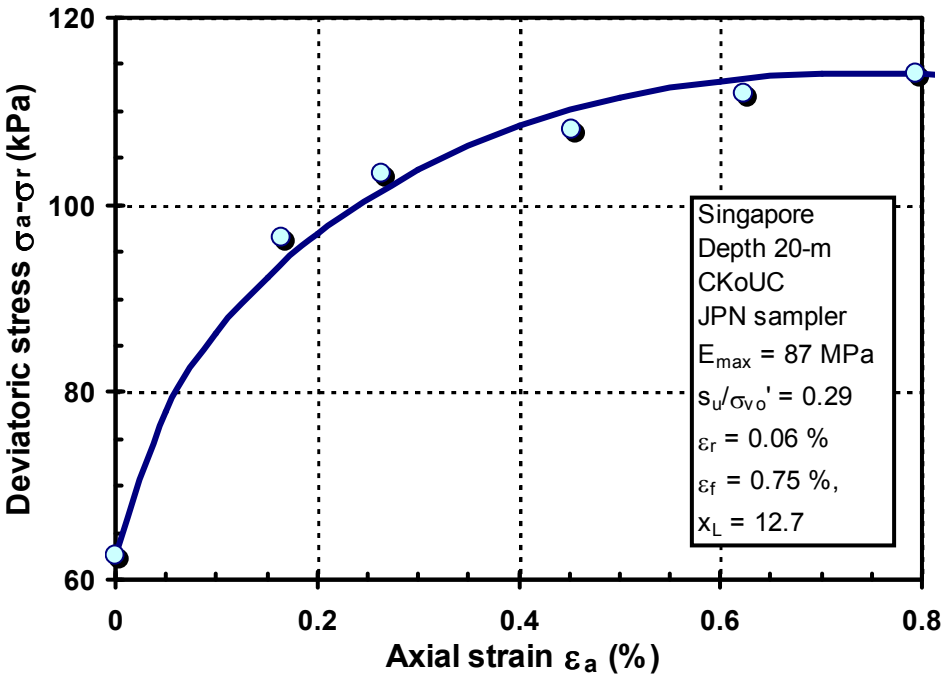


**Figure B-37.** Logarithmic function fitted to stress-strain data from $CK_oUC$ test on a JPN clay sample from Singapore, depth= 20-m (Tanaka et al., 2001, Watabe 1999)

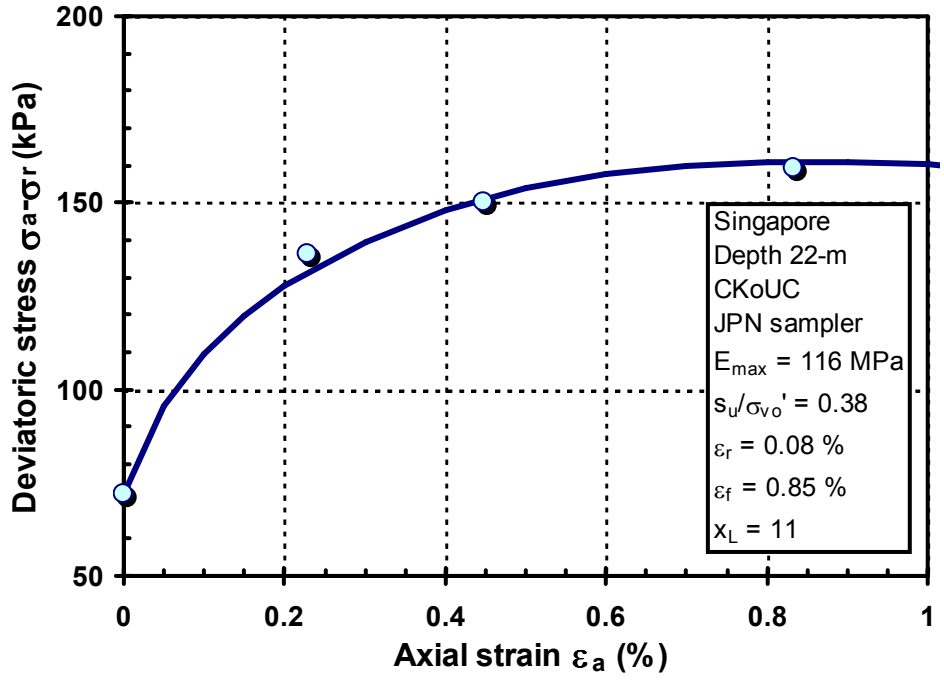


**Figure B-38.** Logarithmic function fitted to stress-strain data from $CK_oUC$ test on a JPN clay sample from Singapore, depth= 22-m (Tanaka et al., 2001, Watabe 1999)

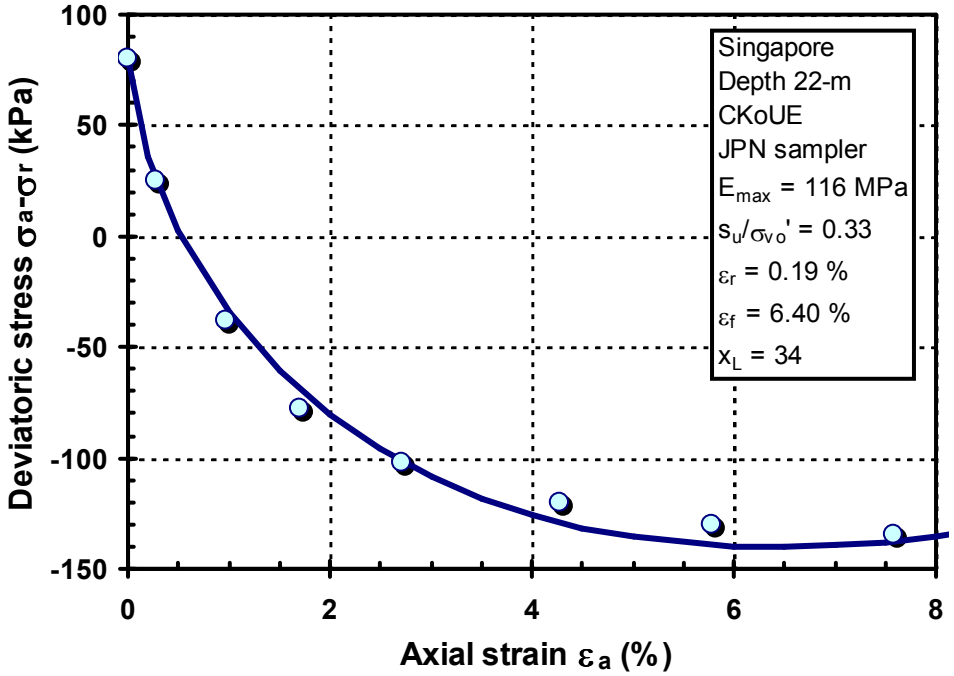


**Figure B-39.** Logarithmic function fitted to stress-strain data from $CK_oUE$ test on a JPN clay sample from Singapore, depth= 22-m (Tanaka et al., 2001, Watabe 1999)

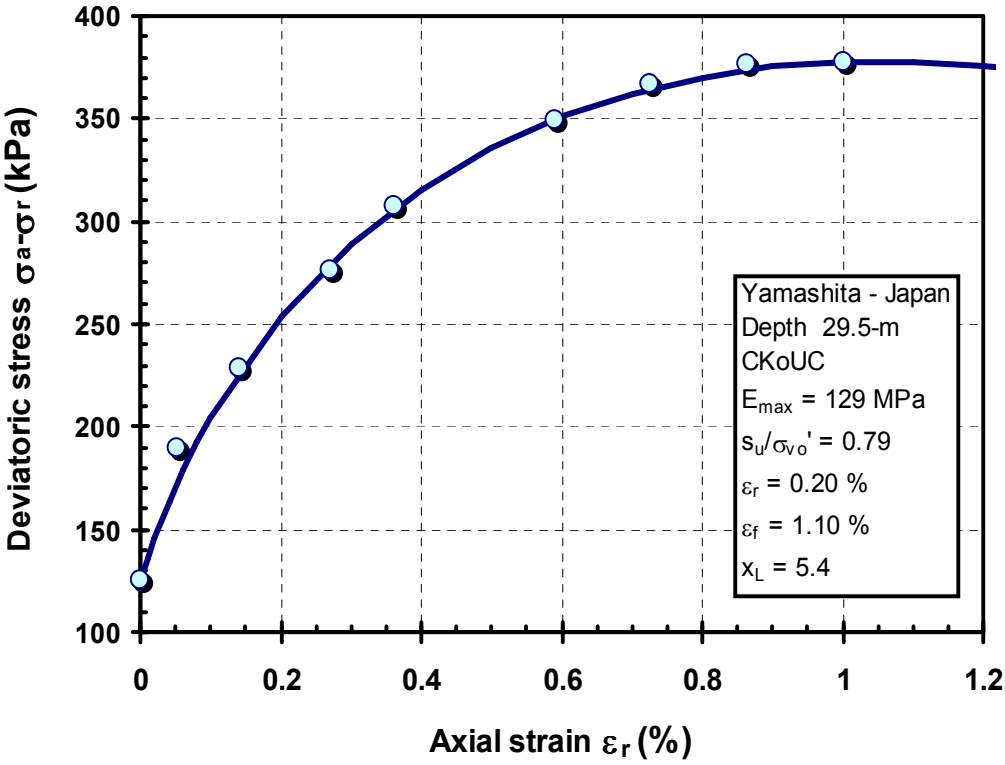


**Figure B-40.** Logarithmic function fitted to stress-strain data from $CK_oUE$ test on a clay sample from Yamashita-Japan, depth= 29.5-m (Tanaka et al., 2001, Watabe 1999)

# APPENDIX C

## SOIL PROFILES AT SHALLOW FOUNDATION CASE STUDY SITES

This appendix contains relevant soil parameters and properties at footing load test sites used for calibrating the proposed method for predicting footing stress-displacement response under vertical loading. A list of footing load test sites is provided in Table C-1. The table includes predominant soil type, groundwater table, footing dimensions, predominant drainage conditions, and relevant references for each site. Relevant soil profiles are plotted in Figures C-1 through C-14. Piezocone and seismic piezocone test results are presented for all sites except Fargo (Figure C-8). The use of the seismic piezocone for obtaining soil properties needed for shallow foundation design is explained in Appendix D.

**Table C-1.** Database of footing load tests under undrained loading conditions

| Site | Soil Type | GWT (m) | Dimensions B x L (mxm) | L/B | Test type | Drainage | Reference | Figure No. |
|---|---|---|---|---|---|---|---|---|
| Bangkok, Thailand | soft clay | 0 | 1.05 x 1.05 | 1 | Full-scale | undrained | Brand et al. (1972) Shibuya & Tamrakar (1999) | C-1 C-2 |
| | | | 0.9 x 0.9 | 1 | Full-scale | undrained | | |
| | | | 0.75 x 0.75 | 1 | Full-scale | undrained | | |
| | | | 0.675 x 0.675 | 1 | Full-scale | undrained | | |
| | | | 0.6 x 0.6 | 1 | Full-scale | undrained | | |
| Belfast, Ireland | soft clayey silt | 0 | 2 x 2 | 1 | Full-scale | undrained | Lehane (2003) | C-3 |
| Bothkennar, UK | clay | 0.2 | 2.2 x 2.2 | 1 | Full-scale | undrained | Hight et al. (1997) Jardine et al. (1995) | C-4 C-5 |
| Cowden, UK | glacial till | 0 | 0.865 x 0.865 | 1 | Plate load test | undrained | Powell & Butcher (2003) | C-6 C-7 |
| Fargo, USA (Grain Elevator) | silty clay (sand layer 4.5 to 6m) | 2.2 | 66.5 x 15.9 | 4.2 | Actual failure | undrained | Nordlund and Deere (1972) | C-8 |
| Shellhaven, UK | soft clay | 0.75 | 5 x 14 | 2.8 | Full-scale | undrained | Schnaid et al. (1993) | C-9 C-10 |
| Labenne, France | dune sand | 3 | 0.7 x 0.7 | 1 | Full-scale | drained | Jardine & Lehane (1993) Amar et al (1994) | C-11 |
| Texas A & M, USA | Eocene deltaic Sand | 4.9 | 1 x 1 | 1 | Full-scale | drained | Briaud and Gibbens (1999) | C-12 |
| | | | 1.5 x 1.5 | 1 | Full-scale | drained | | |
| | | | 2.5 x 2.5 | 1 | Full-scale | drained | | |
| | | | 3 x 3 | 1 | Full-scale | drained | | |
| | | | 3 x 3 | 1 | Full-scale | drained | | |
| Tornhill, Sweden | Sandy silty clay till | 0.2 | 0.5 x 0.5 | 1 | Full-scale | drained | Larsson (2001) | C-13 |
| | | | 1 x 1 | 1 | Full-scale | drained | | |
| | | | 2 x 2 | 1 | Full-scale | drained | | |
| Vagverket, Sweden | Silt | variable | 0.5 x 0.5 | 1 | Full-scale | drained | Larsson (1997) | C-14 |
| | | | 1 x 1 | 1 | Full-scale | drained | | |

GWT is measured below foundation level.

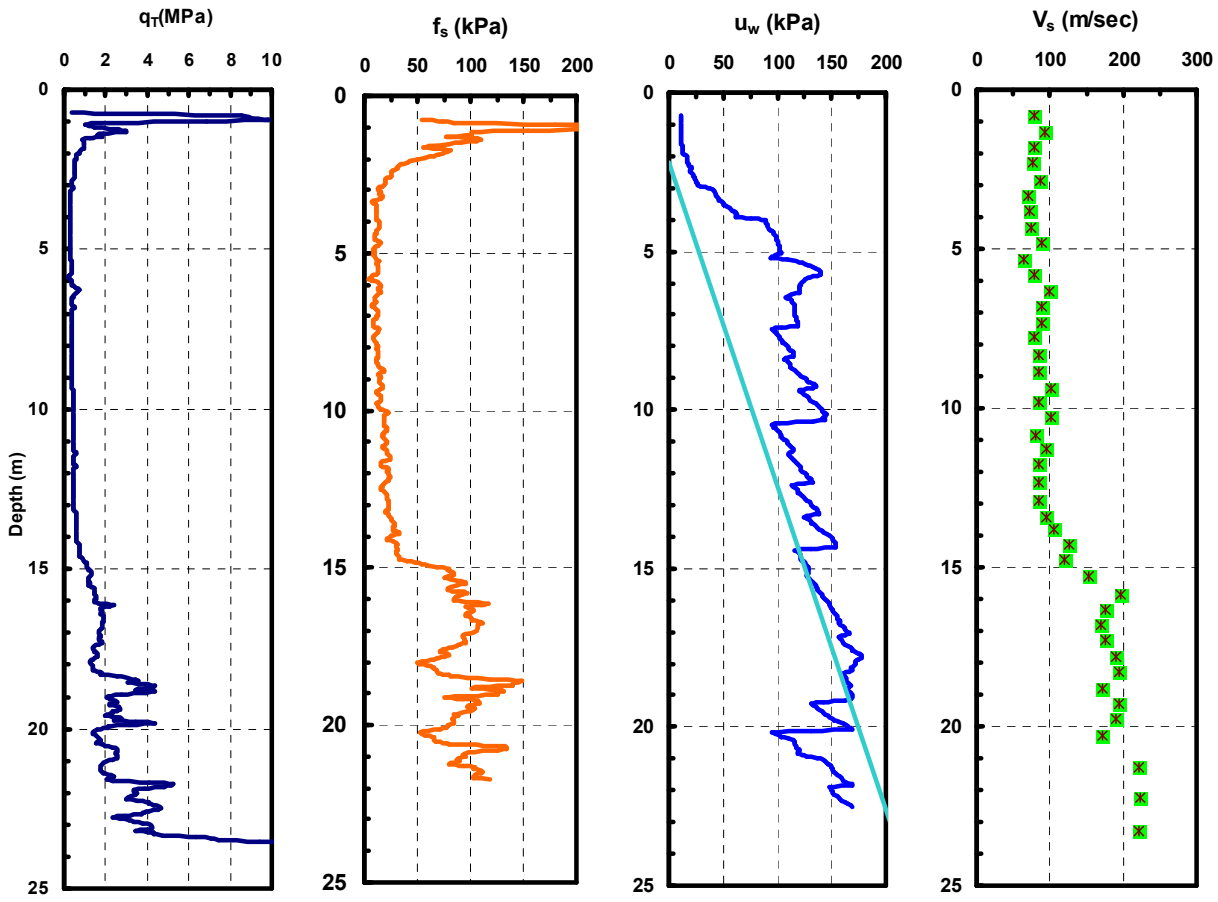


**Figure C-1.** Seismic piezocone test results at Bangkok-AIT (Shibuya and Tamrakar, 1999)

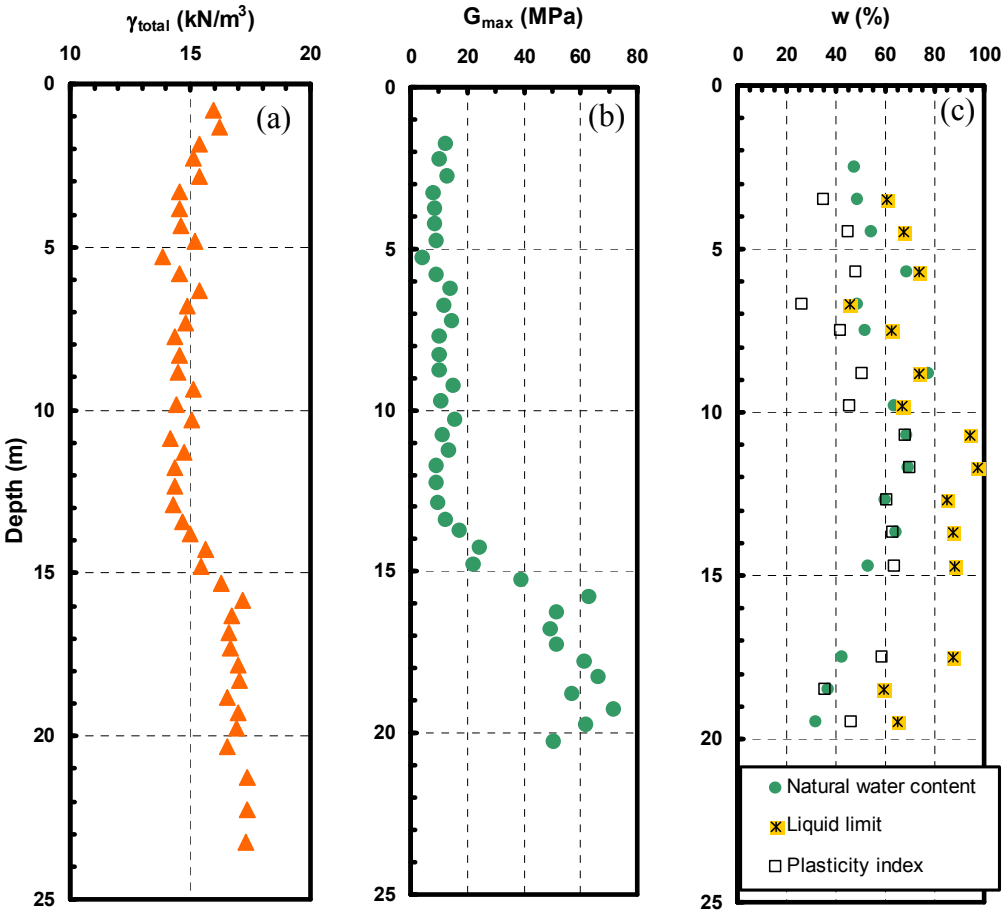


**Figure C-2.** (a) Estimated bulk unit weight $\gamma_{total}$ (using Equation D-3); (b) interpreted small strain stiffness $G_{max}$; (c) Water content and plasticity indices at Bangkok (raw data from Shibuya and Tamrakar, 1999)

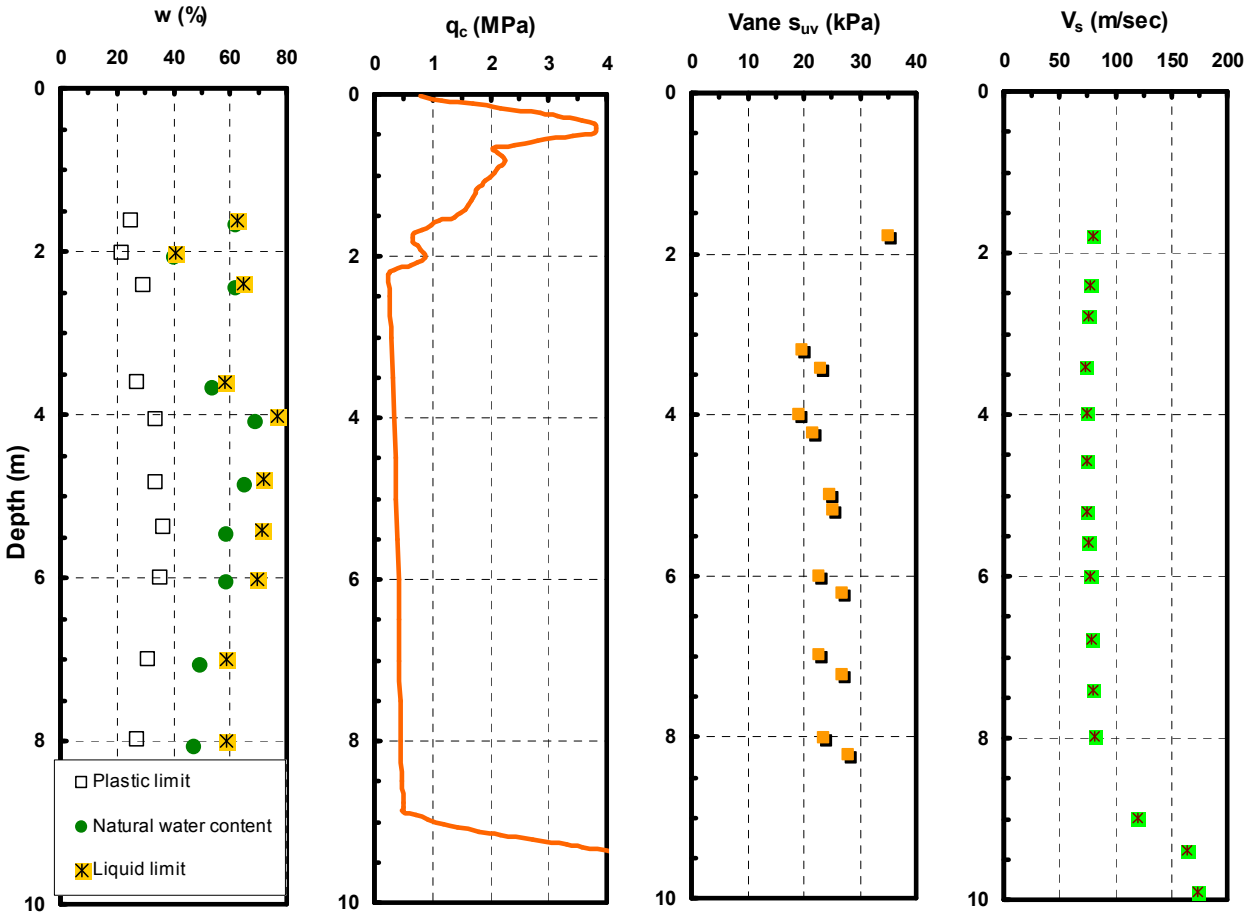


**Figure C-3.** Original test data supplied by Trinity College for the Belfast test site (Lehane, 2003)

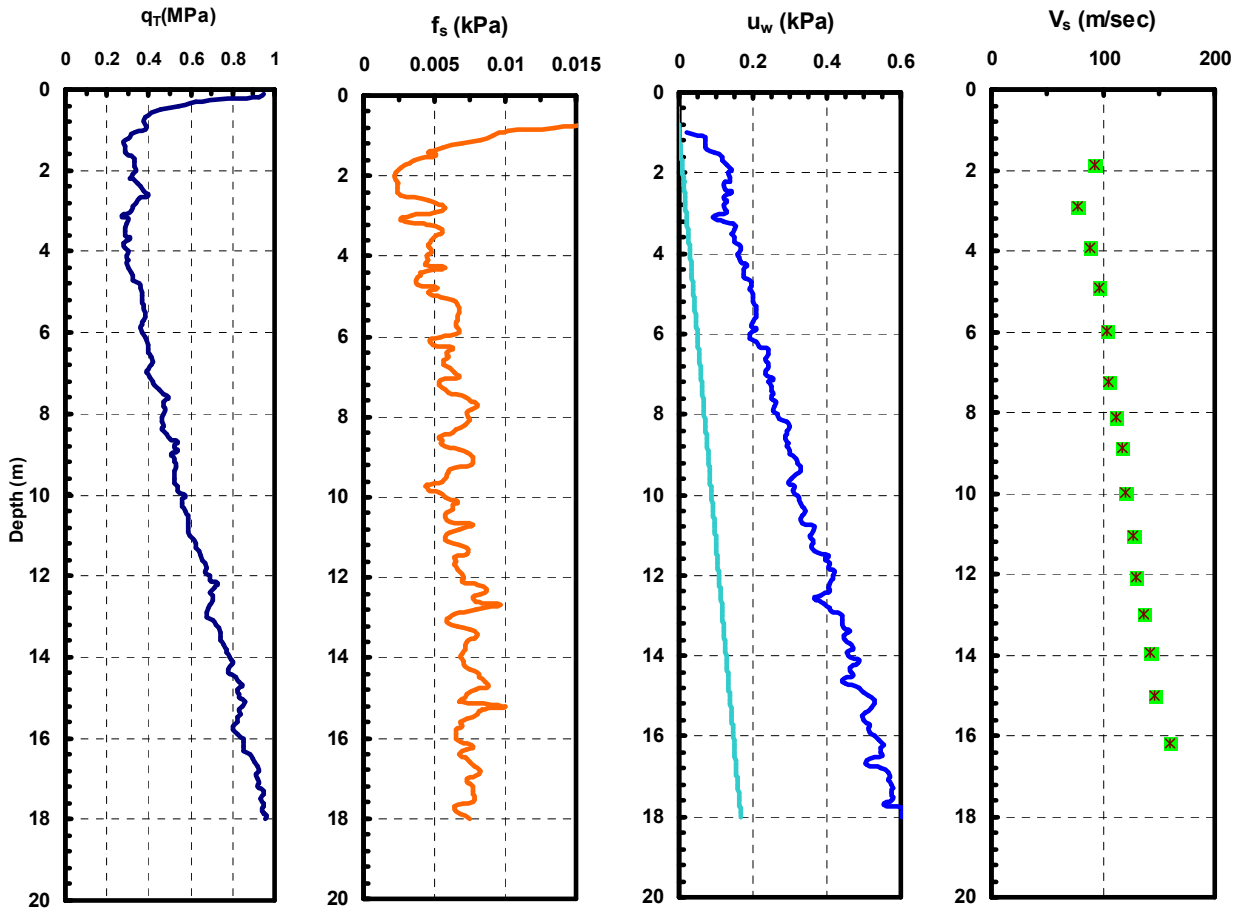


**Figure C-4.** Seismic piezocone test results at Bothkennar (Nash et al., 1992)

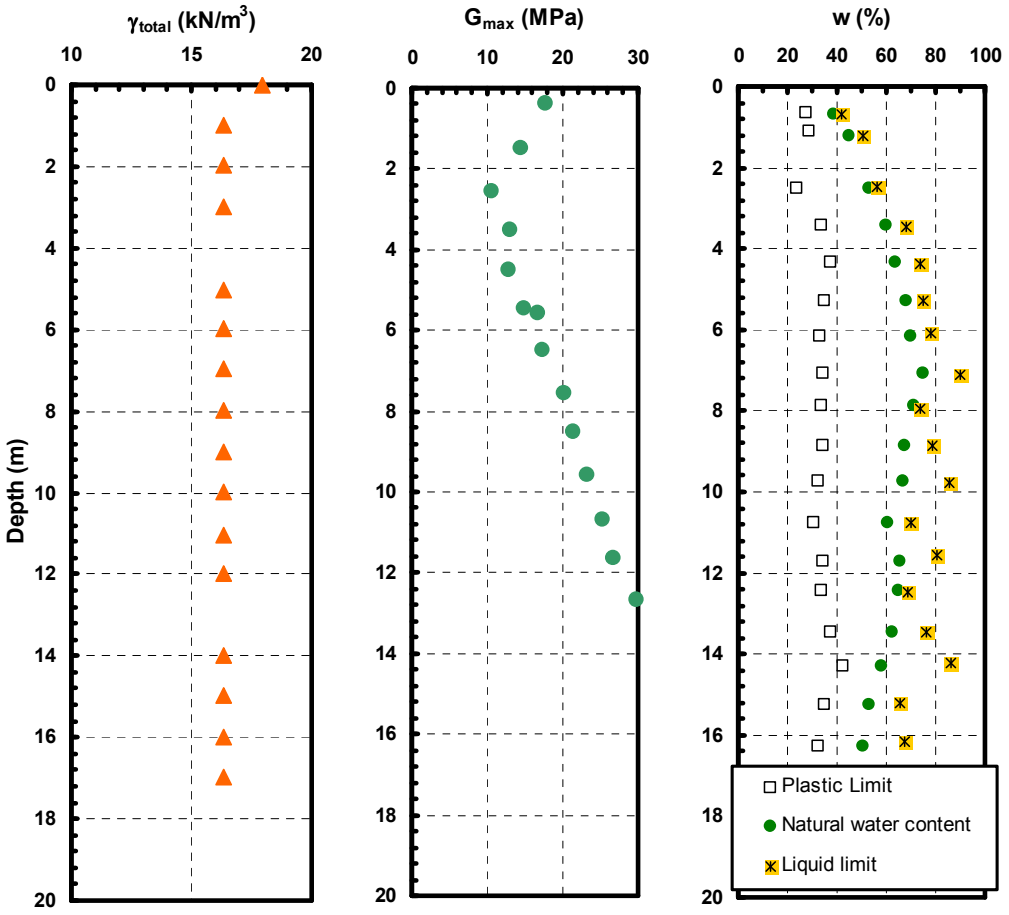


**Figure C-5.** Soil total unit weight, small-strain shear modulus $G_{max}$, and index soil properties at Bothkennar (Hight et al., 1997).

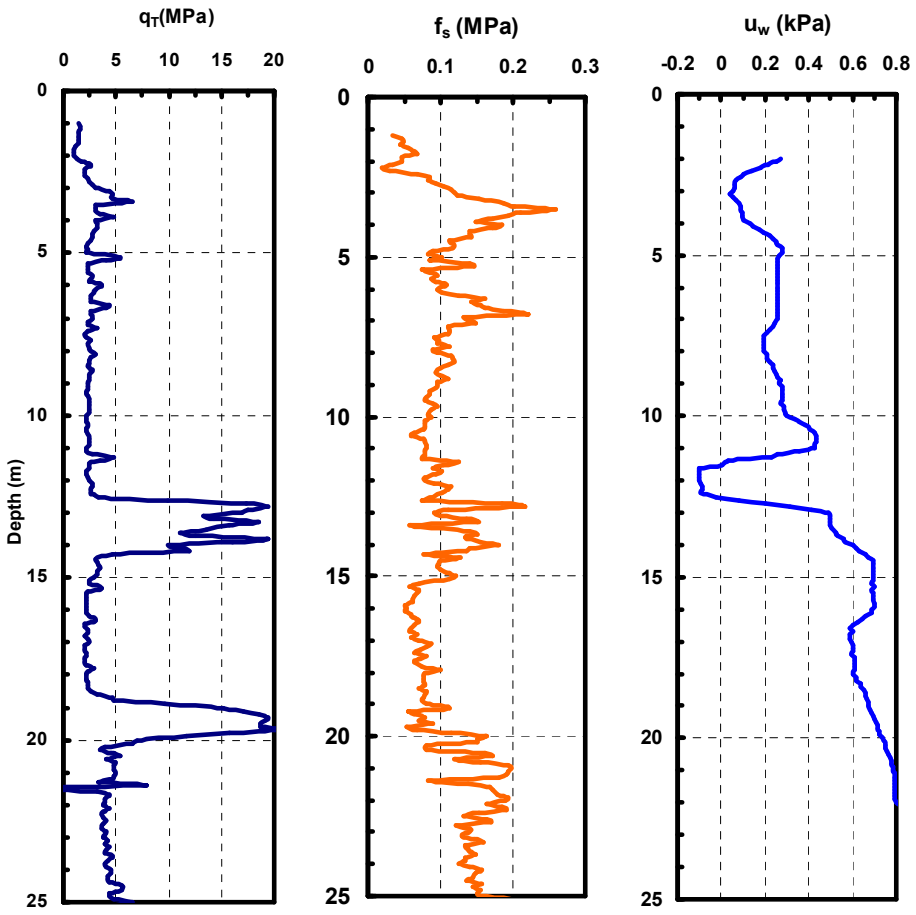


**Figure C-6.** Piezocone test results at Cowden (Powell and Butcher, 2003).

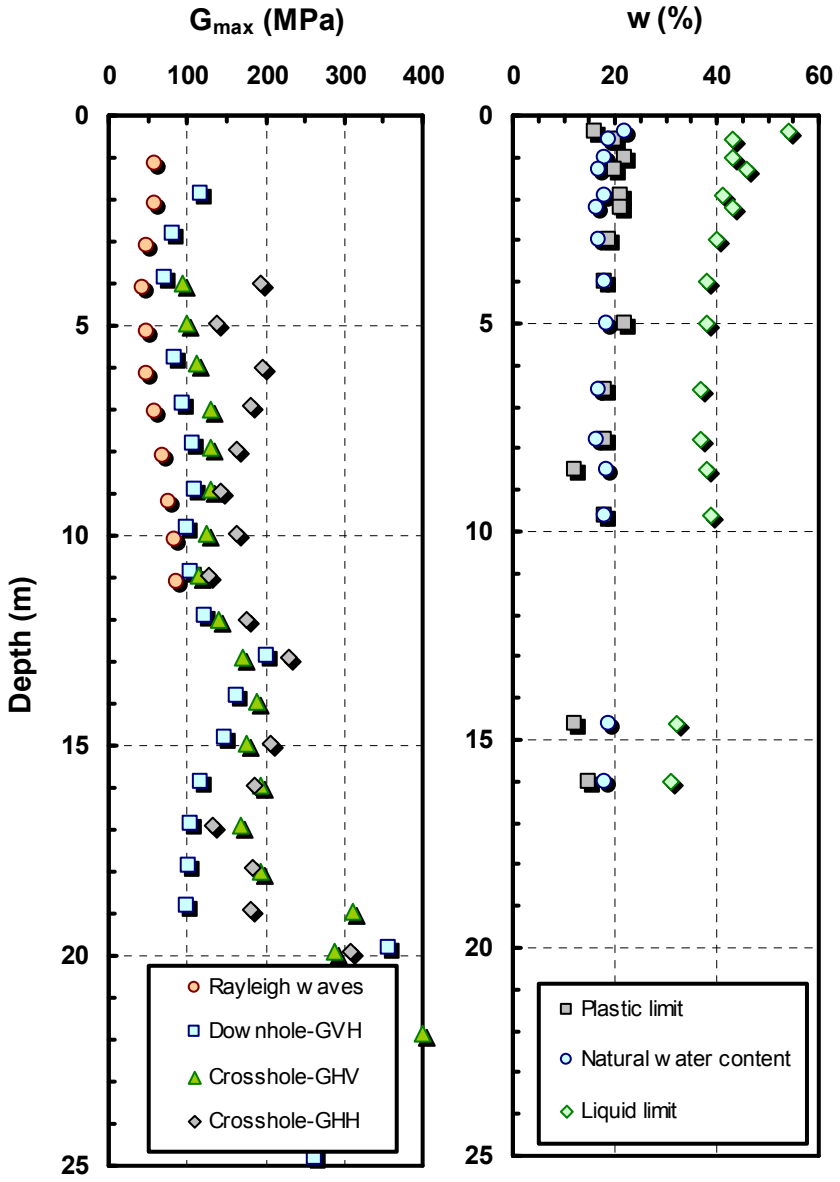


**Figure C-7.** Small-strain shear modulus $G_{max}$ and index soil properties at Cowden (Powell and Butcher, 2003)

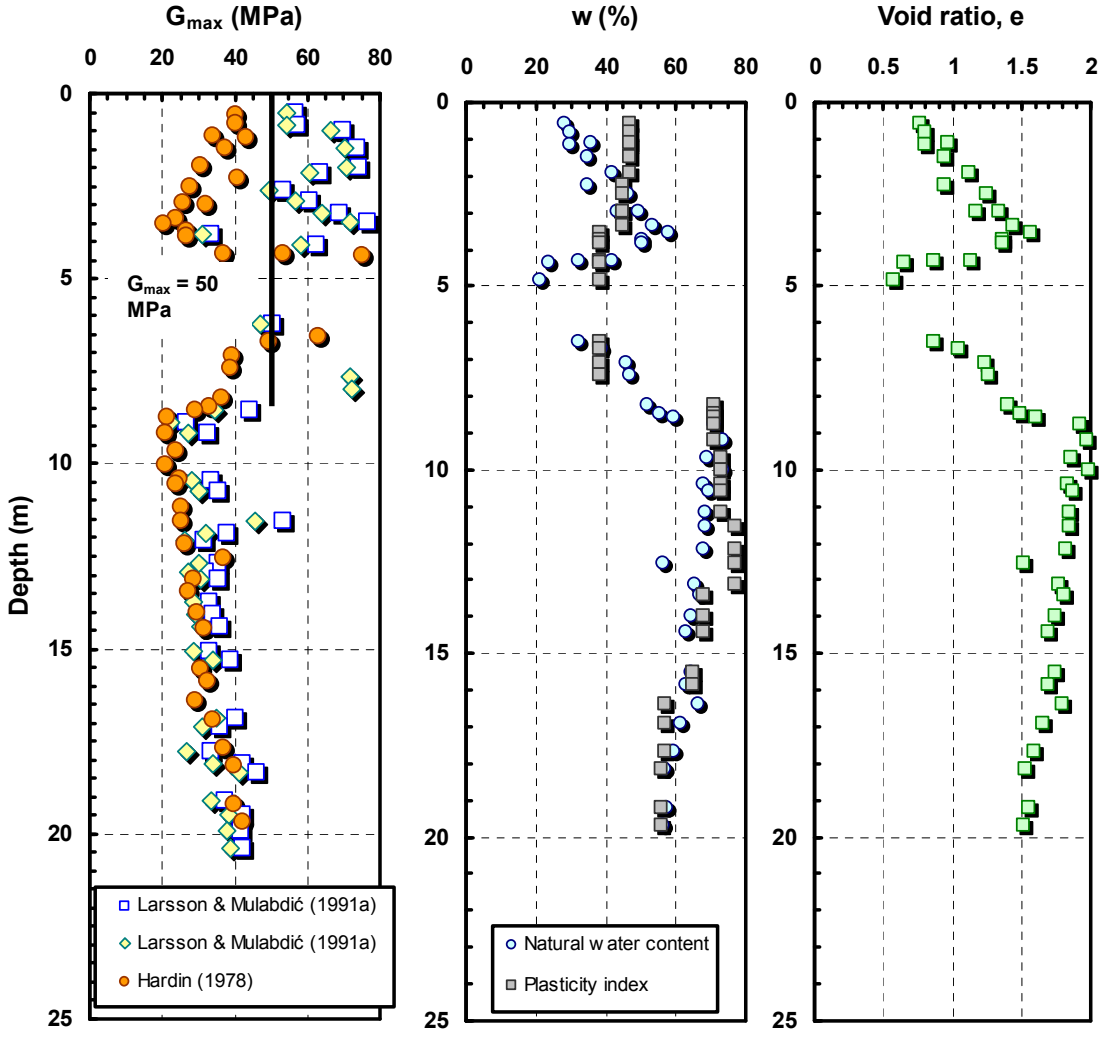


**Figure C-8.** Site specific soil properties at Fargo: a) estimated small-strain shear modulus with depth; b) Natural water content and plasticity index profiles (Nordlund and Deere, 1970); c) void ratio profile (Nordlund and Deere, 1970)

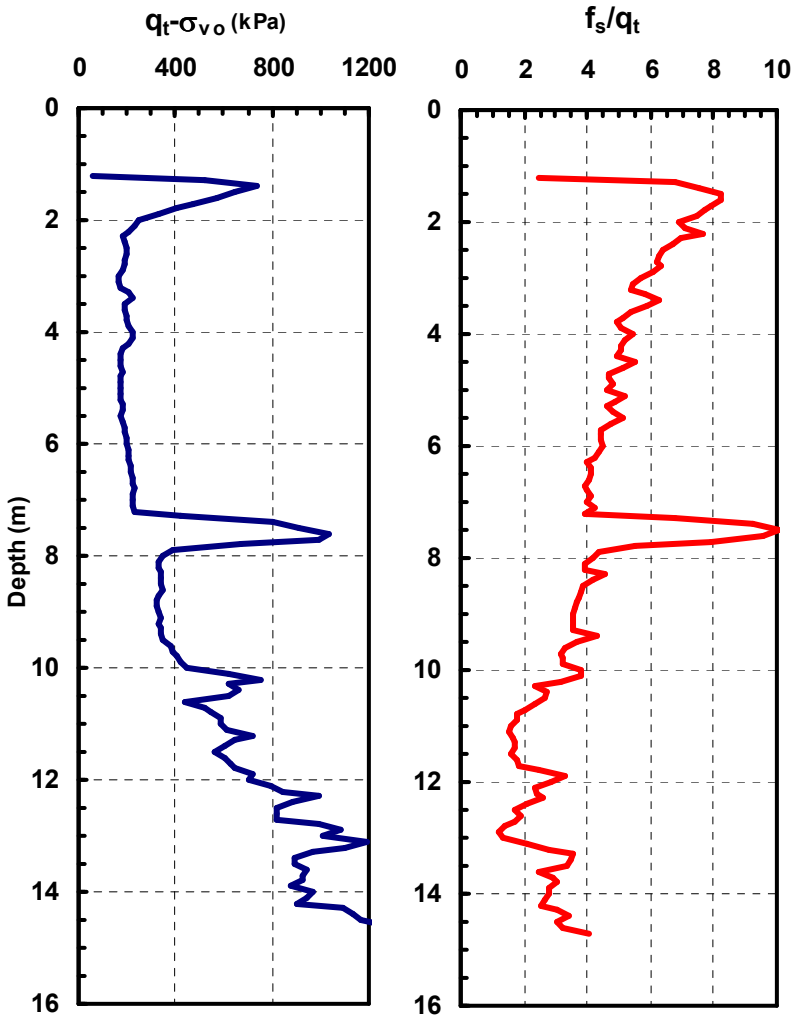


**Figure C-9.** Cone penetration data at Shellhaven site (Schnaid, et al. 1993)

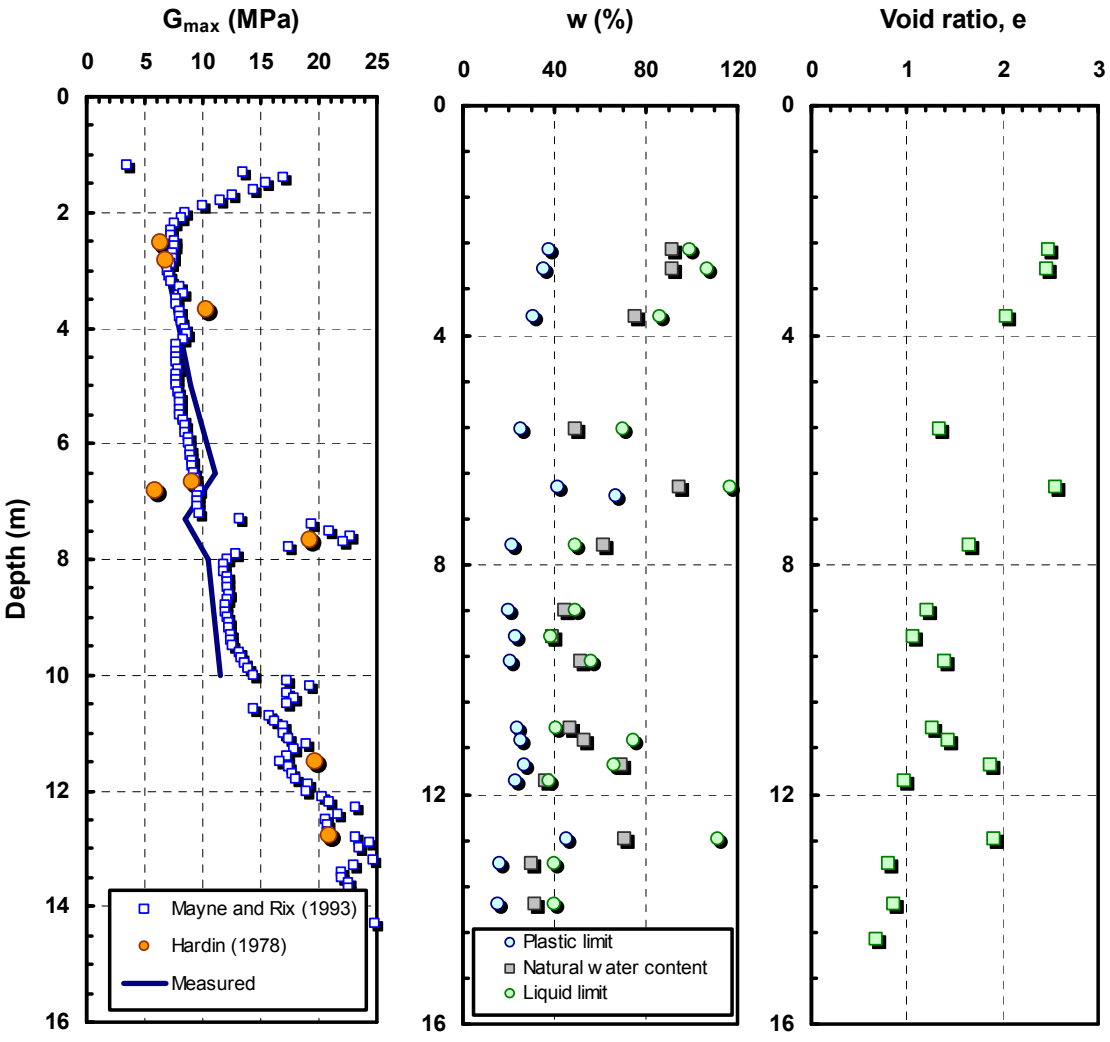


**Figure C-10.** Site specific soil properties at Shellhaven: a) small-strain shear modulus with depth; b) Natural water content, plastic and liquid limits profiles (Schnaid, et al. 1993); c) void ratio profile (Schnaid, et al. 1993)

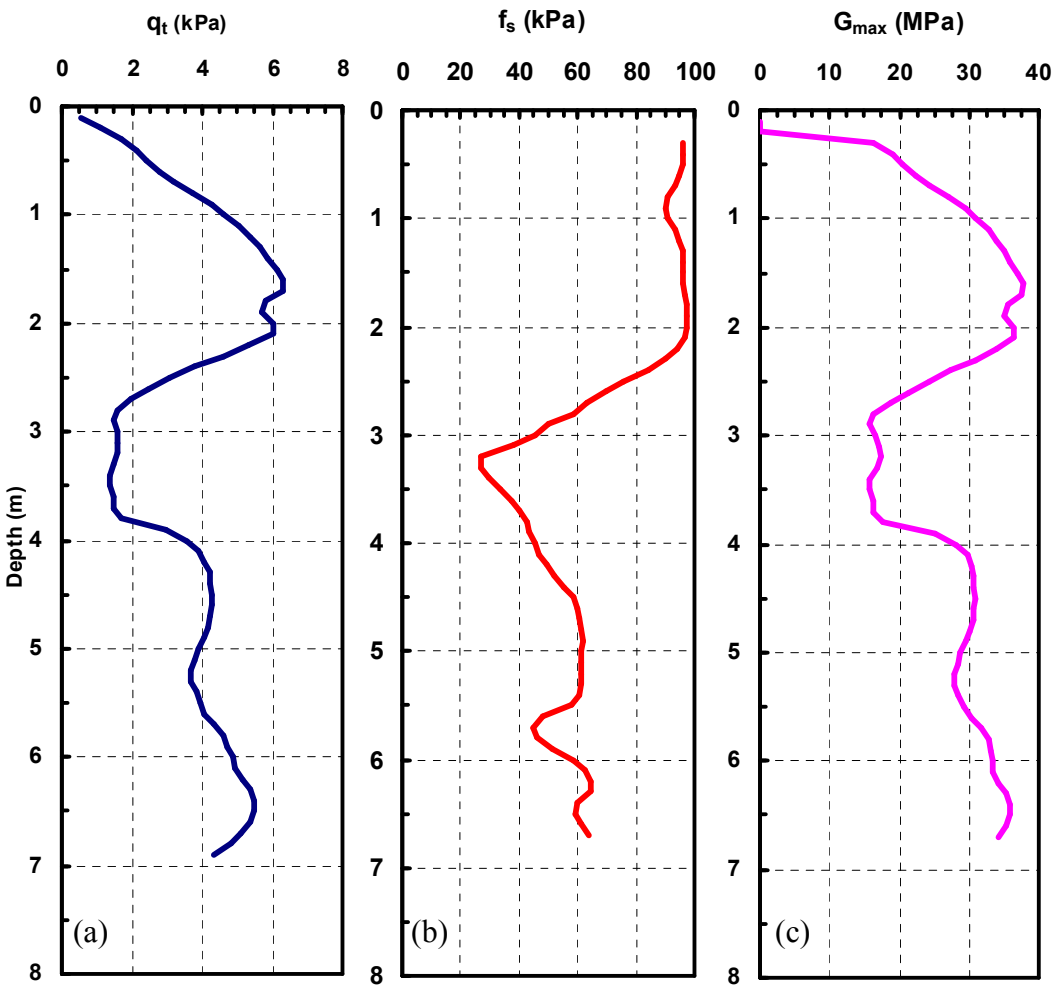


**Figure C-11.** (a) Cone tip resistance (Jardine and Lehane 1993); (b) sleeve friction (Jardine and Lehane, 1993); (c) small-strain stiffness estimated using equation by Hegazy and Mayne (1995)

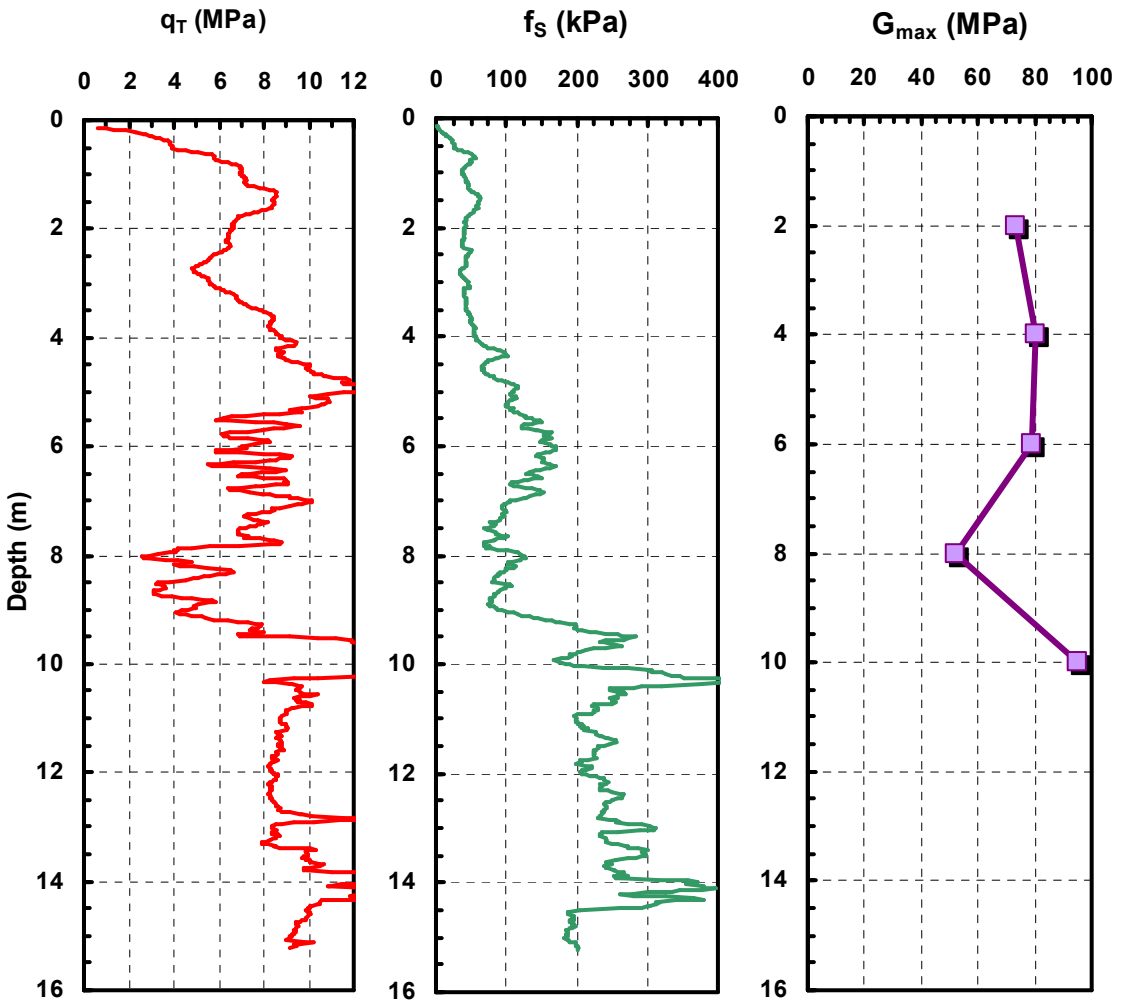


**Figure C-12.** (a) Cone tip resistance; (b) sleeve friction; (c) small-strain stiffness measured from crosshole testing (Briaud and Gibbens, 1994)

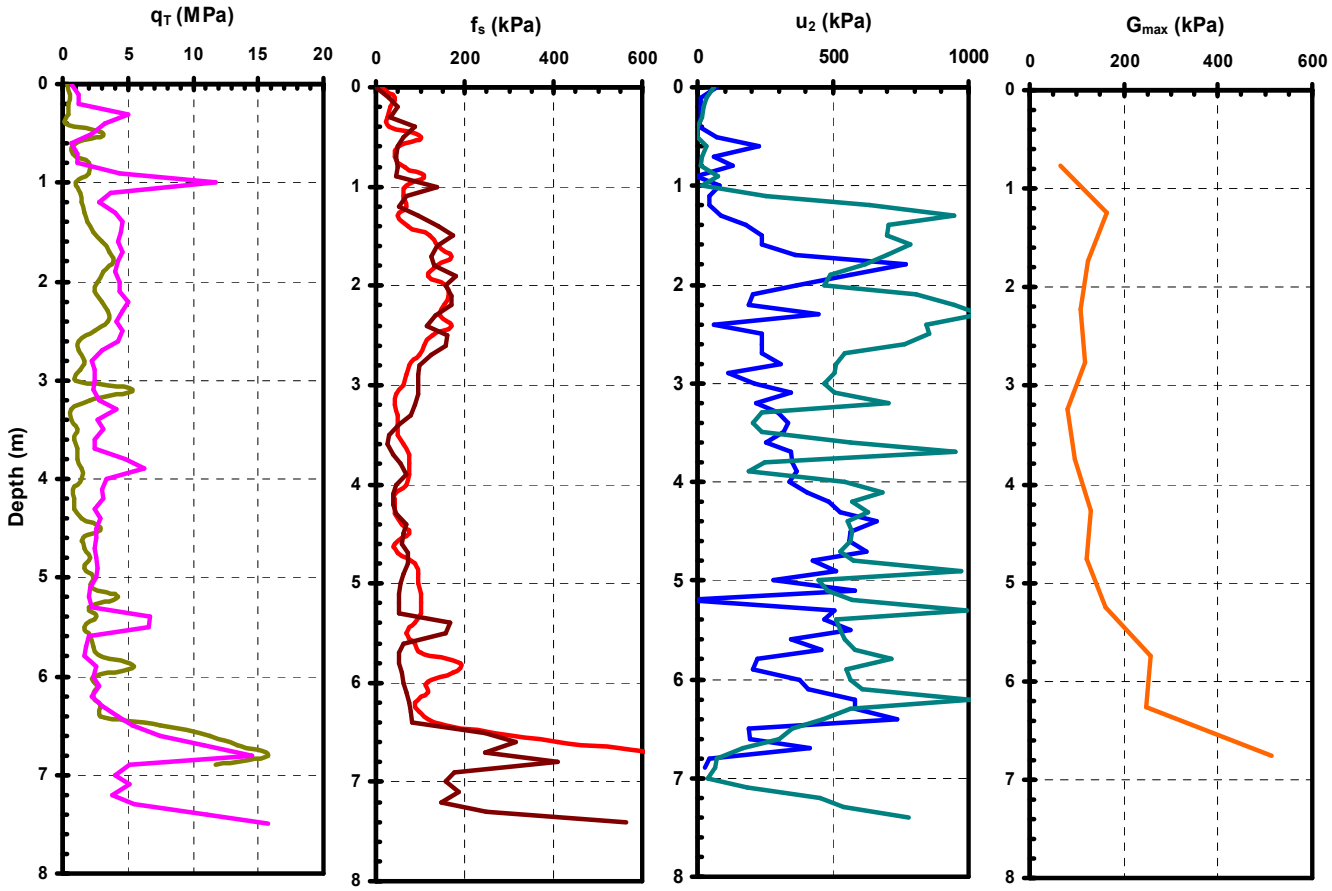


**Figure C-13.** Seismic piezocone data at Tornhill, Sweden site (Larsson, 2001)

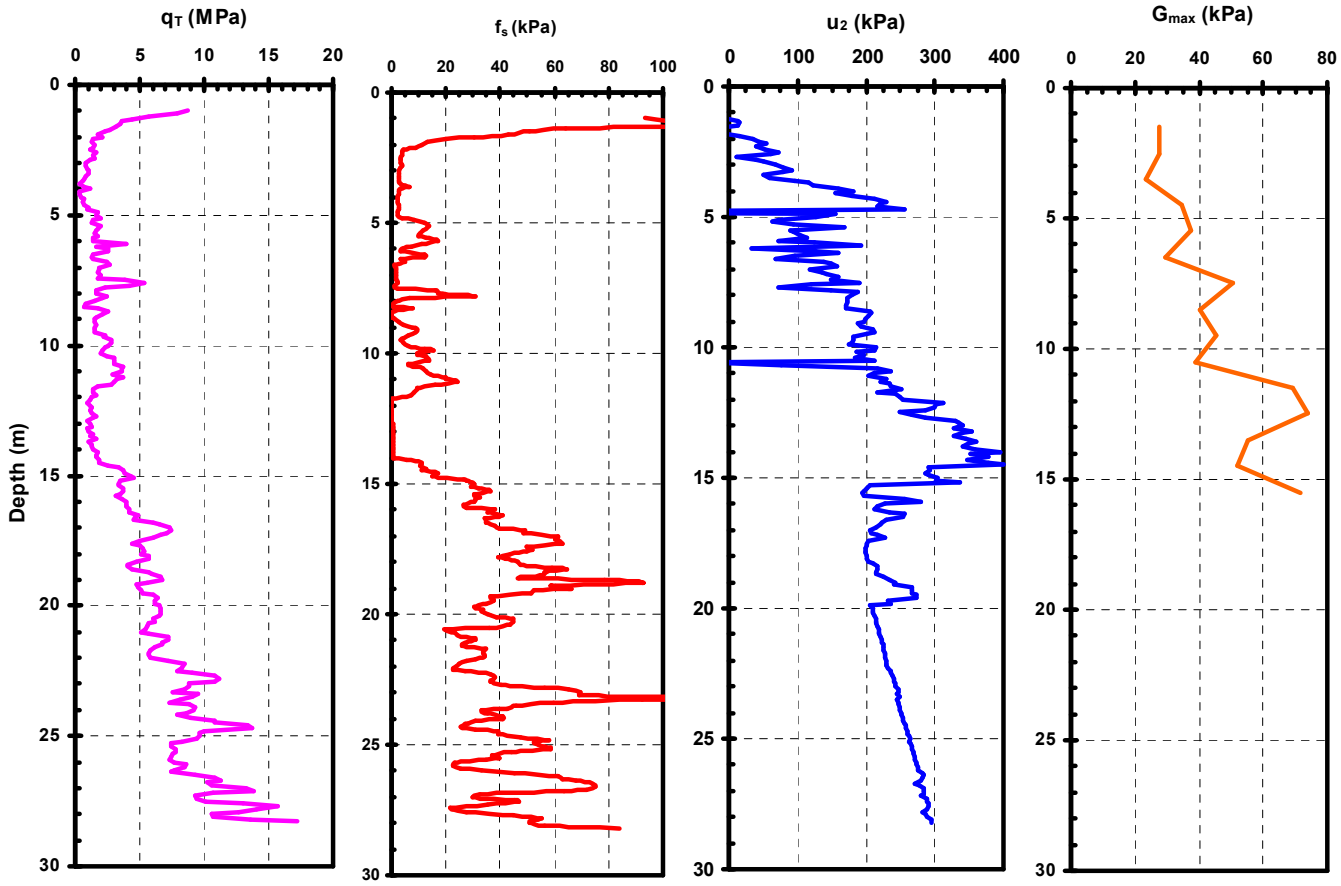


**Figure C-14.** Seismic piezocone data at Vagverket, Sweden site (Larsson, 1997)

# APPENDIX D

## EVALUATION OF SOIL PARAMETERS FROM SEISMIC PIEZOCONE TEST DATA FOR SHALLOW FOUNDATION ANALYSIS

A proper selection of the input soil parameters is a pre-requisite for any reliable analysis of bearing capacity and displacements. The conventional way to characterize a specific site for stratigraphy and assessment of relevant soil properties is to drill borings and extract soil specimens at regular depth increments. Index tests (water content, grain size distribution, plasticity) are performed for classification and stratigraphy purposes. Engineering properties (modulus, strength) are evaluated by testing soil specimens under various boundary and loading conditions (triaxial tests, direct simple shear, torsional shear, consolidation, resonant column).

Alternatively, soil can be characterized from in-situ tests where soil is tested in its natural environment (stress-condition, natural soil structure, chemical and thermal conditions). In-situ tests are classified into penetration and geophysical tests. Penetration tests include standard penetration test (SPT), cone penetrometer (CPT), piezocone (CPTu), flat dilatometer (DMT), field shear vane test (VST), and the pressuremeter (PMT). Geophysical tests are suitable for evaluating the small strain shear modulus $G_{max}$. Crosshole (CHT), downhole (DHT) and spectral analysis of surface waves (SASW) are examples of geophysical testing methods. Results from field penetration tests have long been successfully used to evaluate the shear strength of soils, corresponding to failure strains. Geophysical tests are valuable in computing small-strain stiffness $G_{max}$. It is

therefore significantly useful to collect both small- and high-strain data from a single sounding (i.e., seismic cone; seismic dilatometer) as these represent opposite ends of the stress-strain-strength curve. The seismic piezocone test (SCPTu) with dissipation phases collects data ($q_t$, $f_s$, $u_b$, $t_{50}$, $V_s$) that relates to several aspects of soil behaviour, which are discussed in this chapter.

## D.1 Seismic Piezocone Test

The seismic piezocone test is a hybrid between the piezocone and seismic downhole tests. A seismic receiver is added to the piezocone. The test is conducted as a regular piezocone test with tip, sleeve friction, and pore pressure readings taken every 2 cm. The probe is stopped at given intervals (typically every 1 meter) to add a new rod, at which time; it is convenient to measure the shear wave velocity in a downhole manner. The SCPTu is advanced into the ground at a constant rate of 20-mm/sec and measurements of cone tip resistance $q_c$, sleeve friction $f_s$, and pore water pressure at the shoulder $u_2$ are recorded with depth. Tip resistance is corrected for the porewater effects at the back of the cone tip (Lunne et al, 1997) and designated as $q_T$.

The piezocone provides continuous readings making it very efficient in determining soil strata, boundaries, and the presence of any seams, as well as the determination of strength, stiffness, stress state, and flow characteristics. Piezocone data can be used for soil classification using a number of different methods (e.g. Robertson et al., 1986; Senneset et al., 1989; Olsen & Malone, 1988; and Robertson, 1990). Parameters

evaluated from the piezocone include clay stress history (Chen and Mayne, 1994), clay unit weight (Larsson and Mulabdic, 1993), effective friction angle of sands (Robertson and Campanella, 1983) and clays (Sennest et al., 1989). Figure D-1 (after Mayne et al., 2003) outlines the different properties deduced from the seismic piezocone in clays.

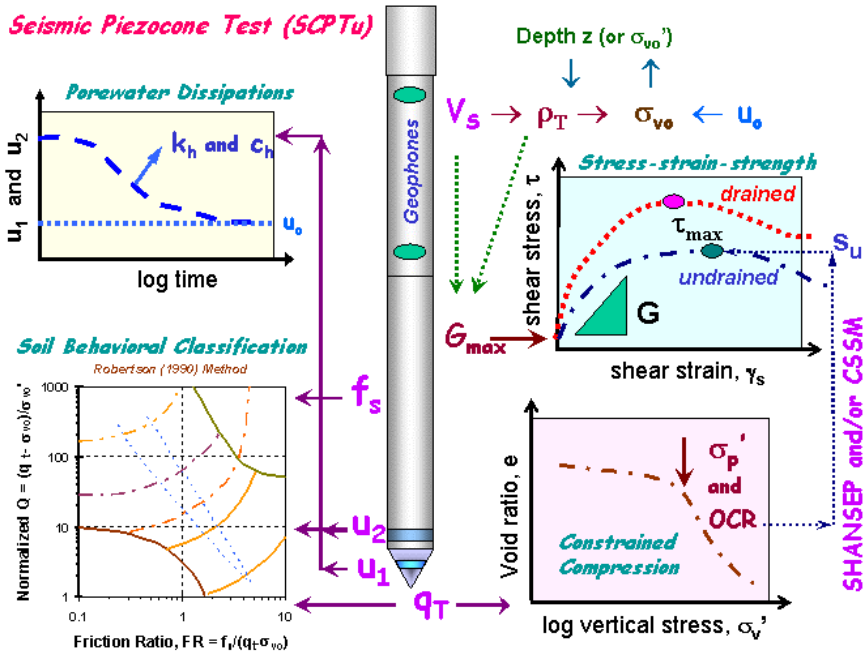


**Figure D-1.** Schematic diagram showing soil properties evaluated from the seismic piezocone in clays (after Mayne et al., 2003)

## D.2 Tip Resistance, Sleeve Friction, and Porewater Pressure Measurements

Both cone tip and sleeve resistance are used together with the porewater pressure for soil classification and evaluating soil properties. The cone tip resistance $q_c$ must be corrected for porewater pressures at the back of the cone tip (Lunne et al., 1997) yielding the total tip resistance known as $q_T$. Therefore, a standard cone penetrometer requires a porewater pressure reading at the shoulder ($u_b$ or $u_2$). For sands, the porewater pressure is very close to hydrostatic making $q_c \sim q_T$. In contrast, high excess porewater pressures are

generated in soft to stiff intact clays when the cone penetrometer is pushed. This makes porewater pressure measurements paramount in clayey soils because $q_T$ is appreciably larger than $q_c$. In fissured and highly overconsolidated clays, the porewater pressure $u_2$ can be negative or nil making the correction small or unnecessary. Results from five seismic piezocone soundings at the Amherst national test site are presented in Figure D-2. The Amherst test site consists of a 24-m thick deposit of soft lightly-overconsolidated lacustrine varved clay overlain by a 3-m desiccated crustal layer and 1-m thick clay fill (Lutenegger, et al. 2000; DeGroot and Lutenegger, 2002). Variability in the upper clay fill and crust are quite evident, while uniformity in the lower soft clay is seen. Sounding B shows dissipations in the porewater channel at the 1-m rod breaks.

The maximum shear modulus is a fundamental soil property and measured either by laboratory or field tests. Results based on field testing are superior to laboratory values that can be affected by sample disturbance during extraction, transportation, and mounting (Hicher, 1996). The maximum shear modulus is obtained from:

$$G_{\max} = \rho_T \cdot V_s^2 \quad \text{.....(D-1)}$$

where $\rho_T$ is the total mass density. The saturated soil mass density can be estimated from the shear wave velocity and depth using an empirical correlation (Mayne, 2001):

$$\rho_{sat} = 0.85 \cdot \log(V_s) - 0.16 \cdot \log(z) \quad \text{.....(D-2)}$$

where $\rho_{sat}$ is in gm/cm$^3$, $V_s$ is in m/s, and z is the depth in meters.

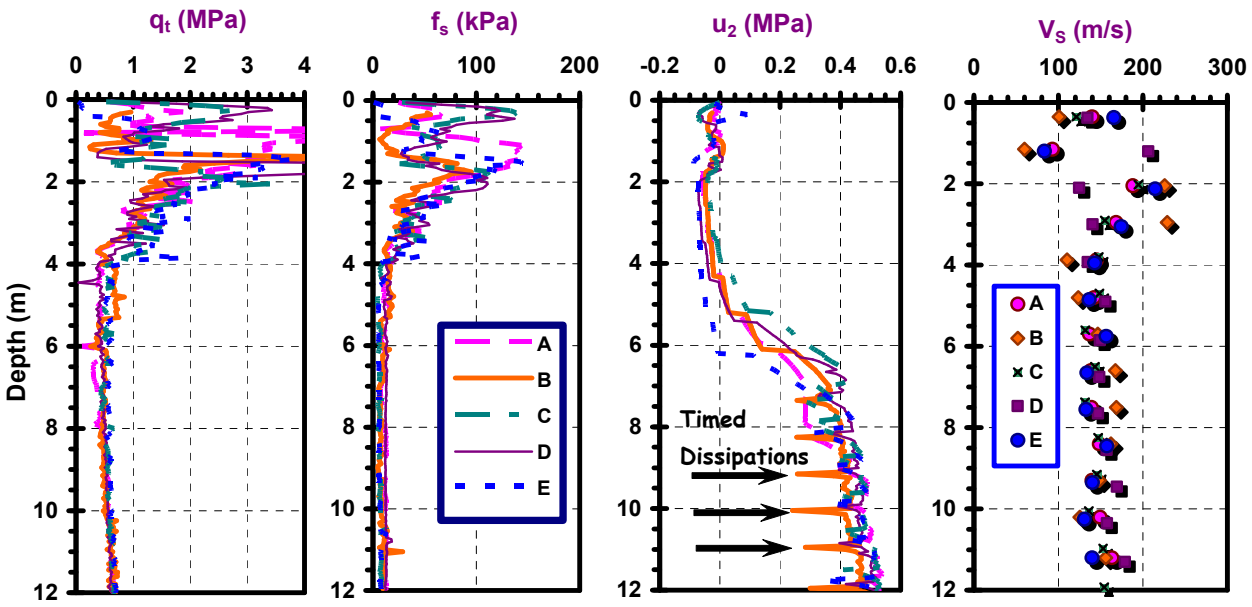


**Figure D-2.** Results of five seismic piezocone tests in varved clay at Amherst national test site (after Mayne et al., 2003)

## D.3 Soil Classification from SCPTu data

Soil classification can be judged either from soil samples extracted from borings or based indirectly on in-situ test readings (e.g. piezocone or flat plate dilatometer tests). Soil classification systems based on laboratory tests (e.g. Unified Soil Classification System, AASHTO) define soil type according to grain size distribution as well as other index properties (e.g. plasticity index). On the other hand, classifications based on in-situ tests are indicative of the soil behavior at the time of testing. The seismic piezocone provides continuous reading making it very valuable for detecting changes in soil stratigraphy and the existence of lenses and inclusions. Typically, visual inspection of the raw penetration records is sufficient for classification. In clean sands, $q_T > 4$ MPa while in soft clays $q_T <$ 1 MPa. In clean sands, no excess porewater pressure is generated during penetration,

while high excess porewater pressures are generated when penetrating low permeability soils (silts and clays). In clean sands, the friction ratio ($FR = \frac{f_s}{q_T}$) is generally small ($FR < 1\%$) while in insensitive clays ($3 < FR < 10\%$). However, in sensitive clays the friction ratio is small ($FR < 1\%$). Alternatively, soil empirical soil classification charts are available (e.g. Begemann, 1965; Douglas and Olsen 1981; Senneset et al., 1989; Robertson, 1990; Olsen and Mitchell, 1995).

## D.4 Evaluation of soil strength from piezocone test results

Soil strength can be determined in the laboratory on undisturbed soil specimens. However, a small number of these tests are typically performed because of cost and time limitations. Also, the issue of sample disturbance arises and is never impossible to avoid. In-situ tests (e.g. VST, DMT, CPTu) offer an alternative and compliment to evaluate soil strength using theoretical and/or empirical relationships, providing an immediate, continuous and economic supplement to laboratory tests.

For saturated soils, it is traditional to assume the soil behaves under either fully drained or fully undrained conditions. Drained soil strength is expressed by the effective friction angle $\phi$'. For undrained loading, no volume change occurs and strength is described by the undrained shear strength $s_u$. The undrained shear strength is not a fundamental material property but depends on several factors including the stress level, stress state, failure mode, strain rate, stress history, and soil anisotropy. The proper value of shear strength used in the analysis depends on the problem type. There are several

relationships (theoretical and/or empirical) for evaluating shear strength in different loading modes ($CK_oUC$, DSS, $CK_oUE$) from piezocone test results. The existence of several approaches to measure the same parameter leads to different interpretations that require interrelationships to tie them together. Therefore it is recommended to relate undrained strength to a more stable parameter such as the overconsolidation ratio, OCR (Mayne, 2001; Mayne et al., 2003). Hence, a stress history based analysis is pursued herein.

It has been shown both experimentally (e.g., Ladd, 1991) and theoretically (e.g., Wroth, 1984) that the normalized undrained shear strength $s_u/\sigma_{vo}'$ depends on the overconsolidation ratio OCR. Kulhawy and Mayne (1990) calibrated this method versus a huge database of laboratory tests including triaxial compression (CIUC and $CK_oUC$), triaxial extension (CIUE and $CK_oUE$), plane strain (PSC and PSE), and direct simple shear (DSS). Because Modified Cam Clay comprises an isotropic yield surface, a more rigorous solution was needed to differentiate between compression and extension loading. This led to the development of a hybrid Wroth-Prevost model, which relates the undrained shear strengths of the different shearing tests to the effective friction angle, as demonstrated in Figure D-3. The undrained shear strength measured from isotropically consolidated undrained compression test CIUC yields the highest strength. While shear strength from anisotropically consolidated undrained extension tests CKoUE represent the lower bound. The direct simple shear test DSS represents an intermediate strength suitable for analysis of slope stability, foundation bearing capacity, and excavation problems.

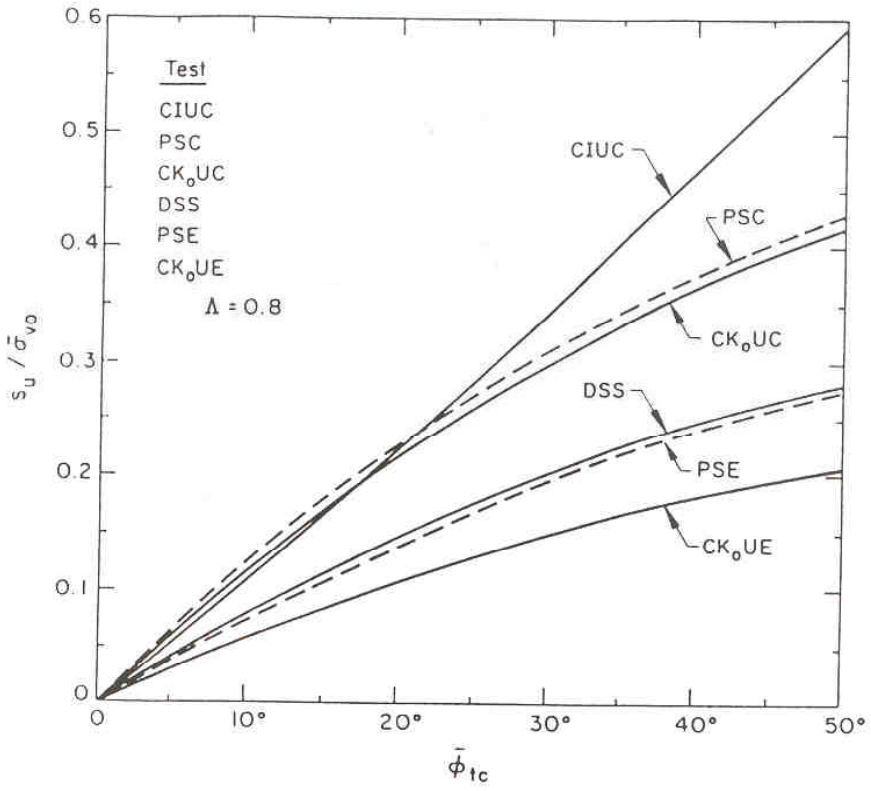


**Figure D-3.** Variation of undrained strength ratio with test type (after Kulhawy and Mayne, 1990)

Ladd et al. (1977) showed the normalized undrained strength to overburden stress $(s_u/\sigma_{vo}')_{OC}$ to increase with overconsolidation ratio OCR according to:

$$\left(s_u / \sigma'_{vo}\right)_{OC} = \left(s_u / \sigma'_{vo}\right)_{NC} OCR^{\Lambda} \quad \text{.....(D-3)}$$

where $\Lambda$ is the plastic volumetric strain ratio = $1\text{-}C_s/C_c$, where $C_s$ and $C_c$ are the swelling and compression indices, respectively; and OCR = $\sigma_p'/\sigma_{vo}'$ is the overconsolidation ratio. The plastic volumetric strain ratio $\Lambda$ is calculated from oedometer test results. Generally, $\Lambda \approx 0.8$ is appropriate for clays of low to medium sensitivity. For highly cemented and

structured clays, $\Lambda \approx 0.9$ up to 1.0 is suitable. Lower values of $\Lambda$ were computed for remolded clays (Mayne, 2001). The dependence of the undrained shear strength on stress history is best represented in normalized form (i.e. $s_u/s_{vo}'$) and known as "Stress History and Normalized Soil Engineering Parameters" or the SHANSEP approach (Ladd et al., 1977).

As mentioned earlier, the undrained shear strength is not a unique value but depends on the mode of loading. For the stability of embankments and shallow footings, it is appropriate to use the undrained shear strength from direct simple shear test DSS, which can be determined from the modified Cam clay model (Wroth, 1984) according to:

$$\left(\frac{s_u}{\sigma_{vo}'}\right)_{DSS} = \frac{\sin\phi'}{2} \cdot OCR^{\Lambda} \quad \text{.....(D-4)}$$

There are similar correlations for the various shear tests. These correlations have been extensively calibrated for use with piezocone data (e.g. Kulhawy and Mayne, 1990; Mayne, 2001). Alternatively, if the effective friction angle is not known, one can make use of the correlation proposed by Ladd (1991):

$$\left(\frac{s_u}{\sigma_{vo}'}\right)_{DSS} = 0.22 \cdot OCR^{0.80} \quad \text{.....(D-5)}$$

Traditionally, the effective friction angle $\phi$' is determined from laboratory shear tests on undisturbed samples. Alternatively, porewater pressure measurements obtained from the piezocone offer the possibility for assessing the effective friction angle $\phi$'. The Norwegian Technical Institute NTH developed a technique for evaluating the effective friction angle from piezocone data (Senneset et al., 1989). The NTH theory is based on the bearing capacity concept, stress field theory, and plane strain conditions. This model can be applied to drained penetration ($\Delta u = 0$) in sandy soils and in fine-grained soils for positive excess pore pressure ($\Delta u > 0$) for saturated soils. There is a special procedure if negative porewater pressures are generated during cone penetration (Sandven, 1990). The method relates the effective friction angle $\phi$' to the cone resistance number $N_m=\Delta q_{net}/(\sigma_{vo}'+a')$ where a' is attraction and the normalized porewater pressure parameter $B_q=\Delta u_2/q_{net}$, where $q_{net}=(q_T-\sigma_{vo})$.

For clean sands, it is common to interpret angle of internal friction from CPT data using the relationship suggested by Kulhawy and Mayne (1990):

$$\phi' = 17.6^{o} + 11.0 \cdot \log\left( q_t \Big/ \sqrt{\sigma_{vo}'} \right) \quad \text{.....(D-6)}$$

where $q_T$ and $\sigma_{vo}$' are in atmospheres. Equation D-4 was developed based on the statistical analysis of corrected calibration chamber test data. Mayne (2004) calibrated Equation D-4 friction angles measured using drained triaxial compression tests on "undisturbed" frozen sand specimens procured at four river sites (Mimura, 2005). As

shown in Figure D-4, friction angles derived using Equation D-4 compare favorably with measured friction angles. More information about the three sands are provided in Chapter 5, where logarithmic functions were fitted to the stress-strain curves from isotropically consolidated triaxial compression tests.

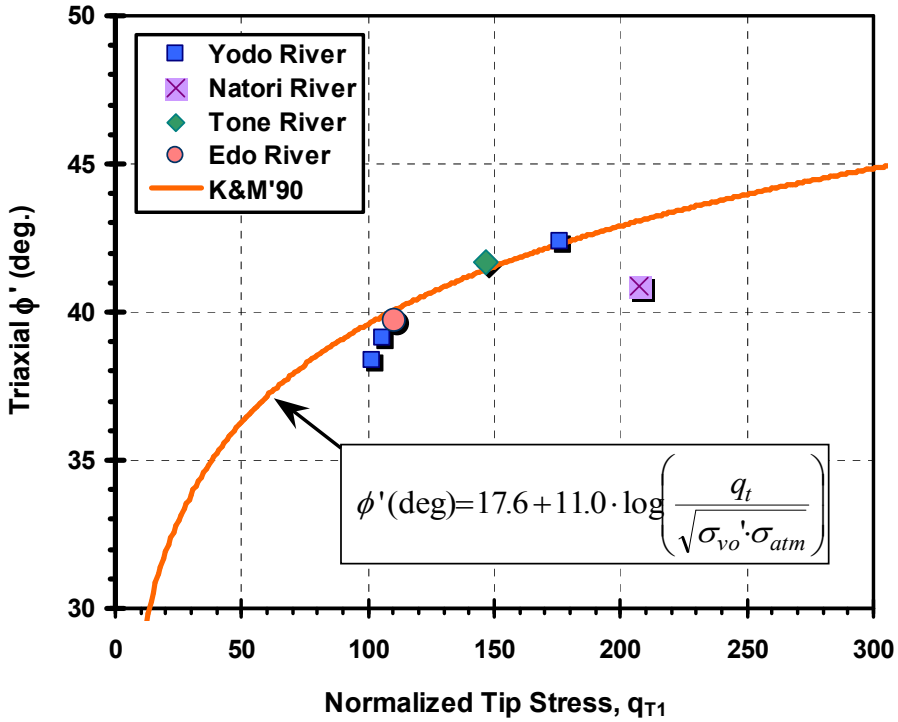


**Figure D-4.** Comparison of measured angle of friction ϕ' from frozen sand samples (Mimura, 2003) with CPT normalized tip stress (after Mayne, 2005)

## D.5 Stress history from piezocone test measurements

The stress history of a specific profile is described by the overconsolidation ratio OCR. Conventionally, OCR is determined from one-dimensional oedometer tests on undisturbed soil specimens. Several methods, both empirical (e.g. Baligh et al., 1980; Mayne & Holtz, 1988) and theoretical (e.g. Wroth, 1988; Mayne and Chen, 1994), have

been developed to evaluate the OCR from piezocone data. An analytical model based on cavity expansion and critical state soil mechanics for piezocone penetrometers with $u_2$ readings gives:

$$OCR = 2\left[\frac{1}{1.95M+1}\left(\frac{q_T - u_2}{\sigma_{vo}^{`}}\right)\right]^{1/\Lambda} \quad \text{.....(D-7)}$$

where M = 6sinϕ'/(3-sinϕ') in triaxial compression. This method has been extensively calibrated (e.g. Mayne and Chen, 1994; Chen and Mayne, 1996). However, as soils vary widely in their characteristics, site-specific calibrations of in-situ methods with laboratory consolidation test results on high quality samples is always warranted (Demers & Leroueil, 2002; Lunne et al., 1997). Another empirical correlation that is used as a first order estimate of the OCR is given by (Chen & Mayne, 1996; Demers & Leroueil, 2002):

$$OCR = \frac{(q_T - \sigma_{vo})}{3 \cdot \sigma'_{vo}} \quad \text{.....(D-8)}$$

Empirical correlations provide means for double-checking the rationality of the interpreted results.

## D.6 Application to case histories to determine DSS undrained shear strength

The aforementioned procedures were applied to four sites where high quality seismic piezocone and laboratory DSS stress-strain data were available to calibrate the methodology (Elhakim and Mayne, 2003; Mayne et al., 2003).

### *D.6.1 Onsøy, Norway*

The soil profile at Onsøy consists of a one-meter thick crust underlain by 44-meters of soft plastic clay with some organic content (Lacasse et al., 1985). Figure D-5 shows seismic piezocone results at the site (Gillespie et al., 1985). Figure D-6 shows laboratory versus piezocone predicted OCR and DSS undrained shear strength values for $\Lambda = 0.8$ and $\phi' = 34^o$.

### *D.6.2 Skå Edeby, Sweden*

The test site is located on an island 25 km west of Stockholm where the soil profile consists of 15 m thick layer of soft clay underlain by till or rock (Larsson and Mulabdić, 1991a). Seismic piezocone test results are shown in Figure D-7. Laboratory and piezocone predicted OCR and DSS undrained shear strengths are presented in Figure D-8 using $\Lambda=0.8$ and $\phi'=34^o$.

### *D.6.3 San Francisco, California, USA*

The soil profile at Islais Creek consists of several layers: (1) fill down to 3.5 m; (2) young Bay Mud from 3.5 to 15.5 m; (3) a clayey sand layer from 15.5 to 17 m; underlain by (4) young Bay Mud down to 33.5 m (Hunt et al., 2002). Seismic piezocone results are presented in Figure D-9. Laboratory versus piezocone predicted profiles of OCR and DSS undrained shear strength are presented in Figure D-10 using $\Lambda = 0.8$ and $\phi' = 36^o$.

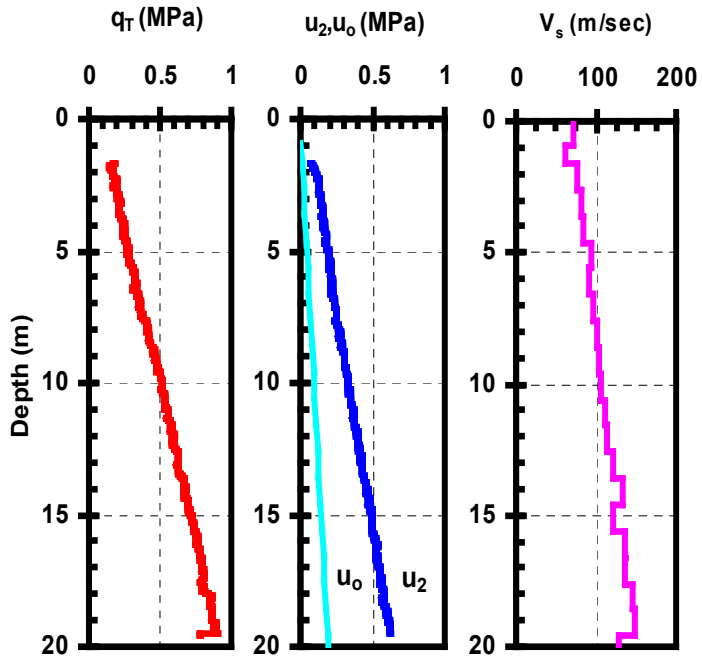


**Figure D-5.** Seismic piezocone profile at Onsøy (after Gillespie et al., 1985)

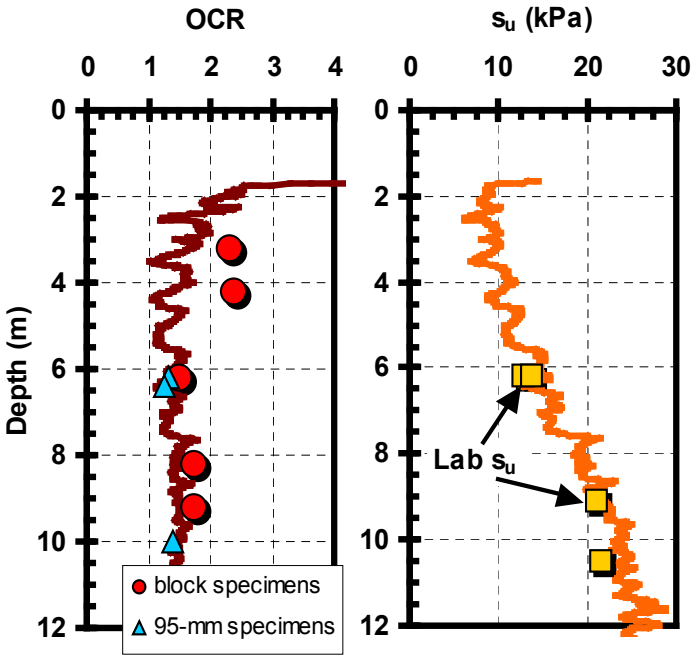


**Figure D-6.** Predicted versus laboratory OCR and DSS strength profiles at Onsøy (laboratory data after Lacasse et al., 1985)

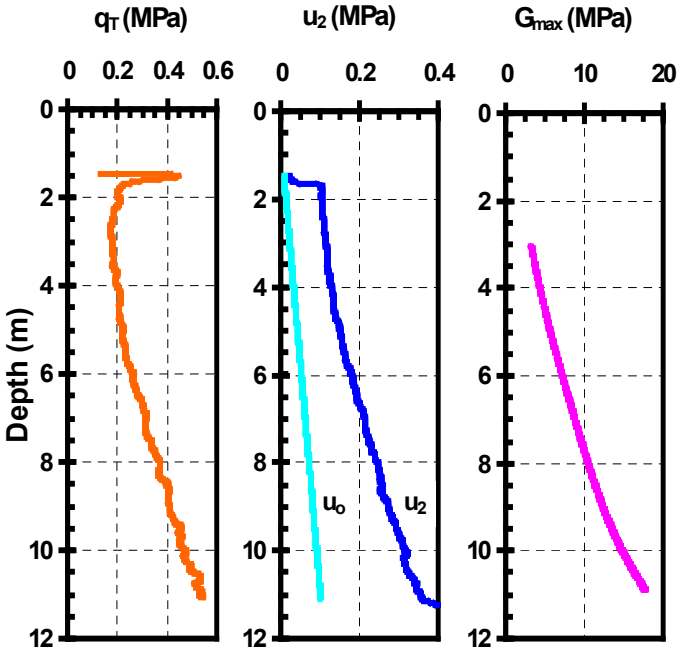


**Figure D-7.** Seismic piezocone profile at Skå Edeby (after Larsson and Mulabdic, 1991a and 1991b)

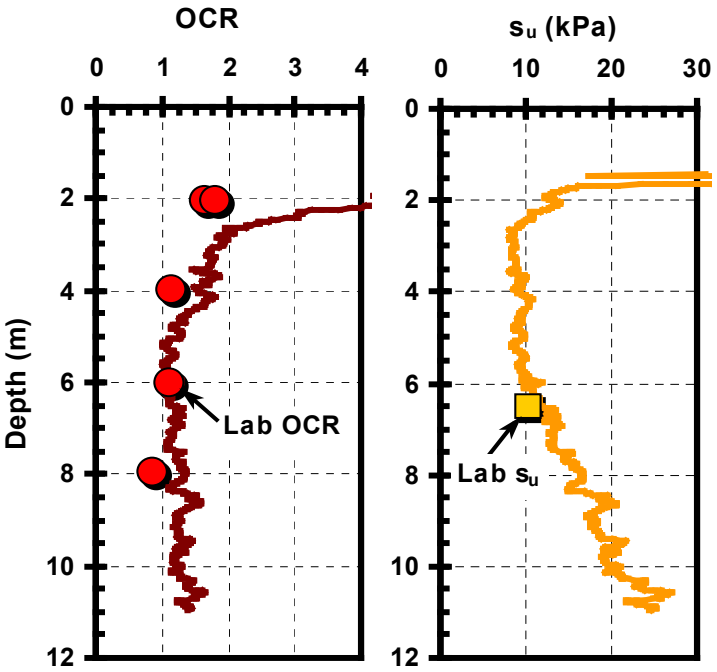


**Figure D-8.** Predicted versus laboratory OCR and DSS strength profiles at Skå Edeby (laboratory OCR from Massarsch et al., 1975; lab DSS from Soydemir, 1976)

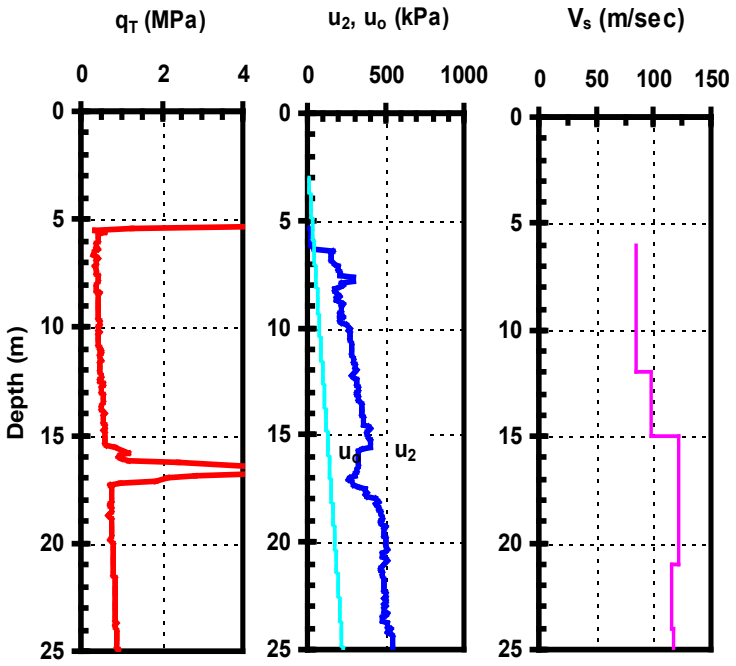


**Figure D-9.** Seismic piezocone profile at San Francisco (after Pestana et al., 2002)

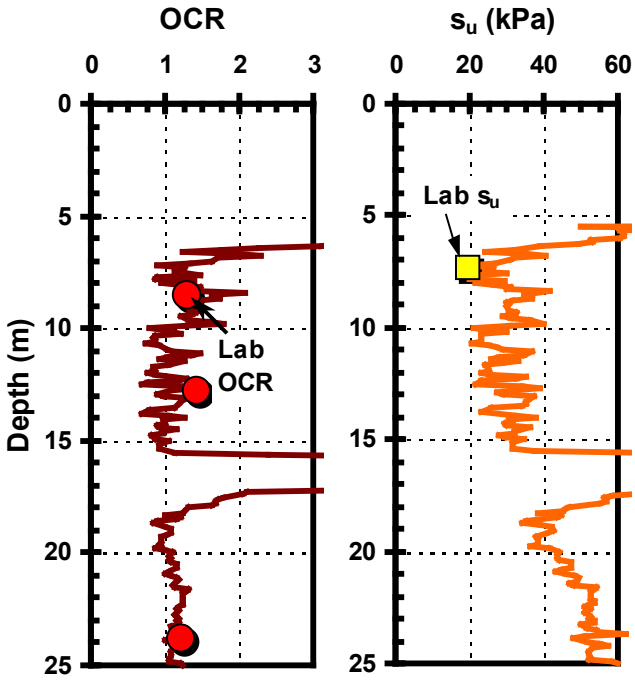


**Figure D-10.** Predicted versus laboratory OCR and DSS strength profiles at San Francisco (laboratory data from Hunt et al., 2002)

### *D.6.4 Amherst NGES, Massachusetts, USA*

The Amherst test site consists of a 24-m thick deposit of soft lightly-overconsolidated lacustrine varved clay overlain by a 3-m desiccated crustal layer and 1-m thick clay fill (Lutenegger, et al. 2000; DeGroot and Lutenegger, 2002). The groundwater table lies one meter deep. Results from several SCPTu soundings are shown in Figure D-11. Variability of the shallow crust is evident from the CPT soundings. Figure D-12 shows comparisons between predicted and laboratory measured OCR and DSS undrained shear strength at the site, using $\Lambda = 0.81$ and $\phi' = 21^o$.

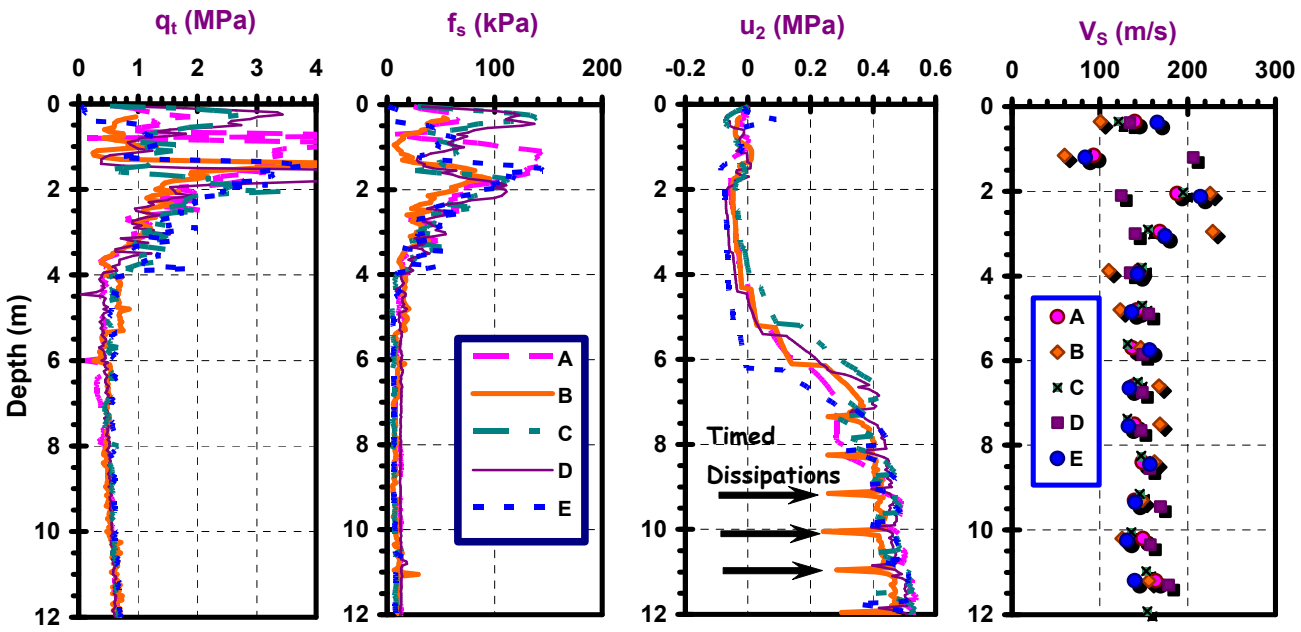


**Figure D-11.** Results of Five Seismic Piezocone Tests in Varved Clay at Amherst National Test Site.

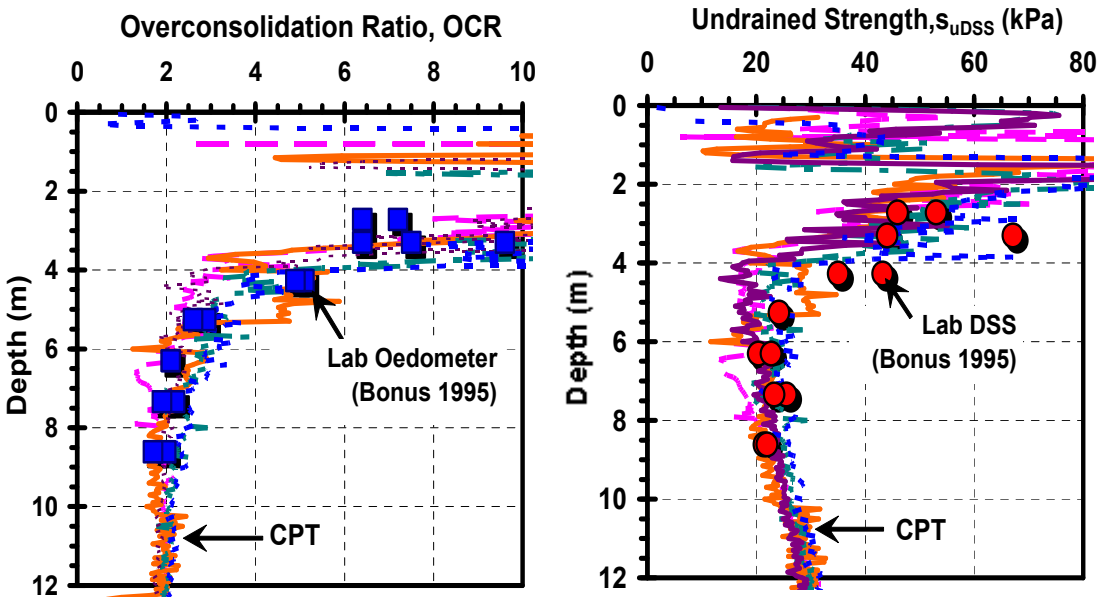


**Figure D-12.** Predicted versus laboratory OCR and DSS strength profiles at Amherst NGES (laboratory data from Bonus, 1995).

# APPENDIX E

## ANALYTICAL EVALUATION OF BEARING CAPACITY

Solutions to calculate theoretical bearing capacity of spread footings have been solved since the beginning of the 20th century. Analytical solutions for the bearing capacity of shallow footings were presented in Chapter 2. A generalized formula for calculating the bearing capacity of vertically-loaded shallow footings of any given shape, at any embedment depth is represented by (Vesić, 1973):

$$q_{ult} = c \cdot N_c \cdot \zeta_{cs} \cdot \zeta_{cd} + \frac{1}{2} \cdot B \cdot \gamma^* \cdot N_\gamma \cdot \zeta_{\gamma s} \cdot \zeta_{\gamma d} + \sigma_{vo}' \cdot N_q \cdot \zeta_{qs} \cdot \zeta_{qd} \quad \text{.....(E-1)}$$

where $q_{ult}$ = the ultimate bearing capacity, c = cohesion, B = footing width, $\sigma_{vo}'$ = effective overburden stress, $N_c$, $N_\gamma$, and $N_q$ are bearing capacity factors for a strip footing, $\zeta_{cs}$, $\zeta_{\gamma s}$, $\zeta_{qs}$ are shape correction factors, and $\zeta_{cd}$, $\zeta_{\gamma d}$, $\zeta_{qd}$ are footing embedment depth correction factors. Available bearing capacity factors $N_c$, $N_\gamma$, and $N_q$ are reviewed. Results are presented graphically in Figures 2-14 through 2-17. More details about the different solutions are provided in Tables E-1 through E-4. Solutions for the bearing factor $N_c$ for surface strip footings are listed in Table E-1. A summary of $N_c$ solutions for the undrained loading conditions "$\phi'=0$" of surface strip footings is provided in Table E-2. The bearing capacity factor $N_q$ for surface strip footings are summarized in Table E-3. Relationships for computing the bearing capacity factor $N_\gamma$ are summarized in Table E-4.

It should be noted that the variation in the values of $N_\gamma$ compared to $N_c$ and $N_q$, as pointed by Vesić (1973); Chen (1975); and Chen and McCarron (1991). The influence of footing shape and embedment depth can be accounted for using correction factors presented in tables E-5 and E-6, respectively.

**Table E-1.** Solutions for the bearing factor $N_c$ for a surface strip footing

| Bearing factor, $N_c$ | Type | Reference |
|---|---|---|
| Prandtl-Reisner bearing factors:<br>$N_c = \cot\phi'\left[e^{\pi\tan\phi'}\tan^2\left(\frac{\pi}{4}+\frac{\phi'}{2}\right)-1\right]$ | Analytical | Chen (1975) |
| Limiting equilibrium analysis of a shallow, rough strip footing | Numerical | Craig & Pariti (1978) |
| Approximate limit equilibrium closed-form solution:<br>$N_c = \left[1+\frac{1}{2}\tan\left(45+\frac{\phi'}{2}\right)\right]\left[2\left(\tan^3\left(45+\frac{\phi'}{2}\right)+\tan\left(45+\frac{\phi'}{2}\right)\right)\right]$ | Analytical | French (1999) |
| Rigorous analysis based on the upper-bound limit analysis theory | Analytical | Soubra (1999) |
| Numerical results presented in Figure E-1 | Numerical | Yin et al. (2001) |

**Table E-2.** Solutions for the bearing factor $N_c$ for a surface strip footing "ϕ'=0"

| Bearing factor, $N_c$ | Type | Reference |
|---|---|---|
| Ideal plastic material under plane strain conditions<br>$N_c = 2+\pi$ | Analytical | Prandtl (1920)* |
| Circular failure surface:<br>$N_c = 5.52$ | Analytical | Fellenius (1929)* |
| Circular failure surface:<br>$N_c = 6.33$ | Analytical | Bjurstrom (1944)* |
| Circular failure surface:<br>$N_c = 2\pi$ | Limit plasticity (upper bound) | Atkinson (1981) |
| Three triangular wedge failure zone<br>$N_c = 6$ | Limit plasticity (upper bound) | Atkinson (1981) |
| Two wedges and a fan slip failure surface<br>$N_c = 2+\pi$ | Limit plasticity (upper bound) | Atkinson (1981) |
| Vertical stress discontinuities<br>$N_c = 4$ | Limit equilibrium (lower bound) | Atkinson (1981) |
| Inclined discontinuities:<br>$N_c = (2+2\sqrt{2})$ | Limit equilibrium (lower bound) | Atkinson (1981) |
| Overlapped inclined discontinuities:<br>$N_c = 2+\pi$ | Limit equilibrium (lower bound) | Atkinson (1981) |

*Foldin and Broms (1981).

**Table E-3.** Solutions for the bearing factor $N_q$ for surface strip footing

| Bearing factor, $N_q$ | Type | Reference |
|---|---|---|
| $N_q = K_p^2$<br>where:<br>$K_p = \frac{1+\sin\phi'}{1-\sin\phi'}$ | Analytical | Lambe and Whitman (1969) |
| Prandtl-Reisner bearing factors:<br>$N_q = e^{\pi \tan\phi'} \tan^2\left(\frac{\pi}{4}+\frac{\phi'}{2}\right)$ | Limit plasticity | Chen (1975) |
| Limiting equilibrium analysis of a shallow, rough strip footing, refer to Figure E-2 | Numerical | Craig & Pariti (1978) |
| $N_q = e^{(\pi-\beta)\tan\phi'} \tan^2\left(\frac{\pi}{4}+\frac{\phi'}{2}\right)$<br>where β =angle of plastification | Limit plasticity | Senneset et al. (1989) |
| Based on Sokolovskii's theory of characteristics: numerical data, refer to Figure E-2 | Analytical | Bolton and Lau (1993) |
| Approximate limit equilibrium closed-form solution:<br>$N_q = \left[1+\frac{1}{2}\tan\left(45+\frac{\phi'}{2}\right)\right]\left[\tan^4\left(45+\frac{\phi'}{2}\right)-1\right]$ | Analytical | French (1999) |
| Rigorous analysis based on the upper-bound limit analysis theory: numerical data – no closed-form solution | Analytical | Soubra (1999) |
| Based on a finite difference program analysis: numerical data – no closed-form solutions | Numerical | Yin et al. (2001) |

**Table E-4.** Methods for calculating the bearing factor $N_\gamma$ for surface strip footings

| Bearing factor, $N_\gamma$ | Type | Reference |
|---|---|---|
| Solution based on the integration of Boussinesq's differential equations using a method of successive approximation: $N_\gamma = \frac{b}{2\sin\left(\frac{\pi}{4}-\frac{\phi}{2}\right)\tan\left(\frac{\pi}{4}-\frac{\phi}{2}\right)}$, for $l$=1, where $b = l\sin\left(\frac{\pi}{2}-\frac{\phi}{2}\right)$ | Analytical | Caquot & Kerisel (1953) |
| $N_\gamma = (N_q - 1)\tan(1.4\phi')$ | | Meyerhof (1961) |
| $N_\gamma = \frac{1}{2}\left(N_\phi^{5/2} - K_p^{1/2}\right)$ where: $K_p = \frac{1+\sin\phi'}{1-\sin\phi'}$ | | Lambe and Whitman (1969) |
| Approximate closed-form equation for numerical data developed by Caquot & Kerisel (1953): $N_\gamma \approx 2(1+N_q)\tan\phi'$ | Approximate | Vesić (1973) |
| Several solutions are presented. The author recommends the solution given by: $N_\gamma = 2(1+N_q)\tan\phi'\tan\left(\frac{\pi}{4}+\frac{\phi'}{5}\right)$, where $N_q = e^{\pi\tan\phi'}\tan^2\left(\frac{\pi}{4}+\frac{\phi'}{2}\right)$ | Limit plasticity | Chen (1975) |
| Approximate closed-form solution of $N_\gamma$ obtained by Lundgren and Mortensen (1953): $N_\gamma = (0.08705 + 0.3231\sin 2\phi' - 0.04836\sin^2 2\phi')\cdot\left(N_q e^{\frac{\pi}{2}\tan\phi'} - 1\right)$ where $N_q = \frac{1+\sin\phi'}{1-\sin\phi'}\cdot e^{\pi\tan\phi'}$ | Empirical fitting | Steenfelt (1977) |
| Limiting equilibrium analysis of a shallow, rough strip footing: numerical data: refer to Figure 3-4 | Analytical | Craig and Pariti (1978) |
| Solution based on statistical analysis of footing load test data with L/B ratio of 6: $N_\gamma = e^{(0.173\phi' - 2.064)}$ | Statistical | Ingra & Baecher (1983) |
| Based on Sokolovskii's theory of characteristics: numerical data. For a rough strip footing, the solution approximated by: $N_\gamma \approx (N_q - 1)\tan(1.5\phi')$, for $30^o<\phi'<50^o$ | Analytical | Bolton and Lau (1993) |
| Finite element and finite difference calculations: numerical data: refer to Figure 3-5 | Numerical | Frydman and Burd (1997) |
| Upper bound solution based on limit analysis. Exact numerical solution approximated by: Rough interface - associative flow: $N_\gamma = e^{0.66+5.11\tan\phi'}\tan\phi'$ Smooth interface - associative flow: $N_\gamma = e^{5.1\tan\phi'}\tan\phi'$ Rough interface – nonassociative flow: $N_\gamma = e^{0.66+5.11\tan\phi^*}\tan\phi^*$ Smooth interface - nonassociative flow: $N_\gamma = e^{5.1\tan\phi^*}\tan\phi^*$ where $\phi^* = \tan^{-1}\frac{\cos\psi\sin\phi}{1-\sin\psi\sin\phi}$ | Numerical | Michalowski (1997) |
| Approximate limit equilibrium closed-form solution: $N_\gamma = \left[1+\frac{1}{2}\tan\left(45+\frac{\phi'}{2}\right)\right]\left[\tan^5\left(45+\frac{\phi'}{2}\right) - \tan\left(45+\frac{\phi'}{2}\right)\right]$ | Analytical | French (1999) |
| Rigorous analysis based on the upper-bound limit analysis theory: numerical data: refer to Figure E-3 | Analytical | Soubra (1999) |
| Least upper-bound solution: numerical data – no closed-form solution | Analytical | Zhu (2000) |
| Finite difference program analysis simulating a rough rigid strip footing: refer to Figure E-3 | Numerical | Yin et al. (2001) |
| Upper and lower bound solutions using a linear Mohr-Coulomb failure envelope with associated flow and finite element discretization: refer to Figure E-3 | Numerical | Ukritchon et al. (2003) |

**Table E-5.** Shape factors for shallow foundations

| Equation | Reference |
|---|---|
| Circular footing on dense or stiff soil:<br>$\zeta_{cs} = 1.2$, $\zeta_{qs} = 1$, $\zeta_{\gamma s} = 0.3$<br>Square footing on dense or stiff soil:<br>$\zeta_{cs} = 1.2$, $\zeta_{qs} = 1$, $\zeta_{\gamma s} = 0.4$ | Terzaghi (1943) |
| $\zeta_{cs} = 1 + 0.2 N_\phi \frac{B}{L}$<br>$\zeta_{qs} = \zeta_{\gamma s} = 1$ for $\phi' = 0^o$<br>$\zeta_{qs} = \zeta_{\gamma s} = 1 + 0.1 N_\phi \frac{B}{L}$ for $\phi' > 10^o$<br>where $N_\phi = \tan^2\left(\frac{\pi}{4} + \frac{\phi}{2}\right)$ | Meyerhof (1963) |
| $\zeta_{cs} = 1 + \frac{B}{L}\frac{N_q}{N_q - 1}\sin\phi$<br>$\zeta_{qs} = 1 + 0.2\frac{B}{L}$<br>$\zeta_{\gamma s} = 1 - 0.4\frac{B}{L}$ | De Beer (1970) |
| $\zeta_{cs} = 1 + \frac{B}{L}\frac{N_q}{N_c}$<br>$\zeta_{qs} = 1 + \frac{B}{L}\tan\phi$<br>$\zeta_{\gamma s} = 1 - 0.4\frac{B}{L}$ | Vesić (1973) |
| Finite element analysis for undrained loading:<br>$\zeta_{cs} = 1 + C_1\frac{B}{L} + C_2\sqrt{\frac{d}{B}}$, where:<br>B/L — $C_1$ — $C_2$<br>1 (circle) — 0.163 — 0.210<br>1 (square) — 0.125 — 0.219<br>0.50 — 0.156 — 0.173<br>0.33 — 0.159 — 0.137<br>0.20 — 0.190 — 0.090 | Salgado et al. (2004) |

**Table E-6.** Depth factors for shallow foundations

| Equation | Reference |
|---|---|
| $\zeta_{cd} = 1 + 0.2\sqrt{N_\phi}\,\frac{z_E}{B}$<br>$\zeta_{qd} = \zeta_{\gamma d} = 1$ for "$\phi' = 0$"<br>$\zeta_{qd} = \zeta_{\gamma d} = 1 + 0.1\sqrt{N_\phi}\,\frac{d}{B}$ for<br>$\phi' > 10^o$<br>where $N_\phi = \tan^2\left(\frac{\pi}{4} + \frac{\phi}{2}\right)$ | Meyerhof (1963) |
| $\zeta_{cd} = \zeta_{qd} - \frac{1 - \zeta_{qd}}{N_q \tan\phi'}$<br>$\zeta_{qd} = 1 + 2\tan\phi'(1 - \sin\phi)^2\,\frac{z_E}{B}$<br>$\zeta_{\gamma d} = 1$<br>For undrained loading "$\phi = 0$",<br>$\zeta_{cd} = 1 + 0.4\frac{z_E}{B}$ | Brinch Hansen factors after Vesić (1973) |
| Finite element analysis for undrained loading:<br>$\zeta_{cd} = 1 + 0.27\sqrt{\frac{z_E}{B}}$ | Salgado et al. (2004) |
| Notes:<br>$z_E$ = depth of foundation embedment<br>B = footing width (smaller dimension)<br>L = footing length. | |

# APPENDIX F

## MODULUS REDUCTION DATABASE

A database of monotonic triaxial and plane strain compression modulus reduction curves is compiled. References, test types, and index soil properties are listed in Table F-1. Data is presented as $E/E_{max}$ versus $q/q_{max}$ shown in Figure F-1. Soils included in the database include both clays and sands that are normally consolidated or overconsolidated. Tests were performed under both drained and undrained conditions.

**Table F-1.** Reference sources for shear modulus reduction data from static (monotonic) triaxial compression tests

| Soil Type | Reference | Test Type | Notes |
|---|---|---|---|
| Bangkok clay | Shibuya and Tamrakar (1999) | $CK_oUC$ | Depth = 13.6 m, $q_{max}$ = 88.6 kPa, $q_o$ = 28.2 kPa, $w_n$ = 65%, LL = 88%, PL = 25%, OCR = 1.6 |
| Bothkennar clay | Clayton et al. (2003) | CKoUC | Depth = 5.4 m, $\Delta q_{max}$ = 30 kPa, $\sigma_{aini}$ = 50 kPa, $\sigma_{rini}$ = 30 kPa, $w_n$ = 68%, LL = 75%, PL = 35%, OCR = 1.5 |
| Bothkennar clay | Clayton et al. (2003) | CKoUC | Depth = 6.0 m, $\Delta q_{max}$ = 44 kPa, $\sigma_{aini}$ = 47 kPa, $\sigma_{rini}$ = 27 kPa, $w_n$ = 68%, LL = 75%, PL = 35%, OCR = 1.5 |
| Bothkennar clay | Clayton et al. (2003) | CIUC | Depth = 7.9-8.3 m, $\Delta q_{max}$ = 36 kPa, $\sigma_{aini}$ = 62 kPa, $\sigma_{rini}$ = 38 kPa, $w_n$ = 71%, LL = 73%, PL = 34%, OCR = 1.4 |
| Pisa clay | Lo Presti et al. (2003) | $CK_oDC$ | LL = 84 %, PL = 33.5 %, $w_n$ = 63 %, OCR = 1.75 |
| Hime sand/gravel | Shibuya and Tamrakar (1999) | CIDC | $K_o$ = 1.0, $q_{max}$ = 182 kPa, $e_o$ = 0.548 |
| Fujinomori clay | Yamashita et al. (2001) | CIUC | $e_o$ = 1.538, $E_{max}$ = 118 MPa, $q_{max}$ = 110 kPa |
| NC SLB sand | Tatsuoka and Kohata (1995) | PSC | Air pluviated dense samples, $e_o$ = 0.557, OCR = 1, $D_{50}$ = 0.62 mm |
| OC SLB sand | Tatsuoka and Kohata (1995) | PSC | Air pluviated dense samples, $e_o$ = 0.563, OCR = 4 |
| Vallericca clay | Georgiannou et al. (1991) | CIUC | LL= 53.2%, PL= 22.2%, $w_n$ = 28.6%, $G_{max}$= 72 MPa, $s_u$ = 200 kPa, $\sigma_3$ = 60 kPa |
| Todi clay | Georgiannou et al. (1991) | CIUC | LL= 47.6%, PL= 19.6%, $w_n$ = 17.2%, $G_{max}$ = 158 MPa, $s_u$ = 649 kPa, $\sigma_3$ = 200 kPa, |
| Pietrafitta clay | Georgiannou et al. (1991) | CIUC | LL= 62.0%, PL= 32.4%, $w_n$ = 41.8%, $G_{max}$ = 158 MPa, $s_u$ = 649 kPa, $\sigma_3$ = 320 kPa |
| Bothkennar clay | Clayton et al. (2003) | CIUC | Depth = 5.4 m, $\Delta q_{max}$ = 30 kPa, $\sigma_{aini}$ = 47 kPa, $\sigma_{rini}$ = 27 kPa, $w_n$ = 68%, LL = 75%, PL = 35%, OCR = 1.5 |
| Bothkennar clay | Clayton et al. (2003) | CIUC | Depth = 6 m, $\Delta q_{max}$ = 44 kPa, $\sigma_{aini}$ = 50 kPa, $\sigma_{rini}$ = 30 kPa, $w_n$ = 68%, LL = 75%, PL = 35%, OCR = 1.5 |
| Kaolin | Tatsuoka and Shibuya (1991) | CIDC | LL= 55%, PL= 29% |
| OC Ticino sand | Tatsuoka and Shibuya (1991) | CIDC | $e_o$ = 0.64, OCR = 4 |
| NC Ticino sand | Tatsuoka and Shibuya (1991) | CIDC | $e_o$ = 0.64, OCR = 1 |
| Toyoura sand | Tatsuoka and Shibuya (1991) | PSC | $e_{max}$ = 0.985, $e_{min}$ = 0.985, $e_o$ = 0.67, $D_{50}$ = 0.22 mm |
| Toyoura sand | Tatsuoka and Shibuya (1991) | PSC | $e_{max}$ = 0.985, $e_{min}$ = 0.985, $e_o$ = 0.83, $D_{50}$ = 0.22 mm |

Notes:
$D_{50}$ = particle size equivalent to 50% passing
$e_o$ = initial void ratio
$E_{max}$ = small-strain Young's modulus
$G_{max}$= small-strain shear modulus
LL= liquid limit
OCR= overconsolidation ratio
PL= plastic limit
$q_{max}$ = soil strength
$s_u$= undrained shear strength
$w_n$= natural water content
$\sigma_{aini}$ = initial axial stress
$\sigma_{rini}$ = initial radial stress
$\sigma_3$ = confining stress

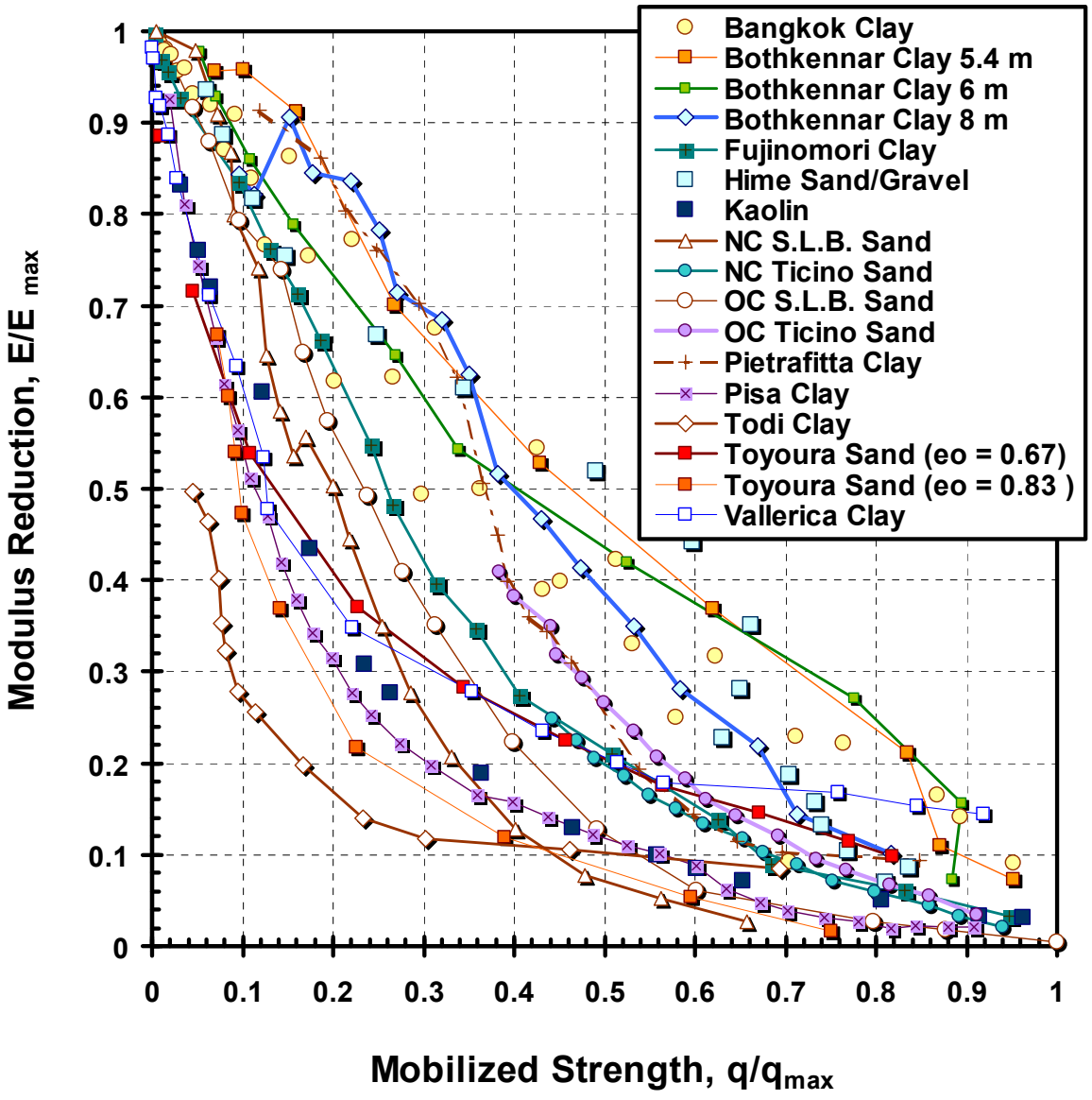


**Figure F-1.** Modulus reduction data from compiled monotonic triaxial and plane strain compression tests plotted versus mobilized stress (note: references in Table F-1)

# APPENDIX G

## NON-LINEAR ELASTIC-PLASTIC MODEL (LOGNEP)

A non-linear elastic-perfectly plastic model was developed and incorporated into FLAC as a user-defined constitutive model using FISH language. The soil shear modulus starts at the small-strain shear modulus $G_{max}$. The shear modulus is reduced with the strain level according to the logarithmic modulus reduction scheme (Puzrin and Burland, 1996; 1998). When the stresses reach the yield surface, the stress-strain behavior is no longer defined by elasticity. A flow rule defines the plastic stress-strain relationship by means of a plastic potential function. The model details are described in Chapter 6. The logarithmic non-linear elastic-plastic model is given herein.

```
;Logarithmic Non-linear Elastic Plastic model (LOGNEP)
;User-defined constitutive model
;FISH
set echo on
def logpuplas
constitutive_model


f_prop dif1_2 dif2_2 dif3_2 gam_2
f_prop $ar $alf $Rf
f_prop m_s11t m_s22t m_s33t m_s12t
f_prop m_s11 m_s22 m_s33 m_s12
f_prop m_g m_k m_gi yield p_ratio
f_prop m_qvol m_qdil m_ind m_ten
f_prop m_gkq m_kq m_tand m_facg
f_prop m_e1 m_e2 m_g2 nls ns kphi m_sv
float $sigi $sign $ds11 $ds22 $ds33 $ds12 $taui
float $lam $taun $sign $s11i $s22i $s33i $s12i
float $fi $ft $apex


case_of  mode
;--- initialization ---
case 1
  if m_g = 0.0 then
    m_g = m_gi
  end_if
  m_e1 = m_k + 4.0 * m_g / 3.0
  m_e2 = m_k - 2.0 * m_g / 3.0
  m_g2 = 2.0 * m_g
  m_kq = m_k * m_qdil
  m_gkq = m_g + m_kq * m_qvol
  m_tand = sqrt(m_qvol * m_qvol + 1.) - m_qvol
  kphi = 1./(3.^0.5)*yield
  m_facg = kphi - (m_qvol + m_tand) * m_ten
  $ar  = (1.+nls)*(LN(1.+nls))/nls/(nls-1.)
  $alf = (nls-1.)/nls/(LN(1.+nls))^$ar


; --- set tension to cone apex if larger than apex ---
  $apex = m_ten
   if m_qvol # 0.0 then
     $apex=kphi/m_qvol
   end_if
     m_ten=min($apex,m_ten)
```

```
;--- running section ---
case 2
    zvisc = 1.0

;--- Strain invariant calculations
  m_s11t = m_s11t + zde11
  m_s22t = m_s22t + zde22
  m_s33t = m_s33t + zde33
  m_s12t = m_s12t + zde12
 if zsub > 0.0 then
    m_s11 = m_s11 + m_s11t/zsub
    m_s11t= 0.0
    m_s22 = m_s22 + m_s22t/zsub
    m_s22t= 0.0
    m_s33 = m_s33 + m_s33t/zsub
    m_s33t= 0.0
    m_s12 = m_s12 + m_s12t/zsub
    m_s12t= 0.0
 end_if
   dif1_2 = (m_s11-m_s22)*(m_s11-m_s22)
   dif2_2 = (m_s22-m_s33)*(m_s22-m_s33)
   dif3_2 = (m_s11-m_s33)*(m_s11-m_s33)
   gam_2  = m_s12*m_s12
   m_sv = sqrt(1./6.*(dif1_2+dif2_2+dif3_2)+gam_2)

;--- Normlized strain
   ns= 2.*m_gi*m_sv/kphi

; --- get new trial stresses from old, assuming elastic increments ---
   $s11i = zs11 + zde11 * m_e1 + (zde22+zde33) * m_e2
   $s22i = zs22 + (zde11+zde33) * m_e2 + zde22 * m_e1
   $s33i = zs33 + (zde11+zde22) * m_e2 + zde33 * m_e1
   $s12i = zs12 + zde12 * m_g2
; --- mean stress ---
   $sigi = ($s11i+$s22i+$s33i)/3.0
; --- deviatoric stresses ---
   $ds11 = $s11i - $sigi
   $ds22 = $s22i - $sigi
   $ds33 = $s33i - $sigi
   $ds12 = $s12i
; --- second deviatoric stress invariant ---
  $taui=sqrt(0.5*($ds11*$ds11+$ds22*$ds22+$ds33*$ds33)+$ds12*$ds12)
; --- Drucker-Prager yield criterion ---
  $fi=$taui+m_qvol*$sigi-kphi
  $ft=$sigi-m_ten
;--- Modulus Degradation
SECTION
; --- plasticity indicator ---
 if $fi > 0.0 then
```

```
  EXIT SECTION
 end_if
  if $fi = 0.0 then
  EXIT SECTION
 end_if

 if $taui - m_tand * $sigi - m_facg > 0.0 then
  EXIT SECTION
 end_if

 if $taui - m_tand * $sigi - m_facg = 0.0 then
  EXIT SECTION
 end_if

 if $ft>0.0 then
   EXIT SECTION
 end_if

 if $ft=0.0 then
   EXIT SECTION
 end_if
if m_g <=1000. then
    m_g = 1000.
 else
  if ns <=1.e-6 then
   m_g = m_gi
    else
     $Rf = 1.-$alf*(LN(1.+ns))^$ar
     $Rf = $Rf-$alf*$ar*ns/(1.+ns)*(LN(1.+ns))^($ar-1.)
     m_g = m_gi*$Rf
   end_if
  end_if
ENDSECTION

     if $ft < 0.0 then
       if $fi > 0.0 then
      m_g   = m_gi
      m_gkq = m_g + m_kq * m_qvol
; --- shear failure ---
      $lam=$fi/m_gkq
; --- correct second deviatoric stress invariant ---
      $taun=$taui-$lam*m_g
; --- correct volumetric stress ---
      $sign=$sigi-$lam*m_kq
; --- correct deviatoric stresses ---
      $ds11 = ($ds11 / $taui) * $taun
      $ds22 = ($ds22 / $taui) * $taun
      $ds33 = ($ds33 / $taui) * $taun
      $ds12 = ($ds12 / $taui) * $taun
```

```
; --- new stresses ---
      zs11 = $ds11 + $sign
      zs22 = $ds22 + $sign
      zs33 = $ds33 + $sign
      zs12 = $ds12
      zvisc = 0.0
      m_ind = 1.0
      else
; --- no failure ---
      zs11 = $s11i
      zs22 = $s22i
      zs33 = $s33i
      zs12 = $s12i
     end_if

  else
     if $taui - m_tand * $sigi - m_facg > 0.0 then
      m_g   = m_gi
      m_gkq = m_g + m_kq * m_qvol
; --- shear failure ---
       $lam = $fi / m_gkq
; --- correct second deviatoric stress invariant ---
       $taun = $taui - $lam * m_g
; --- correct volumetric stress ---
       $sign = $sigi - $lam * m_kq
; --- correct deviatoric stresses ---
       $ds11 = ($ds11 / $taui) * $taun
       $ds22 = ($ds22 / $taui) * $taun
       $ds33 = ($ds33 / $taui) * $taun
       $ds12 = ($ds12 / $taui) * $taun
; --- new stresses ---
       zs11 = $ds11 + $sign
       zs22 = $ds22 + $sign
       zs33 = $ds33 + $sign
       zs12 = $ds12
       zvisc = 0.0
       m_ind = 1.0
      else
; --- tensile failure ---
       zs11 = $s11i - $ft
       zs22 = $s22i - $ft
       zs33 = $s33i - $ft
       zs12 = $s12i
       zvisc = 0.0
       m_ind = 3.0
    end_if
  end_if

   m_g2 = 2.*m_g
```

```
   m_e1 = m_k + 1.333333  * m_g
   m_e2 = m_k - 0.6666667 * m_g
    case 3
;--- max modulus ---
      sm_max = m_g
      cm_max = m_k + 1.333333 * m_g
  end_case
end
opt logpuplas
set echo on
```

## BIBLIOGRAPHY


Adachi, K. (1989). Sampling of cohesionless and gravelly soils. The Art and Science of Geotechnical Engineering, New Jersey, Prentice Hall, pp. 206-220.

Al-Hussaini, M.M. (1973). Influence of relative density on the strength and deformation of sand under plane strain conditions. Evaluation of Relative Density and Its Role in Geotechnical Projects Involving Cohesionless Soils, ASTM STP 523, ASTM, pp. 332-347.

Almeida, S.S.M., and Parry, R.H.G. (1988). Miniature vane and cone penetration tests during centrifuge flight. Vane shear strength testing in soils: field and laboratory studies, ASTM STP 1014, ASTM, Philadelphia, pp. 209-219.

Amar, S., Baguelin, F., and Canepa, Y. (1998). Shallow foundations – experimental study under cyclic loading. Proceedings of Geotechnical Hazards, Rotterdam, pp. 477-483.

Amar, S., Baguelin, F., Canepa, Y., and Frank, R. (1994). Experimental study of the settlement of shallow foundations. Vertical and Horizontal Deformations of Foundations and Embankments, Vol. 2, GSP No. 40, ASCE, Reston, pp. 1602-1610.

Andersen, K.H. and Stenhamar, P. (1982). Static plate loading tests on overconsolidated clay. Journal of the Geotechnical Engineering Division, ASCE, Vol. 108, No. GT7, pp. 919-934.

Atkinson, J.H. (1981). Foundations and Slopes: An Introduction to Applications of Critical State Soil Mechanics. John Wiley and Sons, New York, 382 pages.

Atkinson, J.H. (1993). A note on modeling small strain stiffness in Cam clay. Predictive Soil Mechanics, Oxford University, Thomas Telford, London, pp. 111-120.

Atkinson, J.H. (2000). Non-linear soil stiffness in routine design, Geotechnique, Vol. 50, No. 5, pp. 487-508.

Atkinson, J.H., Lau, W.H. and Powell, J.J.M. (1991). Measurement of soil strength in simple shear. Canadian Geotechnical Journal, Vol. 28, No. 2, pp. 255-262.

Axelsson, K., Yu, Y., Westerberg, B. (1994). Behaviour and modeling of Swedish soft clays. Proceedings of the 13th International Conference of Soil Mechanics and Foundation Engineering, New Delhi, Vol. 1, pp. 57-60.

Baguelin, F., Jezequel, J.F., Shields, D.H. (1978). Pressuremeter and Foundation Engineering, Series on rock and soil mechanics, Vol. 2, No. 4, Trans Tech Publications, Clausthal, 617 pages.

Baldi, G., Bellotti, R., Ghionna, V.N., Jamiolkowski, M., Lo Presti, D.C.F. (1989).

Modulus of sands from CPT's and DMT's. Proceedings of the 12th International Conference on Soil Mechanics and Foundation Engineering, Rio de Janeiro, Vol. 1, pp. 165-170.

Baligh, M.M. (1985). The strain path method. Journal of Geotechnical Engineering, Vol. 111, No. 9, pp. 1108-1136.

Balla, A. (1962). Bearing capacity of foundations, Journal of Soil Mechanics and Foundations Division, ASCE, Vol. 88, No. SM5, pp. 13-34.

Barbour, S.L., and Krahn, J. (2004). Numerical modeling – prediction or process. Geotechnical News, BiTech Publishers, Richmond, British Columbia, pp. 44-52.

Bazant, Z.P. (1978). Endochronic inelasticity and incremental plasticity. International of Solids and Structures, Vol. 14, pp. 691-714.

Begemann, H.K.S. (1965). The friction jacket cone as an aid in determining the soil profile. Proceedings of the 6th International Conference on Soil Mechanics and Foundation Engineering, Montreal, Vol. 1, pp. 17-20.

Berardi, R., and Lancellotta, R. (1991). Stiffness of granular soils from field performance. Geotechnique, Vol. 41, No. 1, pp. 149-157.

Berre, T., Schjetne, K. and Sollie, S. (1969). Sampling disturbance of soft marine clays. Proceedings 7th International Conference of Soil Mechanics and Foundation Engineering, Mexico, Vol. 1, pp. 21-24.

Bjerrum, L. and Landva, A. (1966). Direct simple shear tests on a Norwegian quick clay. Geotechnique, Vol. 16, No. 1, pp. 1-19.

Bolton, M.D. and Lau, C.K. (1993). Vertical bearing capacity factors for circular and strip footings on Mohr-Coulomb soil. Canadian Geotechnical Journal, Vol. 3, No. 6, pp. 1024-1033.

Bolton, M.D. and Whittle, R.W. (1999). A non-linear elastic/perfectly plastic analysis for plane strain undrained expansion tests. Geotechnique, Vol. 49, No. 1, pp. 133-141.

Boswell, L.F., and Scott, C.R. (1975). A flexible circular plate on a heterogeneous elastic half-space: influence coefficients for contact stress and settlement. Geotechnique, Vol. 25, No. 3, pp. 604-610.

Bowey, A.W. and Wood, D.M. (1994). Back analysis of a trial loading on soft clay. Pre-failure Deformation of Geomaterials, Balkema, Rotterdam, Vol. 1, pp. 559-565.

Bowles, J.E. (1988). Foundation Analysis and Design. 4th Edition, McGraw Hill, Inc., New York, 578 pages

Brand, E.W., Muktabhant, C., and Taechathummarak, A. (1972). Load tests on small on small foundations in soft clay, Performance of Earth and Earth-Supported Structures.Vol. 1, Part 2, ASCE, Reston, Virginia, pp. 903-928

Briaud, J.L. (1995). Pressuremeter method for spread footings on sand. The Pressuremeter and its New Avenues, Balkema, Rotterdam, pp. 49-56

Briaud, J.L., and Gibbens, R. (1999). Behavior of five large spread footings in sand. Journal of Geotechnical and Geoenvironmental Engineering, Vol. 125, No. 9, pp. 787-796.

Briaud, J.L., and Jeanjean, P. (1994). Load settlement curve method for spread footings on sand. Vertical and Horizontal Deformations of Foundations and Embankments, ASCE GSP No. 40, Vol. 2, pp. 1774-1804.

Brinch Hansen, J. (1963). Discussion of "Hyperbolic stress-strain response: cohesive soils". Journal of the Soil Mechanics and Foundations Division, Vol. 89, No. SM 4, pp. 241-242.

Brinch Hansen, J. and Christensen, N.H. (1969). Discussion of "Theoretical bearing capacity of very shallow footings". Journal of the Soil Mechanics and Foundations Division, ASCE, Vol. 89, No. SM 6, pp.1568-1572.

Brown, P.T. (1969a). Numerical analyses of uniformly loaded circular rafts on elastic layers of finite depth. Geotechnique, Vol. 19, No.2, pp. 301-306.

Brown, P.T. (1969b). Numerical analyses of uniformly loaded circular rafts on deep elastic foundations. Geotechnique, Vol. 19, No. 3, pp. 399-404.

Burghignoli, A., Pane, V., Cavalera, L. (1991). Monotonic loading. Proceedings 10th European Conference on Soil Mechanics and Foundation Engineering, Vol. 1, Florence, pp. 961-979.

Burland, J.B. (1970). Discussion of Session A. Proceedings of the Conference on In-Situ Investigations in Soils and Rocks, British Geotechnical Society, London, pp. 61-62.

Burland, J.B. (1989). Small is beautiful: the stiffness of soil at small strains. Canadian Geotechnical Journal, Vol. 16, No. 4, pp. 499-516.

Burland, J.B. and Hancock, R.J.R. (1977). Underground car park at the House of Commons: geotechnical aspects, Structural Engineer, Vol. 55, pp. 87-100.

Burland, J.B., Broms, B.B., and De Mello, V.F.B. (1977). Behavior of foundations and structures. Proceedings of the 9th International Conference on Soil Mechanics and Foundation Engineering, Tokyo, Vol. 2, pp. 495-538.

Burland, J.B., Rampello, S., Georgiannou, V.N., and Calabresi, G. (1996). Laboratory study of the strength of four stiff clays. Geotechnique, Vol. 46, No. 3, pp. 491-514.

Campanella, R.G., Robertson, P.K., Gillespie, D. (1986). Seismic cone penetration test. Use of In Situ Tests in Geotechnical Engineering (GSP 6), ASCE, Reston, pp. 116-130.

Campanella, R.G., Robertson, P.K., Gillespie, D.G., and Grieg, J. (1985). Recent developments in in-situ testing of soils. Proceedings 11th International Conference of Soil Mechanics and Foundation Engineering, San Francisco, Vol. 2, pp.849-854.

Campanella, R.G., Stewart, W.P., Roy, D., Davies, M.P. (1994). Low strain dynamic characteristics of soils with the downhole seismic piezocone penetrometer. Dynamic Geotechnical Testing II, ASTM STP 1213, Philadelphia, pp. 73-87.

Caquot, A. and Kerisel, J. (1953). Sur la terme de surface dans le calcul des fondations en milieu pulverulent. Proceedings of the 3rd International Conference on Soil Mechanics and Foundation Engineering, Vol. 1, Zurich, pp. 336-337 (in French).

Carrier, D.W., and Christian, J.T. (1973). Rigid circular plate resting on a non-homogeneous elastic half space. Geotechnique, Vol. 23, No. 1, pp. 67-84.

Chen, B.S-Y. and Mayne, P.W. (1996). Statistical relationships between piezocone measurements and stress history of clays. Canadian Geotechnical Journal, Vol. 33, No. 3, pp. 488-498.

Chen, W.F. (1975). Limit Analysis and Soil Plasticity. Elsevier, Amsterdam, 638 pages.

Chen, W.F. and Han, D.J. (1988). Plasticity for Structural Engineers, Springer-Verlag New York Inc., 606 pages

Chen, W.F. and McCarron, W.O. (1991). Bearing capacity of shallow foundations. Foundation Engineering Handbook, Chapman and Hall, New York, pp. 144-165.

Chen, W.F. and Saleeb, A.F. (1982). Constitutive Equations for Engineering Materials, Vol. 1: Elasticity and Modelling. Wiley-Interscience, New York, NY, 580 pages.

Chen, W.F., and Liu, X.L. (1990). Limit Analysis in Soil Mechanics. Elsevier, Amsterdam, 477 pages.

Chin, F.K. (1971). Discussion to “Pile tests: Arkansas river project”. ASCE Journal of Soil Mechanics and Foundations Division, Vol. 97, SM 6, pp. 930-932.

Christoffersen, H.P., and Lacasse, S. (1984). Report: Offshore Site Investigation Techniques: Laboratory tests on Haga clay, Norwegian Geotechnical Institute, Oslo, 55 pages.

Clarke, B.G. (1995). Pressuremeters in Geotechnical Design. Blackie Academic and Professional, Glasgow, 364 pages.

Clayton, C.R.I., Hight, D.W., and Hopper, R.J. (1992). Progressive destructuring of Bothkennar clay: implications for sampling and reconsolidation procedures. Geotechnique, Vol. 42, No. 2, pp. 219-239.

Consoli, N.C., Schnaid, F., and Milititsky, J. (1998). Interpretation of plate load tests on residual soil site. Journal of Geotechnical and Geoenvironmental Engineering, Vol. 124, No. 9, pp. 857-867.

Craig, R.F. and Pariti, L.N.M. (1978). Limiting equilibrium analysis of strip footings. Journal of the Geotechnical Engineering Division, Vol. 104, No. GT3, pp. 357-368.

Daloglu, A.T. and Vallabhan, C.V.G. (2000). Values of k for slab on Winkler foundation. Journal of Geotechnical and Geoenvironmental Engineering, Vol. 126, No. 5, pp. 463-471.

Davis, E.H. and Poulos, A. (1968). The use of elastic theory for settlement prediction under 3-d conditions. Geotechnique, Vol. 18, No.1, pp. 67-91.

De Beer, E.E. (1970). Experimental determination on the shape factors and the bearing capacity factors of sand. Geotechnique, Vol. 2, No. 4, pp. 387-411.

De Beer, E.E. (1988). Different behavior of bored and driven piles. Proceedings of the 1st International Seminar on Deep Foundation on Bored Piles, Ghent, pp. 47-78.

De Borst, R. and Vermeer, P.A. (1984). Possibilities and limitations of finite elements for limit analysis. Geotechnique, Vol. 34, No. 2, pp. 199-210.

Decourt, L. (1999). Behavior of foundations under working load conditions. Proceedings of the XI Panamerican conference on Soil Mechanics and Geotechnical Engineering, Foz do Iguassu, Brazil, Vol. 4, pp. 453-487.

DeGroot, D.J. and Lutenegger, A.J. (2002). Geology and engineering properties of Connecticut Valley varved clay. Characterization and Engineering Properties of Natural Soils, Vol. 1, Swets & Zeitlinger, Lisse, pp. 695-724.

DeGroot, D.J., Ladd, C.C. and Germaine, J.T. (1992). Direct simple shear testing of cohesive soils. Research Report No. R92-18, Center for Scientific Excellence in Offshore Engineering, Massachusetts, 153 pages.

DeJong, J.T., Frost, D., and Cargill, P.E. (2001). Effect of surface texturing on CPT friction sleeve measurements. Journal of Geotechnical and Geoenvironmental Engineering, ASCE, Vol. 127, No. 2, pp. 158-168.

Demers, D., and Leroueil, S. (2002). Evaluation of preconsolidation pressure and the overconsolidation ratio from piezocone tests of clay deposits in Quebec. Canadian Geotechnical Journal, Vol. 39, No. 1, pp. 174-192.

Desai, C.S. and Siriwardane, H.J. (1984). Constitutive Laws for Engineering Materials with Emphasis on Geologic Materials. Prentice-Hall, Inc., Englewood Cliffs, New Jersey, pp. 169-203.

Detournay, C. (2003). Ph.D. staff member at Itasca Consulting Group, Inc. Personal communication.

DiMillio, A. (2004). A Quarter Century of Geotechnical Research. Federal Highway Administration (FHWA) Research, Development, and Technology, U.S. Department of Transportation, FHWA-RD-98-13X, www.tfhrc.gov/structur/gtr/century/index.htm

Douglas, B.J. and Olsen, R.S. (1981). Soil classification using electric cone penetrometer. Cone Penetration Testing and Experience. Proceedings of the ASCE National Convention, St. Louis, MO, pp. 209-227.

Drnevich, V.P. and Massarsch, K.R. (1979). Sample disturbance and stress-strain behavior. ASCE Journal of Geotechnical Engineering Division, Vol. 105, No. GT9, pp. 1001-1016.

Drucker, D.C., and Prager, W. (1952). Soil mechanics and plastic analysis or limit design. Quarterly of Applied Mathematics, Vol. 10, No. 2, pp. 157-165.

Duncan, J.M., and Buchignani, A.L. (1976), An Engineering Manual for Settlement Studies, Civil Engineering, University of California, Berkeley.

Duncan, J.M., Chang, C.Y. (1970). Nonlinear analysis of stress and strain in soils. Journal of Geotechnical and Geoenvironmental Engineering, Vol. 96, No. 5, pp. 1629-1653.

Dyvik, R, Madshus, C. (1985). Lab measurements of $G_{max}$ using bender elements. Advances in the Art of Testing Soils Under Cyclic Conditions, Detroit, ASCE, pp. 186-196.

Dyvik, R., Berre, T., Lacasse, S. and Raadim, B. (1987). Comparison of truly undrained and constant volume direct simple shear tests. Geotechnique, Vol. 37, No. 1, pp. 3-10.

Eide**,** O., Andersen, K.H. (1984). Foundation engineering for gravity structures in the northern North Sea. Report, Norwegian Geotechnical Institute, Report 154, 54 pages.

Elhakim, A.F., and Mayne, P.W. (2003). Derived stress-strain-strength of clays from seismic cone tests. Deformation Characteristics of Geomaterials, Vol. 1, Balkema, Lisse, pp. 81-87.

England, M. (1993). A method of analysis of stress induced displacement in soils with respect to time. Proceedings of the International Geotechnical Seminar on Deep Foundations on Bored and Auger Piles (BAP 2), Ghent, Vol. 2, pp. 241-246.

Erickson, H.L., and Drescher, A. (2002). Bearing capacity of circular footings. Journal of Geotechnical and Geoenvironmental Engineering, Vol. 128, No. 1, pp. 38-43.

Esquivel, E.R., and Silva, C.H.C. (2000). Miniature piezocone for use in centrifuge testing. Innovations and Applications in Geotechnical Site Characterization. GSP No. 97. ASCE, Reston, Virginia, pp. 118-129.

Fahey, M. (1992). Shear modulus of cohesionless soil: variation with stress and strain level. Canadian Geotechnical Journal, Vol. 29, No. 1, pp. 157-161.

Fahey, M. (1998). Deformation and in situ stress measurement. Geotechnical Site Characterization, ISC '98, Atlanta, Vol. 1, Balkema, Rotterdam, pp. 49-68.

Fahey, M. (2001). Soil stiffness values for foundation settlement analysis. Pre-Failure Deformation Characteristics of Geomaterials, Vol. 2, Balkema, Rotterdam, pp.1325-1332.

Fahey, M. and Carter, J.P. (1993). A finite element study of the pressuremeter test in sand using a nonlinear elastic plastic model. Canadian Geotechnical Journal, Vol. 30, No. 2, pp. 348-362.

Fahey, M., Robertson, P.K., and Soliman, A.A. (1994). Towards a rational method of predicting settlements of spread footings on sand. Vertical and Horizontal Deformations of Foundations and Embankments, Vol. 2, GSP No. 40, ASCE, Reston, pp. 1325-1332.

Fellenius, B.H. (1980). The analysis of results from routine pile load tests. Ground Engineering, Vol. 13, No. 6, pp. 19-29.

Fellenius, B.H. (2002). Basics of Foundation Design. Electronic Edition, eLiB, 212 pages

Fioravante, V., Jamiolkowski, M., and LoPresti, D.C.F. (1994). Stiffness of carbonitic Quiou sand. Proceedings of the 13th International Conference of Soil Mechanics and Foundation Engineering, Vol. 1, New Delhi, pp. 163-167.

Foldin, N., and Broms, B. (1981). Historical development of Civil Engineering in soft clay. Soft Clay Engineering. Developments in Geotechnical Engineering 20, Elsevier Scientific Publishing Company, Amsterdam, pp. 27-156.

Foott, R., Ladd, C.C. (1981). Undrained settlement of plastic and organic clays. Journal of Geotechnical and Geoenvironmental Engineering, Vol. 107, No. GT8, pp. 1079-1094.

French, S.E. (1999). Design of Shallow Foundations. ASCE Press, Reston, Virginia, 374 pages.

Frydman, S. and Burd, H.J. (1997). Numerical studies of bearing-capacity factor $N_\gamma$. Journal of Geotechnical and Geoenvironmental Engineering, Vol. 123, No. 1, pp. 20-29.

Georgiadis, M. and Michalopoulos, A.P. (1985). Bearing capacity of gravity bases on layered soil, ASCE Journal of Geotechnical Engineering, Vol. 111, No. 6, pp. 713-729.

Georgiannou, V.N., Rampello, S., and Silvestri, F. (1991). Static and dynamic measurements of undrained stiffness on natural overconsolidated clays. The Proceedings of the 10th European Conference of Soil Mechanics and Foundation Engineering, Florence, Vol. 1, pp. 91-95.

Ghionna, V.N., Jamiolkowski, M., Pedroni, S., and Salgado, R. (1994). The tip displacement of drilled shafts in sand. Vertical and Horizontal Deformation of Foundations and Embankments, Vol. 2, GSP 40, ASCE, Reston, Virginia, pp. 1039-1057

Gibson, R.E. (1967). Some results concerning displacements and stresses in a non-homogeneous elastic half-space. Geotechnique, Vol. 17, No. 1, pp. 58-67.

Gillespie, D., Lunne, T., and Campanella, R.G. (1985). Tests with UBC seismic cone at three Norwegian research sites. Internal Report No. 59040-1. Norwegian Geotechnical Institute, Oslo, 59 p.

Giroud, J.P. (1970). Stresses under linearly loaded rectangular area. Journal of Soil Mechanics and Foundations Division, ASCE, Vol. 96, No. SM1, pp. 263-268.

Griffiths, D.V., and Prevost, J.H. (1990). Stress-strain curve generation from simple triaxial parameters. International Journal of Numerical and Analytical Methods in Geomechanics, Vol. 14, pp. 587-594.

Griffiths, D.V., Fenton, G.A., and Manoharan, N. (2002). Bearing capacity of rough strip footing on cohesive soil: probabilistic study. Journal of Geotechnical and Geoenvironmental Engineering, ASCE, Vol. 128, No. 9, pp. 743-755.

Hardin, B.O. (1978). The nature of the stress-strain behavior of soils. Earthquake Engineering and Soil Dynamics, ASCE, Vol. 1, pp. 3-90.

Hardin, B.O., and Drnevich, V.P. (1972). Shear modulus and damping in soils: design equations and curves. Journal of the Soil Mechanics and Foundations Division, ASCE, Vol. 98, No. SM 7, pp.667-692.

Harr, M.E. (1966). Foundations of Theoretical Soil Mechanics. McGraw-Hill Book Company, New York, 381 pages.

Hegazy, Y.A. and Mayne, P.W. (1995). Statistical correlations between $V_s$ and CPT Data for different soil types. Proceedings of the International Symposium on Cone Penetration Testing, CPT' 95, Vol. 2, Linköping, Swedish Geotechnical Society, pp. 173-178.

Hepton, P. (1988). Shear wave velocity measurements during penetration testing. Penetration Testing in the UK, Thomas Telford, London, pp. 275-283.

Hicher, P.Y. (1996). Elastic properties of soils. Journal of Geotechnical and Geoenvironmental Engineering, ASCE, Vol. 122, No. 8, pp. 641-648.

Hight, D. and Higgins, K.G. (1995). An approach to the prediction of ground movements in engineering practice: background and application. Proceedings of the International Symposium on Pre-failure Deformations of Geomaterials, IS-Hokkaido, Vol. 2, Balkema, Rotterdam, pp. 909-945.

Hight, D.W. (2003). Personal communication.

Hight, D.W., Bennell, J.D., Chana, B., Davis, P.D., Jardine, R.J., and Porovic, E. (1997). Wave velocity and stiffness measurements of the Crag and Lower London Tertiaries at Sizewell. Geotechnique, Vol. 47, No. 3, pp. 451-474.

Hight, D.W., Boesse, R., Butcher, A.P., Clayton, C.R.I., and Smith, P.R. (1992). Disturbance of the Bothkennar clay prior to laboratory testing. Geotechnique, Vol. 42, No.2, pp. 199-217.

Hight, D.W., Leroueil, S. (2003). Proceedings International workshop on characterization and engineering purposes of natural soils, Vol. 1, Singapore, pp. 255-360

Hoar, R.J. and Stokoe, K.H. (1978). Generation and measurement of shear waves in situ. Dynamic Geotechnical Testing, Special Technical Publication 654, ASTM, Philadelphia, pp. 3-29.

Holtz, R.D. (1991). Stress distribution and settlement of shallow foundations. Foundation Engineering Handbook, 2nd Edition, Chapman and Hall, New York, pp. 166-222.

Holtz, R.D. and Kovacs, W.D. (1981). An Introduction to Geotechnical Engineering, Prentice Hall, New Jersey, 733 pages

Holubec, I. and D'Appolonia, E. (1973). Effect of particle shape on the engineering properties of granular soils. Evaluation of Relative Density and Its Role in Geotechnical Projects Involving Cohesionless Soils, ASTM STP 523, ASTM, pp. 304-318.

Hryciw, R.D. (1990). Small-strain-shear modulus of soil by dilatometer. ASCE Journal of Geotechnical and Geoenvironmental Engineering, Vol. 116, No. 11, pp. 1700-1716.

Hunt, C.E., Pestana, J.M., Bray, J.D., Riemer, M. (2002). Effect of pile driving on static and dynamic properties of soft clay. ASCE Journal of Geotechnical and Geoenvironmental Engineering, Vol. 128, No. 1, pp. 13-24.

Ingra, T.S. and Baecher, G. (1983). Uncertainty in bearing capacity of sands. Journal of Geotechnical Engineering, ASCE, Vol. 109, No. 7, pp. 899-914.

Isenhower, W.M. (1979). Torsional simple shear/resonant column properties of San Francisco bay mud. MS thesis, Civil Engineering Department, University of Texas at Austin, Austin, Texas, 110 pages.

Itasca Consulting Group Inc. (2001a). FLAC: Fast Lagrangian Analysis of Continua User's Guide- Introduction, Section 1, 2nd Edition, 1st Revision, Minneapolis, Minnesota, 24 pages.

Itasca Consulting Group Inc. (2001b). FLAC: Fast Lagrangian Analysis of Continua User's Guide- Problem Solving with FLAC, Section 3, 2nd Edition, 1st Revision, Minneapolis, Minnesota, 148 pages.

Itasca Consulting Group Inc. (2001c). FLAC: Fast Lagrangian Analysis of Continua User's Guide- Theory and Background, Section 2, 2nd Edition, 1st Revision, Minneapolis, Minnesota, 92 pages.

Itasca Consulting Group Inc. (2001d). Estimating limit loads in high friction materials. FLAC: Fast Lagrangian Analysis of Continua Verification Problems, 2nd Edition, 1st Revision, Minneapolis, Minnesota, pp. 1-9.

Jamilokowski, M., Lancellota, R., LoPresti, D.C.F., and Pallara, O. (1994). Stiffness of Toyoura sand at small and intermediate strain. Proceedings of the 13th International Conference of Soil Mechanics and Foundation Engineering, New Delhi, Vol. 3, pp. 169-172.

Jamiolkowski, M. and Pepe, M.C. (2001). Vertical yield stress of Pisa clay from piezocone tests. ASCE Journal of Geotechnical and Geoenvironmental Engineering, Vol. 127, No.10, pp. 893-897.

Jamiolkowski, M., Ghionna, V.N., Lancellotta, R., and Pasqualini, E. (1988). New correlations of penetration tests for design practice, Penetration Testing 1988, ISOPT-1, Vol. 1, Balkema, Rotterdam, pp. 263-296.

Jamiolkowski, M., Lancellotta, R., and LoPresti, D.C.F. (1995). Remarks on the stiffness at small strains of six Italian clays. Pre-failure Deformation of Geomaterials, Vol. 2, Balkema, Rotterdam, pp. 817-836.

Janbu, N. (1969). The resistance concept applied to deformations of soils. Proceedings of the 7th International Conference of Soil Mechanics and Foundation Engineering, Mexico City, Vol. 1, pp. 191-196.

Jardine, R.J. and Lehane, B.M. (1993). Research into the behavior of offshore piles: field experiments in sand and clay. Health and Safety Executive (HSE), London, 136 pages.

Jardine, R.J., Fourie, A., Maswoswe, J., and Burland, J.B. (1985). Field and laboratory measurements of soil stiffness. Proceedings of the 11th International Conference of Soil Mechanics and Foundation Engineering, San Francisco, Vol.2, pp.511-514.

Jardine, R.J., Lehane, B.M., Smith, P.R., Gildea, P.A. (1995). Vertical loading experiments on rigid pad foundations at Bothkennar. Geotechnique, Vol. 45, No. 4, pp. 573-597.

Jardine, R.J., Potts, D.M., Fourie, A.B. and Burland, J.B. (1986). Studies of the influence of non-linear stress-strain characteristics in soil-structure interaction, Geotechnique, Vol. 36, No. 3, pp. 377-396.

Jardine, R.J., Symes, M.J., and Burland, J.B. (1984). The measurement of soil stiffness in the triaxial apparatus. Geotechnique, Vol. 34, No.3, pp. 323-340.

Keaveny, J.M., and Mitchell, J.K. (1986). Strength of fine-grained soils using the piezocone. Use of In Situ Tests in Geotechnical Engineering, GSP 6, ASCE/Reston, Virginia, pp. 668-685.

Kinner, E.B., and Ladd, C.C. (1973). Undrained bearing capacity of clay. Proceedings of the 8th International Conference on Soil Mechanics and Foundation Engineering, Vol. 1, Moscow, pp. 209-215.

Kinner, E.B., and Ladd, C.C. (1973). Undrained bearing capacity of clay. Proceedings 8th International Conference of Soil Mechanics and Foundation Engineering, Vol.1, Moscow, pp.209-215

Kohata, Y., Tatsuoka, F., Wang, L., Jiang, G.L., Hoques, E., and Kodaka, T. (1997). Modeling of the non-linear deformation properties of stiff geomaterials. Geotechnique, Vol. 47, No. 3, pp. 563-580.

Kokusho, T., Yoshida, Y., and Esashi, Y. (1982). Dynamic properties of soft clay for a wide strain range. Soil and Foundations, Vol. 22, No. 4, pp. 1-18.

Kondner, A.M. (1963). Hyperbolic stress-strain response: cohesive soils. Journal of the Soil Mechanics and Foundations Division, ASCE, Vol. 89, No. SM 1, pp.115-143.

Koutsoftas, D.C. (1981). Undrained shear behavior of a marine clay. Laboratory Shear Strength of Soil, STP 740, ASTM, Philadelphia, pp. 254-276.

Koutsoftas, D.C. and Fischer, J.A. (1980). Dynamic properties of two marine clays. Journal of Geotechnical Engineering Division, Vol. 106, No. 6, pp. 645-657.

Koutsoftas, D.C., and Ladd, C.C. (1985). Design strengths for an offshore clay. Journal of the Soil Mechanics and Foundations Division, ASCE, Vol. 111, No. 3, pp.337-355.

Krajcinovic, D. (1976). Rigid-plastic circular plates on elastic foundation. ASCE Journal of Soil Mechanics and Foundations Division, Vol. 102, No. GT2, pp. 213-224.

Kramer, S.L. (1996). Geotechnical Earthquake Engineering, Prentice Hall, New Jersey, 653 pages.

Kulhawy, F.H. and Mayne, P.W. (1990). Manual on Estimating Soil Properties for Foundation Design, Report No. EL-6800, Electric Power Research Institute, Palo Alto, CA, 306 pages.

Kulhawy, F.H., Trautmann, C.H., Beech, J.F., O'Rourke, T.D., and McGuire, W. (1983). Transmission Line Structure Foundations for Uplift-Compression Loading. Report No. EL-2870, Electric Power Research Institute, Palo Alto, CA, 346 pages.

Lacasse, S. and Vucetic, M. (1970). Discussion of state-of-the-art: Laboratory strength testing of soils. Laboratory Shear Strength of Soil, STP 740, ASTM, West Conshohocken, pp. 633-637.

Lacasse, S., Berre, T., and Lefebvre, G. (1985). Block sampling of sensitive clays. Proceedings 11th International Conference on Soil Mechanics and Foundation Engineering, Vol. 2, San Francisco, pp. 887-892.

Ladd, C.C. (1991). Stability evaluation during staged construction. Journal of Geotechnical Engineering, ASCE, Vol. 117, No. 4, pp. 540-615.

Ladd, C.C. and DeGroot, D.J. (2003). Recommended practice for soft ground site characterization: Arthur Casagrande Lecture. The Twelfth Pan American Conference on Soil Mechanics and Geotechnical Engineering, Boston, Vol. 1, Verlag Glückauf GMBH, Essen, pp. 3-57.

Ladd, C.C. and Lambe, T.W. (1963). The strength of "undisturbed" clay determined from undrained tests. Symposium on Laboratory Shear Testing of Soils, ASTM, STP 361, pp. 342-371.

Ladd, C.C., Foott, R., Ishihara, K., Schlosser, F., and Poulos, H.G. (1977). Stress-deformation and strength characteristics. Proceedings of 9th International Conference on Soil Mechanics and Foundation Engineering, Vol. 2, Tokyo, pp. 421-494.

Lambe, T.W. (1968). Behavior of foundations during construction. Journal of the Soil Mechanics and Foundations Division, ASCE, Vol. 94, No. SM 1, pp. 93-130.

Lambe, T.W., and Whitman, R. (1969). Soil Mechanics. John Wiley and Sons, New York, 553 pages.

Landon, M.M., DeGroot, D.J., and Jakubowski, J. (2004). Comparison of shear wave velocity measured in situ and on block samples of a marine clay. Proceedings 57th Canadian Geotechnical Conference, Quebec, pp. 22-28.

Larsson, R. (1977). Basic behavior of Scandinavian soft clays. Report No. 4, Swedish Geotechnical Institute, Linkoping, 125 pages.

Larsson, R. (1980). Undrained shear strength in stability calculation of embankments and foundations on soft clays. Canadian Geotechnical Journal, Vol. 17, No. 4, pp. 591-602.

Larsson, R. (1997), Investigations and Load Tests in Silty Soils. Report 54, Swedish Geotechnical Institute, Linkoping, 257 pages

Larsson, R. (2001). Investigations and Load Tests in Clay Till. Report 59, Swedish Geotechnical Institute, Linkoping, 169 pages.

Larsson, R. and Mulabdić, M. (1991a). Shear moduli in Scandinavian clays: Report No. 40, SGI, Linköping, 127 p.

Larsson, R. and Mulabdić, M. (1991b). Piezocone tests in clays: Report No. 42, SGI, Linköping, 240 p.

Lee, J. (1999). Design of foundations in sand based on CPT results. Ph.D. Thesis, Civil Engineering, Purdue University, West Lafayette, Indiana, 286 pages.

Lee, J., and Salgado, R. (2002). Estimation of footing settlement in sand. International Journal of Geomechanics, Vol. 2, No. 1, pp. 1-20.

Lee, J., Salgado, R., and Carraro, J.A.H. (2004). Stiffness degradation and shear strength of silty sands. Canadian Geotechnical Journal, Vol. 41, No. 5, pp. 831-843.

Lee, J.H., and Salgado, R. (1999). Determination of pile base resistance in sands. Journal of Geotechnical and Geoenvironmental Engineering, ASCE, Vol. 125, No. 8, pp. 673-683.

Lefebvre, G. and Poulin, C. (1979). A new method of sampling in sensitive clay. Canadian Geotechnical Journal, Vol. 16, No. 1, pp. 226-233.

Lefebvre, G., Ladd, C.C. and Pare, J-J. (1988). Comparison of field vane and lab undrained shear strength in soft sensitive clays. Vane Shear Strength Testing in Soils. STP 1014, ASTM, pp. 233-246.

Lehane, B. and Cosgrove, E. (2000). Applying triaxial compression stiffness data to

settlement prediction of shallow foundations on cohesionless soil. Geotechnical Engineering, Vol. 143, Institute of Civil Engineers, October, 191-200.

Lehane, B., and Fahey, M. (2002). Simplified nonlinear settlement prediction model for foundations on sand. Canadian Geotechnical Journal, Vol. 39, No. 2, pp. 293-303.

Lehane, B. (2003). Vertically loaded shallow foundation on soft clayey silt: A case history, Geotechnical Engineering, Vol. 156, No. 1, Institution of Civil Engineers, Thomas Telford, London.

Leonards, G.A. (1976). Estimating consolidation settlements of shallow foundations on overconsolidated clay. Manual of Practice: Estimation of Consolidation Settlement, Special Report 163, Transportation Research Board, National Research Council, Washington D.C., pp. 13-16.

Leroueil, S., and Marques, M.E.S. (1996). Importance of strain rate and temperature effects in geotechnical engineering. Measuring and Modeling Time Dependent Soil Behavior. GSP No. 61, ASCE, New York, pp. 1-60.

Lo Presti, D.C.F. (1994). General Report: measurement of shear deformation of geomaterials in the laboratory. Pre-Failure Deformation Characteristics of Geomaterials, Vol. 2, Balkema, Rotterdam, pp. 1067-1088.

Lo Presti, D.C.F., Jamiolkowski, M., and Pepe, M. (2003). Geotechnical characterization of the subsoil of Pisa Tower. Characterization and Engineering Properties of Natural Soils, Vol. 1, Swets and Zeitlinger, Lisse, pp. 909-946.

Lo Presti, D.C.F., Jamiolkowski, M., Oronzo, P., and Cavallaro (1996). Rate and creep effect on the stiffness of soils. Measuring and Modeling Time Dependent Soil Behavior. GSP No. 61, ASCE, New York, pp. 1263-1280.

Lo Presti, D.C.F., Jamiolkowski, M., Pallara, O., Cavallaro, A., and Pedroni, S. (1997). Shear modulus and damping of soils. Geotechnique, Vol. 47, No. 3, pp 603-617

Lo Presti, D.C.F., Pallara, O., and Puci, I. (1995). A modified commercial triaxial testing system for small strain measurements. Geotechnical Testing Journal, Vol. 18, No. 1, ASTM, pp. 15-31

Lo Presti, D.C.F., Pallara, O., Jamiolkowski, M., and Cavallaro, A. (1999-b). Anisotropy of small stiffness of undisturbed and reconstituted clays. Pre-Failure Deformation Characteristics of Geomaterials, Vol. 1, pp. 3-11

Lo Presti, D.C.F., Pallara, O., Lancellotta, R., Armandi, M. and Maniscalco, R. (1993). Monotonic and cyclic loading behavior of two sands at small strains. Geotechnical Testing Journal, Vol. 16, No. 4, ASTM, pp. 409-424.

Lo Presti, D.C.F., Shibuya, S., and Rix, G.J. (1999-a). Innovation in soil testing. Pre-Failure Deformation Characteristics of Geomaterials, Vol. 2, Balkema, Rotterdam, pp.1027-1076

Lowe, J. and Zaccheo, P.F. (1991). Subsurface explorations and sampling. Foundation Engineering Handbook, 2nd Edition, Chapman and Hall, New York, pp. 1-71.

Lundgren, H. and Mortensen, K. (1953). Determination by the theory of plasticity of the bearing capacity of continuous footings on sand. Proceedings of the 3rd International Conference on Soil Mechanics and Foundation Engineering, Zurich, Vol. 1, pp. 409-412.

Lunne, T. and Lacasse, S. (1999). Geotechnical characteristics of low plasticity clays. Characterization of Soft Marine Clays, Balkema, Rotterdam, pp. 33-56.

Lunne, T., Eidsmoen, T., Gillespie, D., and Howland, J.D. (1986). Laboratory and field evaluation of cone penetrometers. Use of In Situ Tests in Geotechnical Engineering, GSP 6, ASCE, Reston, pp. 714-729.

Lunne, T., Robertson, P.K., and Powell, J.J.M. (1997). Cone Penetration Testing in Geotechnical Practice. E & FN Spon, London, Routledge/New York, 312 pages.

Lutenegger, A.J. (2000). NGES at the University of Massachusetts-Amherst, National Geotechnical Experimentation Sites (GSP 93), ASCE, Reston/VA, pp. 102-129.

Marachi, N. Dean, Duncan, J.M., Chan, C.K., and Seed, H.B. (1981). Plane-strain testing of sand. Laboratory shear strength of soil, ASTM STP 740, ASTM, pp. 294-302.

Marchetti, S. (1980). In situ tests by flat dilatometer. Journal of the Geotechnical Engineering Division, ASCE, Vol. 106, No. 3, pp. 299-321.

Marchetti, S. (1997). Keynote lecture: flat dilatometer design applications. Proceedings of the 3rd International Geotechnical Engineering Conference, Cairo University, Cairo, pp. 421-448.

Marsland, A., Powell, J.J.M. (1980). Cyclic loading tests on 865 mm diameter plates of a stiff clay till. Proceedings of the international symposium on soils under cyclic and transient loading, Vol. 2, Swansea, pp. 837-847.

Massarsch, K.R. (2004). Deformation properties of fine-grained soils from seismic tests. Geotechnical and Geophysical Site Characterization, Vol. 1, Millpress, Rotterdam, pp. 133-146.

Massarsch, K.R., and Drnevich, V.P. (1979). Deformation properties of normally consolidated clays. Proceedings of the 7th European Conference on Soil Mechanics and Foundation Engineering, Vol. 2, Brighton, pp. 251-255.

Massarsch, K.R., Holtz, R.D., and Holm, B.G., and Fredriksson, A. (1975). Measurement of horizontal in situ stresses. In Situ Measurement of Soil Properties, Vol. 1, ASCE, Reston: 266-286.

Mayne, P.W. (1994). CPT-based prediction of footing response. Predicted and Measured Behavior of Five Spread Footings on Sand. Geotechnical Special Publication No. 41, ASCE, Reston, Virginia, pp. 214-217.

Mayne, P.W. (2001). Stress-strain-strength-flow parameters from enhanced in-situ tests. Proceedings of the International Conference on In-Situ Measurement of Soil Properties and Case Histories, Bali, pp. 27-48.

Mayne, P.W. (2003). Class A footing response prediction from seismic cone tests. Deformations Characteristics of Geomaterials, Vol. 1, Balkema, Lisse, pp. 883-888.

Mayne, P.W. (2005). Integrated ground behavior: in-situ and lab tests. Deformation Characteristics of Geomaterials: Recent Investigations and Prospects, Balkema, Lisse, pp. 155-177.

Mayne, P.W. and Poulos, H.G. (1999). Approximate displacement influence factors for elastic shallow foundations. Journal of Geotechnical and Geoenvironmental Engineering, Vol. 125, No. 6, pp. 453-460.

Mayne, P.W. and Poulos, H.G. (2001). Closure: "Approximate Displacement Influence Factors for Elastic Shallow Foundations". Journal of Geotechnical and Geoenvironmental Engineering, Vol. 127, No. 1, pp. 100-102.

Mayne, P.W. and Rix, G.J. (1995). Correlations between shear wave velocity and cone tip resistance in natural clays. Soils and Foundations, Vol. 35, No. 2, pp. 107-110.

Mayne, P.W., and Chen, B.S.Y. (1994). Preliminary calibration of PCPT-OCR model for clays. Proceedings of the 13th International Conference of Soil Mechanics and Foundation Engineering, New Delhi, Vol.1, pp. 199-202.

Mayne, P.W., and Kulhawy, F.H. (1982). $K_o$-OCR relationships in soil. Journal of Geotechnical Engineering, Vol. 108, No. GT6, pp. 851-872.

Mayne, P.W., and Rix, G.J. (1993). $G_{max}$-$q_c$ relationships for clays. ASTM Geotechnical Testing Journal, Vol. 16, No. 1, pp. 54-60.

Mayne, P.W., Christopher, B., and DeJong, J. (2002). Subsurface Investigations: Geotechnical Site Characterization. Publication No. FHWA-NHI-01-031, National Highway Institute, Federal Highway Administration, Washington, D.C., 301 pages.

Mayne, P.W., Puzrin, A., and Elhakim, A.F. (2003). Field characterization of small strain behavior of clays. The Twelfth Pan American Conference on Soil Mechanics and

Geotechnical Engineering, Boston, Vol. 1, Verlag Glückauf GMBH, Essen, pp. 307-313.

Mendelson, A. (1968). Plasticity: Theory and Applications, Macmillan Publishing Co., Inc., New York, 353 pages.

Mesri, G. and Godlewski, P.M. (1977). Time- and stress-compressibility interrelationship. Journal of Geotechnical Engineering, ASCE, Vol. 105, No. 1, pp. 106-113.

Mesri, G. and Rokhsar, A. (1974). Theory of consolidation for clays. Journal of the Geotechnical Engineering Division, ASCE, Vol. 100, GT 8, pp. 889-904.

Meyerhof, G. (1982a). Influence of roughness of base and groundwater conditions on the ultimate bearing capacity of foundations. The bearing capacity and Settlement of foundations. Tech-Press, Halifax, Canada, pp. 53-68.

Meyerhof, G. (1982b). The ultimate bearing capacity of foundations. The bearing capacity and Settlement of foundations. Tech-Press, Halifax, Canada, pp. 2-33.

Meyerhof, G.G. (1951). The ultimate bearing capacity of foundations. Geotechnique, Vol. 2, No. 4, pp. 301-332.

Meyerhof, G.G. (1961). Discussion of "Foundations other than piled foundations". Proceedings of the 5th International Conference of Soil Mechanics and Foundation Engineering, Vol. 3, Paris, pp. 193.

Meyerhof, G.G. (1963). Some recent research on the bearing capacity of foundations. Canadian Geotechnical Journal, Vol. 1, No. 1, pp. 16-26.

Meyerhof, G.G. (1984). Safety factors and limit states analysis in geotechnical engineering. Canadian Geotechnical Journal, Vol. 21, No. 1, pp. 1-7.

Michalowski, R.L. (1997). An estimate of the influence of soil weight on bearing capacity using limit analysis. Soils and Foundations, Vol. 37, No. 4, pp. 57-64.

Milović, D. (1972). Stresses and displacements in an anisotropic layer due to a rigid circular foundation. Geotechnique, Vol. 22, No. 1, pp. 169-174.

Milović, D. (1992). Stresses and Displacements for Shallow Foundations. Elsevier, Amsterdam, 620 pages.

Mimura, M. (2003). Characteristics of some Japanese natural sands - data from undisturbed frozen samples. Characterization and Engineering Properties of Natural Soils, Vol. 2, Balkema, Rotterdam, pp. 1149-1168.

Mitchell, J.K., and Gardner, W.S. (1975). In-situ measurement of volume change characteristics. Proceedings of the ASCE Specialty Conference on In-Situ Measurements of Soil Properties, Raleigh, North Carolina, Vol. 2, pp. 279-345.

Mizuno, E., and Chen, W.F. (1980). Analysis of soil response with different plasticity models. Application of plasticity and generalized stress-strain in geotechnical engineering: Proceedings of the Symposium on Limit Equilibrium, Plasticity, and Generalized Stress-Strain Applications in Geotechnical Engineering, ASCE, Reston, Virginia, pp. 115-138.

Nakase, A., Kusakabe, O., and Takemura, J. (1988). Centrifuge model tests on bearing capacity of clay. Geotechnical Ocean Engineering, Technomic Publishing, Lancaster, pp. 439-455.

Nash, D.F.T., Sills, G.C., and Davidson, L.R. (1992). One-dimensional consolidation testing of soft clay from Bothkennar. Geotechnique, Vol. 42, No. 2, pp. 241-256.

Nigbor, R.L., and Imai, T (1994). The suspension P-S velocity logging method. Proceedings 13th International Conference on Soil Mechanics and Foundation Engineering, TC10, New Delhi, pp. 57-61.

Nordlund, R.L. and Deere, D.U. (1970). Collapse of Fargo grain elevator. Journal of the Soil Mechanics and Foundations Division, Vol. 96, No. SM2, pp. 585-607.

Olsen, R.S. and Malone, G. (1988). Soil classification and site characterization using the CPT. Penetration Testing 1988 (ISOPT-1), Vol. 2, Balkema Publishers, Rotterdam, pp. 886-893.

Olsen, R.S. and Mitchell, J.K. (1995). CPT stress normalization and prediction of soil classification. Proceedings of the International Symposium on Cone Penetration Testing, CPT' 95, Vol. 2, Sweden, Swedish Geotechnical Society, Linkoping, pp. 257-262.

Pestana, J.M., Hunt, C.E., and Bray, J.D. (2002). Soil deformation and excess pore pressure field round a closed-ended pile. ASCE Journal of Geotechnical and Geoenvironmental Engineering, Vol. 128, no. 1, pp. 1-12.

Poulos, H.G. (1967). Stresses and displacements in an elastic layer underlain by a rough rigid base. Geotechnique, Vol. 17, No. 4, pp. 378-410.

Poulos, H.G. (1968). The behaviour of a rigid circular plate resting on a finite elastic layer. Civil Engineering Transactions, Sydney, Vol. 10, pp. 213-219.

Poulos, H.G. (2002). Critical role of ground characterization for foundation deformation prediction. The 5th Annual Sowers Lecture, Georgia Institute of Technology, pp. 1-34.

Poulos, H.G. and Davis, E. (1968). The use of elasticity theory for settlement prediction

under three dimensional conditions. Geotechnique, Vol. 18, No. 1, pp. 67-91.

Poulos, H.G. and Davis, E.H. (1974, 1991). Elastic Solutions for Soil and Rock Mechanics, Center for Geotechnical Research, University of Sydney, Sydney, 410 pages.

Powell, J.J.M. and Butcher, A.P. (2003). Characterization of a glacial clay till at Cowden, Humberside. Characterization and Engineering Properties of Natural Soils, Vol. 2, pp. 983-1020.

Powell, J.J.M., and Uglow**,** I.M. (1988). Interpretation of the Marchetti dilatometer test in UK clays. Penetration Testing in the UK, Thomas Telford, London, pp. 269-273.

Prevost, JH, Keane, CM (1990). Shear stress-strain curve generation from simple material parameters. Journal of Geotechnical and Geoenvironmental Engineering, Vol. 116, No. 8, pp. 1250-1254.

Puzrin, A.M., and Burland, J.B. (1996). A logarithmic stress-strain function for rocks and soils, Geotechnique, Vol. 46, No.1, pp. 157-164.

Puzrin, A.M., and Burland, J.B. (1998). Non-linear model of small-strain behavior of soils, Geotechnique, Vol. 48, No.2, pp. 217-233.

Ramberg, W. and Osgood, W.R. (1943). Description of stress-strain curves by three parameters. Technical Notes: National Advisory committee for Aeronautics No. 902. Washington, 27 pages.

Reese, L.C. and O'Neill, M.W. (1988). Drilled shafts: design procedures and design methods. Report No. FHWA-HI-88-042, Federal Highway Administration, Washington, DC, 564 p.

Richart Jr., F.E. (1977). Dynamic stress-strain relationships for soils, S-O-A. Proceedings 9$^{th}$ International Conference on Soil Mechanics and Foundation Engineering, Vol. 3, Tokyo, pp. 605-612.

Rix, G.J., and E.A. Leipski (1991). Accuracy and Resolution of Surface Wave Inversion. Recent Advances in Instrumentation, Data Acquisition, and Testing in Soil Dynamics, GSP No. 29, ASCE, New York, pp. 17-32.

Robertson, P.K. (1990). Soil classification using the cone penetration test. Canadian Geotechnical Journal, Vol. 27, No. 1, pp. 151-158.

Robertson, P.K., Campanella, R.G., Gillespie, D. and Rice, A. (1986-b). Seismic CPT to measure in situ shear wave velocity, Journal of Geotechnical Engineering, Vol. 112, No. 8, ASCE, pp. 781-803.

Robertson, P.K., Campanella, R.G., Gillespie, D., and Grieg, J. (1986-a). Use of piezometer cone data. Use of In-Situ Tests in Geotechnical Engineering. GSP No. 6, ASCE, New York, pp. 1263-1280.

Salgado, R. Lyamin, A.V., Sloan, S.W., and Yu, H.S. (2004). Two- and three-dimensional bearing capacity of foundations in clay. Geotechnique, Vol. 54, No. 5, pp. 297-306.

Sandven, R. (1990). Strength and deformation properties of fine grained soils obtained from piezocone tests. Ph.D. thesis, Department of Civil Engineering, The Norwegian Institute of Technology, Trondheim, 561 pages.

Santamarina, J.C., Klein, K.A., and, Fam, M.A. (2001). Soils and Waves. John Wiley and Sons, West Sussex, 488 pages.

Schmertmann, J.H. (1970). Static cone to compute static settlement over sand. Journal of Soil Mechanics and Foundations Division, ASCE, Vol. 96, No. SM3, pp. 1011-1043.

Schnaid, F., Wood, W.R., Smith, A.K.C., and Jubb, P. (1993). Investigation of bearing capacity and settlements of soft clay deposits at Shellhaven. Predictive Soil Mechanics, Thomas Telford, UK, pp. 609-627.

Schneider, J.A. (2000). Liquefaction response of soils in mid-America evaluated by seismic Cone Tests. MS Thesis, School of Civil and Environmental Engineering, Georgia Institute of Technology, Atlanta, 273 pages.

Schultz, E. and Melzer, K.J. (1965). The determination of the density and the modulus of compressibility of non-cohesive soils by soundings. Proceedings of the 6$^{th}$ International Conference on Soil Mechanics and Foundation Engineering, Vol. 1, Toronto, pp. 354-358.

Senneset, K. and Janbu, N. (1985). Shear strength parameters obtained from static cone penetration tests. Strength Testing of Marine Sediments: Laboratory and In situ Measurements, STP 883, ASTM, Philadelphia, pp. 41-54.

Senneset, K., Sandven, R. and Janbu, N. (1989). The evaluation of soils parameters from piezocone tests. Transportation Research Record, No. 1235, National Academy Press, pp. 24-37.

Sheahan, T.C., Ladd, C.C., and Germaine, J.T. (1996). Rate-dependent undrained shear behavior of saturated clay. Journal of Geotechnical and Geoenvironmental Engineering, Vol. 122, No. 2, pp. 99-108.

Shibuya, S., and Tamrakar, S.B. (1999). In-situ and laboratory investigations into engineering properties of Bangkok clay. Characterization of Soft Marine Clays, Balkema, Rotterdam, pp. 107-132.

Shibuya, S., Mitachi, T., Fukuda, F., and Hosomi, A. (1997). Modeling of strain-rate dependent deformation of clay at small strains. Proceedings of the 14th International Conference on Soil Mechanics and Geotechnical Engineering, Hamburg, Vol. 1, pp. 409-412.

Shibuya, S., Mitachi, T., Hosomi, A., and Hwang, S.C. (1996). Strain rate effects on stress-strain behavior of clay. Measuring and Modeling Time Dependent Soil Behavior. GSP No. 61, ASCE, New York, pp. 215-227.

Shibuya, S., Mitachi, T., Hosomi, A., and Hwang, S.C. (2000). Case studies of in-situ structure of natural sedimentary clays. Soils and Foundations. Vol. 40, No. 3, pp. 87-100.

Shibuya, S., Mitachi, T., Tanaka, H., Kawaguchi, T., and Lee, I.M. (2001). Measurement and application of quasi-elastic properties in geotechnical site characterization. Proceedings of the 11th International Conference on Soil Mechanics and Geotechnical Engineering, Istanbul, Turkey, Vol. 2, pp. 639-710.

Shibuya, S., Tatsuoka, Fumio, Teachavorasinskun, S., Kong, X.J., Abe, F., Kim, Y.S. and Park, C.S. (1992). Elastic Deformation Properties of Geomaterials. Soils and Foundations, Vol. 32, No. 3, pp. 26-46.

Shibuya, S., Yamashita, S., Watabe, Y., and Lo Presti, D.C.F. (2004). In-situ seismic survey in characterizing engineering properties of natural ground. Geotechnical and Geophysical Site Characterization, Vol. 1, Millpress, Rotterdam, pp. 167-185.

Soubra, A.H. (1999). Upper-bound solutions for bearing capacity of foundations. Journal of Geotechnical and Geoenvironmental Engineering, Vol. 125, No. 1, pp. 59-68.

Soydemir, C. (1976). Strength anisotropy observed through simple shear tests. Laurits Bjerrum Memorial Volume, NGI, Oslo: 99-113.

Stallebrass, S.E., and Taylor, R.N. (1997). The development and evaluation of constitutive model for the prediction of ground movements of overconsolidated clay. Geotechnique, Vol. 47, No 2, pp. 235-253.

Stark, R.F., and Booker, J.R. (1997). Surface displacements of a non homogenous elastic half-space subjected to uniform surface tractions. International Journal of Numerical and Analytical Methods in Geomechanics, Vol. 21, No. 6, pp. 361-378.

Steenfelt, J.S. (1977). Scale effect on bearing capacity factor $N_\gamma$. Proceedings of the 9th International Conference on Soil Mechanics and Foundation Engineering, Tokyo, Vol. 1, pp. 749-752.

Stokoe, K.H., and Santamarina, J.C. (2000). Seismic-wave-bases testing in geotechnical engineering. GeoEng 2000, International Conference on Geotechnical and Geological

Engineering, Melbourne, Vol. 1, pp. 1490-1536.

Stokoe, K.H., Wright, S.G., Bay, J.A., and Roesset, J.M. (1994). Characterization of geotechnical sites by SASW method. Proceedings 13th International Conference on Soil Mechanics and Foundation Engineering, Vol. 1, New Delhi, pp. 15-25.

Stroud, M.A. (1974). The SPT in insensitive clays and soft rocks. Proceedings of the European Symposium on Penetration Testing, Vol. 2.2, Stockholm, pp. 367-375.

Strout, J.M. (1998). Evaluation of the field compressometer test in sand. Doctoral thesis, The Norwegian University of Science and Technology, Trondheim, 238 pages.

Tanaka, H. (1995). National Report–The current state of CPT in Japan. Proceedings of the International Symposium on Cone Penetration Testing (CPT'95), Vol. 1, Linköping, Swedish Geotechnical Society, pp. 115-124.

Tanaka, H. (2000). Sample quality of cohesive soils: lessons from three sites, Ariake, Bothkennar and Drammen. Soils and Foundations, Vol. 40, No. 4, pp. 54-74.

Tanaka, H., and Tanaka, M. (1998). Characterization of sandy soils using CPT and DMT. Soils and Foundations, Vol. 38, No. 3, pp. 55-65.

Tanaka, H., and Tanaka, M. (1999). Key factors governing sample quality. Proceedings of the International Symposium on Characterization of Soft Marine Clays, Balkema, Rotterdam, pp. 57-81.

Tanaka, H., Shiwakoti, D.R., Mishima, O., Watabe, Y., and Tanaka, M. (2001). Comparison of mechanical behavior of two overconsolidated clays: Yamashita and Louiseville clays, Soils and Foundations, Vol. 41, No. 4, pp. 73-87.

Tang, Y.X., Hanzawa, H. and Yasuhara, K. (1994). Direct shear and direct simple shear test results on a Japanese marine clay. Pre-Failure Deformation of Geomaterials, Vol. 1, Balkema, Rotterdam, pp. 107-112.

Tatsuoka, F. (2002). Personal communication.

Tatsuoka, F. and Shibuya, S. (1992). Deformation characteristics of soils and rocks from field and laboratory tests. Institute of Industrial Science, The University of Tokyo, Tokyo, Vol. 37, No. 1, 136 pages.

Tatsuoka, F., Jardine, R.J., LoPresti, D., DiBenedetto, H. and Kodaka, T (1997). Theme Lecture: characterizing the pre-failure deformation properties of geomaterials. Proceedings of the 14th International Conference on Soil Mechanics and Foundation Engineering, Vol. 4, Hamburg, pp. 2129-2164.

Tatsuoka, F., Shibuya, S., and Kuwano, R. (2001): Recent advances in stress-strain testing of geomaterials in the laboratory; background and history of TC-29 for 1994, pp. 1-12.

Tatsuoka, F., Shibuya, S., and Kuwano, R., ed. (2001). Advanced Laboratory Stress-Strain Testing of Geomaterials, Balkema, Rotterdam, 329 pages.

Tatsuoka, F., Teachavorasinkun, S., Dong, J., Kohata, Y., and Sato, T. (1994). Importance of measuring local strains in cyclic triaxial tests on granular materials. Dynamic Geotechnical Testing II (STP 1213), ASTM, Philadelphia, pp. 288-302.

Teachavorasinskun, S., Shibuya, S. and Tatsuoka, F. (1991). Stiffness of sands in monotonic and cyclic torsional simple shear. Geotechnical Engineering Congress 1991, Vol. 2 (GSP No. 27), ASCE, Reston, Virginia, pp. 863-878.

Terzaghi, K. (1943). Theoretical Soil Mechanics, John Wiley and Sons, New York, N.Y., 528 pages.

Terzaghi, K. and Peck, R.B. (1967). Soil Mechanics in Engineering Practice. John Wiley and Sons, New York, 729 pages.

Terzaghi, K., Peck, R.B., and Mesri, G. (1996). Soil Mechanics in Engineering Practice. 3rd Edition, John Wiley and Sons, New York, 549 pages.

Timoshenko, S. and Goodier, J.N. (1951). Theory of Elasticity. McGraw Hill Book Co., New York, 506 pages.

Toki, S., Shibuya, S., and Yamashita, S. (1995). Standardization of laboratory test methods to determine the cyclic deformation properties of geomaterials in Japan. Pre-failure Deformations of Geomaterials, Vol. 2, Balkema, Rotterdam, pp. 741-784.

U.S. Army Corps of Engineers (1996). Engineer Manual EM 1110-1-1906: Soil Sampling, Department of the Army, Washington D.C., 240 pages.

Ueshita, K., and Meyerhof, G.G. (1968). Surface displacement of an elastic layer under uniformly distributed loads. Highway Research Records 228, National Research Council, Washington, D.C., pp. 1-10.

Ukritchon, B., Whittle, A., and Klangvijit, C. (2003). Calculations of bearing capacity factor $N_\gamma$ using numerical limit analyses. Journal of Geotechnical and Geoenvironmental Engineering, Vol. 129, No. 6, pp. 468-474.

Vesić, A.S. (1972). Expansion of cavities in an expanding soil mass. Journal of the Soil Mechanics and Foundations Division, ASCE, Vol. 98, No. SM 3, pp. 265-290.

Vesić, A.S. (1973). Analysis of ultimate loads of shallow foundations. Journal of the Soil Mechanics and Foundations Division, ASCE, Vol. 99, No. SM 1, pp. 45-73.

Vesić, A.S. (1975). Bearing capacity of shallow foundations. Foundation Engineering Handbook, Winkerkorn and Fang eds, Van Nostrand Reinhold Company, New York, N.Y., 751 pages.

Viana da Fonesca, A., and Sousa, J.A. (2002). Hyperbolic model parameters for FEM of footing load test on a residual soil from granite- a database for numerical modeling. Parameters de calcul geotechnique, LCPC, Paris, pp. 429-443.

Vucetic, M. (1994). Cyclic threshold shear strains in soils. Journal of Geotechnical and Geoenvironmental Engineering, Vol. 120, No. 12, pp. 2208-2228.

Vucetic, M., and Dobry, R. (1991). Effect of Soil Plasticity on Cyclic Response. Journal of Geotechnical and Geoenvironmental Engineering, Vol. 117, No. 1, pp.89-107.

Watabe, Y. (1999). Mechanical Properties of Ko-consolidation and shearing behavior observed in triaxial tests for five worldwide clays - Drammen, Louiseville, Singapore, Kansai, and Ariake clay. Characterization of Soft Marine Clays. Balkema, Rotterdam, p. 241-251.

Weiler, W.A. Jr. (1988). Small-strain shear modulus of clay. Earthquake Engineering and Soil Dynamics II - Recent Advances in Ground-motion Evaluation. GSP No. 20, ASCE, Reston, VA, pp. 331-345.

Whitman, R.V., Casagrande, D.R., Karlsrud, K., and Simon, R. (1971). Performance of foundation for ALTAIR radar. ASCE Journal of Soil Mechanics and Foundations Division, Vol. 97, No. SM1, pp. 1-18.

Whittle, A.J. (1993). Evaluation of a constitutive model for overconsolidated clays. Geotechnique, Vol. 43, No. 2, pp. 289-313.

Woods, R.D. (1978). Measurement of dynamic soil properties. Earthquake Engineering and Soil Dynamics, Vol. 1, ASCE, Reston, pp. 91-178.

Woods, R.D. (1994). Laboratory measurement of dynamic soil properties. Dynamic Geotechnical Testing II. Special technical publication STP 1213, American Society for Testing and Materials, ASTM, pp. 165-190

Wroth, C.P. (1984). The interpretation of in-situ soil tests. Geotechnique, Vol. 34, No. 4, pp. 449-489.

Wroth, C.P., and Houlsby, G.T. (1985). Soil mechanics-property characterization and analysis procedures. Proceedings 11th International Conference of Soil Mechanics and Foundation Engineering, San Francisco, Vol. 1, pp.1-55.

Yamashita, S., Hori, T., and Suzuki, T. (2003). Effects of fabric anisotropy and stress condition on small strain, Vol. 1, Swets and Zeitlinger, Lisse, pp. 187-194.

Yamashita, S., Kohata, Y., Kawaguchi, T., and Shibuya, S. (2001). International round-robin test organized by TC-29. Advanced Laboratory Stress-Strain Testing of Geomaterials, Swets and Zeitinger, Lisse, pp. 65-86.

Yin, J.H., Wang, Y.J., and Selvadurai, A.P.S. (2001). Influence of nonassociativity on the bearing capacity of a strip footing. Journal of Geotechnical and Geoenvironmental Engineering, Vol. 127, No. 11, pp. 985-989.

Zhu, D. (2000). The least upper-bound solutions for bearing capacity factor $N_\gamma$. Soils and Foundations, Vol. 40, No. 1, pp. 123-129.

Zhu, H. and Chang, M.F. (2002). Load transfer curves along bored piles considering modulus degradation. Journal of Geotechnical and Geoenvironmental Engineering, Vol. 128, No. 9, pp. 764-774.

# VITA

Amr Elhakim was born on September 22nd, 1972 in Cairo, Egypt. He graduated from El-Horreya Language Schools, Giza, Egypt in July 1990. After that he joined the faculty of Engineering, Cairo University, Cairo, Egypt in September 1990. In July 1995, he earned his B.Sc. in Civil Engineering with honors degree. He worked as a teaching assistant in the Soil Mechanics and Foundations Research Laboratory of Cairo University the in 1995. The same year, he enrolled for a Masters program in Geotechnical Engineering in Cairo University, where he earned his M.Sc. in July 1998. The thesis is titled "Evaluation of the Performance of the Flat Dilatometer in Cohesive Soils".

Amr then joined the Geosystems Engineering Group at Georgia Tech, where he worked under the supervision of Prof. Paul W. Mayne. In May 2001, Amr earned another Masters in Geotechnical Engineering from Georgia Tech. He then finished his doctoral degree in Summer 2005. In May 2001, Amr was awarded the Outstanding Graduate Teaching Award from the School of Civil and Environmental Engineering. Amr is married to Mariam Ghaffar and they have two beautiful children Abdullah and Amina.